The Caltech-Jodrell Bank VLBI Surveys

The Caltech-Jodrell Bank VLBI Surveys

The 'Pearson-Readhead' Survey (PR)

Pearson, T. J., Readhead, A. C. S.
1981, ApJ, 248, 61-81
The milli-arcsecond structure of a complete sample of radio sources. I. VLBI maps of seven sources.

Pearson, T. J., Readhead, A. C. S.
1988, ApJ, 328, 114-142
The milli-arcsecond structure of a complete sample of radio sources. II. First-epoch maps at 5 GHz.

The First Caltech-Jodrell Bank Survey (CJ1)

Polatidis, A.G., Wilkinson, P. N., Xu, W., Readhead, A. C. S., Pearson, T. J., Taylor, G. B., Vermeulen, R. C.
1995, ApJS, 98, 1-32
The first Caltech-Jodrell Bank VLBI survey. I. 18 cm observations of 87 sources.

Thakkar, D. D., Xu, W., Readhead, A. C. S., Pearson, T.J., Taylor, G. B., Vermeulen, R. C., Polatidis, A. G., Wilkinson, P. N.
1995, ApJS, 98, 33-40
The first Caltech-Jodrell Bank VLBI survey. II. 18 cm observations of 25 sources.

Xu, W., Readhead, A. C. S., Pearson, T. J., Polatidis, A.G., Wilkinson, P. N.
1995, ApJS, 99, 297-348
The first Caltech-Jodrell Bank VLBI survey. III. VLBI and MERLIN observations at 5 GHz and VLA observations at 1.4 GHz.

The Second Caltech-Jodrell Bank Survey (CJ2)

Taylor, G. B., Vermeulen, R. C., Pearson, T. J., Readhead, A. C. S., Henstock, D. R., Browne, I. W. A., Wilkinson, P. N.
1994, ApJS, 95, 345-369
The second Caltech-Jodrell Bank VLBI survey. I. Observations of 91 of 193 sources.

Henstock, D. R., Browne, I. W. A., Wilkinson, P. N., Taylor, G. B., Vermeulen, R. C., Pearson, T. J., Readhead, A. C. S.
1995, ApJS, 100, 1-36
The second Caltech-Jodrell Bank VLBI survey. II. Observations of 102 of 193 sources.

THE ASTROPHYSICAL JOURNAL, 248:61–81, 1981 August 15

THE MILLI-ARCSECOND STRUCTURE OF A COMPLETE SAMPLE OF RADIO SOURCES. I. VLBI MAPS OF SEVEN SOURCES

T. J. PEARSON AND A. C. S. READHEAD
Owens Valley Radio Observatory, California Institute of Technology
Received 1980 November 3; accepted 1981 March 2

ABSTRACT

The sample of 51 sources between declinations 35° and 70° with galactic latitude $>10°$ and flux density ≥ 1.3 Jy at 5 GHz contains 36 objects that are suitable for study by very long baseline interferometry (VLBI). Observations have been made of seven of these with a VLBI array of four U.S.A. antennas at a frequency of 5 GHz with full hour-angle coverage. The results show a wide variety of morphologies: two sources (0133+476 and 0859+470) are only slightly resolved, one is a double source (0923+392=4C 39.25) with a constant separation, three (1807+698=3C 371, 1828+487=3C 380, and 2200+420=BL Lac) have an elongated linear structure, and the last (0316+413=3C 84) is complex. Later papers in the series will present the observations of the remaining sources in the sample.

Subject headings: BL Lacertae objects — interferometry — quasars — radio sources: general

I. INTRODUCTION

Recent developments in very long baseline interferometry (VLBI) have made it possible to make aperture synthesis maps of the milli-arcsecond structure of extragalactic radio sources. It is now possible routinely to make reliable observations of high quality at four or more telescopes simultaneously, and the enlargement of the Caltech-JPL Processor to process all 10 baselines from a five-telescope experiment enables us to take full advantage of the extensive (u, v)-plane coverage offered by such observations. The recognition of the value of closure phase (the sum of the visibility phases around a closed loop of baselines: Jennison 1958; Rogers *et al.* 1974) as a good observable, unaffected by the instrumental and atmospheric instabilities that prevent the measurement of visibility phase, and the development of iterative techniques to estimate the true visibility phases from the measured visibility amplitudes and closure phases (Readhead and Wilkinson 1978; Cotton 1979), have made milli-arcsecond aperture synthesis a reality.

So far this technique has been applied to only a small number of sources. For example, Cohen and his colleagues have mapped the "superluminal" sources 3C 273, 3C 345, and 3C 120, which show apparent expansion velocities greater than the speed of light, at two frequencies and at several epochs (Cohen *et al.* 1979); Readhead and Wilkinson and their colleagues have made low-frequency maps of sources which show synchrotron self-absorption at frequencies below 1 GHz, which may be expected to show structure on angular scales of 0.″01–0.″1 (Wilkinson *et al.* 1977; Wilkinson *et al.* 1979; Readhead and Wilkinson 1980; Pearson, Readhead, and Wilkinson 1980; Simon *et al.* 1980). These programs have shown that on the milli-arcsecond scale a large proportion of sources show a characteristic morphology, consisting of a compact, flat-spectrum (presumably self-absorbed) core, with a steeper-spectrum extension on one side, commonly called a jet. The jet appears to be closely related to the large-scale (arc second) structure of the sources: for example, in the classical double radio galaxy NGC 6251 the milli-arcsecond jet is closely aligned with a much larger-scale jetlike feature which extends out of the galaxy toward one of the two outer lobes (Readhead, Cohen, and Blandford 1977; Cohen and Readhead 1979; see also Linfield 1981). In compact sources without classical double structure, the jet is frequently aligned with such arc-second structure as is present; for example, in 3C 273 the radio jet lies within 30° of the position angle of the optical jet. In these sources, however, the alignment is less perfect than in the classical double sources (Readhead *et al.* 1978; Readhead 1980). This has suggested that in the compact sources, the jet represents a beam of energy propagating almost directly toward the observer, with its radiation amplified by relativistic aberration (Readhead *et al.* 1978; Scheuer and Readhead 1979; Blandford and Königl 1979).

It is impossible to assess the statistical significance of these suggestive results without observations of a statistically unbiased sample of sources. Selection on the basis of spectrum, for example, is inadequate as there is known to be a close connection between the angular structure and spectrum of sources. Similarly, to de-

termine how common apparent superluminal expansions are, high-resolution observations are needed of a complete sample at several epochs. The attempts which have been made to determine what fraction of sources show superluminal expansion have suggested that they are quite common, but the estimates are based on very small samples (four superluminal sources in a sample of 10: M. H. Cohen *et al.* 1977).

These are the reasons that led us to make the study of a complete sample of sources that is reported here. This first paper describes the selection of the sample and presents maps of the first seven sources. The maps of the remaining sources, and the discussion of the properties of the sample as a whole, will be the subject of later papers in the series.

II. THE SAMPLE

The choice of a sample for study is governed both by scientific objectives and by observational constraints. To avoid biasing the sample, we chose to select sources by total flux density only. Selection of the sample is thus reduced to three parameters: the frequency of the finding survey, the flux density limit, and the region of sky covered. For the selection frequency we chose 5 GHz, because this is the highest frequency at which full-sky surveys are available, and it is known that the proportion of flat-spectrum, compact objects suitable for study via VLBI increases with selection frequency. 5 GHz is also the frequency of our VLBI mapping observations. The location of suitable telescopes in the northern hemisphere restricts us to northern sources, and in order to achieve the best possible coverage of the (u, v)-plane we further restricted the sample to sources north of declination 35°. The size of the sample is of course restricted by the observing time available and by the sensitivity of the telescopes; it is these constraints that determine the flux density limit.

Our sample is defined by the following criteria:

1. Declination: $35° < \delta < 70°$.
2. Galactic latitude: $|b| > 10°$.
3. Flux density: $S(5\ \mathrm{GHz}) \geq 1.3$ Jy.

The sky coverage of the sample is that of the NRAO–MPIfR[1] ***S4*** survey (Pauliny-Toth *et al.* 1978*a*) from which the values of $S(5\ \mathrm{GHz})$ were taken. The sample so defined contains 51 sources. These sources are listed in Table 1, with their positions, flux densities, optical identifications, and redshifts. The restriction to declinations below 70° was dictated by the absence of a 5 GHz sky survey of higher declinations. With the completion of the MPIfR ***S5*** survey (Kühr *et al.* 1981) this restriction has been lifted, and we intend to enlarge our sample by removing the northern declination limit.

[1]National Radio Astronomy Observatory–Max-Planck-Institut für Radioastronomie.

It is not possible at present to make VLBI maps of all the sources in the sample, because the sensitivity of the VLBI array is insufficient to map sources without a strong compact component. One can decide which sources are mappable on the basis of the observations that have been made with aperture synthesis telescopes, with a resolution of about 1″. The sources are classified in Table 1 according to their arc-second-scale morphology.

The *extended* sources are marked I or II according to their Fanaroff-Riley class (Fanaroff and Riley 1974). The sample includes three of the low-luminosity class I sources (3C 66B, 3C 83.1B=NGC 1265, 3C 449); all of these have compact central components (Preuss *et al.* 1977; van Breugel *et al.* 1981), but at $\lesssim 100$ mJy they are all too weak to be mapped with VLBI. There are 13 high-luminosity class II sources, of which only two (3C 179 and 3C 236) have central components strong enough to map.

There are 34 *compact* sources ($\lesssim 1''$) in the sample. All of these are candidates for mapping. In Table 1 they are marked U (unresolved), or C ("core"-type: Readhead *et al.* 1978) if there is low-brightness resolved structure present. Many of the U sources have not yet been studied with sufficient dynamic range at resolutions of $\sim 1''$ to see if they belong in the C class.

The remaining source is 3C 231, associated with the irregular galaxy M82. VLBI observations of 3C 231 have been made by Geldzahler *et al.* (1977) and Shaffer and Marscher (1979). The 5 GHz flux density of the compact component is ~ 150 mJy, which is too weak for mapping, and as it is a completely different sort of object from the others in the sample we shall not consider it further.

These considerations of the arc-second-scale morphology of the sources thus reduce the sample for which VLBI maps are to be made from 51 to 36 sources: 34 compact sources and two extended doubles.

In order to confirm this conclusion, and to avoid wasting valuable observing time on sources that are too weak to map, we conducted a "finding survey" in 1978 July (1978.51), in which we made brief observations of all 51 sources in the sample. An array of four U.S. antennas was used (Table 2), and each source was observed for two periods of 30 minutes each, separated by about 6^h in hour angle. Thus the visibility of each source was measured at 12 points in the (u, v)-plane. (A small number of sources were observed at fewer points, owing to instrumental failures.) Thirty-five of the 36 sources that we expected to detect showed fringes in this survey, the exception being 1634+628 (3C 343). None of the sources that we did not expect to detect showed fringes. As we intended to make maps of the sources, we did not conduct an elaborate analysis of the results of the finding survey, but simply determined the best-fitting circular Gaussian model of each source. The results are

TABLE 1

THE COMPLETE SAMPLE

Source (1)	(2)	RA (3)	Dec (4)	S(5GHz) (Jy) (5)	Opt type (6)	m_v (7)	z (8)	Radio type (9)	S(core) (Jy) (10)	size (") (11)	Ref (12)
0040+517	3C20	00 40 19.70	51 47 07.2	4.18	G	19	0.350	II	<0.01	-	JPR,L1
0108+388	OC314	01 08 47.27	38 50 32.6	1.35	EF			U			P
0133+476	OC457	01 33 55.13	47 36 13.0	3.26	Q	18.0	(0.86)	U			PW
0220+427	3C66B	02 20 01.73	42 45 54.6	3.75	G	12.9	0.0215	I	0.23	<1.6	N
0314+416	3C83.1B	03 14 56.79	41 40 32.6	3.53	G	12.5	0.0255	I	0.02	<0.1	RP,OBR
0316+413	3C84	03 16 29.56	41 19 51.9	47.2	G	11.9	0.0177	U			ER
0538+498	3C147	05 38 43.51	49 49 42.8	8.18	Q	17.8	0.545	C			L2
0605+480	3C153	06 05 44.46	48 04 49.0	1.35	G	18.5	0.2769	II	<0.01	-	L1,PH
0710+439	OI417	07 10 03.33	43 54 26.2	1.66	G	20.7		U			PW
0711+356	OI318	07 11 05.62	35 39 52.6	1.51	Q	17.0	1.620	U			PW
0723+679	3C179	07 23 04.29	67 54 52.7	1.31	Q	18.0	0.846	II			PW
0804+499	OJ508	08 04 58.40	49 59 23.0	2.07	Q?	19.0		U			PW
0809+483	3C196	08 09 59.42	48 22 07.2	4.35	Q	17.8	0.871	II	<0.05	-	PH
0814+425	OJ425	08 14 51.67	42 32 07.7	1.68	Q	17.7		U			PW
0831+557	4C55.16	08 31 04.37	55 44 41.4	5.60	G	17.5	0.2420	U			L2
0850+581	4C58.17	08 50 50.40	58 08 55.0	1.41	Q	18.0	1.322	C			P
0859+470	4C47.29	08 59 39.97	47 02 56.9	1.78	Q	18.7	1.462	C			PFJ
0906+430	3C216	09 06 17.25	43 05 59.4	1.78	Q	18.5	0.670	U			JPR
0917+458	3C219	09 17 50.67	45 51 43.5	2.29	G	17.2	0.1744	II	0.04	<0.25	B,PBWF
0923+392	4C39.25	09 23 55.31	39 15 23.6	8.90	Q	17.9	0.699	U			ER
0945+408	4C40.24	09 45 50.04	40 53 43.6	1.39	Q	17.5	1.252	C			PFJ
0951+699	3C231,M82	09 51 41.95	69 54 57.5	3.94	G	8.4	0.0009	?			
0954+556	4C55.17	09 54 14.34	55 37 16.4	2.27	Q	17.9	(0.909)	U			PW
0954+658		09 54 57.83	65 48 15.8	1.46	Q	16.7		U			P
1003+351	3C236	10 03 05.39	35 08 48.0	1.32	G	16.0	0.0989	II	1.50	0.2	FMB
1031+567	OL553	10 31 56.00	56 44 18.1	1.31	G	21.3		U			PW
1254+476	3C280	12 54 41.05	47 36 32.1	1.53	G	20		II	<0.01	-	L1,PH
1358+624	4C62.22	13 58 58.32	62 25 06.7	1.77	G	20.9		U			PW
1409+524	3C295	14 09 33.50	52 26 13.0	6.48	G	20.1	0.4614	II	<0.02	-	L1,PE
1609+660	3C330	16 09 16.16	66 04 30.0	2.35	G	20.8	0.549	II	<0.02	-	JPR,L1
1624+416	4C41.32	16 24 18.22	41 41 23.4	1.31	EF			U			PW
1633+382	4C38.41	16 33 30.63	38 14 09.9	4.08	Q	18.0	1.814	U			PW
1634+628	3C343	16 34 01.06	62 51 41.8	1.50	Q	20.6	0.988	U			ER
1637+574	OS562	16 37 17.43	57 26 15.8	1.44	Q	17.0	0.745	C			P
1641+399	3C345	16 41 17.60	39 54 10.8	10.9	Q	16.0	0.595	U			ER
1642+690	4C69.21	16 42 18.03	69 02 13.7	1.43	Q	19.2		C			PFJ
1652+398	4C39.49	16 52 11.75	39 50 24.6	1.42	G	13.8	0.0337	U			
1739+522	4C51.37	17 39 29.00	52 13 10.3	1.99	Q	18.5	1.375	U			PW
1807+698	3C371	18 07 18.54	69 48 57.1	2.33	G	14.8	0.050	C			PFJ
1823+568	4C56.27	18 23 14.93	56 49 18.1	1.67	Q?	18.9		U			PW
1828+487	3C380	18 28 13.54	48 42 40.5	6.19	Q	16.8	0.692	C			L2
1842+455	3C388	18 42 35.45	45 30 21.6	1.77	G	15.3	0.0908	II	0.10	<1.3	PH
1939+605	3C401	19 39 38.84	60 34 32.6	1.52	G	18.0	0.201	II	0.04	<2	JPR
1954+513	OV591	19 54 22.46	51 23 46.3	1.43	Q	18.5	1.230	U			PW
2021+614	OW637	20 21 13.31	61 27 18.1	2.31	SO	19.5		U			PW
2153+377	3C438	21 53 45.49	37 46 12.9	1.54	G	19.3	0.292	II	0.01	<0.5	JPR,L1
2200+420	OY401	22 00 39.36	42 02 08.6	4.75	Q	14.5	0.069	U			ER
2229+391	3C449	22 29 07.63	39 06 03.5	1.39	G	13.2	0.0171	I	0.04	<0.4	PWS
2243+394	3C452	22 43 32.81	39 25 27.6	3.26	G	16.0	0.0811	II	0.13	<0.8	RP
2351+456	4C45.51	23 51 49.96	45 36 22.9	1.41	G?	20.6		U			PW
2352+495	OZ488	23 52 37.78	49 33 26.8	1.77	G	19.0	0.2370	U			ER,FB

EXPLANATION OF TABLE 1

Col. (1).—Source name according to IAU convention.

Col. (2).—Alternative name.

Cols. (3), (4).—Right ascension and declination (1950.0); from Peacock and Wall (1981) when available or from Pauliny-Toth *et al.* (1978*a*). All are measured with interferometers and have uncertainties typically less than 0".3.

Col. (5).—Flux density at 5 GHz (Jy), from the S4 survey (Pauliny-Toth *et al.* 1978*a*), epoch 1974 December.

TABLE 1—*Continued*

Col. (6).—Optical identification: EF, Empty field. G, Galaxy. Q, Quasar or BL Lac object. SO, Stellar object.
Col. (7).—Optical magnitude, m_v.
Col. (8).—Redshift. The data in columns (6)–(8) are from the compilations of Burbidge and Crowne (1979), Hewitt and Burbidge (1980), and Peacock and Wall (1981), with the following exceptions: 0040+417 (Laing 1981*b*), 0108+388 (Johnson 1974), 0954+658 (Walsh, Wills and Wills 1979), 1642+690 (Perley, Fomalont, and Johnston 1980).
Col. (9).—Radio morphology: I, Extended double, Fanaroff-Riley class I. II, Extended double, Fanaroff-Riley class II. C, "Core" source with dominant central component. U, Unresolved by aperture-synthesis telescopes.
Col. (10).—Flux density of central component at 5 GHz (Jy), for class I and class II sources only.
Col. (11).—Angular size of central component (arc seconds), for class I and class II sources only, determined using synthesis telescopes.
Col. (12).—References for radio data in columns (9)–(11): B, Burch 1979. ER, Elsmore and Ryle 1976. FMB, Fomalont, Miley, and Bridle 1979. JPR, Jenkins, Pooley, and Riley 1977. L1, Laing 1981*b*. L2, Laing 1981*a*. N, Northover 1973. OBR, Owen, Burns, and Rudnick 1978. P, R. A. Perley, private communication. PBWF, Perley *et al.* 1980. PFJ, Perley, Fomalont, and Johnston 1980. PH, Pooley and Henbest 1974. PW, Peacock and Wall 1981. PWS, Perley, Willis, and Scott 1979. RP, Riley and Pooley 1975.

TABLE 2

THE ANTENNAS

	Location	Diameter (m)	System Temp (K)[a]	Sensitivity (K/Jy)[b]
NRAO ...	National Radio Astronomy Observatory, Green Bank, West Virginia	43	70	0.31
FDVS	Harvard Radio Astronomy Station, Fort Davis, Texas	26	140	0.082
OVRO ...	Owens Valley Radio Observatory, Big Pine, California	40	120	0.22
HCRK ...	University of California, Hat Creek, California	26	70	0.074

[a]System temperatures are typical values for the run.
[b]Sensitivities are peak values: there is some variation with the attitude of the antenna.

given in Table 3. Owing to problems calibrating the Fort Davis antenna, we were forced to omit three baselines from this analysis; the fit is thus based on six 30-minute tracks on each source.

Table 3 lists the flux density and diameter (FWHM) of the Gaussian model, obtained by least-squares fit of a straight line of the form

$$\log(S) = a + b(u^2 + v^2),$$

where S is the correlated flux density at the point (u, v). This is the correct statistical procedure to use when the data are affected primarily by multiplicative calibration errors rather than additive noise errors. The linear correlation coefficient r is also listed: a value of -1 indicates perfect correlation, i.e. exact fit to a Gaussian, while positive values of r imply that the visibility increases with increasing baseline, in which case the corresponding diameter is imaginary. The Gaussian parameters should not be taken too literally for sources with $r > -0.7$.

III. THE FIRST SEVEN SOURCES: OBSERVATIONS AND ANALYSIS

The remainder of this paper is concerned with the observations made in 1978 December of seven sources from the complete sample. The observational technique will be the same for all the sources. In the first observing session we studied seven of the strongest sources: 0133+476, 0316+413, 0859+470, 0923+392, 1807+698, 1828+487, and 2200+420.

The observations, made on 1978 December 11–14 (1978.95), in the frequency band 5.010–5.012 GHz, utilized the same four telescopes as the finding survey (Table 2). This array gives six baselines, ranging in length from 6.2 million to 58 million wavelengths (equatorial component). Hydrogen-maser frequency standards were used at all four stations. The data were recorded on NRAO Mark II terminals (Clark 1973). The feeds were linearly polarized with the E-vector in position angle 90°, so the resulting maps represent the distribution of $I-Q$ rather than the total intensity I.

TABLE 3

RESULTS OF THE FINDING SURVEY

Source	Flux Density (Jy)	FWHM (milli-arcsec)	Linear Correlation Coefficient (r)
0108+388	1.14	1.16	−0.63
0133+476	1.77	1.22	−0.93
0316+413	38.3	3.05	−0.73
0538+498	1.52	2.96	−0.89
0710+439	0.79	1.18	−0.47
0711+356	0.96	1.07	−0.58
0723+679	0.31	0.29	−0.04
0804+499	0.49	1.13	−0.77
0814+425	1.60	1.15	−0.87
0831+557	3.23	3.05	−0.99
0850+581	0.88	0.53	−0.32
0859+470	0.98	0.83	−0.48
0906+430	0.70	...	+0.25
0923+392	8.89	2.42	−0.90
0945+408	1.03	1.21	−0.72
0954+556[a] ...	...	...	...
0954+658	0.49	0.39	−0.15
1003+351	0.29	1.71	−0.52
1031+567[a] ...	...	...	...
1358+624	0.49	1.60	−0.53
1624+416	0.83	2.05	−0.75
1633+382	1.59	1.35	−0.88
1634+628[b] ...	...	...	...
1637+574	0.81	...	+0.20
1641+399	4.91	1.50	−0.43
1642+690	1.52	...	+0.13
1652+398	0.65	1.19	−0.82
1739+522	0.39	0.56	−0.10
1807+698	1.21	1.40	−0.58
1823+568	0.79	...	+0.19
1828+487	0.68	...	+0.52
1954+513	0.73	0.97	−0.26
2021+614	1.52	1.70	−0.48
2200+420	2.24	1.77	−0.69
2351+456	0.95	2.09	−0.96
2352+495	1.62	1.00	−0.96

[a]Less than 3 (u, v) points detected: these sources are heavily resolved.

[b]Not detected in the finding survey.

The data were cross-correlated using the Caltech/JPL Interferometry Processor. The processor output was integrated coherently for 120 s. The visibility amplitudes were calibrated in the usual way (Cohen *et al.* 1975) and used with the closure phase to make hybrid maps by the method of Readhead and Wilkinson (1978). The calibrated visibility amplitudes and closure phases are presented in the Appendix.

The accuracy of the maps depends on the (u, v)-coverage, sensitivity, and dynamic range of the observations.

a) (u, v)-*Coverage*

As far as possible, each source was observed continuously for the full period for which it was visible from all four telescopes, generally between 9.5 and 11.5 hours; 0133+476 was observed for only 5 hours and 1807+698 for 8 hours. A typical example of the (u, v)-coverage obtained is shown in Figure 1. While this coverage is good by comparison with what has been available in past VLBI experiments, it does not approach the completeness of coverage achieved with purpose-built aperture synthesis instruments. In the absence of any *a priori* information about the source, the sampling theorem tells us that to map a source of size less than θ with resolution $\delta\theta$, we need to sample the (u, v)-plane every $1/\theta$ wavelengths out to a maximum of $1/\delta\theta$ wavelengths. This sampling requirement on the uniformity of the (u, v)-coverage is not satisfied in the present observations, and we must therefore remember that there may be real features of the source which are not represented or are incorrectly represented in the maps. Blind tests, like those conducted by Readhead and Wilkinson (1978), give us some confidence that the (u, v)-coverage is adequate to map simple sources, but of course we do not know *a priori* that the sources *are* sufficiently simple. The sampling requirement is unlikely to be satisfied with any array of presently existing telescopes, and fully reliable VLBI maps must await the construction of a carefully designed VLBI array.

b) *Sensitivity*

In the present observations the coherent integration time was 120 s and the bandwidth was 2 MHz; the system temperatures and sensitivities of the antennas are given in Table 2. From these data one can calculate the rms noise in a single integration, following the procedure described by Cohen *et al.* (1975): the noise varied from 0.14 Jy on the least sensitive baseline (FDVS–HCRK) to 0.04 Jy on the best baseline (NRAO–OVRO).

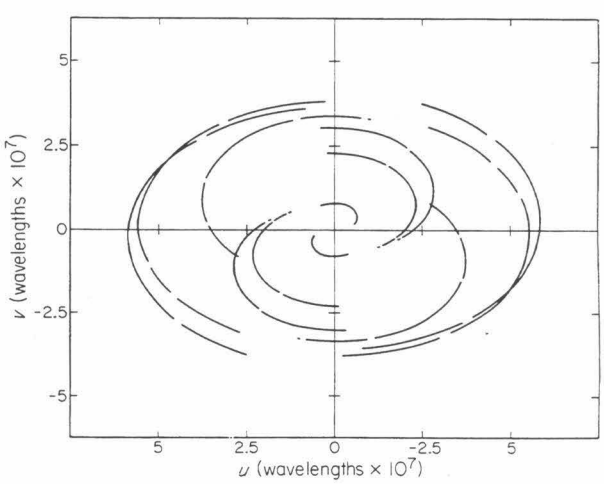

FIG. 1.—Tracks of the six baselines in the (u, v)-plane for the observation of 3C 84 (0316+413). The conjugate tracks are also shown. Occasional gaps are due to tape changes.

The correlated flux density should be at least 3 times the noise level for a reliable detection. The system noise gives rise to errors in the map, but these errors are always much smaller than the errors due to poor dynamic range (Readhead *et al.* 1979).

c) *Dynamic Range*

The dynamic range (the ratio of the strongest feature to the weakest believable feature) of the maps is limited by the gaps in the (u, v)-coverage and by uncertainties in the calibration. The relative scaling of the different baselines is uncertain by about 5%. From experiments with simulated observations (cf. Readhead and Wilkinson 1978) and by comparing the results of real observations with four and five stations, we have found that the dynamic range of the maps is usually about 20:1. This means that contours at 5% and below in the maps presented in the figures are unreliable.

IV. DISCUSSION OF INDIVIDUAL SOURCES

The seven sources observed are listed in Table 4, which gives the total flux density of each source at the epoch of observation, the effective resolution, and the linear scale of each map. The effective resolution is specified by the parameters of the restoring beam used in the hybrid mapping. The restoring beam is an elliptical Gaussian with FWHM chosen to match as closely as possible the FWHM of the "dirty beam" produced by the Fourier inversion. Use of a smaller restoring beam is dangerous, in that it can produce a map with incorrect features. The linear scale of the maps (in parsecs per milli-arcsecond) was calculated assuming a Hubble constant $H_0 = 55$ km s^{-1} Mpc^{-1} and deceleration parameter $q_0 = 0.05$; these values were used for all the linear dimensions quoted in this paper. Spectral index is defined by $S \propto \nu^{\alpha}$.

a) *0133+476 (OC 457, DA 55)*

The radio source 0133+476 is compact and has an unusually flat radio spectrum. It has been identified with an 18-mag blue stellar object (A. M. Cohen *et al.* 1977). The optical spectrum of this object has been observed by Strittmatter *et al.* (1974), who found only one possible emission line, at 520 nm; it is therefore generally described as a BL Lacertae object. A redshift of 0.86 has been quoted in the literature (Medd *et al.* 1972; Hewitt and Burbidge 1980), but it is not clear on what evidence this is based. 0133+476 is a strongly variable source: Andrew *et al.* (1978) measured its flux density at 10.7 GHz and 6.7 GHz between 1966 and 1976, in which period its flux density varied between 2 and 6 Jy; in recent years its 5 GHz flux density has been decreasing, from 3.26 Jy (***S4*** survey, 1974 December), through 2 Jy (Weiler and Johnston 1980, 1978 March–June) to 1.8 Jy at the epoch of our observations (1978 December). VLBI observations have been made at 5 GHz by Weiler and Johnston (1980), who included it in their study of BL Lacertae objects, and at 1.67 GHz and 10.7 GHz by Marscher and Shaffer (1980).

Owing to the constraint of the observing schedule, we observed 0133+476 for only 5 hours, but the structure of the source appears to be sufficiently simple that this is not a serious limitation. The closure phases do not depart from zero by more than 15°, and the correlated flux densities range between 1.8 Jy on the shortest baseline and 1.2 Jy on the longest baseline. This behavior indicates that the source is only slightly resolved. It is conventional in such cases to model the brightness distribution as an elliptical Gaussian. The best-fitting Gaussian model has a total flux density of 1.7 Jy and axes (FWHM) 1.5 and 1.0 milli-arcsec, with the longer axis in position angle 144°. This implies that the maximum brightness temperature is greater than 55 GK (1 GK = 10^9 kelvin). The 5 GHz observations of Weiler and Johnston were made with a longer baseline (Germany–West Virginia) than those used here, and with very restricted (u, v)-coverage, but they found a position angle of 140°, in excellent agreement with our 144°. The equivalent Gaussian diameter (0.7 milli-arcsec) is smaller than ours, perhaps indicating the presence of an unresolved core.

TABLE 4

THE FIRST SEVEN SOURCES

SOURCE	TOTAL FLUX DENSITY (Jy)	EFFECTIVE RESOLUTION[a]			REDSHIFT	SCALE[b]
		Major	Minor	PA (°)	z	(pc/milli-arcsec)
0133+476	1.8	4.0	1.8	−18	0.86?	9.2
0316+413	57.0	2.8	2.2	+11	0.0177	0.46
0859+470	1.7	2.9	2.1	+11	1.462	10.5
0923+392	7.5	3.0	2.2	+15	0.699	8.5
1807+698	2.4	2.8	1.7	−10	0.05	1.2
1828+487	3.0	2.9	2.1	+10	0.692	8.4
2200+420	2.3	2.9	2.4	+11	0.069	1.7

[a] FWHM of the Gaussian restoring beam (milli-arcsec).
[b] $H_0 = 55$ km s^{-1} Mpc^{-1}, $q_0 = 0.05$.

TABLE 5

GAUSSIAN MODELS

SOURCE	COMPONENT	FLUX DENSITY (Jy)	DISPLACEMENT FROM A		MAJOR AXIS FWHM (mas)	AXIAL RATIO	PA OF MAJOR AXIS (°)
			(mas)	in PA(°)			
0133+476	A 1.67 GHz[a]	2.06	...	...	5.1	0.42	170
	A 5 GHz	1.7	...	...	1.5	0.63	144
	A 10.7 GHz[a]	2.6	...	...	0.82	0.53	125
0859+470	A	1.15	...	...	2.1	0.43	0
0923+392	A	4.65	...	...	1.1	1	...
	B	2.34	1.89	−83	0.30	1	...
2200+420	A	1.19	...	...	0.53	1	...
	B	0.65	3.0	183	1.6	1	...
	C	0.15	6.7	174	3.0	1	...

[a]Marscher and Shaffer 1980.

Table 5 compares our 5-GHz model with the 10.7 GHz and 1.67 GHz models (derived from observations made about a year before ours) of Marscher and Shaffer (1980). It is clear that the position angle rotates as the frequency increases and the angular scale decreases. This behavior has been observed in other sources by Readhead *et al.* (1978), but in the present case it is particularly marked. The new 5 GHz observations also confirm the observation of Marscher and Shaffer that the effective angular size of the source increases linearly with wavelength. The spectrum of 0133+476 was measured at epoch 1978.0 by Owen, Spangler, and Cotton (1980): its flux density was almost constant at 2.15 Jy throughout the observed frequency range (750 MHz to 90 GHz). Marscher and Shaffer show that this flat spectrum and the linear increase of size with wavelength can be interpreted most simply in terms of a single, inhomogeneous synchrotron component (Marscher 1977).

It would be of great value to have measurements of the spectrum of 0133+476 at several epochs, to determine whether the decrease in flux density during 1978 that was observed at 5 GHz occurred throughout the spectrum. Further VLBI observations of the source are also required to determine how the structure of the source varies while the total flux density changes.

b) 0316+413 (3C 84, NGC 1275)

The radio source 3C 84 is the strongest in our sample. It has received considerable attention from VLBI observers because of its intensity and variability. It has been studied particularly well at 2.8 cm (10.6 GHz) (Pauliny-Toth *et al.* 1976; Preuss *et al.* 1979) and 1.35 cm (22 GHz) (Pauliny-Toth *et al.* 1978*b*; Matveenko *et al.* 1980); the papers cited give full references to earlier observations. The majority of these observations have measured amplitude only. At lower frequencies, a hybrid map based on amplitude and closure phase has been made by Wilkinson *et al.* (1979) at 50 cm (609 MHz). This map (of necessity) has a much lower resolution (FWHM 10 milli-arcsec) than the higher-frequency observations.

Our 6 cm (5 GHz) map, with a resolution (FWHM) of about 2.5 milli-arcsec, is shown in Figure 2, and the delta-function model that this map represents is compared with the measured data in the Appendix (Fig. 9). Comparison of this map with published maps at higher and lower frequencies is difficult owing to the varying resolution of the observations, and because the structure of 3C 84 is highly frequency-dependent, with several centers of high-frequency emission embedded in a larger, steeper-spectrum halo ~20 milli-arcsec (9 pc) across. The galaxy also exhibits radio emission on scales of 30″ and ~5′. A full discussion of the 5 GHz map and a comparison with data from other epochs and at different frequencies is deferred to a separate paper. It is clear, however, that the radio structure of 3C 84 is markedly different from the structure of any other object mapped with VLBI. The majority of these objects show a linear structure, consisting either of a core with a one-sided jet, or of two roughly equal components, sometimes connected by a bridge of emission. The radio source 3C 84 does not have a linear structure, and it shows no evidence of the collimation required to produce the core-jet morphology.

The associated optical galaxy, NGC 1275, is also an unusual object. Its optical classification is subject to uncertainty: it is generally called a Seyfert galaxy, but there is no evidence for spiral structure; it is sometimes classified as an elliptical, although the Balmer absorption-line spectrum suggests that the stellar population is younger than that of a typical elliptical galaxy. The main emission-line system is at 5300 km s^{-1}, but there is filamentary structure on one side of the nucleus at 8300 km s^{-1}. These two systems were identified by Minkowski (1957), who suggested that they are two colliding galaxies—a hypothesis which might explain the unusual radio structure. In a detailed discussion of more recent optical and radio observations, however,

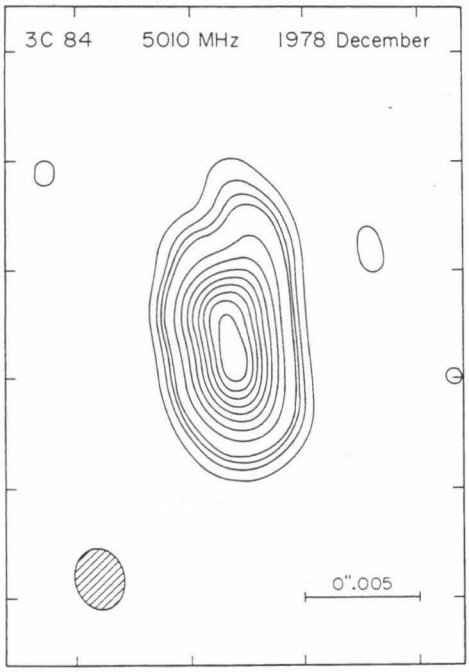

FIG. 2.—Hybrid map of 3C 84 (0316+413). The contour levels are 2.5, 5, 7.5, 10, 20, 30, 40, 50, 60, 70, 80, and 90% of the maximum, which has a brightness temperature of 120 GK. There are no negative contours at −2.5% or below. The hatched ellipse shows the half-power contour of the restoring beam. The frame is marked at intervals of 5 milli-arcsec. In this figure and the other maps (Figs. 3, 4 and 5) north is up and east to the left.

Kent and Sargent (1979) have shown that the 8300 km s^{-1} system is probably an unrelated spiral galaxy seen in projection against NGC 1275.

c) 0859+470 (4C 47.29, OJ 499)

The radio source 0859+470 is identified with a 19-mag quasar with a redshift of 1.462 (Carswell and Walsh, quoted by Hewitt and Burbidge 1980). A 5 GHz map from the VLA published by Perley, Fomalont, and Johnston (1980) shows that the source consists of a core emitting about 90% of the flux density, an extension 2″ to the north, and a possible extension 1″ to the southeast.

Our VLBI data show no large variations in visibility, and the closure phases do not depart significantly from zero. The data can be closely reproduced by the elliptical-Gaussian model shown in Table 5. This model accounts for only 70% of the total flux density of the source measured at the same epoch, so the remaining 30% must be attributed to extended components. The hybrid map is essentially identical to this Gaussian model, so we do not present it here.

d) 0923+392 (4C 39.25, DA 267)

The radio source 0923+392 is an 18-mag quasar with a redshift of 0.699. It has been observed many times in VLBI experiments (e.g., Shaffer *et al.* 1977; Bååth *et al.* 1980) and has always appeared to consist of two components. Although the strengths of the two components have varied, their separation has remained fixed at about 2 milli-arcsec (55 lt-yr).

Our observations can be closely reproduced by a model consisting of two circular Gaussian components (Table 5). The hybrid mapping procedure produces a delta-function model that fits the data slightly better than the two-component model but is otherwise indistinguishable. In the map itself the double structure is not clearly apparent, owing to the convolution with the restoring beam, so we do not present it here. The angular separation of the two components is determined fairly precisely by the location of the minima in the visibility function, but the other parameters of the deconvolution are less certain. It is difficult to estimate the uncertainty in the measured separation owing to the possible presence of systematic errors, but the error is certainly not greater than 0.1 milli-arcsec.

The model of Table 5 can be directly compared only with other observations at 5 GHz, of which there have been very few. In 1974.05 the components had flux densities 6.9 Jy and 1.6 Jy and separation 2.02 milli-arcsec in position angle 96° (or −84°) (Pauliny-Toth *et al.*, quoted by Shaffer *et al.* 1977). Thus between 1974.05 and 1978.95 the position angle has remained constant, the separation has, if anything, decreased, and the flux densities of both components have changed. It is reasonable to assume that the stronger component of 1974.05 is still the stronger component, although this cannot be proved because no phase measurements were made in 1974.05; if this is the case, the stronger component, A, has weakened and component B has strengthened since 1974.

More observations are available at higher frequencies. Bååth *et al.* (1980) report 7.85 GHz observations for 16 epochs between 1972.3 and 1975.1, with varying quality of (u, v)-coverage, and Shaffer *et al.* (1977) report observations at 10.7 GHz and 14.8 GHz between 1972.3 and 1974.5. In all cases the separation was 2.0 milli-arcsec, with a maximum possible error of 0.1 milli-arcsec. The apparent decrease in separation between 1972.3 and 1978.9 is thus 0.1 ± 0.1 milli-arcsec, corresponding to a velocity of $(0.4 \pm 0.4)c$.

Both Shaffer *et al.* and Bååth *et al.* have attempted to analyse the spectrum of 0923+392 in terms of three homogeneous, self-absorbed synchrotron components and a transparent steep-spectrum component. Two of these components correspond to the VLBI components A and B. The changes in 5 GHz flux density of A and B since 1974.05 appear to be consistent with the evolution-

ary scheme postulated by Shaffer *et al.*, but observations at a higher frequency would be helpful to confirm this.

The steep-spectrum component has been detected by Perley and Johnston (1979) using the Very Large Array (VLA) at 1400 MHz. It has the appearance of a halo or asymmetric double with a position angle of $30° \pm 10°$, which is apparently unrelated to the VLBI position angle. An unpublished 5 GHz VLA map by Perley shows two secondary components $\approx 1\farcs5$ away from the nucleus in position angles 80° and −120°; again the relationship between this structure and the milli-arcsecond double is unclear.

e) 1807+698 (3C 371)

The radio source 3C 371 is identified with a 14–15 mag N galaxy in a small cluster (Sandage 1966). The spectrum of this object has weak emission lines with a redshift of 0.05, the stellar absorption lines normally seen in E galaxies, and a highly variable nonthermal continuum (Miller 1975), which has led to comparisons with BL Lacertae objects (Miller 1975; Miller, French, and Hawley 1978).

The arc-second-scale radio structure of 3C 371 has recently been studied by Perley and Johnston (1979) and by Perley, Fomalont, and Johnston (1980), using the VLA. It is an asymmetric, D2 (Miley 1971) object with a strong, flat-spectrum core, and a weaker, steep-spectrum component extending away from the core on one side, in position angle −115°. There is also a low-brightness "halo."

The hybrid map of the flat-spectrum core, derived from our VLBI observations, is shown in Figure 3. The structure is linear, consisting of a strong component with a maximum brightness temperature in excess of 9 GK, a secondary component 4.5 milli-arcsec (18 lt-yr) away in position angle −97°, and an extension from the strong component toward the weaker one. Both the secondary component and the extension define the same position angle, which is remarkably close to the position angle of component A on the 5 GHz VLA map (Perley, Fomalont, and Johnston 1980), −115°. The difference of 8° is significant, however. Thus 3C 371 appears to resemble other D2 sources, such as 3C 273 and 3C 345, in showing a one-sided "jet" directed approximately, but not exactly, toward the outer arc-second-scale structure. Unfortunately the dynamic range of the present observations does not permit us to determine whether the structure is really a continuous "jet," or how far it extends from the strong component. Further VLBI observations at other frequencies are needed to determine the spectra of the various components; there is also a prospect of measuring an expansion velocity, but this may be difficult because the visibility does not show sharp minima like those that have been used to trace the superluminal expansion of 3C 273 and 3C 345.

A number of previous VLBI detections of 3C 371 have been reported (Wittels *et al.* 1978 and references therein; Shaffer 1978), but they are all measurements of visibility at a single point in the (u, v)-plane and cannot be compared with the present observations because of the variations in the source.

The spectrum of 3C 371 for 1978.0 (Owen, Spangler, and Cotton 1980) is fairly flat and smooth between 1 GHz and 90 GHz, which would be more consistent with the inhomogeneous synchrotron models of Marscher (1977) than with a model consisting of a small number of discrete, homogeneous components.

f) 1828+487 (3C 380)

The radio source 3C 380 is a 17-mag quasar with a redshift of 0.692. Observations with the Cambridge 5 km telescope (Laing 1981*a*) and with the VLA

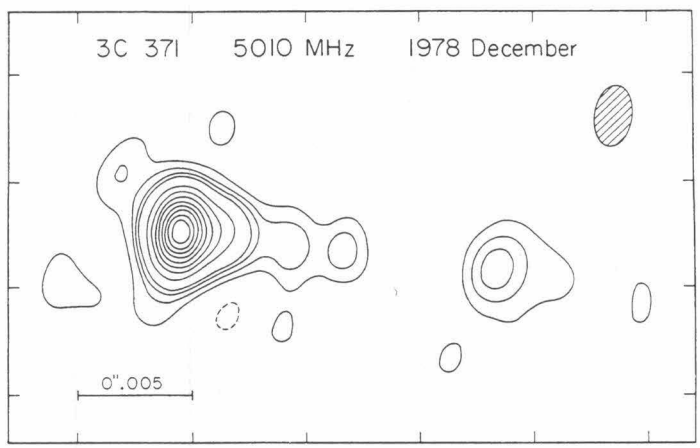

FIG. 3.—Hybrid map of 3C 371 (1807+698). The contour levels are −2.5 (*dashed*), 2.5, 5, 7.5, 10, 20, 30, 40, 50, 60, 70, 80, and 90% of the maximum, which has a brightness temperature of 9.4 GK. The hatched ellipse shows the half-power contour of the restoring beam. The frame is marked at intervals of 5 milli-arcsec.

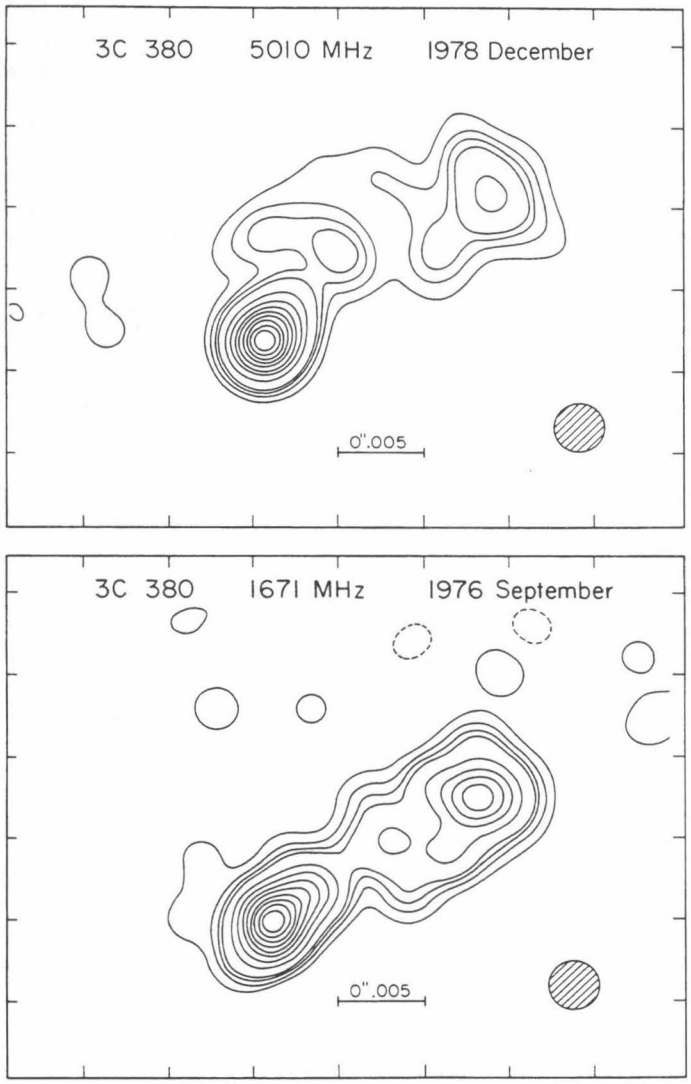

FIG. 4.—Hybrid maps of 3C 380 (1828+487). The 5010 MHz map (*top*) is from the present work; the 1671 MHz map (*bottom*) has been redrawn from the data of Readhead and Wilkinson (1980). The same restoring beam, a circular Gaussian of FWHM 3 milli-arcsec, has been used for both maps (*hatched ellipse*). The contour levels are −2.5 (*dashed*), 2.5, 5, 7.5, 10, 20, 30, 40, 50, 60, 70, 80, and 90% of the maximum, which has a brightness temperature of 5.7 GK at 5010 MHz and 46 GK at 1671 MHz. The frame is marked at intervals of 5 milli-arcsec.

(Wilkinson *et al.* 1981) have shown that it has a strong, compact central component with a jetlike structure extending to a distance of about 1".5 from the nucleus in position angle −47°. There is also a steeper-spectrum halo extending about 3" on both sides of the nucleus. A VLBI map of 3C 380 with a resolution of 3 milli-arcsec (FWHM) has been made by Readhead and Wilkinson (1980) at a frequency of 1671 MHz; this map can be directly compared with the new 5 GHz map derived from observations made 2.2 yr later. Both maps are shown in Figure 4; to facilitate the comparison, the same restoring beam has been used for both maps.

The 5 GHz observations had less complete (u, v)-coverage than the 1671 MHz observations, so the dynamic range is slightly worse; and even on the shortest baseline the source is strongly resolved, so large-scale structure is poorly represented in the map. The two maps are remarkably similar, however: both show a strong component A to the southeast and a weaker, more diffuse component B to the northwest, and in both maps the position angle of the line joining the components is −57°. The separation of A and B is different, though: 14 milli-arcsec at 1671 MHz and 16 milli-arcsec at 5 GHz (about 400 lt-yr). In both maps A is more

resolved on the northwest side than on the southeast side. The low-brightness structure between the two components is less constrained by the data, and it is not clear to what extent the differences should be considered significant. The distant component detected at 1671 MHz, 0".73 from the nucleus, was not and could not have been detected in the 5 GHz observations owing to the lack of short baselines.

Figure 5 shows profiles of the brightness temperature along the axis of the source at the two frequencies. The two profiles have been aligned so that the peak and southeast edge of component A coincide at the two frequencies. This is the most plausible alignment, but the correct way to align the profiles is unknown because of the lack of absolute phase measurements. A shift of one profile relative to the other of more than 2 milli-arcsec can be ruled out because it would give component A an implausible spectrum.

If component A is aligned as in Figure 5, however, the peak of component B does not coincide at the two frequencies; B must have an inverted spectrum ($\alpha \approx 0.6$) on its "leading" (northwest) edge and a steep spectrum ($\alpha \approx -1.0$) on its trailing edge. In this respect it resembles the knots in the jet of 3C 147 (Readhead and Wilkinson 1978).

An alternative but less plausible alignment would be for the peak of component B to coincide at the two frequencies. This is just permitted by the constraints discussed above. In this case B has a spectral index of -0.7, while A has a steeply rising spectrum on the southeast side and a steeply falling spectrum on the northwest side.

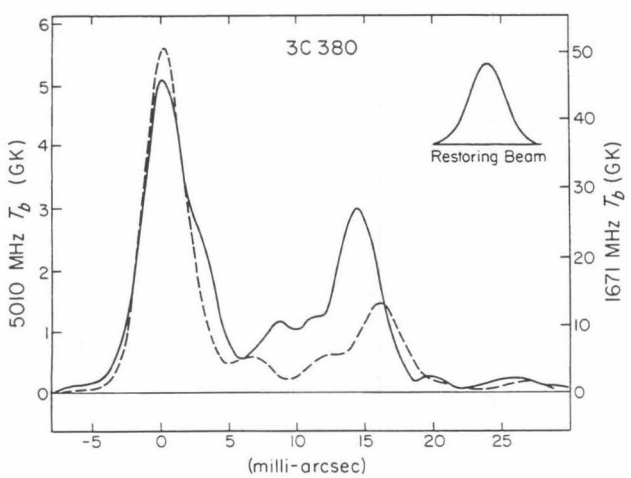

FIG. 5.—Profiles of brightness temperature T_b along the axis of 3C 380 (position angle $-57°$) at 5010 MHz (*dashed line*) and 1671 MHz (*full line*). The brightness temperature scales (*left*: 5010 MHz; *right*: 1671 MHz) have been chosen so that an unresolved point source with a flat spectrum ($\alpha = 0$) would give equal deflections at both frequencies. Where the dashed line lies above the full line, $\alpha > 0$ (inverted spectrum); where the dashed line lies below the full line, $\alpha < 0$. Spectral index is defined by $S \propto \nu^{\alpha}$. The profile of the restoring beam (FWHM = 3 milli-arcsec) is indicated.

There is another problem in comparing the two profiles, in that the effects of spectrum cannot be distinguished from variations in structure between the 1974.7 (1671 MHz) and 1976.9 (5 GHz) observations. For example, it is possible that the separation has increased due to the motion of one of the components: the apparent velocity would be ~ 0.8 milli-arcsec per year, or about $40c$. Further observations are required to rule out structural changes.

The maps of 3C 380 can be interpreted most simply in terms of the "core-jet" picture of compact sources (Readhead *et al.* 1978). Component A is the core, with a flat spectrum indicative of synchrotron self-absorption, and the jet extends toward component B in about the same position angle as the arc-second scale jet seen in the Cambridge and VLA maps. Component B is a "knot" in the jet. Readhead and Wilkinson (1980) discussed two alternative origins for the knot: a shock wave in the jet (Rees 1978) and an interaction between the jet and interstellar matter (Blandford and Königl 1979). The fact that the knot has a flatter spectrum on its outer edge, which is sharper than the trailing edge, perhaps favors the first alternative.

g) 2200+420 (BL Lacertae)

BL Lacertae has received considerable attention from VLBI observers; the observations up to the end of 1977 have been summarized by Shaffer (1978). Kellermann *et al.* (1977) made observations on six baselines at 10.6 GHz and one baseline at 15 GHz and found the radio source to be elongated in position angle 10°. They interpreted the data in terms of a two-component model with separation 1.25 milli-arcsec. Comparison with earlier observations showed that in spite of the large changes in the total flux density, the position angle had remained nearly constant over a period of four years. The separation of the components had apparently varied, but the detailed behavior is unclear owing to the ambiguities of model-fitting with limited (u, v)-coverage. More recent observations of BL Lacertae at 5 GHz (epoch 1979.2, Bååth *et al.* 1981) continue to show a north-south elongation.

Our 5 GHz map of BL Lacertae is shown in Figure 6. It too has a predominant position angle close to zero. The resolution of this map is about a factor of 4 worse than the observations of Kellermann *et al.* made in 1974.5. The map appears to show continuous emission along a trail extending about 7 milli-arcsec (40 lt-yr) south from the brightest point. The profile of brightness temperature along a north-south line (Fig. 7) shows two clear shoulders, indicating that the source consists of at least three distinguishable components. In order to make this deconvolution more quantitative, we derived a three-component model by least-squares fitting to the

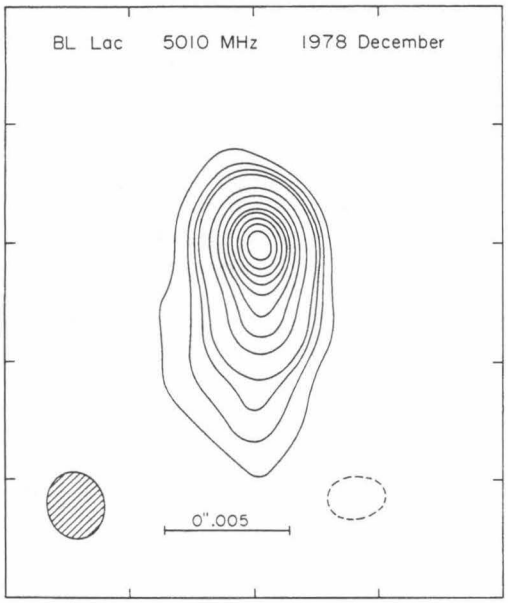

FIG. 6

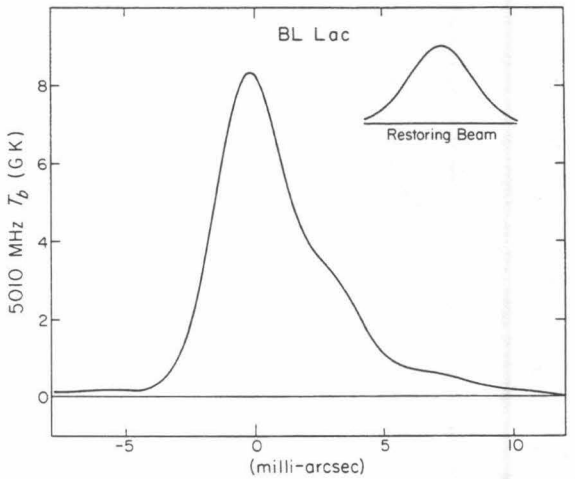

FIG. 7

FIG. 6.—Hybrid map of BL Lac (2200+420). The contour levels are −2.5, 2.5, 5, 7.5, 10, 20, 30, 40, 50, 60, 70, 80, and 90% of the maximum, which has a brightness temperature of 8.3 GK. The hatched ellipse shows the half-power contour of the restoring beam. The frame is marked at intervals of 5 milli-arcsec.

FIG. 7.—Profile of brightness temperature T_b along a north-south line through the peak of emission from BL Lac. The profile of the restoring beam is indicated.

visibility amplitudes (Table 5). The fit of this model to both the amplitudes and closure phases is virtually indistinguishable from the fit of the hybrid map.

It should be remembered that this model is a deconvolution, and therefore subject to some uncertainty, but it is suggestive: the components lie almost on a straight line with a position angle that has remained more or less constant for several years, and the progression from A to B to C is one of both decreasing flux density and increasing size. It would be attractive to identify each component with a single expanding synchrotron cloud, with A being the youngest and B and C relics of earlier outbursts, which have moved away from their origin at A along a channel which is preserved between outbursts. If A, B, and C represent successive outbursts separated by less than a year, then apparent velocities considerably in excess of c would be involved. At present, this picture must be regarded as speculation, but it can be confirmed or disproved by regular VLBI monitoring of BL Lacertae at a single frequency (or, preferably, two frequencies) at intervals comparable with the time scale of the total flux density variations, that is, a few months. The observations presented here were made while the flux density was unusually low, and it has since increased by more than a factor of 4. It is particularly important to find out whether the rapid flux density variations affect the whole source or only one component.

V. DISCUSSION

It would be premature to attempt to draw general, quantitative conclusions from the observations presented here, which refer to a nonrandom subset of seven sources from the complete sample. These seven should be representative of the strongest sources in the sample, however.

The source 3C 84 is (at present) the most intense in the sample, and also one of the closest. It is a very peculiar object in both its optical and its radio properties, and is apparently far from being a typical source.

Among the other sources the "core-jet" morphology occurs in at least two of the seven sources, 3C 371 and 3C 380, and perhaps in a third, BL Lacertae. To these we can add 3C 345, which is the second most intense source in the sample. We did not observe 3C 345 because it has already been well studied, and maps have been made at several epochs (Readhead *et al.* 1979; Cohen *et al.* 1981). In spite of their similar radio morphology, however, these four sources are a very mixed bunch; two are quasars with redshifts 0.595 (3C 345) and 0.692 (3C 380), one is a low-redshift BL Lac object (BL Lacertae), and one is a low-redshift N galaxy (3C 371).

The source 0923+392 (4C 39.25) is the third most intense in the sample and, as a compact double source, appears to represent a second morphology. Whether this

is common morphology remains to be seen, and we cannot yet say whether the distinction between such sources and the core-jet sources is not an artificial one due to inadequate dynamic range.

The remaining two sources (0133+476, 0859+470) were only partially resolved in our observations, with angular sizes $\lesssim 2$ milli-arcsec. Intercontinental baselines and higher frequencies are needed to resolve such sources.

The observations described here were made under the auspices of the U.S.A. VLBI Network Users Group. We thank the many people involved in scheduling the observations, recording the data at the participating observatories, and processing the tapes, for their indispensable contributions to this paper. We also thank R. A. Laing, J. A. Peacock, and R. A. Perley for communicating results in advance of publication, and the referee for his helpful comments. The work was supported by the National Science Foundation via grants AST 77-00247 and AST 79-13249 to the Owens Valley Radio Observatory; the National Radio Astronomy Observatory is operated by Associated Universities, Inc., under contract with the NSF; astronomical VLBI at Harvard Radio Astronomy Station and Hat Creek Radio Astronomy Observatory is supported by the NSF.

APPENDIX

Figures 8–14 reproduce the measured visibility amplitudes on each of the six interferometer baselines and the closure phases for each of the four baseline triangles; only three of these four closure phases are independent. The measurements are represented by 2σ error bars. The curves superposed on the data points are derived from either Gaussian models or the hybrid maps, as indicated in the figure legends. In the case of the hybrid maps, the curves are derived from the delta-function models (not convolved with the restoring beam). In most cases the hybrid maps reproduce the data exactly. The worst discrepancies occur in the closure phase for 3C 84—the closure phase errors are worst where the amplitudes are small, and can be attributed to the limited dynamic range.

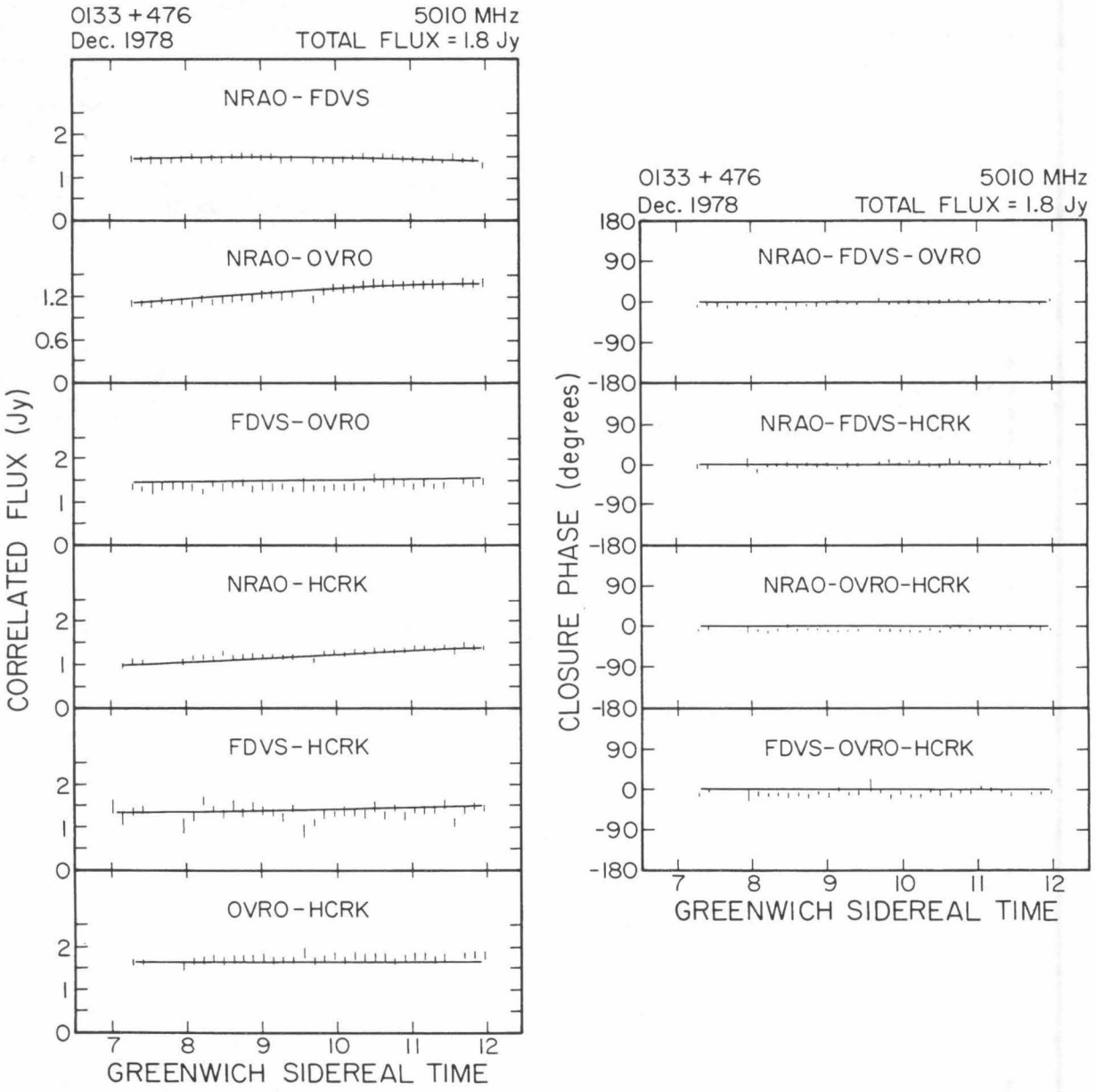

FIG. 8.—Visibility amplitudes and closure phases for 0133+476. The model is an elliptical Gaussian (Table 5).

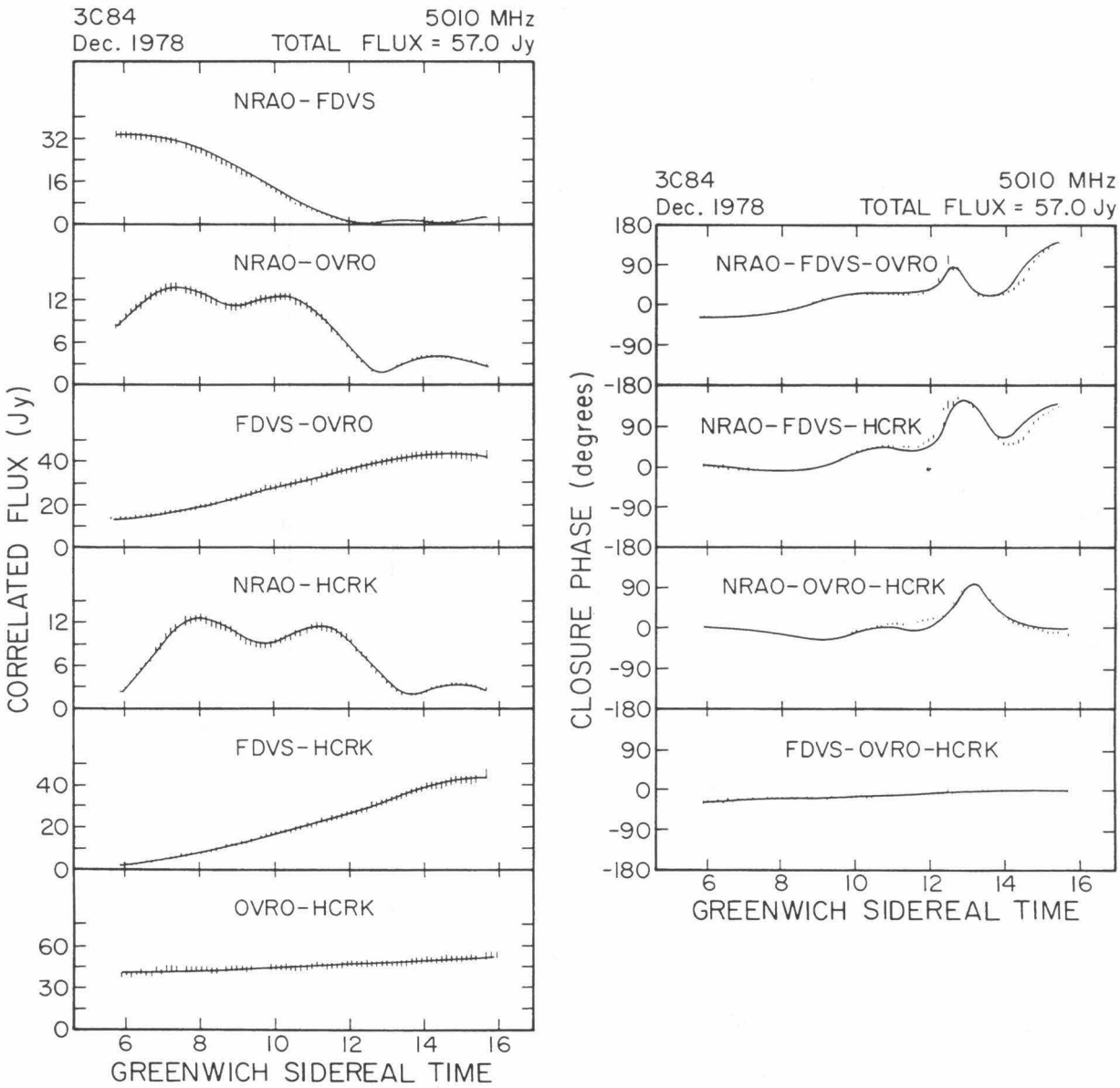

FIG. 9.—Visibility amplitudes and closure phases for 3C 84 (0316+413). The model is the hybrid map (Fig. 2).

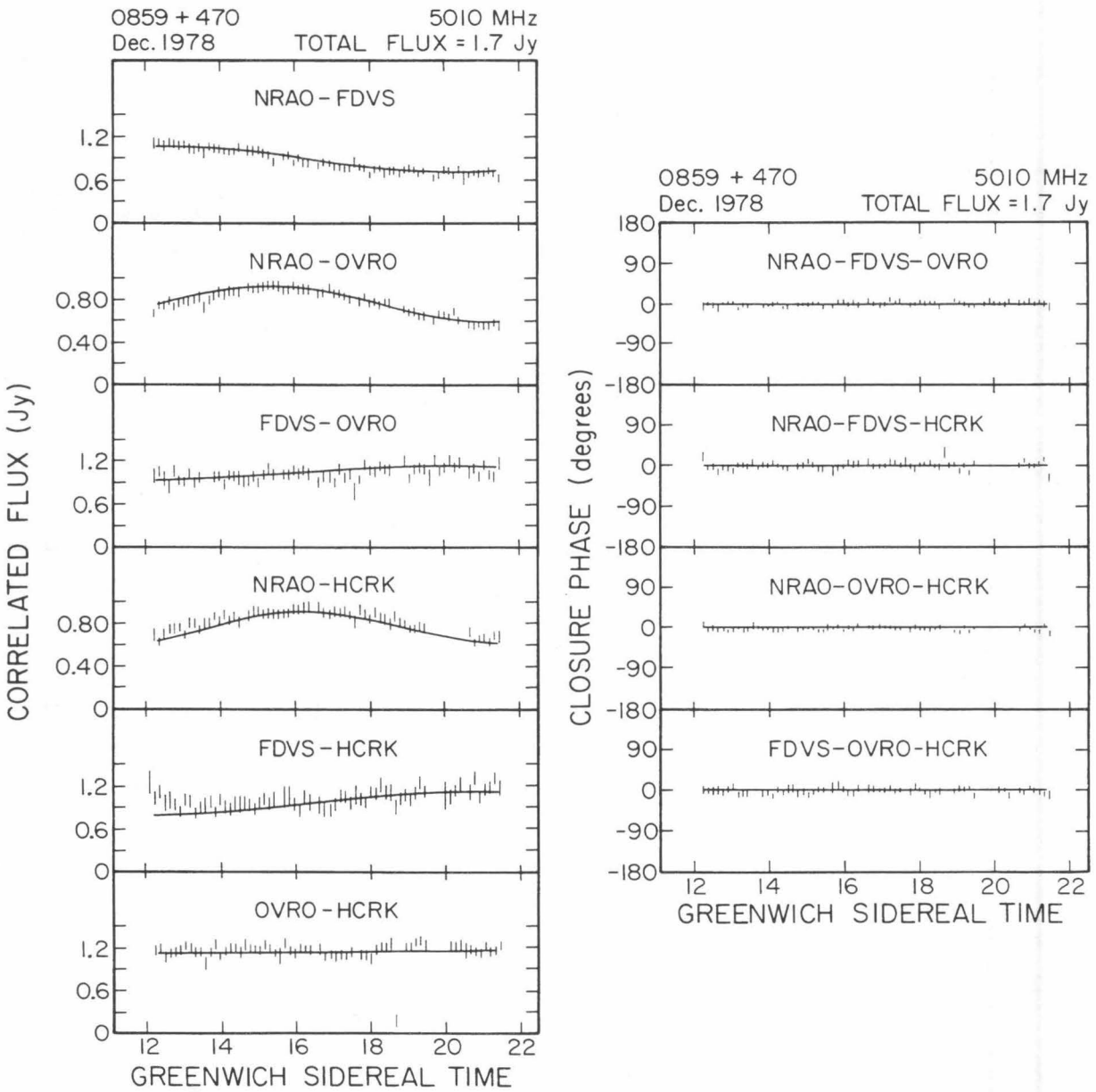

FIG. 10.—Visibility amplitudes and closure phases for 0859+470. The model is an elliptical Gaussian (Table 5).

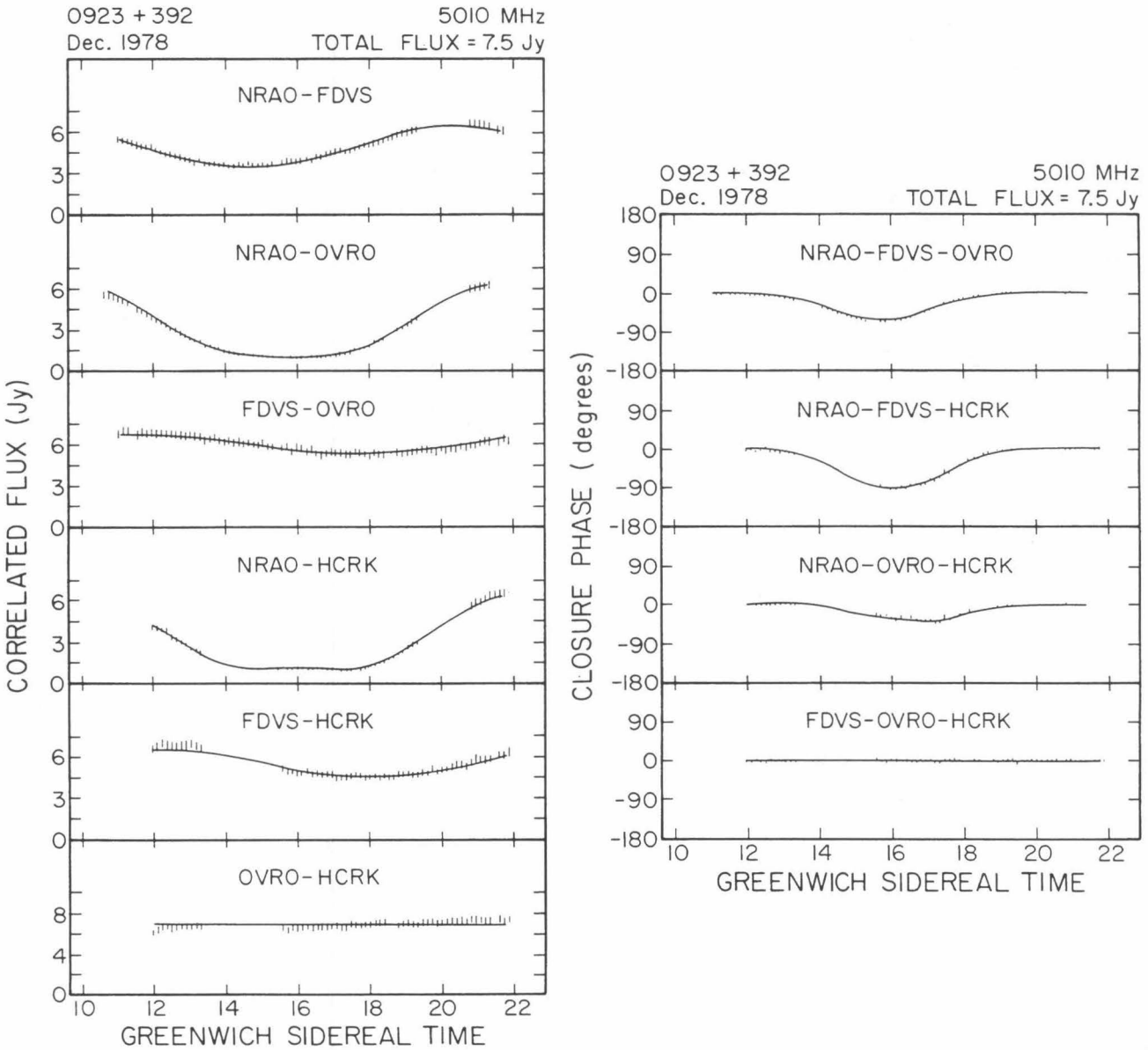

FIG. 11.—Visibility amplitudes and closure phases for 0923+392. The model consists of two circular Gaussian components (Table 5).

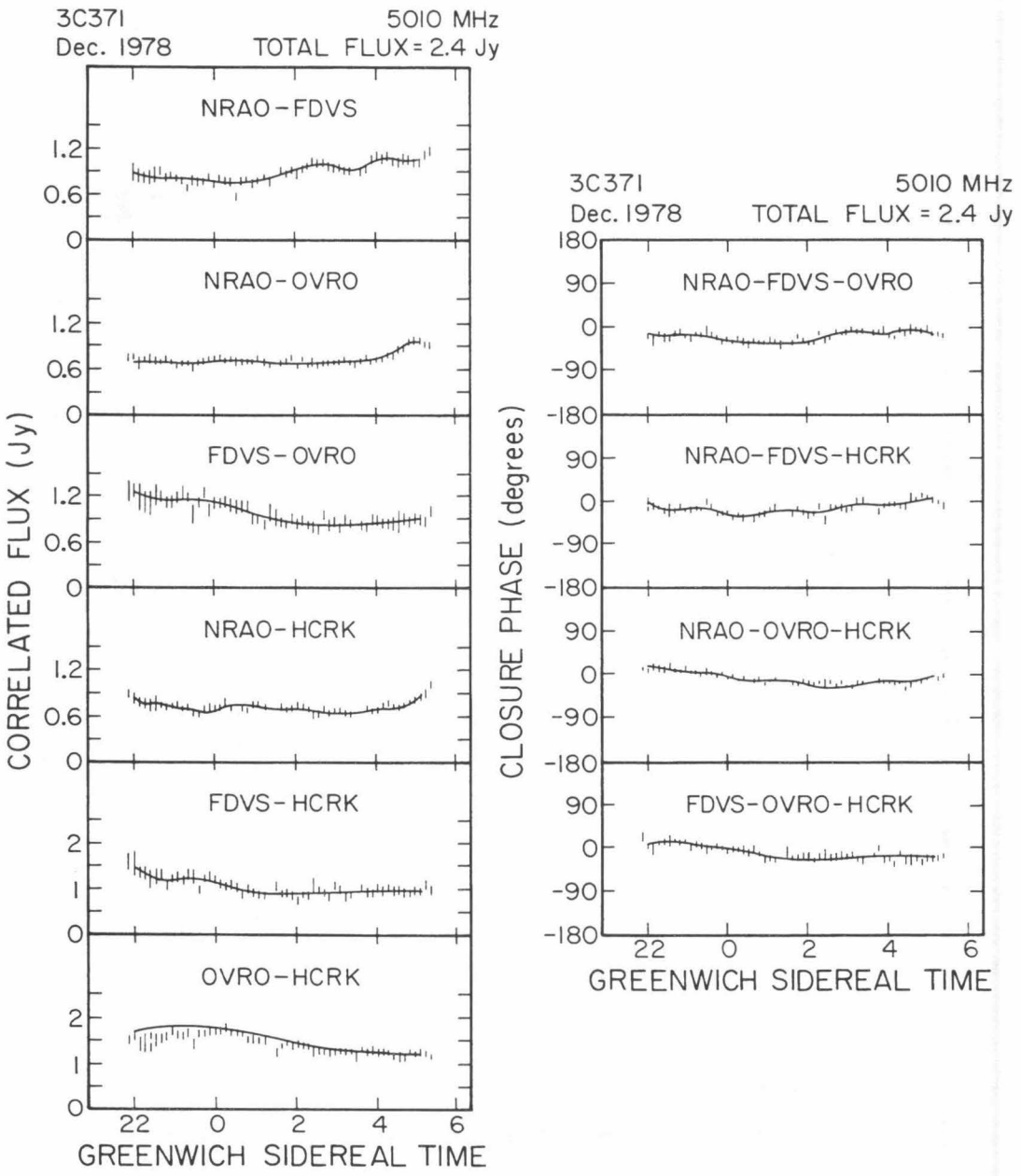

FIG. 12.—Visibility amplitudes and closure phases for 3C 371 (1807+698). The model is the hybrid map (Fig. 3).

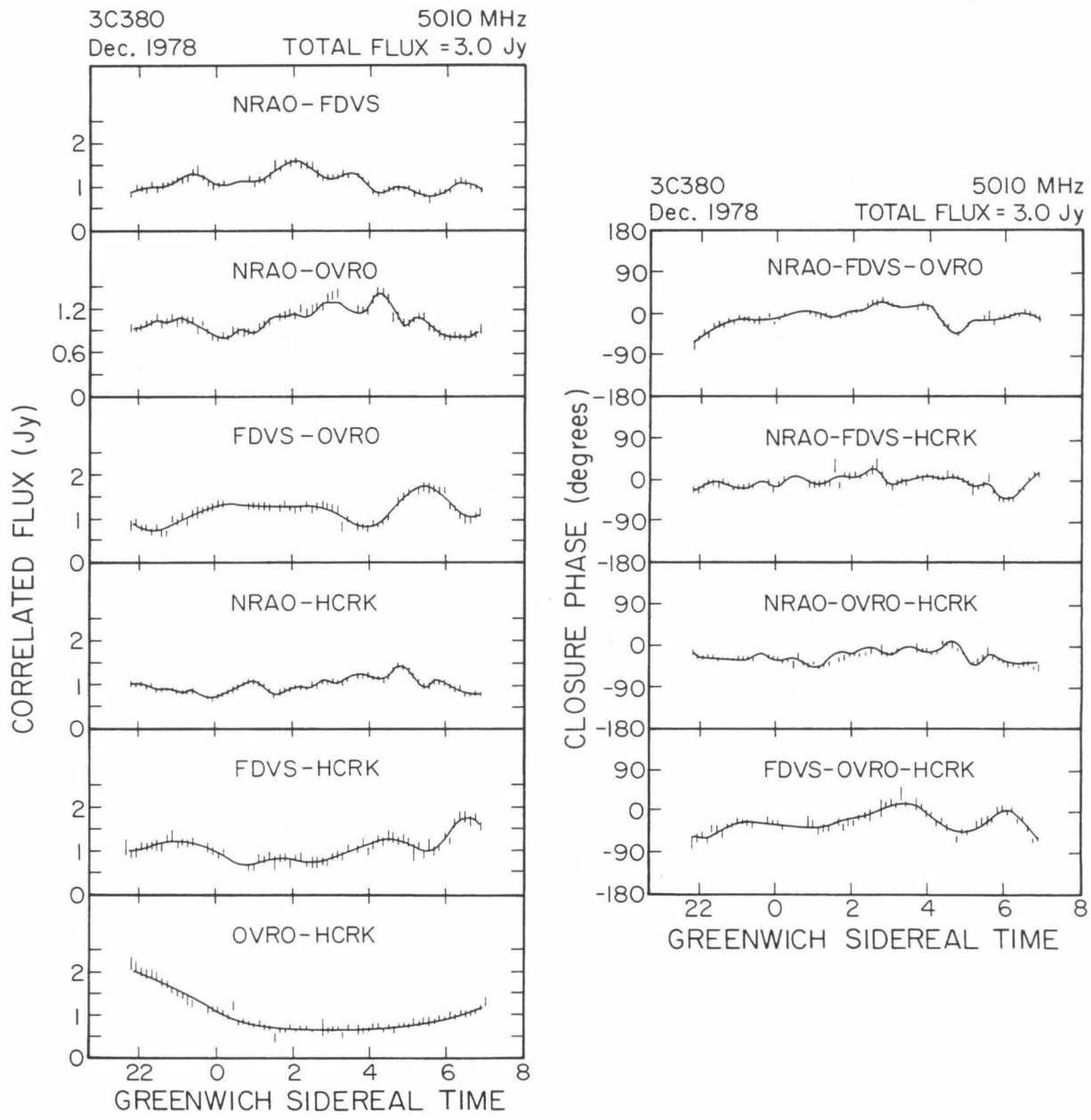

FIG. 13.—Visibility amplitudes and closure phases for 3C 380 (1828+487). The model is the hybrid map (Fig. 4).

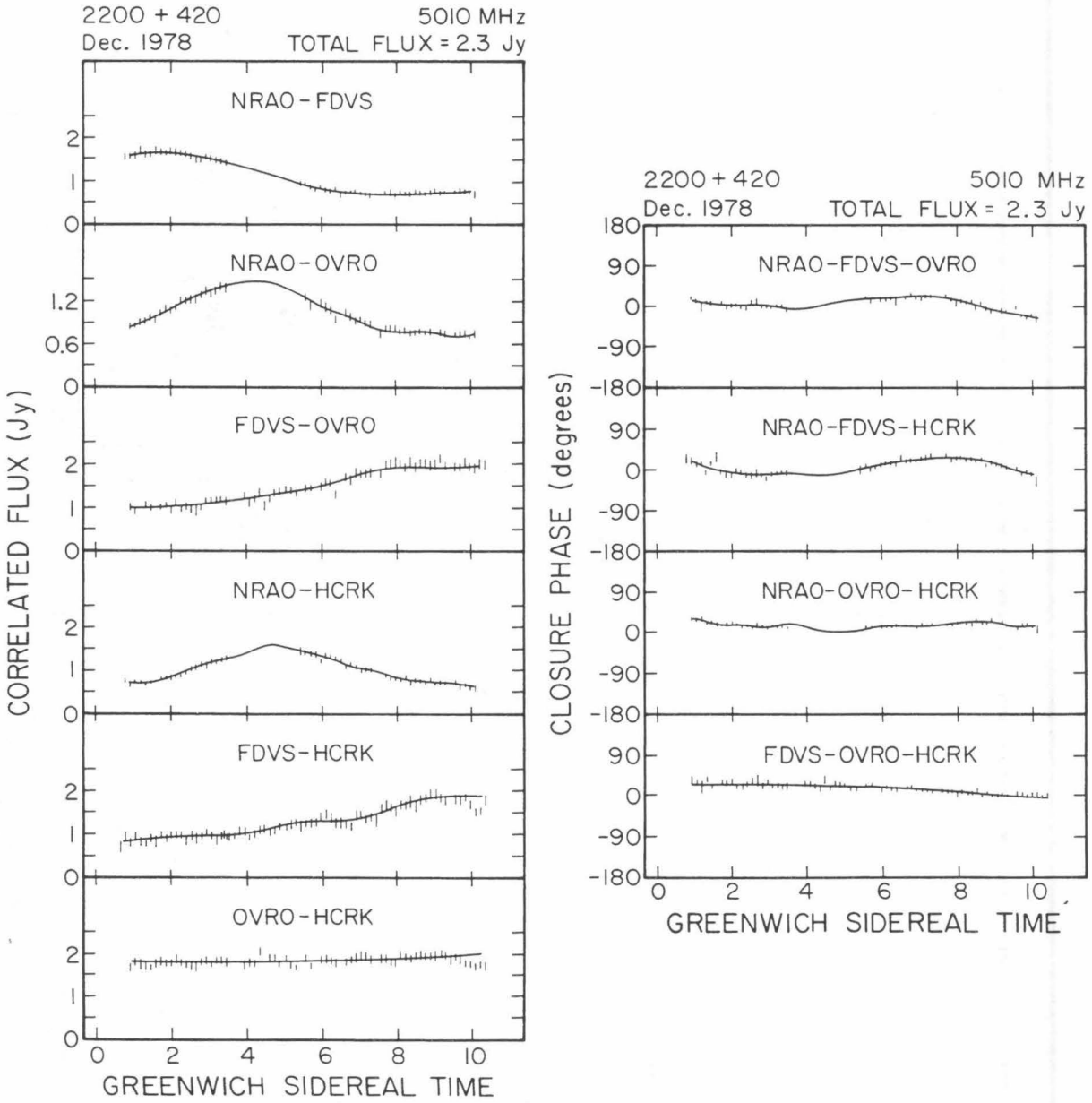

FIG. 14.—Visibility amplitudes and closure phases for BL Lac (2200+420). The model is the hybrid map (Fig. 6).

REFERENCES

Andrew, B. H., Macleod, J. M., Harvey, G. A., and Medd, W. J. 1978, *A.J.*, **83**, 863.
Bååth, L. B., *et al.* 1980, *Astr. Ap.*, **86**, 364.
Bååth, L. B., Elgered, G., Lundqvist, G., Graham, D., Weiler, K. W., Seielstad, G. A., Tallqvist, S., and Schilizzi, R. T. 1981, *Astr. Ap.*, **96**, 316.
Blandford, R. D., and Königl, A. 1979, *Ap. J.*, **232**, 34.
Burbidge, G. R., and Crowne, A. H. 1979, *Ap. J. Suppl.*, **40**, 583.
Burch, S. F. 1979, *M.N.R.A.S.*, **186**, 293.
Clark, B. G. 1973, *Proc. IEEE*, **61**, 1242.
Cohen, A. M., Porcas, R. W., Browne, I. W. A., Daintree, E. J., and Walsh, D. 1977, *Mem. R.A.S.*, **84**, 1.
Cohen, M. H., *et al.* 1975, *Ap. J.*, **201**, 249.
Cohen, M. H., *et al.* 1977, *Nature*, **268**, 405.
Cohen, M. H., Pearson, T. J., Readhead, A. C. S., Seielstad, G. A., Simon, R. S., and Walker, R. C. 1979, *Ap. J.*, **231**, 293.
Cohen, M. H., and Readhead, A. C. S. 1979, *Ap. J.* (*Letters*), **233**, L101.
Cohen, M. H., Unwin, S. C., Simon, R. S., Seielstad, G. A., Pearson, T. J., Linfield, R. P., and Walker, R. C. 1981, *Ap. J.*, **247**, 774.
Cotton, W. D. 1979, *A.J.*, **84**, 1122.
Elsmore, B., and Ryle, M. 1976, *M.N.R.A.S.*, **174**, 411.
Fanaroff, B. L., and Riley, J. M. 1974, *M.N.R.A.S.*, **167**, 31P.
Fomalont, E. B., Miley, G. K., and Bridle, A. H. 1979, *Astr. Ap.*, **76**, 106.
Geldzahler, B. J., Kellermann, K. I., Shaffer, D. B., and Clark, B. G. 1977, *Ap. J.* (*Letters*), **215**, L5.
Hewitt, A., and Burbidge, G. R. 1980, *Ap. J. Suppl.*, **43**, 57.
Jennison, R. C. 1958, *M.N.R.A.S.*, **118**, 276.
Jenkins, C. J., Pooley, G. G., and Riley, J. M. 1977, *Mem. R.A.S.*, **84**, 61.
Johnson, K. H. 1974, *A.J.*, **79**, 1006.
Kellermann, K. I., *et al.* 1977, *Ap. J.*, **211**, 658.
Kent, S. M., and Sargent, W. L. W. 1979, *Ap. J.*, **230**, 667.
Kühr, H., Pauliny-Toth, I. I. K., Witzel, A., and Schmidt, J. 1981, 1981, *A.J.*, in press.
Laing, R. A. 1981*a*, *M.N.R.A.S.*, **194**, 301.
_____. 1981*b*, *M.N.R.A.S.*, **195**, 261.
Linfield, R. P. 1981, *Ap. J.*, **244**, 436.
Marscher, A. P. 1977, *Ap. J.*, **216**, 244.
Marscher, A. P., and Shaffer, D. B. 1980, *A.J.*, **85**, 668.
Matveenko, L. I., *et al.* 1980, *Pis'ma Astr. Zh.*, **6**, 77 (English transl. *Soviet Astr. Letters*, **6**, 42).
Medd, W. J., Andrew, B. H., Harvey, G. A., and Locke, J. L. 1972, *Mem. R.A.S.*, **77**, 109.
Miley, G. K. 1971, *M.N.R.A.S.*, **152**, 477.
Miller, J. S. 1975, *Ap. J.* (*Letters*), **200**, L55.
Miller, J. S., French, H. B., and Hawley, S. A. 1978, in *Pittsburgh Conference on BL Lac Objects*, ed. A. M. Wolfe (Pittsburgh: University of Pittsburgh), p. 176.
Minkowski, R. 1957, in *IAU Symposium 4, Radio Astronomy*, ed. H. C. van de Hulst (Cambridge: Cambridge University Press), p. 107.
Northover, K. J. E. 1973, *M.N.R.A.S.*, **165**, 369.
Owen, F. N., Burns, J. O., and Rudnick, L. 1978, *Ap. J.* (*Letters*), **226**, L119.
Owen, F. N., Spangler, S. R., and Cotton, W. D. 1980, *A.J.*, **85**, 351.
Pauliny-Toth, I. I. K., *et al.* 1976, *Nature*, **259**, 17.
Pauliny-Toth, I. I. K., Witzel, A., Preuss, E., Kühr, H., Kellermann, K. I., Fomalont, E. B. and Davis, M. M. 1978*a*, *A.J.*, **83**, 451.
Pauliny-Toth, I. I. K., *et al.* 1978*b*, *Pis'ma Astr. Zh.*, **4**, 64 (English transl. *Soviet Astr. Letters*, **4**, 32).
Peacock, J. A., and Wall, J. V. 1981, *M.N.R.A.S.*, **194**, 331.
Pearson, T. J., Readhead, A. C. S., and Wilkinson, P. N. 1980, *Ap. J.*, **236**, 714.
Perley, R. A., Bridle, A. H., Willis, A. G., and Fomalont, E. B. 1980, *A.J.*, **85**, 499.
Perley, R. A., Fomalont, E. B., and Johnston, K. J. 1980, *A.J.*, **85**, 649.
Perley, R. A., and Johnston, K. J. 1979, *A.J.*, **84**, 1247.
Perley, R. A., Willis, A. G., and Scott, J. S. 1979, *Nature*, **281**, 437.
Pooley, G. G., and Henbest, S. N. 1974, *M.N.R.A.S.*, **169**, 477.
Preuss, E., Pauliny-Toth, I. I. K., Witzel, A., Kellermann, K. I., and Shaffer, D. B. 1977, *Astr. Ap.*, **54**, 297.
Preuss, E., Kellermann, K. I., Pauliny-Toth, I. I. K., Witzel, A., and Shaffer, D. B. 1979, *Astr. Ap.*, **79**, 268.
Readhead, A. C. S. 1980, in *IAU Symposium 92, Objects of High Redshift*, ed. G. O. Abell and P. J. E. Peebles (Dordrecht-Holland: D. Reidel), p. 165.
Readhead, A. C. S., Cohen, M. H., and Blandford, R. D. 1978, *Nature*, **272**, 131.
Readhead, A. C. S., Cohen, M. H., Pearson, T. J., and Wilkinson, P. N. 1978, *Nature*, **276**, 768.
Readhead, A. C. S., Pearson, T. J., Cohen, M. H., Ewing, M. S., and Moffet, A. T. 1979, *Ap. J.*, **231**, 299.
Readhead, A. C. S., and Wilkinson, P. N. 1978, *Ap. J.*, **223**, 25.
_____. 1980, *Ap. J.*, **235**, 11.
Rees, M. J. 1978, *M.N.R.A.S.*, **184**, 61P.
Riley, J. M., and Pooley, G. G. 1975, *Mem. R.A.S.*, **80**, 105.
Rogers, A. E. E., *et al.* 1974, *Ap. J.*, **193**, 293.
Sandage, A. 1966, *Ap. J.*, **145**, 1.
Scheuer, P. A. G., and Readhead, A. C. S. 1979, *Nature*, **277**, 182.
Shaffer, D. B. 1978, in *Pittsburgh Conference on BL Lac Objects*, ed. A. M. Wolfe (Pittsburgh: University of Pittsburgh), p. 68.
Shaffer, D. B., and Marscher, A. P. 1979, *Ap. J.* (*Letters*), **233**, L105.
Shaffer, D. B., *et al.* 1977, *Ap. J.*, **218**, 353.
Simon, R. S., Readhead, A. C. S., Moffet, A. T., Wilkinson, P. N., and Anderson, B. 1980, *Ap. J.*, **236**, 707.
Strittmatter, P. A., Carswell, R. F., Gilbert, G., and Burbidge, E. M. 1974, *Ap. J.*, **190**, 509.
van Breugel, W. J. M., Schilizzi, R. T., Hummel, E., and Kapahi, V. K. 1981, *Astr. Ap.*, in press.
Walsh, D., Wills, B. J., and Wills, D. 1979, *M.N.R.A.S.*, **189**, 667.
Weiler, K. W., and Johnston, K. J. 1980, *M.N.R.A.S.*, **190**, 269.
Wilkinson, P. N., Readhead, A. C. S., Anderson, B., and Purcell, G. H. 1979, *Ap. J.*, **232**, 365.
Wilkinson, P. N., Readhead, A. C. S., Purcell, G. H., and Anderson, B. 1977, *Nature*, **269**, 764.
Wilkinson, P. N., Readhead, A. C. S., Napier, P. J., and Bignell, C. 1981, in preparation.
Wittels, J. J., *et al.* 1978, *A.J.*, **83**, 560.

T. J. PEARSON and A. C. S. READHEAD: California Institute of Technology, Mail Code 102-24, Pasadena CA 91125

THE ASTROPHYSICAL JOURNAL, 328:114–142, 1988 May 1

THE MILLIARCSECOND STRUCTURE OF A COMPLETE SAMPLE OF RADIO SOURCES. II. FIRST-EPOCH MAPS AT 5 GHz

T. J. PEARSON AND A. C. S. READHEAD
Owens Valley Radio Observatory, California Institute of Technology
Received 1987 July 15; accepted 1987 October 20

ABSTRACT

We have conducted a VLBI survey of a complete, flux-density–limited sample of 65 extragalactic radio sources, selected at 5 GHz. We have made 5 GHz images with a resolution $\sim 0\overset{''}{.}001$ of 37 of the sources using the Mark II system, and VLBI images are available for a further five sources. We have classified the sources into a number of groups with similar characteristics, based on the VLBI maps of the sources, their large-scale structure, and their radio spectra.

We have examined the radio polarization, variability, largest angular size, alignment of large-scale and small-scale structure, and optical identification of the sources in each of the classes. One class, compact double sources with steep high-frequency spectra, is distinguished from the other classes by all these criteria: they show low polarization, little variability, and no large-scale structure, and are identified with galaxies. The majority of sources, however, can be grouped into classes that show a regular progression of properties consistent with the increasing prominence of the jet in a "core-jet" structure.

One-sided jetlike structures are found in all classes except the very compact sources and the compact S doubles. No two-sided jets are found. In cases where both a VLBI (parsec-scale) jet and a kiloparsec jet are seen, the VLBI jet is on the same side as, or is connected with, the kiloparsec jet. Large misalignments are common. Superluminal motion is common and has been found in many of the classes, with the notable exception of the compact double sources.

Subject headings: galaxies: jets — interferometry — polarization — radio sources: galaxies — radio sources: general — radio sources: identifications — radio sources: variable

I. INTRODUCTION

The technique of very long baseline interferometry (VLBI) can image the compact radio sources in active galactic nuclei with a resolution 3–4 orders of magnitude greater than can presently be obtained with any other technique at any frequency. The resolution approaches a scale of 10^{16} cm in nearby galactic nuclei, and permits critical observations that provide new insights into the nature of the central energy source. It is true that VLBI cannot give direct observations of the energy source itself, which may be a supermassive black hole with dimensions 2 or 3 orders of magnitude smaller still than the best available resolution (e.g., Begelman, Blandford, and Rees 1984), and that the radio radiation detected in VLBI observations represents only a small part of the energy output of the central engine (e.g., Phinney 1985). Nonetheless, VLBI is the only available high-resolution imaging technique that can probe active galactic nuclei with subparsec resolution, and such observations have great promise for improving our understanding of the central engines. For example, VLBI observations have already shown that the initial collimation of material ejected from the nuclei takes place on a scale of less than a parsec, and that, at least in some cases, the ejected material is moving at close to the speed of light (e.g., Kellermann and Pauliny-Toth 1981).

VLBI observations have demonstrated that many of the compact radio sources in active galactic nuclei are one-sided jets, and several have shown apparent superluminal motion. But some objects have different morphologies: some are symmetric double sources with an overall extent of less than a kiloparsec, and with no obvious nucleus; some are central components of large, double-lobed radio galaxies or quasars; and others are steep-spectrum sources with a complex structure. The relationships between the various types of source and the underlying causes of the different morphologies remain unclear. It is not known, for example, whether the morphological differences reflect fundamental differences in the central engines, or are caused by environmental differences in the parent galaxies or the surrounding medium. In order to study these questions, we must first determine the full range of morphological types of compact radio structure and the frequencies with which they occur. Such a study complements the detailed studies of individual sources that are already in progress.

This paper is the second reporting results of a project that we began in 1977 to determine the milliarcsecond structure of a complete sample of radio sources. We chose to observe a flux-density–limited sample selected at 5 GHz. The high selection frequency ensures that in many of the objects the dominant radio emission arises in the compact nuclear component. If the radio emission from the compact components is relativistically beamed, the sample may be biased in orientation, with many sources directed toward us. To investigate this possibility, it is important to observe samples such as the one that we have chosen here, which depend to the minimum on theoretical speculation, and also samples in which any possible orientation bias is minimized (Barthel *et al.* 1984; Cawthorne *et al.* 1986; Zensus and Porcas 1986; Hough and Readhead 1987). Our approach here has the practical advantage that the sample contains many compact objects that can be studied by Mark II VLBI. The observational selection criteria used for our sample are well defined and allow it to be used for statistical tests of any theories that make quantitative predictions, including the

popular beaming theories. In addition to providing a uniform body of data for statistical studies, our objectives in undertaking this study were to determine the full spectrum of morphologies exhibited by the compact radio sources, and to attempt a physical classification of the morphological types. A further aim was to discover more superluminal sources in order better to determine their statistical properties.

In an earlier paper (Pearson and Readhead 1981, hereafter Paper I) we described the selection of the sample and presented maps of seven sources. This second paper includes first-epoch maps of a further 30 sources, and discusses the properties of the sample as a whole. The observations required to make second-epoch maps of most of the sources have been completed; these maps will enable us to measure changes in the structure of the sources and will be the subject of future papers in the series. Some of the second-epoch results on particularly interesting sources have already been published (Eckart *et al.* 1985; Pearson *et al.* 1986; Barthel *et al.* 1986). In parallel with the radio observations, we are obtaining high-quality optical spectra of all 65 sources in the sample using the Palomar 200 inch (5 m) telescope; some preliminary results have been published (Lawrence *et al.* 1986, 1987). A program is also underway to measure the optical polarization of all the sources (C. Impey and C. Lawrence, in preparation).

Since the publication of Paper I, we have enlarged the sample from 51 to 65 sources. The revised sample is defined in § II. Forty-five of the 65 sources have milliarcsecond-scale emission detectable with the Mark II VLBI system, and we have undertaken to map all of these, excluding only a few that have been studied by other workers. The observations and the resulting maps are the subjects of § III and § IV, and we attempt to classify the source morphologies in § V. In § VI we discuss some trends and correlations, and in § VII we review the properties of the sources in the various classes and discuss the impact of these results on our physical understanding of these objects. Finally we summarize our conclusions in § VIII. An appendix includes notes on each of the sources and references to other work.

A preliminary report on this work was presented at IAU Symposium 110 (Pearson and Readhead 1984*a*; Readhead, Pearson, and Unwin 1984), and a more recent summary at the Workshop on Superluminal Radio Sources (Pearson, Readhead, and Barthel 1987).

II. THE COMPLETE SAMPLE

In Paper I we defined a complete sample of 51 sources. Since the publication of Paper I, we have enlarged the sample to 65 sources by removing the northern declination limit. The revised sample is defined by the following criteria: (1) declination (1950.0) $\delta < 35°$; (2) Galactic latitude $|b| > 10°$; and (3) total 5 GHz flux density $S \geq 1.3$ Jy. The flux densities used in the selection were those measured in the NRAO–MPIfR 6 cm strong source surveys (Pauliny-Toth *et al.* 1978, hereafter S4; Kühr *et al.* 1981*a*, hereafter S5). Since many of the sources are variable, a selection based on flux densities measured at a different epoch would produce a rather different sample. (One source, 1749+701, was measured in both S4 and S5. It is included in the sample on the basis of its S5 flux density, not its S4 flux density, which was below the limit.)

This sample has eight sources in common with a sample of 13 sources that is being studied intensively by a group at the Max-Planck-Institut für Radioastronomie (Eckart *et al.* 1982, 1986, 1987).

The complete sample of 65 sources is listed in Table 1, which gives for each source the name, the 1950.0 coordinates, the nature of the associated optical object, and the redshift where available. The table also gives the date of the mapping observation reported here, the antennas used, and the flux density at the time of observation. Table 1 also includes the fraction F_c of the flux density in a compact core, and the assignment of each source to a morphological class; these entries are discussed in § V.

Not all the sources in the sample contain a strong, compact component that can be mapped with VLBI. In Paper I we described a "finding survey" in which we detected 35 of the 51 sources south of declination 70°. We subsequently made similar observations of 12 of the 14 northern sources that were added to the sample, and detected 11. (We did not observe two sources, 0210+864 and 1157+732, in which the cores were known to be too weak for VLBI observation.) Thus we detected 46 of the complete sample of 65 sources.

Of these 46 sources, we have completed first-epoch maps of 37, seven of which were published in Paper I. Of the nine sources that we have not mapped, four (3C 147, 3C 179, 3C 236, and 3C 345) have been observed extensively by other workers. The remaining five (0404+768, 0954+556, 0954+658, 1031+567, 1358+624) were detected in the finding survey but were too strongly resolved to be mapped with the US VLBI network; we have observed four of these with the European VLBI network, which has better sensitivity at the required resolution, and we shall report the results elsewhere.

We can make a simple subdivision of the sample sources into two classes, "compact" and "lobe-dominated," based on published observations with resolution $\sim 1''$. To some extent this division depends on the dynamic range of the observations, but there is a fairly clear distinction between the compact sources dominated by an unresolved core (45 examples in the sample) and the extended sources dominated by emission from lobes (19 examples); one very low-luminosity source (M82) is unusual and does not fit this classification. The 19 lobe-dominated sources can be further separated into three low-luminosity class I sources and 16 high-luminosity class II sources (Fanaroff and Riley 1974). The results of the finding survey can be summarized as follows:

	Total	Detected	Not Detected
Compact sources	45	43	2
Lobe-dominated sources	19	3	16
M82	1	0	1
Total	65	46	19

The three lobe-dominated sources that *were* detected are class II sources with strong cores (3C 179, 3C 236, and 3C 390.3). The two compact sources that were *not* detected are both steep-spectrum sources (1634+628 and 2342+821); see the notes in the Appendix.

All 65 sources in the complete sample have been optically identified, and redshifts have been measured for 60 (Lawrence *et al.* 1987). The sample is dominated by high-luminosity objects; there are a few low-redshift objects (e.g., Markarian 501, 3C 371), but low-luminosity objects such as Seyfert galaxies are very underrepresented compared with a volume-limited sample.

III. OBSERVATIONS

The first-epoch maps of 37 sources were made using the Mark II VLBI system (Clark 1973). Observations were sched-

TABLE 1

THE COMPLETE SAMPLE

Source (1)	Other Designation (2)	R.A. (3)	Decl. (4)	Reference for Cols. (3) and (4) (5)	Optical Identification (6)	V (7)	z (8)	Scale (pc mas^{-1}) (9)	Reference for Cols. (6) and (8) (10)
0016+731	...	00^{h}16^{m}54^s.20	73°10′51″.5	1	Q	18	1.781	4.2	1, 2
0040+517	3C 20	00 40 19.70	51 47 07.2	2	G	19	0.174	1.9	1
0108+388	OC 314	01 08 47.25	38 50 32.8	1	G	22	...	...	3
0133+476	OC 457	01 33 55.11	47 36 12.8	1	Q	19	0.859	4.2	1, 2
0153+744	...	01 53 04.35	74 28 05.7	1	Q	17	2.338	3.9	1, 2
0210+860	3C 61.1	02 10 40.00	86 05 20.0	2	G	19	0.184	2.0	2, 3
0212+735	...	02 12 49.94	73 35 40.1	1	Q	19	2.367	3.9	1, 2
0220+427	3C 66B	02 20 01.73	42 45 54.6	2	G	12.9	0.0215	0.30	4
0314+416	3C 83.1B	03 14 56.79	41 40 32.6	2	G	12.5	0.0181	0.26	4
0316+413	3C 84	03 16 29.56	41 19 51.9	1	G	11.9	0.0172	0.24	4
0404+768	4C 76.03	04 04 00.13	76 48 52.5	2	G	22	...	...	5
0454+844	...	04 54 57.16	84 27 53.0	1	BL	18	...	...	2
0538+498	3C 147	05 38 43.51	49 49 42.8	1	Q	17.8	0.545	3.7	2
0605+480	3C 153	06 05 44.46	48 04 49.0	2	G	18.5	0.2769	2.6	4
0710+439	OI 417	07 10 03.36	43 54 26.0	1	G	20.7	0.518	3.6	1
0711+356	OI 318	07 11 05.60	35 39 52.6	1	Q	17	1.62	4.2	2
0723+679	3C 179	07 23 04.29	67 54 52.7	2	Q	18.0	0.846	4.2	2
0804+499	OJ 508	08 04 58.40	49 59 23.1	1	Q	17.5	1.43	4.3	2
0809+483	3C 196	08 09 59.42	48 22 07.2	2	Q	17.8	0.871	4.2	2
0814+425	OJ 425	08 14 51.67	42 32 07.7	1	BL	17.7	...	...	5
0831+557	4C 55.16	08 31 04.38	55 44 41.4	1	G	17.5	0.2420	2.4	4
0836+710	4C 71.07	08 36 21.56	71 04 22.4	1	Q	16.5	2.17	4.0	2
0850+581	4C 58.17	08 50 50.15	58 08 55.7	1	Q	18	1.322	4.3	2
0859+470	4C 47.29	08 59 39.98	47 02 56.8	1	Q	18.7	1.462	4.3	2
0906+430	3C 216	09 06 17.25	43 05 59.4	2	Q	18.5	0.67	3.9	2
0917+458	3C 219	09 17 50.66	45 51 43.6	3	G	17.2	0.1744	1.9	4
0923+392	4C 39.25	09 23 55.32	39 15 23.5	1	Q	17.9	0.699	4.0	2
0945+408	4C 40.24	09 45 50.08	40 53 43.4	1	Q	17.5	1.252	4.3	2
0951+699	M82 (3C 231)	09 51 41.95	69 54 57.5	2	G	8.4	0.0009	0.013	4
0954+556	4C 55.17	09 54 14.36	55 37 16.4	1	Q	17.7	0.909	4.2	2
0954+658	...	09 54 57.85	65 48 15.5	1	BL	16.7	0.368	3.1	1, 2
1003+351	3C 236	10 03 05.39	35 08 48.0	2	G	16.0	0.0989	1.2	4
1031+567	OL 553	10 31 55.96	56 44 18.1	1	G	21.3	0.45	3.4	3, 5
1157+732	3C 268.1	11 57 49.89	73 17 27.5	4	G	21.5	0.97	4.2	6
1254+476	3C 280	12 54 41.05	47 36 32.1	2	G	20	0.994	4.3	7
1358+624	4C 62.22	13 58 58.36	62 25 06.7	1	G	20.9	0.431	3.3	1
1409+524	3C 295	14 09 33.50	52 26 13.0	2	G	20.1	0.4614	3.4	4
1458+718	3C 309.1	14 58 56.64	71 52 11.2	2	Q	16.8	0.905	4.2	2
1609+660	3C 330	16 09 16.16	66 04 30.0	2	G	20.3	0.549	3.7	4
1624+416	4C 41.32	16 24 18.25	41 41 23.5	1	Q	22	2.55	3.8	3
1633+382	4C 38.41	16 33 30.63	38 14 10.0	1	Q	18	1.814	4.2	2
1634+628	3C 343	16 34 01.08	62 51 41.6	1	Q	20.6	0.988	4.3	2
1637+574	OS 562	16 37 17.43	57 26 15.7	1	Q	17	0.745	4.1	2
1641+399	3C 345	16 41 17.61	39 54 10.8	1	Q	16.0	0.595	3.8	2
1642+690	4C 69.21	16 42 18.08	69 02 13.2	1	Q	19.2	0.751	4.1	1, 2
1652+398	4C 39.49	16 52 11.73	39 50 25.1	4	G	13.8	0.0337	0.46	2
1739+522	4C 51.37	17 39 29.00	52 13 10.4	1	Q	18.5	1.375	4.3	2
1749+701	...	17 49 03.40	70 06 39.6	1	BL	17.0	...	...	2
1803+784	...	18 03 39.18	78 27 54.3	1	Q	17	0.68	4.0	2, 3
1807+698	3C 371	18 07 18.54	69 48 57.1	1	G	14.2	0.050	0.67	2
1823+568	4C 56.27	18 23 14.95	56 49 18.1	1	BL	18.4	0.664	3.9	1, 2
1828+487	3C 380	18 28 13.54	48 42 40.5	2	Q	16.8	0.692	4.0	2
1842+455	3C 388	18 42 35.45	45 30 21.6	2	G	15.3	0.0908	1.1	4
1845+797	3C 390.3	18 45 37.57	79 43 06.4	2	G	15	0.0569	0.75	4
1928+738	4C 73.18	19 28 49.35	73 51 44.9	1	Q	16.5	0.302	2.8	1, 2
1939+605	3C 401	19 39 38.84	60 34 32.6	2	G	18.0	0.201	2.1	4
1954+513	OV 591	19 54 22.47	51 23 46.4	1	Q	18.5	1.22	4.3	2
2021+614	OW 637	20 21 13.30	61 27 18.1	1	G	19.5	0.2266	2.3	8
2153+377	3C 438	21 53 45.49	37 46 12.9	2	G	19.2	0.292	2.7	4
2200+420	BL Lac	22 00 39.36	42 02 08.6	1	BL	14.5	0.07	0.90	2
2229+391	3C 449	22 29 07.60	39 06 03.4	2	G	13.2	0.0171	0.24	4
2243+394	3C 452	22 43 32.81	39 25 27.6	2	G	16.0	0.0811	1.0	4
2342+821	...	23 42 06.35	82 10 01.3	5	Q	20.5	0.735	4.0	3
2351+456	4C 45.51	23 51 49.96	45 36 22.9	2	Q	20.6	2.0	4.1	3
2352+495	OZ 488	23 52 37.78	49 33 26.8	1	G	19	0.237	2.4	4

TABLE 1—*Continued*

VLB? (11)	Mapped (12)	Antennas (13)	S_t (14)	S_0 (15)	F_c (16)	Classification (17)
Y	1982 Apr	BKGFO	1.65	1.7	0.95	Very compact
N	...	...	4.18	...	<0.003	F-R II
Y	1979 Jul	GFOH	1.35	1.6	...	Compact S double
Y	1978 Dec	GFOH	3.26	1.8	0.89	Compact
Y	1982 Apr	BGFO	1.51	1.5	...	Compact F double
N	...	...	1.68	...	<0.007	F-R II
Y	1980 Sep	BKFO	2.20	2.3	0.59	Asymmetric I
N	...	...	3.75	...	<0.06	F-R I
N	...	...	3.53	...	<0.01	F-R I
Y	1978 Dec	GFOH	47.2	57.	...	Irregular
Y	...	...	2.79	...	...	Steep-spectrum compact
Y	1981 Aug	BKGFO	1.40	1.0	0.51	Asymmetric I
Y	...	...	8.18	...	...	Steep-spectrum compact
N	...	...	1.35	...	<0.004	F-R II
Y	1980 Jul	BKGFO	1.66	1.6	...	Compact S double
Y	1980 Jul	BKGFO	1.51	1.1	0.24	Compact F double
Y	...	...	1.31	...	0.31	F-R II
Y	1979 Dec	BKGFO	2.07	1.4	0.99	Very compact
N	...	...	4.35	...	<0.012	F-R II
Y	1979 Jul	GFOH	1.68	1.9	0.84	Compact
Y	1979 Dec	KGFO	5.60	5.3	...	Irregular
Y	1980 Sep	BKFO	2.57	2.6	0.40	Asymmetric II
Y	1980 Jul	BKFO	1.41	1.1	0.85	Compact
Y	1978 Dec	GFOH	1.78	1.7	0.68	Asymmetric I
Y	1979 Dec	BKGFO	1.78	1.9	0.45	Steep-spectrum compact
N	...	...	2.29	...	<0.018	F-R II
Y	1978 Dec	GFOH	8.90	7.5	...	Compact F double
Y	1979 Jul	GFOH	1.39	1.5	0.48	Asymmetric II
N	...	...	3.94	...	...	(Not classified)
Y	...	...	2.27	...	...	(Not observed)
Y	...	...	1.46	...	...	(Not observed)
Y	...	...	1.32	...	<0.28	F-R II
Y	...	...	1.31	...	...	(Not observed)
N	...	...	2.63	...	<0.015	F-R II
N	...	...	1.53	...	<0.007	F-R II
Y	...	...	1.77	...	...	(Not observed)
N	...	...	6.48	...	<0.009	F-R II
Y	1981 Aug	BKGFO	3.34	3.3	0.18	Steep-spectrum compact
N	...	...	2.35	...	<0.032	F-R II
Y	1980 Jul	BKGFO	1.31	1.2	0.35	Asymmetric II
Y	1979 Apr	BKGFO	4.08	2.3	0.37	Asymmetric II
N	...	...	1.50	...	...	Steep-spectrum compact
Y	1979 Jul	GFOH	1.44	1.9	0.96	Very compact
Y	...	...	10.9	7.5	0.35	Asymmetric II
Y	1980 Jul	BKGFO	1.43	1.9	0.86	Compact
Y	1980 Jul	BKGFO	1.42	1.3	0.35	Asymmetric II
Y	1982 Apr	BGFO	1.99	1.0	0.91	Very compact
Y	1982 Apr	BKGFO	1.81	1.3	0.67	Asymmetric I
Y	1982 Apr	BKGFO	2.63	2.9	0.74	Asymmetric I
Y	1978 Dec	GFOH	2.33	2.4	0.40	Asymmetric II
Y	1979 Dec	BKGFO	1.67	1.5	0.74	Asymmetric I
Y	1978 Dec	GFOH	6.19	3.0	...	Steep-spectrum compact
N	...	...	1.77	...	<0.03	F-R II
Y	1982 Apr	BKGFO	4.32	2.3	0.13	F-R II
Y	1980 Sep	BKFO	3.34	3.3	0.64	Asymmetric I
N	...	...	1.52	...	<0.028	F-R II
Y	1979 Jul	GFOH	1.43	1.5	0.57	Asymmetric I
Y	1979 Dec	KGFO	2.31	2.2	...	Compact F double
N	...	...	1.54	...	<0.007	F-R II
Y	1978 Dec	GFOH	4.75	2.3	0.52	Asymmetric I
N	...	...	1.39	...	<0.027	F-R I
N	...	...	3.26	...	<0.04	F-R II
N	...	...	1.30	...	...	Steep-spectrum compact
Y	1980 Jul	BKGFO	1.41	1.1	0.29	Asymmetric II
Y	1979 Dec	BKGFO	1.77	1.6	0.45	Compact S double

uled by the US VLBI network in seven sessions between 1978 and 1982 (Table 2). Most sources were scheduled to be observed continuously for about 11 hours using five antennas (four antennas of the US network and the 100 m antenna of the Max-Planck-Institut für Radioastronomie at Effelsberg), but owing to a variety of technical problems not all the observations were successful, so the coverage of the (u, v)-plane obtained varied considerably from source to source. Table 2 gives details of the observations of each source. The typical resolution is 1–2 mas (1 mas = $0''.001 = 4.85 \times 10^{-9}$ radians).

The data were cross-correlated on the Caltech–JPL Mark II VLBI processor. Estimates of the cross-correlation coefficients were obtained by a least-squares fit on each baseline independently; in most cases a coherent integration time of 120 s was used (Table 2). The "global fringe-fitting" procedure (Schwab and Cotton 1983) was not used. The data were calibrated in the usual way (Cohen *et al.* 1975) using measurements of antenna system temperatures and either antenna temperatures or antenna gain curves. The *a priori* amplitude calibration was adjusted in some cases to achieve agreement at baseline crossing points in the (u, v)-plane; in the later observations, the calibration was further improved by using a self-calibration technique.

Images of the sources were obtained by model fitting and hybrid mapping methods. Most of the sources had a fairly simple brightness distribution that could be well represented by a simple model consisting of one, two, or three elliptical Gaussian components. The model parameters were initially guessed by inspection of the visibility amplitudes and closure phases, and then improved estimates were made by an iterative least-squares fitting program. The Gaussian model was used as a starting model for an iterative self-calibration and mapping procedure (Pearson and Readhead 1984*b*). The art of VLBI image reconstruction has progressed rapidly in the years since this project was begun. The earliest images were made by the method of Readhead and Wilkinson (1978) that uses self-calibration of visibility phases only; in later observations, amplitude self-calibration was also applied using an adaptation by S. C. Unwin of the CORTEL program (Cornwell and Wilkinson 1981). Thus the quality of the resulting images varied, depending on the extent of the (u, v)-plane coverage and the analysis methods used. Typically the dynamic range of the images (the ratio of the brightness of the brightest feature in the map to the rms noise in an area of blank sky) varied from about 50:1 for observations with four antennas and without amplitude self-calibration to about 300:1 for observations with five antennas and amplitude self-calibration. It is clear that in many cases it would be possible to achieve an improvement in image quality by reanalyzing the data, but it is unlikely that such an effort would result in substantial changes in the apparent structure of the sources. We shall reanalyze the data presented here using the best available methods when we analyze the second-epoch observations (in preparation). The second-epoch maps should in most cases be greatly superior to the first-epoch maps, owing both to improved analysis methods and to the use of more antennas.

IV. RESULTS

The resulting VLBI images of 37 sources are presented as contour maps in Figure 1. For completeness, we include the seven maps published in Paper I. All the images have been restored with Gaussian clean beams, the FWHM contours of which are shown as hatched ellipses in Figure 1. The parameters of the restoring beam, the peak brightness, and the contour levels used for each map are listed in Table 3.

The notes on each source in the Appendix draw attention to interesting features of the VLBI images and discuss their relationship to other observations. References are given to observations of the sources that were not mapped in this project.

The contour maps are not the most convenient presentation of the data for quantitative analysis. In Table 4 we present the parameters of Gaussian models of all but the most complex sources. In cases where self-calibration was used to make the maps, these models were derived by least-squares fitting of the *self-calibrated* data. The agreement factors (reduced χ^2) in columns (8) and (9) indicate the quality of the fit. When the agreement factor is less than 2, the model is a moderately accurate representation of the source structure; larger agreement factors indicate that the model is overly simple.

We have not attempted to estimate errors in the model parameters. The best-determined parameters are the flux densities and relative positions of well-separated, barely resolved components; in such cases the positions should be accurate to $\lesssim 0.1$ beamwidth (i.e., 0.1 mas in most cases). When two or more components are blended, the uncertainties are greater

NOTES TO TABLE 1

Col. (1).—Source name according to IAU convention.
Col. (2).—Alternative source name.
Col. (3).—Right ascension (1950.0).
Col. (4).—Declination (1950.0).
Col. (5).—Reference for radio position in cols. (3) and (4): (1) Perley 1982; (2) Peacock and Wall 1981; (3) Perley *et al.* 1980; (4) VLA position (R. A. Laing and R. A. Perley, private communications); (5) Peacock and Wall (VLA position; 1985, private communication).
Col. (6).—Optical identification: G = galaxy, Q = quasar, BL = blazar. The distinction between Q and BL is sometimes unclear.
Col. (7).—Approximate visual magnitude of the optical object.
Col. (8).—Redshift.
Col. (9).—Linear scale (pc mas^{-1}), assuming $H_0 = 100$ km s^{-1} Mpc^{-1} and $q_0 = 0.5$.
Col. (10).—Reference for optical identification and redshift: (1) Lawrence *et al.* 1986; (2) Hewitt and Burbidge 1987; (3) unpublished work by C. R. Lawrence, S. C. Unwin, and the authors (see also Lawrence *et al.* 1987) [0108+388, 1624+416; 1803+784; 2342+821, 2351+456]; (4) Burbidge and Crowne 1979; (5) Peacock *et al.* 1981 [0404+768, 0814+425, 1031+567]; (6) H. Spinrad 1986, private communication [1157+732]; (7) Spinrad 1982 [1254+476]; (8) Bartel *et al.* 1984*b* [2021+641].
Col. (11).—"Y" if the source was detected in the VLBI finding survey, "N" if it was not.
Col. (12).—Date of first-epoch mapping observation.
Col. (13).—Antennas used in map (for abbreviations see notes to Table 2).
Col. (14).—Total 5 GHz flux density (Jy) of the source in the published survey (S4 or S5).
Col. (15).—Total 5 GHz flux density (Jy) of the source at the time of the VLBI observation.
Col. (16).—Fraction F_c of the total flux density in an unresolved core (see § V).
Col. (17).—Morphological class (see § V).

TABLE 2

JOURNAL OF OBSERVATIONS

Source	Epoch	Antennas[a]	Frequency (MHz)	Integration Time (s)	Polarization[b]	Total Time Scheduled (hr)
			1978 Dec 11–14			
0133+476.....	1978.95	GFOH	5011	120	Lin 90	5
0316+413.....	1978.95	GFOH	5011	120	Lin 90	10.5
0859+470.....	1978.95	GFOH	5011	120	Lin 90	9.5
0923+392.....	1978.95	GFOH	5011	120	Lin 90	11.5
1633+382.....	1978.95	GFOH	5011	120	Lin 90	2
1807+698.....	1978.95	GFOH	5011	120	Lin 90	8.5
1828+487.....	1978.95	GFOH	5011	120	Lin 90	9.5
2200+420.....	1978.95	GFOH	5011	120	Lin 90	10
			1979 Apr 1[c]			
1633+382.....	1979.25	BGFOH	4996	120	Lin 90	6.5
			1979 Jul 24–26			
0108+388.....	1979.56	GFOH	5011	60	Lin 90	12
0814+425.....	1979.56	GFOH	5011	60	Lin 90	13
0945+408.....	1979.56	GFOH	5011	60	Lin 90	12.5
1637+574.....	1979.56	GFOH	5011	60	Lin 90	12.5
1823+568.....	1979.56	GFOH	5011	60	Lin 90	3
1954+513.....	1979.56	GFOH	5011	60	Lin 90	11.5
			1979 Nov 30–Dec 2[d]			
0804+499.....	1979.92	BKGFO	5009	240	Lin 90	11
0831+557.....	1979.91	KGFO	5009	240	Lin 90	11
0906+430.....	1979.92	BKGFO	5009	240	Lin 90	8
1358+624.....	1979.92	BG	5009	240	Lin 90	9
1823+568.....	1979.92	BKGFO	5009	240	Lin 90	10.5
2021+614.....	1979.91	KGFO	5009	240	Lin 90	12
2352+495.....	1979.91	BKGFO	5009	240	Lin 90	10
			1980 Jul 11–14			
0710+439.....	1980.53	BKGFO	5011	120	LCP	11
0711+356.....	1980.53	BKGFO	5011	120	LCP	10
0850+581.....	1980.53	BKFO	5011	120	LCP	11.5
1624+413.....	1980.53	BKGFO	5011	120	LCP	9.5
1642+690.....	1980.53	BKGFO	5011	120	LCP	12
1652+398.....	1980.53	BKGFO	5011	120	LCP	10
2351+456.....	1980.53	BKGFO	5011	120	LCP	5
			1980 Sep 19–26[e]			
0016+731.....	1980.74	BKFO	5009	120	LCP	1
0153+744.....	1980.74	BKFO	5009	120	LCP	1
0212+735.....	1980.72	BKFO	5009	120	LCP	9
0404+768.....	1980.74	B(KF)O	5009	120	LCP	1
0454+844.....	1980.73	BKFO	5009	120	LCP	8.5
0538+498.....	1980.74	(K)FO	5009	120	LCP	1
0836+710.....	1980.72	BKFO	5009	120	LCP	6.5
1749+701.....	1980.74	BKFO	5009	120	LCP	0.5
1803+784.....	1980.74	BKFO	5009	120	LCP	0.5
1928+738.....	1980.72	BKFO	5009	120	LCP	9
2342+821.....	1980.74	(BKFO)	5009	120	LCP	1
			1981 Aug 22–23			
0454+844.....	1981.64	BKGFO	4989	120	LCP	11
1458+718.....	1981.64	BKGFO	4989	120	LCP	11
			1982 Apr 1–5			
0016+731.....	1982.25	BKGFO	4989	120	LCP	14
0153+744.....	1982.26	BGFO	4989	120	LCP	11
1739+522.....	1982.26	BGFO	4989	120	LCP	9
1749+701.....	1982.26	BKGFO	4989	120	LCP	6
1803+784.....	1982.26	BKGFO	4989	120	LCP	6
1845+797.....	1982.25	BKGFO	4989	120	LCP	8.5

TABLE 3

MAP PARAMETERS

SOURCE	OBSERVATION	BEAM[a] a	b	θ (degrees)	PEAK (Jy beam^{-1})	CONTOUR LEVELS (% OF PEAK)
0016+731	1982 Apr	1.8	1.1	77	1.44	±0.5, ±1, 2, 5, 10, 20, 30, 40, 50, 60, 70, 80, 90
0108+388	1979 Jul	2.9	2.1	11	0.99	±1, 3, 5, 7, 10, 15, 20, 30, 40, 50, 60, 70, 80, 90
0133+476	1978 Dec	4.0	1.8	−18	1.35	±1, 2, 3, 4, 5, 10, 20, 30, 40, 50, 60, 70, 80, 90
0153+744	1982 Apr	1.5	1.1	−40	0.49	±5, 10, 20, 30, 40, 50, 60, 70, 80, 90
0212+735	1980 Sep	1.3	1.0	110	1.14	±1, ±2, 3, 4, 6, 8, 10, 20, 30, 40, 50, 60, 70, 80, 90
0316+413	1978 Dec	2.8	2.2	11	15.50	±2.5, 5, 7.5, 10, 20, 30, 40, 50, 60, 70, 80, 90
0454+844	1981 Aug	1.3	1.3	0	0.72	±2, 5, 10, 20, 30, 40, 50, 60, 70, 80, 90
0710+439	1980 Jul	1.4	1.0	−25	0.32	±2, ±5, 10, 20, 30, 40, 50, 60, 70, 80, 90
0711+356	1980 Jul	1.8	0.8	−24	0.48	±2, ±5, 10, 20, 30, 40, 50, 60, 70, 80, 90
0804+499	1979 Dec	1.3	1.0	90	1.29	±0.25, ±0.5, 1, 2, 3, 4, 5, 10, 20, 30, 40, 50, 60, 70, 80, 90
0814+425	1979 Jul	3.2	2.1	23	1.49	±1, ±3, 6, 10, 20, 30, 40, 50, 60, 70, 80, 90
0831+557	1979 Dec	2.0	2.0	0	0.77	±1, ±2, 3, 4, 5, 10, 20, 30, 40, 50, 60, 70, 80, 90
0836+710	1980 Sep	1.3	1.0	90	0.88	±2, 4, 6, 8, 10, 20, 30, 40, 50, 60, 70, 80, 90
0850+581	1980 Jul	1.5	0.8	−63	0.68	±2, ±5, 10, 20, 30, 40, 50, 60, 70, 80, 90
0859+470	1978 Dec	2.9	2.1	11	0.85	±1, 2, 3, 4, 5, 10, 20, 30, 40, 50, 60, 70, 80, 90
0906+430	1979 Dec	1.5	1.0	145	0.87	±0.5, ±1, 2, 3, 4, 5, 10, 20, 30, 40, 50, 60, 70, 80, 90
0923+392	1978 Dec	3.0	2.2	15	4.28	±1, 2, 3, 4, 5, 10, 20, 30, 40, 50, 60, 70, 80, 90
0945+408	1979 Jul	2.9	2.1	11	0.70	±1, ±3, 5, 7, 10, 15, 20, 30, 40, 50, 60, 70, 80, 90
1458+718	1981 Aug	1.3	1.3	0	0.31	±2, ±5, 10, 20, 30, 40, 50, 60, 70, 80, 90
1624+416	1980 Jul	1.8	0.8	−63	0.41	±2, ±5, 10, 20, 30, 40, 50, 60, 70, 80, 90
1633+382	1979 Apr	1.8	1.0	−24	1.21	±0.5, 1, 2, 3, 4, 5, 10, 20, 30, 40, 50, 60, 70, 80, 90
1637+574	1979 Jul	2.7	2.1	31	1.65	±1, ±3, 6, 10, 20, 30, 40, 50, 60, 70, 80, 90
1642+690	1980 Jul	1.2	1.1	0	1.39	±0.4, ±1.2, 2, 5, 10, 20, 30, 40, 50, 60, 70, 80, 90
1652+398	1980 Jul	1.9	0.9	−26	0.53	±0.5, ±1, ±2, 5, 10, 20, 30, 40, 50, 60, 70, 80, 90
1739+522	1982 Apr	1.1	0.8	−45	0.80	±0.5, 1, 2, 5, 10, 20, 30, 40, 50, 60, 70, 80, 90
1749+701	1982 Apr	1.1	1.1	0	0.82	±1, 2, 5, 10, 20, 30, 40, 50, 60, 70, 80, 90
1803+784	1982 Apr	1.1	1.1	0	2.17	±1, 2, 5, 10, 20, 30, 40, 50, 60, 70, 80, 90
1807+698	1978 Dec	2.8	1.7	−10	0.92	±2.5, 5, 7.5, 10, 20, 30, 40, 50, 60, 70, 80, 90
1823+568	1979 Dec	1.1	1.1	0	1.08	±0.5, ±1, 2, 3, 4, 5, 10, 20, 30, 40, 50, 60, 70, 80, 90
1828+487	1978 Dec	2.9	2.1	10	1.01	±2.5, 5, 7.5, 10, 20, 30, 40, 50, 60, 70, 80, 90
1845+797	1982 Apr	1.8	1.5	90	0.27	±2, 5, 10, 20, 30, 40, 50, 60, 70, 80, 90
1928+738	1980 Sep	1.3	1.0	140	1.46	±1, 2, 3, 4, 6, 8, 10, 20, 30, 40, 50, 60, 70, 80, 90
1954+513	1979 Jul	2.9	2.0	−19	0.71	±2, 6, 10, 20, 30, 40, 50, 60, 70, 80, 90
2021+614	1979 Dec	2.0	2.0	0	0.90	±2, 4, 6, 8, 10, 20, 30, 40, 50, 60, 70, 80, 90
2200+420	1978 Dec	2.9	2.4	11	1.20	±1, ±2, ±3, 4, 5, 10, 20, 30, 40, 50, 60, 70, 80, 90
2351+456	1980 Jul	3.8	0.9	−15	0.27	±5, 15, 25, 35, 45, 55, 65, 75, 85, 95
2352+495	1979 Dec	1.4	1.0	−36	0.52	±2, 4, 6, 8, 10, 20, 30, 40, 50, 60, 70, 80, 90

[a] The restoring beam is an elliptical Gaussian with FWHM major axis a mas and minor axis b mas, with major axis in position angle θ.

and the model should only be regarded as a *possible* deconvolution of a complex structure. Such deconvolutions are not unique, and can be misleading.

V. CLASSIFICATION

The new observations presented in this paper enable us to classify powerful extragalactic radio sources on the basis of the morphology of the compact radio emission regions close to the central engine. The objects exhibit a variety of radio morphologies and spectrum shapes. This variety may arise from fundamental differences in the central engine or the host galaxy, or it may be due to environmental effects. A detailed study of the differences may be able to show whether the objects are drawn from a single parent population with a continuum of properties, or whether there are more fundamental differences, and will give us some insight into the relationship between mor-

NOTES TO TABLE 2

[a] Antennas: Only antennas that made successful observations are listed. The source was not detected at stations listed in parentheses. B: 100 m antenna at Effelsberg, near Bonn, Federal Republic of Germany (Max-Planck-Institut für Radioastronomie). F: 26 m antenna at Fort Davis, Texas (George R. Agassiz Station of the Harvard College Observatory). G: 43 m antenna at Green Bank, West Virginia (National Radio Astronomy Observatory). H: 26 m antenna near Cassel, California (Hat Creek Observatory, University of California). K: 37 m antenna near Westford, Massachusetts (Haystack Observatory, Northeast Radio Observatory Corporation). O: 40 m antenna near Big Pine, California (Owens Valley Radio Observatory, California Institute of Technology).

[b] Polarization: Lin 90—linear, E-vector in P.A. 90°. LCP—left circular (IEEE convention).

[c] The 1979 April observations were made by R. C. Walker and M. H. Cohen as part of another program.

[d] In 1979 November–December K observed right circular polarization.

[e] In 1980 September antenna G was scheduled but failed.

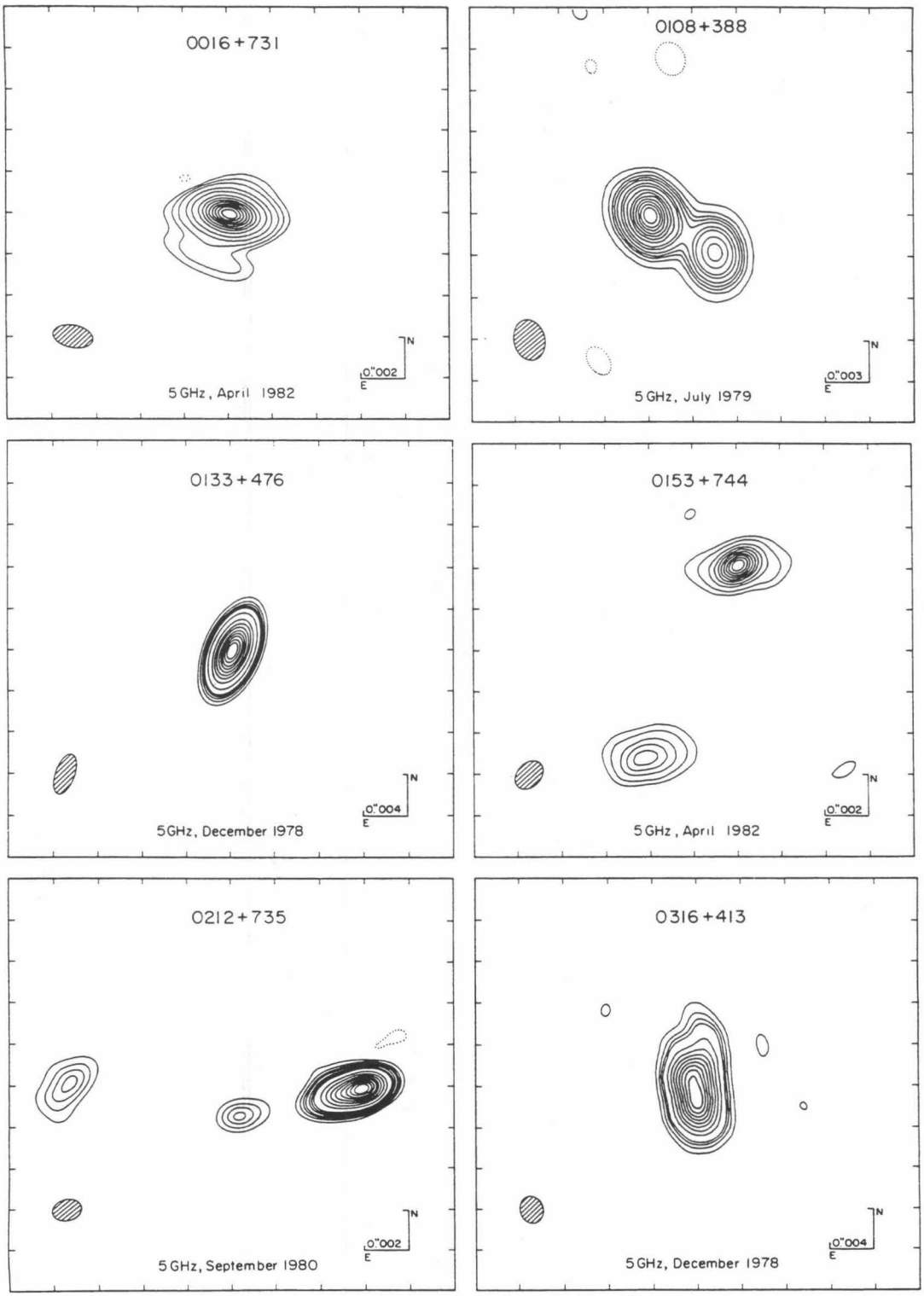

FIG. 1.—First-epoch VLBI maps of 37 sources. The scale of each map is indicated in the lower right-hand corner, and the FWHM contour of the elliptical Gaussian restoring beam is shown as a hatched ellipse in the lower left-hand corner. The peak flux density, contour levels, and parameters of the restoring beam used for each map are listed in Table 3.

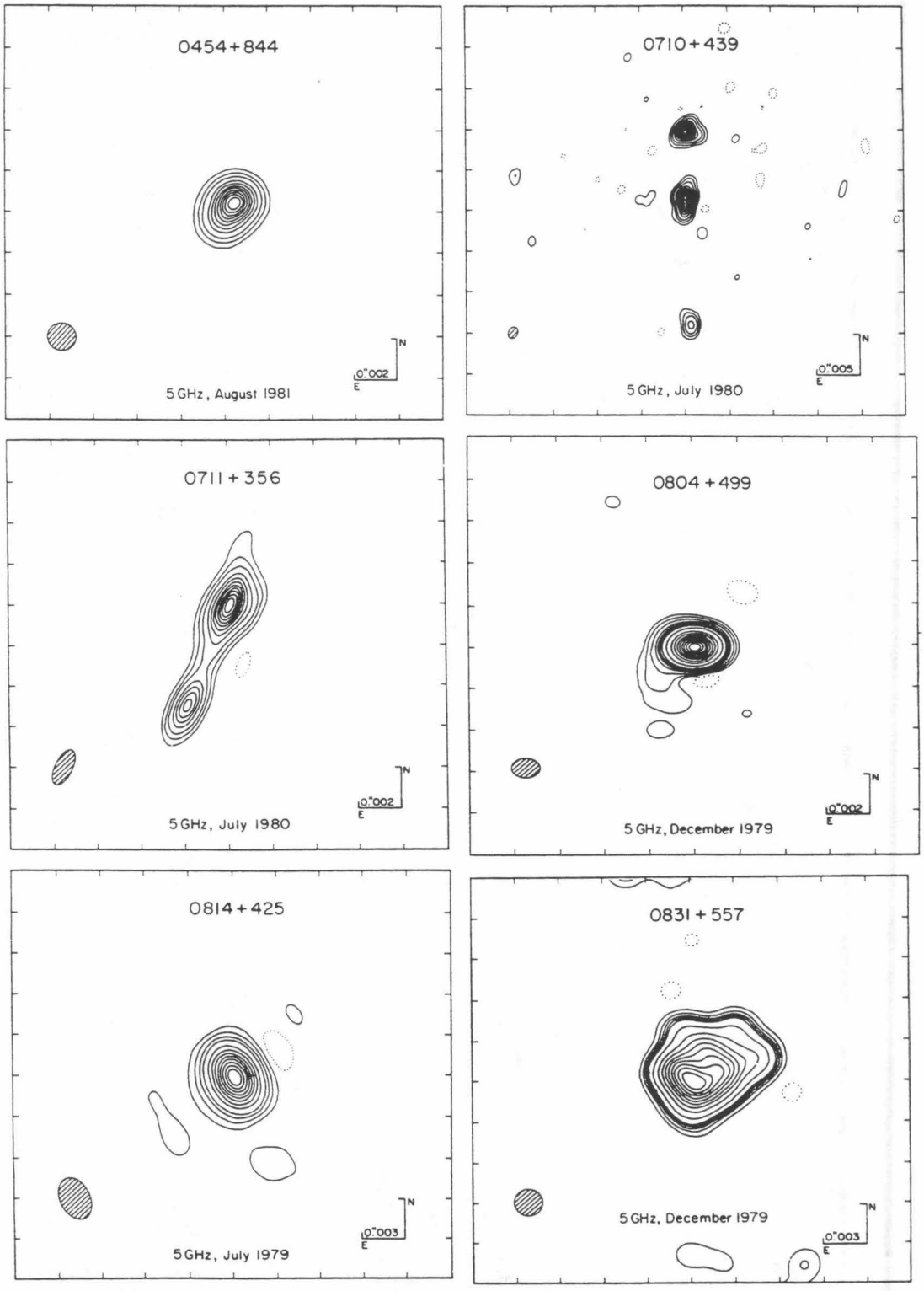

FIG. 1.—*Continued*

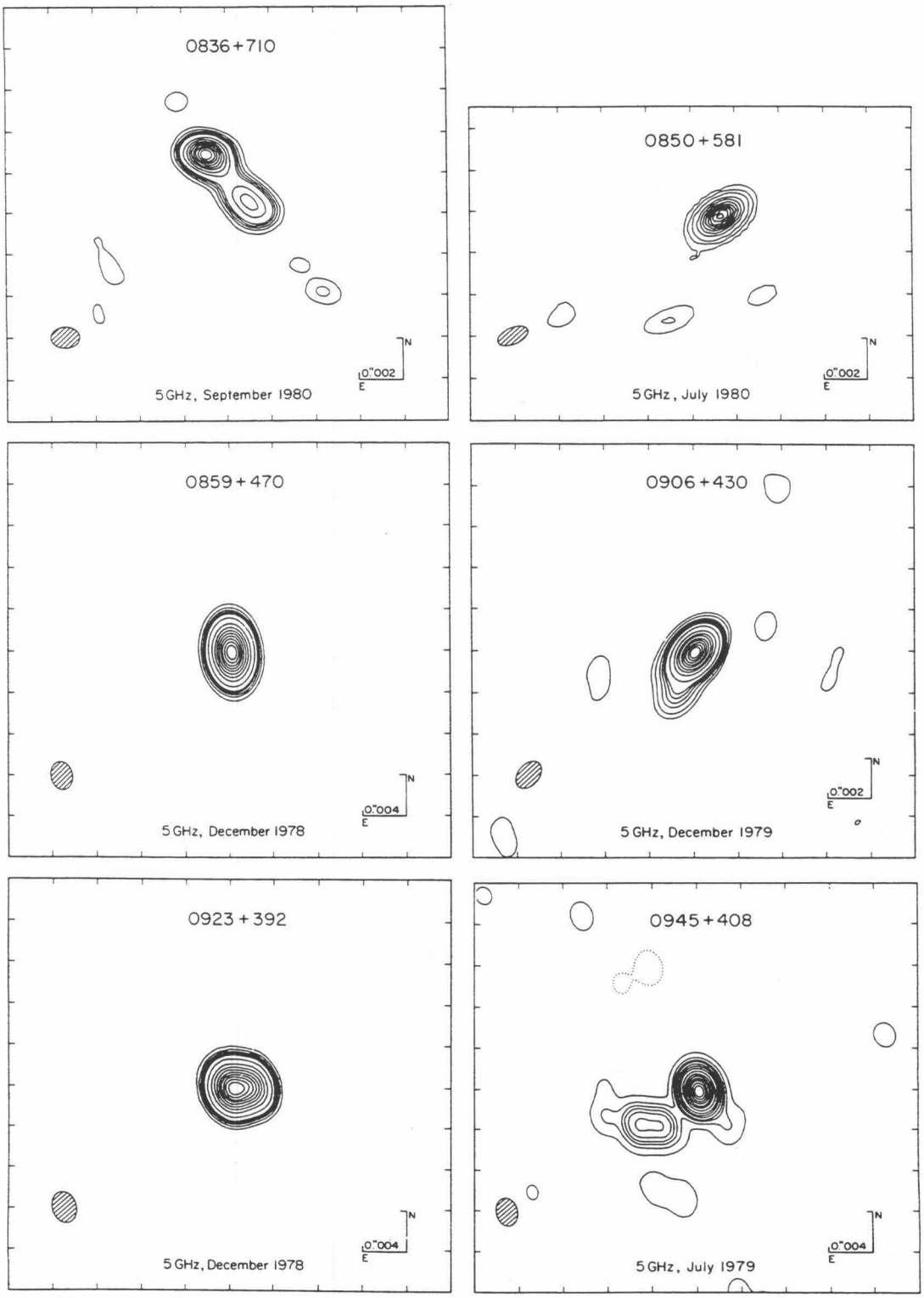

FIG. 1.—*Continued*

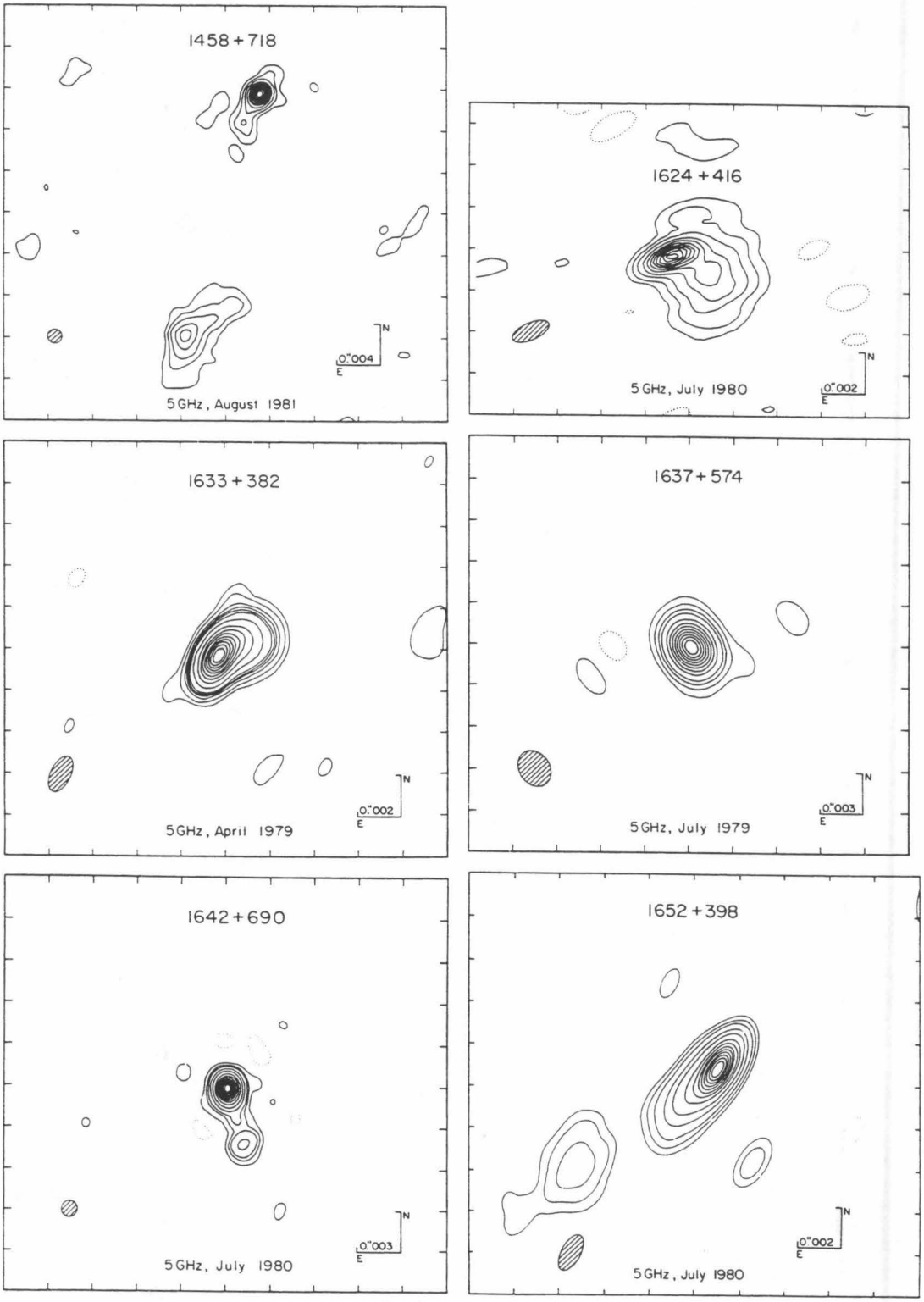

FIG. 1.—*Continued*

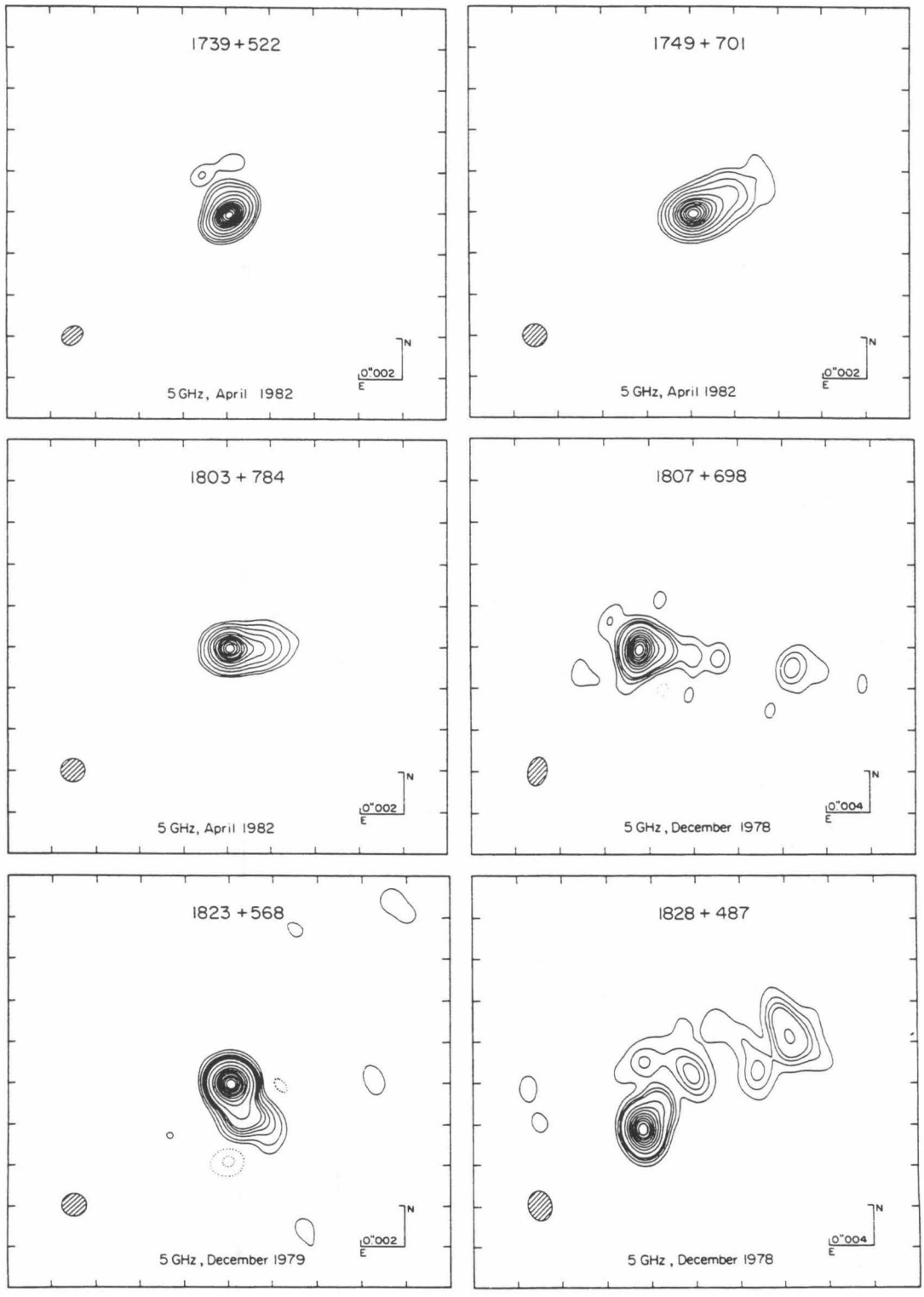

FIG. 1.—*Continued*

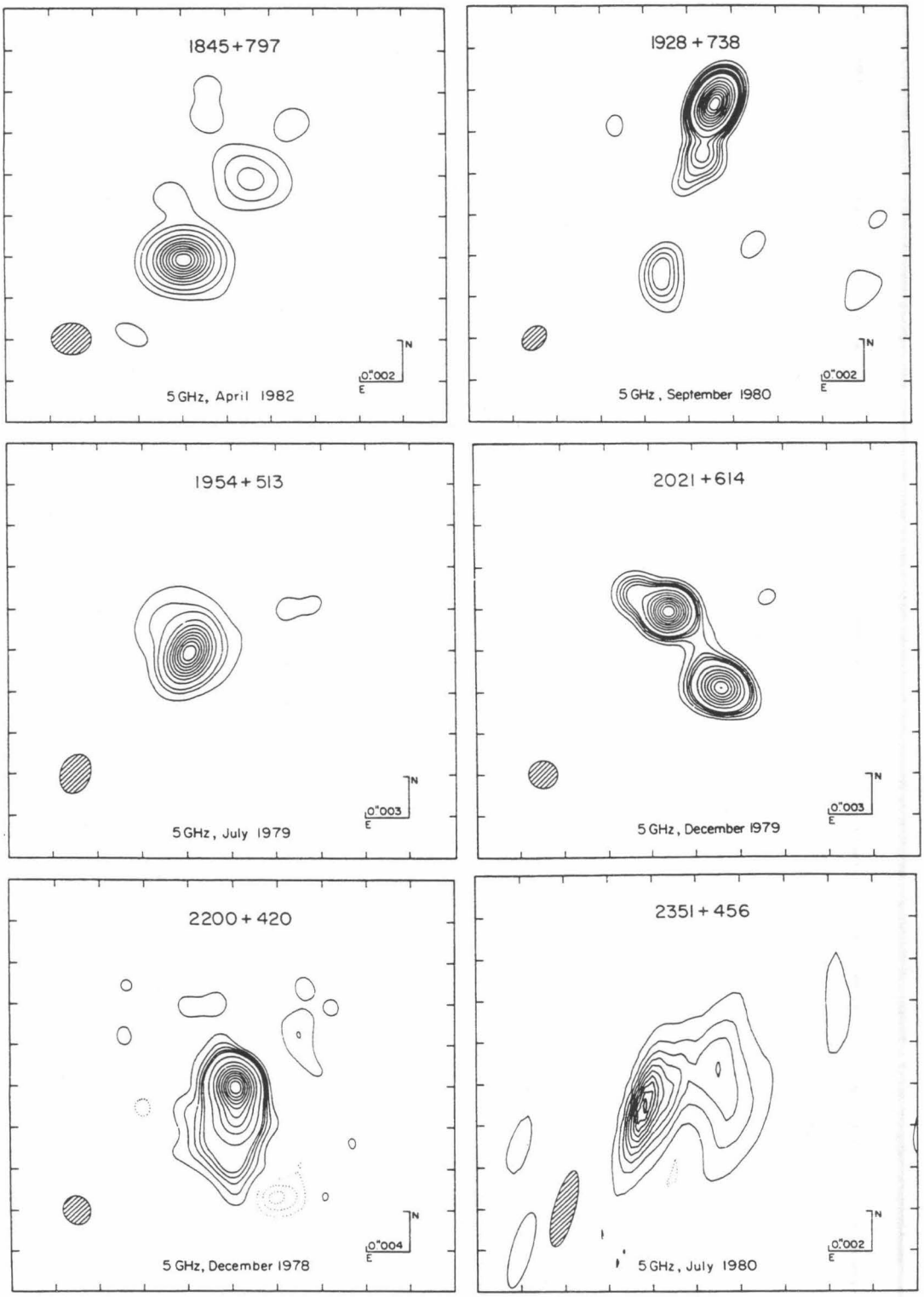

FIG. 1.—*Continued*

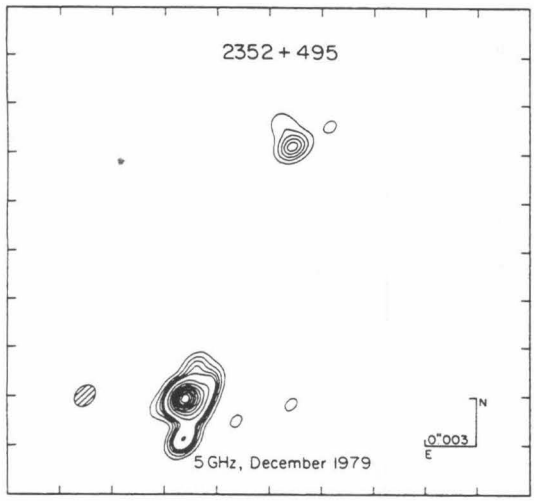

FIG. 1.—*Continued*

phology and the underlying physical processes that may be occurring in the objects.

We have therefore attempted to separate the sources into a number of groups with similar characteristics, based on the VLBI maps of the sources, their large-scale structure, and their radio spectra (Kühr *et al.* 1981*b*). Our assignment of these sources to classes is indicated in Table 1 and summarized in Table 5. The classification is based primarily on the morphology of the dominant radio component; we then apply a secondary criterion based on radio spectrum, and, finally, a tertiary criterion based on the size of the dominant radio emission region.

The most obvious distinguishing feature is the presence, or absence, of a strong compact component. It seems likely that the feature with the highest surface brightness is most closely associated with the central engine, and we therefore refer to this as the "core" component. We have used the results of model fitting (see Table 4) to determine the strength of the core, and hence the fraction F_c of the total flux density in the core. In a few objects there are weak unresolved components for which we can derive only lower limits to the surface brightness, but in most of these cases there is also a very high surface brightness feature which dominates the nuclear radio emission and which we identify with the core. Two significant results are that all the cores are situated at one end of the nuclear structure, and they are all resolved, i.e., there is not a single case of a strong compact component which is completely unresolved.

We consider first the sources with $F_c > 0.5$. All these sources have, by definition, a large fraction of their flux density in an unresolved core. We divide them into three classes:

1*a*. *Very compact* objects ($F_c > 0.9$);

1*b*. *Compact* objects ($0.8 < F_c \leq 0.9$);

1*c*. *Asymmetric I* objects ($0.5 < F_c \leq 0.8$).

All of the objects in these three classes (except perhaps 0859+470) are asymmetric, and, as pointed out above, none is completely unresolved. It is possible that they all have a similar asymmetric, "core-jet" structure, and differ only in the relative prominence of the core. All the sources with $F_c > 0.5$ have flat high-frequency spectra ($\alpha > -0.5$ in the range 1–10 GHz, $S \propto \nu^{\alpha}$), and further subdivision by spectrum is not productive.

Among the objects with $F_c \leq 0.5$, the extended radio emission is more prominent, and a wider variety of morphologies and spectra are found. We first identify

1*d*. *Asymmetric II* objects: these are well-resolved, asymmetric objects with a bright compact component at one end of an extended jetlike feature, and a flat high-frequency spectrum.

A different morphology is exhibited by a class of "compact double" objects, which have two or more well-separated components of comparable brightness. For reasons which will be made clear in § VI, we divide these into two subclasses:

2*a*. *Compact S double* objects, with a compact double morphology and a *steep* high-frequency spectrum; these exhibit maxima in their spectra around 1 GHz.

2*b*. *Compact F double* objects, with a compact double morphology and a *flat* high-frequency spectrum.

Most of the remaining sources have steep high-frequency spectra. We next select the remaining flat-spectrum sources:

3. *Irregular flat-spectrum* objects: sources with complex milliarcsecond morphology and flat high-frequency spectra.

Finally we divide the remaining steep-spectrum sources according to the extent of the extended emission:

4. *Steep-spectrum compact* objects, in which most of the emission arises in a region with a projected size smaller than 15 kpc.

5*a*. *Lobe-dominated* objects of *Fanaroff-Riley class I*;

5*b*. *Lobe-dominated* objects of *Fanaroff-Riley class II*.

This completes the classification. It is notable that some possible morphologies do not occur. For example, there are no sources with a flat-spectrum core and two oppositely directed nuclear jets.

VI. TRENDS AND CORRELATIONS

In order to test the physical significance of the morphological classification that we have proposed, we have examined correlations of other observable properties of the sources with morphological class. In this section we discuss the polarization, variability, largest angular size, alignment, and optical identification of the objects in the various classes.

a) Polarization

Measurements of the integrated polarization at 5 GHz of many of the objects in our sample have been made by Perley (1982) and by Rudnick and Jones (1982, 1983). Many of the objects show variations in both polarization strength and position angle, and detailed comparisons with VLBI observations made at a different epoch could be misleading. However, there is a clear difference in the mean level of polarization of objects in different classes (Table 5). Two interesting points should be noted:

1. In the very compact, compact, and asymmetric sources the mean level of polarization increases as we progress from class 1*a* to class 1*d*, in the direction of increasing prominence of the jet. This suggests that the jets are responsible for most of the observed polarization. This result for a large sample of objects is consistent with the few VLBI polarization images that have been made so far, in which it is found that the jets are polarized and the cores have low levels of polarization (Roberts and Wardle 1987).

2. The compact double sources of both classes 2*a* and 2*b* have levels of polarization which are, on average, about an order of magnitude below those of the asymmetric objects. This suggests that the basic structures of the compact double

TABLE 4

GAUSSIAN MODELS

Source	S (Jy)	r (mas)	θ (degrees)	a (mas)	b/a	ϕ (degrees)	A.F. (amplitude)	A.F. (closure phase)
0016+731.....	1.582	0.00	0.0	0.55	0.70	99.6	2.01	1.16
	0.091	1.66	155.7	1.84	0.23	100.2		
0108+388.....	0.558	0.00	0.0	1.02	0.69	82.1	1.21	1.20
	1.156	5.06	59.1	1.41	0.36	65.6		
0133+476.....	1.596	0.00	0.0	1.41	0.64	147.6	0.87	1.17
	0.199	3.67	316.9	3.90	0.59	−13.7		
0153+744.....	0.374	4.66	−25.0	0.00	...	...	5.55	2.12
	0.270	4.95	−26.1	2.65	0.00	93.5		
	0.620	5.49	157.2	2.23	0.43	96.3		
0212+735.....	1.358	0.00	0.0	0.79	0.35	118.9	1.75	1.67
	0.529	1.25	103.5	0.74	0.63	137.0		
	0.117	5.74	102.9	1.21	0.68	103.7		
	0.062	14.22	106.9	1.72	0.61	25.6		
0454+844.....	0.523	0.00	0.0	1.16	0.40	−25.3	1.79	0.90
	0.507	0.83	−36.4	0.15	1.00	...		
0710+439.....	0.625	8.45	−0.1	1.25	0.59	90.0	3.83	4.48
	0.713	0.00	0.0	2.36	0.30	0.0		
	0.167	15.42	182.2	1.14	0.73	0.0		
0711+356.....	0.268	0.00	0.0	0.11	1.00	...	1.53	1.45
	0.776	5.35	−21.7	1.21	0.62	−23.4		
	0.150	2.40	−25.1	1.86	0.26	−24.9		
	0.051	5.67	−34.6	0.00	...	...		
0804+499.....	1.344	0.00	0.0	0.23	1.00	...	1.53	1.16
	0.075	2.78	140.4	3.96	0.32	0.0		
	0.075	1.00	85.9	1.32	0.20	0.0		
0814+425.....	1.599	0.00	0.0	0.55	0.00	98.4	2.94	1.17
	0.100	1.97	148.7	0.00	...	...		
0836+710.....	1.045	0.00	0.0	0.75	0.20	35.3	1.63	1.77
	0.554	1.84	214.2	3.00	0.00	36.6		
	0.425	3.35	220.2	1.25	0.57	42.5		
	0.384	8.40	217.3	3.03	0.47	26.4		
0850+581.....	0.936	0.00	0.0	0.87	0.31	162.5	1.14	1.50
	0.087	5.30	156.1	0.96	0.63	63.7		
0859+470.....	1.151	0.00	0.0	2.14	0.43	0.6	1.05	1.10
0906+430.....	0.875	0.00	0.0	0.11	0.89	30.8	0.87	1.26
	0.091	1.88	154.5	1.48	0.29	14.6		
0923+392.....	4.710	0.00	0.0	1.15	0.96	85.9	0.82	1.31
	2.331	1.89	276.9	0.80	0.00	−14.9		
0945+408.....	0.746	0.00	0.0	0.50	0.00	97.9	1.61	1.70
	0.363	5.77	127.1	4.40	0.18	83.7		
1624+416.....	0.429	0.00	0.0	0.70	0.22	95.0	1.87	1.23
	0.688	2.02	238.9	2.84	0.70	4.5		
1633+382.....	0.425	0.00	0.0	1.17	0.24	138.8	0.58	1.20
	0.857	0.34	115.1	0.00	...	...		
	0.428	1.08	−63.8	1.16	0.59	−106.3		
1637+574.....	1.830	0.00	0.0	1.02	0.00	7.1	2.65	1.11
1642+690.....	1.625	0.00	0.0	0.73	0.00	1.9	3.77	2.43
	0.158	4.23	194.9	1.40	0.38	121.9		
	0.087	0.97	206.1	0.75	0.00	87.8		
1652+398.....	0.449	0.00	0.0	0.35	0.42	135.1	1.71	1.41
	0.320	0.98	133.3	2.47	0.33	134.6		
	0.119	7.93	127.6	6.51	0.32	124.8		
1739+522.....	0.891	0.00	0.0	0.40	0.84	−22.9	1.26	0.98
	0.074	1.74	3.2	2.14	0.88	−17.9		
1749+701.....	0.836	0.00	0.0	0.61	0.00	−75.4	1.41	1.16
	0.432	1.13	−64.3	2.01	0.38	−56.1		
1803+784.....	2.157	0.00	0.0	0.16	0.00	−93.8	2.67	1.37
	0.696	1.24	−92.2	0.87	0.38	−80.2		
1807+698.....	0.952	0.00	0.0	0.93	0.72	−115.0	0.96	1.14
	0.200	14.13	−96.8	4.10	0.54	−82.0		
	0.287	1.79	−90.7	2.19	0.00	−94.0		
	0.165	5.72	−102.0	4.61	0.00	−100.0		
1823+568.....	1.132	0.00	0.0	0.35	0.00	16.4	1.28	1.24
	0.146	1.35	197.4	0.82	0.00	23.0		
1845+797.....	0.309	0.00	0.0	0.80	0.39	−49.7	1.15	1.05
	0.073	4.86	−37.5	1.71	0.47	−43.4		
1928+738.....	2.114	0.00	0.0	1.16	0.18	164.0	2.23	1.42
	0.168	1.98	166.0	1.30	0.40	24.3		
	0.202	3.57	163.0	2.03	0.38	145.6		
	0.240	8.25	163.0	1.90	0.55	−1.6		
	0.111	16.23	173.0	2.14	0.85	13.5		

TABLE 4—*Continued*

Source	S (Jy)	r (mas)	θ (degrees)	a (mas)	b/a	θ (degrees)	A.F. (amplitude)	A.F. (closure phase)
1954+513.....	0.854	0.00	0.0	1.22	0.76	−50.1	1.28	1.76
	0.217	3.44	7.8	7.23	0.20	−60.9		
2021+614.....	1.012	0.00	0.0	0.77	0.61	57.0	1.33	1.78
	0.997	6.57	212.4	1.45	0.70	48.4		
	0.162	2.66	63.8	1.00	0.58	61.0		
2200+420.....	1.186	0.00	180.0	0.53	1.00	...	1.06	1.47
	0.648	2.99	182.7	1.63	1.00	...		
	0.154	6.70	173.8	2.97	1.00	...		
2351+456.....	0.323	0.00	0.0	0.77	0.80	−56.0	1.52	1.88
	0.166	1.46	−72.9	1.04	0.71	−48.1		
	0.302	3.88	−62.2	2.35	0.62	−10.7		
2352+495.....	0.730	0.00	0.0	0.86	0.90	54.9	2.44	2.93
	0.212	2.13	177.8	1.05	0.00	0.2		
	0.146	16.77	−21.7	1.18	0.83	105.6		

NOTE.—Parameters of each elliptical Gaussian component of the model brightness distribution: S, flux density; r, θ, polar coordinates of the center of the component relative to an arbitrary origin, with polar angle measured from north through east; a, b major and minor axes of the FWHM contour; ϕ, position angle of the major axis, measured from north through east. The agreement factors (reduced χ^2) between the model and the data are denoted by A.F. (amplitude) and A.F. (closure phase). The following sources were too complex for modeling: 0316+413, 0831+557, 1458+718, 1828+487.

sources are different from those of the core-jet sources; e.g., the observed features are probably not parts of invisible underlying jets.

In an inhomogeneous sample of 26 radio sources, Rusk and Seaquist (1985) found a strong trend for the *E*-vector of the radio polarization to lie normal to the VLBI structural axis. Rusk (1987) has suggested that there is a difference between BL Lac objects, in which the polarization tends to lie parallel to the structural axis, and quasars and radio galaxies, in which the polarization tends to lie normal to the axis. In our sample the distribution is bimodal, with the polarization position angles tending to lie either perpendicular or parallel to the structural axis. However, only a small number of sources have data of sufficient quality for this investigation, and more observations of the polarization of the cores of the objects and their Faraday rotation measures are needed before a definitive statement can be made.

b) Variability

Seielstad, Pearson, and Readhead (1983) measured the 10.7 GHz flux density variability over a period of 4 years of all the sources in our sample south of declination 70°. Their

TABLE 5

CLASSIFICATION OF THE 65 SOURCES IN THE COMPLETE SAMPLE

Class	Description	Core Fraction F_c	Number	Members	Mean Polarization (5 GHz)[a]	Fraction with $V > 0.4$[a]
1*a*.....	Very compact	$0.9 \le F_c < 1.0$	4	0016+731, 0804+499, 1637+574, 1739+522	1.6 ± 0.5 (4)	1.00 (3)
1*b*.....	Compact	$0.8 \le F_c < 0.9$	4	0133+476, 0814+425, 0850+581, 1642+690	1.4 ± 0.9 (4)	1.00 (4)
1*c*.....	Asymmetric I	$0.5 \le F_c < 0.8$	9	0212+735, 0454+844, 0859+470, 1749+701, 1803+784, 1823+568, 1928+738, 1954+513, 2200+420	2.9 ± 1.8 (9)	0.80 (5)
1*d*.....	Asymmetric II	$F_c < 0.5$	8	0836+710, 0945+408, 1624+416, 1633+382, 1641+399, 1652+398, 1807+698, 2351+456	3.3 ± 2.6 (8)	0.43 (7)
2*a*.....	Compact S double	$F_c < 0.5$	3	0108+388, 0710+439, 2352+495	0.3 ± 0.1 (3)	0.00 (3)
2*b*.....	Compact F double	$F_c < 0.5$	4	0153+744, 0711+356, 0923+392, 2021+614	0.5 ± 0.4 (4)	0.33 (3)
3.....	Irregular flat-spectrum	$F_c < 0.5$	2	0316+413, 0831+557	0.1 ± 0.1 (2)	...
4.....	Steep-spectrum compact	$F_c < 0.5$	7	0404+768, 0538+498, 0906+430, 1458+718, 1634+628, 1828+487, 2342+821	2.4 ± 2.2 (4)	0.00 (4)
5*a*.....	Lobe-dominated, F-R I	$F_c < 0.5$	3	0220+427, 0314+416, 2229+391	...	...
5*b*.....	Lobe-dominated, F-R II	$F_c < 0.5$	16	0040+517, 0210+860, 0605+480, 0723+679, 0809+483, 0917+458, 1003+351, 1157+732, 1254+476, 1409+524, 1609+660, 1842+455, 1845+797, 1939+605, 2153+377, 2243+394	...	...
...	Not classified (M82)	...	1	0951+699	...	...
...	Not yet observed	...	4	0954+556, 0954+658, 1031+567, 1358+624	...	...

[a] Number of sources for which data are available given in parentheses.

results show that there is a clear difference in the variability of the sources in the different classes. Rather than estimate the "mean variability" in each class, which is rather sensitive to the behavior of a few highly variable sources, we have determined the fraction of objects in each class for which the fractional variability estimated by Seielstad *et al.*, $V = \Delta S/\langle S \rangle$, is greater than 0.4 (Table 5). The great majority of compact and asymmetric sources in classes 1*a*–1*c* are variable at this level, but a significantly smaller fraction of the sources in class 1*d* ("asymmetric II") exceed this level. Very few of the compact double sources (classes 2*a* and 2*b*) or steep-spectrum compact sources (class 4) exceed this level of variability.

Only the most compact emission regions are expected to be variable on a time scale of 4 yr. Thus the lower level of variability in objects of class 1*d* can be attributed to the greater prominence of the resolved jet components in these objects. The projected sizes of these features are greater than a few parsecs, and therefore they have a number of different emission regions separated by distances of this order. Thus we would expect variations in brightness of the different components to occur at different times even if they are causally connected. The same explanation applies to the low variability of the steep-spectrum compact objects (class 4) in which the dominant emission regions are also large.

The low variability observed in the compact double sources, which contain two small dominant emission regions, cannot be explained in this way. It appears that the low variability must be an intrinsic feature of these objects, again suggesting that they are intrinsically different from the core-jet sources.

c) *Largest Angular Size*

We have collected information on the largest angular size of the objects in our sample from the literature. The references are given in the Appendix. In recent years, very high dynamic range maps made with the VLA and MERLIN have revealed low-level extended structure in many of the objects, and we can expect that further observations will find more. In every morphological class except for 2*a* (the steep-spectrum compact doubles), some sources have low-brightness features considerably larger than 1″. This is true even of the very compact objects. Among the compact double sources, however, only one, 0923+395 (4C 39.25), has a largest angular size greater than 0″.2. This source has some similarities to the asymmetric core-jet sources, e.g., it shows superluminal motion, and it raises doubts as to whether the flat-spectrum compact doubles should not be considered more akin to the asymmetric sources than to the steep-spectrum compact doubles.

d) *Alignment of Large-Scale and Small-Scale Structures*

It is generally believed that the small-scale jets observed in VLBI images are the sources of, and are continuous with, the large-scale jets that supply the outer lobes. To investigate this hypothesis, we have compared the position angle of the radio structure revealed in the VLBI maps with the position angle of the larger scale structure. The distribution of the differences between these two angles reflects the distribution of the deviations of the jets from straight lines, and, in the beaming picture, larger deviations should be observed in the sources with stronger cores, owing to projection effects (e.g., Moore *et al.* 1981; Readhead *et al.* 1983; Readhead, Pearson, and Barthel 1987). The observed distribution is sensitive to both the magnitude of the intrinsic deviations and the Lorentz factor of the jets, but it is not possible to disentangle these two contributions on the basis of the misalignments alone (Rusk and Rusk 1986).

TABLE 6

ALIGNMENT OF LARGE-SCALE AND SMALL-SCALE STRUCTURE

Source	Large-Scale P.A.	Small-Scale P.A.	Difference $\lvert\Delta(\text{P.A.})\rvert$
0723+679	260°	272°	12°
0836+710	204	214	10
0850+581	139	156	17
0906+430	241	155	86
0923+392	259	277	18
0945+408	32	127	95
1003+351	304	292	12
1458+718	73	164	91
1624+416	351	239	112
1641+399	328	230	98
1642+690	168	195	27
1749+701	209	296	87
1803+784	195	268	73
1807+698	241	263	22
1823+568	98	197	99
1828+480	316	328	12
1845+797	323	322	1
1928+738	189	166	23

In Table 6 we list the 18 objects in the sample for which both a small-scale and a large-scale position angle are available. For the small scale we have taken the position angle of the feature closest to the VLBI core (the brightest, most compact component in the map), while for the large scale we have taken the position angle relative to the core of either a portion of the large-scale jet or a compact hot spot, choosing the angle which maximizes the position-angle difference Δ(P.A.) between the inner and the outer structure. The resulting distribution of position-angle differences (Fig. 2) is remarkable and quite unexpected. There are two distinct peaks in the distribution, one at zero as expected if intrinsic misalignments are small, and a second centered at 90°. The peak at 90° is difficult to explain, but if it is a real feature of the parent population of radio sources, it could provide an important constraint on models of the jet, the central engine, and the host galaxy.

In a similar study of a larger, inhomogeneous sample (including many of the sources in Table 6), Rusk and Rusk (1986) found a smooth distribution of Δ(P.A.) peaked at zero. This suggests that the bimodal distribution found in our sample could be due to statistical fluctuation, or it could be a result of the different selection criteria. A chi-square test of the null hypothesis that both samples are taken from the same parent population shows that the differences between the two samples are not statistically significant. The bimodality of our distribution is sufficiently striking, however, to encourage us to investigate the implications of a real preference for Δ(P.A.) values close to 90°.

It is straightforward to calculate the expected distribution of Δ(P.A.) for a given intrinsic bend between the inner and the outer jets, both when relativistic beaming is a dominant effect and when it is not. The expected distribution is always peaked around the intrinsic angle of bend in the nonrelativistic case, although the distribution is broadened by projection (examples for intrinsic bends of 15° and 90° are shown in Fig. 2). If relativistic beaming is important, the peak is broadened, the width increasing with Lorentz factor γ, and an almost uniform distribution is obtained if $1/\gamma$ is smaller than the intrinsic angle of deviation. (If relativistic beaming is important in the large-scale

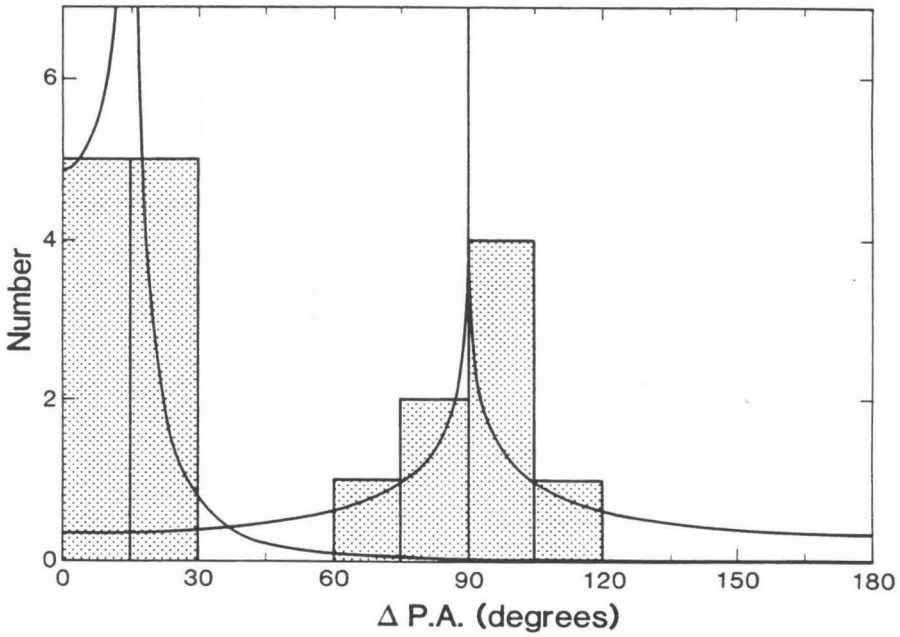

FIG. 2.—Distribution of the absolute value of the difference in position angle Δ(P.A.) between small-scale (VLBI) structure and extended structure, in the sample of 18 sources for which information is available (Table 6). Two theoretical probability distributions are plotted, assuming that the objects are randomly oriented with respect to the line of sight and that they all have the same intrinsic bend angle (15° and 90° for the two distributions). The probability distributions are normalized to 10 objects (15° curve) and eight objects (90° curve), in accordance with the apparent distribution of objects between the two peaks.

structure, however, observational selection will discriminate against objects in which the emission from large-scale structure is beamed away from the line of sight. Such effects are very model-dependent.) Other effects will also broaden the distribution, including a distribution of intrinsic bend angles and observational errors. We conclude that in order to produce a sharp peak in the distribution around $\Delta(\text{P.A.}) \sim 90°$, the sources must have an intrinsic bend angle of 90°, with little variance, and relativistic beaming cannot introduce a strong orientation bias in the observed sample.

It is difficult to conceive of mechanisms for bending jets that will result in a preferred intrinsic misalignment of 90° between the small-scale and large-scale structure. For example, models which attribute the bending to precession of the central engine have no preferred misalignment. If the jets are bent by a pressure gradient in the host galaxy, then we can identify the axis of the large-scale structure with that of the galaxy pressure gradient, while the axis of the small-scale structure is that of the central engine (black hole). With this interpretation, our observations would suggest that there is a class of sources in which these two axes are perpendicular.

It is therefore important to test the reality of the bimodal distribution by observing larger, independent samples, and by making high dynamic range maps with resolution 0.″1–1″ of the objects in our sample for which large-scale structure has not yet been detected.

e) Optical Identification and Spectrum

The published optical data on the objects are very inhomogeneous, and, in particular, there has been no systematic attempt to distinguish between quasars and BL Lac objects. We have nearly completed a program (with C. R. Lawrence and S. C. Unwin) to obtain high-quality spectra of all the objects using the Palomar 200 inch telescope, which we hope will improve the situation. With such information as is available, some trends are apparent. Approximately 75% of the core-dominated sources for which we have maps are quasars or BL Lac objects. It is therefore notable that all 17 of the sources in classes 1*a*, 1*b*, and 1*c* are quasars or BL Lac objects, and even more remarkable that all three of the steep-spectrum compact double sources are identified with galaxies. Here we also see a distinction between the flat-spectrum and the steep-spectrum compact doubles: only one out of the four flat-spectrum compact doubles is identified with a galaxy.

VII. DISCUSSION

In this section we discuss the different classes of object in more detail.

a) Very Compact and Compact Sources

The *very compact* and *compact* sources have, by definition, a single unresolved component (smaller than a milliarcsecond) which emits $> 80\%$ of the flux density. All the sources in these two classes are highly variable, changing by 50% or more in 4 yr or less (at 10.7 GHz). All are fairly strongly polarized ($> 1\%$), and all are quasars.

The "very compact" sources can be regarded as "naked cores," that is, flat-spectrum core sources without an associated jet; and it is possible that we shall find a jet by making images of higher dynamic range, or by making images when these highly variable sources are in a low state. In some cases the images show some low-brightness emission at a very low level, $< 1\%$ of the peak, but this is at the limit of the VLBI imaging process. (These sources are thus good phase calibrators for VLBI arrays.)

The "compact" sources are intermediate between the "very compact" sources and the "asymmetric" sources. Where low-brightness nuclear emission is found, it is one-sided. At least

two "compact" sources are known to be superluminal (0850+581: Barthel *et al.* 1986; 1642+690: Pearson *et al.* 1986), and it is likely that others will be found to be superluminal, although in some cases the observations are very difficult owing to the high dynamic range required.

b) *Asymmetric Sources*

The *asymmetric I* sources are defined, analogously to the compact sources, by the relative strength of the unresolved core, which is between 50% and 80% of the total flux density. All of these sources have an asymmetric structure with a compact core and a lower brightness extension (or "jet") on one side only. The *asymmetric II* sources are defined by morphology; the one-sided structure is similar to that of the asymmetric I sources, but the fraction of flux density in the core is $<50\%$. In the few sources for which spectral information is available, the core is found to have a flat (self-absorbed) spectrum and the "jet" a steeper spectrum.

It is possibly misleading to use the word "jet" to describe the asymmetric features in these sources. It is reasonable to use it for the long linear structures seen in objects like Cygnus A and NGC 6251, where there must be a flow of material along the jet to supply the energy requirement of the outer lobes. In the VLBI sources, the word is used to describe almost any feature that is slightly longer than it is wide, with no evidence for any material flow at all. The justification comes from the analogy—and at this stage it is only an analogy—between these sources and the few where there is good evidence for a jet; the evidence is (1) continuity of the parsec-scale VLBI structure with a large-scale jet supplying an outer lobe and (2) apparent bulk relativistic motion outward along the jets in superluminal sources.

Many of these sources have extensive large-scale structure. Although they were at first thought to be small sources of subgalactic dimensions, very high dynamic range observations with the VLA and MERLIN have shown up extensive large-scale features. In some cases the VLBI structure is well aligned with outer arcsecond-scale structure (e.g., 1807+698); in others, the misalignment can be as large as 90° (e.g., 0945+408). Lack of alignment does not imply that there is no connection, however, as 3C 345 illustrates (Browne *et al.* 1982*a*). Sometimes, as in 1823+568, the large-scale "jet" seen in the VLA map is highly contorted, but even in these cases the milliarcsecond VLBI jet appears to be connected to the large-scale jet. Note that in all the "asymmetric" sources where there is a large-scale jet, the milliarcsecond jet is either on the same side as the large-scale jet or it connects up with the large-scale jet.

The "prototype" source of this class is 3C 345, the well-known superluminal, which is also in the sample. Another superluminal source in the asymmetric class is 1928+738 (Eckart *et al.* 1985). It is likely that many more of the asymmetric and compact sources—possibly all of them—will be found to be superluminal when they are studied sufficiently carefully. The similarities between the asymmetric source 1928+738 and the two superluminal sources in the "compact" class emphasize that the distinction between the two classes is probably artificial. In all three cases there is a compact core, and one or more weaker components moving superluminally away from the core. The direction of superluminal expansion is in all cases closely aligned with a kiloparsec-scale jet. What is perhaps most remarkable is that all three sources have a very similar large-scale structure. The VLA images show (1) a bright, dominant, unresolved core—this is the feature that we are resolving in the VLBI images; (2) a curved continuous jet on one side—in all cases, this is contiguous with the VLBI jet; and (3) a diffuse lobe on the *opposite* side of the core. The overall angular sizes are similar to those of the "classical double" radio galaxies and quasars, which have a similar structure but with a much weaker core. The similarity of the structures suggests that they are related.

c) *Compact Double Sources*

Unlike previous authors, we have distinguished two different classes of compact double sources: one with steep high-frequency spectra, called *compact S doubles* or class 2*a*, and one with flat high-frequency spectra, called *compact F doubles* or class 2*b*. The clearest result of the correlations discussed in § VI is that the compact double sources, and particularly the steep-spectrum ones, stand apart from the other objects in our sample in almost every respect: (1) they do not look like parts of one- or two-sided jets, whereas all of the other categories do fit this simple model; (2) they have an order of magnitude less polarization; (3) they exhibit a very low level of variability; and (4) they have no detectable structure on the scale of a second of arc. In the compact S doubles, we see no evidence of a compact core, and we conclude that in these objects we are not seeing emission from a core and jet. In the case of the compact F doubles this is not so clear. For example, 0711+439 has a compact flat-spectrum component at one end, and this could therefore be a one-sided jet. We believe that the distinction between these two types of compact double is real.

Compact double sources were first identified as a distinct class by Phillips and Mutel (1982). Phillips and Mutel, with their colleagues, have made an intensive study of four members of the class (Phillips and Mutel 1980, 1981, 1982; Mutel, Phillips, and Skuppin 1981; Phillips and Shaffer 1983; Hodges, Mutel, and Phillips 1984; Mutel, Hodges, and Phillips 1985; Biretta, Schneider, and Gunn 1985; Mutel and Hodges 1986; Hodges and Mutel 1987). In these four sources the radio emission comes from two, roughly equal, well-separated components, 50–150 mas apart; both components have similar spectra, and there is no obvious compact flat-spectrum core. A distinctive feature is that all these sources have "humped" spectra, with a peak at about 1 GHz, a steep falloff to higher frequencies ($\alpha \gtrsim 1$), and little emission at low frequencies. They therefore fall into the class that we call "compact S doubles." At higher resolution some of the components show internal structure; for example, in 2050+364 the two components show "tails" pointing back toward the center. This has led Phillips and Mutel to suggest that these may be "infant" classical double radio sources, in which we are seeing the two heads of two counterprojecting beams, that have not yet escaped from the parent galaxy. In that case, we might expect to see a central component in the middle, marking the central engine; no such components have yet been seen, but that may just be because they are too faint.

In the compact S doubles, the correlation between humped spectrum, low variability, and low polarization that we discussed in § VI was first noticed by Rudnick and Jones (1982). While all our compact S doubles have humped spectra, the converse is not true; sources with such spectra can show a variety of structures. Our observations suggest that both morphology and spectrum must be taken into account in defining this class.

The class of compact F doubles is rather less well defined.

The sources in this class share some, but not all, of the distinguishing features of the compact S doubles. It is not clear whether the class is homogeneous or is an accidental mixture of sources of a variety of types.

d) Irregular Flat-Spectrum Sources

These are flat-spectrum sources with complex resolved structures that can be classified neither as "asymmetric" nor as "double." Only two sources fall into this class, 0315+413 (3C 84) and 0831+557. Both are peculiar (see the notes in the Appendix), but perhaps the only thing they have in common is that they cannot be placed in any of the other classes. At higher frequencies 3C 84 shows many of the characteristics of the asymmetric II class (Readhead *et al.* 1983).

e) Steep-Spectrum Compact Sources

Seven sources are classified as *steep-spectrum compact sources*. These sources are characterized by a steep, straight spectrum, usually with a low-frequency turnover near 100 MHz, and sometimes flattening at high frequencies. The spectrum indicates that if such a source has a core, it is much less prominent than in the flat-spectrum sources. This class of sources has been studied by several investigators (e.g., van Breugel, Miley, and Heckman 1984; Fanti *et al.* 1985). These sources are quite common; for example, Peacock and Wall (1982) studied a sample of 168 sources selected at 2.7 GHz. Contrary to their expectations, they found that a large proportion (44%) of the compact sources (smaller than 2″) in their sample had steep high-frequency spectra. (Selection by spectrum alone would also find the compact S doubles; in the current sample, 10 out of 65 [15%] fall into one of the two classes with steep high-frequency spectra.)

The steep-spectrum compact sources show structure on all angular scales from 1 mas to 1″. The VLBI structure is complex, showing a compact, flat-spectrum core, and in some cases a central "jet" which may be misaligned by as much as 90° from the large-scale structure. These sources are unlikely to be normal extended double sources seen "end-on," because in many cases no flat-spectrum core is observed and the overall sizes are smaller than the lobe widths of normal double sources (though 3C 380 may be an exception). There is some evidence from inverse-Compton arguments that relativistic bulk motion is occurring in two of these sources (3C 147 and 3C 309.1; Simon 1982; Wilkinson *et al.* 1986) and superluminal motion has been detected in 3C 216 (Pearson, Readhead, and Barthel 1987).

f) Lobe-dominated Sources

We have classified 19 of the sources in the complete sample as "lobe-dominated." Three of these are low-luminosity sources of Fanaroff-Riley class I, and 16 are high-luminosity "classical" sources of class II. Almost all such sources have a compact core associated with the parent galaxy or quasar. Most of the cores are very weak, however, <100 mJy at 5 GHz, and we detected VLBI fringes from only the three strongest. The results are thus biased toward sources with unusually strong central components. Two of the three sources, 3C 179 and 3C 236, were excluded from our observations because they have been extensively studied by others (see § IV); the third is 3C 390.3, which has also been mapped by Preuss *et al.* (1980) and Linfield (1981). All three sources show good alignment between the nuclear structure and the outer lobes. One (3C 179) is definitely superluminal (Porcas 1981), and another (3C 390.3) may be (see the notes in the Appendix). It is of interest that 3C 390.3 shows possible evidence for two-sided ejection: Linfield's 10.7 GHz map shows a "core-jet" structure directed toward the bright, compact southeast lobe, while both our 5 GHz map and that of Preuss *et al.* show another component 5 mas away on the northwest side of the "core."

g) General Remarks

It now seems clear that relativistic bulk motion is a common feature in nuclear components of powerful objects. This must therefore affect the appearance of these objects at some level. Nevertheless, as we have seen, most of the objects in our sample and nearly all the objects that we have mapped have compact, presumably flat-spectrum, cores. In the context of the beaming theories, this suggests either that the cores have broad emission cones or that we have selected objects in which the axis of a narrow emission cone is close to the line of sight. The role of relativistic beaming in these objects is thus far from clear, but this knowledge is essential to understanding the basic physics and statistics of these objects. The determination of the distribution of apparent velocities in this sample, and in other samples selected to minimize the possible effects of beaming on the sample constitution, should help to determine the role of beaming, and lead eventually to a thorough understanding of the physics of these remarkable objects.

The rare exceptions to this unifying picture are the compact S double objects which seem to require an altogether different explanation. These are high-luminosity objects with little if any energy in extended radio components. They must therefore be relatively short-lived, or the energies of the synchrotron-emitting electrons must be dissipated by means other than pure synchrotron radiation (e.g., adiabatic expansion).

VIII. CONCLUSIONS

In this paper we have presented VLBI observations of the compact radio structure in a sample of 65 powerful extragalactic radio sources. This is the largest sample for which such a systematic study has yet been undertaken. We have classified the sources as very compact, compact, asymmetric, compact double, irregular flat-spectrum, compact steep-spectrum, and lobe-dominated. One new result is that we have identified two different types of "compact double" source. Other major results include the following:

1. One-sided jets are common features in active galactic nuclei. They are found in every class of object except the compact double objects. The jets typically have steep spectra and are optically thin.

2. Compact optically thick cores are found in all objects except the compact S doubles and a few steep-spectrum compact objects; i.e., "naked jets" are rare.

3. No two-sided jet has yet been found in an active galactic nucleus (although 3C 390.3 may be an exception to this rule).

4. The nuclear jets lie on the same side of the core as the large-scale jets, or, in cases where there are large changes in position angle between the small-scale and the large-scale jet, the two jets connect, sometimes after bending through an angle greater than 90°. No counterexample has been found in which a large-scale jet joins the nucleus on the side opposite a nuclear jet.

5. The nuclear jets are fairly highly polarized, with polarizations typically in the range 1%–5%. The nuclear cores have low polarization, typically below 0.5%.

6. Superluminal motion is common in active galactic nuclei and is found in all classes of object except the compact S double objects.

7. The compact S double sources seem to be a completely different kind of object. The evidence suggests that the radio structures that we see are not parts of cores or jets, and they have low polarization and variability.

8. A wide variety of morphologies is seen among the compact, asymmetric, steep-spectrum compact, and lobe-dominated objects. It is therefore remarkable that nearly all of these structures can be resolved into the three basic constituents—nuclear core, contiguous nuclear and large-scale jets, and outer lobes. The complexities and contortions that are seen can all be explained in terms of projection effects, relativistic beaming effects, and interactions with the surrounding medium. It seems therefore that these are all examples of the same underlying mechanism in which power is generated and collimated into two oppositely directed channels on a scale smaller than a parsec and then propagated by means of a remarkably stable and well-defined channel over distances ranging from a few parsecs to megaparsecs.

This work at the Owens Valley Radio Observatory was supported by National Science Foundation grants AST 82-10259 and AST 85-09822. We are grateful to the US VLBI network and the Max-Planck-Institut für Radioastronomie for generous allocations of observing time, and we wish especially to thank the personnel of the observatories and the Caltech VLBI Processor for their careful attention that made the observations successful. We are also grateful to many colleagues (unfortunately too numerous to name) for providing data in advance of publication and for their stimulating comments on the paper.

APPENDIX

NOTES ON INDIVIDUAL SOURCES

Where necessary, we have assumed $H_0 = 100h$ km s^{-1} Mpc^{-1} and $q_0 = 0.5$ to convert angles to projected distances.

0016+731.—VLA observations at 5 GHz (Perley 1982) show no structure on angular scales between 0".2 and 6" at a level of 0.2 mJy; the fractional polarization is 1.5%. VLBI observations at 5 GHz (Eckart *et al.* 1986, 1987) show that 70% of the flux density originates a component <3 mas in extent. VLBI observations at 22 GHz (Lawrence *et al.* 1985) yield a mean visibility of 0.5 between OVRO and Effelsberg.

From our observations there is no evidence of extended structure above a level of 0.1 Jy. The correlated amplitudes and closure phases indicate a slightly resolved and asymmetric structure. We obtained a good fit to the observations with a simple two-component model (Table 4), with a core component slightly extended in P.A. 100° and a weak secondary component 1.7 mas from the core in P.A. 156°.

0040+517 (3C 20).—3C 20 is a double radio source with no compact core (an upper limit of about 12 mJy can be placed on the 5 GHz flux density of the core: Laing 1981). Not surprisingly, it was not detected in the finding survey, and we have not attempted to map it.

0108+388.—There is no evidence of any large-scale structure in this object from VLA and Westerbork observations at 5 GHz (Perley 1982; Kapahi 1981). Perley's observations place an upper limit of 0.2 mJy in any component within 6" of the core. Low levels of polarization (0.2%) have been detected at both 1.4 and 5 GHz. The object is not strongly variable (Seielstad, Pearson, and Readhead 1983).

From our observations at 5 GHz, there is no evidence for any structure on angular scales greater than 10 mas, and the flux density of any possible larger feature must be less than 0.1 Jy. A two-component model gave a very good fit to the observations (Table 4). The components are separated in P.A. 60° and both are extended along P.A. 65°–85°. Second-epoch observations (Readhead, Pearson, and Unwin 1984) show no evidence for variations in structure.

0133+476.—There is no evidence of any large-scale structure in this object (Kapahi 1981; Perley 1982). Perley's observations place an upper limit of 0.2 mJy on any structure in the range 0".2–6", and they show that the level of polarization is 1.5% at both 1.4 and 5 GHz. Altschuler (1980) observed a significant rotation in the polarization position angle at 8 GHz during a radio outburst. The source is strongly variable on a time scale of months (Andrew *et al.* 1978; Seielstad, Pearson, and Readhead 1983). VLBI observations at 5 and 15 GHz (Weiler and Johnston 1980) yielded a visibility of 0.7 between Green Bank and Effelsberg, indicating a size of 0.7 mas. There is also some evidence in their observations for an elongation in P.A. 140°. Marscher and Shaffer (1980) made VLBI observations at 1.7 and 10 GHz; at 1.7 GHz, an elliptical Gaussian model with FWHM 5 mas × 2 mas elongated in P.A. 170° fits well and accounts for all of the flux density of the source; at 10 GHz, an elliptical Gaussian with FWHM 0.8 mas × 0.5 mas elongated in P.A. 123° fits well.

In our observations the closure phases indicate that the object is resolved and asymmetric. A two-component model fits the data well, and shows that there is a resolved component northwest of the unresolved core. A slightly better fit is obtained with the three-component model given in Table 4, which indicates larger structure extending about 10 mas to the west.

0153+744.—No large-scale structure has been detected in this object. VLA observations indicate no structure above a level of 0.2 mJy between 0".2 and 6", and they show that the polarization level is low (0.2%) at both 1.4 and 5 GHz (Perley 1982). Eckart *et al.* (1986, 1987) have made VLBI observations at 1.7 and 5 GHz. At both frequencies they find a double source embedded in a halo. The northern component has an inverted spectrum and is therefore identified with the core. The southern component and halo both have steep spectra. Witzel (1987) has placed an upper limit of 0.03 mas yr^{-1} ($v/c < 1.3h^{-1}$) on proper motion between the two components.

Our map is in reasonable agreement with the 5 GHz map by Eckart *et al.*; we find two bright components embedded in a halo. However, it is clear that this is a complex object, and we did not obtain a good fit to the data with simple three- and four-component

models. Our best-fitting model (Table 4) does not give a satisfactory fit to the data, but it does reproduce correctly the gross features of the source. About 25% of the flux density originates in a resolved component larger than 5 mas.

0210+860 (3C 61.1).—The central component of this Fanaroff-Riley class II source is weaker than ~12 mJy (Laing 1981). We have not attempted to observe it.

0212+735.—There is no evidence for extended structure in this object: Antonucci *et al.* (1986), using the VLA at 1.49 GHz with a 1".2 beam, found no extended emission at a dynamic range of 2700:1. Perley (1982) measured a level of polarization of 2.4% at 5 GHz. The associated optical object is a 19 mag quasar with $z = 2.367$ (Argue and Sullivan 1980; Lawrence *et al.* 1986), not a BL Lac object as earlier reported (Biermann *et al.* 1981). Eckart *et al.* (1986, 1987) have made VLBI observations at 1.7, 5, and 22 GHz, and found a core-jet structure, with the jet extending 12.5 mas away from the core in P.A. 91° on the 1.7 GHz map. Further VLBI observations (Witzel 1987) have shown that this is a superluminal source.

We obtained a fair fit to our data with a four-component model (Table 4). Our map shows the core-jet structure clearly. Since this object has a number of well-separated bright features, it is an excellent candidate for monitoring superluminal motion.

0220+427 (3C 66B).—3C 66B is a low-luminosity (Fanaroff-Riley class I) radio galaxy. The central core has a flux density of about 0.21 Jy at 5 GHz (Northover 1973); it was not detected in the finding survey, and we did not attempt to map it. (The nearby BL Lac object 3C 66A does contain a milliarcsecond core, but it is too weak for inclusion in the complete sample.)

0314+416 (3C 83.1B, NGC 1265).—NGC 1265 is a famous "twin tail" source of Fanaroff-Riley class I. A recent VLA study is that of O'Dea and Owen (1986), which indicates that the nuclear component has a flux density of ~25 mJy at 5 GHz. This component has been detected in a VLBI observation at 5 GHz (37 ± 6 mJy on the Westerbork-Effelsberg baseline: van Breugel *et al.* 1981), but it is too weak for detection in our finding survey, and it was not included in the mapping observations.

0316+413 (3C 84, NGC 1275).—This complex object has been intensively studied in all accessible spectral bands. A detailed discussion of the compact radio component has been given by Readhead *et al.* (1983), who showed on the basis of VLBI observations at 22 GHz that it has a core-jet structure extended in the north-south direction, and that the core is situated at the extreme northern end of the jet. At the resolution of the present observations, the structure is dominated by the jet and surrounding halo.

0404+768.—This is a steep-spectrum compact radio source, smaller than ~2" (Peacock and Wall 1982). We made a short observation in 1980 September, and detected fringes on the most sensitive baseline only. We have not yet attempted to map the source.

0454+844.—There is no evidence for extended structure in this object. Antonucci *et al.* (1986), using the VLA at 1.49 GHz with a 1".2 beam, found no extended emission at a dynamic range of 1500:1. Perley (1982) found no structure in the range 0".2–6" above 0.3 mJy at 5 GHz, and he found that the object had a polarization level of 3% at both 1.4 and 5 GHz. The object is highly variable on a time scale of months (Seielstad, Pearson, and Readhead 1983). The nearby radio and X-ray source 0450+844 (Biermann *et al.* 1982) is probably unrelated (Johnston *et al.* 1984). The associated optical object is a 16.5 mag BL Lac object with unknown redshift (Argue and Sullivan 1980; Biermann *et al.* 1981). VLBI observations by Eckart *et al.* (1986, 1987) at 1.7, 5, and 22 GHz show that the object has a double structure with a separation at 5 GHz of 0.52 mas in P.A. 146° (epoch 1979.93).

Our observations are well fitted by a simple double model consisting of a compact component and an extended component (Table 4). Comparing our results with those of Eckart *et al.*, we find that the separation has increased by 0.3 mas in 1.7 yr, implying superluminal motion if the redshift is greater than 1.3.

0538+498 (3C 147).—3C 147 is an archetypal example of a steep-spectrum compact source, and it has been well studied by many workers. In view of this, we did not make 5 GHz observations of this object as part of our survey. Nevertheless, it is part of our complete sample, and we therefore discuss it here for completeness.

The large-scale structure of 3C 147 has been mapped using the VLA at 4.9 and 15.0 GHz by Readhead, Napier, and Bignell (1980), at 15.0 GHz by van Breugel, Miley, and Heckman (1984), and at 5 GHz by Pearson, Perley, and Readhead (1985). There is also a 5 GHz MERLIN map by Wilkinson *et al.* (1984*c*). In addition there are observations at 81.5 MHz, both by interplanetary scintillations (Readhead and Hewish 1974) and by long-baseline interferometer (Hartas *et al.* 1983). These observations all reveal emission over about 0".5 (2 kpc), with greatest extension in P.A. 20°. There is no evidence of any larger scale structure, so the radio source is presumably much smaller than any host galaxy (in projection, at least). The spectrum has a peak at 120 MHz, and a low-frequency cutoff which is generally attributed to synchrotron self-absorption (Scott and Readhead 1977).

There have been many VLBI observations of 3C 147, including the first hybrid maps to be made by VLBI (Wilkinson *et al.* 1977). It has been mapped at 327 MHz (Simon *et al.* 1983), 609 MHz (Wilkinson *et al.* 1977), 1661 and 1671 MHz (Readhead and Wilkinson 1980; Simon, Readhead, and Wilkinson 1984), and 5 GHz (Preuss *et al.* 1984). Above 5 GHz it is heavily resolved, and therefore difficult to observe. The VLBI observations at frequencies up to 1671 MHz reveal a one-sided core-jet structure, with the jet extending 0".2 (~1 kpc) to the southwest of the core. At the extreme southwestern end the jet bends through 90° northward over a distance comparable to the width of the jet and then rapidly fades. Such rapid fading in the vicinity of a bend is also seen in 3C 309.1. The width of the jet is ~20 mas (75 pc), and is well resolved. There are a number of distinct regions of higher brightness along the jet. The core is heavily resolved in all directions. It is about 5 mas across and roughly circular. The structure of the core changes at both low frequencies (Simon *et al.* 1983) and high frequencies (Preuss *et al.* 1984), but it is complex, and no simple pattern has emerged. The low-frequency variability may be attributable to refractive effects in the interstellar medium (Rickett, Coles, and Bourgois 1984; Blandford and Narayan 1985), or it could represent intrinsic variations enhanced by Dopper boosting (Simon *et al.* 1983).

The VLA and MERLIN maps show that the "large-scale," 0".5, structure is on the side of the core opposite the jet. There are also faint extensions toward the east. The overall morphology of 3C 147 is mysterious. With its well-collimated jet, diffuse core, and apparent lack of outer lobes, it does not fit into the pattern of either the extended double sources or the compact objects.

0605+480 (3C 153).—Any nuclear component in this Fanaroff-Riley class II source is weaker than 5 mJy (Laing 1981). We did not detect it in the finding survey, and have not attempted to map it.

0710+439.—We obtained a relatively poor fit to the data on this source with a simple three-component model (Table 4), but this model does give the flux densities and relative positions of the three major components. Less than 0.1 Jy is unaccounted for in the model; this is consistent with the observations of Kapahi (1981) and Perley (1982), who found less than 0.2 Jy in extended emission on scales 0".2–6".

The map shows that there are three well-separated components, lying very close to a straight line. The component in the middle is extended along the axis; the other components are resolved, but not along any particular line. All three components have similar spectra: there is no obvious flat-spectrum core embedded in any of them (Readhead, Pearson, and Unwin 1984). The source is identified with a faint (20 mag) narrow-emission-line galaxy with redshift $z = 0.517$ (Lawrence *et al.* 1986), implying that the maximum size of the source is 25 mas or $100h^{-1}$ pc. The source has a spectrum peaking at about 2 GHz, and has low polarization (0.1% at 5 GHz; Perley 1982) and low variability (Seielstad, Pearson, and Readhead 1983); these properties, along with the similarity of the component spectra, suggest that it should be placed in the class of "compact double steep spectrum" sources, in spite of the fact that it has three components rather than two. The linearity of the source suggests strongly that the components are in some way associated, but it is not obvious that any of them is a "central engine." The point in the source with the flattest spectrum is at the southern end of the central component. It is possible that this point marks the central engine, and that the source is an infant double radio galaxy (Hodges and Mutel 1987), but that is not the only possible interpretation. It is also notable that the southernmost component is rather weak and might have been missed in observations of low dynamic range, in which case we might have been inclined to look for a "central component" midway between the other two. The linear structure makes it plausible to postulate that there is a "jet" in this galaxy, but the three peaks we happen to see may just be accidents—where shock fronts happen to occur, for example. We have studied this source sufficiently well to be able to look for internal motions (Readhead, Pearson, and Unwin 1984). There is no evidence for any changes in component separation in the 2.5 years between our two 5 GHz images. Formally, there is an insignificant subluminal expansion.

0711+356.—VLA observations of this object by Perley (1982) show no evidence for any structure above a level of 0.3 mJy between 0".2 and 6". The radio spectrum has a broad maximum, with a peak at about 2 GHz (Kühr *et al.* 1981*b*). It was not significantly variable in the observations of Seielstad, Pearson, and Readhead (1983) on time scales of months to years, but it does vary significantly on a 10 yr timescale. Perley observed a level of polarization of 0.6% at 5 GHz.

We found that a two-component model gives a poor fit to our data, but a fair fit can be obtained with three components, and a good fit with four components (Table 4). There is a strong, very compact component and a one-sided extension to the northwest. Our model fitting shows that the data do require an additional component to the west of northern extension, as seen in the map. We have also made 10 GHz observations of this object (unpublished), which show that the compact southern component has a flat spectrum and should therefore be associated with the core. We have reported second-epoch observations which show that the two major components are not separating, and formally there is an insignificant superluminal contraction (Readhead, Pearson, and Unwin 1984).

0723+679 (3C 179).—3C 179 is a Fanaroff-Riley class II source with a strong central core. An excellent series of VLBI observations revealing superluminal expansion within the core has been conducted by Porcas (1987, and references therein), and we therefore did not include 3C 179 in our observations.

0804+499.—No evidence of extended structure in this object has been found in Westerbork observations (Kapahi 1981) or in VLA observations (Perley 1982), which place an upper limit of 0.2 mJy on structure in the range 0".2–6". The radio source is highly variable on a time scale of a few months (Seielstad, Pearson, and Readhead 1983), and it has a polarization level of 1%–2% at 5 GHz (Perley 1982; Rudnick and Jones 1983).

VLBI observations at 22 GHz (Lawrence *et al.* 1985) give a visibility of 0.82 on the OVRO–Effelsberg baseline, indicating very compact structure at this frequency. The structure is likewise very compact in our observations, which show a very compact unresolved component with a weak extension to the southeast. The closure phases indicate clearly that the object is extended and asymmetric. A two-component model did not give a good fit, but the three-component model listed in Table 4 gave an excellent fit to both the closure phases and amplitudes.

0809+483 (3C 196).—This is a double radio source with an unusual contorted structure which may be due to interaction of a precessing jet with the circumgalactic medium (Lonsdale and Morison 1980, 1983). The flux density of the nuclear component is only $\sim$6 mJy (Cawthorne *et al.* 1986, quoting a private communication from R. Laing), so it is not surprising that we did not detect it in our pilot observations. Brown, Broderick, and Mitchell (1986) have made VLBI observations of the compact hot spot in the northern lobe.

0814+425.—VLA observations by Perley (1982) reveal a secondary component, of 1.2 mJy, 7".8 from the core in P.A. $-40°$. This component is double with a separation of 2".8 in P.A. 45°. Perley also measured the level of polarization at 5 GHz to be 0.5%. The total flux density varies by about 50% on a time scale of a few months (Seielstad, Pearson, and Readhead 1983).

We have only a small amount of closure phase data, but they indicate that the object is slightly extended and asymmetric. We obtained a good fit to the data with a two-component model extended in P.A. $-31°$ (Table 4), i.e., toward the secondary component. Observations with higher dynamic range and higher resolution thus may reveal this to be a core-jet source.

0831+557.—The arcsecond-scale emission of this object has been studied with MERLIN (Whyborn *et al.* 1985). It has a linear triple structure dominated by a core with a steep high-frequency spectrum. The core is straddled by components 5" to the north and 6" to the south. The overal size is 11", corresponding to a projected size of 27 kpc at a redshift of 0.242. Thus the projected distances of the outer components from the core are about 13 kpc, within the host galaxy, but modest deprojection would place them outside the galaxy. The object has also been studied with low-resolution VLBI (Whyborn *et al.* 1985). In these observations the central component is resolved into two subcomponents separated by 0".16 and aligned with the large-scale structure, and there is evidence of a bridge or jet between the two subcomponents. Our high-resolution VLBI observations resolve the southern subcomponent, revealing it to be amorphous with a roughly circular outline. This is one of the more curious morphologies found in the survey.

0836+720.—VLA observations at 5 GHz by Perley (1982) and C. O'Dea (1986, private communication) show that this object has a single secondary component 1".3 from the core in P.A. 200°, and that it is highly polarized (7.6%). VLBI observations by Eckart *et al.* (1986, 1987) show that this is a core-jet object, and, on the basis of observations at two epochs, it appears to be a superluminal source.

We obtained a reasonable fit to our data with the four-component model given in Table 4. This model and the map show a core-jet structure, with the core at the northeastern end of the jet. The jet is roughly aligned with the secondary component seen in the VLA maps.

0850+581.—Figure 1 shows the first-epoch map of 0850+581. We have already published this map and maps from two further epochs (Barthel *et al.* 1986), presenting evidence that this source is the bright core of an extended triple radio source, and shows superluminal motion with an apparent speed $v/c = (4.5 \pm 1.6)h^{-1}c$ along the axis defined by a kiloparsec-scale jet. We obtained a good fit to the first-epoch data with the model given in Table 4.

0859+470.—Perley (1982) has detected a faint secondary component in this object at 5 GHz, 1".5 from the core in P.A. −25°, with a flux density of 5.2 mJy. This component is also seen in MERLIN maps at 408 MHz (D. Shone 1986, private communication) along with a weaker component about 1" from the core in P.A. 155°. The flux density varies by about 50% on a time scale of months (Seielstad, Pearson, and Readhead 1983), and the polarization is 2% at 5 GHz (Perley 1982). VLBI observations at 22 GHz by Lawrence *et al.* (1985) yielded a mean visibility of 0.46 on the OVRO–Effelsberg baseline. Our observations show that the source is clearly resolved in P.A. 0°, and we obtained an excellent fit to the data with a single elliptical Gaussian component with FWHM ~2 mas (Table 4).

0906+430 (3C 216).—The large-scale structure of 3C 216 has been mapped at the VLA by Schilizzi, Kapahi, and Neff (1982) and by Pearson, Perley, and Readhead (1985). These maps show a bright core straddled by two weaker, resolved components. The core has a flat spectrum and dominates the emission at high frequencies. IPS observations at 81.5 MHz (Readhead and Hewish 1974) show that 50% of the emission originates in components 0".5 in size, and interferometric observations at 81.5 MHz (Hartas *et al.* 1983) show that about 30% of the emission comes from a region as large as 1'—a projected size of 236 kpc. If this large-scale emission comes from the outer lobes of a classical triple source viewed end-on, then the deprojected size is enormous and the source has some morphological similarities to the giant radio galaxy 3C 236. No other steep-spectrum compact source has been found to have emission on such a large scale, but few such objects have been studied with sufficient sensitivity to detect very faint extended features. This object clearly warrants very high dynamic range VLA observations.

We have made 5 GHz VLBI observations of 3C 216 at three epochs. The first-epoch map (Fig. 1) shows a compact core with a faint extension to the southeast, in a direction almost perpendicular to the large-scale structure. The later maps show superluminal motion at $2.4h^{-1}c$ along this direction, indicative of bulk relativistic motion in the source (Pearson, Readhead, and Barthel 1987). MERLIN and EVN maps (Porcas 1986 and private communication) suggest that the extension seen in the 5 GHz maps is a jet that connects the central core to the western lobe (not the stronger eastern lobe).

The source 3C 216 has several striking similarities to the steep-spectrum compact source 3C 309.1 (1458+718; see the discussion below). The large-scale morphologies are almost identical (Pearson, Perley, and Readhead 1985), the small-scale structure is misaligned with the large-scale structure and shows a compact core and one-sided jet, and there is likely bulk relativistic motion along the jets of both objects. Since very large scale structure has been seen in 3C 216, it is clearly important to make high dynamic range VLA maps to search for such structure in 3C 309.1.

0917+458 (3C 219).—This is a Fanaroff-Riley class II source. The central component has a flux density of 51 mJy at 4.9 GHz (Bridle, Perley, and Henriksen 1986), and it was therefore not detected in our VLBI pilot survey. It has, however, been detected at 10.7 GHz using the more sensitive Mark III VLBI system, and has FWHM $\approx$ 0.5 mas (D. H. Hough, J. O. Burns, and W. A. Christiansen 1987, private communication).

0923+392 (4C 39.25).—MERLIN observations of this object by Browne *et al.* (1982*b*) reveal a complex structure extending over 5" in P.A. −115° relative to the core. Perley (1982) identified three components, and measured a polarization level of 1% at 5 GHz. The object is not highly variable, but it does show 25% variability over a 10 yr time scale (Seielstad, Pearson, and Readhead 1983).

We obtained a good fit to the data with the two-component model given in Table 4. This model is consistent with the extensive series of observations by Shaffer and Marscher (1987), who find that these two components are stationary and that, subsequent to our observations, a new component has emerged from the western component and is moving toward the eastern component at a superluminal speed.

0945+408.—The large-scale structure of this object has been mapped using the VLA by Perley, Fomalont, and Johnston (1980). It consists of a resolved core embedded in a halo 13" (56 kpc) in extent. The core has been mapped using MERLIN by Foley (1982) and is resolved into a very compact core with a one-sided jet extending over 4" (18 kpc). The compact structure revealed by our VLBI observations shows a strong core and a one-sided resolved feature, which may be part of a jet. This feature is roughly perpendicular to the 4" jet; in this respect the object is similar to 3C 216 and 3C 309.1.

The source has a high degree of polarization (6% at 5 GHz) (Perley 1982), and varies on a time scale of a few months (Seielstad, Pearson, and Readhead 1983).

0951+699 (M82, 3C 231).—This irregular galaxy contains a number of discrete, compact radio sources (Unger *et al.* 1984). The strongest of these, 41.9+58, has been detected in several VLBI observations (e.g., Wilkinson and de Bruyn 1984). This source has been found to have a shell structure and is probably a supernova remnant rather than an active nucleus (Bartel *et al.* 1987; Wilkinson and de Bruyn 1987). We therefore do not consider it further here.

0954+556.—Although this source was detected in the finding survey, it has not yet been mapped. We are currently analyzing observations made with the EVN.

0954+658.—Although this source was detected in the finding survey, it has not yet been mapped. We are currently analyzing observations made with the EVN.

1003+351 (3C 236).—3C 236 is a giant Fanaroff-Riley class II source with a strong, steep-spectrum central component. We did not include it in our observations, since it has been studied extensively by other workers (Barthel *et al.* 1985, and references therein).

1031+567.—Although this source was detected in the finding survey, it has not yet been mapped. We are currently analyzing observations made with the EVN.

1157+752 (3C 268.1).—This is a Fanaroff-Riley class II source with a weak central component (1.7 mJy at 5 GHz; R. A. Laing 1986, private communication; see also Cawthorne *et al.* 1986). We have not attempted to observe it.

1254+476 (3C 280).—This is a Fanaroff-Riley class II source with a weak central component (<10 mJy; Laing 1981). It was not detected in the finding survey.

1358+624.—Although this source was detected in the finding survey, it has not yet been mapped. We are currently analyzing observations made with the EVN.

1409+524 (3C 295).—This is a Fanaroff-Riley class II source with a weak central component (<60 mJy; Laing 1981). It was not detected in the finding survey.

1458+718 (3C 309.1).—The large-scale structure of 3C 309.1 has been mapped with the VLA (van Breugel, Miley, and Heckman 1984; Pearson, Perley, and Readhead 1985) and with MERLIN (Kus, Wilkinson, and Booth 1981; Wilkinson *et al.* 1984*b*). It consists of a very bright core straddled by two weaker components. The separation between the outer components is 2″ (8.7 kpc). Thus even the deprojected size is presumably much smaller than that of the parent galaxy.

VLBI observations (Wilkinson *et al.* 1984*b*, 1986) reveal a compact core with a fairly flat spectrum, and a jet which extends southward from the core for a distance of 60 mas (260 pc) and then bends eastward through 90° in a distance comparable to the width of the jet, which is about 7 mas (30 pc). The jet fades rapidly at the bend, and, as in the case of 3C 147, there is a bright component at the position where the jet begins to bend. No evidence of a jet is seen on the other side of the core. Wilkinson *et al.* (1986) show that the low X-ray flux of 3C 309.1 provides evidence for bulk relativistic motion of the radiating material in the brightest knot along the jet; the proper motion of this knot has not yet been measured.

1609+660 (3C 330).—This is a Fanaroff-Riley class II source with a weak central component (<75 mJy; Laing 1981). It was not detected in the finding survey.

1624+416.—Kapahi (1981) found no evidence for extended structure in this object on scales larger than 2″. Perley (1982) has detected a weak (7 mJy) component 0.″7 from the core in P.A. 352°. The object varies on a time scale of months (Seielstad, Pearson, and Readhead 1983) and has a polarization level of 0.2% at 5 GHz (Perley 1982).

We obtained a fair fit to our VLBI data with the two-component model given in Table 4. This model and the map show a structure extending from the core and curving away from the direction defined by the 0.″7 secondary component. Owing to instrumental failures (which are not infrequent in VLBI), our data were much more sparse than for most of the objects which we mapped. Nevertheless, the curving core-jet structure is quite clear.

1633+382.—Kapahi (1981) observed this object on the Westerbork synthesis radio telescope (WSRT) and found it to be unresolved. Perley's VLA observations (1982) show it to be essentially unresolved, with a possible short extension 0.″2 to the southeast. It is highly variable on time scales of a few months (Seielstad, Pearson, and Readhead 1983) and has a polarization level of about 1.5% at 5 GHz (1982).

There have been a number of VLBI observations of this object. Kellermann *et al.* (1977) fitted their observations with an elliptical Gaussian model with FWHM 0.5 mas × 0.3 mas extended in P.A. 160°. Marscher and Shaffer (1980) fitted their 1.6 GHz observations with a circular Gaussian with FWHM 1.2 mas.

We obtained an excellent fit to our data with the three-component model given in Table 4. This shows a dominant unresolved core with an extension in P.A. $-65°$.

1634+628 (3C 343).—This compact steep-spectrum object has been mapped with VLBI at 1.66 GHz by Fanti *et al.* (1985). It has no extended structure and consists of a single complex component 200 mas in diameter. It was not detected in our finding survey, suggesting that any compact feature at 5 GHz is weaker than ~ 300 mJy, and too weak to map with Mark II VLBI on the US network.

1637+574.—No high-quality map of the large-scale structure of this object has been published. In observations at 2.7 GHz on the Green Bank interferometer Owen, Porcas, and Neff (1978) detected a secondary component 8″ from the core, and Kapahi (1981) observed it at 5 GHz using the WSRT and found it to be elongated by 2″ in P.A. 144°. Perley (1982) detected diffuse structures extending approximately 6″ northwest and west at 5 GHz. The flux density is highly variable on a time scale of months (Seielstad, Pearson, and Readhead 1983), and the fractional polarization is about 2% at 5 GHz (Perley 1982).

Observations at 22 GHz by Lawrence *et al.* (1985) yielded a mean visibility of 0.59 on the OVRO–Effelsberg baseline. Our observations were made with stations in the US only and show no strong evidence of extended structure; the closure phases do not depart significantly from zero. The data are reasonably well fitted by a circular Gaussian brightness distribution. We obtained a slightly but not significantly better fit with an elliptical Gaussian (Table 4).

1641+399 (3C 345).—This archetypal superluminal source has been the subject of an extensive VLBI study by M. H. Cohen and his collaborators (Biretta, Moore, and Cohen 1986 and references therein). For this reason we did not observe it as part of the survey, although we do include it in the classification and analysis. The large-scale structure consists of a faint halo (Schilizzi and de Bruyn 1983) and a 3″ jet (Browne *et al.* 1982*a*).

1642+690.—The first-epoch map presented here and our second-epoch map are discussed in detail by Pearson *et al.* (1986). It is an asymmetric core-jet source showing superluminal expansion. A fair fit which reproduced all the major features in the data was obtained with the three-component model given in Table 4.

1652+398 (Markarian 501).—We obtained a good fit to our data with the three-component core-jet model given in Table 4. Van Breugel and Schilizzi (1986) observed this galaxy on the European VLBI network. Their map, which has lower resolution but greater sensitivity than ours, shows that the jet extends at least 55 mas from the core. In our data, there are variations in the

amplitudes on the US baselines which suggest that there is a more distant component than those in our map, in agreement with van Breugel and Schilizzi's results. It is not clear how the VLBI jet is related to the large-scale radio emission, which is extended 1′ in P.A. 45° (Ulvestad, Johnston, and Weiler 1983). Observations at 10.7 GHz by Seielstad, Pearson, and Readhead (1983) show no evidence of variability.

1739+522.—In 1.7 GHz observations on the VLA Perley (1982) and Shone (1986) found that this core-dominated object has a weak secondary component situated 3″.5 from the core in P.A. 260°. There is no other evidence for extended structure above a level of 0.3 mJy within 6″ of the core. The fractional polarization at 5 GHz is 1% (Perley 1982), and the source is strongly variable (Seielstad, Pearson, and Readhead 1983).

We found that a single component gave a fair fit to our data, but there were systematic deviations in the closure phases of up to 10°, indicating that a more complex, asymmetric model was required. We obtained an excellent fit with the two-component model given in Table 4, which shows that the object is extended in the north-south direction, i.e., roughly orthogonal to the large-scale structure. Observations at 22 GHz by Lawrence *et al.* (1985) give a mean visibility on the OVRO–Effelsberg baseline of 0.65.

1749+701.—VLA observations at 14.9 GHz by O'Dea (1986, private communication) reveal a 5 mJy component 0″.4 from the core in P.A. 209°. Perley (1982) found evidence for a 0″.4 halo in his 5 GHz observations, and he measured a polarization level of 0.4%. The object is highly variable on a time scale of a few months (Seielstad, Pearson, and Readhead 1983).

Bååth (1984) has made VLBI observations at three epochs, and finds a variable core-jet structure extending in P.A. ~ 300°. Observations by Eckart *et al.* (1986, 1987) at 1.7 GHz reveal that the object is just resolved at their resolution of 3.4 mas, in P.A. 296°. There is some evidence that the object may be superluminal (Witzel 1987).

Our observations reveal a clear core-jet structure extended in P.A. 296°. The data are fitted well by the two-component model given in Table 4.

1803+784.—Antonucci *et al.* (1986) have made high dynamic range observations of this core-dominated source using the VLA at 1.49 GHz. Their map shows emission extending ~2″ west and south of the core, and a secondary component of 8.6 mJy ~45″ south of the core in P.A. 194°. Perley (1982) has measured 5% polarization at 5 GHz. The associated optical object is a 16.4 mag BL Lac object with a redshift of 0.68 (C. R. Lawrence 1987, private communication). A number of other nearby radio and X-ray sources (Biermann *et al.* 1982) are probably unrelated (Johnston *et al.* 1984).

VLBI observations by Eckart *et al.* (1986, 1987) show a core-jet structure at 1.66 GHz extending 30 mas in P.A. 260°. Our map has higher dynamic range than the 5 GHz maps of Eckart *et al.*, and also shows a clear core-jet structure. We obtained a fair fit to the data with the two-component model given in Table 4. Witzel (1987) has placed a subluminal upper limit on any internal proper motion in this source between 1979.9 and 1985.8.

1807+698 (3C 371).—This nearby N galaxy or BL Lac object has been intensively studied in the radio, optical and X-ray bands. A high dynamic range VLA map at 1.7 GHz by Ulvestad and Johnston (1984) reveals that the compact radio source is embedded in an elliptical halo 2′ × 1′.5 in extent with the major axis in the east-west direction. Higher resolution VLA observations by Perley, Fomalont, and Johnston (1980) and MERLIN observations by Browne *et al.* (1982*b*) reveal a one-sided jet structure, similar to that seen in 3C 120, extending at least 3″ in P.A. 240°. The object is highly variable on time scales of a few months (Seielstad, Pearson, and Readhead 1983), and Perley's observations (1982) reveal that it is polarized at the level of 2.7% at 5 GHz.

Numerous VLBI observations have been made of the nucleus of 3C 371. Our first-epoch map, shown here in Figure 1, has already been published (Pearson and Readhead 1981). The map reveals an asymmetric core-jet structure extending 14 mas in P.A. −97°. We obtained a good fit to the data with the four-component model given in Table 4. Our second-epoch map (Readhead, Pearson, and Unwin 1984) has been reanalyzed, together with third-epoch data, by Lind (1987). The source has a complex, variable, core-jet structure, but no clear evidence has been found for superluminal motion. There is, however, evidence for bulk relativistic motion from X-ray and radio variability arguments (Worrall *et al.* 1984).

1823+568.—MERLIN observations at 408 MHz of this object by Foley (1982) reveal a triple structure extended in P.A. 95°, consisting of a bright core straddled by two components 1″.1 and 1″.4 away, and connected to the core by bridges of emission. MERLIN 1666 MHz observations (Foley 1982) show a curved jet extending southward from the core and turning to the east 1″ south of the core. VLA observations at 5 GHz by O'Dea, Barvainis, and Challis (1986) show the core and the eastern components, but not the western component, indicating that the latter has a steeper spectrum. The object is highly variable on a time scale of a few months and has a polarization level of 5% at 5 GHz (Perley 1982).

Our map shows a one-sided core-jet structure with the jet extending to the south, i.e., in the direction of the large-scale jet. The two-component model given in Table 4 provides a good fit to the data.

1828+487 (3C 380).—The large-scale structure of 3C 380 has been mapped a number of times. VLA observations at 5 GHz by Pearson, Perley, and Readhead (1985) show a complex structure extending over 9″. This structure is similar to that mapped at 1.7 GHz using MERLIN (Wilkinson *et al.* 1984*a*, *b*; Flatters 1987). Four components can be distinguished in these maps: a compact flat-spectrum core, a short "jet" extending to the northwest, a bright ridge of emission 3″ east of the core, and a diffuse halo in which these features are embedded.

The compact component has been studied in several VLBI observations (Readhead and Wilkinson 1980; Wilkinson *et al.* 1984*a*), and was observed in the course of this survey. These observations show a compact, flat-spectrum core with a steeper elongated component, generally identified as a "jet," extended 15 mas in P.A. −57°, close to the position angle of the VLA and MERLIN maps (−45°).

The projected radius of the halo is $20h^{-1}$ kpc; thus even modest deprojection by a factor of 2 would probably place these regions outside the parent galaxy. The spectrum of 3C 380 is steep between 20 MHz and 5 GHz, but flattens above 5 GHz owing to the flat-spectrum core component, which dominates the spectrum at frequencies above 10 GHz.

It is possible that 3C 380 may be a classical triple source seen end-on. There are 20 steep-spectrum double or triple sources in our sample, so that the probability of having one of these objects aligned within 5° of the line of sight is about 10%, which is not too

unlikely for consideration. The size and power of the halo are typical of the outer lobes of powerful triple sources, and the dominance of the flat-spectrum core could be due to relativistic boosting of a weak core component. An alternative possibility, advocated by Wilkinson *et al.* (1984*a*), is that the morphology of 3C 380 is due to interaction with the interstellar medium. Observations of the broad and narrow optical emission lines may help to discriminate between these two possibilities.

1842+455 (3C 388).—This is a Fanaroff-Riley class II source with a core component of ~60 mJy at 4.9 GHz (Burns and Christiansen 1980). This component was too weak for detection in our VLBI pilot survey, but it has been detected at 10.7 GHz using the Mark III system, and its angular size is ~0.5 mas (D. H. Hough, J. O. Burns, and W. A. Christiansen 1987, private communication).

1845+797 (3C 390.3).—This is one of the few Fanaroff-Riley class II sources in our sample with a central component that is bright enough to map with the Mark II VLBI system. It has been observed previously by Linfield (1981) and by Preuss *et al.* (1980). Our observations reveal a dominant component which is just resolved and is extended in P.A. −50°, and a resolved component 4.9 mas away in P.A. −38°, extended in P.A. −43°. The small differences in these position angles are probably not significant. Our observations are in agreement with those of Preuss *et al.* in showing that there is structure in this object on the northwest side of the core, in contrast to the extension of the core to the southeast found in the higher resolution observations by Linfield at 10.7 GHz. This may therefore be a two-sided nuclear jet. Alef *et al.* (1987) have made several 5 GHz observations, and have suggested that they indicate superluminal motion of the northeastern component. However, the position of the strongest jet component in their best maps (1980.4 and 1985.4) is almost the same as the position of the northeastern component in our map (1982.2). It seems to us that the data are consistent with no net motion of this component. Further observations spaced more closely will help to clarify this.

1928+738.—Recent VLA maps of 1928+738 made with very high dynamic range (Rusk and Rusk 1986; Johnston *et al.* 1987) show that this source, previously thought to be unresolved, is actually an extended double-lobed object. The maps show a curved jet to the south, a counterjet to the north, and a large amorphous lobe of diameter 15″ situated 25″ north of the core. The whole object is embedded in a halo 1′.5 in size.

The first-epoch VLBI map of the core presented here and maps from other epochs are discussed in detail by Eckart *et al.* (1985). The VLBI maps reveal an asymmetric core-jet source showing superluminal motion along a knotty milliarcsecond jet aligned with the southern jet seen in the VLA maps. A five-component model was published by Eckart *et al.*; we have refitted the data and obtain a slightly better fit with the model given in Table 4.

1939+605 (3C 401).—This Fanaroff-Riley class II source was not detected in our VLBI pilot survey. The flux density of the central component is ~20 mJy (Laing 1981).

1954+513.—VLA observations of this object by O'Dea (1986, private communication) show a possible jet extending 10″ north (P.A. 350°) and a component 7″ south of a bright unresolved core. The flux density varies by about 20% on time scales of a few months (Seielstad, Pearson, and Readhead 1983), and the fractional polarization is about 0.3% at 5 GHz (Perley 1982).

In our VLBI observations of the core, the closure phases show systematic deviations of up to 10° from zero, indicating that it is resolved and asymmetric. This object has a fairly complex structure extending to the north of the core, and we were unable to obtain a good fit to the closure phase data, although the two-component model given in Table 4 fits the amplitudes well. More observations are needed.

2021+614.—VLA observations by Perley (1982) reveal no structure on scales greater than 0″.2 above a level of 0.3 mJy. The source varies only by about 20% on a 10 yr time scale (Seielstad, Pearson, and Readhead 1983), and the polarization is very low (0.1% at 5 GHz; Perley 1982).

Our observations show two almost equal components, placing the object in the "compact double flat spectrum" class. The two components are each resolved into two subcomponents at higher resolution (Bartel *et al.* 1984*a*). Two of these are optically thin, one has a flat spectrum, and the other appears to be synchrotron self-absorbed in the frequency range 2.3–8.3 GHz. We obtained a fair fit to the data with the three-component model given in Table 4. By comparison with a second-epoch 5 GHz map, we have placed a subluminal limit on the proper motion between the two bright components, $v = (0.2 \pm 0.2)h^{-1}c$ (Readhead, Pearson, and Unwin 1984).

2153+377 (3C 438).—This Fanaroff-Riley class II source has a weak central component (~10 mJy; Laing 1981), too weak for detection in our finding survey.

2200+420 (BL Lac).—As the archetypal BL Lac object, this source has been studied intensively at all accessible wavelengths, and we do not attempt to review all these observations here. The radio structure is very core-dominated, but a high dynamic range VLA map by Ulvestad and Johnston (1984) reveals a very weak amorphous halo 20″ in extent. This halo is slightly elongated in the north-south direction and has a flux density of 40 mJy. No other components are seen above a level of 0.3 mJy at 1.7 GHz and 5 GHz (Perley 1982). The radio source is highly variable on time scales of a few days. At 5 GHz the fractional polarization varies between 1% and 2.5% (Perley 1982; Rudnick and Jones 1982).

There have been numerous VLBI observations of BL Lac (e.g., Kellermann *et al.* 1977; Weiler and Johnston 1980). Our 5 GHz map shows an asymmetric structure extended in P.A. 180°. We obtained a good fit with the three-component model shown in Table 4. Mutel and Phillips (1987, and references therein) have mapped this object at a number of epochs and found a series of components moving superluminally along this north-south direction.

2229+391 (3C 449).—This Fanaroff-Riley class I source has a weak central component that was not detected in our finding survey. VLA observations at 5 GHz (Perley, Willis, and Scott 1979) give the core strength as 37 mJy. The core was detected in a VLBI observation by van Breugel *et al.* (1981), which showed that it is smaller than 40 mas.

2243+394 (3C 452).—This Fanaroff-Riley class II source has a weak central component (130 mJy; Riley and Pooley 1975), too weak for detection in our finding survey.

2342+821.—This is a compact steep-spectrum source (Peacock and Wall 1982). We made a pilot observation of this source in 1980 September, but did not detect it, owing to a typographical error in the position given by Peacock and Wall; the correct position is given in Table 1.

2351+456.—WSRT observations of this object by Kapahi (1979) revealed no structure larger than 2″. It is variable on a time scale of a few months (Seielstad, Pearson, and Readhead 1983) and Rudnick and Jones (1982) have measured a fractional polarization of 1.6% at 5 GHz.

We obtained a reasonable fit to all but the shortest baselines with the three-component model given in Table 4. There is clearly some larger scale structure, since 0.3 Jy is unaccounted for in our model.

2352+495.—This object has no detected radio structure on scales larger than 0″.2 (Perley 1982). It exhibits weak variability (15%) on time scales of a few months (Seielstad, Pearson, and Readhead 1983) and 0.2%–0.7% polarization at 5 GHz (Perley 1982).

Our observations show that this is a complex source with a significant amount of emission on scales larger than 10 mas. We tried fitting the data with three- and four-component models, and achieved a fairly poor fit to the data with the three-component model given in Table 4. The map shows two distinct components, one of which has a simple structure while the other is complex. We have classified this as a "compact double steep spectrum" source, but further observations are needed to confirm this classification.

REFERENCES

Alef, W., Götz, M. M. A., Preuss, E., and Kellermann, K. I. 1987, *Astr. Ap.*, submitted.
Altschuler, D. R. 1980, *A.J.*, **85**, 1559.
Andrew, B. H., MacLeod, J. M., Harvey, G. A., and Medd, W. J. 1978, *A.J.*, **83**, 863.
Antonucci, R. R. J., Hickson, P., Olszewski, E. W., and Miller, J. S. 1986, *A.J.*, **92**, 1.
Argue, A. N., and Sullivan, C. 1980, *M.N.R.A.S.*, **192**, 779.
Bååth, L. B. 1984, in *IAU Symposium 110, VLBI and Compact Radio Sources*, ed. R. Fanti, K. Kellermann, and G. Setti (Dordrecht: Reidel), p. 127.
Bartel, N., *et al.* 1984*a*, *Ap. J.*, **279**, 116.
Bartel, N., *et al.* 1987, *Ap. J.*, **323**, 505.
Bartel, N., Shapiro, I. I., Huchra, J. P., and Kühr, H. 1984*b*, *Ap. J.*, **279**, 112.
Barthel, P. D., Miley, G. K., Schilizzi, R. T., and Preuss, E. 1984, *Astr. Ap.*, **140**, 399.
Barthel, P. D., Pearson, T. J., Readhead, A. C. S., and Canzian, B. J. 1986, *Ap. J. (Letters)*, **310**, L7.
Barthel, P. D., Schilizzi, R. T., Miley, G. K., Jägers, W. J., and Strom, R. G. 1985, *Astr. Ap.*, **148**, 243.
Begelman, M. C., Blandford, R. D., and Rees, M. J. 1984, *Rev. Mod. Phys.*, **56**, 255.
Biermann, P., *et al.* 1981, *Ap. J. (Letters)*, **247**, L53.
Biermann, P., Fricke, K., Johnston, K. J., Kühr, H., Pauliny-Toth, I. I. K., Strittmatter, P. A., Urbanik, M., and Witzel, A. 1982, *Ap. J. (Letters)*, **252**, L1.
Biretta, J. A., Moore, R. L., and Cohen, M. H. 1986, *Ap. J.*, **308**, 93.
Biretta, J. A., Schneider, D. P., and Gunn, J. E. 1985, *A.J.*, **90**, 2508.
Blandford, R., and Narayan, R. 1985, *M.N.R.A.S.*, **213**, 591.
Bridle, A. H., Perley, R. A., and Henriksen, R. N. 1986, *A.J.*, **92**, 534.
Brown, R. L., Broderick, J. J., and Mitchell, K. J. 1986, *Ap. J.*, **306**, 107.
Browne, I. W. A., Clark, R. R., Moore, P. K., Muxlow, T. W. B., Wilkinson, P. N., Cohen, M. H., and Porcas, R. W. 1982*a*, *Nature*, **299**, 788.
Browne, I. W. A., Orr, M. J. L., Davis, R. J., Foley, A., Muxlow, T. W. B., and Thomasson, P. 1982*b*, *M.N.R.A.S.*, **198**, 673.
Burbidge, G., and Crowne, A. H. 1979, *Ap. J. Suppl.*, **40**, 583.
Burns, J. O., and Christiansen, W. A. 1980, *Nature*, **287**, 208.
Cawthorne, T. V., Scheuer, P. A. G., Morison, I., and Muxlow, T. W. B. 1986, *M.N.R.A.S.*, **219**, 883.
Clark, B. G. 1973, *Proc. IEEE*, **61**, 1242.
Cohen, M. H., *et al.* 1975, *Ap. J.*, **201**, 249.
Cornwell, T. J., and Wilkinson, P. N. 1981, *M.N.R.A.S.*, **196**, 1067.
Eckart, A., Hill, P. Johnston, K. J., Pauliny-Toth, I. I. K., Spencer, J. H., and Witzel, A. 1982, *Astr. Ap.*, **108**, 157.
Eckart, A., Witzel, A., Biermann, P., Johnston, K. J., Simon, R., Schalinski, C., and Kühr, H. 1986, *Astr. Ap.*, **168**, 17.
———. 1987, *Astr. Ap. Suppl.*, **67**, 121.
Eckart, A., Witzel, A., Biermann, P., Pearson, T. J., Readhead, A. C. S., and Johnston, K. J. 1985, *Ap. J. (Letters)*, **296**, L23.
Fanaroff, B. L., and Riley, J. M. 1974, *M.N.R.A.S.*, **167**, 31P.
Fanti, C., Fanti, R., Parma, P., Schilizzi, R. T., and van Breugel, W. J. M. 1985, *Astr. Ap.*, **143**, 292.
Flatters, C. 1987, *Nature*, **326**, 683.
Foley, A. R. 1982, Ph.D. thesis, Victoria University of Manchester.
Hartas, J. S., Rees, W. G., Scott, P. F., and Duffett-Smith, P. J. 1983, *M.N.R.A.S.*, **205**, 625.
Hewitt, A., and Burbidge, G. 1987, *Ap. J. Suppl.*, **63**, 1.
Hodges, M. W., and Mutel, R. L. 1987, in *Superluminal Radio Sources*, ed. J. A. Zensus and T. J. Pearson (Cambridge: Cambridge University Press), p. 168.
Hodges, M. W., Mutel, R. L., and Phillips, R. B. 1984, *A.J.*, **89**, 1327.
Hough, D. H., and Readhead, A. C. S. 1987, in *Superluminal Radio Sources*, ed. J. A. Zensus and T. J. Pearson (Cambridge: Cambridge University Press), p. 114.
Johnston, K. J., Biermann, P., Eckart, A., Kühr, H., Strittmatter, P. A., Strom, R. G., Witzel, A., and Zensus, A. 1984, *Ap. J.*, **280**, 542.
Johnston, K. J., Simon, R. S., Eckart, A., Biermann, P., Schalinski, C., Witzel, A., and Strom, R. G. 1987, *Ap. J. (Letters)*, **313**, L85.
Kapahi, V. K. 1979, *Astr. Ap.*, **74**, L11.
———. 1981, *Astr. Ap. Suppl.*, **43**, 381.
Kellermann, K. I., and Pauliny-Toth, I. I. K. 1981, *Ann. Rev. Astr. Ap.*, **19**, 373.
Kellermann, K. I., *et al.* 1977, *Ap. J.*, **211**, 658.
Kühr, H., Pauliny-Toth, I. I. K., Witzel, A., and Schmidt, J. 1981*a*, *A.J.*, **86**, 854 (S5).
Kühr, H., Witzel, A., Pauliny-Toth, I. I. K., and Nauber, U. 1981*b*, *Astr. Ap. Suppl.*, **45**, 367.
Kus, A. J., Wilkinson, P. N., and Booth, R. S. 1981, *M.N.R.A.S.*, **194**, 527.
Laing, R. A. 1981, *M.N.R.A.S.*, **195**, 261.
Lawrence, C. R., Pearson, T. J., Readhead, A. C. S., and Unwin, S. C. 1986, *A.J.*, **91**, 494.
Lawrence, C. R., *et al.* 1985, *Ap. J.*, **296**, 458.
Lawrence, C. R., Readhead, A. C. S., Pearson, T. J., and Unwin, S. C. 1987, in *Superluminal Radio Sources*, ed. J. A. Zensus and T. J. Pearson (Cambridge: Cambridge University Press), p. 260.
Lind, K. R. 1987, in *Superluminal Radio Sources*, ed. J. A. Zensus and T. J. Pearson (Cambridge: Cambridge University Press), p. 180.
Linfield, R. 1981, *Ap. J.*, **244**, 436.
Lonsdale, C. J., and Morison, I. 1980, *Nature*, **288**, 66.
———. 1983, *M.N.R.A.S.*, **203**, 833.
Marscher, A. P., and Shaffer, D. B. 1980, *A.J.*, **85**, 668.
Moore, P. K., Browne, I. W. A., Daintree, E. J., Noble, R. G., and Walsh, D. 1981, *M.N.R.A.S.*, **197**, 325.
Mutel, R. L., and Hodges, M. W. 1986, *Ap. J.*, **307**, 472.
Mutel, R. L., Hodges, M. W., and Phillips, R. B. 1985, *Ap. J.*, **290**, 86.
Mutel, R. L., and Phillips, R. B. 1987, in *Superluminal Radio Sources*, ed. J. A. Zensus and T. J. Pearson (Cambridge: Cambridge University Press), p. 60.
Mutel, R. L., Phillips, R. B., and Skuppin, R. 1981, *A.J.*, **86**, 1600.
Northover, K. J. E. 1973, *M.N.R.A.S.*, **165**, 369.
O'Dea, C. P., Barvainis, R., and Challis, P. 1986, in *IAU Symposium 119, Quasars*, ed. G. Swarup and V. K. Kapahi (Dordrecht: Reidel), p. 217.
O'Dea, C. P., and Owen, F. N. 1986, *Ap. J.*, **301**, 841.
Owen, F. N., Porcas, R. W., and Neff, S. G. 1978, *A.J.*, **83**, 1009.
Pauliny-Toth, I. I. K., Witzel, A., Preuss, E., Kühr, H., Kellermann, K. I., Fomalont, E. B., and Davis, M. M. 1978, *A.J.*, **83**, 451 (S4).
Peacock, J. A., Perryman, M. A. C., Longair, M. S., Gunn, J. E., and Westphal, J. A. 1981, *M.N.R.A.S.*, **194**, 601.
Peacock, J. A., and Wall, J. V. 1981, *M.N.R.A.S.*, **194**, 331.
———. 1982, *M.N.R.A.S.*, **198**, 843.
Pearson, T. J., Barthel, P. D., Lawrence, C. R., and Readhead, A. C. S. 1986, *Ap. J. (Letters)*, **300**, L25.
Pearson, T. J., Perley, R. A., and Readhead, A. C. S. 1985, *A.J.*, **90**, 738.
Pearson, T. J., and Readhead, A. C. S. 1981, *Ap. J.*, **248**, 61 (Paper I).
———. 1984*a*, in *IAU Symposium 110, VLBI and Compact Radio Sources*, ed. R. Fanti, K. Kellermann, and G. Setti (Dordrecht: Reidel), p. 15.
———. 1984*b*, *Ann. Rev. Astr. Ap.*, **22**, 97.
Pearson, T. J., Readhead, A. C. S., and Barthel, P. D. 1987, in *Superluminal Radio Sources*, ed. J. A. Zensus and T. J. Pearson (Cambridge: Cambridge University Press), p. 94.
Perley, R. A. 1982, *A.J.*, **87**, 859.
Perley, R. A., Bridle, A. H., Willis, A. G., and Fomalont, E. B. 1980, *A.J.*, **85**, 499.
Perley, R. A., Fomalont, E. B., and Johnston, K. J. 1980, *A.J.*, **85**, 649.
Perley, R. A., Willis, A. G., and Scott, J. S. 1979, *Nature*, **281**, 437.
Phillips, R. B., and Mutel, R. L. 1980, *Ap. J.*, **236**, 89.
———. 1981, *Ap. J.*, **244**, 19.
———. 1982, *Astr. Ap.*, **106**, 21.
Phillips, R. B., and Shaffer, D. B. 1983, *Ap. J.*, **271**, 32.
Phinney, E. S. 1985, in *Astrophysics of Active Galaxies and Quasi-stellar Objects*, ed. J. S. Miller (Mill Valley: University Science Books), p. 453.
Porcas, R. W. 1981, *Nature*, **294**, 47.
———. 1986, in *IAU Symposium 119, Quasars*, ed. G. Swarup and V. K. Kapahi (Dordrecht: Reidel), p. 131.
———. 1987, in *Superluminal Radio Sources*, ed. J. A. Zensus and T. J. Pearson (Cambridge: Cambridge University Press), p. 12.

Preuss, E., Alef, W., Whyborn, N., Wilkinson, P. N., and Kellermann, K. I. 1984, in *IAU Symposium 110, VLBI and Compact Radio Sources*, ed. R. Fanti, K. Kellermann, and G. Setti (Dordrecht: Reidel), p. 29.
Preuss, E., Kellermann, K. I., Pauliny-Toth, I. I. K., and Shaffer, D. B. 1980, *Ap. J. (Letters)*, **240**, L7.
Readhead, A. C. S., and Hewish, A. 1974, *Mem. R.A.S.*, **78**, 1.
Readhead, A. C. S., Hough, D. H., Ewing, M. S., Walker, R. C., and Romney, J. D. 1983, *Ap. J.*, **265**, 107.
Readhead, A. C. S., Napier, P. J., and Bignell, R. C. 1980, *Ap. J. (Letters)*, **237**, L55.
Readhead, A. C. S., Pearson, T. J., and Barthel, P. D. 1987, in *IAU Symposium 129, The Impact of VLBI on Astrophysics and Geophysics*, ed. M. J. Reid and J. M. Moran (Dordrecht: Reidel), in press.
Readhead, A. C. S., Pearson, T. J., and Unwin, S. C. 1984, in *IAU Symposium 110, VLBI and Compact Radio Sources*, ed. R. Fanti, K. Kellermann, and G. Setti (Dordrecht: Reidel), p. 131.
Readhead, A. C. S., and Wilkinson, P. N. 1978, *Ap. J.*, **223**, 25.
———. 1980, *Ap. J.*, **235**, 11.
Rickett, B. J., Coles, W. A., and Bourgois, G. 1984, *Astr. Ap.*, **134**, 390.
Riley, J. M., and Pooley, G. G. 1975, *Mem. R.A.S.*, **80**, 105.
Roberts, D. H., and Wardle, J. F. C. 1987, in *Superluminal Radio Sources*, ed. J. A. Zensus and T. J. Pearson (Cambridge: Cambridge University Press), p. 193.
Rudnick, L., and Jones, T. W. 1982, *Ap. J.*, **255**, 39.
———. 1983, *A.J.*, **88**, 518.
Rusk, R. 1987, in *IAU Symposium 129, The Impact of VLBI on Astrophysics and Geophysics*, ed. M. J. Reid and J. M. Moran (Dordrecht: Reidel), in press.
Rusk, R., and Rusk, A. C. M. 1986, *Canadian J. Phys.*, **64**, 440.
Rusk, R., and Seaquist, E. R. 1985, *A.J.*, **90**, 30.
Schilizzi, R. T., and de Bruyn, A. G. 1983, *Nature*, **303**, 26.
Schilizzi, R. T., Kapahi, V. K., and Neff, S. G. 1982, *J. Ap. Astr.*, 3, 173.
Schwab, F. R., and Cotton, W. D. 1983, *A.J.*, **88**, 688.
Scott, M. A., and Readhead, A. C. S. 1977, *M.N.R.A.S.*, **180**, 539.
Seielstad, G. A., Pearson, T. J., and Readhead, A. C. S. 1983, *Pub. A.S.P.*, **95**, 842.
Shaffer, D. B., and Marscher, A. P. 1987, in *Superluminal Radio Sources*, ed. J. A. Zensus and T. J. Pearson (Cambridge: Cambridge University Press), p. 67.
Shone, D. L. 1986, Ph.D. thesis, Victoria University of Manchester.
Simon, R. S. 1982, Ph.D. thesis, California Institute of Technology.
Simon, R. S., Readhead, A. C. S., Moffet, A. T., Wilkinson, P. N., Allen, B., and Burke, B. F. 1983, *Nature*, **302**, 487.
Simon, R. S., Readhead, A. C. S., and Wilkinson, P. N. 1984, in *IAU Symposium 110, VLBI and Compact Radio Sources*, ed. R. Fanti, K. Kellermann, and G. Setti (Dordrecht: Reidel), p. 111.
Spinrad, H. 1982, *Pub. A.S.P.*, **94**, 397.
Ulvestad, J. S., and Johnston, K. J. 1984, *A.J.*, **89**, 189.
Ulvestad, J. S., Johnston, K. J., and Weiler, K. W. 1983, *Ap. J.*, **266**, 18.
Unger, S. W., Pedlar, A., Axon, D. J., Wilkinson, P. N., and Appleton, P. N. 1984, *M.N.R.A.S.*, **211**, 783.
van Breugel, W., Miley, G., and Heckman, T. 1984, *A.J.*, **89**, 5.
van Breugel, W., and Schilizzi, R. 1986, *Ap. J.*, **301**, 834.
van Breugel, W. J. M., Schilizzi, R. T., Hummel, E., and Kapahi, V. K. 1981, *Astr. Ap.*, **96**, 310.
Weiler, K. W., and Johnston, K. J. 1980, *M.N.R.A.S.*, **190**, 269.
Whyborn, N. D., Browne, I. W. A., Wilkinson, P. N., Porcas, R. W., and Spinrad, H. 1985, *M.N.R.A.S.*, **214**, 55.
Wilkinson, P. N., Booth, R. S., Cornwell, T. J., and Clark, R. R. 1984*a*, *Nature*, **308**, 619.
Wilkinson, P. N., Cornwell, T. J., Kus, A. J., Readhead, A. C. S., and Pearson, T. J. 1984*b*, in *NRAO Workshop No. 9, Physics of Energy Transport in Extragalactic Radio Sources*, ed. A. H. Bridle and J. A. Eilek (Green Bank: National Radio Astronomy Observatory), p. 76.
Wilkinson, P. N., and de Bruyn, A. G. 1984, *M.N.R.A.S.*, **211**, 593.
———. 1987, in *IAU Symposium 129, The Impact of VLBI on Astrophysics and Geophysics*, ed. M. J. Reid and J. M. Moran (Dordrecht: Reidel), in press.
Wilkinson, P. N., Kus, A. J., Pearson, T. J., Readhead, A. C. S., and Cornwell, T. J. 1986, in *IAU Symposium 119, Quasars*, ed. G. Swarup and V. K. Kapahi (Dordrecht: Reidel), p. 165.
Wilkinson, P. N., Readhead, A. C. S., Purcell, G. H., and Anderson, B. 1977, *Nature*, **269**, 764.
Wilkinson, P. N., Spencer, R. E., Readhead, A. C. S., Pearson, T. J., and Simon, R. S. 1984*c*, in *IAU Symposium 110, VLBI and Compact Radio Sources*, ed. R. Fanti, K. Kellermann, and G. Setti (Dordrecht: Reidel), p. 25.
Witzel, A. 1987, in *Superluminal Radio Sources*, ed. J. A. Zensus and T. J. Pearson (Cambridge: Cambridge University Press), p. 83.
Worrall, D. M., *et al.* 1984, *Ap. J.*, **278**, 521.
Zensus, J. A., and Porcas, R. W. 1986, in *IAU Symposium 119, Quasars*, ed. G. Swarup and V. K. Kapahi (Dordrecht: Reidel), p. 167.

T. J. PEARSON and A. C. S. READHEAD: Owens Valley Radio Observatory, 105-24 California Institute of Technology, Pasadena, CA 91125

THE ASTROPHYSICAL JOURNAL SUPPLEMENT SERIES, 98:1–32, 1995 May

THE FIRST CALTECH–JODRELL BANK VLBI SURVEY. I. λ = 18 CENTIMETER OBSERVATIONS OF 87 SOURCES

A. G. POLATIDIS AND P. N. WILKINSON
University of Manchester, Nuffield Radio Astronomy Laboratories, Jodrell Bank, Macclesfield, Cheshire SK11 9DL, UK

AND

W. XU, A. C. S. READHEAD, T. J. PEARSON, G. B. TAYLOR, AND R. C. VERMEULEN
Owens Valley Radio Observatory, California Institute of Technology 105-24, Pasadena, CA 91125
Received 1993 December 30; accepted 1994 November 2

ABSTRACT

We present the first results from the first Caltech–Jodrell Bank VLBI survey (the CJ1 survey). The CJ1 sample includes 135 radio sources with total flux density 1.3 Jy > $S_{6\,cm} \geq 0.7$ Jy, declination $\delta_{1950} \geq 35°$, and Galactic latitude $|b^{II}| > 10°$. It extends the flux density limit of the complete "PR" sample studied by Pearson & Readhead from 1.3 to 0.7 Jy and increases the total number of sources from 65 to 200.

The complete survey includes VLBI images at both λ-18 and 6 cm of all the objects in the extended sample that have cores strong enough to be mapped with the Mark II VLBI system. These images provide a large enough sample to study, for example, the variety of morphologies exhibited by compact radio sources, cosmological evolution, superluminal motion, and misalignment between parsec-scale and kiloparsec-scale radio structures.

In this paper we present λ-18 cm VLBI observations of 56 CJ1 and 31 PR sources made in 1990–1991, including images of 82 sources. The observations were made with a "snapshot" technique in which each source was observed in three 20–30-minute scans using an array of 12–16 antennas. The images have resolution 3–10 mas and dynamic range greater than 100:1. Later papers in the series will present the remaining λ-18 cm observations, the λ-6 cm observations, and the analysis and interpretation of the results.

Subject headings: quasars: general — radio continuum: galaxies — surveys — techniques: interferometric

1. PARSEC-SCALE OBSERVATIONS OF COMPACT RADIO SOURCES

VLBI observations have revealed a variety of radio structures in active galactic nuclei (AGNs) ranging from asymmetric core–jets to compact symmetric objects (CSOs) (e.g., Readhead, Pearson, & Unwin 1984; Conway et al. 1994; Wilkinson et al. 1994) and the complex structures observed in some compact steep-spectrum sources (CSS) (e.g., Fanti et al. 1990a). It is not yet known whether these morphological differences reflect fundamental differences in the central engines or environmental differences in the parent galaxies. To clarify the relationships between the various types of source and to elucidate the underlying causes of the different radio structures one can study either a few representative sources in detail or well-defined samples of sources to investigate their statistical properties.

So far, largely due to the limited observing time devoted to VLBI, the first approach has dominated VLBI efforts. However, several groups have observed complete, albeit small, samples of AGNs. The largest complete sample to date has been the "PR" sample (Pearson & Readhead 1981, 1988 [PR88]). This sample contains 65 objects, selected from the MPIfR-NRAO S4 and S5 surveys (Pauliny-Toth et al. 1978; Kühr et al. 1981) of which 45 have been imaged with VLBI. The S4 and S5 surveys were made at a short wavelength (λ-6 cm) and hence the selection favors objects where the dominant radio emission arises in a compact, flat-spectrum component. PR88 proposed a classification scheme for all 65 sources in the sample based on the milliarcsecond-scale morphology of the sources, their large-scale radio structure and their radio spectra. There are five major classes of radio-loud AGNs, some of which are divided into subclasses.

Other significant surveys have also been made. For example a sample of 13 flat-spectrum sources, selected from the S5 survey with $\delta > 70°$ and $S_{6\,cm} > 1$ Jy, has been studied by astronomers from MPIfR (Eckart et al. 1987; Witzel et al. 1988). The weak cores of lobe-dominated sources have been studied by several sets of workers; thus far results on more than 30 objects have been published (e.g., Zensus & Porcas 1987; Hooimeyer et al. 1992; Giovannini et al. 1992; Hough, Vermeulen, & Readhead 1993). Samples of ~50 compact steep-spectrum sources selected from the 3CR and the Peacock & Wall (1982) catalogs have been observed at multiple wavelengths by an international group of astronomers (e.g., Fanti et al. 1985, 1990b; Sanghera 1992; Dallacasa et al. 1994). A group mainly from Brandeis University has been investigating the milliarcsecond-scale polarization of quasars and BL Lac objects; observations of 24 objects have been published so far (e.g., Cawthorne et al. 1993a,b). Finally Wehrle et al. (1992) have been studying a sample of 41 sources with flux density that has exceeded 4.5 Jy at λ-3.8 cm at any epoch.

These studies, and follow-up work on individual objects, have begun to delineate the different morphological classes of compact objects in AGNs and their distinctive properties, have demonstrated that the phenomenon of superluminal motion is common in most of these classes, and have focused attention on a number of particularly interesting objects. However it is

clear that a larger complete sample of sources is required to tackle a variety of interesting astronomical questions, many of which arose from these smaller surveys.

2. THE FIRST CALTECH-JODRELL BANK VLBI SURVEY (CJ1)

The large number of apparently different classes of AGNs, as revealed by the PR88 analysis, first raises the question of whether the full range of morphologies has been observed and identified. In addition the size of the PR sample is too small for many interesting statistical studies to be performed; in particular some classes contain only one or two members and statistical tests *within* these classes are impossible. We therefore decided to expand PR's work by making observations of a significantly larger, complete flux-density–limited sample of radio sources. The program is a collaboration between the California Institute of Technology (Caltech) and N.R.A.L. Jodrell Bank (University of Manchester). Since it is the first such survey we identify it as the first Caltech–Jodrell Bank or CJ1 survey.[1]

Our principal astronomical aims are (1) To test the PR classification scheme and to add to it any new types of objects we might observe. (2) To provide a sample large enough to make interesting statistical studies both as a whole and within and between different classes. In particular, we can investigate the distribution of misalignments between the milliarcsecond scale and the arcsecond scale (PR88) and study the cosmological evolution of different classes using the luminosity-volume test. The relation between VLBI angular size and redshift can also be used as a probe of universal geometry (Kellermann 1993; Gurvits 1993). Testing the applicability of "Unified Schemes" is another goal of this study. (3) To provide first-epoch observations of a large sample of candidate sources for superluminal motion studies (Vermeulen & Cohen 1994). (4) To look for possible small-separation gravitational lens systems.

In order to have a large enough sample of sources for statistical studies, we decided to select a set of sources which, when combined with the PR sample, would treble the total number of objects available for study. We therefore selected sources from the S4 and S5 surveys by lowering the flux density limit used by PR, but otherwise following PR's two remaining selection criteria. Our sample thus obeys the following selection criteria: (1) flux density at 6 cm: 1.3 Jy $> S_{6\ \mathrm{cm}} \geq$ 0.7 Jy; (2) declination (B1950.0) $\delta \geq 35°$; and (3) Galactic latitude $|b^{\mathrm{II}}| > 10°$. The selection was based on the flux densities measured at the epoch of the S4 and S5 surveys, and since many of the sources are variable a selection made from measurements at another epoch would result in a slightly different sample.

There are 137 objects in the S4 and S5 surveys which conform to the above criteria. Of them one, 1758+666, is identified with a planetary nebula and another, 1038+528, consists of two independent quasars (Owen, Wills, & Wills 1980), neither of which is strong enough to satisfy, on its own, the flux density selection criterion. These two sources have been excluded and thus our final *CJ1 sample* contains 135 objects. Together with the PR sample we therefore have a total of 200 objects for statistical studies.

Complementary observing programs have been undertaken to obtain arcsecond scale radio maps of CJ1 sources for which an adequate map was not available in the literature and to complete the optical identifications and measure redshifts. Redshifts for 26 objects were reported by Xu et al. (1994); further results will be reported in later papers in this series.

The PR survey was made at λ-6 cm but for the CJ1 survey we decided to make VLBI observations both at λ-6 cm and λ-18 cm in order to take advantage of the complementary resolution and surface brightness sensitivity provided at these two wavelengths. Maps at two wavelengths were expected to clarify ambiguous cases and hence to increase the reliability of the classification.

In order to complete the dual-wavelength observations of such a large sample within a practical time span, we used a "snapshot" observing technique, which will be explained in detail below. The observations were made using the NRAO Mark II recording system, principally because of the availability of the JPL/Caltech Block II correlator which can process data from 16 telescopes simultaneously.

The sensitivity of the narrowband (1.8 MHz) Mark II system limits the number of sources that can be imaged to those with a compact component stronger than ~100 mJy. For reasons of time economy, we did not perform a "finding" survey like PR; instead, we collated from the literature arcsecond and subarcsecond resolution maps, mainly made with the VLA and MERLIN, for all the sources in the sample. We also collected radio spectral information for all the sources, mainly from Kühr et al. (1979). Using the radio structure and radio spectral information we sorted the sources into the following categories:

1. Sources which were almost certain to have structure that can be mapped with the Mark II system. These include sources with overall angular size less than 2″ and all objects observed with VLBI by Preston et al. (1985) for which at least 20% of the total flux density is detected on intercontinental baselines.
2. Sources which had been previously observed with VLBI and for which the maps were of sufficient quality to allow us to classify the source unambiguously.
3. Sources which do not contain strong enough compact components to be mapped by Mark II VLBI. These sources are predominantly large, lobe-dominated sources with weak or nondetected core.

Table 1 lists the 135 sources in the CJ1 sample. Of these, there are 81 sources in category 1 that we have observed at λ-18 cm. Furthermore, to complete the information on the PR sample, we decided to observe the 28 objects from the PR sample that had not been observed previously with VLBI at λ-18 cm. We also included the previously mapped objects 0538+498, 1458+518, and 1807+698 as a check on the snapshot technique (see Appendix A). The 31 PR sources observed are listed in Table 2.

The observations took place in nine observing sessions, four at λ-18 cm and five at λ-6 cm wavelength, and were completed within two and a half years starting in 1990 March. In this paper we discuss the observations and the data analysis for 87 sources observed in three of the four λ-18 cm observing ses-

[1] The second Caltech–Jodrell Bank or CJ2 survey of 193 flat- and peaked-spectrum sources is reported by Taylor et al. (1994) and Henstock et al. (1995).

TABLE 1

THE COMPLETE CJ1 SAMPLE

Source (1)	Other (2)	R.A. (3)	Declination (4)	S_{11cm} (5)	S_{6cm} (6)	$S_{2.8cm}$ (7)	ID (8)	V (9)	z (10)	Ref (11)	λ18 cm VLBI (12)
0010+405 ...	4C40.01	00 13 31.131	40 51 37.15	1.18	1.05	0.78	G	17.9	0.255	2	1990 Sep
0010+775 ...	...	00 13 11.7	77 48 47	1.32	0.781	0.48	G	18.0	0.326	1	1991 Nov
0013+790 ...	3C6.1	00 16 32.3	79 16 52	2.01	1.044	0.46	G	22.0	0.840	3	...
0022+390 ...	OA 026	00 25 26.157	39 19 35.45	0.78	0.859	0.91	Q	19.8	1.946	1	1991 Sep
0048+509 ...	3C22.0	00 50 56.2	51 12 04	1.28	0.760	0.33	G	22.0	0.937	2	...
0102+480 ...	...	01 05 49.930	48 19 03.18	1.09	0.982	0.75	EF	...	...	2	1991 Jun
0106+729 ...	3C33.1	01 09 44.3	73 11 57	1.86	0.890	...	G	19.5	0.181	4	...
0206+355 ...	4C35.03	02 09 38.6	35 47 51	1.43	0.894	0.58	G	13.0	0.0373	2	...
0218+357 ...	OD 330	02 21 05.470	35 56 13.72	1.03	1.17	0.90	BL	20.0	>0.685	2,5	1991 Nov
0220+397 ...	3C65.0	02 23 42.8	40 00 52	1.59	0.770	0.31	G	23.0	1.176	2	...
0248+430 ...	...	02 51 34.537	43 15 15.83	0.96	1.21	1.20	Q	18.6	1.316	2	1991 Jun
0258+350 ...	4C34.09	03 01 42.37	35 12 20.7	1.31	0.926	0.65	G	13.5	0.0165	2	...
0307+444 ...	4C44.07	03 10 31.2	44 35 48	0.98	0.733	...	Q	18.8	1.165	2	...
0309+390 ...	4C39.11	03 12 26.7	39 16 30	1.12	0.728	0.34	G	18.2	0.161	2	...
0402+379 ...	4C37.11	04 05 49.263	38 03 32.24	1.47	1.15	0.69	G	18.5	0.055	1	1990 Sep
0407+747 ...	4C74.08	04 13 17.0	74 51 07	1.67	0.962	0.49	G	19.1	–	1	...
0602+673 ...	...	06 07 52.672	67 20 55.42	0.83	1.07	1.08	Q	20.6	...	2	1990 Sep
0615+820 ...	...	06 26 03.007	82 02 25.57	1.02	0.999	0.86	Q	17.5	0.710	3	10
0620+389 ...	...	06 24 19.022	38 56 48.72	0.89	0.874	...	Q	20.0	3.470	1	1991 Nov
0642+449 ...	OH 471	06 46 32.026	44 51 16.59	1.27	0.778	0.90	Q	18.5	3.406	2	1991 Nov
0646+600 ...	OH 577.1	06 50 31.256	60 01 44.55	0.69	0.788	0.46	Q	18.9	0.455	2	1991 Sep
0650+371 ...	...	06 53 58.283	37 05 40.61	0.77	0.971	0.71	Q	18.2	1.982	2	1991 Sep
0651+542 ...	3C171.0	06 55 14.9	54 09 00	1.99	1.16	0.53	G	18.9	0.2384	2	...
0702+749 ...	3C173.1	07 09 18.4	74 49 32	1.46	0.789	0.32	G	18.9	0.292	4	...
0703+426 ...	4C42.23	07 06 41.9	42 31 58	1.67	0.985	0.60	G	15.0	0.060	2	...
0707+476 ...	...	07 10 46.105	47 32 11.14	1.29	0.998	1.37	Q	18.2	1.292	2	1991 Sep
0707+689 ...	4C68.08	07 13 14.1	68 52 09	1.13	0.749	0.42	Q	20.5	1.141	1	11
0716+714 ...	...	07 21 53.449	71 20 36.36	0.97	1.121	2.00	BL	13.2	–	1	1991 Nov
0734+805 ...	3C184.1	07 43 01.4	80 26 26	1.92	1.134	0.27	G	17.0	0.118	3	...
0740+828 ...	...	07 50 57.764	82 41 58.03	1.29	0.931	0.65	Q	18.5	1.991	1	1991 Jun
0746+483 ...	OI 478	07 50 20.438	48 14 53.56	0.70	0.796	0.79	Q	18.4	1.951	2	1991 Nov
0755+379 ...	3C189	07 58 28.8	37 47 12	1.79	1.26	0.86	G	14.9	0.0433	2	1991 Jun
0805+410 ...	...	08 08 56.652	40 52 44.88	0.94	0.766	1.08	Q	19.0	1.420	1	1991 Nov
0812+367 ...	OJ 320	08 15 25.945	36 35 15.14	1.03	1.01	0.98	Q	18.0	1.025	2	1990 Sep
0816+526 ...	4C52.18	08 19 47.7	52 32 26	1.22	0.776	0.42	G	18.0	0.189	2	...
0818+472 ...	3C197.1	08 21 33.6	47 02 37	1.16	0.860	0.30	G	16.5	0.1301	2	...
0820+560 ...	OJ 535	08 24 47.237	55 52 42.67	1.08	0.917	0.88	Q	18.0	1.417	2	1991 Sep
0821+394 ...	4C39.23	08 24 55.484	39 16 41.90	1.10	0.993	1.18	Q	18.5	1.216	2	1991 Sep
0827+378 ...	4C37.24	08 31 10.0	37 42 10	1.37	0.930	0.57	Q	18.1	0.914	2	(1991 Sep)
0828+493 ...	OJ 448	08 32 23.217	49 13 21.04	1.17	1.02	0.96	BL	18.8	0.548	2	1991 Jun
0833+585 ...	...	08 37 22.410	58 25 01.84	0.50	1.11	1.23	Q	18.0	2.101	2	1991 Jun
0844+540 ...	4C54.17	08 47 53.9	53 52 35	1.07	0.732	0.43	G	15.0	0.0453	2	...
0900+428 ...	4C42.28	09 04 15.628	42 38 04.77	0.97	0.761	0.72	G	19.9	...	2	1991 Nov
0917+449 ...	...	09 20 58.459	44 41 53.98	0.54	0.803	1.01	Q	19.0	2.18	2	1991 Nov
0917+624 ...	OK 630	09 21 36.231	62 15 52.18	0.87	0.996	1.36	Q	19.5	1.446	2	1991 Sep
0936+361 ...	3C223.0	09 39 52.7	35 53 58	2.06	1.29	0.72	G	17.1	0.1368	2	...
0938+399 ...	3C223.1	09 41 24.0	39 44 42	1.23	0.870	0.49	G	16.4	0.1075	2	...
0945+664 ...	4C66.09	09 49 12.165	66 14 59.59	1.62	1.22	0.77	G	21.6	...	2	(1991 Jun)
0955+476 ...	OK 492	09 58 19.670	47 25 07.83	0.71	0.739	0.75	Q	18.0	1.873	2	1991 Nov
1003+830 ...	...	10 10 15.774	82 50 14.38	0.78	0.716	0.66	G	20.5	0.322	1	1991 Sep
1007+416 ...	4C41.21	10 10 27.6	41 32 38	1.04	0.706	0.50	Q	16.5	0.611	2	...
1015+359 ...	OL 326	10 18 10.988	35 42 39.44	0.63	0.916	1.04	Q	18.5	1.226	2	1991 Sep
1020+400 ...	4C40.25	10 23 11.566	39 48 15.38	1.06	0.866	1.18	Q	17.5	1.254	1	1991 Nov
1030+415 ...	...	10 33 03.708	41 16 06.23	1.02	1.13	1.48	Q	18.2	1.120	2	1991 Jun
1030+585 ...	3C244.1	10 33 33.7	58 14 43	1.95	1.12	0.51	G	19.0	0.428	2	...

TABLE 1—*Continued*

Source (1)	Other (2)	R.A. (3)	Declination (4)	S_{11cm} (5)	S_{6cm} (6)	$S_{2.8cm}$ (7)	ID (8)	V (9)	z (10)	Ref (11)	λ18 cm VLBI (12)
1039+811 ...	...	10 44 23.063	80 54 39.44	0.90	1.144	0.78	Q	16.5	1.254	3	10
1044+719 ...	...	10 48 27.620	71 43 35.93	0.74	0.707	0.96	Q	19	1.15	6	1991 Sep
1053+704 ...	...	10 56 53.619	70 11 45.90	0.65	0.710	0.96	Q	18.5	2.492	1	1991 Sep
1053+815 ...	...	10 58 11.539	81 14 32.67	0.96	0.770	1.20	G	18.5	0.706	1	1991 Sep
1056+432 ...	3C247	10 58 58.8	43 01 24	1.55	0.949	0.40	G	21.5	0.7489	2	...
1058+726 ...	4C72.16	11 01 48.807	72 25 37.11	1.07	0.778	0.56	Q	17.4	1.45	7	1991 Sep
1100+772 ...	3C249.1	11 04 13.9	76 58 58	1.33	0.772	0.45	Q	15.7	0.311	4	...
1101+384 ...	Mkr 421	11 04 27.315	38 12 31.79	0.77	0.725	0.79	BL	13.1	0.0308	2	1991 Nov
1111+408 ...	3C254	11 14 38.7	40 37 20	1.45	0.790	0.32	Q	18.0	0.734	2	...
1128+385 ...	OM 346.9	11 30 53.282	38 15 18.55	0.89	0.771	0.93	Q	16.0	1.733	1	1991 Nov
1137+660 ...	3C263.0	11 39 57.1	65 47 49	1.73	1.04	0.57	Q	16.3	0.649	2	...
1138+594 ...	4C59.16	11 40 48.9	59 12 31	1.23	0.767	0.43	EF	...	...	2	(1991 Nov*)
1144+402 ...	...	11 46 58.298	39 58 34.30	1.05	0.941	1.55	Q	18.5	1.088	1	1991 Sep
1144+542 ...	...	11 46 44.204	53 56 43.09	0.71	0.878	0.73	Q	20.5	2.201	1	1991 Nov
1150+497 ...	4C49.22	11 53 24.466	49 31 08.83	1.56	1.11	1.48	Q	17.1	0.334	2	1991 Nov
1150+812 ...	...	11 53 12.499	80 58 29.15	1.25	1.181	1.10	Q	18.5	1.250	3	10
1152+551 ...	4C55.22	11 55 28.2	54 53 34	1.33	0.843	0.52	G	16.0	0.050	2	...
1203+645 ...	3C268.3	12 06 24.7	64 13 37	2.00	1.16	0.51	G	20.0	0.371	2	12
1213+350 ...	4C35.28	12 15 55.602	34 48 15.21	1.21	1.01	0.79	Q	20.1	0.851	2	1991 Jun
1213+538 ...	4C53.24	12 15 29.6	53 35 58	1.40	0.904	0.37	Q	18.0	1.065	2	...
1216+487 ...	ON 428	12 19 06.415	48 29 56.17	0.96	1.08	1.05	Q	18.5	1.076	2	1991 Jun
1225+368 ...	ON 343	12 27 58.726	36 35 11.82	1.58	0.767	0.26	Q	21.5	1.974	1	13
1242+410 ...	ON470.5	12 44 49.188	40 48 06.14	1.16	0.744	0.53	Q	19.0	0.813	1	1991 Nov
1250+568 ...	3C277.1	12 52 26.3	56 34 20	1.53	1.05	0.41	Q	17.9	0.321	2	14
1311+678 ...	4C67.22	13 13 27.3	67 36 05	1.45	0.923	0.50	EF	...	...	2	1991 Sep
1317+520 ...	4C52.27	13 19 46.196	51 48 05.76	0.92	0.716	0.45	Q	17.0	1.060	2	1991 Nov
1319+428 ...	3C285	13 21 17.8	42 35 14	1.23	0.760	0.48	G	16.0	0.0794	2	...
1333+459 ...	...	13 35 21.960	45 42 38.25	0.57	0.757	0.66	Q	18.5	2.449	1	1991 Nov
1333+589 ...	4C58.26	13 35 25.928	58 44 00.29	0.72	0.826	0.74	EF	...	...	2	1991 Sep
1336+391 ...	3C288	13 38 49.9	38 51 09	1.76	0.992	0.37	G	16.5	0.2459	2	...
1342+663 ...	...	13 44 08.679	66 06 11.65	0.61	0.817	0.89	Q	19.4	1.351	1	1991 Sep
1347+539 ...	4C53.28	13 49 34.657	53 41 17.04	1.00	0.962	0.91	Q	17.3	0.978	1	1991 Jun
1349+647 ...	3C292	13 50 42.0	64 29 35	1.06	0.720	0.75	G	20.7	0.713	2	...
1357+769 ...	...	13 57 55.370	76 43 21.05	0.58	0.844	0.60	SO	19.0	...	8	1991 Sep
1418+546 ...	OQ 530	14 19 46.598	54 23 14.79	0.94	1.09	1.43	BL	15.5	0.152	2	1990 Sep
1419+419 ...	3C299	14 21 05.6	41 44 49	1.61	0.900	0.39	G	18.4	0.367	2	...
1435+638 ...	...	14 36 45.803	63 36 37.87	1.41	1.24	1.01	Q	15.0	2.068	2	1990 Sep
1437+624 ...	OQ 663	14 38 44.8	62 11 55	1.39	0.862	0.44	Q	19.0	1.090	2	1991 Sep
1438+385 ...	OQ 363	14 40 22.337	38 20 13.63	0.88	0.770	0.56	Q	21.6	...	2	1991 Nov
1441+522 ...	3C303	14 43 02.7	52 01 38	1.55	0.940	0.81	G	17.0	0.141	2	...
1448+634 ...	3C305	14 49 21.5	63 16 14	1.60	0.920	0.47	G	13.7	0.041	2	...
1504+377 ...	OR 306	15 06 09.530	37 30 51.13	0.97	1.10	1.56	G	21.2	0.674	2	1990 Sep
1547+507 ...	OR 580	15 49 17.468	50 38 05.79	0.69	0.738	0.65	Q	18.5	2.169	2	1991 Sep
1549+628 ...	3C325	15 49 58.4	62 41 22	1.84	0.830	0.42	G	21.0	0.86	2	...
1557+708 ...	4C70.19	15 57 31.0	70 41 25	1.76	1.02	...	G	14.0	0.026	1	...
1627+444 ...	3C337	16 28 53.1	44 19 14	1.57	0.910	0.50	G	21.0	0.635	2	...
1637+626 ...	3C343.1	16 38 28.2	62 34 44	2.23	1.20	0.50	G	20.7	0.750	2	12
1637+826 ...	NGC6251	16 32 31.971	82 32 16.38	1.37	0.978	0.73	G	14.3	0.0243	3	15
1638+398 ...	NRAO512	16 40 29.633	39 46 46.03	1.08	1.16	1.72	Q	16.5	1.666	2	1990 Sep
1656+477 ...	...	16 58 02.779	47 37 49.24	0.73	0.923	0.86	Q	18.2	1.622	2	1991 Sep
1656+482 ...	4C48.41	16 57 46.879	48 08 33.05	0.89	0.776	0.81	EF	...	...	2	1991 Sep
1658+471 ...	3C349.0	16 59 29.5	47 02 44	1.88	1.14	0.58	G	19.0	0.205	2	...
1704+608 ...	3C351.0	17 04 41.3	60 44 30	2.03	1.21	0.59	Q	15.3	0.371	2	...
1719+357 ...	OT 332	17 21 09.491	35 42 16.07	0.64	0.859	0.84	Q	17.5	0.263	2	1991 Nov
1732+389 ...	OT 355	17 34 20.579	38 57 51.45	0.67	1.15	0.89	Q	19.0	0.976	2	1991 Jun

TABLE 1—*Continued*

Source (1)	Other (2)	R.A. (3)	Declination (4)	S_{11cm} (5)	S_{6cm} (6)	$S_{2.8cm}$ (7)	ID (8)	V (9)	z (10)	Ref (11)	λ18 cm VLBI (12)
1734+508 ...	...	17 35 49.005	50 49 11.57	0.60	0.803	0.72	EF	...	...	2	1991 Sep
1738+476 ...	OT 465	17 39 57.130	47 37 58.37	0.84	0.904	0.85	BL	19.5	0.316	1	1991 Jun
1751+441 ...	OT 486.4	17 53 22.650	44 09 45.67	0.59	1.04	1.22	Q	19.5	0.871	2	1990 Sep
1758+388 ...	OT 398	18 00 24.765	38 48 30.70	0.42	0.916	1.62	Q	17.8	2.092	2	1991 Jun
1800+440 ...	OU 401	18 01 32.315	44 04 21.90	0.63	1.02	1.12	Q	16.8	0.663	2	1990 Sep
1819+396 ...	4C39.56	18 21 20.9	39 42 45	1.78	0.971	0.38	G	19.0	...	2	16
1825+743 ...	3C379.1	18 24 33.0	74 20 57	1.05	0.728	0.35	G	18.0	0.256	4	...
1832+474 ...	3C381	18 33 46.2	47 27 21	2.30	1.29	0.79	G	17.2	0.1605	2	...
1833+653 ...	3C383	18 33 43.6	65 21 38	1.23	0.799	0.38	G	17.0	0.161	2	...
1842+681 ...	...	18 42 33.642	68 09 25.23	0.87	0.810	1.50	Q	17.9	0.473	1	1991 Jun
1843+356 ...	OU 373	18 45 35.110	35 41 16.72	0.95	0.812	0.49	G	21.9	...	2	1991 Nov
1926+611 ...	...	19 27 30.443	61 17 32.88	–	0.721	0.80	BL	17.5	–	1	1991 Jun
1940+504 ...	3C402	19 41 46.0	50 35 45	1.72	0.933	–	G	14.0	0.0239	2	...
1943+546 ...	OV 573	19 44 31.514	54 48 07.07	1.20	0.850	0.50	G	17.7	0.263	2	1991 Jun
2007+777 ...	...	20 05 30.999	77 52 43.25	0.82	1.279	1.10	BL	16.5	0.342	9	10
2010+723 ...	4C72.28	20 09 52.302	72 29 19.35	1.08	0.917	0.75	BL	19.0	–	1	(1991 Jun*)
2104+763 ...	3C427.1	21 04 07.5	76 33 07	1.93	0.997	0.37	G	21.1	0.572	3	...
2207+374 ...	4C37.65	22 09 21.424	37 42 18.23	1.23	0.791	0.48	Q	18.5	1.493	1	1991 Sep
2214+350 ...	OY 324	22 16 20.011	35 18 14.18	0.74	0.824	0.56	Q	18.0	0.510	2	1991 Jun
2229+695 ...	...	22 30 36.468	69 46 28.07	0.62	0.812	0.80	G	19.6	–	1	1991 Jun
2253+417 ...	OY 489	22 55 36.708	42 02 52.54	1.17	0.990	1.00	Q	18.8	1.476	2	1991 Jun
2255+416 ...	4C41.45	22 57 22.072	41 54 16.52	1.42	0.993	0.62	Q	20.9	1.724	1	1991 Jun
2311+469 ...	4C46.47	23 13 48.1	47 12 16	1.11	0.726	0.43	Q	17.9	0.742	1	(1991 Jun*)
2323+435 ...	OZ 438	23 25 42.3	43 46 58	1.35	1.01	0.58	G	18.0	0.145	2	17
2324+405 ...	3C462	23 26 55.9	40 48 09	1.51	1.12	0.57	G	19.9	0.394	2	(1990 Sep)

NOTES.—Table 1 is published in computer-readable form in the AAS CD-ROM Series, Vol. 4.

Col. (1): Source name according to IAU convention. Col. (2): Alternative source name. Cols. (3)–(4): J2000.0 right ascension and declination. Positions specified with a precision of 0.″01 are from the Jodrell Bank–VLA Astrometric Survey (Patnaik et al. 1992, Tables 2 and 4; and unpublished observations); the remaining positions have been compiled from a variety of publications via the NASA Extragalactic Database (NED). Cols. (5)–(7): Total flux density (Jy) at λ-11, 6, and 2.8 cm (Pauliny-Toth et al. 1978; Kühr et al. 1981). Col. (8): Optical identification: BL, BL Lac object; EF, empty field; G, galaxy; Q, quasar; SO, stellar object. Col. (9): Visual magnitude. Col. (10): Redshift; "–" indicates a featureless spectrum. Col. (11): Reference for optical identification, magnitude, and redshift. Col. (12): Date of λ-18 cm VLBI observation or reference to published observation. Parentheses indicate that the source was observed but was not mapped; in three cases (marked with an asterisk) this is because the a priori position assumed for correlations was wrong, while in the other cases the source was too heavily resolved. An ellipsis indicates that the source was not observed because it does not contain a compact component strong enough for detection with Mark-II VLBI.

REFERENCES.—(1) Xu et al. 1994; (2) Stickel & Kühr 1994; (3) Stickel, Meisenheimer, & Kühr 1994; (4) Spinrad et al. 1985; (5) Browne et al. 1993; (6) Henstock, Browne, & Wilkinson 1995; (7) Jackson 1989; (8) Palomar Observatory Sky Survey; (9) Hewitt & Burbidge 1993; (10) Eckart et al. 1987; (11) Sanghera 1992; (12) Fanti et al. 1985; (13) Dallacasa et al. 1994; (14) Foulsham 1989; (15) Jones et al. 1986; (16) Dallacasa et al. 1990; (17) Sanghera 1989; (18) Lawrence et al. 1995.

sions. The observations of the 25 sources in the remaining λ-18 cm session are discussed in the accompanying Paper II (Thakkar et al. 1995). The λ-6 cm results will be presented in Paper III (Xu et al. 1995).

3. OBSERVATIONS

3.1. *Snapshot Method*

The images obtained in the PR survey have a typical resolution of 1–2 mas and a dynamic range (defined as the ratio of the peak brightness to the rms noise in an area of blank sky) between 50:1 and 300:1. To achieve our astronomical goals the CJ1 images at the two wavelengths had to be of comparable or better quality. However a project as large as the CJ1 survey would be impractical with the long track observations used by PR. It would require ~1600 hr of observing time and, given the limited amount of time available to VLBI networks, would take at least 8 years to complete. In view of the large number of telescopes that now regularly take part in VLBI observations we decided instead to use a "snapshot" observing scheme.

We carried out a series of tests and simulations to determine the optimum combination of scans required to achieve our observational goals with an array of 12–16 telescopes (see our Appendix; Polatidis 1993). We found that with three 20 minute scans, sources of rather greater complexity than those in PR's maps could reliably be mapped with a dynamic range greater than 100:1. Although a larger number of shorter scans would provide more uniform u, v coverage, and hence even better images, the loss of data each time the telescopes slew from source to source would decrease the number of data points severely. Because of this reduction in observing efficiency our actual observations were made with scans of 30 minutes each. This provided us with at least 20 minutes of data for most scans, and at least a few minutes of data even from scans where a telescope has to unwind completely in azimuth.

TABLE 2

SOURCES FROM THE PR SAMPLE OBSERVED AT λ = 18 CENTIMETERS

Source (1)	Other (2)	R.A. (3)	Declination (4)	S_{11cm} (5)	S_{6cm} (6)	$S_{2.8cm}$ (7)	ID (8)	V (9)	z (10)	Ref (11)	λ18 cm VLBI (12)
0108+388 ...	OC 314	01 11 37.319	39 06 28.09	1.00	1.35	0.86	G	22	0.6703	18	1990 Sep
0133+476 ...	OC 457	01 36 58.595	47 51 29.10	2.19	3.26	...	Q	19	0.859	18	1990 Sep
0404+768 ...	4C 76.03	04 10 45.0	76 56 47	4.00	2.79	1.80	G	22	0.5985	18	1990 Sep
0538+498 ...	3C 147	05 42 36.1	49 51 07	13.0	8.18	4.14	Q	17.8	0.545	18	1990 Sep
0711+356 ...	OI 318	07 14 24.818	35 34 39.79	1.83	1.51	0.97	Q	17	1.620	18	1991 Jun
0723+679 ...	3C 179	07 28 10.9	67 48 48	1.58	1.31	0.98	Q	18.0	0.8436	18	1990 Sep
0804+499 ...	OJ 508	08 08 39.667	49 50 36.53	1.53	2.07	1.62	Q	17.5	1.4321	18	1990 Sep
0814+425 ...	OJ 427	08 18 16.000	42 22 45.41	2.21	1.68	2.47	BL	17.7	0.2453	18	1990 Sep
0831+557 ...	4C 55.16	08 34 54.903	55 34 21.09	7.45	5.60	2.82	G	17.5	0.2404	18	1990 Sep
0850+581 ...	4C 58.17	08 54 41.996	57 57 29.92	0.87	1.41	1.55	Q	18	1.322	18	1991 Jun
0859+470 ...	4C 47.29	09 03 03.990	46 51 04.14	1.87	1.78	1.47	Q	18.7	1.462	18	1990 Sep
0906+430 ...	3C 216	09 09 33.5	42 53 46	2.39	1.78	1.41	Q	18.5	0.670	18	1990 Sep
0923+392 ...	4C 39.25	09 27 03.014	39 02 20.85	4.82	8.90	12.2	Q	17.9	0.699	18	1991 Jun
0945+408 ...	4C 40.24	09 48 55.339	40 39 14.58	1.26	1.39	1.29	Q	17.5	1.252	18	1991 Jun
1458+718 ...	3C 309.1	14 59 07.6	71 40 20	5.04	3.34	1.96	Q	16.8	0.9021	18	1990 Sep
1624+416 ...	4C 41.32	16 25 57.670	41 34 40.63	1.58	1.31	1.14	Q	22	2.550	18	1990 Sep
1633+382 ...	4C 38.41	16 35 15.493	38 08 04.50	2.50	4.08	6.03	Q	18	1.807	18	1990 Sep
1637+574 ...	OS 562	16 38 13.457	57 20 23.98	0.98	1.44	1.73	Q	17	0.7487	18	1990 Sep
1642+690 ...	4C 69.21	16 42 07.849	68 56 39.76	1.42	1.43	1.90	Q	19.2	0.751	18	1990 Sep
1652+398 ...	4C 39.49	16 53 52.217	39 45 36.61	1.44	1.42	1.19	G	13.8	0.0328	18	1990 Sep
1739+522 ...	4C 51.37	17 40 36.978	52 11 43.40	1.93	1.99	1.37	Q	18.5	1.381	18	1990 Sep
1749+701 ...	...	17 48 32.841	70 05 50.77	1.89	1.09	1.39	BL	17.0	0.7699	18	1991 Nov
1807+698 ...	3C 371	18 06 50.681	69 49 28.11	2.21	2.33	1.81	G	14.2	0.050	18	1990 Sep
1823+568 ...	4C 56.27	18 24 07.069	56 51 01.49	1.51	1.67	2.28	BL	18.4	0.6634	18	1990 Sep
1845+797 ...	3C 390.3	18 42 08.9	79 46 18	6.61	4.32	2.02	G	15	0.0569	18	1990 Sep
1954+513 ...	OV 591	19 55 42.739	51 31 48.55	1.57	1.43	1.33	Q	18.5	1.2230	18	1990 Sep
2021+614 ...	OW 637	20 22 06.682	61 36 58.81	2.17	2.31	1.95	G	19.5	0.228	18	1990 Sep
2200+420 ...	BL Lac	22 02 43.292	42 16 39.98	5.15	4.75	5.82	BL	14.5	0.0688	18	1990 Sep
2342+821 ...	...	23 44 03.7	82 26 40	2.30	1.30	0.65	Q	20.5	0.7344	18	1990 Sep
2351+456 ...	4C 45.51	23 54 21.678	45 53 04.24	1.48	1.41	1.04	Q	20.6	1.9864	18	1990 Sep
2352+495 ...	OZ 488	23 55 09.459	49 50 08.34	2.18	1.77	1.12	G	19.7	0.2383	18	1990 Sep

NOTES.—Table 2 is published in computer-readable form in the AAS CD-ROM Series, Vol. 4.

Col. (1): Source name according to IAU convention. Col. (2): Alternative source name. Cols. (3)–(4): J2000.0 right ascension and declination. Positions specified with a precision of 0.01 are from the Jodrell Bank–VLA Astrometric Survey (Patnaik et al. 1992, Tables 2 and 4; and unpublished observations); the remaining positions have been compiled from a variety of publications via the NASA Extragalactic Database (NED). Cols. (5)–(7): Total flux density (Jy) and λ-11, 6, at 2.8 cm (Pauliny-Toth et al. 1978; Kühr et al. 1981). Col. (8): Optical identification: BL, BL Lac object; G, galaxy; Q, quasar; SO, stellar object. Col. (9): Visual magnitude. Col. (10): Redshift. Col. (11): Reference for optical identification, magnitude, and redshift. Col. (12): Date of λ-18 cm VLBI observation.

REFERENCE.—(18) Lawrence et al. 1995.

To maximize the u, v coverage we tried to schedule three scans as widely spaced as possible within the mutual visibility "window" during which the source could be seen by all the antennas. For some low-declination sources ($\delta \approx 35°$–$37°$) the mutual visibility window was quite short ($\approx$4 hr) and the resulting u, v coverage contains significant gaps, although the image quality is still adequate for our purposes (see Fig. 1). The source changes were optimized to provide the shortest slewing time between sources in order to avoid significant data loss from some of the slower telescopes. The equatorially mounted telescopes in the array, WSRT and Green Bank, posed additional constraints in scheduling. In the case of WSRT, where the hour angle coverage is limited to ±6 hr from the meridian, we inevitably scheduled a few scans when the source could not be observed, but this did not affect the image quality significantly.

3.2. *λ-18 Centimeter Observations*

The λ-18 cm VLBI observations for the CJ1 survey were completed in four observing sessions. Here we present the observations of 87 sources taken in 1990 September, in 1991 June, and in 1991 November; the observations of the remaining 25 objects taken in 1991 September are presented in Paper II (Thakkar et al. 1995). All available telescopes of the European (EVN) and the US (USVN) VLBI networks, including the partly completed VLBA (Napier et al. 1994), were scheduled to participate.[2] In addition, telescopes in the Soviet Union participated in some of the observations.

The data were recorded using the NRAO Mark II system with an effective bandwidth of 1.8 MHz centered at 1.665 GHz. Left circular polarization (LCP) (IEEE convention) was recorded. All telescopes of the EVN and the USVN were

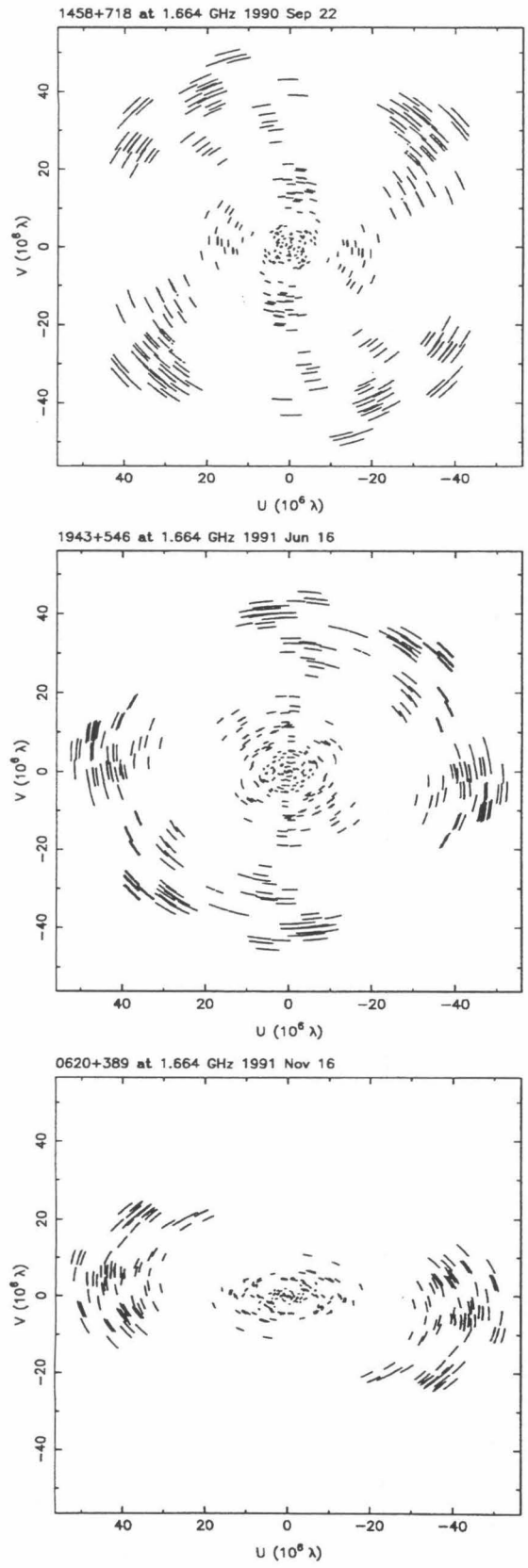

FIG. 1.—Examples of the sampling of the projected-baseline (u, v) plane obtained in the snapshot observations at declinations 71°, 54°, and 38°.

equipped with hydrogen masers as frequency and timing standards, and rubidium atomic clocks were used at the telescopes of the Soviet Union.

In 1990 September, 13 telescopes were scheduled to observe 37 sources in a 60 hr observing session. Useful data were obtained from 12 telescopes for most of the observing session. In 1991 June, 17 telescopes took part in the 42 hr observations of 27 sources. In 1991 November, 13 telescopes participated successfully and 23 sources were observed in a 41 hour session. The participating telescopes and their characteristics are listed in Table 3. Examples of the u, v coverage obtained are shown in Figure 1.

3.3. *Correlation and Fringe Fitting*

The data were correlated with the JPL/Caltech Block II correlator which enabled us to process nearly all the observations in a single correlation pass. The output of the correlator is an estimate of complex fringe visibility sampled at intervals of 2 s on each baseline, at four frequencies within the 2 MHz band, with the phase referenced to an *a priori* model of the source position, antenna locations, and atmosphere. Before the data can be averaged over the full bandwidth and longer time-intervals, the residual phase gradients in time and frequency due to delay and rate errors in the *a priori* model must be estimated and removed. This is the process of "fringe fitting." Fringe fitting was performed using the NRAO Astronomical Image Processing System (AIPS) task FRING, an implementation of the Schwab & Cotton (1983) algorithm. A solution interval of 5 minutes—comparable with the coherence time—and a point-source model were used. The "reference telescope" was chosen to be Effelsberg whenever possible, otherwise the Green Bank telescope was used. After correction of the delays and rates found by FRING, the visibilities were coherently averaged across the observing band, and then the phases were self-calibrated using a point-source model with a solution interval of 10 s, using the program DIFMAP in the Caltech VLBI package (Pearson 1991; Shepherd, Pearson, & Taylor 1994). In the 1991 June observing session, the coherence time was much shorter than in the other sessions, apparently as a result of ionospheric scintillation. For this session it was found that a shorter self-calibration interval of 2 s improved the signal-to-noise ratio for sources with more than 350 mJy in a compact component.

For the three sources 1138+594, 2010+723, and 2311+469, we were unable to find fringes on all baselines. This was due to large errors ($\geq 10''$) in the *a priori* source positions used for the correlator model. We were thus unable to map these three sources. Three other sources, 0010+775, 0945+664, and 2324+405, were heavily resolved and were detected only on

[2] The VLBA, the VLA, and the 140 foot (43 m) Green Bank telescope are instruments of the National Radio Astronomy Observatory, which is operated by Associated Universities, Inc., under cooperative agreement with the National Science Foundation.

TABLE 3

TELESCOPE CHARACTERISTICS

Telescope	Code	Location	Diam (m)	1990 Sep	1991 Jun	1991 Nov	T_{sys} (K)	T_{sys} (Jy)	Sensitivity (K/Jy)
Onsala	S	Sweden	25		√		32	348	0.093
Effelsberg	B	Germany	100	√	√	√	54[a]	36	1.5[a]
WSRT	W	Netherlands	5×25			√	58	125	0.46
Lovell	J	Jodrell Bank, UK	76	√	√	√	38	44	0.86
Medicina	L	Bologna, Italy	32	√	√	√	53	530	0.1
Simeiz	R	Crimea, USSR	22	√	√	√	104	1155	0.09
Evpatoria	Ev	Crimea, USSR	70		√		100	143	0.7
Pushchino	Pu	Moscow, USSR	22		√		450	5000	0.09
Bear Lake	Bl	Moscow, USSR	64		√		89	118	0.75
NRAO	G	Green Bank, WV, USA	43	√	√	√	21	70	0.3
Haystack	K	Westford, MA, USA	36	√	√		96	1116	0.086
VLBA_PT	PT	Pie Town, NM, USA	25	√	√	√	31	321	0.097
VLBA_KP	KP	Kitt Peak, AZ, USA	25	√	√	√	33	334	0.099
VLBA_LA	LA	Los Alamos, NM, USA	25	√	√	√	31	295	0.104
VLBA_NL	NL	North Liberty, IA, USA	25		√	√	32	366	0.088
VLA[b]	Y	Socorro, NM, USA	25	√	√	√	34	378	0.089
OVRO	O	Owens Valley, CA, USA	40	√	√	√	53	254	0.21

[a] Estimate only; actual performance quoted in janskys.

[b] the VLA was used in single antenna mode.

Cols. (1)–(3): The name, the code used and the location of each telescope. Affiliations: S: Onsala Space Observatory; B: Max-Planck-Institüt für Radioastronomie; W: Westerbork Synthesis Radio Telescope, NFRA; J Nuffield Radio Astronomy Laboratories; L: Istituto di Radioastronomia; R, Ev, Bl, Pu: IKI Moscow; G: National Radio Astronomy Observatory; K: Haystack Observatory; PT, KP,LA, FD, NL: National Radio Astronomy Observatory VLBA; Y: National Radio Astronomy Observatory VLA; O: Owens Valley Radio Observatory. Col. (4): The diameter of each telescope (in meters). Cols. (5)–(7): A tick indicates whether the telescope participated in that session. Cols. (8)–(10): The system temperature in kelvins and in janskys and the sensitivity in kelvins per jansky of each telescope. The values quoted are representative of the three sessions.

short baselines (less than ~500 km). We were able to make a low-resolution map of 0010+775 but were not able to make useful maps of the other two sources.

After fringe fitting and phase self-calibration the visibility data were first averaged coherently across the observing band and then averaged in time intervals of 60 s. The uncertainties of the averaged data were estimated from the scatter of the points within the averaging interval.

3.4. *Amplitude Calibration*

Calibration of the data was performed using the method described by Cohen et al. (1975). The calibration of the correlation coefficients was based on the peak telescope sensitivity and a normalized gain-elevation curve for each telescope. At λ-18 cm telescope gains are very weakly dependent on elevation so flat gain curves were adequate for most of the telescopes. The system temperature values supplied by each observatory were inspected and any obviously erroneous values, probably due to radio interference, were deleted. The Caltech program CAL was used to apply the amplitude calibration to the raw visibilities.

In practice the *a priori* amplitude calibration is rarely much better than ~5% and is often 10% in error, hence it is necessary to observe calibrator sources with known structures (but only slightly resolved) which are strong enough to be detected with high signal-to-noise ratio on all baselines. For our observations we used the sources 0552+398 and 1739+522 as calibrators. The observations of the calibrators were spread out over the entire time span of each session to monitor changing conditions in the array. Although neither calibrator is unresolved at λ-18 cm, their visibilities can be fitted by single Gaussians. The calibration source data were self-calibrated with the program DIFMAP using the Gaussian models; the gain of each telescope was allowed to vary by a single multiplicative factor for the complete run on the calibrator. DIFMAP produced a set of correction factors to be applied on a telescope-by-telescope basis in CAL.

FIG. 2.—The λ = 18 cm VLBI maps of 82 sources. For each source the top panel shows the naturally weighted, higher resolution map, and the bottom panel the tapered map. Logarithmic contour levels are used in all maps, drawn at $-2, -1, 1, 2, 4, 8, 16, \cdots 1024 \times 3\ \sigma$ (where σ is the rms noise measured in an empty region of the map). The FWHM contour of the elliptical Gaussian restoring beam is shown hatched in the lower left-hand corner. The peak flux density, rms noise, and parameters of the restoring beam are given in Table 4. The angular scale is marked in milliarcseconds and, where the source redshift is known, the linear scale of each map is indicated in the lower right-hand corner (assuming $H_0 = 100$ km s^{-1} Mpc^{-1} and $q_0 = 0.5$). Note that the field of view of the tapered map is usually larger than that of the uniformly weighted map. For 0010 + 775, which was heavily resolved, we present only a low-resolution map. FITS images corresponding to the maps presented in Fig. 2 are published in the AAS CD-ROM Series, Vol. 4.

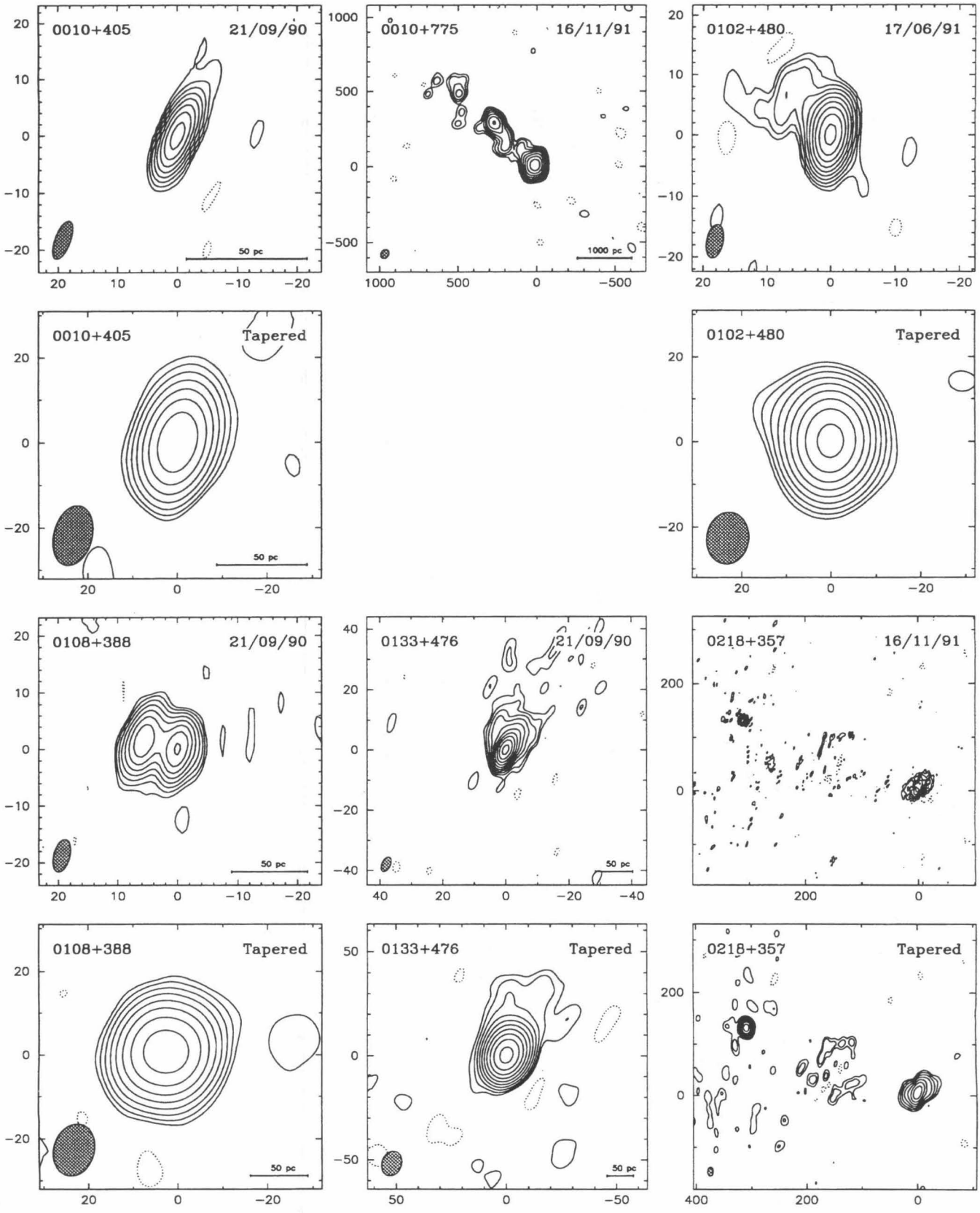
0010+405
21/09/90
50 pc
0010+775
16/11/91
1000 pc
0102+480
17/06/91
0010+405
Tapered
50 pc
0102+480
Tapered
0108+388
21/09/90
50 pc
0133+476
21/09/90
50 pc
0218+357
16/11/91
0108+388
Tapered
50 pc
0133+476
Tapered
50 pc
0218+357
Tapered

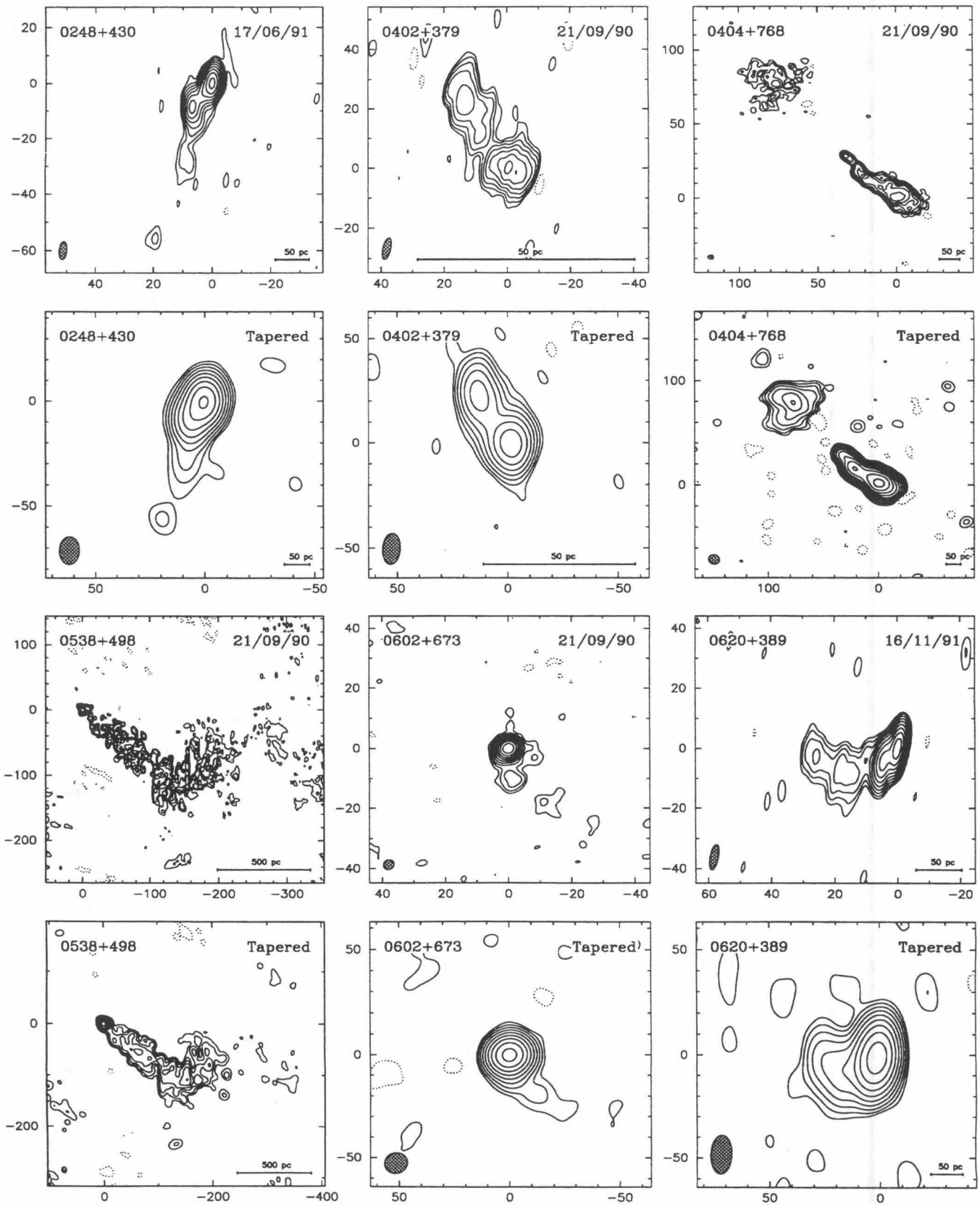

FIG. 2.—*Continued*

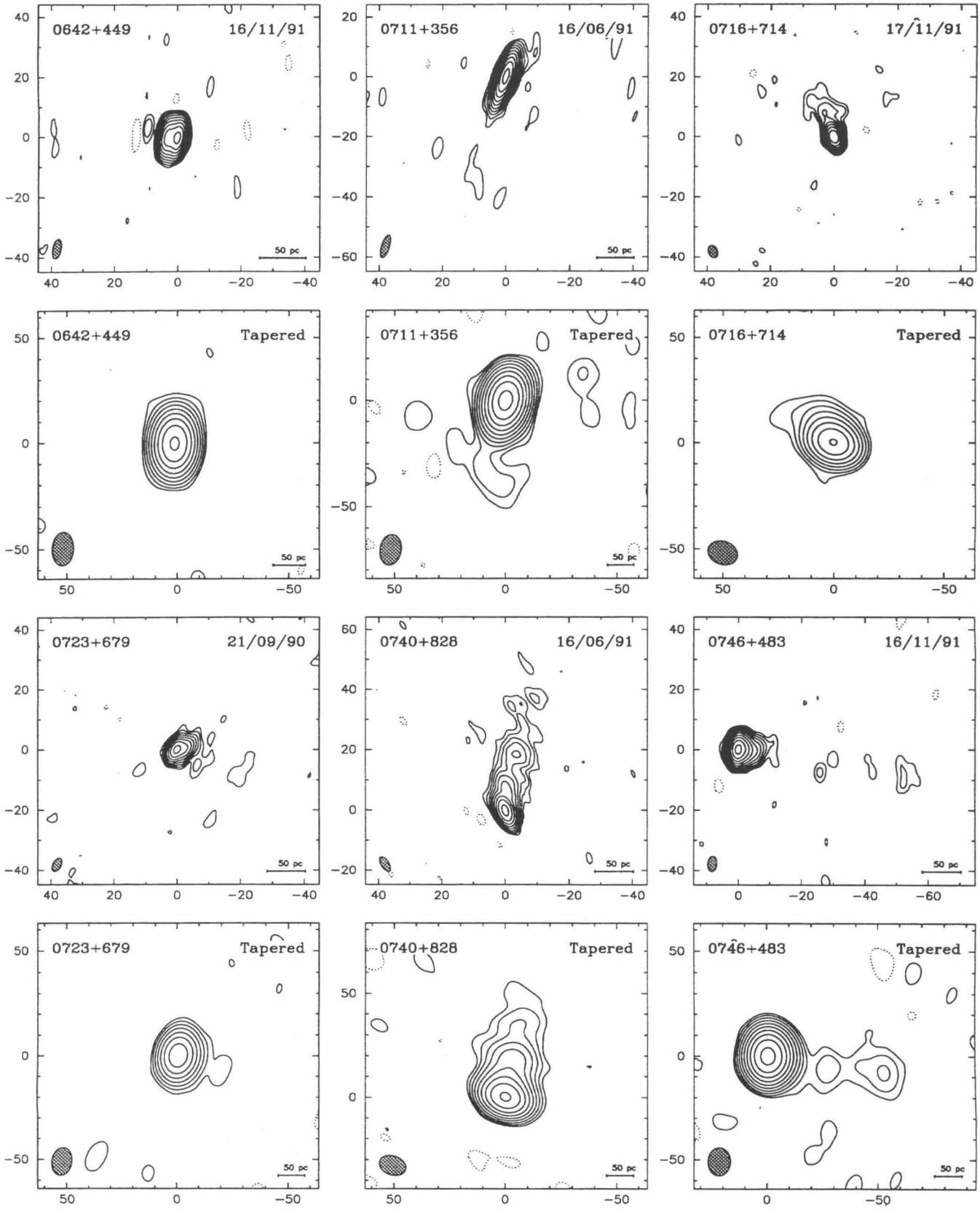

FIG. 2.—*Continued*

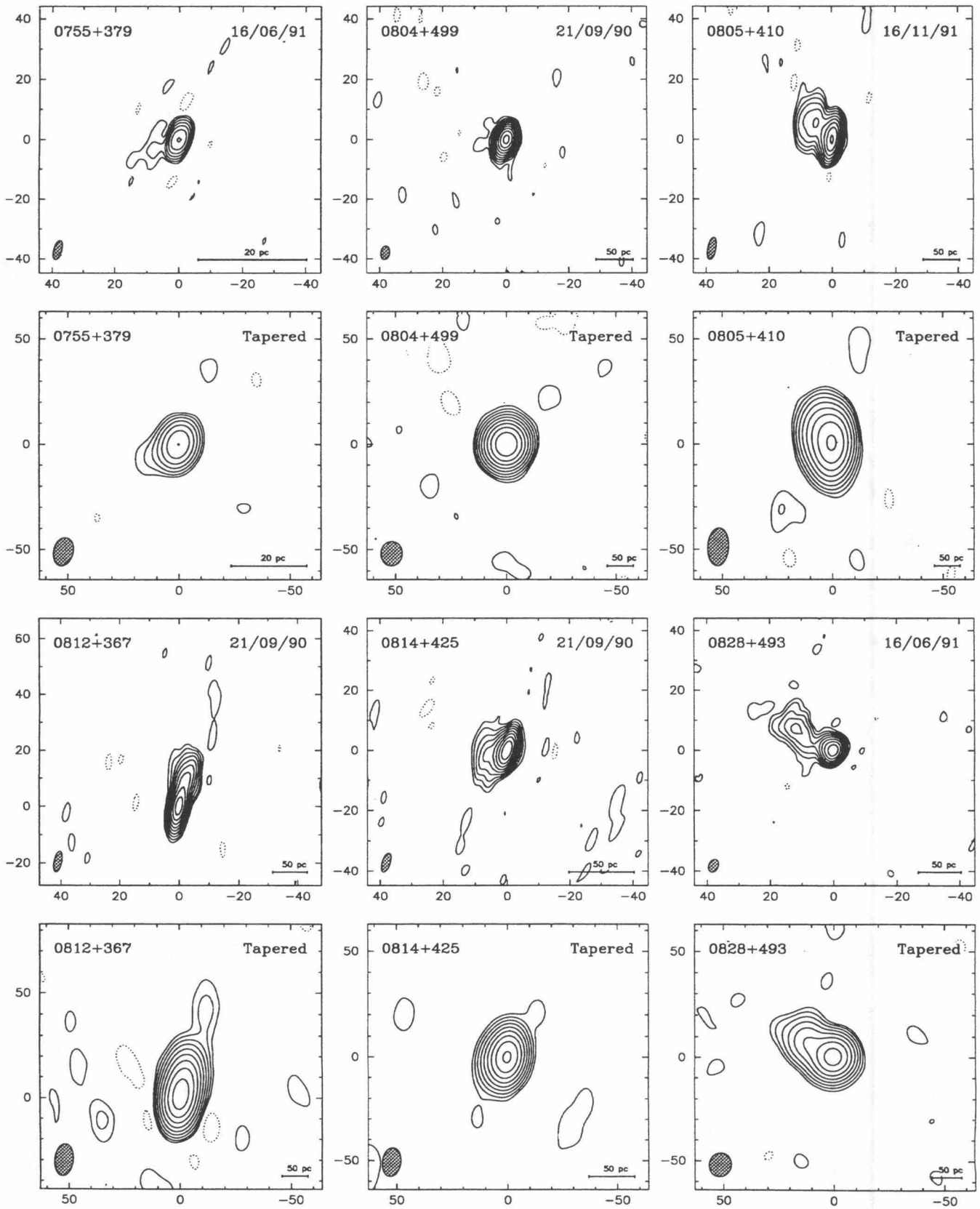

FIG. 2.—*Continued*

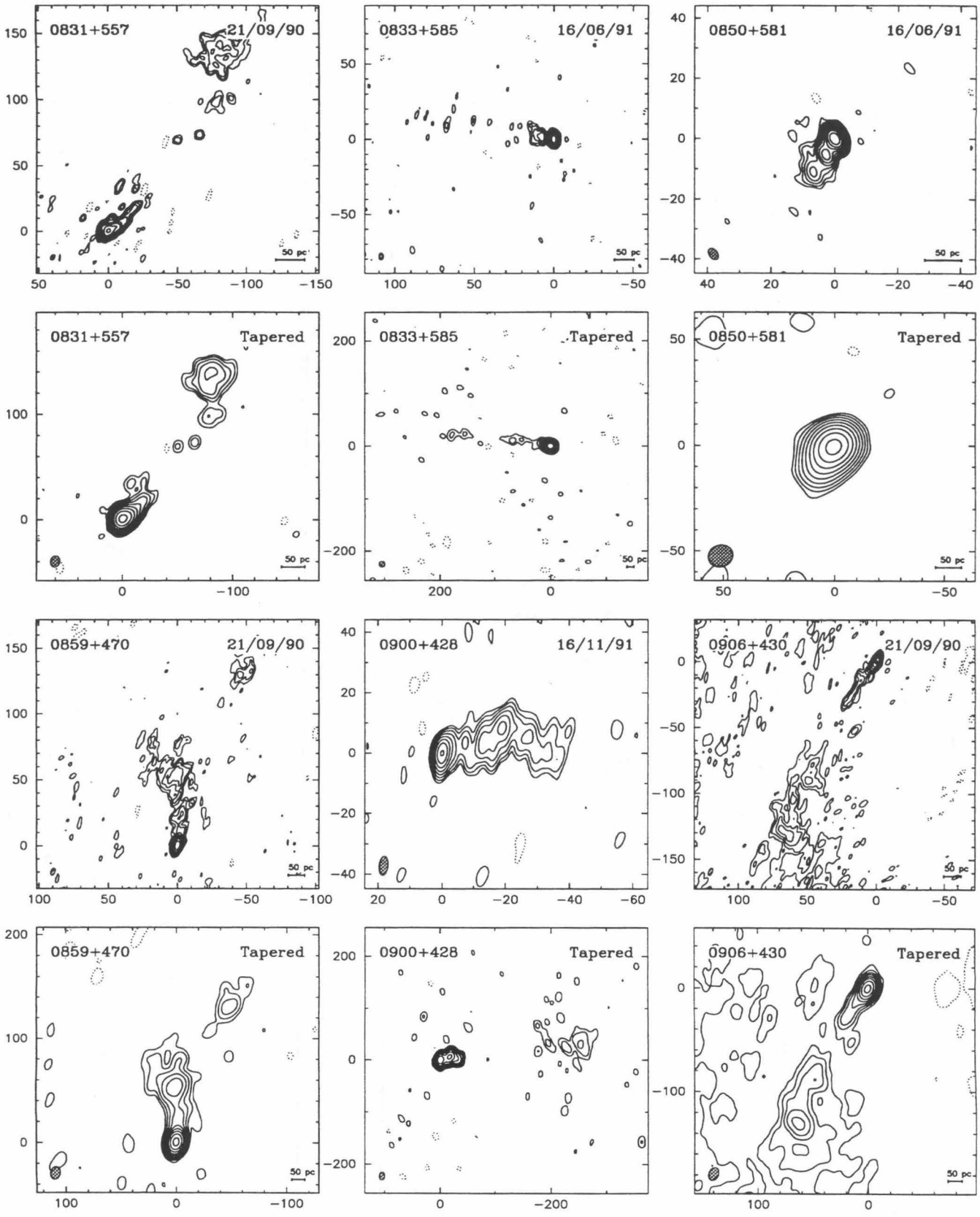

FIG. 2.—*Continued*

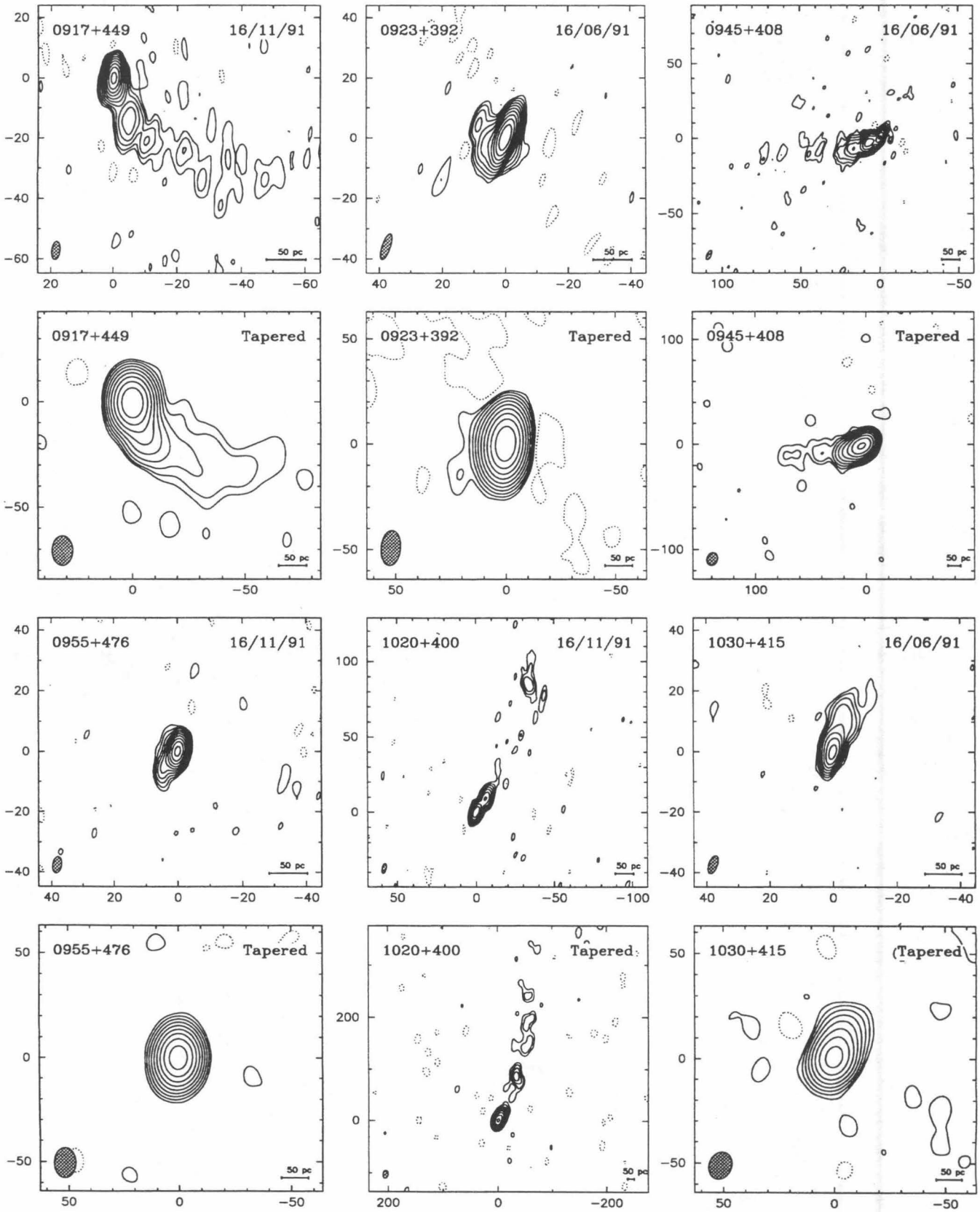

FIG. 2.—*Continued*

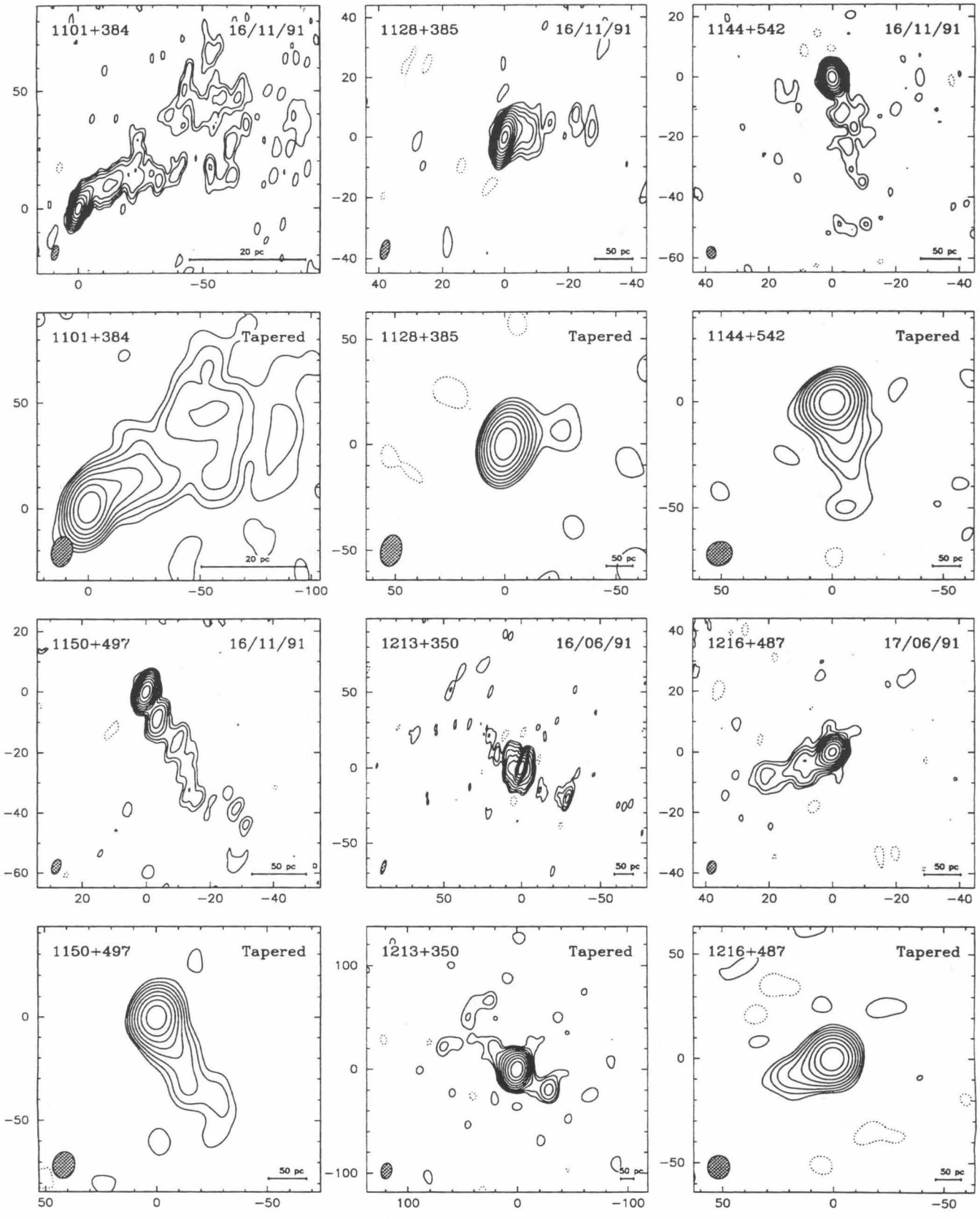

FIG. 2.—*Continued*

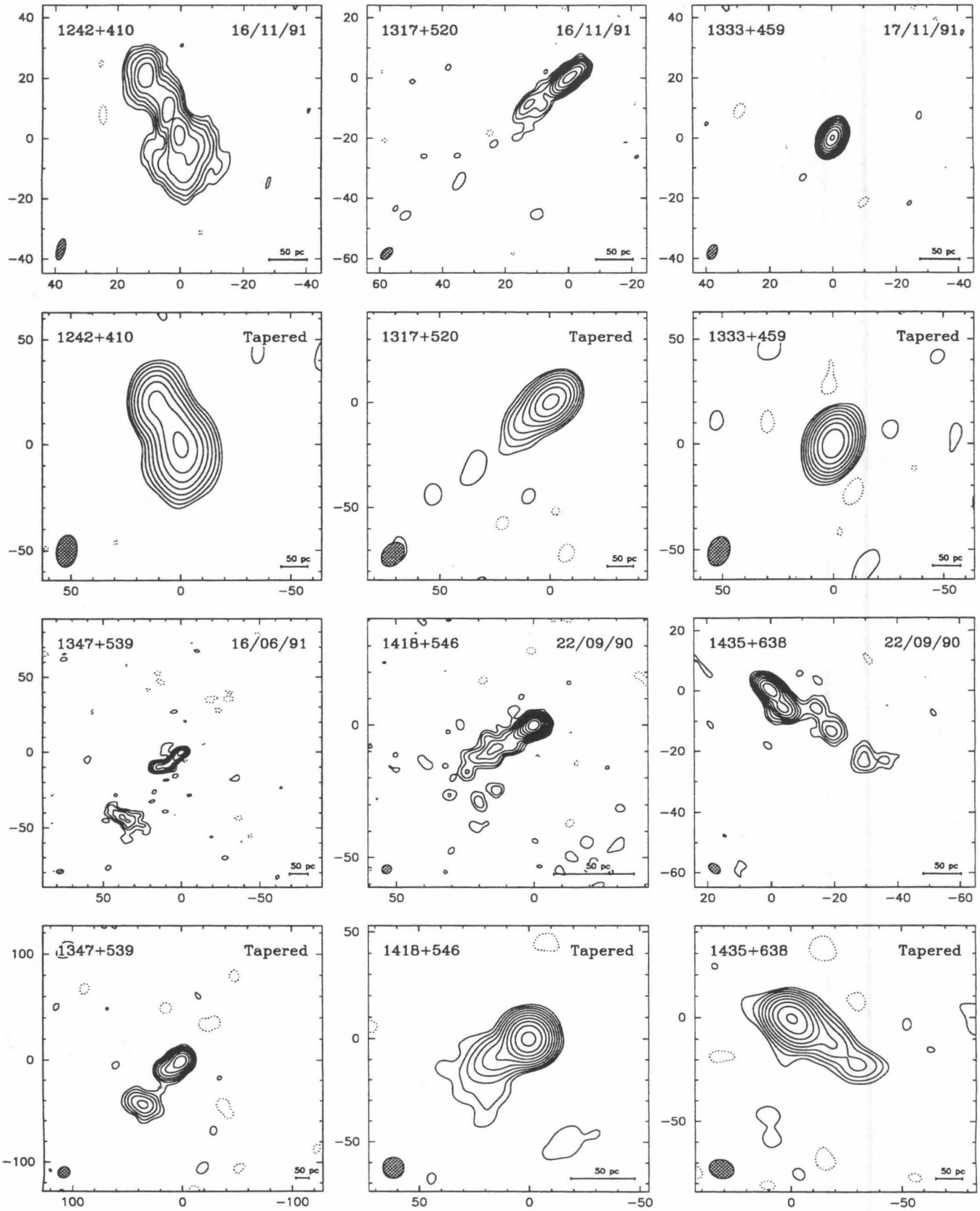

FIG. 2.—*Continued*

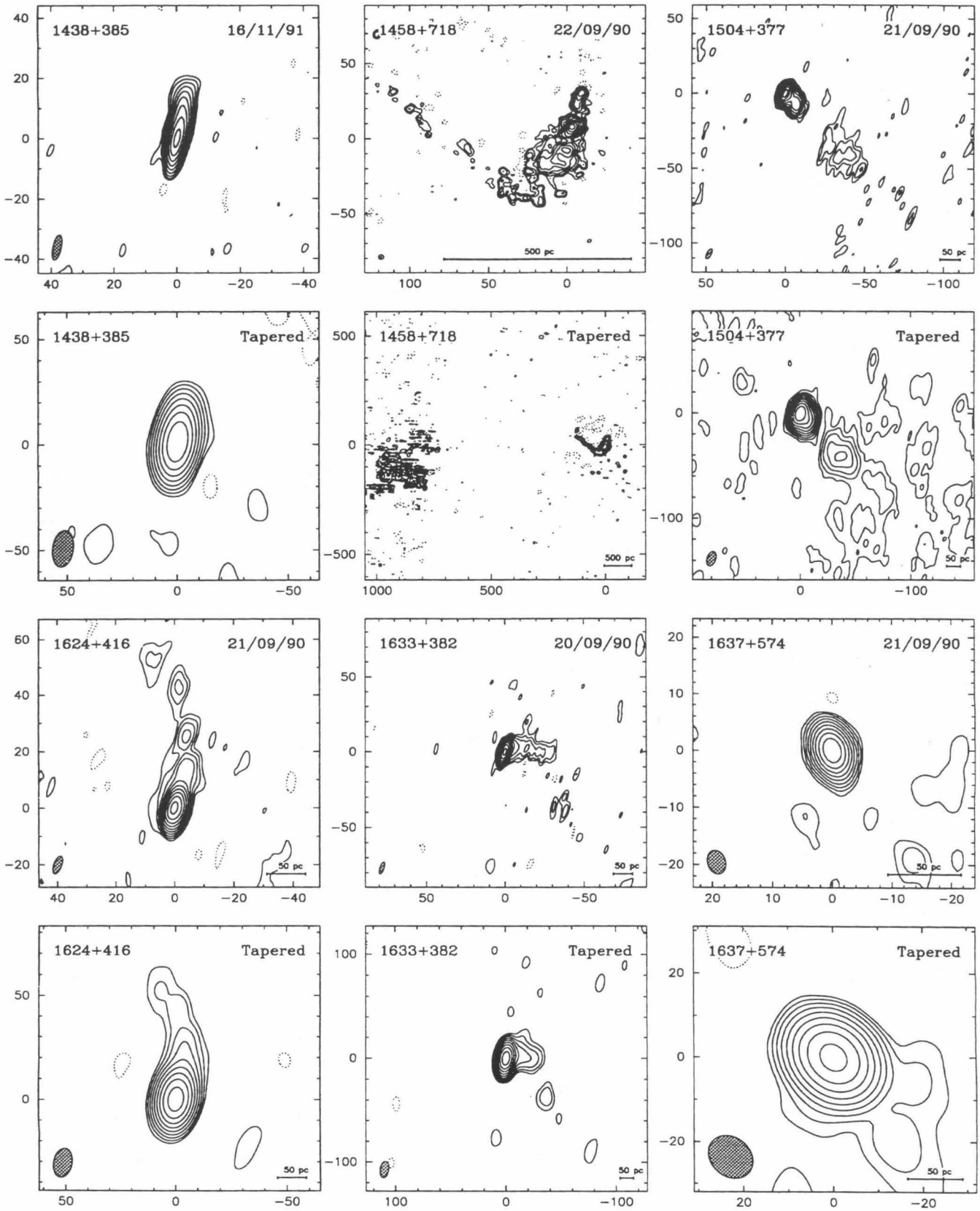

FIG. 2.—*Continued*

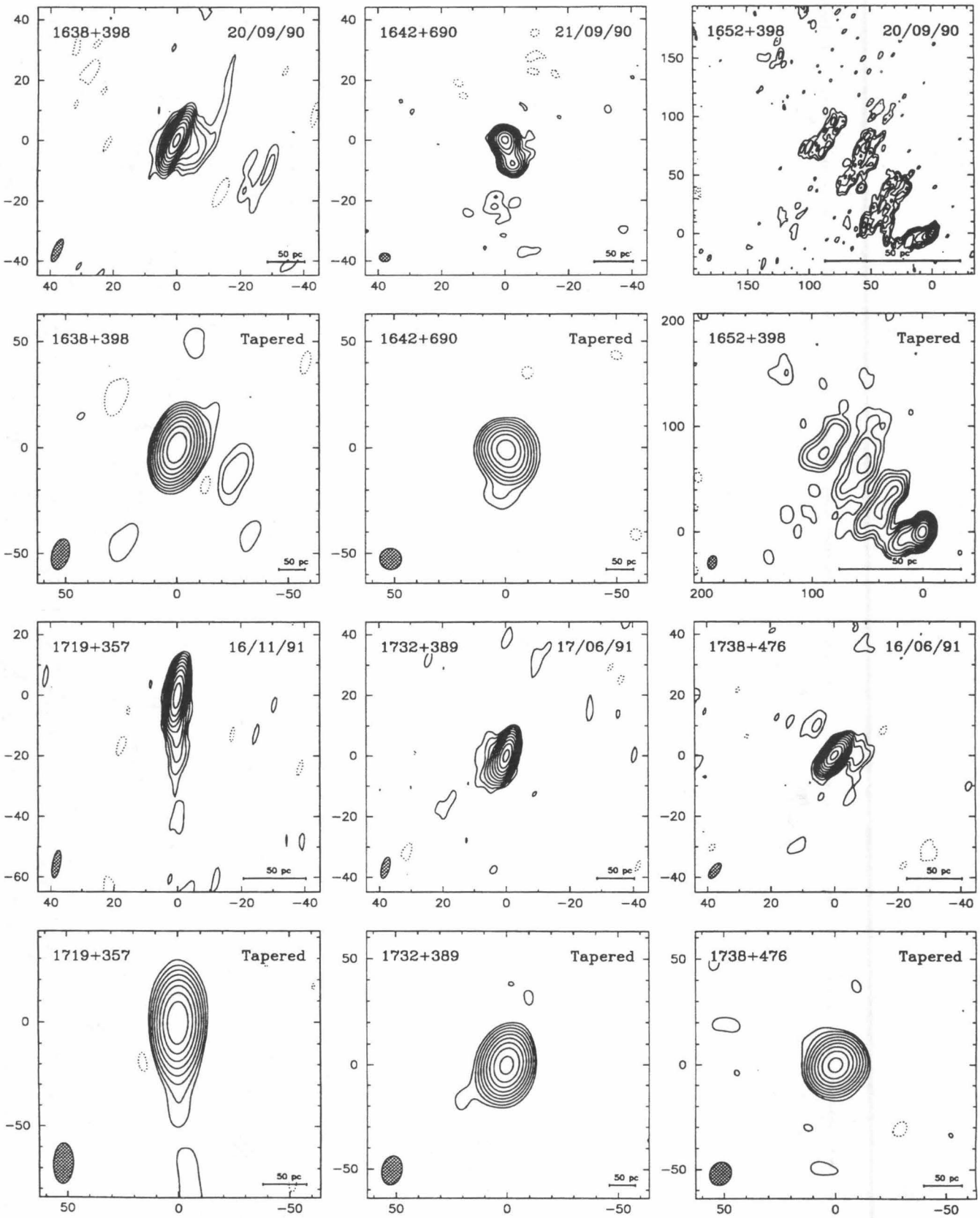

FIG. 2.—*Continued*

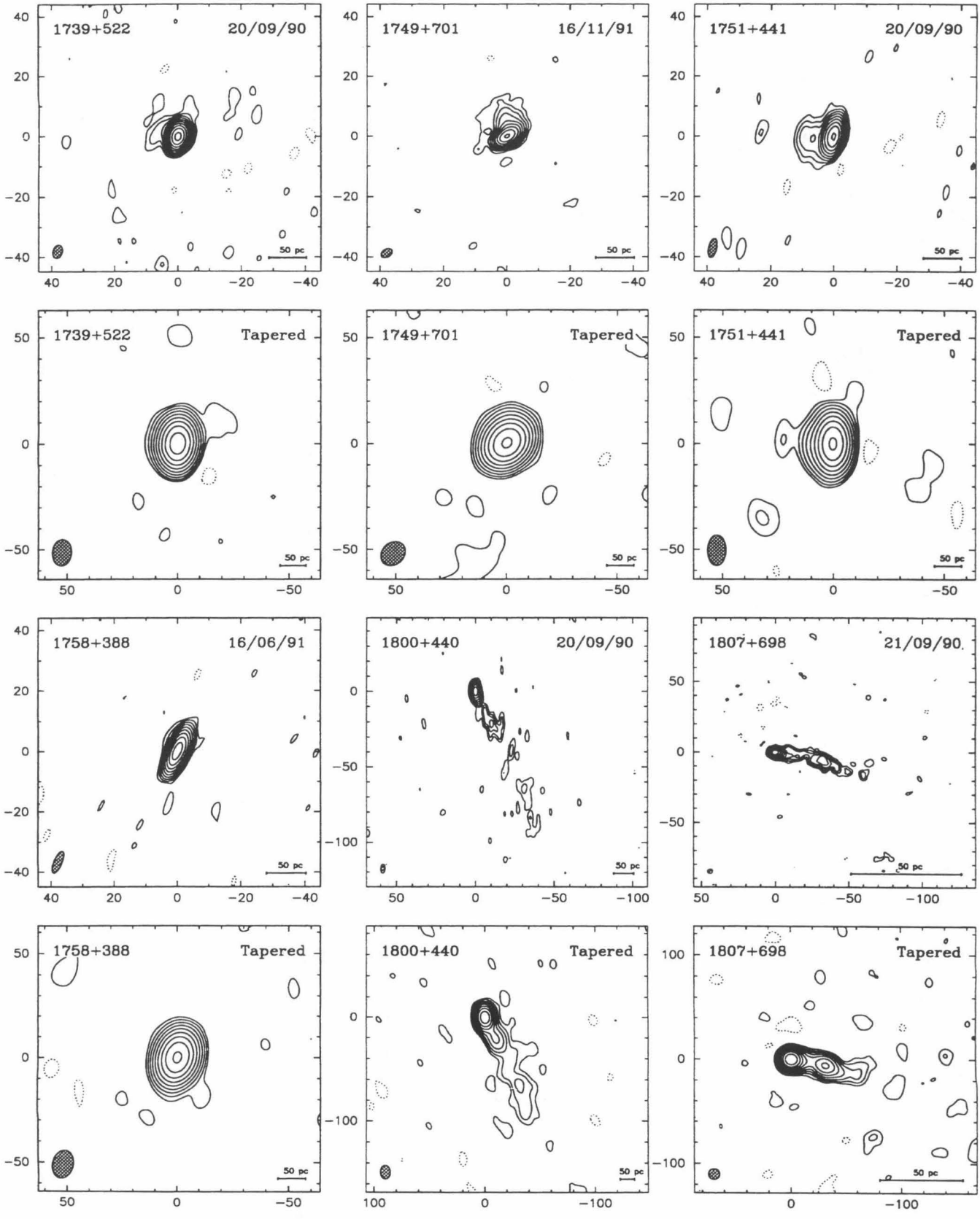

FIG. 2.—*Continued*

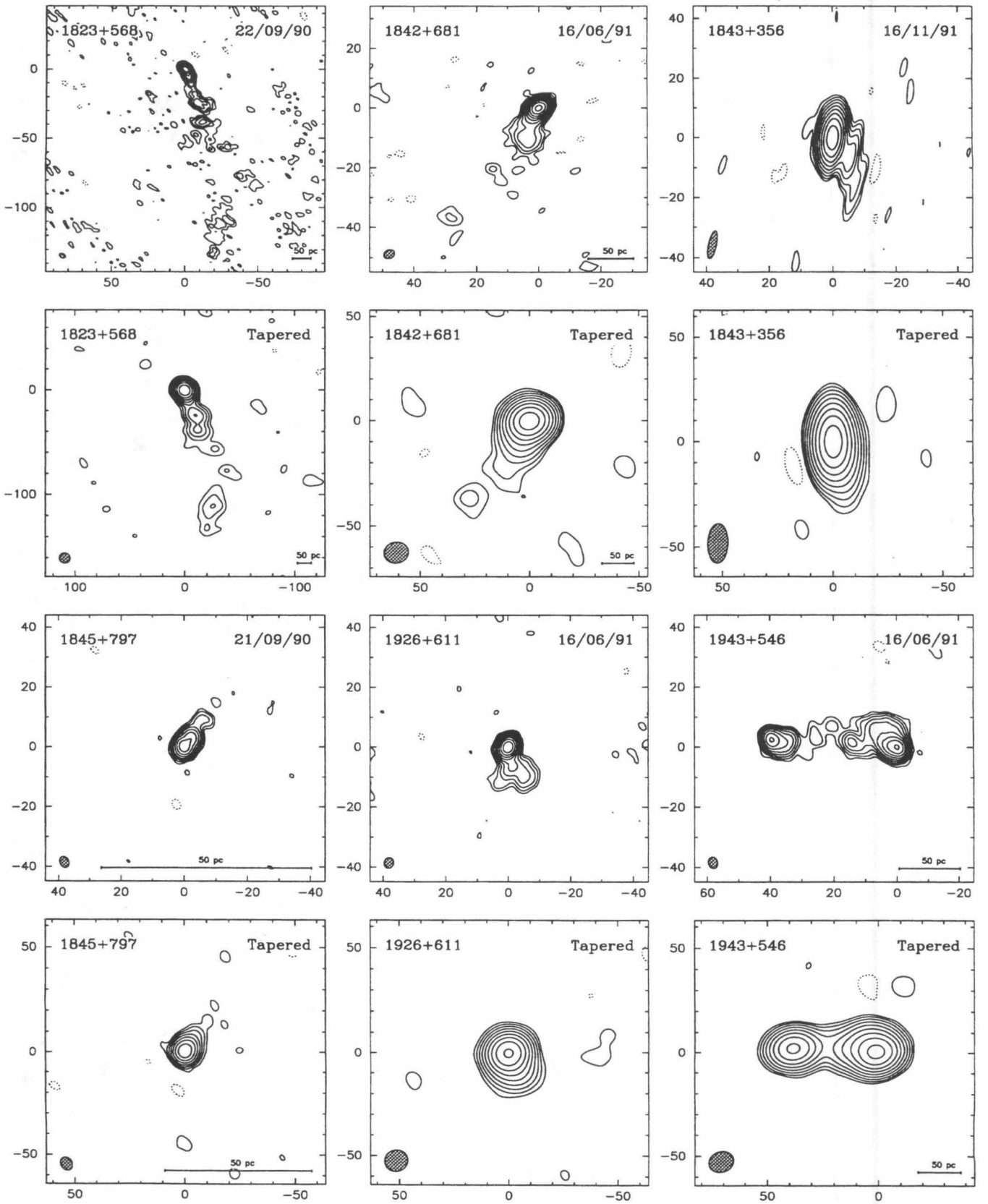

FIG. 2.—*Continued*

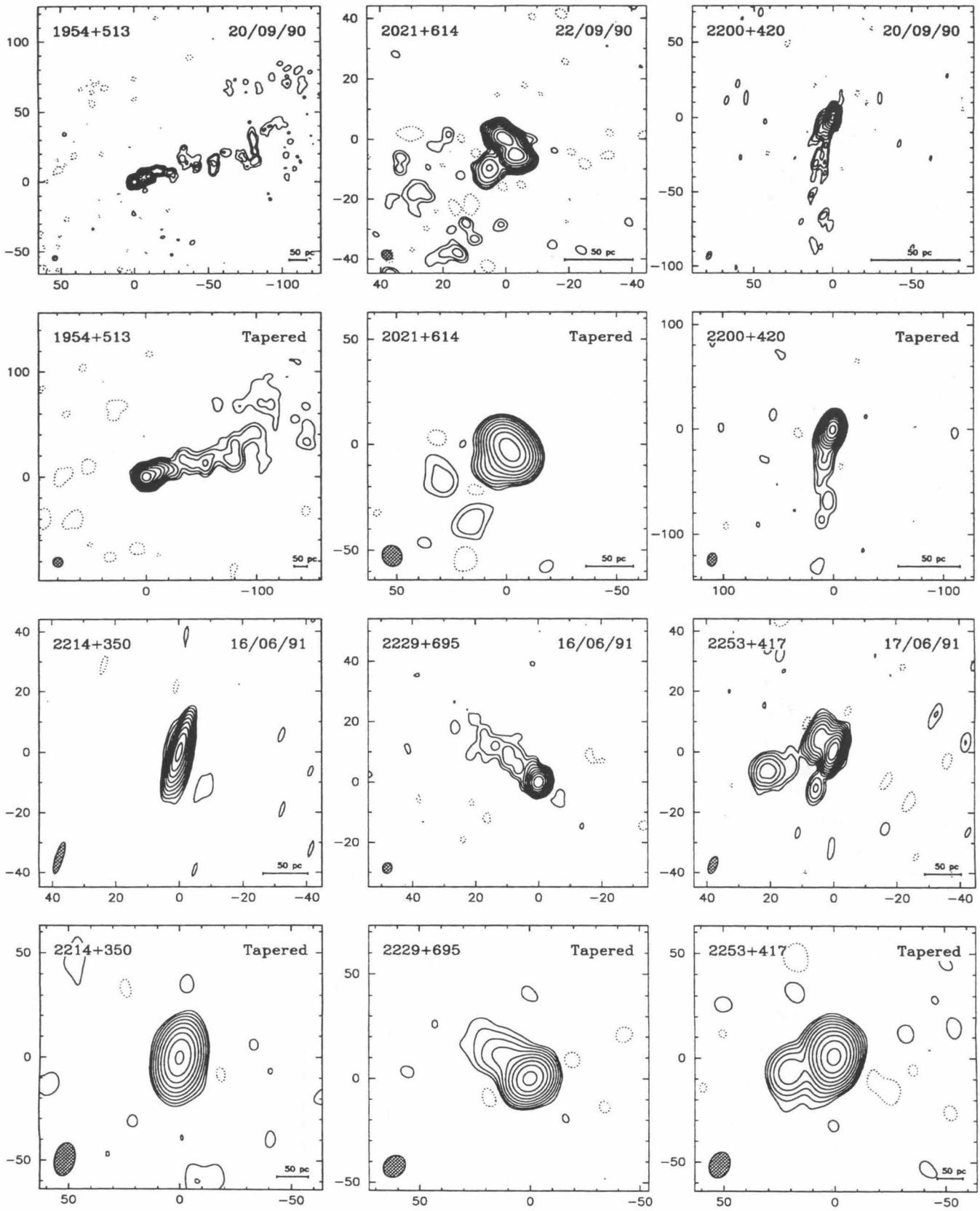

FIG. 2.—*Continued*

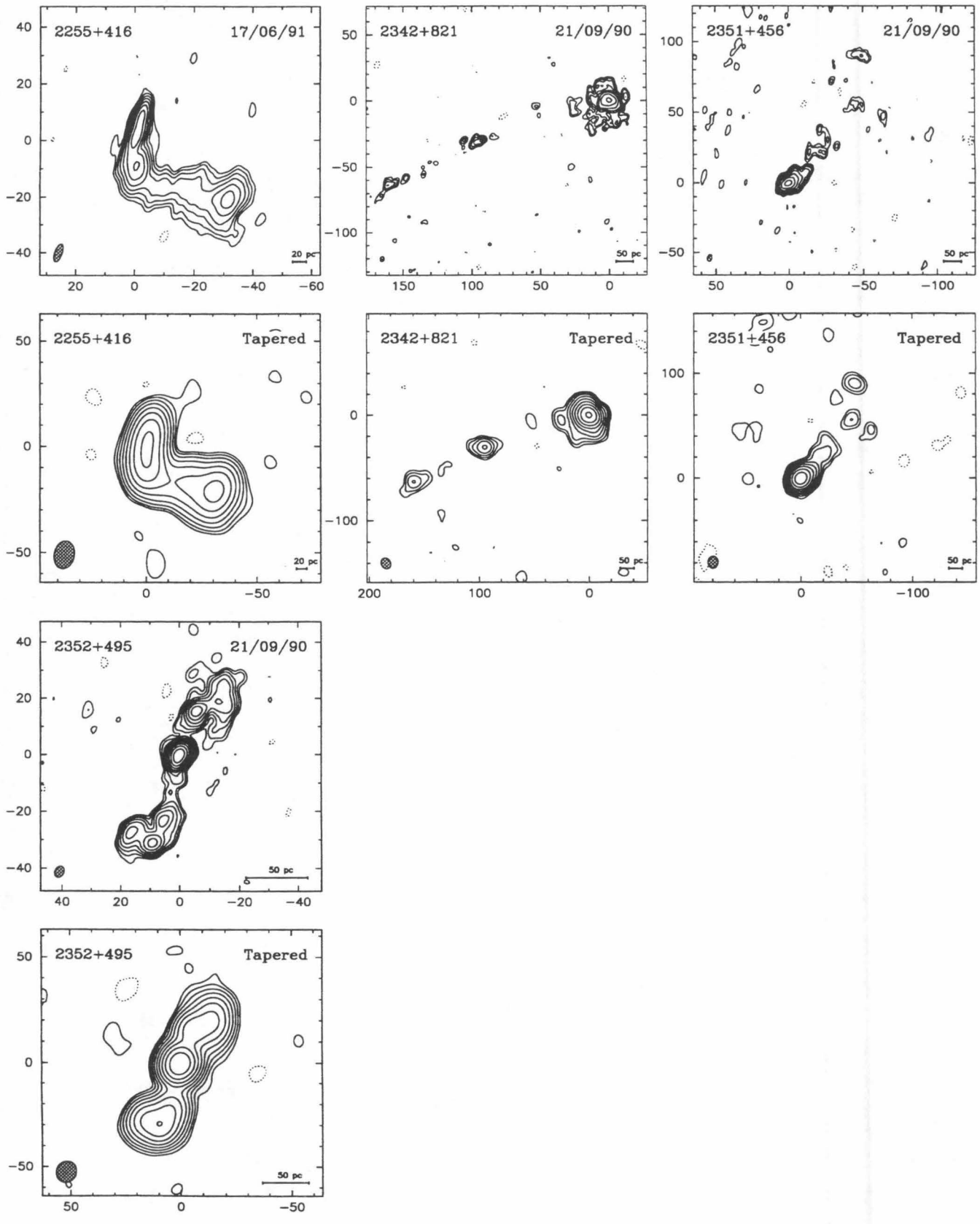

FIG. 2.—*Continued*

TABLE 4

MAP PARAMETERS

Name	Sample	Observation	Naturally Weighted Maps					Tapered Maps				
			Beam[a]			S_{peak}	rms	Beam[a]			S_{peak}	rms
			a (mas)	b (mas)	θ (°)	(mJy/beam)		a (mas)	b (mas)	θ (°)	(mJy/beam)	
0010+405...	CJ1	1990 Sep	7.10	2.56	−19	227	0.44	14.34	8.59	−13	243	0.65
0010+775...	CJ1	1991 Nov	64.50	49.19	−24	530	0.80					
0102+480...	CJ1	1991 Jun	5.60	2.55	−10	990	0.54	12.35	9.38	−5	1180	1.13
0108+388...	PR	1990 Sep	5.89	2.72	−13	249	0.59	12.59	9.08	−14	427	0.74
0133+476...	PR	1990 Sep	5.18	2.71	−24	1000	0.50	12.07	8.91	−16	1290	0.74
0218+357...	CJ1	1991 Nov	7.78	2.86	−15	79	0.35	17.21	9.67	−2	175	0.53
0248+430...	CJ1	1991 Jun	6.41	2.55	−6	593	0.57	13.04	9.12	−2	788	0.96
0402+379...	CJ1	1990 Sep	7.27	2.49	−13	165	0.68	14.63	7.96	−4	395	1.27
0404+768...	PR	1990 Sep	3.45	2.85	75	311	0.86	9.79	8.74	68	1220	0.69
0538+498...	PR	1990 Sep	4.78	2.76	−1	1070	1.40	11.10	8.90	11	2230	4.18
0602+673...	CJ1	1990 Sep	3.54	3.12	−49	479	0.35	10.48	9.86	−57	539	0.57
0620+389...	CJ1	1991 Nov	8.49	2.50	−11	390	0.30	18.62	9.40	−2	569	0.48
0642+449...	CJ1	1991 Nov	6.63	2.59	−10	268	0.25	15.92	9.58	−2	431	0.50
0711+356...	PR	1991 Jun	7.92	2.52	−16	1350	0.60	14.72	9.72	−8	1590	0.93
0716+714...	CJ1	1991 Nov	4.28	2.79	19	198	0.26	13.66	10.91	65	217	0.54
0723+679...	PR	1990 Sep	4.79	2.58	−26	161	0.33	13.35	8.98	−8	230	0.72
0740+828...	CJ1	1991 Jun	5.45	2.46	30	479	0.45	12.51	8.98	67	693	0.81
0746+483...	CJ1	1991 Nov	5.15	2.82	−5	557	0.26	13.45	9.94	0	700	0.40
0755+379...	CJ1	1991 Jun	6.67	2.50	−14	102	0.52	13.52	8.93	−13	160	0.83
0804+499...	PR	1990 Sep	4.63	2.81	−10	807	0.43	11.34	9.78	−2	912	0.66
0805+410...	CJ1	1991 Nov	17.76	9.56	−3	377	0.44	17.76	9.56	−3	377	0.44
0812+367...	CJ1	1990 Sep	7.54	2.57	−11	420	0.32	15.33	8.44	−6	521	0.47
0814+425...	PR	1990 Sep	6.55	2.58	−16	813	0.49	13.87	8.40	−7	946	1.11
0828+493...	CJ1	1991 Jun	4.43	2.95	−21	215	0.34	11.48	10.05	−10	269	0.48
0831+557...	PR	1990 Sep	4.61	2.53	−26	1230	1.50	10.76	8.02	−12	3600	3.44
0833+585...	CJ1	1991 Jun	4.69	2.59	0	628	0.40	10.91	10.40	23	727	0.50
0850+581...	PR	1991 Jun	4.21	2.65	30	643	0.41	11.24	10.17	−55	792	0.83
0859+470...	PR	1990 Sep	5.50	2.64	−21	618	0.45	12.29	8.39	−13	893	0.86
0900+428...	CJ1	1991 Nov	6.23	2.70	−6	143	0.36	15.14	9.56	−2	180	0.47
0906+430...	PR	1990 Sep	5.96	2.65	−22	320	0.40	12.61	8.51	−17	387	0.78
0917+449...	CJ1	1991 Nov	6.13	2.65	−6	700	0.35	14.03	9.49	0	790	0.48
0923+392...	PR	1991 Jun	9.07	2.61	−17	2510	0.87	16.68	8.89	−5	3040	1.16
0945+408...	PR	1991 Jun	6.67	2.60	−23	508	0.58	12.55	9.61	−16	905	1.07
0955+476...	CJ1	1991 Nov	5.50	2.77	−9	504	0.28	14.25	9.77	−1	540	0.48
1020+400...	CJ1	1991 Nov	6.66	2.64	−12	205	0.26	15.18	9.18	−7	295	0.36
1030+415...	CJ1	1991 Jun	6.24	2.71	−19	296	0.54	13.07	10.16	−18	403	0.74
1101+384...	CJ1	1991 Nov	6.62	2.69	−13	236	0.18	14.57	9.33	−10	282	0.39
1128+385...	CJ1	1991 Nov	6.70	2.69	−14	619	0.31	15.24	9.39	−12	678	0.92
1144+542...	CJ1	1991 Nov	4.10	2.94	6	261	0.24	12.15	11.06	−41	324	0.43
1150+497...	CJ1	1991 Nov	5.23	2.68	−19	306	0.27	12.70	9.83	−11	346	0.54
1213+350...	CJ1	1991 Jun	9.79	2.44	−16	867	0.53	15.16	9.49	−11	1220	0.87
1216+487...	CJ1	1991 Jun	4.39	2.87	−11	394	0.43	11.18	9.82	−5	545	0.76
1242+410...	CJ1	1991 Nov	7.28	2.57	−14	162	0.58	15.12	9.30	−8	423	0.94
1317+520...	CJ1	1991 Nov	4.92	2.80	−42	148	0.28	12.68	9.01	−39	228	0.45
1333+459...	CJ1	1991 Nov	5.13	2.87	−21	276	0.30	14.12	9.47	−17	324	0.45
1347+539...	CJ1	1991 Jun	4.23	2.91	−83	236	0.66	11.37	10.41	−40	383	1.15
1418+546...	CJ1	1990 Sep	3.70	3.28	−54	1010	0.35	10.32	9.79	0	1220	0.67
1435+638...	CJ1	1990 Sep	4.22	2.80	48	400	0.54	11.15	9.08	70	593	0.73
1438+385...	CJ1	1991 Nov	8.55	2.59	−11	344	0.34	17.25	9.21	−7	468	0.65
1458+718...	PR	1990 Sep	3.26	3.13	85	618	0.54	11.77	11.19	−53	1320	0.48
1504+377...	CJ1	1990 Sep	7.37	2.64	−24	464	0.36	14.08	7.84	−18	579	0.40
1624+416...	PR	1990 Sep	6.64	2.60	−19	900	0.52	14.17	8.36	−10	1350	1.04
1633+382...	PR	1990 Sep	8.33	2.56	−18	2060	0.99	16.13	7.91	−8	2370	1.88
1637+574...	PR	1990 Sep	4.18	2.97	16	898	0.57	11.06	8.97	39	989	0.92
1638+398...	CJ1	1990 Sep	8.25	2.53	−22	1150	0.64	14.84	7.89	−14	1240	0.80

TABLE 4—*Continued*

Name	Sample	Observation	Naturally Weighted Maps					Tapered Maps				
			Beam[a]			S_{peak}	rms	Beam[a]			S_{peak}	rms
			a (mas)	b (mas)	θ (°)	(mJy/beam)		a (mas)	b (mas)	θ (°)	(mJy/beam)	
1642+690...	PR	1990 Sep	3.44	2.99	88	481	0.50	10.01	9.93	14	741	1.23
1652+398...	PR	1990 Sep	5.83	2.81	−19	484	0.26	12.97	8.26	−12	592	0.51
1719+357...	CJ1	1990 Sep	9.31	2.51	−10	326	0.30	19.44	9.20	−1	384	0.51
1732+389...	CJ1	1991 Jun	7.21	2.54	−14	876	0.47	14.11	9.18	−10	973	0.94
1738+476...	CJ1	1991 Jun	5.89	2.62	−35	783	0.42	11.56	9.67	−23	881	0.89
1739+522...	PR	1990 Sep	4.52	2.94	−15	1020	0.53	12.51	8.55	−3	1170	0.92
1749+701...	PR	1991 Nov	3.87	2.71	−53	339	0.38	12.31	9.99	−39	496	0.56
1751+441...	CJ1	1990 Sep	6.60	2.55	−11	335	0.40	14.48	8.21	0	425	0.52
1758+388...	CJ1	1991 Jun	7.85	2.50	−22	326	0.25	13.53	9.33	−14	392	0.46
1800+440...	CJ1	1990 Sep	6.09	2.67	−2	220	0.32	13.15	8.87	2	279	0.44
1807+698...	PR	1990 Sep	3.49	3.08	−59	633	0.39	10.32	10.04	−9	838	0.56
1823+568...	PR	1990 Sep	4.45	2.94	50	449	0.33	9.90	9.37	47	518	0.71
1842+681...	CJ1	1991 Jun	3.66	2.86	−62	747	0.41	11.22	9.91	−75	859	0.77
1843+356...	CJ1	1991 Nov	9.40	2.48	−12	447	0.34	18.83	9.13	−2	771	0.60
1845+797...	PR	1990 Sep	3.81	2.84	24	148	0.41	6.57	5.16	30	183	0.51
1926+611...	CJ1	1991 Jun	3.58	2.99	−14	506	0.30	10.74	10.16	−48	583	0.65
1943+546...	CJ1	1991 Jun	3.86	2.86	12	612	0.73	11.55	9.71	−66	1060	1.03
1954+513...	PR	1990 Sep	3.70	3.26	−20	647	0.42	9.49	8.81	10	729	0.60
2021+614...	PR	1990 Sep	3.66	2.99	46	554	0.35	10.13	8.99	24	1360	1.04
2200+420...	PR	1990 Sep	5.79	2.72	−18	1440	0.68	12.72	8.23	−9	2110	0.99
2214+350...	CJ1	1991 Jun	10.97	2.41	−16	335	0.33	16.24	9.12	−10	375	0.45
2229+695...	CJ1	1991 Jun	3.64	2.94	−17	709	0.46	11.38	9.36	−38	803	0.79
2253+417...	CJ1	1991 Jun	6.01	2.56	−18	1210	0.39	12.83	9.03	−16	1460	0.80
2255+416...	CJ1	1991 Jun	6.62	2.50	−19	256	0.78	13.25	9.24	−11	519	1.13
2342+821...	PR	1990 Sep	3.87	2.70	−14	320	0.70	10.75	8.52	25	1280	1.39
2351+456...	PR	1990 Sep	5.03	2.73	−12	265	0.53	11.62	8.82	−1	702	1.10
2352+495...	PR	1990 Sep	4.08	3.01	−24	747	0.49	10.29	9.00	−18	1060	0.64

[a] The restoring beam is an elliptical gaussian with FWHM major axis a and minor axis b, with major axis at position angle θ.

Col. (1): Source name. Col. (2): Sample: PR if $S_{6\,cm} > 1.3$ Jy, CJ1 if 1.3 Jy $> S_{6\,cm} > 0.7$ Jy; there are 31 PR sources and 51 CJ1 sources. Col. (3): Date of observations. Cols. (4)–(6). The beam characteristics of the naturally weighted maps. Col. (7): The peak flux density of the naturally weighted maps (milijansky per beam). Col. (8): The rms noise in the naturally weighted maps (millijansky per beam). Cols. (9)–(11): The beam characteristics of the tapered maps. Col. (12): The peak flux density of the tapered maps (millijansky per beam). Col. (13): The rms noise in the tapered maps (millijansky per beam).

Table 4 is published in computer-readable form in the AAS CD-ROM Series, Vol. 4.

An independent estimate of the calibration was acquired by examining the ratios of baseline amplitudes at "crossing points" in the u, v plane using the Caltech program UVCROSS. A "crossing point" was assumed to exist where points of two baselines were within 3 Mλ of each other in the u, v plane. If the calibration was perfect the ratios of the amplitudes at these points would be unity.

The correction factors derived by DIFMAP and UVCROSS were usually in excellent agreement ($\leq$3%) and were therefore combined to derive an average correction factor for each telescope. Successive iterations of this procedure were performed until the correction values obtained by DIFMAP and UVCROSS were close to unity. The calibration information provided by most telescopes was good enough for this procedure to converge rapidly. In general the corrections applied to the telescope gains were less than 15% although corrections of up to 66% were occasionally found.

Finally we examined the closure phases for any obvious baseline-dependent errors. Since the calibrators are barely resolved the closure phases should be close to zero and any major deviation from zero should be examined carefully. In the 1990 September and 1991 June sessions closure phases involving WSRT differed from zero by up to 30° in some cases. This can probably be attributed to polarization contamination (Bartel et al. 1985). We discarded all data from WSRT for these two sessions.

The calibrated data were then inspected and discrepant points deleted using DIFMAP. As far as possible, editing was antenna-based; i.e., the error could be attributed to a single antenna and all baselines involving that antenna were flagged. Caution was exercised not to delete points that might result from extended structure. Most deleted points were located at the beginning of the scan when telescopes were slewing to source.

3.5. *Imaging*

The maps were made with a standard iterative self-calibration procedure (e.g., Pearson & Readhead 1984; Wilkinson 1989) implemented in the Caltech program DIFMAP (Shepherd, Pearson, & Taylor 1994). In addition to self-calibration, Fourier inversion, and deconvolution using the

TABLE 5

GAUSSIAN MODELS

Source	S (Jy)	r (mas)	θ (°)	a (mas)	b/a	Φ (°)	χ^2
0010+405...CJ1	0.241	0.00	0.0	1.45	0.30	−54.8	1.067
	0.008	7.30	−29.5	4.84	0.30	−68.1	
0102+480...CJ1	1.136	0.00	0.0	1.78	0.69	12.3	0.835
	0.081	3.19	30.2	2.87	0.00	60.0	
	0.035	9.79	45.4	8.97	0.39	−58.0	
0108+388...PR	0.297	0.00	0.0	1.91	0.58	71.6	1.048
	0.271	5.66	75.5	2.56	0.60	−51.6	
0133+476...PR	1.226	0.00	0.0	2.78	0.45	−13.8	1.042
	0.085	4.06	−53.8	5.08	0.15	18.7	
	0.153	6.96	−7.5	9.75	0.50	−74.5	
	0.036	20.01	−36.2	33.05	0.08	−17.7	
0218+357...CJ1	0.309	0.00	0.0	21.36	0.40	−26.8	1.531
	0.259	10.74	−16.9	36.31	0.51	−57.8	
	0.113	154.12	77.4	154.34	0.48	58.0	
	0.199	334.58	67.4	7.44	0.48	73.0	
	0.113	358.95	69.6	114.21	0.57	−53.0	
0248+430...CJ1	0.691	0.00	0.0	1.51	0.93	81.3	1.072
	0.138	4.57	139.0	3.40	0.34	−41.5	
	0.207	11.03	142.4	2.19	0.40	48.9	
0602+673...CJ1	0.517	0.00	0.0	1.31	0.68	71.9	0.895
	0.050	4.25	177.9	11.49	0.27	68.4	
0620+389...CJ1	0.388	0.00	0.0	0.83	0.80	−21.4	0.969
	0.102	3.43	116.8	7.93	0.00	−49.9	
	0.187	6.49	135.7	2.52	0.62	−38.6	
	0.077	20.07	108.4	16.02	0.43	56.6	
0642+449...CJ1	0.289	0.00	0.0	1.30	0.00	81.0	1.032
	0.178	3.16	87.9	1.51	0.75	69.9	
0711+356...PR	0.841	0.00	0.0	1.38	0.00	64.6	0.881
	0.842	2.00	156.6	6.02	0.00	−23.5	
0716+714...CJ1	0.201	0.00	0.0	1.62	0.00	10.0	1.038
	0.035	5.71	17.1	9.84	0.30	24.2	
0723+679...PR	0.161	0.00	0.0	1.47	0.00	−83.3	1.126
	0.087	2.80	−87.2	2.72	0.34	−65.3	
0740+828...CJ1	0.335	0.00	0.0	1.77	0.43	−3.2	0.941
	0.351	2.26	−6.6	1.38	0.65	−24.9	
	0.146	8.05	−4.1	4.87	0.50	5.8	
	0.097	19.27	−10.0	8.99	0.55	−16.4	
	0.021	37.37	−9.6	14.72	0.39	−71.2	
0746+483...CJ1	0.452	0.00	0.0	0.90	0.34	−66.3	0.788
	0.267	1.60	−96.5	3.56	0.28	87.5	
	0.026	6.25	−93.7	4.15	0.00	−52.8	
	0.014	44.46	−99.8	35.36	0.21	80.6	
0755+379...CJ1	0.167	0.00	0.0	3.31	0.00	−89.4	1.324
	0.010	11.78	111.7	22.83	0.00	−62.6	
0804+499...PR	0.827	0.00	0.0	1.14	0.69	−53.9	0.882
	0.108	2.49	142.2	3.39	0.51	3.6	
0805+410...CJ1	0.331	0.00	0.0	2.12	0.63	5.1	1.123
	0.119	7.67	44.6	6.00	0.16	89.4	
0812+367...CJ1	0.469	0.00	0.0	3.12	0.27	−12.7	0.958
	0.161	9.70	−14.3	4.77	0.49	−30.1	
	0.016	13.37	−1.8	5.46	0.00	24.9	

TABLE 5—*Continued*

Source	S (Jy)	r (mas)	θ (°)	a (mas)	b/a	Φ (°)	χ^2
0814+425...PR	0.709	0.00	0.0	1.21	0.46	−35.1	0.978
	0.261	1.36	107.2	4.19	0.63	−49.0	
	0.062	6.63	101.6	6.74	0.39	−38.4	
0828+493...CJ1	0.230	0.00	0.0	1.29	0.29	70.1	1.020
	0.043	2.76	55.6	1.35	0.38	75.9	
	0.079	12.82	60.8	9.90	0.49	41.3	
0833+585...CJ1	0.714	0.00	0.0	1.53	0.45	80.9	1.178
	0.071	7.86	77.6	8.38	0.52	63.2	
0850+581...PR	0.712	0.00	0.0	1.40	0.55	−24.3	0.995
	0.171	6.00	152.7	2.46	0.00	−32.1	
	0.058	12.35	146.5	8.74	0.17	6.0	
0900+428...CJ1	0.178	0.00	0.0	2.50	0.57	−17.0	1.476
	0.021	8.92	−63.5	8.12	0.00	6.2	
	0.103	15.34	−79.4	12.04	0.48	−51.5	
	0.059	20.96	−65.8	3.13	0.29	−67.6	
	0.045	30.30	−85.2	12.20	0.51	59.8	
	0.061	252.21	−83.0	53.35	0.68	−12.1	
0917+449...CJ1	0.747	0.00	0.0	1.53	0.43	−4.9	0.975
	0.062	4.49	−158.0	2.57	0.93	−11.4	
	0.072	15.58	−161.1	8.61	0.38	−4.3	
	0.009	24.09	−156.0	2.46	0.00	−53.6	
	0.049	32.92	−138.5	40.06	0.27	59.8	
0923+392...PR	2.854	0.00	0.0	1.71	0.34	−87.2	1.168
	0.348	2.71	84.5	9.24	0.13	−59.9	
	0.021	5.95	−145.9	10.92	0.00	−28.9	
	0.010	8.59	68.2	12.85	0.00	−20.3	
0945+408...PR	0.518	0.00	0.0	1.16	0.00	−77.2	1.354
	0.837	7.94	117.5	5.52	0.54	−77.9	
	0.179	19.23	114.5	7.51	0.88	−57.4	
	0.076	41.77	102.4	59.14	0.23	−86.7	
0955+476...CJ1	0.516	0.00	0.0	0.99	0.58	−23.6	0.830
	0.043	4.54	132.8	8.54	0.19	−23.9	
1020+400...CJ1	0.185	0.00	0.0	2.38	0.27	−31.0	1.125
	0.098	2.88	−45.0	1.60	0.00	−32.3	
	0.117	11.63	−35.1	6.56	0.44	−27.7	
	0.062	90.08	−21.5	85.59	0.15	−4.7	
1030+415...CJ1	0.280	0.00	0.0	1.57	0.45	5.5	1.141
	0.131	3.54	2.7	2.98	0.62	68.5	
	0.086	11.83	−17.2	8.64	0.59	3.2	
1101+384...CJ1	0.224	0.00	0.0	0.73	0.00	−66.9	0.901
	0.064	3.04	−37.9	8.99	0.17	−31.0	
	0.090	17.59	−53.0	21.50	0.32	−60.5	
	0.103	64.45	−53.8	49.29	0.73	3.3	
1128+385...CJ1	0.627	0.00	0.0	1.21	0.52	5.3	1.084
	0.068	2.76	−66.2	6.21	0.65	−32.1	
	0.030	11.48	−81.4	21.33	0.47	−65.4	
1144+542...CJ1	0.315	0.00	0.0	2.32	0.48	12.1	1.028
	0.019	3.44	−158.4	7.96	0.00	−61.6	
	0.032	17.11	−161.4	22.84	0.55	10.6	
1150+497...CJ1	0.337	0.00	0.0	1.71	0.21	19.6	1.019
	0.030	9.48	−158.6	4.35	0.51	−6.4	
	0.046	23.16	−152.9	40.62	0.11	24.0	
1213+350...CJ1	0.959	0.00	0.0	1.77	0.83	32.7	1.373
	0.173	3.23	−150.2	8.01	0.66	72.0	
	0.369	4.73	95.5	11.56	0.43	27.5	
	0.031	35.58	−125.6	2.67	0.59	−55.4	

TABLE 5—*Continued*

Source	S (Jy)	r (mas)	θ (°)	a (mas)	b/a	Φ (°)	χ^2
1216+487...CJ1	0.509	0.00	0.0	2.64	0.36	−76.6	1.326
	0.099	5.17	116.2	8.22	0.31	−77.3	
	0.043	16.34	116.7	15.38	0.24	87.2	
1242+410...CJ1	0.286	0.00	0.0	6.46	0.48	6.2	1.288
	0.271	7.44	−145.2	6.87	0.59	−25.0	
	0.225	8.63	23.8	3.53	0.89	88.2	
	0.117	13.11	174.1	8.74	0.43	61.4	
	0.268	22.12	28.1	4.49	0.84	44.3	
1317+520...CJ1	0.255	0.00	0.0	6.32	0.16	−51.1	1.392
	0.004	8.00	109.3	13.17	0.00	−19.8	
	0.019	15.55	123.6	22.19	0.00	−10.3	
1333+459...CJ1	0.330	0.00	0.0	2.12	0.51	−64.6	1.033
1347+539...CJ1	0.218	0.00	0.0	1.64	0.76	−40.9	1.459
	0.199	4.06	137.3	5.92	0.00	−38.4	
	0.194	14.63	130.3	10.73	0.29	−78.0	
	0.126	57.30	140.2	14.72	0.44	49.8	
1418+546...CJ1	0.931	0.00	0.0	1.10	0.00	−54.4	0.946
	0.347	1.82	130.4	4.64	0.36	−64.3	
	0.112	17.07	122.9	16.43	0.00	−66.2	
1435+638...CJ1	0.558	0.00	0.0	3.74	0.35	43.0	1.142
	0.214	7.09	−146.7	2.32	0.77	72.5	
	0.071	19.83	−120.8	14.02	0.20	31.1	
	0.025	39.26	−128.7	5.33	0.46	−40.7	
1438+385...CJ1	0.423	0.00	0.0	4.53	0.29	−14.6	1.535
	0.119	9.12	−11.1	4.68	0.00	23.2	
1504+377...CJ1	0.499	0.00	0.0	1.39	0.66	54.4	0.918
	0.109	3.25	−132.1	3.14	0.68	−36.9	
	0.176	9.85	−135.2	6.62	0.25	31.6	
	0.077	54.87	−137.5	25.39	0.49	47.8	
1624+416...PR	0.859	0.00	0.0	1.63	0.45	63.5	1.092
	0.392	0.98	−52.4	6.28	0.51	−5.1	
	0.184	2.64	−136.6	2.81	0.00	−37.9	
	0.109	18.19	−11.0	25.03	0.24	−0.2	
1633+382...PR	1.855	0.00	0.0	0.98	0.49	43.5	1.419
	0.548	1.57	−63.6	3.10	0.00	85.3	
	0.296	12.29	−77.7	24.12	0.43	85.8	
	0.042	53.64	−135.0	15.90	0.61	18.1	
1637+574...PR	0.994	0.00	0.0	1.86	0.42	17.8	0.999
	0.050	10.38	−145.7	28.30	0.66	77.2	
1638+398...CJ1	1.186	0.00	0.0	0.89	0.49	61.6	0.922
	0.108	2.87	−116.4	9.25	0.00	75.8	
1642+690...PR	0.450	0.00	0.0	1.69	0.30	1.3	1.094
	0.307	2.54	−165.0	3.46	0.26	12.4	
	0.146	8.43	−163.3	2.76	0.41	9.7	
	0.010	22.39	173.1	4.80	0.53	−33.6	
1652+398...PR	0.439	0.00	0.0	2.25	0.18	−27.8	1.484
	0.163	2.43	117.1	4.40	0.00	−63.8	
	0.202	14.22	114.8	24.31	0.17	−58.7	
	0.180	41.46	57.3	44.19	0.38	−17.9	
	0.220	95.70	44.0	72.15	0.83	−5.6	
1719+357...CJ1	0.390	0.00	0.0	5.30	0.09	−1.5	0.925
	0.020	13.28	−178.1	13.06	0.14	−3.2	

TABLE 5—*Continued*

Source	S (Jy)	r (mas)	θ (°)	a (mas)	b/a	Φ (°)	χ^2
1732+389...CJ1	0.862	0.00	0.0	0.78	0.65	70.8	1.057
	0.138	2.38	121.7	4.53	0.43	−44.2	
1738+476...CJ1	0.803	0.00	0.0	1.29	0.85	−40.1	1.024
	0.090	1.43	−69.4	2.63	0.51	43.8	
	0.019	7.25	−99.3	12.44	0.22	−14.1	
1739+522...PR	1.133	0.00	0.0	1.37	0.88	79.0	1.042
	0.074	2.56	8.5	7.80	0.21	−75.1	
1749+701...PR	0.449	0.00	0.0	3.05	0.37	−59.7	1.156
	0.088	3.55	−25.3	6.66	0.36	56.5	
	0.012	8.17	−3.2	2.34	0.00	18.3	
1751+441...CJ1	0.329	0.00	0.0	1.53	0.05	−73.1	0.967
	0.095	1.69	70.8	2.70	0.16	−39.7	
	0.038	6.61	84.0	8.20	0.53	−80.7	
1758+388...CJ1	0.333	0.00	0.0	1.19	0.71	73.1	0.999
	0.066	1.71	−91.4	1.61	0.56	−55.7	
1800+440...CJ1	0.181	0.00	0.0	1.70	0.00	33.1	1.136
	0.096	1.57	−134.3	4.09	0.22	19.4	
	0.084	25.98	−153.1	50.02	0.15	29.0	
1807+698...PR	0.632	0.00	0.0	1.88	0.25	87.9	1.346
	0.263	2.53	−98.3	4.79	0.11	81.8	
	0.274	28.15	−101.7	31.30	0.19	73.5	
	0.041	33.06	−96.9	2.99	0.66	60.2	
1823+568...PR	0.494	0.00	0.0	1.54	0.44	15.4	0.962
	0.081	5.52	−160.2	4.00	0.00	14.1	
	0.056	27.41	−159.9	9.29	0.57	47.8	
	0.025	39.06	−163.9	4.15	0.51	−77.4	
	0.046	112.96	−169.2	41.06	0.71	−16.6	
1842+681...CJ1	0.668	0.00	0.0	1.07	0.09	−20.1	0.992
	0.168	1.29	121.9	1.64	0.00	−6.2	
	0.036	4.29	149.3	2.79	0.54	−64.2	
	0.067	10.38	157.9	6.82	0.77	4.8	
1843+356...CJ1	0.807	0.00	0.0	4.54	0.43	32.3	1.022
	0.054	7.81	−134.5	4.86	0.00	−31.8	
	0.010	20.75	−163.3	14.25	0.17	−14.7	
1845+797...PR	0.156	0.00	0.0	2.02	0.00	−44.9	0.972
	0.070	3.75	−39.9	1.86	0.00	−19.8	
	0.048	5.96	−36.0	19.32	0.12	−37.2	
1926+611...CJ1	0.562	0.00	0.0	1.49	0.55	−45.4	1.035
	0.092	7.19	−163.4	9.44	0.39	46.8	
1943+546...CJ1	0.518	0.00	0.0	1.71	0.65	58.4	1.186
	0.468	2.25	84.5	3.39	0.48	83.6	
	0.125	6.08	70.1	9.95	0.00	−68.2	
	0.259	7.71	40.4	8.26	0.56	89.6	
	0.063	15.03	82.8	1.79	0.44	−82.5	
	0.016	23.04	75.1	4.09	0.00	25.8	
	0.216	35.94	87.5	6.20	0.56	−68.3	
	0.344	40.08	86.3	1.74	0.62	85.1	
2200+420...PR	1.053	0.00	0.0	6.56	0.48	−26.2	1.380
	1.306	2.07	−28.0	3.29	0.00	13.0	
	0.127	7.79	129.0	9.69	0.18	−21.8	
	0.093	24.95	168.1	27.85	0.24	−16.5	
	0.019	66.47	176.8	14.05	0.00	35.6	
2214+350...CJ1	0.277	0.00	0.0	1.63	0.00	−17.9	0.998
	0.110	1.96	−173.2	5.11	0.33	13.4	

TABLE 5—*Continued*

Source	S (Jy)	r (mas)	θ (°)	a (mas)	b/a	Φ (°)	χ^2
2229+695...CJ1	0.711	0.00	0.0	0.98	0.67	−81.0	0.921
	0.105	1.35	23.2	4.80	0.00	21.4	
	0.011	6.07	43.0	9.87	0.18	13.2	
	0.059	15.67	49.7	16.24	0.35	54.7	
2253+417...CJ1	1.334	0.00	0.0	2.02	0.45	−6.6	1.203
	0.322	5.67	41.4	4.71	0.50	43.2	
	0.013	12.70	152.7	2.65	0.51	22.2	
	0.078	21.70	108.3	5.96	0.67	−73.9	
2255+416...CJ1	0.277	0.00	0.0	9.34	0.48	−23.4	1.744
	0.423	11.00	76.4	22.94	0.35	76.6	
	0.033	28.29	71.6	2.08	0.00	45.9	
	0.429	33.38	69.4	7.07	0.60	31.2	
	0.397	38.37	54.1	4.76	0.37	−19.7	
	0.222	41.98	44.0	2.86	0.26	−7.8	
2352+495...PR	0.820	0.00	0.0	3.01	0.70	−36.0	1.683
	0.322	1.52	164.8	3.38	0.00	−16.0	
	0.057	12.92	−26.8	19.64	0.00	−29.5	
	0.221	16.71	−20.2	3.11	0.53	−58.9	
	0.092	22.41	174.2	23.41	0.00	−12.5	
	0.137	24.15	166.5	4.14	0.26	−22.5	
	0.285	24.53	−36.2	11.99	0.45	−7.7	
	0.181	32.07	150.6	5.11	0.78	85.9	
	0.205	32.33	163.2	3.86	0.00	68.1	

NOTES.—Table reports parameters of each Gaussian component of the model brightness distribution: S, flux density; r, θ, polar coordinates of the center of the component relative to an arbitrary origin, with polar angle measured from north through east; a, b, major and minor axes of the FWHM contour; Φ, position angle of the major axis measured from north through east. The sources 0010+775, 0402+379, 0404+768, 0538+498, 0831+557, 0859+470, 0906+430, 1458+718, 1954+513, 2021+614, 2342+821, and 2351+456 were too complicated to model.

Table 5 is published in computer-readable form in the AAS CD-ROM Series, Vol. 4.

CLEAN algorithm, DIFMAP incorporates data editing, display, and model fitting. In the self-calibration step, antenna phase solutions were determined with a 1 minute interval, and antenna amplitude solutions were determined with a 1 minute interval for sources stronger than 500 mJy or a 30 minute interval for weaker sources.

For each source we made several maps using different weighting and tapering of the visibility data. In Figure 2, we present two maps for each source. The first is a "naturally weighted" map, in which each measured visibility is weighted by the inverse square-root of its estimated variance. This weighting gives better results than using weighting by inverse variance, which overemphasizes the few high-sensitivity antennas and tends to give high sidelobe responses. The interferometer baselines range from 0.3 to 55 Mλ giving a minimum restoring beamwidth of ~3 mas (FWHM). However, at declinations near our southern limit of 35° the beam is elongated by about a factor of 3. In order to detect any additional low-brightness components located away from the center of the map we also mapped a field 1″ square using natural weighting with an additional Gaussian taper dropping to 20% at baseline 20 Mλ. In these maps the FWHM beamwidth is typically ~10 mas. In Figure 2 we present only the central part of the field of view where significant emission was detected.

The restoring beam, peak brightness, and rms noise for each of the maps presented in Figure 2 are given in Table 4. All the maps are convolved with the "formal beam" (an estimate of the FWHM of the central lobe of the dirty map) which is calculated in DIFMAP from the second moments of the visibility weighting function. In the majority of the maps the dynamic range is limited by thermal noise; the typical rms noise (σ) in the naturally weighted images away from the source is ~0.5–1 mJy beam^{-1}. As the core strength is usually a few hundred mJy the dynamic range in the maps is typically a few hundred-to-one. In general the rms noise is lower in the maps made from the 1991 June observations, which had the largest number of telescopes.

3.6. *Model Fitting*

Quantitative parameters of the source brightness distributions were estimated by fitting elliptical Gaussian models to the real and imaginary parts of the self-calibrated visibility data using a nonlinear least-squares algorithm in DIFMAP. The quality of the agreement between the model and the visibilities is expressed in the form of reduced χ^2: a value close to unity indicates that the model is an accurate representation of the data (although not necessarily a unique one).[3] On the whole,

[3] χ^2 is the sum of the squares of the deviations between the model and the measured visibilities, normalized by the errors estimated from the scatter in the data within a coherent integration. Reduced χ^2 is χ^2 divided by the number of degrees of freedom, here taken to be twice the number of visibilities (for independent real and imaginary parts). This is an overestimate of the number of degrees of freedom, because a small number of model parameters and a larger number of antenna calibration parameters have been estimated from the data.

most of the structures observed in the survey were simple and reduced χ^2 values close to unity were obtained with simple models comprised of a few Gaussian components. For complicated sources model fitting is very time-consuming and of limited utility; for these sources no models are presented.

The models are listed in Table 5. For multicomponent models the center of the most compact component was chosen as the coordinate origin. Comparisons with the λ-6 cm models (PR88; Xu et al. 1995) show that this component usually has a flat or inverted spectrum and can thus be identified with the optically thick core.

4. CONCLUSION

In this first paper of the series we have defined the sample of sources studied in the first Caltech–Jodrell Bank VLBI survey (CJ1). The complete sample of 135 sources is listed in Table 1. We have shown that we can make reliable images using Mark II VLBI in an efficient "snapshot" mode, and have reported on λ-18 cm snapshot observations of 56 of the CJ1 sources and 31 sources from the PR sample (Table 2). From these observations we were able to make images of 51 CJ1 sources and 31 PR sources (Table 4 and Fig. 2), and Gaussian models of 49 CJ1 sources and 21 PR sources (Table 5).

Observations at λ-18 cm of a further 25 sources are presented in Paper II (Thakkar et al. 1995), which completes the λ-18 cm part of the CJ1 survey. In addition, we have made higher resolution λ-6 cm observations of 87 CJ1 sources, which will be presented in Paper III (Xu et al. 1995). The interpretation of the results from the CJ1 survey will be given in later papers in the series.

We thank the staffs at the observations in the European and the U.S. VLBI Networks for their efforts during the CJ1 survey. We also thank Dr. Leonid Matveyenko and the staffs of the telescopes in the former Soviet Union who made special efforts to participate in these observations. A. G. P. acknowledges the receipt of a British Council Fellowship for the year 1991. The work at the California Institute of Technology was supported by the National Science Foundation (grants AST-8814554 and AST-9117100). Some of the data in Table 1 were obtained by way of the NASA/IPAC Extragalactic Database (NED), which is operated by the Jet Propulsion Laboratory, Caltech, under contract with the National Aeronautics and Space Administration. We are grateful to the referee, Margo Aller, for helpful comments.

APPENDIX
FIDELITY AND RELIABILITY OF SNAPSHOT IMAGES

It is important to demonstrate that the images are of a sufficient quality for classification purposes. Even for perfectly calibrated data, "reconstruction" errors are present on-source, arising from the inability of the deconvolution algorithms to interpolate over unsampled regions of the u, v plane. In addition the surface brightness sensitivity of any array is limited and hence weak extended features can be missed.

In 1990 September we observed the well-known sources 0538+498 (3C 147), 1458+718 (3C 309.1), and 1807+698 (3C 371) as a direct test of the reliability of the images produced by snapshot observations. For 0538+498 and 1458+718 maps made from full track observations at λ-18 cm with 10 and 8 stations, respectively, were available for comparison (Simon, Readhead, & Wilkinson 1984; Wilkinson et al. 1984). For 1807+698 a 12 station map made at λ-6 cm was available (Lind 1987). All three sources have core-jet structures in which the jet has complex substructure. The comparisons between the full-track maps and our snapshot maps are very good. Even in the case of such a large diffuse source as 0538+498 where the jet extends for ~200 mas (~70 beams) the main features of the full-track maps are reproduced. The tapered maps of 0538+498 and 1458+718 actually trace the diffuse extensions of the jets better than the full-track maps, mainly due to data from many short baselines in 1990 September. Long-track maps of several other complex sources became available after we had completed the mapping of the CJ1 data (0404+768 and 2342+821, Dallacasa et al. 1994; 1652+398, Conway & Wrobel 1995). Again the principal features of the snapshot maps agree well with these recent maps and we can therefore be confident that our maps are good enough for the astronomical purposes outlined in § 2.

In order to acquire a semiquantitative view of our ability to detect extended, low surface-brightness components in a map which contains a bright compact component, we carried out some further imaging simulations. To simplify the process we did not include bright compact components in the test images and did not introduce telescope-dependent errors in the data. This allowed us to dispense with self-calibration when making images from the simulated data. Using the FAKE program in the Caltech VLBI software package, datasets corresponding to observations with a 12 telescope array (as in the 1990 September observations) were created for single Gaussian models having a range of flux densities and angular sizes. A map was made from each data set using the programs in the Caltech package. For the larger angular sizes (≥30 mas), tapering in the u, v plane and larger map and beam sizes were used.

A summary of our results is shown in Figure 3. For strong components (flux density ≥ 300 mJy), Gaussian components with sizes as large as 100 mas (FWHM) are easily detected. As the flux density decreases, larger sources become difficult to detect, for example a 30 mJy, 30 mas source is barely detected, and a 30 mJy, 100 mas source cannot be detected even on a heavily tapered map. These estimates of surface brightness sensitivity are likely to be conservative, since useful data were obtained from more than 12 telescopes in the other observing sessions. It is important to stress that in order to achieve the performance summarized in Figure

FIG. 3.—A summary of the results from the simulations to assess the sensitivity of the snapshot observing technique to weak extended components. Since in practice the data have to be self-calibrated one can achieve this performance only if the source also contains a compact component whose flux density is ~100 mJy. A tickmark in each square indicates that a Gaussian component of that size and flux density is clearly detected in the maps, a "?" that the component has probably been detected and a "χ" that there is no evidence for the component in the map.

3, with a phase-uncorrected VLBI array using Mark II equipment, the source must also contain a compact component with a flux density ~ 100 mJy. This bright component enables the data to be self-calibrated easily.

These simulations were for source components at the center of the map. Away from the source center two major effects limit the field of view: the finite bandwidth and the coherent averaging time (Thompson, Moran, & Swenson 1986). For a ~1% bandwidth and a 1 minute coherent integration time, which we used for all our data, the dominant effect is time averaging. For a reduction in amplitude of 10% the field of view for our observations is ±0.″45 from the map center.

REFERENCES

Bartel, N., Ratner, M. I., Shapiro, I. I., Cappallo, R. J., Rogers, A. E. E., & Whitney, A. R. 1985, AJ, 90, 2532
Browne, I. W. A., Patnaik, A. R., Walsh, D., & Wilkinson, P. N. 1993, MNRAS, 263, L32
Cawthorne, T. V., Wardle, J. F. C., Roberts, D. H., & Gabuzda, D. C. 1993a, ApJ, 416, 519
Cawthorne, T. V., Wardle, J. F. C., Roberts, D. H., Gabuzda, D. G., & Brown, L. F. 1993b, ApJ, 416, 496
Cohen, M. H., et al. 1975, ApJ, 201, 249.
Conway, J. E., Myers, S. T., Pearson, T. J., Readhead, A. C. S., Unwin, S. C., & Xu, W. 1994, ApJ, 425, 568
Conway, J. E., & Wrobel, J. M. 1995, ApJ, 439, 98
Dallacasa, D., Fanti, C., Fanti, R., Schilizzi, R. T., Spencer, R. E., & Venturi, T. 1990, in Compact Steep-Spectrum and GHz-peaked Spectrum Radio Sources, ed. C. Fanti, R. Fanti, C. P. O'Dea, & R. T. Schilizzi (Bologna: Consiglio Nazionale delle Ricerche), 77
Dallacasa, D., Fanti, C., Fanti, R., Schilizzi, R. T., & Spencer, R. E. 1994, A&A, in press
Eckart, A., Witzel, A., Biermann, P., Johnston, K. J., Simon, R. S., Schalinski, C., & Kühr, H. 1987, A&AS, 67, 121
Fanti, C., Fanti, R., Parma, P., Schilizzi, R. T., & van Breugel, W. J. M. 1985, A&A, 143, 292
Fanti, R., Fanti, C., Schilizzi, R. T., Rendong, N., Parma, P., van Breugel, W. J. M., & Venturi, T. 1990a, A&A, 231, 333
Fanti, R., Fanti, C., Stanghellini, C., Schilizzi, R. T., Spencer, R. E., & van Breugel, W. J. M. 1990b, in Compact Steep-Spectrum and GHz-Peaked Spectrum Radio Sources, ed. C. Fanti, R. Fanti, C. P. O'Dea, & R. T. Schilizzi (Bologna: Consiglio Nazionale delle Ricerche), 48
Foulsham, P. A. 1989, M.Sc. thesis, Univ. of Manchester
Giovannini, G., Comoretto, G., Feretti, L., Marcaide, J., Venturi, T., Vermeulen, R., & Wehrle, A. E. 1992, in Physics of Active Galactic Nuclei, ed. W. J. Duschl & S. J. Wagner (Berlin: Springer), 561
Gurvits, L. I. 1993, in Subarcsecond Radio Astronomy, ed. R. J. Davis & R. S. Booth (Cambridge: Cambridge Univ. Press), 380
Henstock, D. R., Browne, I. W. A., Wilkinson, P. N., Taylor, G. B., Vermeulen, R. C., Pearson, T. J., & Readhead, A. C. S. 1995, ApJS, submitted
Hewitt, A., & Burbidge, G. 1993, ApJS, 87, 451
Hooimeyer, J. R. A., Barthel, P. D., Schilizzi, R. T., & Miley, G. K. 1992, A&A, 261, 61
Hough, D. H., Vermeulen, R. C., & Readhead, A. C. S. 1993, in Subarcsecond Radio Astronomy, ed. R. J. Davis & R. S. Booth (Cambridge: Cambridge Univ. Press), 193
Jackson, N. J. 1989, Ph.D. thesis, Univ. of Manchester
Jones, D. L., et al. 1986, ApJ, 305, 684
Kellermann, K. I. 1993, Nature, 361, 134
Kühr, H., Nauber, U., Pauliny-Toth, I. I. K., & Witzel, A. 1979, A catalog of radio sources, MPIfR preprint 55
Kühr, H., Pauliny-Toth, I. I. K., Witzel, A., & Schmidt, J. 1981, AJ, 86, 854 (S5)
Lawrence, C. R., Zucker, J. R., Readhead, A. C. S., Unwin, S. C., Pearson, T. J., & Xu, W. 1995, ApJS, submitted
Lind, K. R. 1987, in Superluminal Radio Sources, ed. J. A. Zensus & T. J. Pearson (Cambridge: Cambridge Univ. Press), 180
Napier, P. J., Bagri, D. S., Clark, B. G., Rogers, A. E. E., Romney, J. D., Thompson, A. R., & Walker, R. C. 1994, Proc. IEEE, 82, 658
Owen, F. N., Wills, B. J., & Wills, D. 1980, ApJ, 235, L57
Patnaik, A. R., Browne, I. W. A., Wilkinson, P. N., & Wrobel, J. M. 1992, MNRAS, 254, 655
Pauliny-Toth, I. I. K., Witzel, A., Preuss, E., Kühr, H., Kellermann, K. I., Fomalont, E. B., & Davis, M. M. 1978, AJ, 83, 451 (S4)
Peacock, J. A., & Wall, J. V. 1982, MNRAS, 198, 843
Pearson, T. J. 1991, BAAS, 23, 991
Pearson, T. J., & Readhead, A. C. S. 1981, ApJ, 248, 61

Pearson, T. J., & Readhead, A. C. S. 1984, ARA&A, 22, 97
———. 1988, ApJ, 328, 114 (PR88)
Polatidis, A. G. 1993, Ph.D. thesis, Univ. of Manchester
Preston, R. A., Morabito, D. D., Williams, J. G., Faulkner, J., Jauncey, D., & Nicholson, G. D. 1985, AJ, 90, 1599
Readhead, A. C. S., Pearson, T. J., & Unwin, S. C. 1984, in IAU Symp. 110, VLBI and Compact Radio Sources, ed. R. Fanti, K. I. Kellermann, & G. Setti (Dordrecht: Reidel), 131
Sanghera, H. S. 1989, M.Sc. thesis, Univ. of Manchester
———. 1992, Ph.D. thesis, Univ. of Manchester
Schwab, F. R., & Cotton, W. D. 1983, AJ, 88, 688
Shepherd, M. C., Pearson, T. J., & Taylor, G. B. 1994, BAAS, 26, 987
Simon, R. S., Readhead, A. C. S., & Wilkinson, P. N. 1984, in IAU Symp. 110, VLBI and Compact Radio Sources, ed. R. Fanti, K. I. Kellermann, & G. Setti (Dordrecht: Reidel), 111
Spinrad, H., Djorgovski, S., Marr, J., & Aguilar, L. 1985, PASP, 97, 932
Stickel, M., & Kühr, H. 1994, A&AS, 103, 349
Stickel, M., Meisenheimer, K., & Kühr, H. 1994, A&AS, 105, 211
Taylor, G. B., Vermeulen, R. C., Pearson, T. J., Readhead, A. C. S., Henstock, D. R., Browne, I. W. A., & Wilkinson, P. N. 1994, ApJS, 95, 345
Thakkar, D. D., Pearson, T. J., Readhead, A. C. S., Xu, W., Taylor, G. B., Vermeulen, R. C., Polatidis, A. G., & Wilkinson, P. N. 1995, ApJS, 98, 33
Thompson, A. R., Moran, J. M., & Swenson, G. W. 1986, Interferometry and Synthesis in Radio Astronomy (New York: Wiley)
Vermeulen, R. C., & Cohen, M. H. 1994, ApJ, 430, 467
Wehrle, A. E., Cohen, M. H., Unwin, S. C., Aller, H. D., Aller, M. F., & Nicolson, G. 1992, ApJ, 391, 589
Wilkinson, P. N. 1989, in Very Long Baseline Interferometry Techniques and Applications, ed. M. Felli & R. E. Spencer (Dordrecht: Kluwer), 69
Wilkinson, P. N., Spencer, R. E., Readhead, A. C. S., Pearson, T. J., & Simon, R. S. 1984, in IAU Symp. 110, VLBI and Compact Radio Sources, ed. R. Fanti, K. I. Kellermann, & G. Setti (Dordrecht: Reidel), 25
Wilkinson, P. N., Polatidis, A. G., Readhead, A. C. S., Xu, W., & Pearson, T. J. 1994, ApJ, 432, L87
Witzel, A., Schalinski, C. J., Johnston, K. J., Biermann, P. L., Krichbaum, T. P., Hummel, C. A., & Eckart, A. 1988, A&A, 206, 245
Xu, W., Lawrence, C. R., Readhead, A. C. S., & Pearson, T. J. 1994, AJ, 108, 395
Xu, W., Readhead, A. C. S., Pearson, T. J., Polatidis, A. G., & Wilkinson, P. N. 1995, ApJS, submitted
Zensus, J. A., & Porcas, R. W. 1987, in Superluminal Radio Sources, ed. J. A. Zensus & T. J. Pearson (Cambridge: Cambridge Univ. Press), 126

THE ASTROPHYSICAL JOURNAL SUPPLEMENT SERIES, 98:33–40, 1995 May

THE FIRST CALTECH–JODRELL BANK VLBI SURVEY. II. λ = 18 CENTIMETER OBSERVATIONS OF 25 SOURCES

D. D. THAKKAR, W. XU, A. C. S. READHEAD, T. J. PEARSON, G. B. TAYLOR, AND R. C. VERMEULEN
Owens Valley Radio Observatory, California Institute of Technology 105-24, Pasadena, CA 91125

AND

A. G. POLATIDIS AND P. N. WILKINSON
University of Manchester, Nuffield Radio Astronomy Laboratories, Jodrell Bank, Macclesfield, Cheshire SK11 9DL, UK
Received 1993 December 30; accepted 1994 November 2

ABSTRACT

We report λ-18 cm VLBI observations made in 1991 September of a further 25 objects from the first Caltech–Jodrell Bank VLBI Survey (the CJ1 survey). The CJ1 sample is a complete, flux-density limited sample of 135 radio sources with total flux density at λ-6 cm between 0.7 and 1.3 Jy. These observations complete the λ-18 cm part of the survey. Together with the results of Paper I (Polatidis et al.), we have now observed 81 CJ1 sources at λ-18 cm. Later papers in the series will present λ-6 cm observations and the analysis and interpretation of the results.

Subject headings: quasars: general — radio continuum: galaxies — surveys — techniques: interferometric

1. INTRODUCTION

In this paper we present λ-18 cm VLBI observations of a further 25 sources from the first Caltech–Jodrell Bank VLBI Survey (hereafter the CJ1 survey). These observations complete the λ-18 cm part of the survey. The scientific objectives of the survey and the selection of the sample were described in Paper I (Polatidis et al. 1995). The CJ1 sample consists of all the sources in the NRAO-MPIfR S4 and S5 surveys (Pauliny-Toth et al. 1978; Kühr et al. 1981) which satisfy the following criteria: declination (1950.0) $\delta > 35°$; Galactic latitude $|b| > 10°$; total λ-6 cm flux density 1.3 Jy $> S_{6\,cm} > 0.7$ Jy.

There are 135 sources in this sample of which 92 are observable with the Mark II VLBI system. The other 43 objects have weak compact central components with flux density of less than 0.2 Jy. Most of these sources have been optically identified and redshifts have been measured. We have mapped 81 of the sources at λ-18 cm (Paper I and this paper) and 87 at λ-6 cm (Xu et al. 1995). A list of all the sources in the complete sample, together with their redshifts, optical identifications, and total radio flux densities was given in Paper I.

2. OBSERVATIONS

The 25 sources presented in this paper were observed in one contiguous global VLBI network run of 48 hr in 1991 September. The participating telescopes are listed in Table 1, with their system temperatures and sensitivities.[1] The data were recorded using the NRAO Mark II system with an effective bandwidth of 1.8 MHz centered at 1.665 GHz in left circular polarization (LCP). Hydrogen masers were used as time and frequency standards at each telescope.

[1] The VLBA, the VLA, and the 140 foot (43 m) Green Bank telescope are instruments of the National Radio Astronomy Observatory, which is operated by Associated Universities, Inc., under cooperative agreement with the National Science Foundation.

To use the network time efficiently, we used the "snapshot" technique. Instead of using a few antennas and a long track, this technique uses a large number of antennas (13 for this observation). Each source was observed in three or four scans of 30 minutes each, as described in Paper I. The map quality is limited by thermal noise rather than the loss of u, v coverage resulting from the use of the snapshot technique. The images of most of the sources in the sample have dynamic range greater than 100:1.

The correlation of the data was carried out at Caltech using the JPL–Caltech Block II correlator. The 16 station correlator allowed us to correlate the data for all the telescopes in a single pass. This eliminates nonclosing errors caused by errors in tape reading. The sources 0552+398 and 1739+522 were used as fringe finders. The fringe fitting was done using the AIPS task FRING, and calibration, editing, and mapping were done using the Caltech VLBI package and DIFMAP, as described in Paper I.

3. RESULTS

The source list and map parameters are given in Table 2, and the maps are shown in Figure 1. As in Paper I, for each source we present a "naturally weighted" maps with a resolution of ~3 mas (FWHM), and a "tapered" map with a resolution of ~10 mas. We could not obtain a reliable image for the source 0827+378, since it is completely resolved on baselines longer than 15 Mλ. From the visibility data, we can put an upper limit of 75 mJy on the core flux density.

We attempted to model the brightness distribution of each source with simple elliptical Gaussian components, using the least-squares model-fitting algorithm in DIFMAP. The model components are listed in Table 3. We do not list models for four sources for which we could not obtain agreement factors of less than 1.5 with fewer than five components.

TABLE 1

TELESCOPE CHARACTERISTICS

Telescope	Code	Location	Diam (m)	T_{sys} (K)	T_{sys} (Jy)	Sensitivity (K/Jy)
Effelsberg	B	Germany	100	—	28	—[a]
WSRT	W	Netherlands	5×25	—	168	—[a]
Lovell	J	Jodrell Bank, UK	76	47	56	0.8
NRAO	G	Green Bank, WV, USA	43	21	72	0.3
Haystack	K	Westford, MA, USA	36	172	1066	0.16
VLBA_PT	PT	Pie Town, NM, USA	25	34	340	0.1
VLBA_KP	KP	Kitt Peak, AZ, USA	25	35	350	0.1
VLBA_LA	LA	Los Alamos NM, USA	25	33	330	0.1
VLBA_NL	NL	North Liberty, IA, USA	25	35	350	0.1
VLBA_FD	FD	Fort Davis, TX, USA	25	34	340	0.1
VLBA_BR	BR	Brewster, WA, USA	25	29	291	0.1
VLA[b]	Y	Socorro, NM, USA	25	45	450	0.1
OVRO	O	Owens Valley, CA, USA	40	53	254	0.21

[a] T_{sys} measurements supplied in janskys.

[b] The VLA was used in single antenna mode.

NOTES.—Cols. (1)–(3): the name, the code used and the location of each telescope. Col. (4): the diameter of each telescope (in meters). Cols. (5)–(7): The system temperature in kelvins and in janskys and the sensitivity in kelvins per jansky of each telescope.

AFFILIATIONS.—B, Max-Planck-Institüt für Radioastronomie; W, Westerbork Synthesis Radio Telescope, NFRA; J, Nuffield Radio Astronomy Laboratories; G, National Radio Astronomy Observatory; K, Haystack Observatory; PT, KP, LA, FD, NL, BR, National Radio Astronomy Observatory VLBA; Y, National Radio Astronomy Observatory VLA; O, Owens Valley Radio Observatory.

TABLE 2

MAP PARAMETERS

Name	Naturally Weighted Maps					Tapered Maps				
	Beam[a]			S_{peak}	rms	Beam[a]			S_{peak}	rms
	a (mas)	b (mas)	θ (°)	(mJy/beam)		a (mas)	b (mas)	θ (°)	(mJy/beam)	
0022+390...	7.88	2.72	−18	521	0.49	15.18	8.00	−7	601	1.01
0646+600...	4.98	3.02	32	580	0.35	11.56	9.46	72	670	0.52
0650+371...	7.76	2.71	−15	963	0.46	15.23	8.59	−7	1030	0.76
0707+476...	7.76	2.64	0	859	0.44	16.46	8.69	17	956	0.74
0820+560...	5.13	3.40	−76	755	0.43	12.28	8.81	−44	862	0.64
0821+394...	7.52	2.58	−11	216	0.73	14.90	8.30	−3	311	1.87
0917+624...	4.08	3.15	−17	751	0.57	11.08	9.51	−22	1010	0.68
1003+830...	3.83	2.91	−73	192	0.36	12.67	10.09	−39	394	0.66
1015+359...	11.05	2.53	−17	561	0.39	19.48	8.30	−8	632	0.53
1044+719...	3.62	3.03	−71	900	0.35	13.70	11.54	−29	970	0.63
1053+704...	3.56	3.37	−54	607	0.38	12.23	9.94	−41	669	0.75
1053+815...	3.54	3.12	−26	594	0.33	13.06	12.67	5	635	0.65
1058+726...	4.21	3.17	−89	476	0.33	11.38	9.34	−31	665	0.92
1144+402...	9.04	2.65	−10	334	0.29	16.23	8.68	1	391	0.48
1311+678...	3.85	2.92	−38	161	0.62	10.65	8.75	−20	519	1.10
1333+589...	3.93	3.12	3	207	0.26	11.48	10.76	−14	293	0.49
1342+663...	4.39	2.76	−11	662	0.32	12.52	9.76	−2	784	0.72
1357+769...	3.53	3.26	−65	583	0.29	12.07	10.32	−60	639	0.52
1437+624...	3.98	2.92	4	323	0.59	12.39	10.21	50	1000	0.94
1547+507...	4.42	3.09	−27	298	0.51	10.66	9.18	−15	655	0.80
1656+477...	5.46	2.64	−13	805	0.32	15.46	11.19	3	1030	0.68
1656+482...	5.52	2.93	−8	459	0.26	13.12	9.64	−1	563	0.51
1734+508...	4.31	3.10	−33	415	0.30	11.31	10.02	−36	575	0.70
2207+374...	8.91	2.59	−19	333	0.37	15.04	7.57	−8	635	0.77

[a] The restoring beam is an elliptical Gaussian with FWHM major axis a and minor axis b, with major axis at position angle θ.

NOTES.—Col. (1): source name. Cols. (2), (3), and (4): the beam characteristics of the naturally weighted maps. Col. (5): the peak flux density of the naturally weighted maps (mJy beam^{-1}). Col. (6): the rms noise in the naturally weighted maps (mJy beam^{-1}). Cols. (7), (8), and (9): the beam characteristics of the tapered maps. Col. (10): the peak flux density of the tapered maps (mJy beam^{-1}). Col. (11): the rms noise in the tapered maps (mJy beam^{-1}).

Table 2 is published in computer-readable form in the AAS CD-ROM Series, Vol. 4.

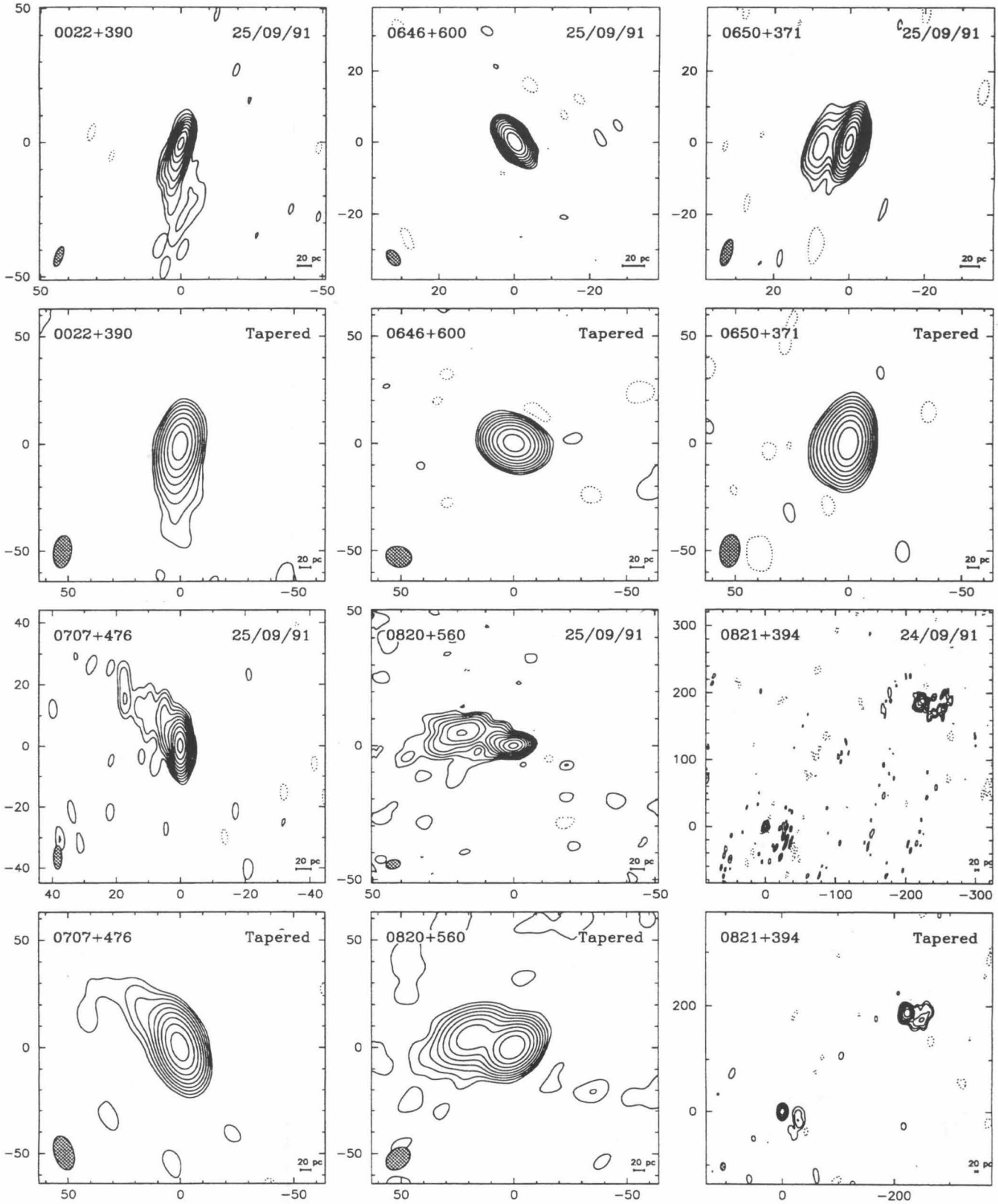

FIG. 1.—The λ-18 cm VLBI maps of 24 sources. For each source the top panel shows the naturally weighted, higher resolution map, and the bottom panel shows the tapered map. Logarithmic contour levels are used in all maps, drawn at $-2, -1, 1, 2, 4, 8, 16, \cdots 1024 \times 3\ \sigma$ (where σ is the rms noise measured in an empty region of the map). The FWHM contour of the elliptical Gaussian restoring beam is shown hatched in the lower left-hand corner. The peak flux density, rms noise and parameters of the restoring beam are given in Table 2. The angular scale is marked in milliarcsec and, where the source redshift is known, the linear scale of each map is indicated in the lower right-hand corner (assuming $H_0 = 100$ km s^{-1} Mpc^{-1} and $q_0 = 0.5$). Note that the field of view of the tapered map is usually larger than that of the uniformly weighted map.

FITS images corresponding to the maps presented in Fig. 1 are published in the AAS CD-ROM Series, Vol. 4.

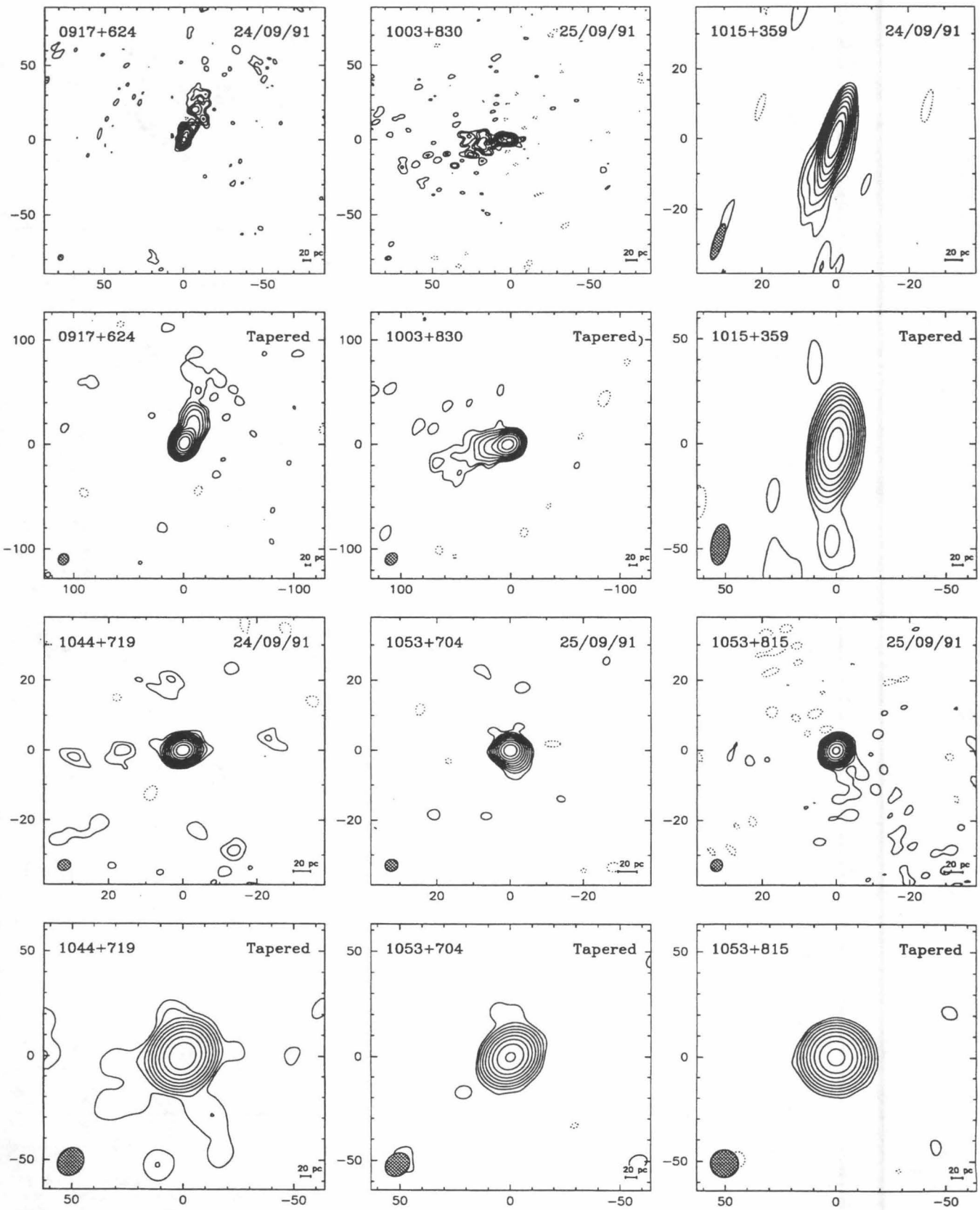

FIG. 1.—*Continued*

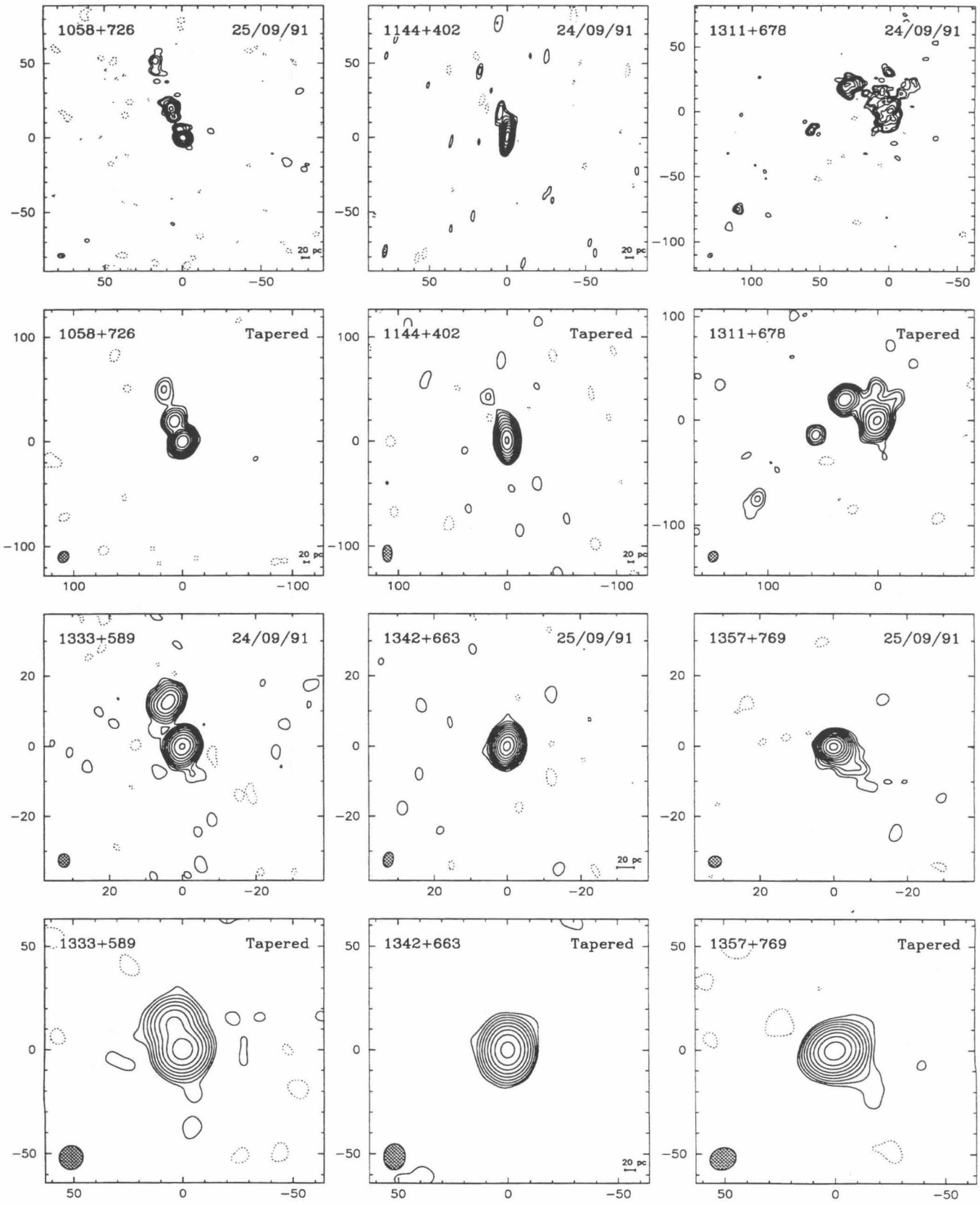

FIG. 1.—*Continued*

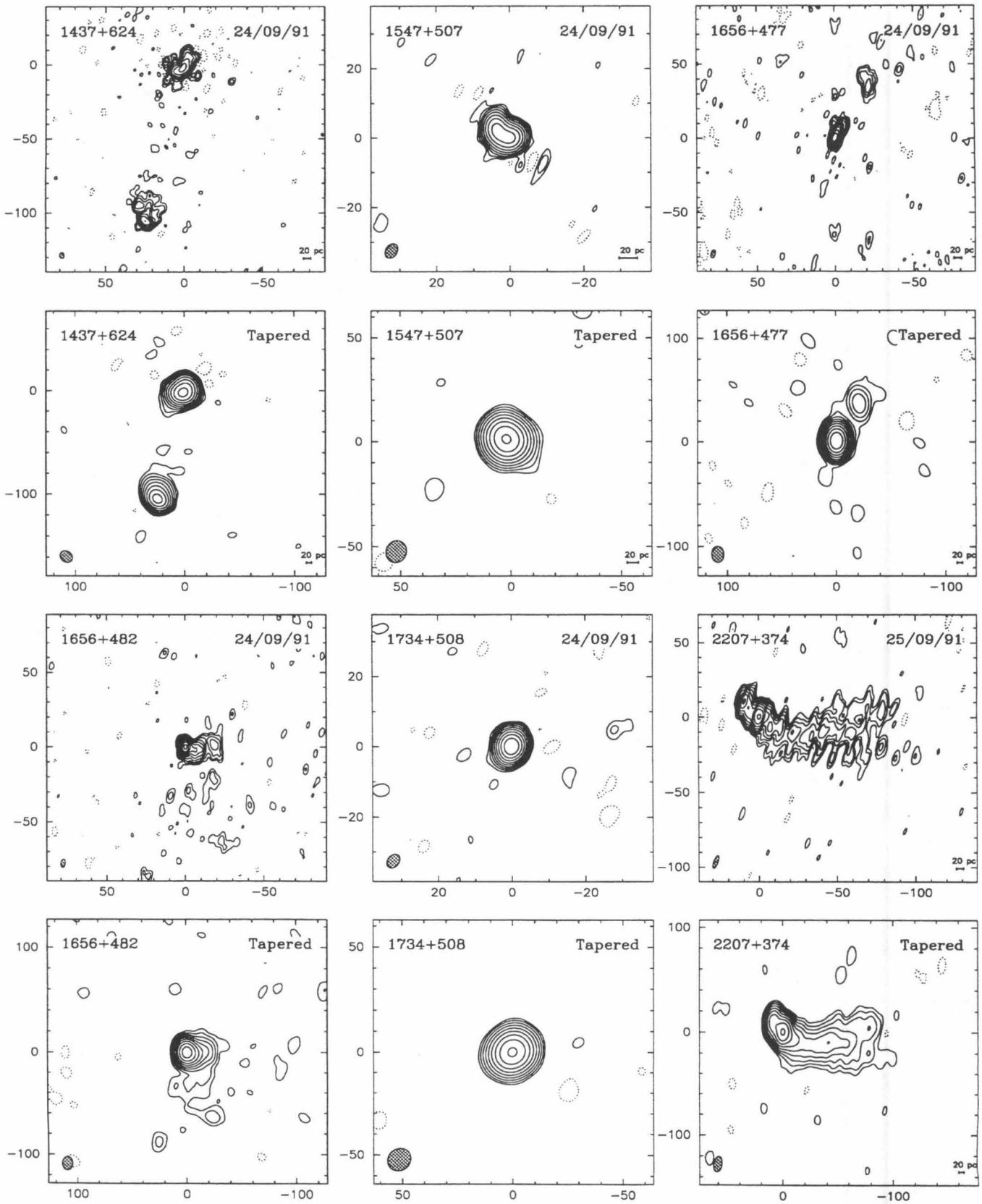

FIG. 1.—*Continued*

TABLE 3

GAUSSIAN MODELS

Source	S (Jy)	r (mas)	θ (°)	a (mas)	b/a	Φ (°)	χ^2
0022+390...	0.504	0.00	0.0	1.30	0.00	17.2	1.086
	0.185	6.49	168.6	11.22	0.28	−10.3	
0646+600...	0.700	0.00	0.0	3.23	0.18	32.3	1.279
0650+371...	1.011	0.00	0.0	1.26	0.69	6.4	0.931
	0.088	6.91	95.5	7.38	0.44	−51.7	
0707+476...	0.930	0.00	0.0	1.34	0.50	44.0	1.130
	0.089	10.69	34.3	9.13	0.00	−38.2	
0820+560...	0.728	0.00	0.0	1.98	0.00	86.7	1.282
	0.234	3.72	75.7	5.45	0.27	65.6	
	0.266	18.16	72.7	8.59	0.59	−81.8	
	0.059	23.73	83.7	7.39	0.45	30.6	
0917+624...	0.775	0.00	0.0	1.28	0.53	−9.7	1.269
	0.378	4.95	−20.3	2.44	0.82	26.8	
	0.159	20.73	−24.8	21.12	0.44	−7.5	
1003+830...	0.251	0.00	0.0	2.01	0.84	62.6	1.282
	0.217	5.15	85.3	2.20	0.83	72.5	
	0.103	18.97	98.0	14.67	0.67	−47.5	
1015+359...	0.596	0.00	0.0	2.73	0.25	−1.3	0.844
	0.068	6.97	169.2	10.84	0.22	−22.7	
1044+719...	0.975	0.00	0.0	1.04	0.88	−63.8	0.797
1053+704...	0.674	0.00	0.0	1.35	0.69	65.4	1.037
1053+815...	0.638	0.00	0.0	0.97	0.87	−71.4	0.767
1058+726...	0.681	0.00	0.0	3.04	0.32	15.1	1.290
	0.037	3.71	−146.0	13.06	0.00	−72.3	
	0.017	11.29	25.1	13.52	0.00	−56.1	
	0.068	20.44	21.4	5.00	0.26	−85.1	
	0.019	24.07	19.9	5.09	0.00	85.6	
	0.016	53.74	19.1	7.27	0.39	−45.3	
1144+402...	0.320	0.00	0.0	1.36	0.69	6.7	0.823
	0.087	3.60	1.0	3.20	0.57	70.2	
	0.012	17.29	15.5	3.38	0.18	−64.1	
1333+589...	0.301	0.00	0.0	2.86	0.61	−51.7	1.044
	0.126	13.31	16.0	4.58	0.27	−41.9	
1342+663...	0.798	0.00	0.0	1.72	0.71	−85.1	0.795
1357+769...	0.648	0.00	0.0	1.28	0.67	68.8	1.071
1547+507...	0.360	0.00	0.0	2.96	0.47	65.9	1.025
	0.430	4.22	58.2	4.02	0.11	28.7	
	0.009	11.27	−131.0	8.54	0.00	−20.1	
1656+477...	0.820	0.00	0.0	1.12	0.52	23.3	0.982
	0.301	5.04	−23.1	3.72	0.59	−17.3	
	0.047	42.09	−30.9	22.25	0.41	−22.8	
1656+482...	0.467	0.00	0.0	1.38	0.51	63.9	1.091
	0.240	6.22	−102.9	10.74	0.59	87.1	
1734+508...	0.631	0.00	0.0	2.99	0.59	27.7	0.999

NOTE.—Parameters of each Gaussian component of the model brightness distribution: S, flux density; r, θ, polar coordinates of the center of the component relative to an arbitrary origin, with polar angle measured from north through east; a, b, major and minor axes of the FWHM contour; Φ, position angle of the major axis measured from north through east. The sources 0821+394, 1311+678, 1437+624, and 2207+374 were too complicated to model.

Table 3 is published in computer-readable form in the AAS CD-ROM Series, Vol. 4.

We thank the staff at the observatories in the European and the US VLBI Networks, and AGP acknowledges the receipt of British Council Fellowship for the year 1991. The work at Caltech is supported by the National Science Foundation (grants AST-8814554 and AST-9117100). We are grateful to the referee, Margo Aller, for helpful comments.

REFERENCES

Kühr, H., Pauliny-Toth, I. I. K., Witzel, A., & Schmidt, J. 1981, AJ, 86, 854

Pauliny-Toth, I. I. K., Witzel, A., Preuss, E., Kühr, H., Kellermann, K. I., Fomalont, E. B., & Davis, M. M. 1978, AJ, 83, 451

Polatidis, A. G., Wilkinson, P. N., Xu, W., Readhead, A. C. S., Pearson, T. J., Taylor, G. B., & Vermeulen, R. C. 1995, ApJS, 98, 1

Xu, W., Readhead, A. C. S., Pearson, T. J., Polatidis, A. G., & Wilkinson, P. N. 1995, ApJS, submitted

THE ASTROPHYSICAL JOURNAL SUPPLEMENT SERIES, 99:297–348, 1995 August

THE FIRST CALTECH–JODRELL BANK VLBI SURVEY. III. VLBI AND MERLIN OBSERVATIONS AT 5 GHz AND VLA OBSERVATIONS AT 1.4 GHz

W. XU, A. C. S. READHEAD, AND T. J. PEARSON
Owens Valley Radio Observatory, California Institute of Technology, Pasadena, CA 91125

AND

A. G. POLATIDIS AND P. N. WILKINSON
University of Manchester, Nuffield Radio Astronomy Laboratories, Jodrell Bank, Macclesfield, Cheshire SK11 9DL, England, UK
Received 1994 November 28; accepted 1995 January 26

ABSTRACT

We present the 5 GHz results from the first Caltech–Jodrell Bank (CJ1) VLBI survey. The 1.6 GHz maps were presented in two separate papers (Polatidis et al. 1995; Thakkar et al. 1995). These three papers complete the first stage of this program to map at both 1.6 and 5 GHz all objects accessible to Mark II VLBI in the complete sample of 135 objects with $1.3 > S_{5\,\mathrm{GHz}} \geq 0.7$ Jy, $\delta(1950) \geq 35°$, and $|b| > 10°$. The combination of the CJ1 sample with the Pearson-Readhead (PR) sample provides a complete, flux density–limited sample of 200 objects with $S_{5\,\mathrm{GHz}} \geq 0.7$ Jy, $\delta(1950) \geq 35°$, and $|b| > 10°$ for which all of the objects accessible to Mark II VLBI have been mapped at both 5 GHz (129 objects) and 1.6 GHz (132 objects).

In addition to the 5 GHz VLBI maps, we present in this paper 5 GHz MERLIN observations of 20 objects and 1.4 GHz VLA observations of 92 objects in the combined CJ1 + PR sample. The VLA maps, together with *L*-band (1.3–1.7 GHz) maps available in the literature, provide a complete set of VLA maps for the combined CJ1 + PR sample. Finally, we present the radio spectra of the objects in the CJ1 sample.

The combined CJ1 + PR VLBI surveys provide a sample which is large enough for a number of important astrophysical and cosmological studies. These will be presented in further papers in this series.

Subject headings: quasars: general — radio continuum: galaxies — surveys

1. INTRODUCTION

This is the third paper in a series presenting results of the first Caltech–Jodrell Bank VLBI survey (the CJ1 Survey). The CJ1 sample comprises the 135 objects from the S4 and S5 surveys (Pauliny-Toth et al. 1978; Kühr et al. 1981a) with $1.3\ \mathrm{Jy} > S_{5\,\mathrm{GHz}} \geq 0.7$ Jy, $\delta(1950) \geq 35°$, and $|b| \geq 10°$. Together with the Pearson-Readhead sample (Pearson & Readhead 1988, hereafter PR) of objects with $S_{5\,\mathrm{GHz}} \geq 1.3$ Jy, the CJ1 + PR sample has a combined total of 200 objects with $S_{5\,\mathrm{GHz}} \geq 0.7$ Jy, $\delta(1950) \geq 35°$, and $|b| \geq 10°$.

Some of the objects in the sample do not contain a bright, compact component and thus are not suitable for imaging with the global Mark II VLBI network. As described in Paper I (Polatidis et al. 1995), we used previous VLBI and VLA observations to exclude unsuitable sources, that is, sources that were known to contain no component smaller than 2″ and stronger than 300 mJy at centimeter wavelengths. We did include some sources with weaker compact cores when there was prior evidence of milliarcsecond-scale structure.

In Papers I and II (Polatidis et al. 1995; Thakkar et al. 1995) we cataloged the sample and presented the results of 1.6 GHz VLBI observations of 81 objects in the CJ1 sample accessible to Mark II VLBI imaging and 31 objects from the PR sample that had not previously been imaged with VLBI at 1.6 GHz. In this paper we present the 5 GHz VLBI observations of the 87 objects in the CJ1 sample and the one remaining object in the PR sample accessible to Mark II VLBI. These three papers, combined with the 5 GHz maps of PR and maps available in the literature, provide a complete set of VLBI maps at 1.6 and 5 GHz of all objects accessible to Mark II VLBI in the CJ1+PR sample.

In addition to the 5 GHz VLBI maps of CJ1 objects, we present radio spectra of all CJ1 objects, 1.4 GHz VLA maps of 92 objects, and five GHz MERLIN maps of 20 objects from the combined CJ1+PR sample. The objects mapped with the VLA are those CJ1+PR objects for which no adequate VLA maps exist in the literature. Thus, the VLA maps presented here, plus those available in the literature, provide an almost uniform set of ~1.4 GHz maps of the large-scale radio structure of the complete CJ1+PR sample.

The VLBI maps presented in these three papers were made with the "snapshot" technique, which has proved extremely effective in mapping compact structure in radio sources and increases the efficiency of VLBI arrays by over a factor ~20. The technique is described in detail by Polatidis et al. (1995).

The results of the combined CJ1+PR surveys provide a sample which is large enough for a number of important astrophysical and cosmological studies—including determination of physically distinct classes, proper motion–redshift tests, angular diameter–redshift tests, and misalignment between parsec-scale and kiloparsec-scale radio structures. In particular, there were some classes of object in the PR sample with very few members, and these have now been augmented significantly by the addition of the CJ1 objects. The dual-wavelength observations presented in these three papers provide for a much more secure classification of radio-loud active galaxies than do single-frequency observations. The classification of these objects

will be discussed in a later paper in this series. In addition, a number of interesting objects—including compact symmetric objects and possible gravitational lenses—have been discovered in the course of the 1.6 and 5 GHz VLBI surveys. These topics will be addressed in a number of papers describing follow-up studies of the CJ1 survey.

2. OBSERVATIONS AND DATA REDUCTION

2.1. *VLBI Observations and Data Reduction*

We observed 87 objects in the CJ1 sample with the global VLBI network at 5 GHz. Observations were recorded with left circular polarization (IEEE convention) and with a bandwidth of 1.8 MHz, using the Mark II VLBI format (Clark 1973), and cross-correlated with the JPL/Caltech Block 2 correlator. One object, 0404+768, in the PR sample was also observed since it had not been mapped previously at 5 GHz. All objects, except 0218+357 and 0404+768, were observed with the snapshot technique (Polatidis et al. 1995)—generally with three 20–30 minute scans, but a few objects had one or two extra scans; 0218+357 was observed for 4.5 hr and 0404+768 for 3 hr. The observations were completed in six sessions between 1990 and 1992 (Table 1). Thirteen to 17 stations participated in each session. The locations and parameters of the stations are listed in Table 1. In the session of 1991 September we obtained simultaneous MERLIN observations. Data from three of the six MERLIN stations (Cambridge, Mark II at Jodrell Bank, and Knockin) were recorded in Mark II format for cross-correlation with the non-MERLIN stations. The MERLIN data were combined with VLBI data, giving 21 stations in this session. The length of the snapshots was shortened from 30 minutes to 20 minutes during the course of this project as we gained confidence in the technique. To optimize the *uv* coverage, the three snapshots were scheduled as follows: for objects with mutual observing time of 8 hr or longer, the snapshots were separated by about 4 hr, which provided very good *uv* coverage; for other objects, three snapshots were taken at the beginning, the middle, and the end of the mutual observing time. For objects with a declination near 35°, the lower limit of our sample, the mutual observing time is only ~4 hr, which leaves large holes in the *uv* coverage and may lead to uncertainties in the map. In these cases one or two stations were often given up in order to gain ~1.5 hr or more in mutual observing time. Figure 1 shows the *uv* coverage for three representative objects, at $\delta \simeq 38°$, $\delta \simeq 52°$, and $\delta \simeq 77°$.

After correlation, data were fringe-fitted with the NRAO Astronomical Image Processing System (AIPS) program FRING (1994 July edition), the global fringe-fitting algorithm developed by Schwab & Cotton (1983). Nyquist search windows, i.e., 2000 ns in delay and 500 mHz in rate centered on zero, were used. The Effelsberg 100 m antenna was chosen as the reference antenna whenever possible; otherwise, the Green Bank 140 foot (43 m) telescope was selected. The solution interval was set to 4–6 minutes in most cases, but values up to 15 minutes were used for weak objects. For 0218+357, a 2 minute interval was used since this object is a large double of separation ~330 mas. After fringe-fitting, the 2 s data were phase-self-calibrated in DIFMAP (Shepherd, Pearson, & Taylor 1994) with a 10 s solution time to remove the residual phase errors. A point source model was used for all objects except 0218+357, for which a model with two Gaussian components, derived from EVN observations (A. R. Patnaik, private communication), was used. The data were then averaged coherently for 60 s in all but two cases. An averaging interval of 10 s was used for 0218+357 and 30 s for 0404+768 to avoid significant time-average smearing. The error bars of the averaged data were calculated from the scatter of individual data points within the averaging period.

Amplitude calibration was performed with the program CAL in the Caltech VLBI package, which calibrates the correlation coefficients using measurements of antenna system temperatures and antenna gain curves (Cohen et al. 1975). Station-dependent calibration gain factors were derived from the observations of the strong, barely resolved, or highly core-dominated calibrator objects 0133+476, 0552+398, 1638+398, and 1739+522. These gain factors were applied to the entire observing session. We believe that the final calibration is good to ~5%. Time-dependent calibration errors were later corrected by self-calibration. After calibration, the data were edited in DIFMAP.

All of the objects were first mapped and self-calibrated non-interactively using an automatic script, called AUTOMAP, to drive DIFMAP. In AUTOMAP the data are first phase-self-calibrated with a point source model, and then a "dirty" image is produced by Fourier inversion. The position of the highest surface brightness feature on the dirty map is then identified, and a small rectangular window is centered on this position. The map is then "CLEANed" (Högbom 1974) for a number of iterations, with a loop gain of typically ~0.01. In each CLEAN iteration the highest surface brightness feature remaining within the window in the residual or "difference" map is subtracted from the data. AUTOMAP then performs another phase self-calibration using the clean-component model and makes a new difference map. It finds the position of the highest surface brightness feature in this map, adds another window centered on this position, and repeats the above process. In later loops amplitude self-calibration is allowed in addition to phase self-calibration. After some experimentation we developed a final version of AUTOMAP in which (1) the CLEAN loop had a cutoff at 6 σ, where σ is the residual rms noise in the difference map; (2) a Gaussian taper with a value of 0.3 at a spacing of 50 Mλ in the *uv* plane was applied to the visibility amplitudes—this helped to show up any faint extended structure; and (3) amplitude self-calibration was applied, followed by more CLEAN loops with a cutoff at 4.5 σ. Note that the rms noise on the residual map was changing during the above process, so the CLEAN cutoff was adjusted for each step. After choosing adequate map sizes, ~60% of the maps generated by AUTOMAP are equivalent to those made interactively, and ~35% contain slight errors at low levels and can be corrected interactively with ease. The rest had to be mapped interactively with care. Even for these objects, the structure revealed by AUTOMAP is basically correct. AUTOMAP failed entirely on only one—complex—object, 1311+678.

Our final procedure generated three images: a uniformly weighted map, a naturally weighted map, and a map made from data which had been tapered with a Gaussian function with a value 0.3 at 50 Mλ. The tapered maps have map sizes 4 times as large as the others to search for structure on larger scales. The final maps are limited by thermal noise in most

TABLE 1

TELESCOPE CHARACTERISTICS

Telescope	Code	Location	Diameter (meter)	Sensitivity (K/Jy)	T_{sys} (K)	Network	1990 Mar	1991 Jun	1991 Sep	1992 Mar	1992 Jun	1992 Sep
Onsala	S	Sweden	26	0.059	150	EVN	√	√	√	√	√	√
Effelsberg	B	Germany	100	2.38	45	EVN	√	√	√		√	√
WSRT	W	Netherlands	14×25	—[a]	110	EVN	√	√	√	√	√	√
JBNK	J2	Jodrell Bank, UK	25	0.12	46	EVN, MERLIN		√	√	√		
Medicina	L	Bologna, Italy	32	0.16	45	EVN	√	√	√	√	√	√
Noto	No	Noto, Italy	32	0.146	45	EVN	√	√	√	√	√	√
Cambridge	C	Cambridge, UK	32	0.23	32	MERLIN			√	√		
Knockin	Kn	Knockin, UK	25	0.12	33	MERLIN			√			
Tabley	T	Tabley, UK	25	0.13	34	MERLIN			√			
Defford	De	Defford, UK	25	0.032	55	MERLIN			√			
Darnhall	Da	Darnhall, UK	25	0.12	32	MERLIN			√			
Haystack	K	Westford, MA, USA	36	0.16	74	US	√	√	√	√	√	√
NRAO	G	Green Bank, WV, USA	43	0.27	33	US	√	√	√	√	√	√
FDVS	F	Fort Davis, TX, USA	26	0.095	88	US	√					
VLBA_Nl	Nl	North Liberty, IA, USA	25	0.142	40	VLBA		√	√	√	√	√
VLBA_Fd	Fd	Fort Davis, TX, USA	25	0.131	42	VLBA		√	√	√	√	√
VLBA_La	La	Los Alamos, NM, USA	25	0.139	40	VLBA	√	√	√	√	√	√
VLBA_Pt	Pt	Pie Town, NM, USA	25	0.126	42	VLBA	√	√	√	√	√	√
VLBA_Kp	Kp	Kitt Peak, AZ, USA	25	0.128	43	VLBA	√	√	√	√	√	√
VLBA_Ov	Ov	Owens Valley, CA, USA	25	0.124	36	VLBA				√	√	√
VLBA_Br	Br	Brewster, WA, USA	25	0.130	34	VLBA			√	√	√	√
VLA[b]	Y	Socorro, NM, USA	25	0.119	37	US	√	√	√	√	√	√
OVRO	O	Owens Valley, CA, USA	40	0.201	70	US	√	√	√			

[a] WSRT provided T_{sys} in K and Jy, from which the sensitivity could be derived. The value varied from 0.3 to 1, depending on the number of antennas actually used.

[b] The VLA was used in single-antenna mode.

NOTES.—Cols. (1)–(3): The name, code, and location of each telescope. Col. (4): The diameter of each telescope (in meters). Cols. (5)–(6): The sensitivity in kelvins per jansky and system temperature in kelvins of each telescope. Col. (7): The network with which each telescope is associated. Cols. (8)–(13): A tick indicates whether the telescope participated in that session.

AFFILIATIONS.—O, Onsala Space Observatory; B, Max-Planck-Institute für Radiostronomie; W, Westerbork Synthesis Radio Telescope; J2, MK II telescope, Nuffield Radio Astronomy Laboratories; L, No, Instituto di Radioastronomia; C, Kn, T, De, Da, Nuffield Radio Astronomy Laboratories; K, Haystack Observatory; G, National Radio Astronomy Observatory; F, George A. Agassiz Station of Harvard University; Nl, Fd, La, Pt, Kp, Ov, Br, National Radio Astronomy Observatory, VLBA; Y, National Radio Astronomy Observatory, VLA; O, Owens Valley Radio Observatory.

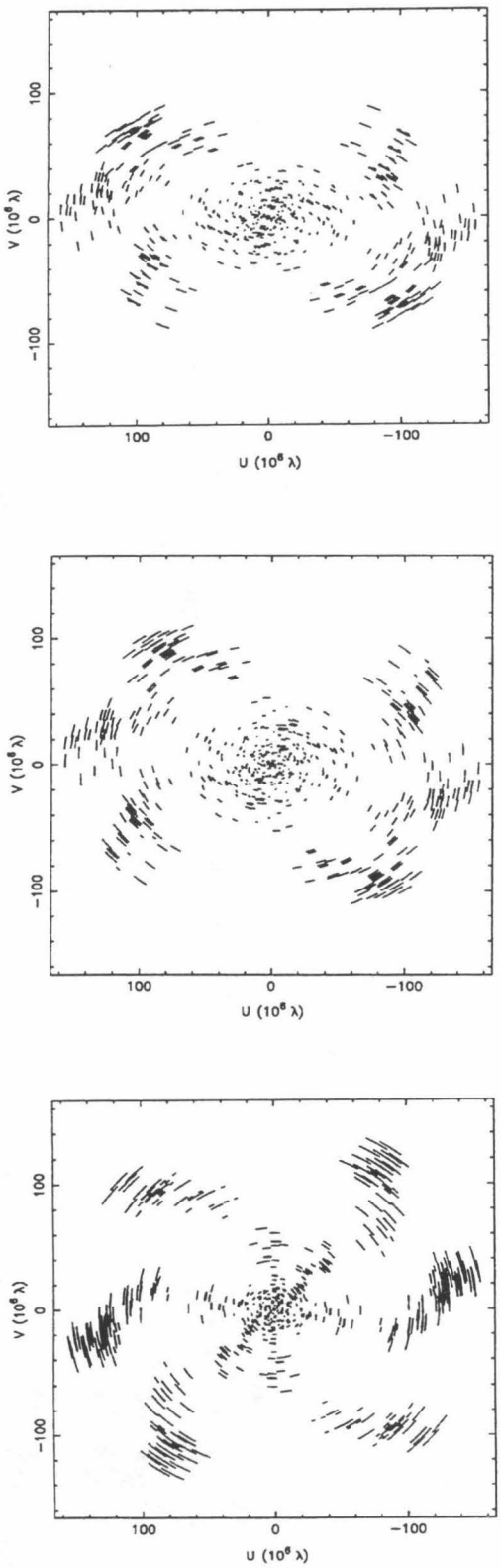

FIG. 1.—Typical *uv* coverages for VLBI observations. *Top:* $\delta \simeq 38°$ (1438+385 observed on 1992 June 6); *middle:* $\delta \simeq 52°$ (1317+520 observed on 1992 June 6); *bottom:* $\delta \simeq 77°$ (1357+769 observed on 1991 June 8).

cases. The typical rms noise in a blank area in the map is ~0.5 mJy with natural weighting and ~1 mJy with uniform weighting. The dynamic range of the images (i.e., the ratio of the brightest feature in the map to rms noise in a blank area) is larger than 300:1 in most cases. Four objects, 0707+689, 0827+378, 1203+645, and 1637+626, were very heavily resolved and detected on only a few short baselines and were not mapped. The naturally weighted and tapered maps of the other 84 objects are presented in Figure 2. The objects 0218+357, 0821+394, 1138+594, and 1437+624 have large angular sizes, and we present maps of individual components so that more detail can be seen. The parameters of the maps are listed in Table 2.

The final step in the data analysis was to fit the closure phases and self-calibrated amplitudes with elliptical Gaussian models using the program MODELFIT in the Caltech VLBI package (Pearson 1991). Such models provide a parameterization of the object structure, which is useful both for comparing structural changes between epochs and for estimating physical parameters. The models and agreement factors (square root of reduced χ^2) between the models and observed visibilities are listed in Table 3. Separate agreement factors are given for amplitude and closure phase. In addition a "total" agreement factor (a weighted average of the amplitude and closure phase agreement factors) is given; this is the quantity that is minimized in the least-squares model-fitting procedure. A detailed description of the agreement factor is given by Henstock et al. (1995).

In addition to the 87 CJ1 objects discussed in this paper, six other CJ1 objects have been observed with global VLBI or the EVN at 1.6 GHz (Paper I and references therein). A good quality 5 GHz map of 1637+826 (NGC 6251) has been published by Jones et al. (1986); thus, we did not observe it. The objects 0010+775, 0945+664, and 2324+405 were heavily resolved at 1.6 GHz, while 1250+568 and 2323+435 have no bright compact feature in their 1.6 GHz EVN images and hence are not accessible to Mark II VLBI observations. Therefore, we did not attempt to observe these five objects at 5 GHz.

2.2. *MERLIN Observations and Data Reduction*

MERLIN observations at 5 GHz of 20 objects in the CJ1 and PR samples were made in 1992 February. Parameters for the MERLIN telescopes are summarized in Table 1. The object list is given in Table 4. Each object was observed with many 20–30 minute scans spanning ~12 hr, with a total integration time from 4 to 6 hr. Our observations were made with left circular polarization (IEEE convention) and recorded with a bandwidth of 7 MHz separated into seven 1 MHz channels. The data were calibrated with the OLAF package of the Nuffield Radio Astronomy Laboratories. The objects 3C 286 and OQ 208 were used as the flux density calibrators. Bandpass corrections were made with the AIPS package. The maps were made with DIFMAP. Typical *uv* coverages are shown in Figure 3. Uniformly weighted maps are presented in Figure 4. For four objects with large-scale structure, naturally weighted maps restored with a circular Gaussian beam of FWHM 100 mas are also presented. For the object 0812+367 we include a map of the central and southern component to show more detail. Its northern component is slightly resolved. The parameters of the maps are listed in Table 4.

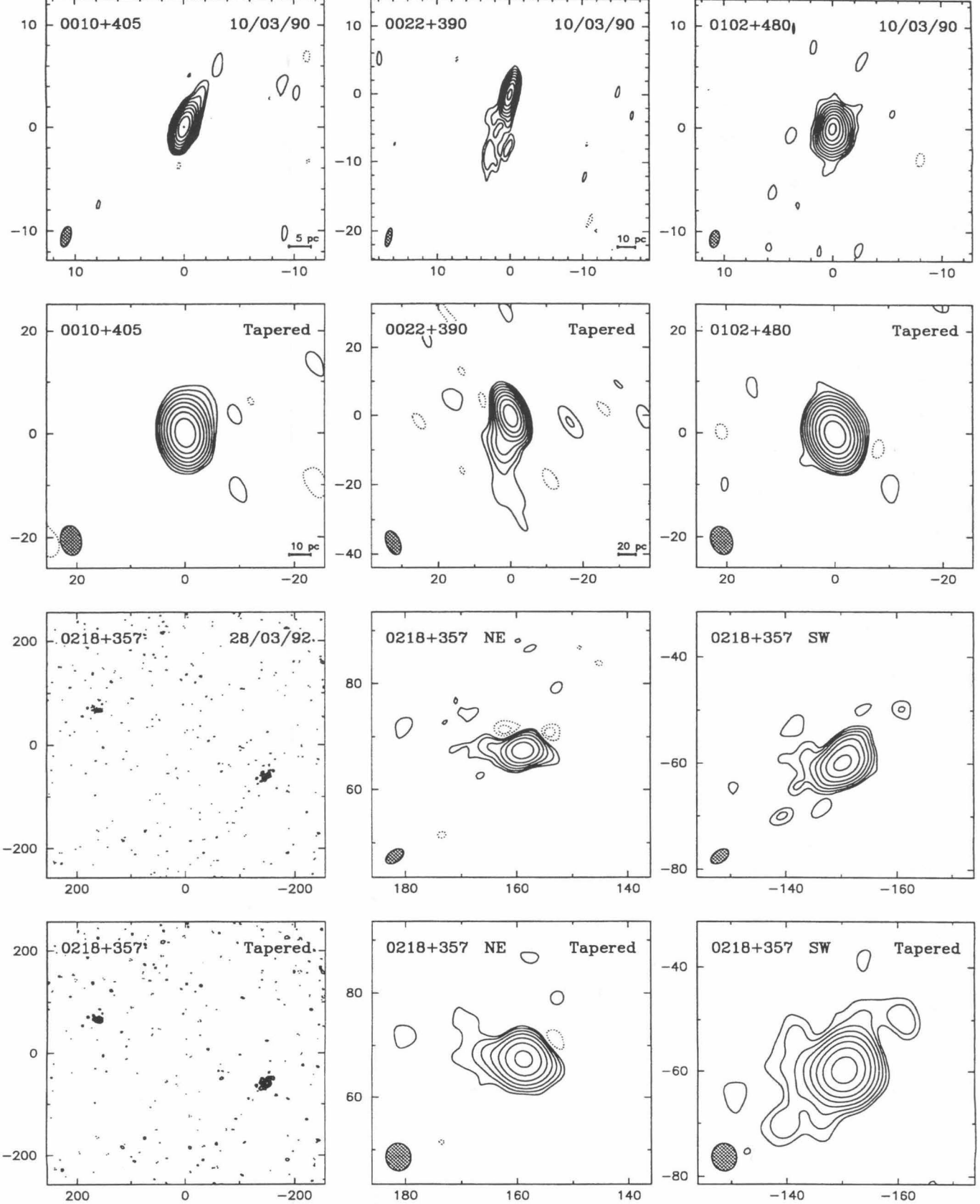

FIG. 2.—The 5 GHz VLBI maps of 84 objects. For each object the upper panel shows the naturally weighted map, and the lower panel shows the tapered map. Logarithmic contour levels are used in all maps, at $-2, -1, 1, 2, 4, 8, 16, \cdots 1024 \times 3\ \sigma$ (where σ is the rms noise measured in a blank region of the map). The objects 0218+357, 0821+394, 1138+594, and 1437+624 have large angular sizes, and maps of individual components are also presented. The FWHM contour of the elliptical Gaussian restoring beam is shown hatched in the lower left-hand corner. The peak intensity, rms noise, and parameters of the restoring beam are listed in Table 3. The angular scale is marked in milliarcseconds, and, where the redshift is known, the linear scale of each map is indicated in the lower right-hand corner (assuming $H_0 = 100$ km s^{-1} Mpc^{-1} and $q_0 = 0.5$). FITS images corresponding to the maps presented in Fig. 2 are published in the AAS CD-ROM Series, Vol. 5.

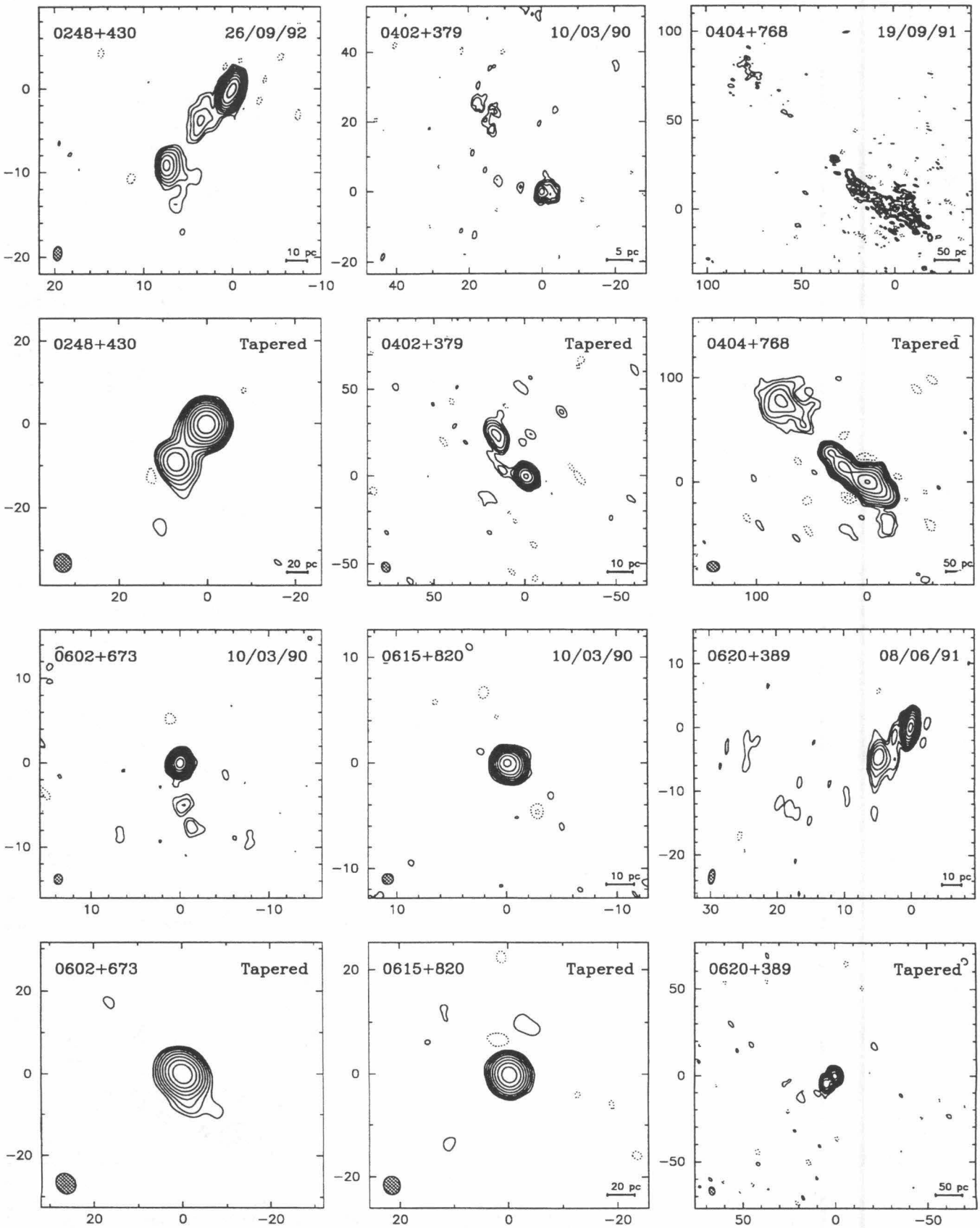

FIG. 2—*Continued*

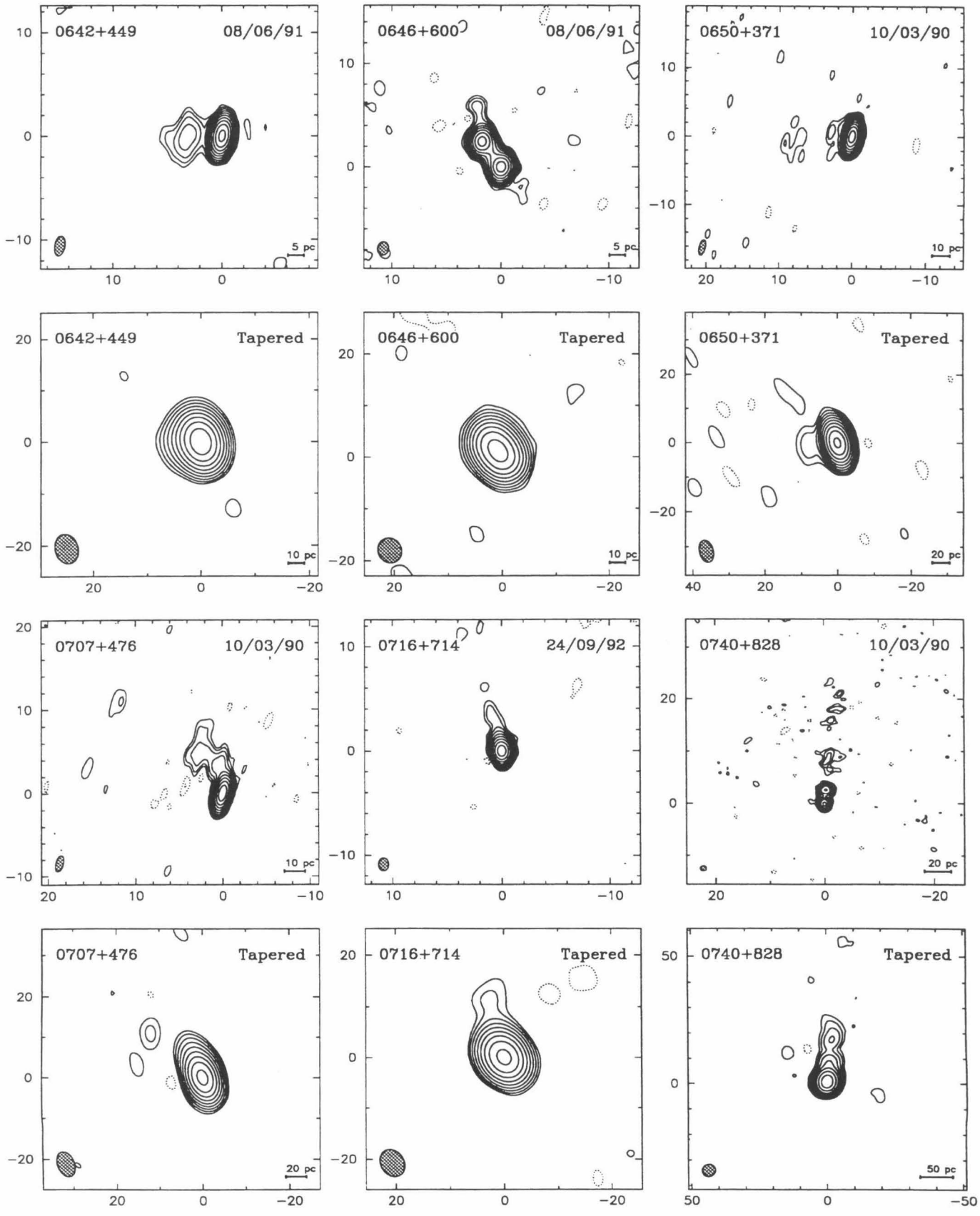

FIG. 2—*Continued*

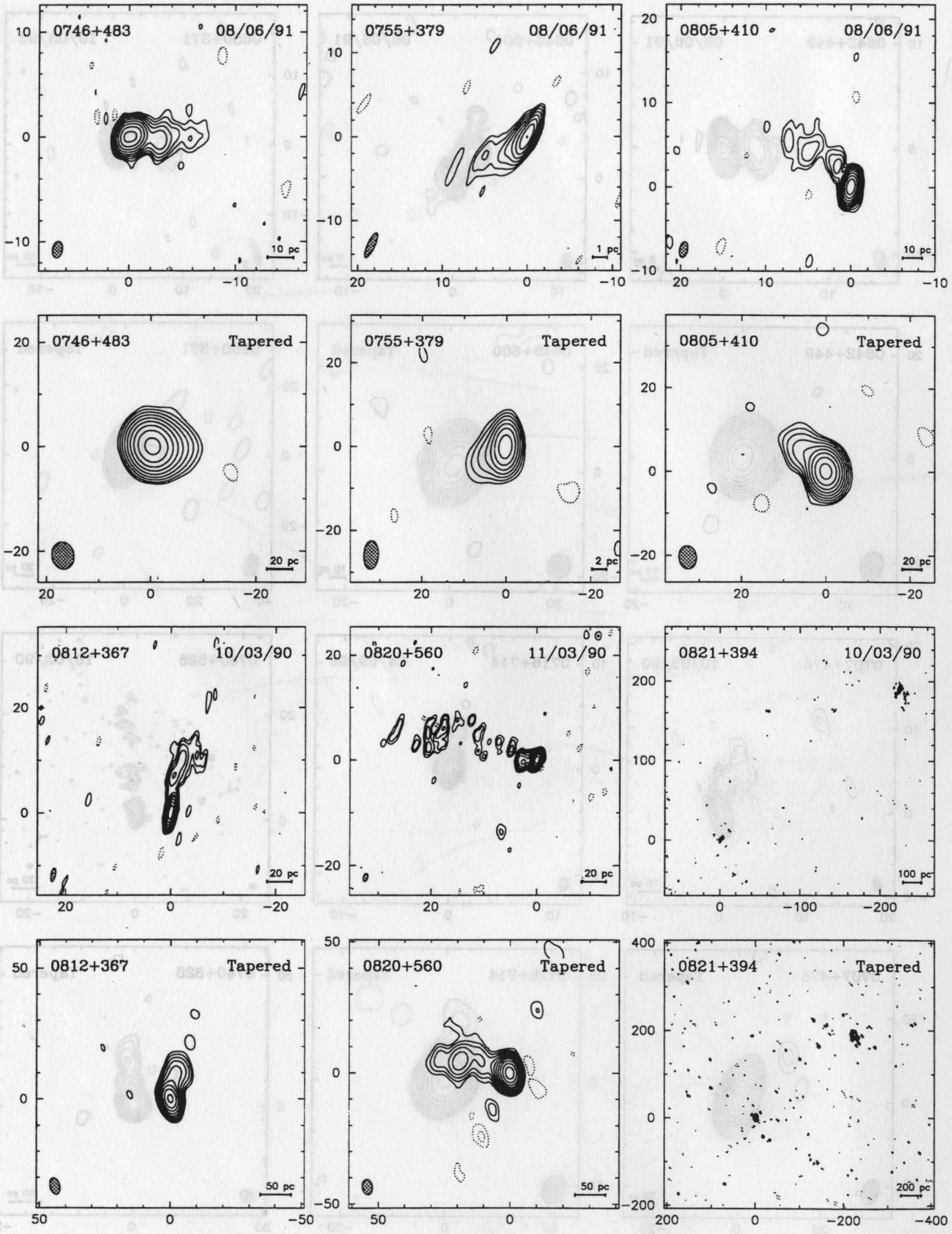

FIG. 2—*Continued*

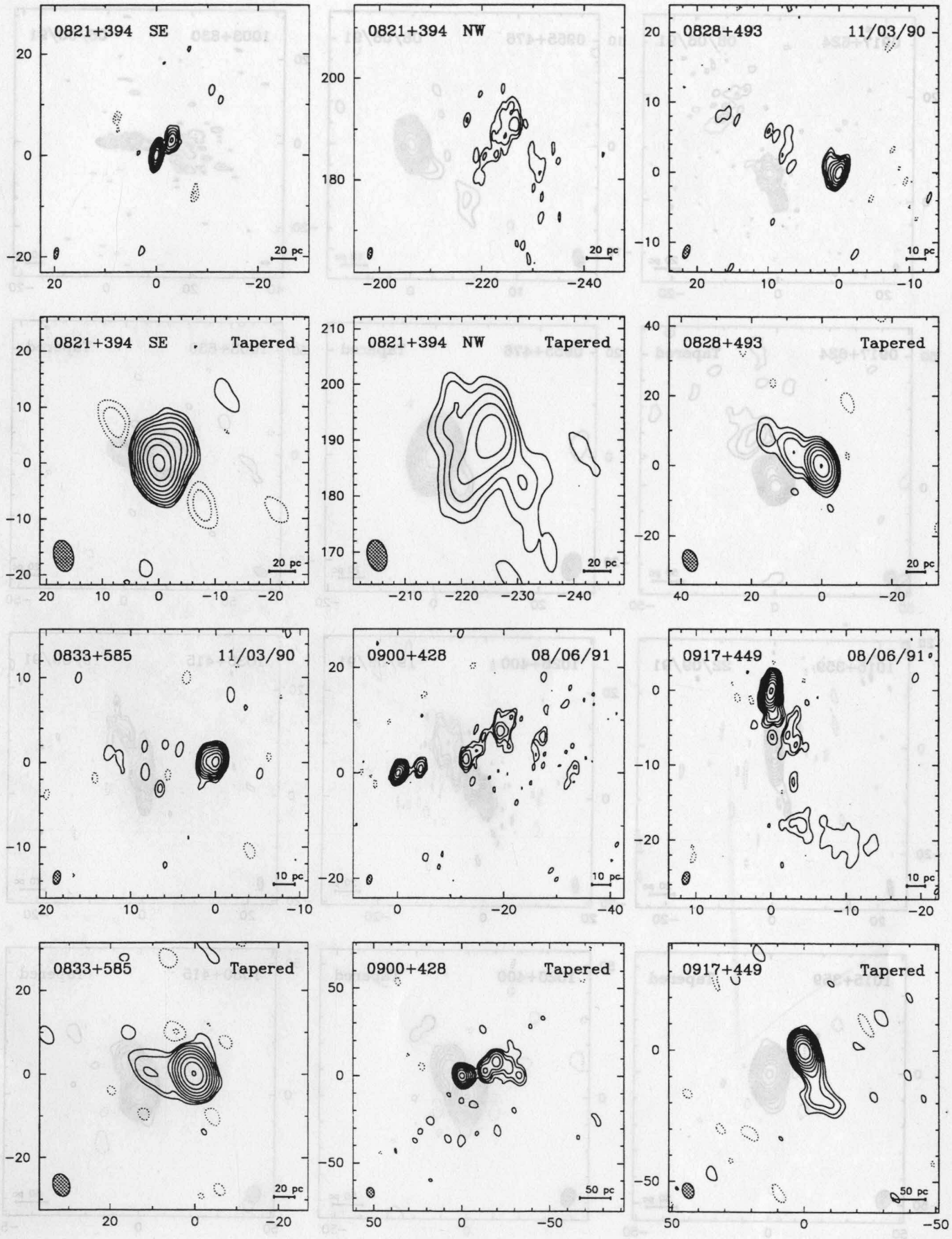

FIG. 2—*Continued*

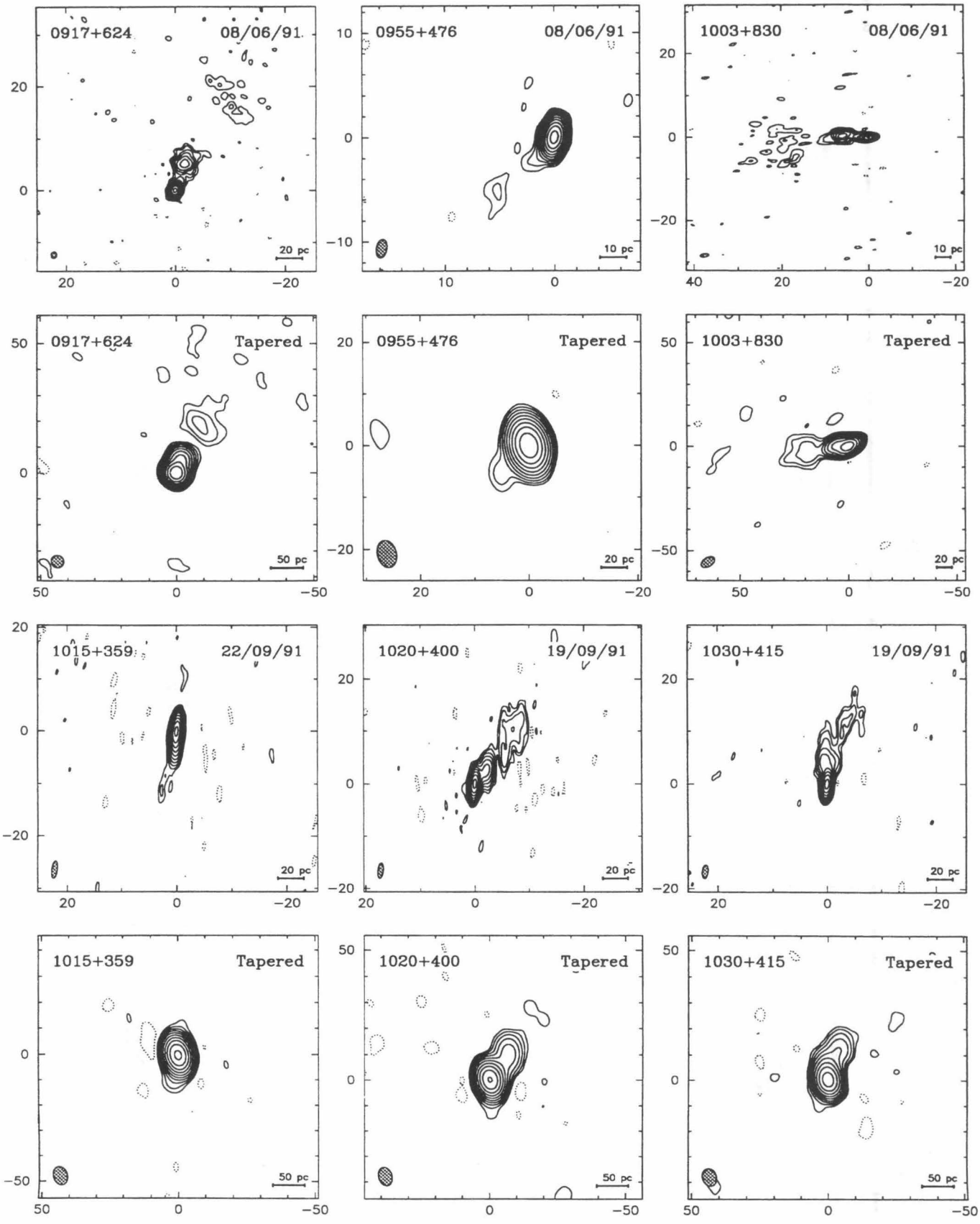

FIG. 2—*Continued*

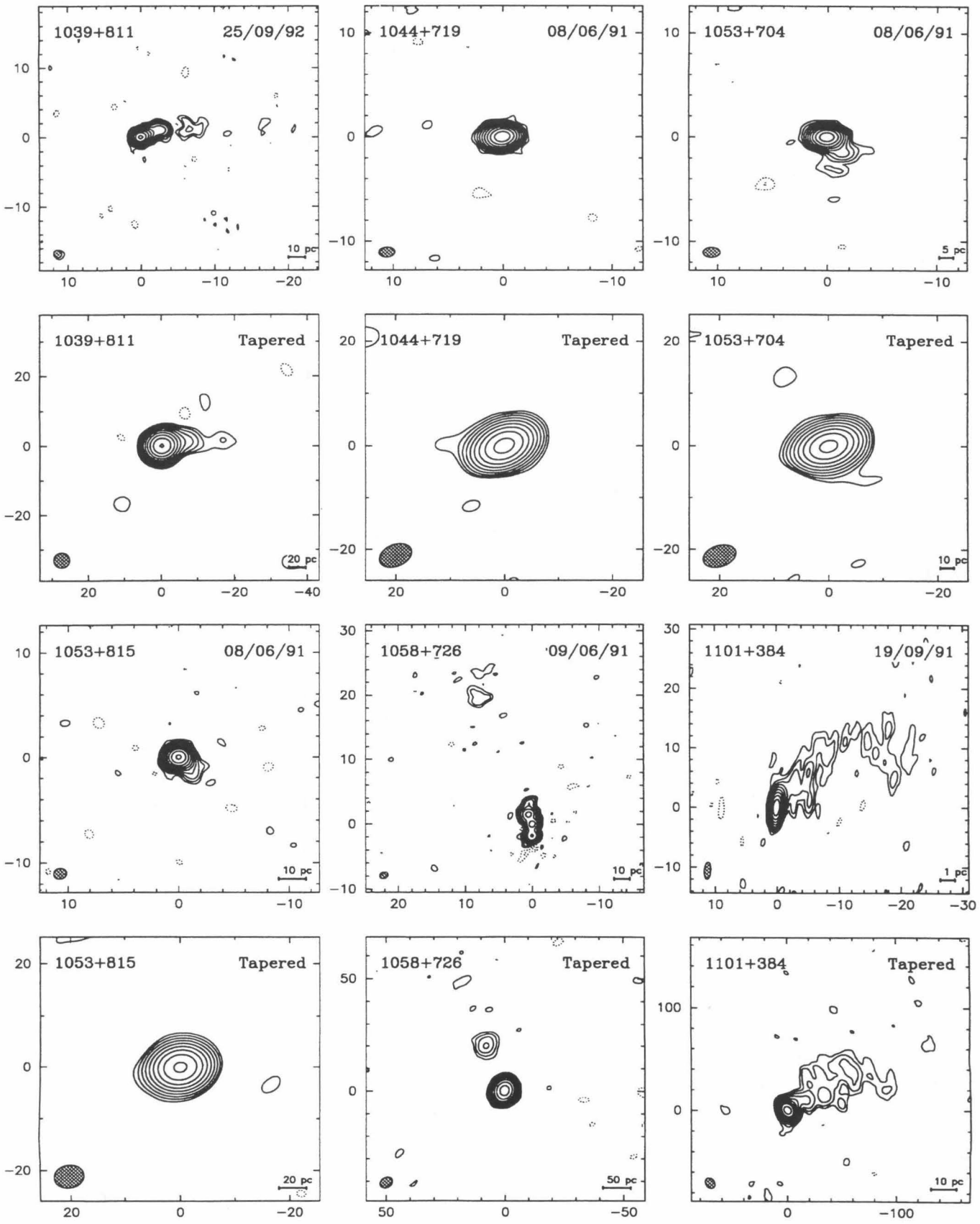

FIG. 2—*Continued*

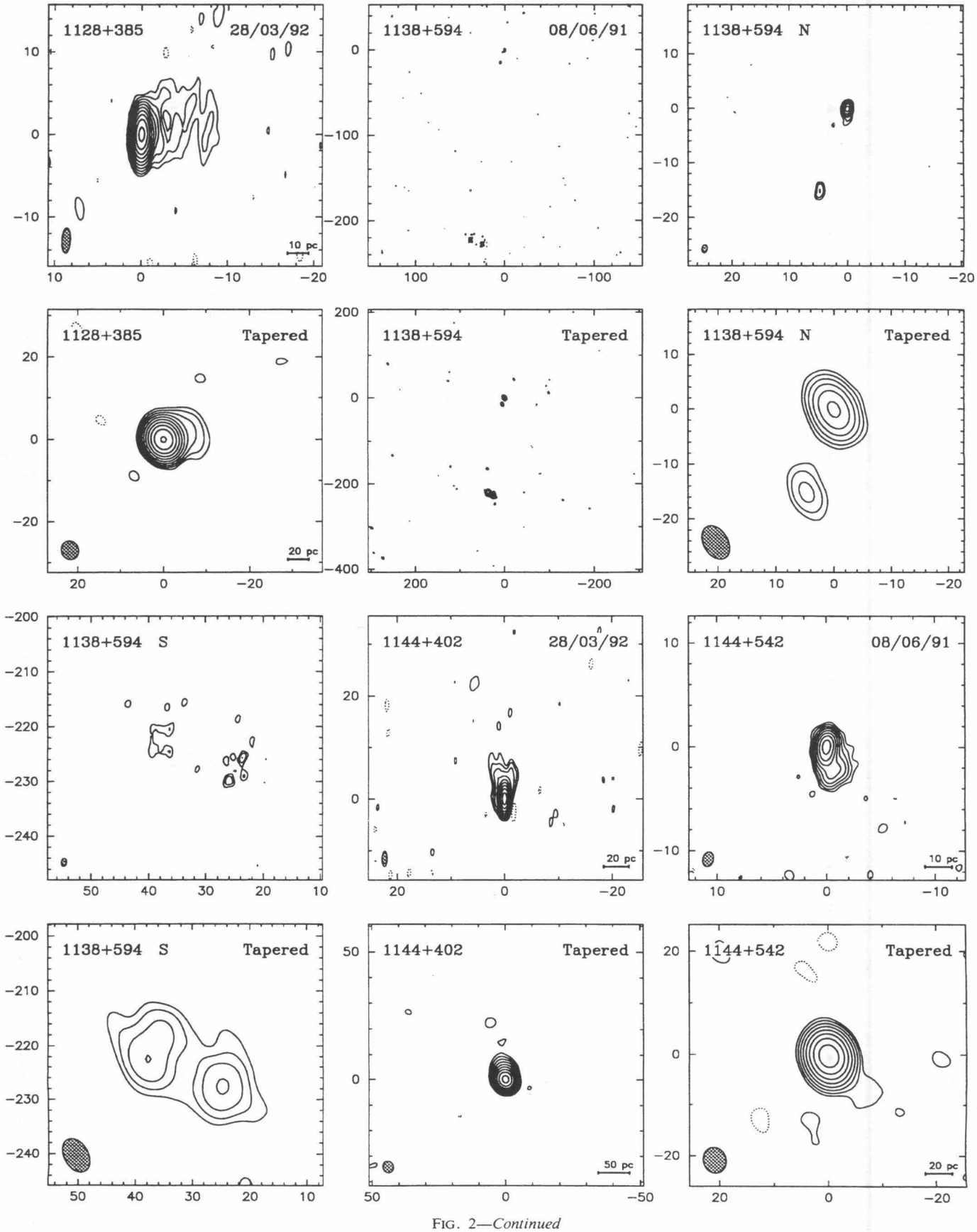

FIG. 2—*Continued*

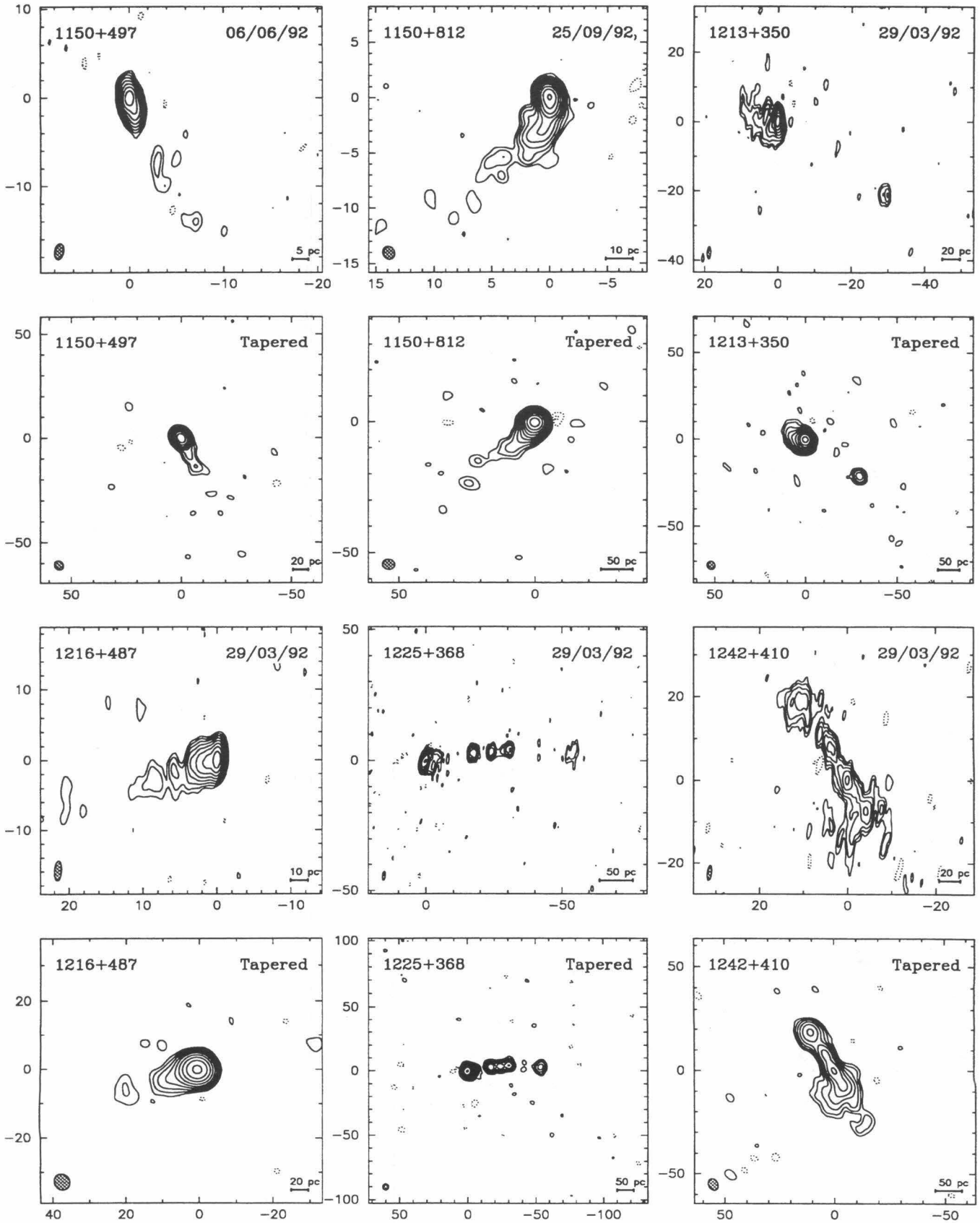

FIG. 2—*Continued*

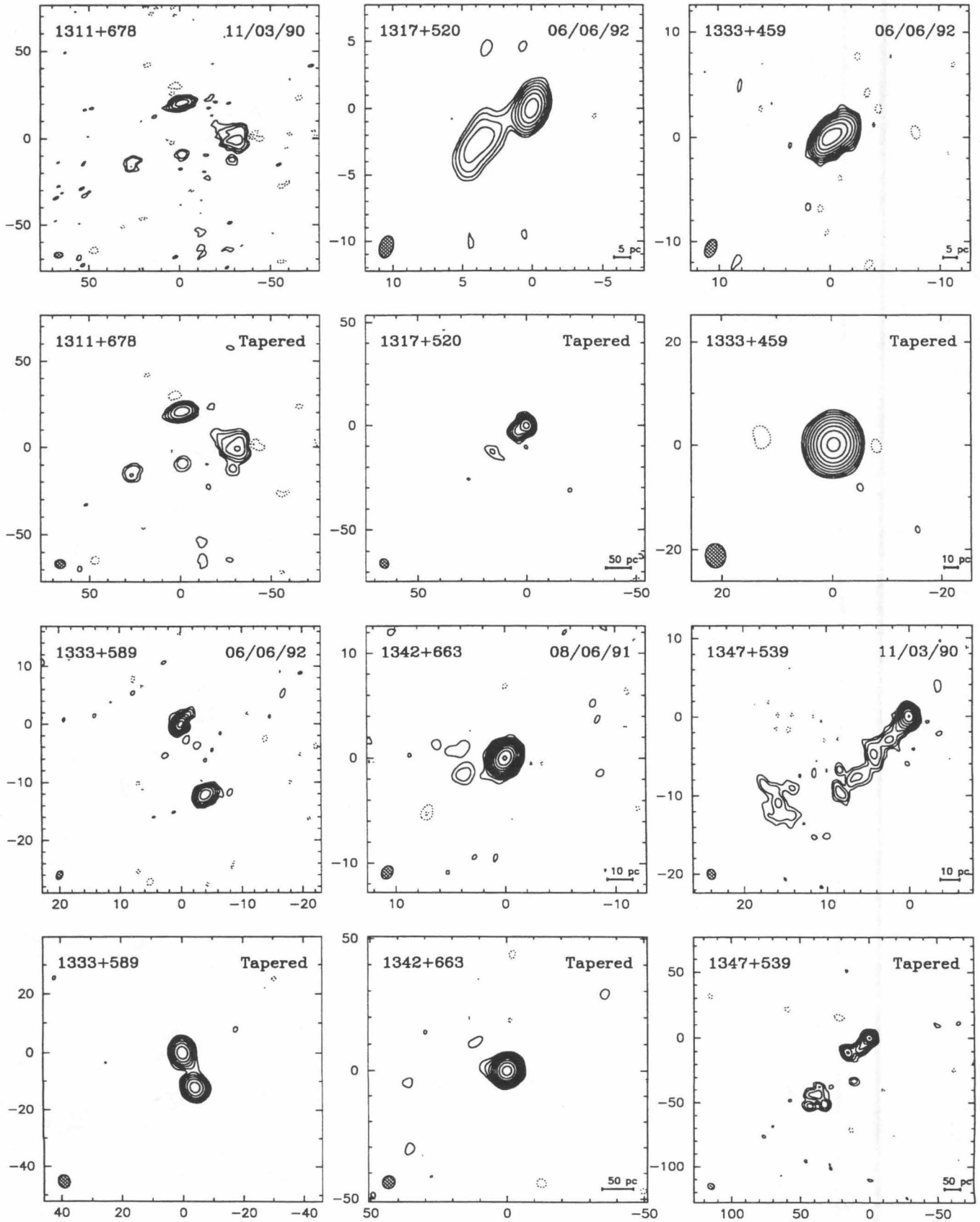

FIG. 2—*Continued*

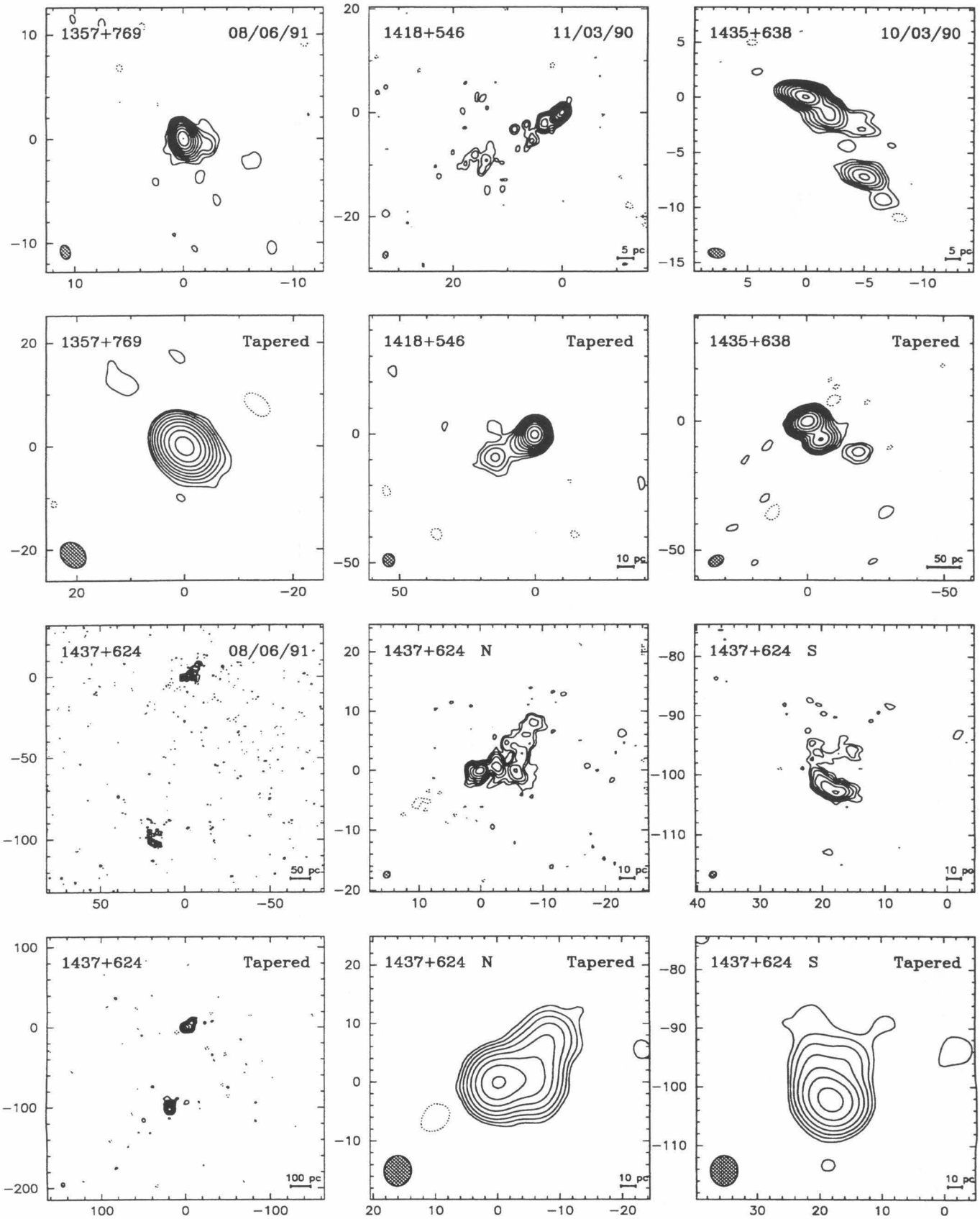

FIG. 2—*Continued*

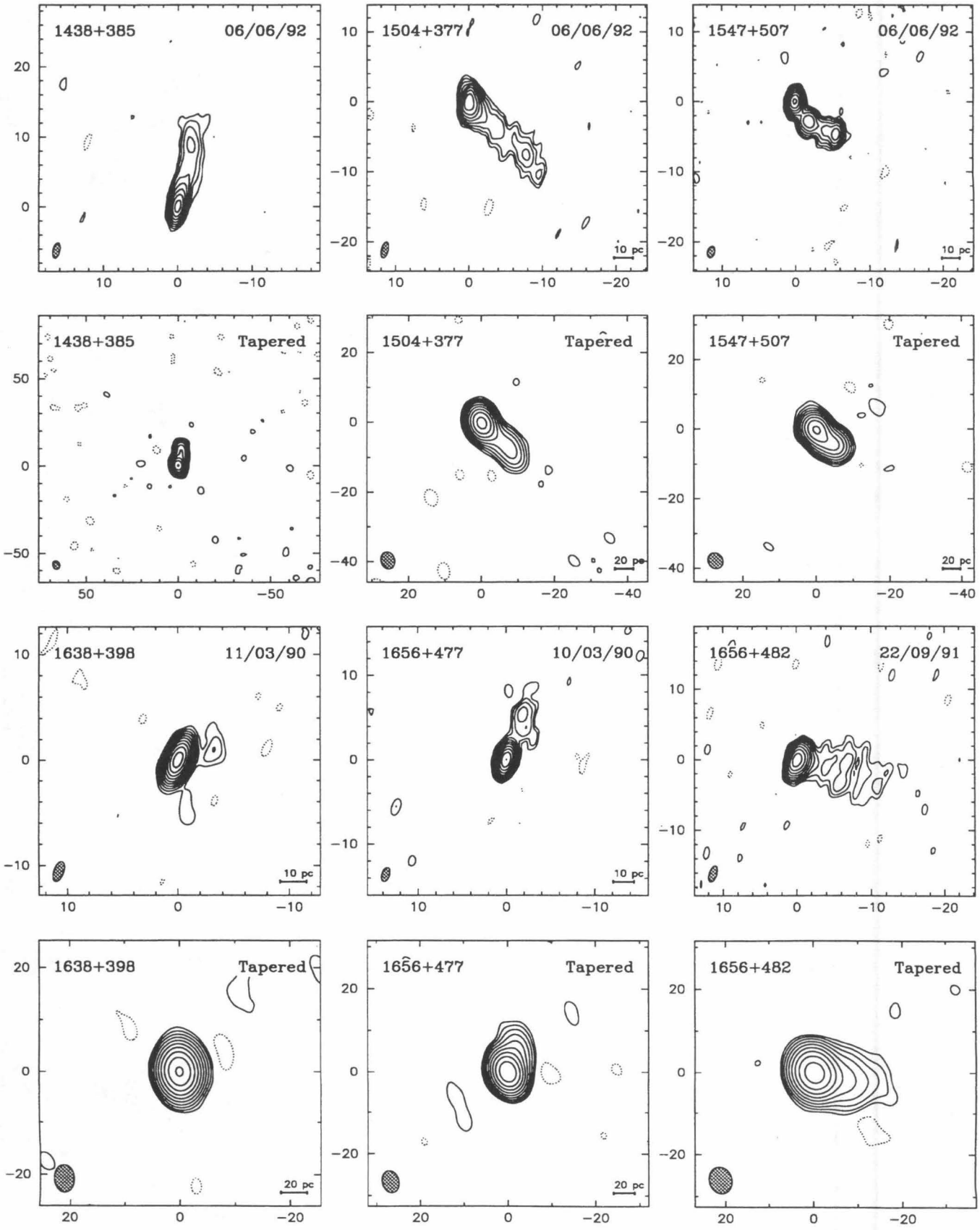

FIG. 2—*Continued*

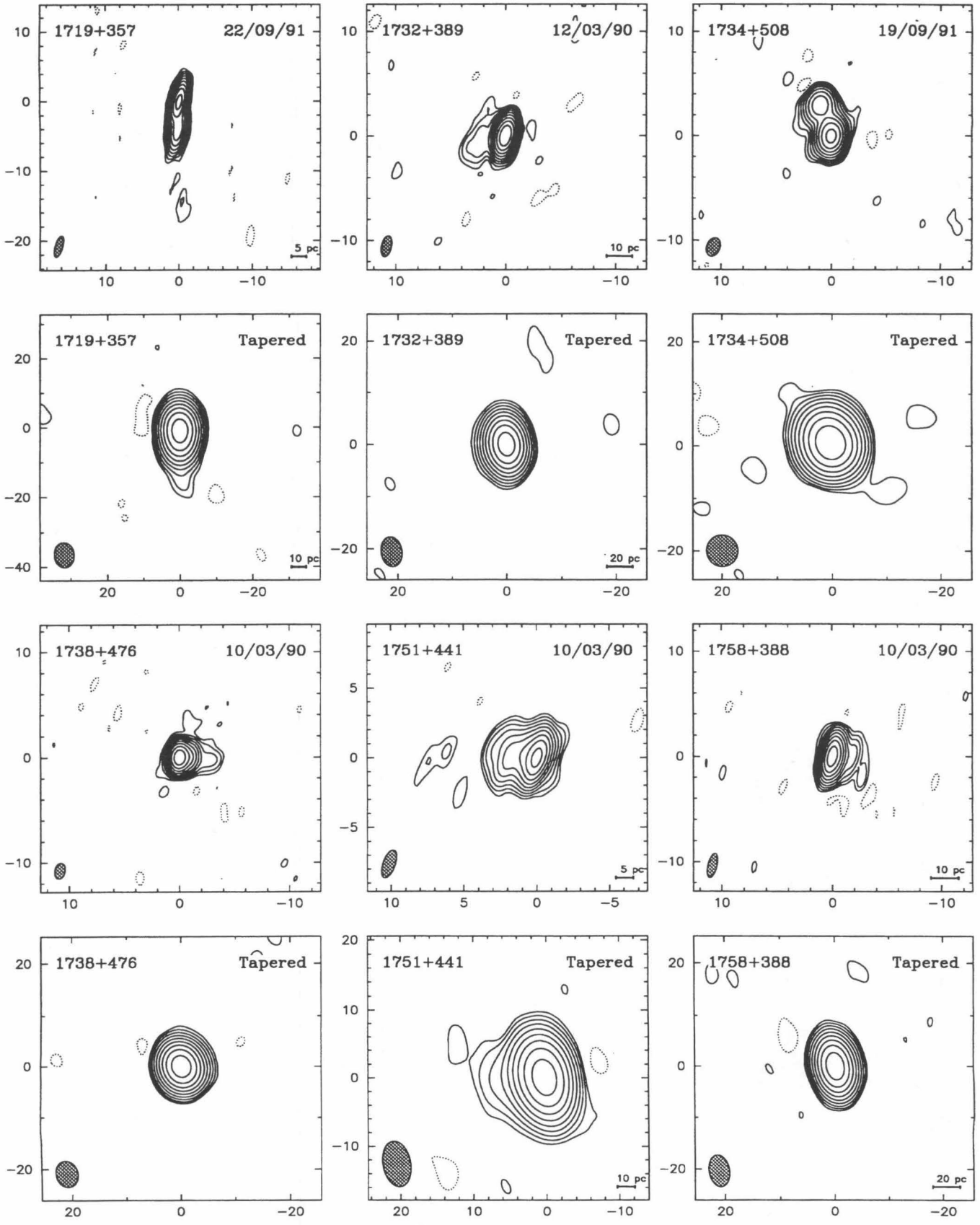

FIG. 2—*Continued*

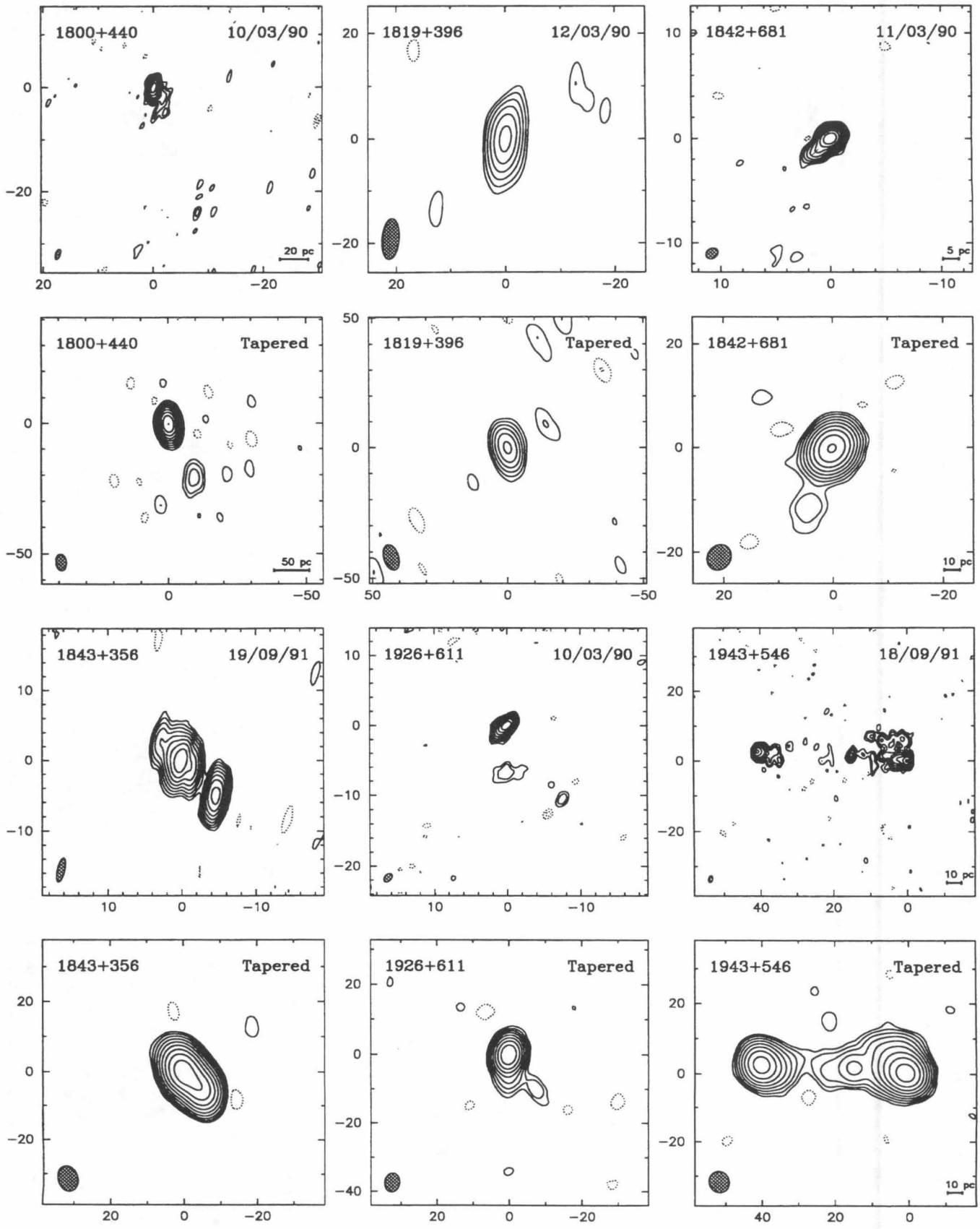

FIG. 2—*Continued*

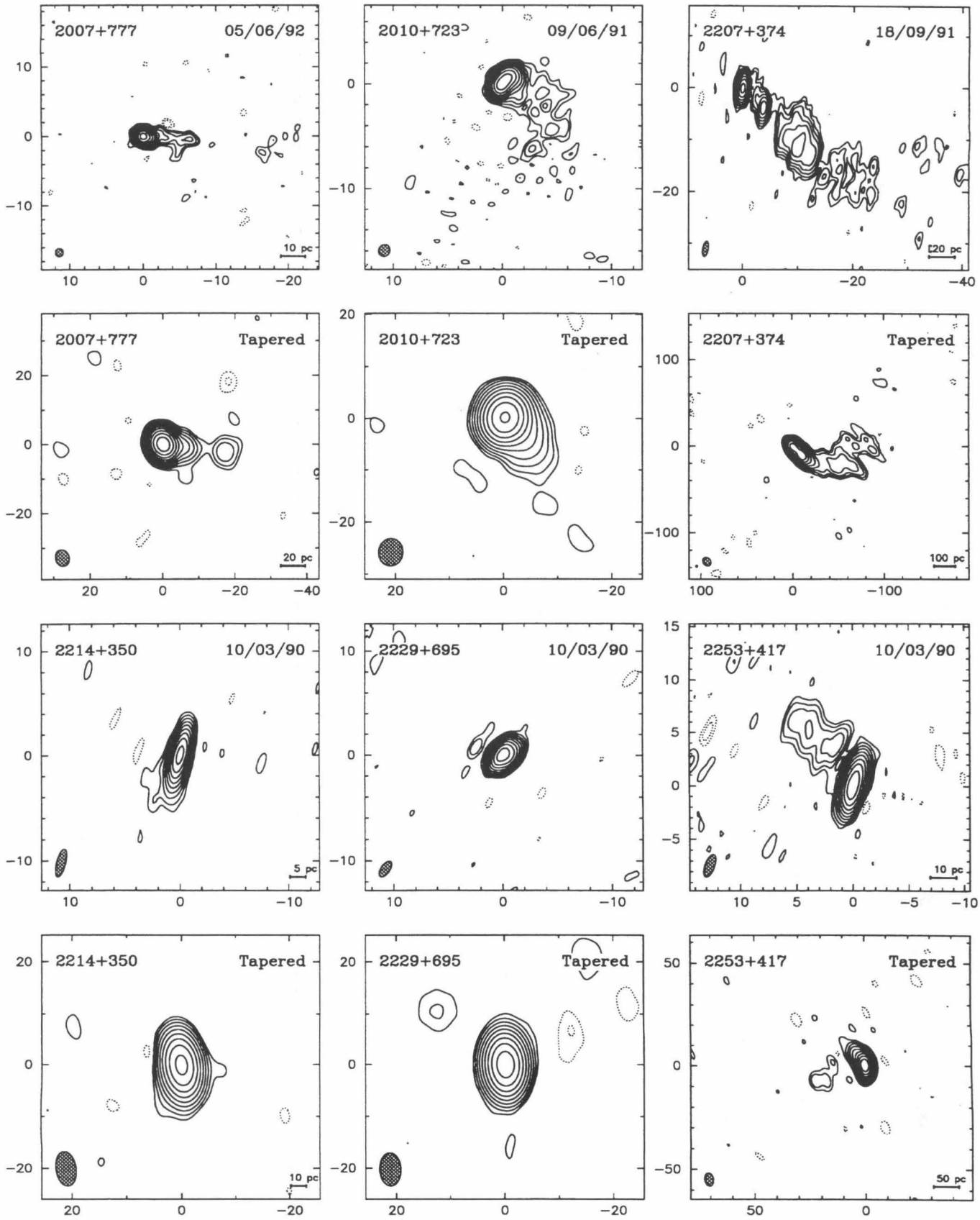

FIG. 2—*Continued*

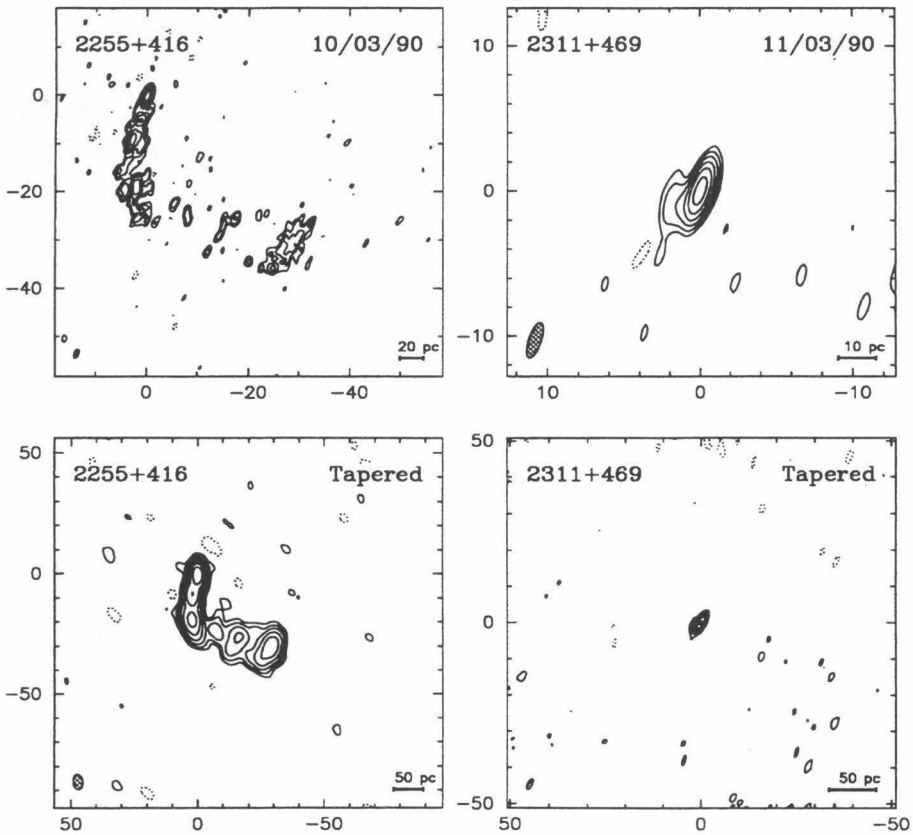

FIG. 2—*Continued*

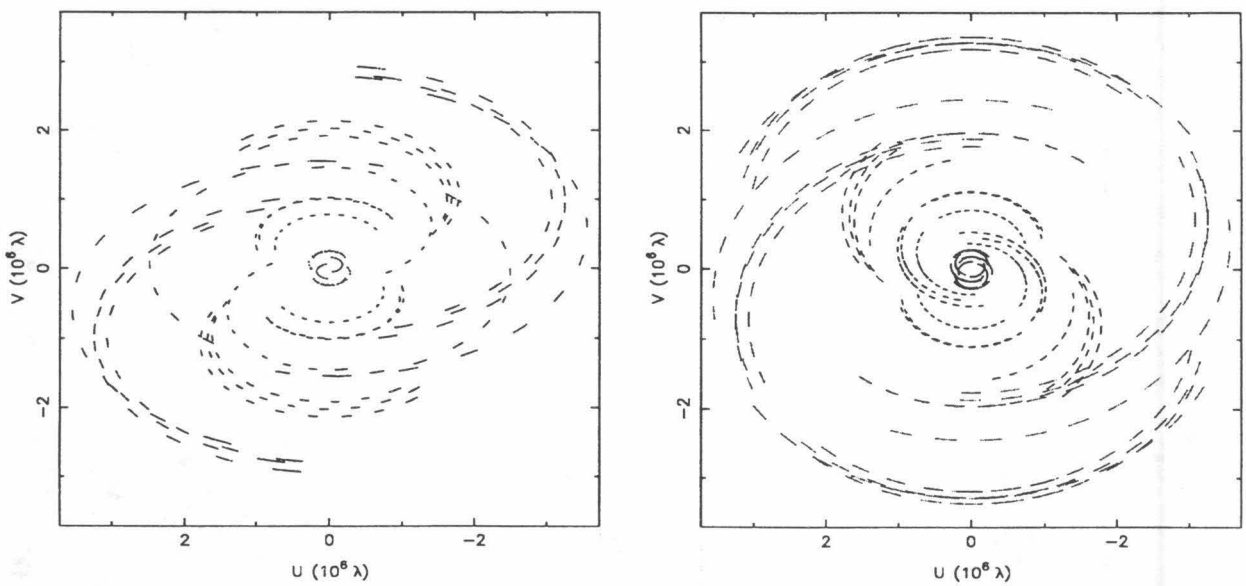

FIG. 3.—Typical *uv* coverages for MERLIN observations. *Left:* $\delta \simeq 37°$ (0812+367 observed on 1992 February 4); *right:* $\delta \simeq 54°$ (1347+539 observed on 1992 February 6).

TABLE 2

VLBI MAP PARAMETERS

Source	Observation	Naturally Weighted Maps					Tapered Maps				
		Beam[a]			S_{peak}	rms	Beam			S_{peak}	rms
		a (mas)	b (mas)	θ (°)			a (mas)	b (mas)	θ (°)		
0010+405	1990 Mar	2.0	0.9	−14	417.0	0.5	5.8	3.9	10	466.0	0.6
0022+390	1990 Mar	2.7	0.8	−12	395.0	0.8	7.3	3.8	20	518.0	0.8
0102+480	1990 Mar	1.7	0.9	−11	695.0	0.7	5.6	3.9	18	1060.0	0.8
0218+357[c]	1992 Mar	3.7	2.2	−52	221.3	0.7	5.2	4.5	6	380.0	0.7
0248+430	1992 Sep	1.7	1.0	−7	609.0	0.6	4.5	4.0	12	982.0	0.7
0402+379	1990 Mar	2.1	0.9	−17	143.0	1.0	6.0	4.6	22	413.0	0.9
0404+768	1991 Sep	1.9	1.2	70	153.0	1.0	11.4	10.1	84	997.6	1.2
0602+673	1990 Mar	1.2	1.0	−7	560.0	0.4	5.2	4.3	30	649.0	0.9
0615+820	1990 Mar	1.1	1.0	−29	458.0	0.5	3.6	3.1	9	717.0	1.1
0620+389	1991 Jun	2.4	0.9	−9	403.0	0.4	4.8	3.2	12	464.0	0.8
0642+449	1991 Jun	1.9	0.9	−10	1470.0	0.7	5.8	4.2	14	1580.0	1.2
0646+600	1991 Jun	1.3	1.0	−11	430.0	0.4	4.9	4.3	24	813.0	0.7
0650+371	1990 Mar	2.3	0.8	−14	959.0	0.4	6.5	3.8	14	1280.0	0.7
0707+476	1990 Mar	2.0	0.8	−14	645.0	0.5	6.3	3.8	18	770.0	0.8
0707+689[b]	1991 Jun										
0716+714	1992 Sep	1.3	0.9	1	598.0	0.5	5.6	4.4	28	640.0	0.7
0740+828	1990 Mar	1.1	1.0	−82	310.0	0.6	5.0	4.7	−44	573.0	0.9
0746+483	1991 Jun	1.6	1.0	−11	439.0	0.4	5.2	4.3	13	757.0	0.8
0755+379	1991 Jun	3.2	0.8	−24	143.0	0.4	6.8	3.5	−4	175.0	0.6
0805+410	1991 Jun	1.9	0.9	−12	910.0	0.6	5.5	4.1	7	966.0	0.9
0812+367	1990 Mar	2.6	0.8	−11	701.0	0.5	6.4	3.7	15	782.0	0.9
0820+560	1990 Mar	1.6	0.9	−17	1160.0	0.5	5.9	3.9	10	1320.0	0.6
0821+394[c]	1990 Mar	2.3	0.8	−9	642.0	0.9	5.6	3.5	12	694.0	0.7
0827+378[b]	1991 Jun										
0828+493	1990 Mar	2.0	0.8	−18	192.0	0.6	6.4	4.0	17	265.0	0.7
0833+585	1990 Mar	1.6	0.9	−10	386.0	0.7	5.5	3.9	19	604.0	0.8
0900+428	1991 Jun	1.8	0.9	−12	218.0	0.4	5.8	4.2	14	273.0	0.6
0917+449	1991 Jun	1.8	0.9	−12	973.0	0.6	6.0	4.2	17	1260.0	0.8
0917+624	1991 Jun	1.2	1.1	−8	843.0	0.4	4.9	4.6	28	1020.0	0.7
0955+476	1991 Jun	1.8	1.0	−10	993.0	0.5	5.3	3.5	14	1050.0	0.8
1003+830	1991 Jun	1.9	0.8	−81	258.0	0.3	6.9	4.1	−55	304.0	0.5
1015+359	1991 Sep	3.3	1.0	−7	569.0	0.3	7.3	5.1	15	668.0	0.4
1020+400	1991 Sep	3.0	1.0	−6	698.0	0.4	7.3	4.9	15	762.0	0.5
1030+415	1991 Sep	2.7	1.0	−6	282.0	0.3	6.9	5.1	16	324.0	0.3
1039+811	1992 Sep	1.1	1.1	61	869.0	0.5	4.4	4.3	−85	1090.0	0.7
1044+719	1991 Jun	1.5	0.9	−86	757.0	0.6	6.2	4.1	−65	958.0	0.9
1053+704	1991 Jun	1.6	0.9	−89	480.0	0.4	6.3	4.0	−70	556.0	0.6
1053+815	1991 Jun	1.2	1.0	−80	492.0	0.3	5.5	4.4	−77	554.0	0.6
1058+726	1991 Jun	1.3	1.0	−70	105.0	0.4	5.7	4.4	−54	311.0	0.6
1101+384	1991 Sep	2.9	1.1	−5	374.0	0.3	10.8	8.0	30	421.0	0.4
1128+385	1992 Mar	3.1	1.0	−3	823.0	0.4	4.6	4.0	14	936.0	0.6
1138+594[c]	1991 Jun	1.5	0.9	−9	79.2	0.6	6.6	4.2	27	90.0	0.8
1144+402	1992 Mar	3.0	1.0	−1	532.0	0.5	4.6	4.0	17	580.0	0.6
1144+542	1991 Jun	1.4	1.0	−14	230.0	0.4	5.1	4.2	14	349.0	0.6
1150+497	1992 Jun	1.8	0.9	−8	325.0	0.5	4.6	3.8	31	440.0	0.6

TABLE 2—*Continued*

Source	Observation	Naturally Weighted Maps					Tapered Maps				
		Beam[a]			S_{peak}	rms	Beam			S_{peak}	rms
		a (mas)	b (mas)	θ (°)			a (mas)	b (mas)	θ (°)		
1150+812	1992 Sep	1.2	1.0	25	727.0	0.4	4.6	3.9	79	1050.0	0.5
1203+645[b]	1990 Mar										
1213+350	1992 Mar	3.5	0.9	−3	433.0	0.7	4.9	4.2	18	691.0	0.7
1216+487	1992 Mar	2.9	1.0	−4	312.0	0.5	4.8	4.2	22	498.0	0.5
1225+368	1992 Mar	3.4	1.0	−6	226.0	0.6	4.8	4.1	8	457.0	0.6
1242+410	1992 Mar	3.6	0.9	−6	66.5	0.6	6.0	4.3	25	157.0	0.7
1311+678	1990 Mar	4.8	3.3	−84	148.0	2.0	5.8	5.0	82	184.0	2.2
1317+520	1992 Jun	1.7	1.0	−16	161.0	0.5	4.6	3.9	23	179.0	0.7
1333+459	1992 Jun	1.8	1.0	−21	350.0	0.6	4.6	3.7	4	579.0	0.6
1333+589	1992 Jun	1.6	1.0	−25	219.0	0.8	4.6	3.7	18	307.0	1.9
1342+663	1991 Jun	1.3	1.0	−28	597.0	0.4	5.0	4.5	−14	682.0	0.6
1347+539	1990 Mar	1.3	1.0	15	437.0	0.6	5.1	4.3	49	505.0	0.6
1357+769	1991 Jun	1.4	0.9	14	584.0	0.4	5.4	4.2	40	643.0	0.6
1418+546	1990 Mar	1.3	0.9	−15	1470.0	0.6	5.1	4.3	6	1930.0	1.0
1435+638	1990 Mar	1.4	0.9	79	536.0	0.6	5.9	4.0	−61	733.0	0.6
1437+624[c]	1991 Jun	1.2	1.0	−29	129.0	0.4	5.2	4.4	−4	267.0	0.6
1438+385	1992 Jun	2.2	0.9	−12	321.0	0.6	4.9	3.8	14	429.0	0.5
1504+377	1992 Jun	2.3	0.9	−13	349.0	0.5	5.0	3.8	13	534.0	0.5
1547+507	1992 Jun	1.7	1.0	−13	438.0	0.5	4.7	4.0	24	557.0	0.6
1637+626[b]	1991 Jun										
1638+398	1990 Mar	2.0	0.9	−19	1570.0	0.7	5.3	3.7	5	1760.0	1.0
1656+477	1990 Mar	1.7	0.9	−16	1230.0	0.8	5.3	3.8	14	1440.0	1.0
1656+482	1991 Sep	2.4	1.0	−18	393.0	0.3	6.5	5.2	15	566.0	0.5
1719+357	1991 Sep	3.1	1.0	−16	288.0	0.3	7.3	5.4	4	387.0	0.3
1732+389	1990 Mar	2.0	0.9	−12	1040.0	0.7	5.8	3.8	8	1230.0	1.0
1734+508	1991 Sep	1.8	1.2	−20	465.0	0.4	6.1	5.7	8	722.0	0.5
1738+476	1990 Mar	1.5	0.9	−11	797.0	0.6	5.1	4.0	14	1030.0	0.8
1751+441	1990 Mar	2.1	0.8	−18	604.0	0.6	6.7	3.8	10	843.0	0.7
1758+388	1990 Mar	2.4	0.8	−13	691.0	0.6	6.2	3.7	9	889.0	0.7
1800+440	1990 Mar	2.1	0.8	−19	389.0	0.6	6.3	3.8	5	501.0	0.7
1819+396	1990 Mar	7.8	3.1	−5	228.0	1.8	10.0	5.5	17	245.0	2.2
1842+681	1990 Mar	1.2	0.9	−50	622.0	0.8	5.0	4.2	−26	801.0	1.0
1843+356	1991 Sep	3.5	1.0	−12	245.0	0.3	7.5	5.3	14	528.0	0.4
1926+611	1990 Mar	1.4	0.9	−38	399.0	0.6	5.6	4.1	−7	551.0	0.7
1943+546	1991 Sep	1.9	1.1	−12	245.0	0.3	6.3	5.4	13	481.0	0.4
2007+777	1992 Jun	1.2	1.1	−8	1540.0	0.7	4.8	3.8	16	1950.0	0.7
2010+723	1991 Jun	1.1	1.0	−18	519.0	0.4	5.3	4.4	−4	919.0	0.5
2207+374	1991 Sep	2.9	1.0	−10	152.0	0.3	10.5	8.0	27	277.0	0.4
2214+350	1990 Mar	2.7	0.8	−14	527.0	0.5	6.7	3.7	9	586.0	0.6
2229+695	1990 Mar	1.7	0.8	−33	650.0	0.5	6.4	3.8	2	949.0	0.8
2253+417	1990 Mar	2.2	0.8	−19	624.0	0.4	6.3	3.8	9	958.0	0.7
2255+416	1990 Mar	2.0	0.9	−20	236.0	0.7	6.3	3.8	8	304.0	0.8
2311+469	1990 Mar	2.6	0.8	−17	71.8	0.5	3.1	1.2	−25	78.0	0.7

[a] The restoring beam is an elliptical Gaussian with FWHM major axis a and minor axis b, with major axis in position angle θ.
[b] Heavily resolved.
[c] The same contour levels are used for maps of individual components.

NOTES.—Col. (1): Source name. Col. (2): Observation date. Cols. (3)–(5): The beam characteristics of the naturally weighted maps. Col. (6): The peak intensity of the naturally weighted maps (mJy beam^{-1}). Col. (7): The rms noise in the naturally weighted maps (mJy beam^{-1}). Cols. (8)–(10): The beam characteristics of the tapered maps. Col. (11): The peak intensity of the tapered maps (mJy beam^{-1}). Col. (12): The rms noise in the tapered maps (mJy beam^{-1}).

Table 2 is published in computer-readable form in the AAS CD-ROM Series, Vol. 5.

TABLE 3

GAUSSIAN MODELS

Source	S (Jy)	r (mas)	θ (°)	a (mas)	b/a	ϕ (°)	Amp. A.F.	Cl.Phs. A.F.	Total A.F.
0010+405	0.423	0.00	0.0	0.55	0.40	144.8	1.004	1.059	1.029
	0.058	0.97	−30.2	1.41	0.30	−31.2			
0022+390	0.395	0.00	0.0	0.55	0.86	109.8	1.041	1.077	1.057
	0.087	5.28	168.8	9.19	0.11	153.9			
	0.118	1.04	159.6	0.68	0.41	44.8			
0102+480	0.664	0.50	194.1	1.63	0.72	11.2	1.035	1.041	1.038
	0.453	0.00	0.0	0.28	0.34	111.3			
0248+430	0.718	0.00	0.0	0.99	0.41	150.2	1.261	1.127	1.201
	0.353	1.29	145.5	0.51	0.00	61.5			
	0.044	5.43	154.3	4.80	0.00	150.5			
	0.128	11.93	140.8	1.30	0.64	10.9			
0402+379	0.403	0.65	235.0	2.90	0.78	89.6	1.017	1.354	1.172
	0.094	0.24	158.3	0.75	0.00	29.9			
	0.048	2.72	91.3	1.07	0.81	178.4			
	0.162	27.72	35.3	11.68	0.34	23.2			
0602+673	0.642	0.00	0.0	0.53	0.66	−19.7	1.052	1.061	1.056
	0.036	3.46	187.3	6.84	0.21	173.7			
0615+820	0.528	0.00	0.0	0.67	0.64	154.1	1.027	1.105	1.063
	0.254	0.84	238.9	1.12	0.56	−5.6			
0620+389	0.436	0.00	0.0	0.47	0.68	−62.2	0.949	0.997	0.971
	0.049	1.20	149.8	1.98	0.00	27.0			
	0.089	6.68	134.2	2.22	0.67	−32.9			
0642+449	1.566	0.00	0.0	0.34	0.76	82.3	0.998	0.975	0.987
	0.086	3.03	92.1	1.57	0.81	25.4			
0646+600	0.449	0.00	0.0	0.51	0.64	38.1	1.018	1.106	1.059
	0.493	3.03	−144.8	0.53	0.81	12.4			
	0.102	1.35	−139.1	1.59	0.08	12.6			
	0.012	3.39	13.0	0.58	0.33	153.8			
0650+371	1.288	0.00	0.0	0.77	0.57	43.8	1.109	1.214	1.157
	0.022	3.01	87.3	1.23	0.30	99.5			
0707+476	0.434	0.00	0.0	0.29	0.95	−52.4	1.041	1.032	1.037
	0.279	0.62	−16.0	0.44	0.68	48.7			
	0.040	5.16	23.4	2.28	0.38	134.9			
	0.087	1.80	6.1	4.19	0.21	−0.9			
	0.014	15.94	51.7	10.36	0.50	−34.7			
0716+714	0.631	0.00	0.0	0.34	0.22	28.1	1.078	1.035	1.058
	0.018	1.99	6.5	0.00	0.10	0.0			
0740+828	0.319	0.00	0.0	0.36	0.74	9.9	1.141	1.149	1.145
	0.119	0.87	10.3	0.00	0.01	105.2			
	0.258	2.76	−5.5	1.18	0.85	101.1			
	0.049	8.63	−4.2	3.10	0.29	19.4			
	0.048	17.67	−5.1	10.29	0.23	−2.7			
0746+483	0.363	0.00	0.0	0.47	0.35	93.4	1.075	1.129	1.100
	0.391	0.82	−85.4	0.74	0.59	−75.0			
	0.087	3.10	−92.4	1.52	0.60	81.3			
0755+379	0.120	0.00	0.0	0.26	0.00	54.6	1.028	1.087	1.055
	0.031	0.72	127.8	0.54	0.00	−93.8			
	0.048	1.52	119.8	2.85	0.26	118.9			
0805+410	0.956	0.00	0.0	0.42	0.60	10.4	1.127	1.002	1.071
	0.025	2.46	27.8	1.51	0.00	13.1			
	0.070	6.54	46.8	5.73	0.37	58.1			

TABLE 3—*Continued*

Source	S (Jy)	r (mas)	θ (°)	a (mas)	b/a	ϕ (°)	Amp. A.F.	Cl.Phs. A.F.	Total A.F.
0812+367	0.549	0.00	0.0	0.21	0.51	−91.3	1.089	1.043	1.069
	0.231	1.00	−12.2	0.35	0.96	−27.6			
	0.170	8.61	−9.5	9.22	0.21	−20.1			
0820+560	1.168	0.00	0.0	0.28	0.66	115.2	1.164	1.095	1.134
	0.126	0.73	97.4	0.73	0.00	59.9			
	0.133	2.63	97.6	1.93	0.47	88.7			
	0.159	18.88	75.0	12.98	0.44	90.5			
0821+394	0.597	0.00	0.0	0.29	0.95	34.0	1.305	1.068	1.205
	0.115	0.61	−22.0	0.81	0.66	−36.8			
	0.095	4.28	−44.8	1.58	0.48	133.4			
	0.257	294.64	−49.8	10.91	0.81	35.5			
0828+493	0.202	0.00	0.0	0.37	0.63	88.2	1.008	1.063	1.033
	0.070	0.74	67.6	1.27	0.71	−43.2			
	0.038	9.93	61.4	11.18	0.34	67.5			
0833+585	0.396	0.00	0.0	0.47	0.64	69.8	1.103	1.114	1.108
	0.246	0.94	85.1	0.95	0.61	61.5			
0900+428	0.175	0.00	0.0	0.20	0.86	111.1	1.039	1.064	1.051
	0.106	0.70	−62.1	0.91	0.01	−79.4			
	0.017	4.54	−79.6	0.71	0.67	−25.0			
	0.025	13.29	−76.6	1.51	0.59	−16.9			
	0.047	21.41	−67.1	2.89	0.82	142.6			
	0.098	23.20	−76.2	21.41	0.59	90.8			
0917+449	0.705	0.00	0.0	0.50	0.07	−30.5	1.020	1.031	1.025
	0.578	0.91	176.1	1.02	0.50	3.9			
	0.080	5.92	−162.7	7.07	0.44	26.1			
	0.043	19.59	−161.3	8.79	0.26	80.1			
0917+624	0.811	0.00	0.0	0.42	0.43	145.0	1.035	1.030	1.033
	0.213	0.72	−21.0	0.60	0.18	20.6			
	0.236	5.56	−18.6	2.57	0.78	−19.5			
	0.042	20.78	−25.9	10.72	0.64	27.1			
0955+476	1.051	0.00	0.0	0.33	0.80	114.6	0.988	1.008	0.997
	0.022	1.85	132.6	2.08	0.56	144.3			
1003+830	0.278	0.00	0.0	0.51	0.26	71.1	1.056	1.040	1.049
	0.041	2.67	83.1	1.10	0.00	64.5			
	0.111	5.88	85.1	2.20	0.43	114.3			
	0.048	18.98	96.5	14.04	0.63	104.0			
1015+359	0.426	0.00	0.0	0.13	0.00	87.3	1.143	1.028	1.092
	0.176	0.82	187.0	0.55	0.66	39.0			
	0.099	2.75	181.9	1.51	0.46	175.7			
1020+400	0.694	0.00	0.0	0.21	0.01	−69.7	1.150	1.055	1.108
	0.118	2.73	−40.7	3.13	0.23	−41.9			
	0.060	12.14	−33.9	7.11	0.41	−22.8			
1030+415	0.223	0.00	0.0	0.00	1.00	120.6	1.040	1.033	1.036
	0.060	0.69	−4.5	0.41	0.15	−56.9			
	0.073	3.70	3.8	4.50	0.33	9.7			
	0.035	8.95	−15.0	14.76	0.09	−17.4			
1039+811	0.833	0.00	0.0	0.30	0.40	−60.3	1.183	1.010	1.107
	0.244	0.83	−64.8	0.81	0.40	−63.8			
	0.072	2.56	−68.2	1.19	0.55	−89.2			
	0.043	6.10	−78.0	5.70	0.28	−88.1			
1044+719	0.234	0.00	0.0	0.00	1.00	−54.4	1.041	1.019	1.031
	0.737	0.36	113.2	0.69	0.93	−36.3			

TABLE 3—*Continued*

Source	S (Jy)	r (mas)	θ (°)	a (mas)	b/a	ϕ (°)	Amp. A.F.	Cl.Phs. A.F.	Total A.F.
1053+704	0.269	0.00	0.0	0.29	0.94	172.2	1.047	1.017	1.033
	0.264	0.25	199.5	0.44	0.57	13.8			
	0.043	1.62	−144.5	1.83	0.40	56.3			
1053+815	0.372	0.00	0.0	0.19	0.98	178.1	1.033	1.030	1.032
	0.175	0.21	−143.0	0.76	0.35	−140.8			
	0.017	1.61	−129.8	1.66	0.62	150.4			
1058+726	0.122	0.00	0.0	0.59	0.26	−3.1	1.015	1.172	1.090
	0.034	0.76	−4.7	0.00	1.00	0.0			
	0.101	1.95	3.2	0.59	0.00	−127.3			
	0.148	3.40	9.9	0.95	0.62	23.7			
	0.024	23.74	19.8	4.81	0.44	−1.2			
1101+384	0.366	0.00	0.0	0.32	0.54	142.1	1.126	1.069	1.101
	0.072	1.39	−24.1	3.40	0.26	−21.8			
	0.144	42.16	−52.6	80.97	0.41	−68.9			
1128+385	0.759	0.00	0.0	0.70	0.04	3.4	1.032	1.011	1.023
	0.191	0.73	−136.1	1.03	0.41	−1.9			
	0.055	3.34	−81.0	7.72	0.58	−49.1			
1138+594	0.087	0.00	0.0	0.00	0.07	−97.4	0.928	1.224	1.068
	0.019	15.57	162.0	1.96	0.28	13.0			
	0.147	225.41	171.7	24.02	0.39	61.2			
1144+402	0.457	0.00	0.0	0.06	0.96	153.1	1.036	1.027	1.032
	0.087	2.70	−0.0	4.00	0.56	2.4			
	0.095	0.65	1.0	0.63	0.87	58.5			
1144+542	0.162	0.00	0.0	0.00	1.00	12.2	0.996	1.079	1.035
	0.044	0.60	177.1	0.12	0.00	−3.5			
	0.121	1.10	177.7	0.85	0.70	−2.3			
	0.060	2.63	196.3	1.92	0.37	122.9			
1150+497	0.327	0.00	0.0	0.46	0.22	25.1	1.044	1.068	1.055
	0.149	1.55	−157.5	0.75	0.22	23.4			
	0.037	9.41	−156.0	14.62	0.17	−154.3			
1150+812	0.702	0.00	0.0	0.36	0.43	−4.3	0.987	1.009	0.997
	0.316	0.99	182.1	0.53	0.54	136.7			
	0.188	2.97	168.4	2.74	0.38	150.2			
	0.036	7.60	144.5	8.28	0.26	133.6			
1213+350	0.420	0.00	0.0	0.72	0.00	−70.9	1.064	1.104	1.082
	0.325	1.15	204.3	2.44	0.59	138.4			
	0.233	3.38	117.3	9.51	0.44	46.6			
	0.025	36.84	−125.5	0.97	0.00	36.3			
1216+487	0.265	0.00	0.0	0.13	0.00	30.5	1.000	1.065	1.030
	0.287	1.48	102.1	2.00	0.25	100.1			
	0.066	4.95	103.9	8.12	0.24	116.2			
1225+368	0.351	0.00	0.0	1.37	0.73	−153.4	1.154	1.341	1.241
	0.240	2.27	−32.8	1.78	0.45	−16.1			
	0.117	18.48	−78.1	2.41	0.30	−101.8			
	0.050	25.08	−80.0	1.62	0.00	−71.9			
	0.062	31.80	−80.7	2.10	0.00	89.0			
	0.040	54.78	−85.5	4.75	0.69	−29.3			
1242+410	0.116	0.00	0.0	0.78	0.92	152.3	1.005	1.526	1.261
	0.152	7.81	25.7	4.86	0.20	24.6			
	0.160	21.11	29.4	4.79	0.74	37.2			
	0.056	3.37	−140.8	1.64	0.24	131.2			
	0.229	8.66	−154.8	9.33	0.76	−23.8			

TABLE 3—*Continued*

Source	S (Jy)	r (mas)	θ (°)	a (mas)	b/a	ϕ (°)	Amp. A.F.	Cl.Phs. A.F.	Total A.F.
1311+678	0.166	0.00	0.0	1.43	0.41	67.4	1.141	1.892	1.504
	0.157	4.66	−67.2	5.07	0.45	−83.8			
	0.410	37.12	−121.0	11.13	0.74	−13.2			
	0.065	41.35	144.6	3.50	0.00	165.5			
	0.035	29.12	175.0	5.26	0.28	34.7			
1317+520	0.181	0.00	0.0	0.47	0.38	116.5	0.985	1.078	1.029
	0.067	4.52	124.4	2.91	0.35	135.5			
	0.007	19.90	129.9	3.46	0.00	6.6			
1333+459	0.345	0.00	0.0	0.82	0.33	113.2	1.058	1.178	1.115
	0.298	1.19	−62.7	1.16	0.26	108.4			
1333+589	0.097	0.00	0.0	0.50	0.71	−44.9	1.140	1.304	1.218
	0.227	0.01	−108.9	1.21	0.64	−35.1			
	0.325	12.73	−161.7	1.69	0.67	117.4			
1342+663	0.685	0.00	0.0	0.48	0.80	110.8	1.058	1.005	1.034
	0.007	2.78	107.6	1.66	0.00	−35.7			
	0.006	4.79	81.1	1.47	0.01	−21.1			
1347+539	0.419	0.00	0.0	0.23	0.00	−53.4	1.111	1.048	1.083
	0.034	0.84	145.0	0.01	0.49	4.7			
	0.063	1.44	141.2	1.76	0.00	132.2			
	0.072	5.41	141.0	3.86	0.20	−41.9			
	0.102	15.98	128.2	13.82	0.34	105.0			
	0.094	58.94	141.3	16.12	0.75	37.4			
1357+769	0.635	0.00	0.0	0.34	0.86	125.3	1.027	1.025	1.026
	0.025	2.87	−111.2	2.84	0.10	−5.5			
1418+546	1.470	0.00	0.0	0.34	0.42	−68.8	1.097	1.042	1.073
	0.415	1.07	129.3	0.55	0.56	110.6			
	0.230	2.92	128.2	4.34	0.35	128.5			
	0.083	16.59	121.0	9.25	0.86	72.3			
1435+638	0.418	0.00	0.0	0.75	0.38	63.6	1.166	1.125	1.148
	0.241	0.46	−134.8	0.00	0.00	133.5			
	0.202	2.61	−125.9	1.64	0.25	26.6			
	0.124	9.08	−144.6	0.94	0.70	52.1			
	0.006	22.41	−133.4	1.97	0.05	30.0			
1437+624	0.193	0.00	0.0	1.01	0.65	105.5	1.068	1.286	1.172
	0.093	2.11	−74.5	2.58	0.62	100.4			
	0.183	5.74	−68.3	13.29	0.23	−35.8			
	0.058	104.24	170.4	2.47	0.15	65.1			
	0.198	103.32	169.9	4.53	0.49	63.2			
	0.057	6.64	−93.9	2.72	0.62	−5.4			
1438+385	0.244	0.00	0.0	0.33	0.78	47.2	1.025	1.073	1.048
	0.140	0.72	8.9	1.03	0.69	−5.6			
	0.093	2.24	−13.8	2.01	0.50	−0.4			
	0.106	8.15	−12.0	6.74	0.26	−2.5			
1504+377	0.413	7.07	44.9	0.67	0.15	37.0	0.989	1.066	1.025
	0.116	5.92	45.4	0.00	0.30	42.0			
	0.149	0.57	40.3	11.28	0.16	45.2			
1547+507	0.430	0.00	0.0	0.18	0.85	168.6	1.052	1.044	1.048
	0.088	1.01	−152.1	0.79	0.00	3.8			
	0.159	3.50	−147.2	1.78	0.28	41.0			
	0.106	7.26	−130.5	1.13	0.41	−0.2			
	0.063	5.84	−136.4	1.58	0.21	71.1			
1638+398	1.752	0.00	0.0	0.47	0.85	−41.0	1.103	1.056	1.083
	0.034	1.40	−58.4	2.54	0.00	11.2			

TABLE 3—*Continued*

Source	S (Jy)	r (mas)	θ (°)	a (mas)	b/a	ϕ (°)	Amp. A.F.	Cl.Phs. A.F.	Total A.F.
1656+477	1.122	0.00	0.0	0.56	0.49	−1.5	1.138	1.085	1.115
	0.325	0.51	1.9	0.86	0.60	−24.4			
	0.063	4.38	−25.5	3.38	0.28	−46.1			
	0.043	5.86	−18.7	0.99	0.83	28.7			
1656+482	0.392	0.00	0.0	0.37	0.00	84.8	1.084	1.052	1.069
	0.116	0.81	−108.6	0.29	0.00	−16.7			
	0.046	0.94	−108.4	1.40	0.00	−119.9			
	0.036	3.27	−104.5	6.41	0.41	−111.0			
	0.059	7.50	−98.8	9.87	0.56	82.1			
1719+357	0.212	0.00	0.0	0.00	1.00	0.0	1.045	1.028	1.037
	0.103	0.93	184.0	0.00	0.50	0.0			
	0.138	4.27	178.3	2.06	0.28	−1.5			
1732+389	0.995	0.00	0.0	0.52	0.52	174.1	1.278	1.062	1.187
	0.234	0.54	105.6	0.00	0.50	100.0			
1734+508	0.416	0.00	0.0	0.41	0.87	−121.7	1.182	1.162	1.173
	0.188	0.88	21.7	0.61	0.72	−174.1			
	0.223	3.36	19.3	1.02	0.67	30.4			
1738+476	0.924	0.00	0.0	0.59	0.47	51.2	0.915	1.113	1.008
	0.139	1.05	−86.4	0.64	0.83	9.0			
	0.017	2.70	−94.2	0.73	0.46	50.8			
1751+441	0.695	0.00	0.0	0.53	0.67	80.3	1.088	1.041	1.067
	0.232	1.48	87.3	1.39	0.53	−82.2			
	0.026	8.30	80.5	8.44	0.63	79.8			
1758+388	0.828	0.00	0.0	0.60	0.53	82.3	1.051	1.082	1.065
	0.091	1.05	−99.1	1.23	0.00	79.1			
1800+440	0.331	0.00	0.0	0.17	0.68	73.4	1.045	1.058	1.051
	0.090	0.52	−160.0	0.33	0.00	44.7			
	0.088	1.36	−156.8	0.65	0.62	−177.0			
	0.047	14.58	−155.7	30.54	0.10	24.3			
1819+396	0.273	0.00	0.0	1.61	0.43	−56.5	1.435	1.414	1.426
1842+681	0.647	0.00	0.0	0.45	0.57	107.0	1.149	1.075	1.117
	0.181	1.32	134.3	1.31	0.53	−28.0			
	0.024	3.64	148.4	6.96	0.09	−35.5			
1843+356	0.173	0.00	0.0	0.49	0.98	51.9	1.075	1.251	1.159
	0.116	0.91	53.5	0.62	0.45	3.1			
	0.313	7.06	43.3	1.29	0.70	157.8			
	0.101	5.15	43.8	1.58	0.50	39.6			
	0.140	8.30	45.6	1.67	0.03	54.2			
1926+611	0.394	0.00	0.0	0.43	0.72	121.2	1.038	1.091	1.062
	0.133	0.94	118.7	0.73	0.22	130.4			
	0.049	1.53	141.0	1.88	0.53	166.0			
	0.024	6.76	179.6	2.64	0.69	102.5			
	0.008	12.83	−145.8	0.69	0.02	3.5			
1943+546	0.024	0.00	0.0	6.18	0.06	125.7	1.161	1.170	1.165
	0.234	16.80	−91.8	0.63	0.69	63.1			
	0.248	15.33	−91.0	2.98	0.27	−98.0			
	0.184	13.07	−79.8	7.42	0.85	2.0			
	0.038	19.06	85.9	4.70	0.74	75.1			
	0.122	23.11	85.0	2.00	0.78	161.3			
	0.118	24.13	84.7	0.49	0.00	74.1			
2007+777	1.698	0.00	0.0	0.45	0.49	73.8	1.098	1.040	1.071
	0.268	1.00	−107.5	0.00	0.00	−117.2			
	0.124	3.90	−94.5	5.23	0.25	−99.9			
	0.023	17.68	−97.0	3.18	0.50	−171.8			

TABLE 3—*Continued*

Source	S (Jy)	r (mas)	θ (°)	a (mas)	b/a	ϕ (°)	Amp. A.F.	Cl.Phs. A.F.	Total A.F.
2010+723	0.350	0.00	0.0	0.27	0.00	−36.4	1.071	1.088	1.079
	0.142	0.23	−25.1	1.29	0.00	−30.4			
	0.426	0.99	−39.2	0.82	0.47	110.5			
	0.021	2.52	−128.1	1.61	0.00	111.5			
	0.089	3.93	−118.6	7.44	0.47	27.7			
2207+374	0.143	0.00	0.0	0.57	0.34	45.4	1.080	1.169	1.121
	0.048	0.57	−140.6	1.28	0.00	−129.1			
	0.073	5.24	−133.6	1.43	0.52	8.1			
	0.090	14.98	−138.9	2.47	0.57	−40.8			
	0.238	14.92	−134.3	8.36	0.47	−153.5			
	0.048	21.89	−130.2	12.74	0.26	−84.8			
	0.187	57.08	−105.7	48.57	0.55	116.0			
2214+350	0.551	0.00	0.0	0.35	0.82	−22.1	1.015	1.038	1.026
	0.049	1.96	169.4	1.13	0.55	−30.3			
2229+695	0.523	0.00	0.0	0.44	0.97	28.2	1.027	1.053	1.039
	0.456	0.56	−108.3	0.87	0.26	81.5			
	0.003	2.66	79.1	0.01	0.49	20.0			
2253+417	0.507	0.00	0.0	0.81	0.18	28.0	1.075	1.059	1.068
	0.487	1.33	−10.6	1.24	0.42	−25.7			
	0.042	4.63	21.1	1.16	0.33	47.8			
	0.064	6.65	36.3	4.11	0.35	12.3			
2255+416	0.242	0.00	0.0	0.65	0.34	−17.2	1.125	1.152	1.137
	0.054	1.13	170.3	2.15	0.36	−27.2			
	0.050	5.09	167.4	1.70	0.23	−61.2			
	0.180	8.85	165.1	3.23	0.52	−36.9			
	0.276	19.13	172.8	8.70	0.59	16.1			
	0.138	31.96	−151.5	14.69	0.65	70.3			
	0.193	42.24	−136.6	8.28	0.55	152.5			
2311+469	0.055	0.00	0.0	0.39	0.00	114.4	0.979	1.350	1.152
	0.039	0.31	121.9	0.42	0.68	6.1			
	0.012	1.72	133.9	1.66	0.65	173.2			

NOTE.—Parameters of each Gaussian component of the model brightness distribution; S, flux density; r, θ, polar coordinates of the center of the component relative to an arbitrary origin, with polar angle measured from north through east; a, b, major and minor axes of the FWHM contour; ϕ, position angle of the major axis measured from north through east. The sources 0218+357 and 0404+768 are too complicated to model.

Table 3 is published in computer-readable form in the AAS CD-ROM Series, Vol. 5.

TABLE 4

MERLIN MAP PARAMETERS

Source	Sample	BEAM[a]			S_{peak}	rms
		a (mas)	b (mas)	θ (°)		
0707+476	CJ1	49.7	37.8	37	948	1.52
0812+367	CJ1	100.0	100.0	0	747	0.23
0814+425	PR	56.8	37.7	30	906	0.59
0820+560	CJ1	51.2	37.8	26	1753	0.52
0900+428	CJ1	49.0	41.0	44	376	0.23
		100.0	100.0	0	430	0.15
0917+624	CJ1	48.5	38.2	30	1059	0.46
0945+408	PR	53.4	38.8	33	1232	0.82
		100.0	100.0	0	1317	0.47
0954+556	PR	47.7	38.1	32	967	0.91
1039+811	CJ1	47.0	40.9	7	1000	0.36
1150+812	CJ1	47.3	38.5	26	979	0.32
1347+539	CJ1	44.2	36.3	−48	592	0.33
1418+546	CJ1	44.0	36.0	−48	1429	0.49
1633+382	PR	47.5	38.9	33	2113	0.94
1638+398	CJ1	48.4	38.7	31	1230	0.68
1749+701	PR	47.6	37.7	8	469	0.44
1800+440	CJ1	63.7	43.7	−37	402	0.20
		100.0	100.0	0	412	0.21
1803+784	PR	47.0	38.6	−64	1951	0.56
1819+396	CJ1	56.9	41.1	−39	324	0.53
1943+546	CJ1	50.6	38.9	24	655	0.58
1954+513	PR	50.0	38.1	25	1403	0.51

[a] The restoring beam is an elliptical Gaussian with FWHM major axis a and minor axis b, with major axis in position angle θ.

NOTES.—Col. (1): Source name. Col. (2): Sample. Cols. (3)–(5): The beam characteristics of the maps. Cols. (6)–(7): The peak intensity and rms noise of the maps (mJy beam^{-1}).

Table 4 is published in computer-readable form in the AAS CD-ROM Series, Vol. 5.

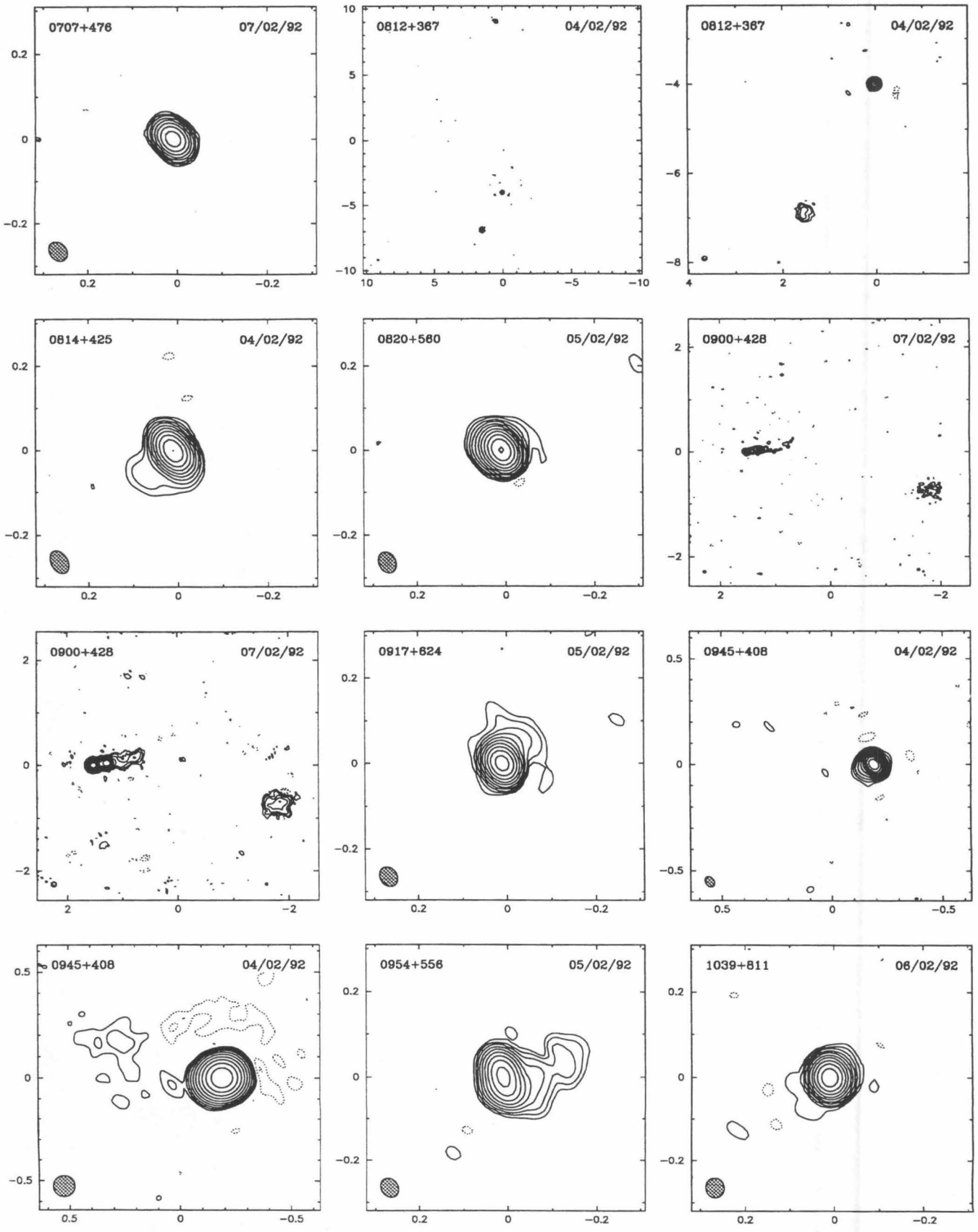

FIG. 4.—The 5 GHz MERLIN uniformly weighted maps of 20 objects. Logarithmic contour levels are used in all maps, at $-2, -1, 1, 2, 4, 8, 16, \cdots 1024 \times 3\ \sigma$ (where σ is the rms noise measured in a blank region of the map). The FWHM contour of the elliptical Gaussian restoring beam is shown hatched in the lower left-hand corner. For 0812+367, 0900+428, 0945+408, and 1800+440, which have large angular sizes, the naturally weighted map restored with a circular beam of FWHM 100 mas is also shown. In addition, an enlarged map of 0812+367 is presented to show the central and southern components in more detail. The peak intensity, rms noise, and parameters of the restoring beam are listed in Table 5. The angular scale is marked in arcseconds. *FITS* images corresponding to the maps presented in Fig. 4 are published in the AAS CD-ROM Series, Vol. 5.

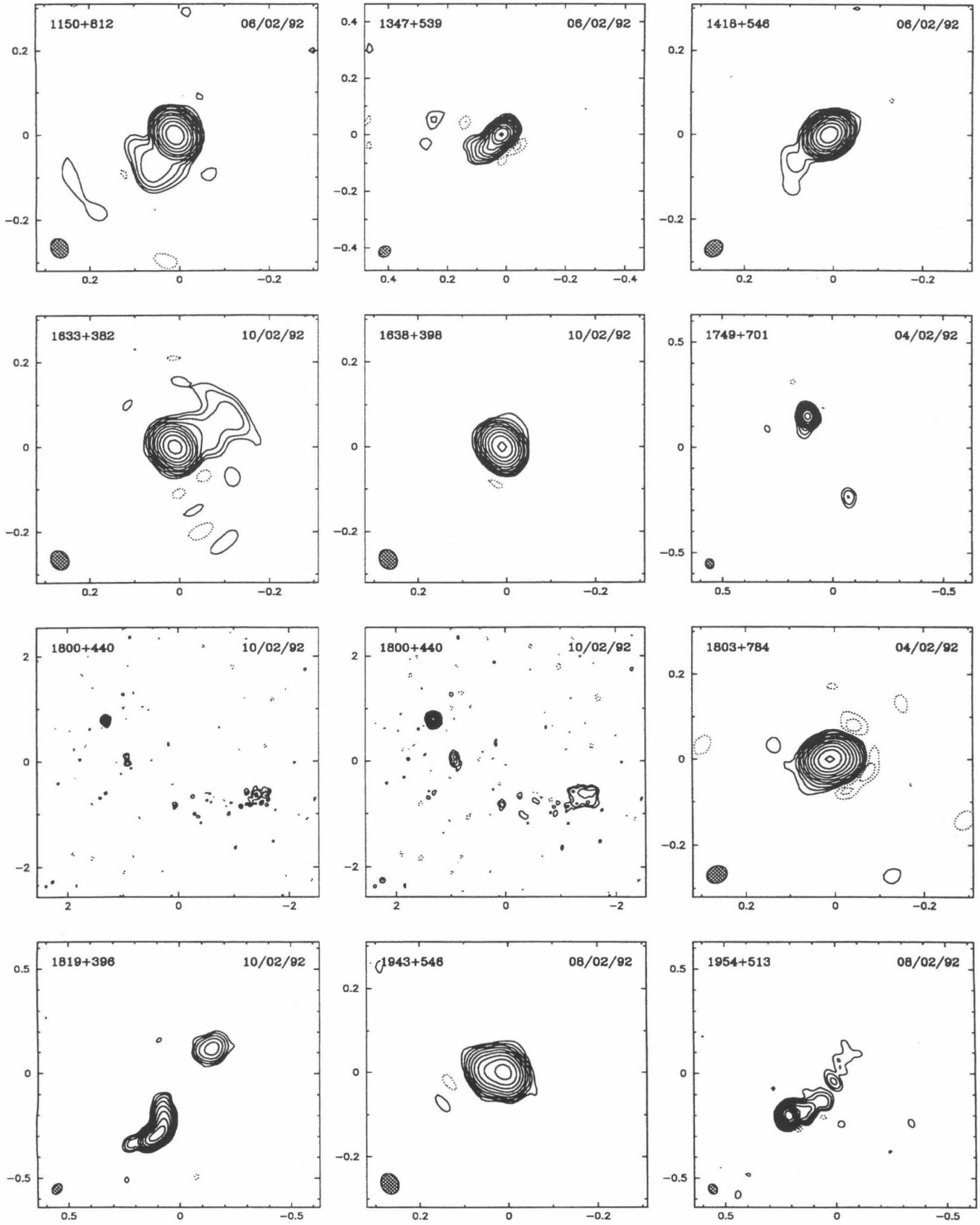

FIG. 4—*Continued*

TABLE 5

VLA MAP PARAMETERS

Source	Sample	S_{peak} (mJy)	rms (mJy)	Structure
0010+775	CJ1	1979.8	0.36	E
0016+731	PR	969.0	0.21	E?[a]
0022+390	CJ1	738.9	0.18	E
0102+480	CJ1	751.9	0.17	U
0133+476	PR	1172.8	0.41	U
0153+744	PR	1794.3	0.29	U
0212+735	PR	2443.6	0.36	U
0248+430	CJ1	1052.3	0.18	E
0309+390	CJ1	68.5	0.35	E[c]
0402+379	CJ1	1092.3	0.21	E
0404+768	PR	5639.2	0.82	U
0454+844	PR	392.1	0.10	U
0602+673	CJ1	519.1	0.18	U
0620+389	CJ1	834.3	0.27	E?
0642+449	CJ1	475.6	0.15	U
0650+371	CJ1	836.6	0.20	U
0703+426	CJ1	39.8	0.50	E[d]
0707+689	CJ1	1450.5	0.42	E
0710+439	PR	2005.3	0.28	U
0740+828	CJ1	1325.7	0.54	E
0746+483	CJ1	704.1	0.22	U
0755+379	CJ1	149.6	0.60	E[f]
0755+379	CJ1	208.3	0.64	E[e]
0805+410	CJ1	528.4	0.22	E
0818+472	CJ1	101.1	0.53	E
0821+394	CJ1	1257.0	0.56	E
0827+378	CJ1	1755.1	0.29	E
0827+378	CJ1	1920.2	0.37	E[c]
0831+557	PR	8064.7	1.28	E
0844+540	CJ1	22.9	0.36	E[c]
0900+428	CJ1	811.1	0.43	E
0917+449	CJ1	913.7	0.18	E
0945+664	CJ1	1490.7	0.24	E
0954+658	PR	636.6	0.29	E
0955+476	CJ1	650.3	0.37	U
1003+351	PR	2824.6	0.70	E[g]
1003+830	CJ1	476.3	0.15	E
1015+359	CJ1	622.0	0.31	E
1020+400	CJ1	680.6	0.21	E
1030+415	CJ1	417.8	0.16	E
1031+567	PR	1815.6	0.32	U
1044+719	CJ1	785.9	0.19	E
1053+704	CJ1	441.4	0.11	E
1053+815	CJ1	392.9	0.13	E
1058+726	CJ1	748.4	0.21	E
1101+384	CJ1	626.2	0.17	E
1138+594	CJ1	1982.0	0.43	E
1144+542	CJ1	373.4	0.14	U
1216+487	CJ1	616.9	0.15	E
1225+368	CJ1	2072.2	0.43	U
1242+410	CJ1	1366.1	0.28	U
1254+476	PR	2414.1	0.64	E
1311+678	CJ1	2427.1	0.35	E?
1333+459	CJ1	253.9	0.18	U
1333+589	CJ1	305.3	0.26	U
1336+391	CJ1	97.7	0.37	E
1342+663	CJ1	581.5	0.26	E?
1347+539	CJ1	935.2	0.21	E
1357+769	CJ1	471.0	0.12	U
1358+624	PR	4426.1	0.54	U
1437+624	CJ1	2322.4	0.32	E?
1438+385	CJ1	580.0	0.17	E
1547+507	CJ1	624.3	0.11	E?
1557+708	CJ1	24.1	0.20	E
1609+660	PR	2813.5	0.93	E
1624+416	PR	1632.4	0.89	E
1634+628	PR	4900.0	0.63	E?[h]
1638+398	CJ1	1118.2	0.31	E
1652+398	PR	1428.2	0.25	E
1656+482	CJ1	788.1	0.16	E
1719+357	CJ1	402.6	0.25	E
1732+389	CJ1	992.4	0.15	U
1734+508	CJ1	485.1	0.28	U
1738+476	CJ1	848.1	0.15	E?[b]
1749+701	PR	725.8	0.15	E
1751+441	CJ1	554.0	0.17	E
1758+388	CJ1	281.7	0.74	E
1800+440	CJ1	450.6	0.39	E
1833+653	CJ1	200.5	0.50	E
1842+681	CJ1	886.0	0.13	E
1843+356	CJ1	947.3	0.22	U
1926+611	CJ1	825.4	0.15	E?
1943+546	CJ1	1710.3	0.24	U
1954+513	PR	1377.3	0.47	E
2010+723	CJ1	1388.3	0.26	E
2021+614	PR	2169.8	0.32	U
2207+374	CJ1	1674.2	0.28	E
2214+350	CJ1	363.6	0.19	E
2229+695	CJ1	757.1	0.12	E
2253+417	CJ1	1333.7	0.29	U
2255+416	CJ1	2069.3	0.34	U
2342+821	PR	3736.2	0.47	E?[h]
2351+456	PR	1684.5	0.28	E?[h]
2352+495	PR	2515.8	0.34	U

[a] Faint component $\sim 12''$ to the north.
[b] Faint component $\sim 1'$ to the west.
[c] Logarithmic contour levels in steps of $\sqrt{2}$.
[d] Convolved with $3''$ circular Gaussian beam.
[e] Convolved with $5''$ circular Gaussian beam.
[f] The lowest contour is $2\ \sigma$.
[g] The lowest contour is $4\ \sigma$.
[h] Source resolved at long baselines.

NOTES.—Col. (1): Source name. Col. (2): Sample. Cols. (3)–(4): The peak intensity and rms noise in the map, in mJy beam^{-1}. Col. (5): Structure: U, unresolved; E, extended structure detected; E?, hint of extended structure (see notes).

Table 5 is published in computer-readable form in the AAS CD-ROM Series, Vol. 5.

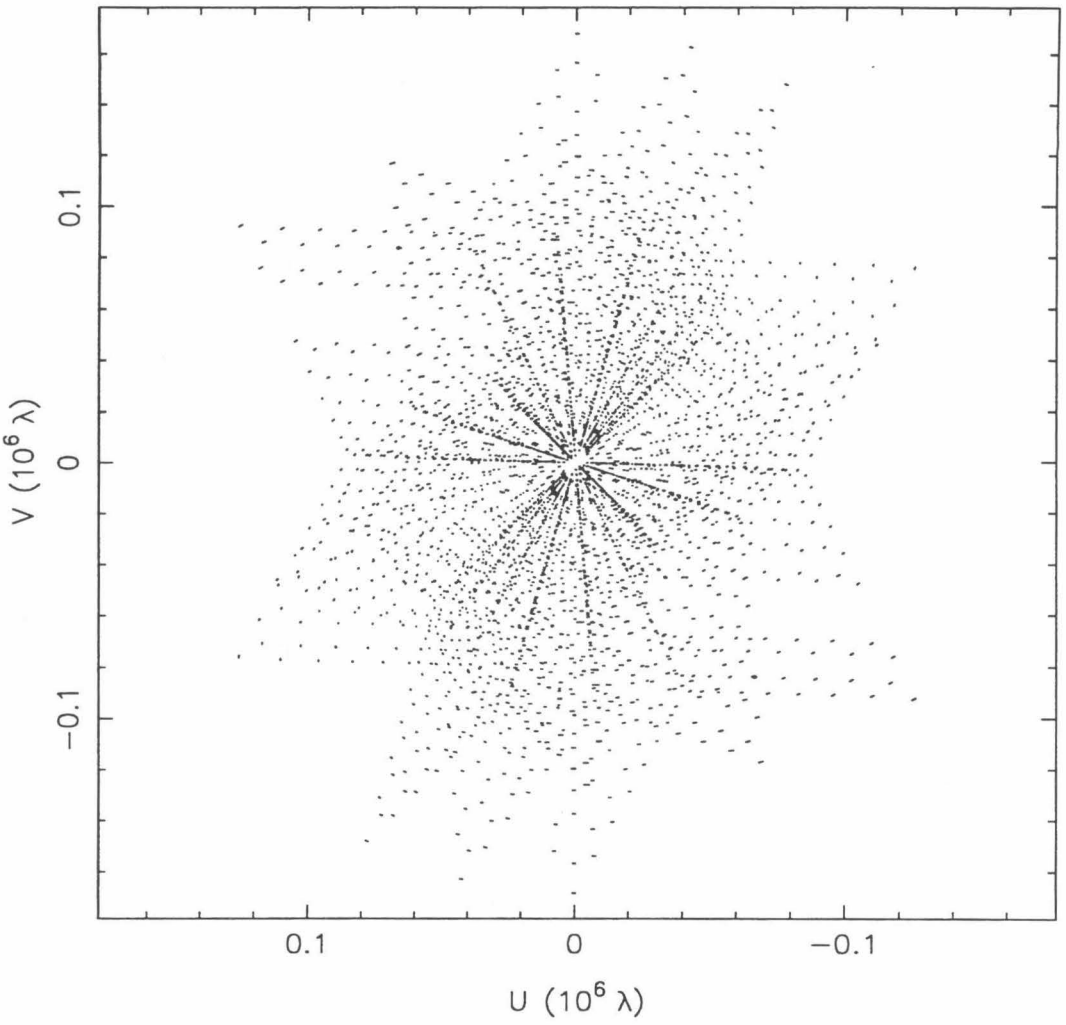

FIG. 5.—Typical *uv* coverage for VLA observations: $\delta \simeq 41°$ (1242+410 observed on 1992 November 5 at 1.365 GHz).

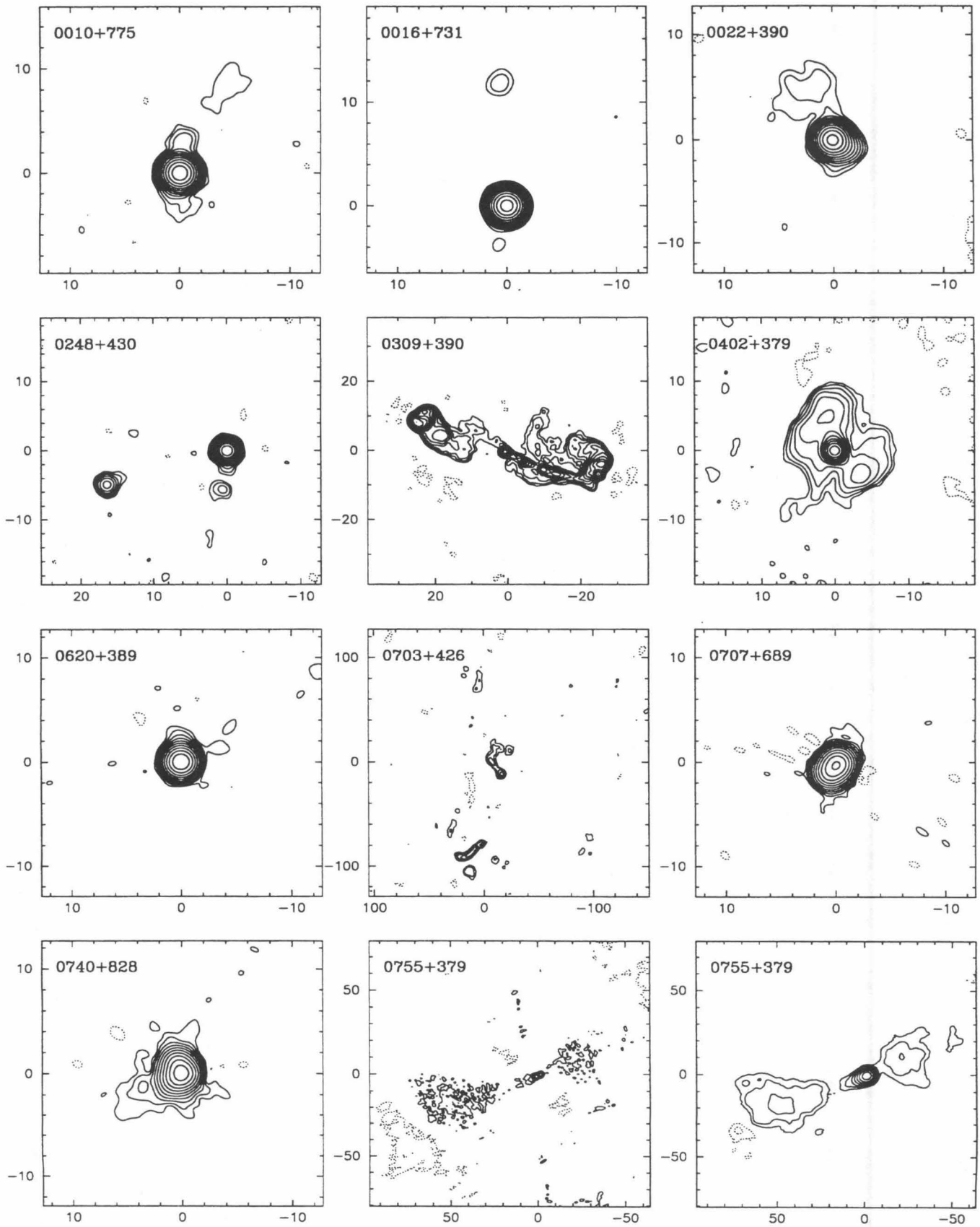

FIG. 6.—The 1.4 GHz VLA maps of 64 objects with extended structure. The naturally weighted map is shown for each object. Unless noted otherwise in Table 6, logarithmic contour levels are used in all maps, drawn at $-2, -1, 1, 2, 4, 8, 16, \cdots 1024 \times 3\ \sigma$ (where σ is the rms noise measured in a blank region of the map), and the maps are restored with a circular Gaussian beam of FWHM 1".5. For 0755+379 and 0827+378, the map restored with a larger beam is also shown. The peak intensity and rms noise are given in Table 6. The angular scale is marked in arcseconds. FITS images corresponding to the maps presented in Fig. 6 are published in the AAS CD-ROM Series, Vol. 5.

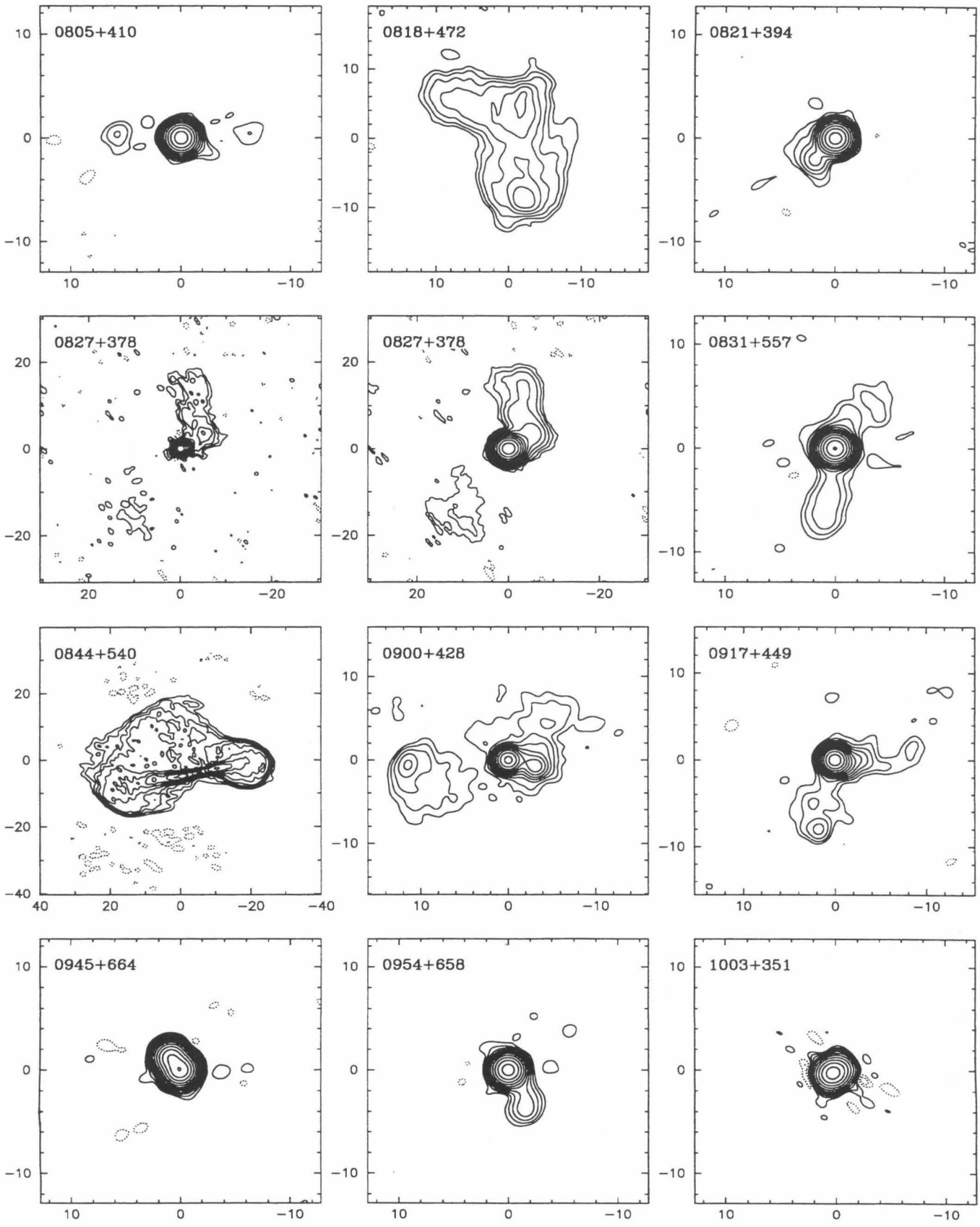

FIG. 6—*Continued*

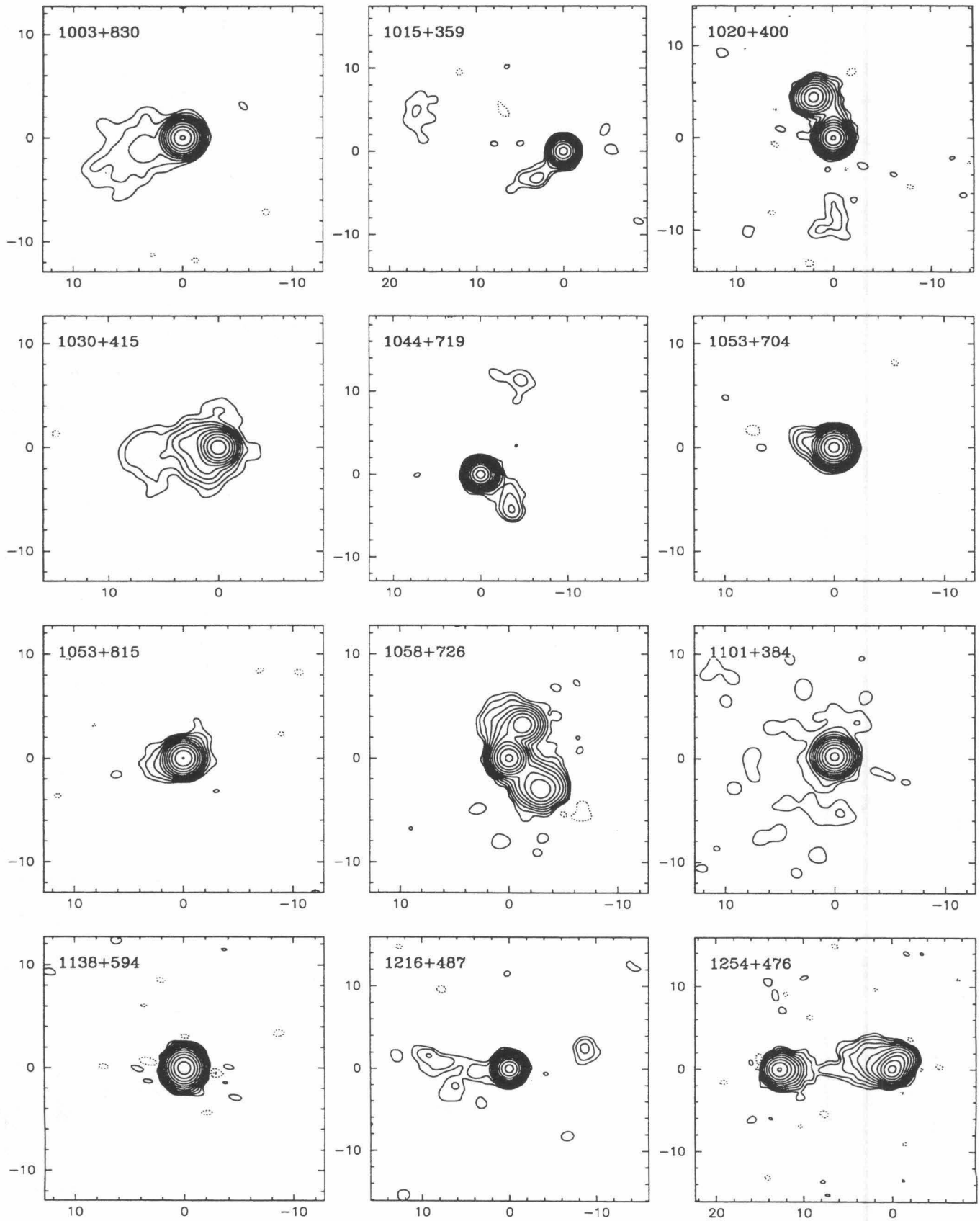

FIG. 6—*Continued*

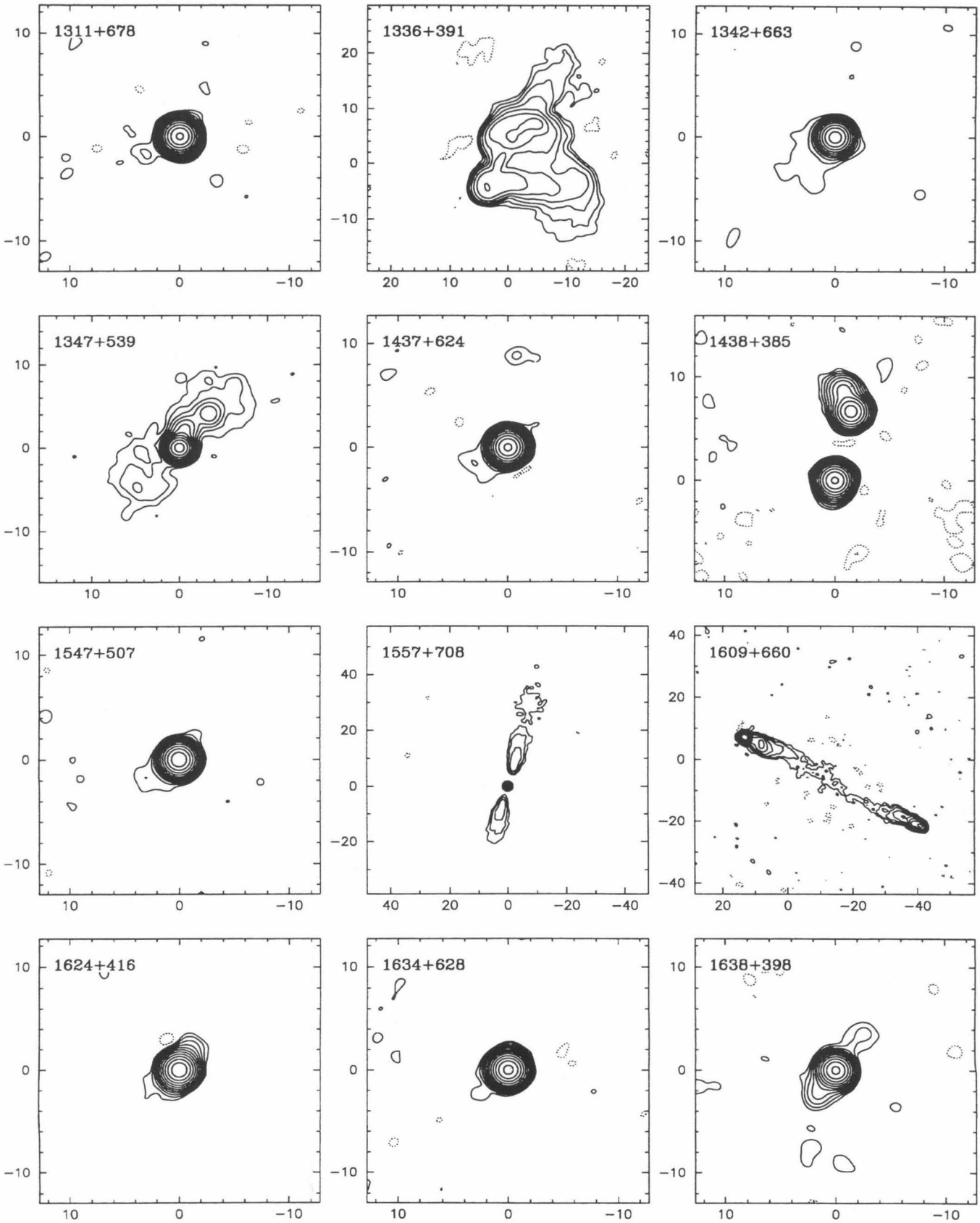

FIG. 6—*Continued*

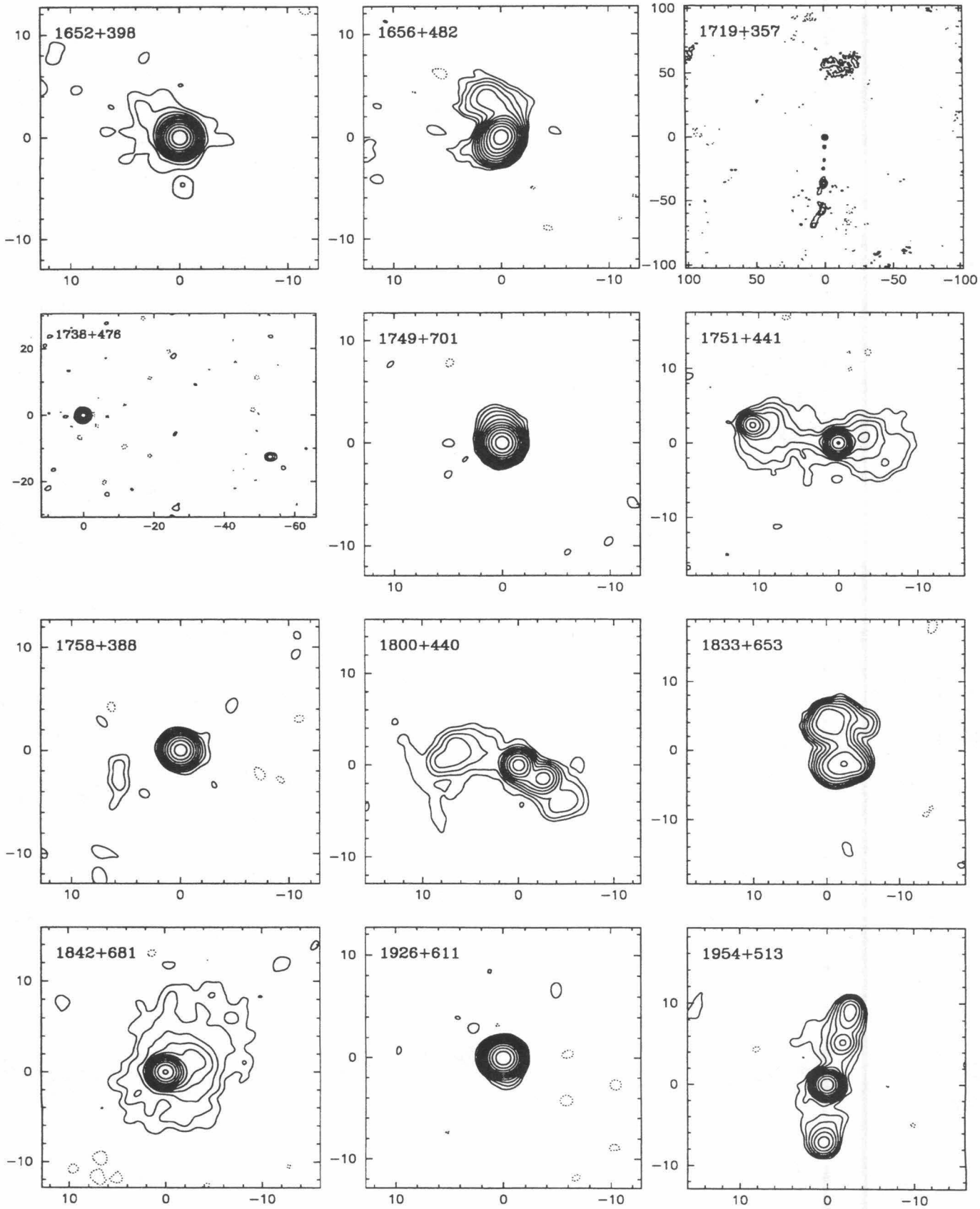

FIG. 6—*Continued*

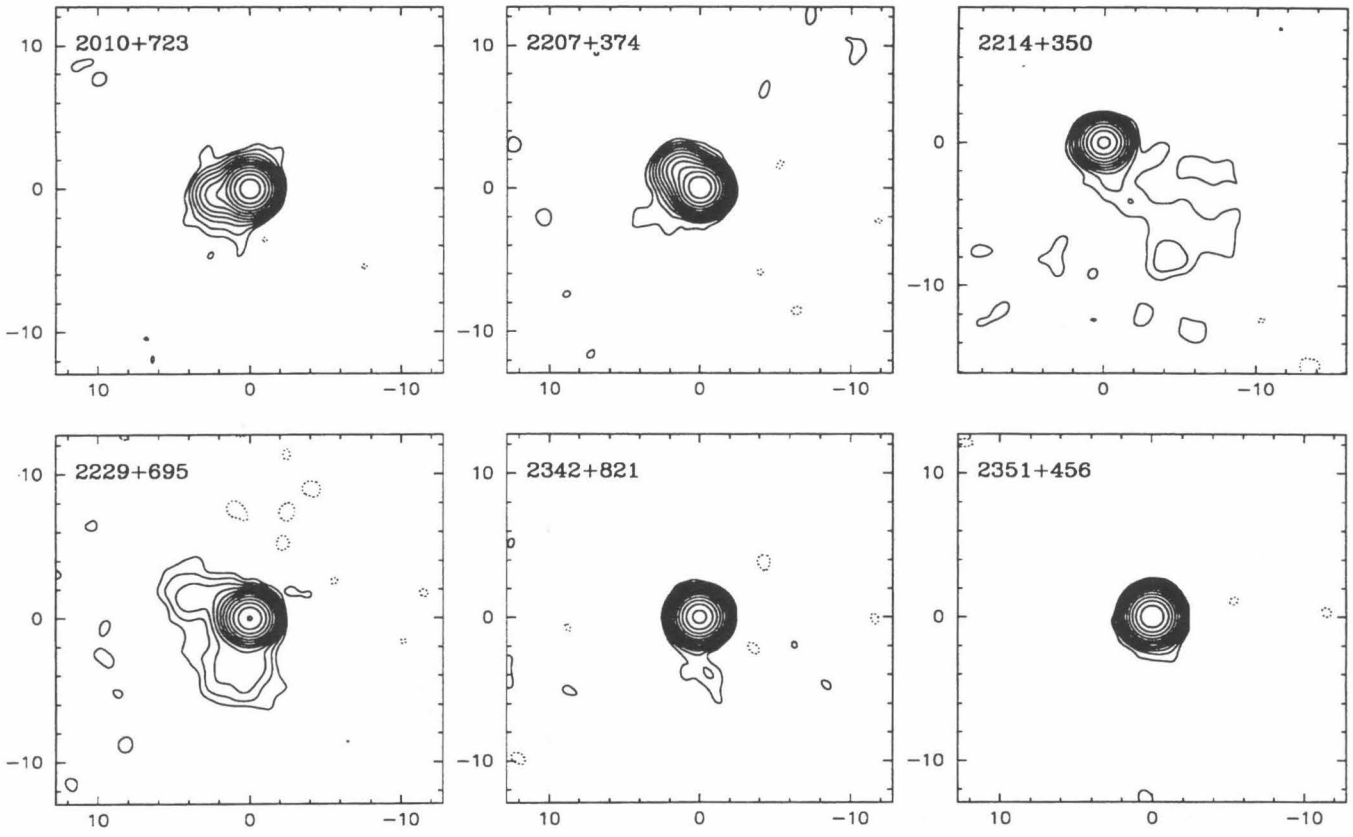

FIG. 6—*Continued*

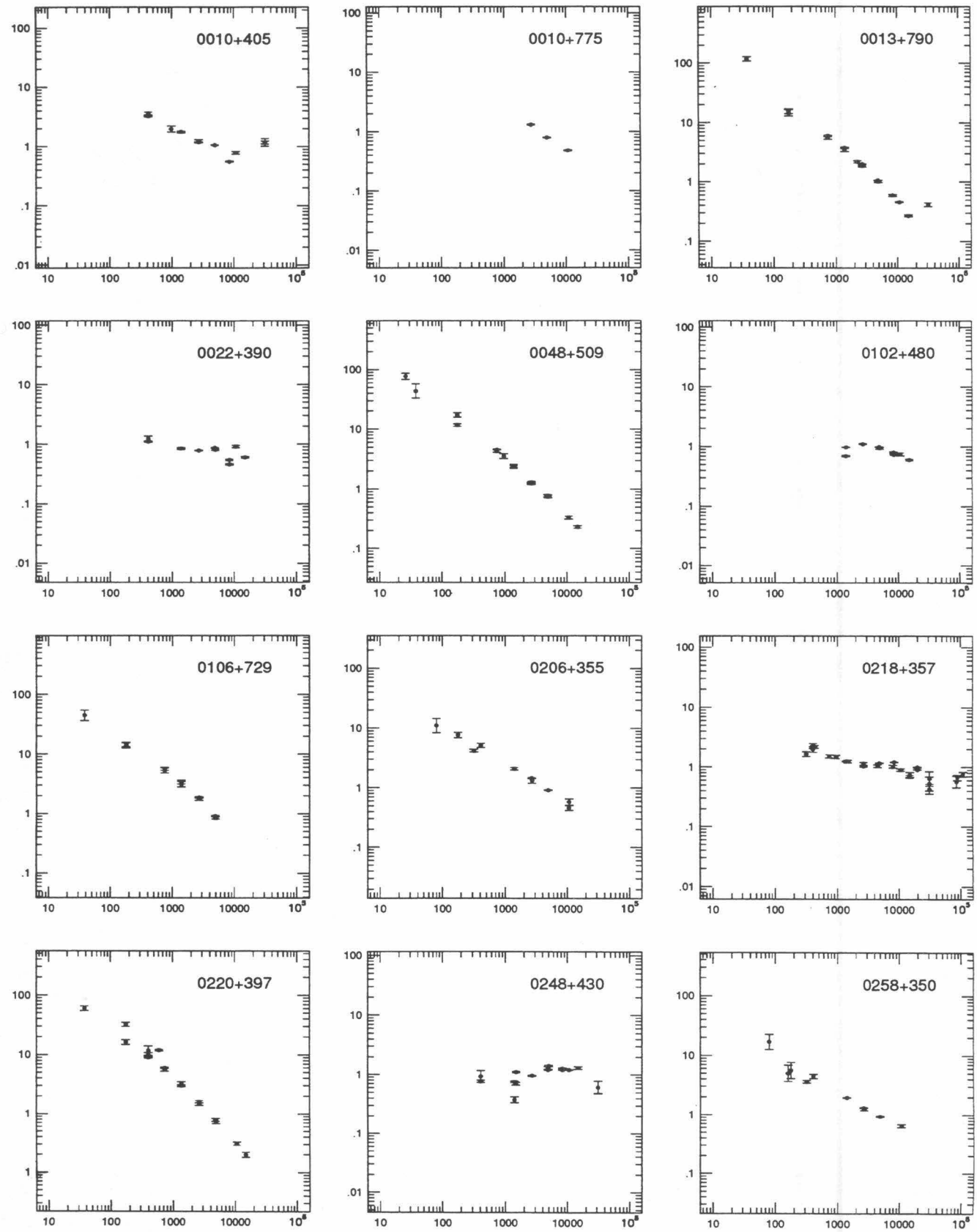

FIG. 7.—Spectra of all objects in the CJ1 sample. The data points are from the references cited in the text.

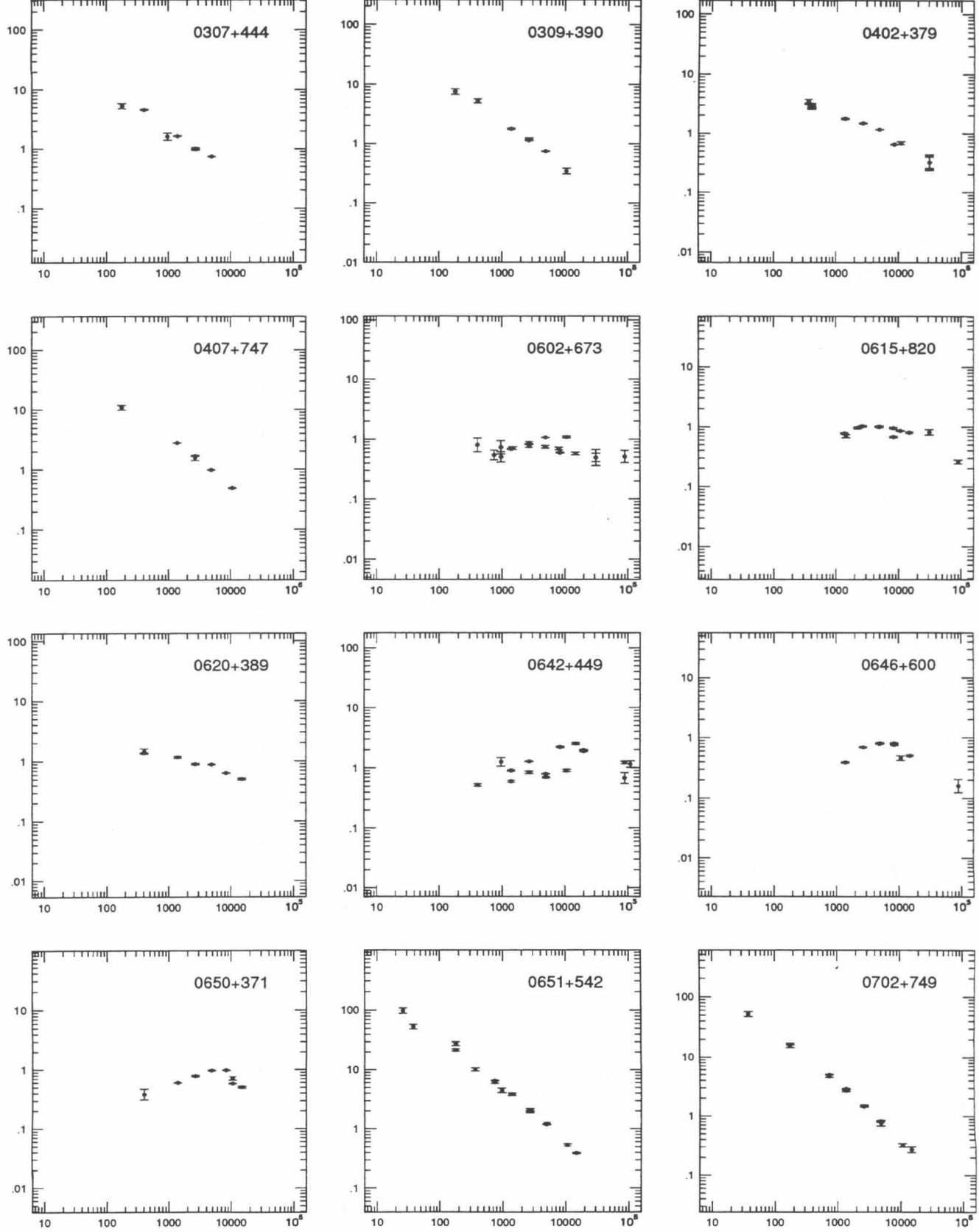

FIG. 7—*Continued*

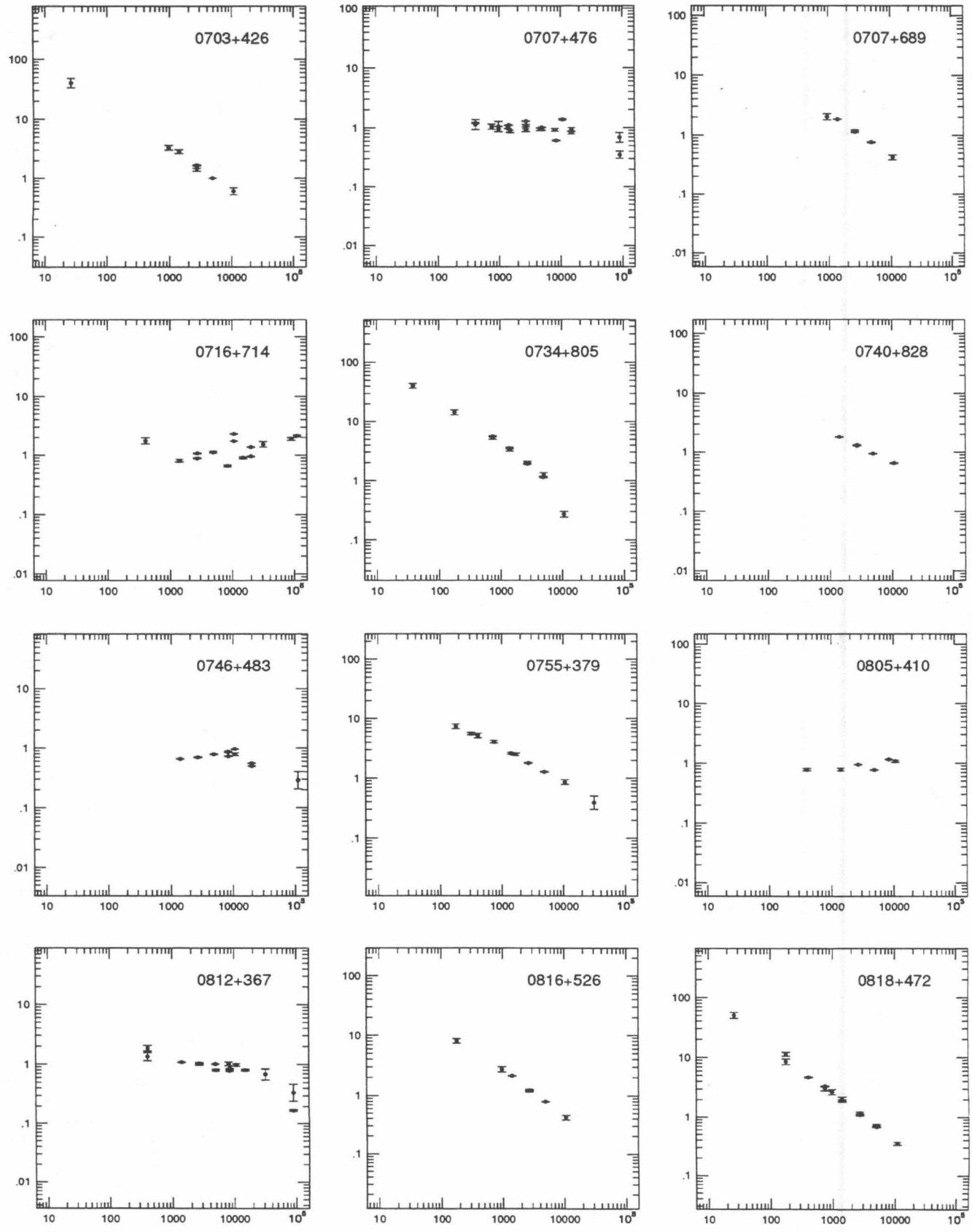

FIG. 7—*Continued*

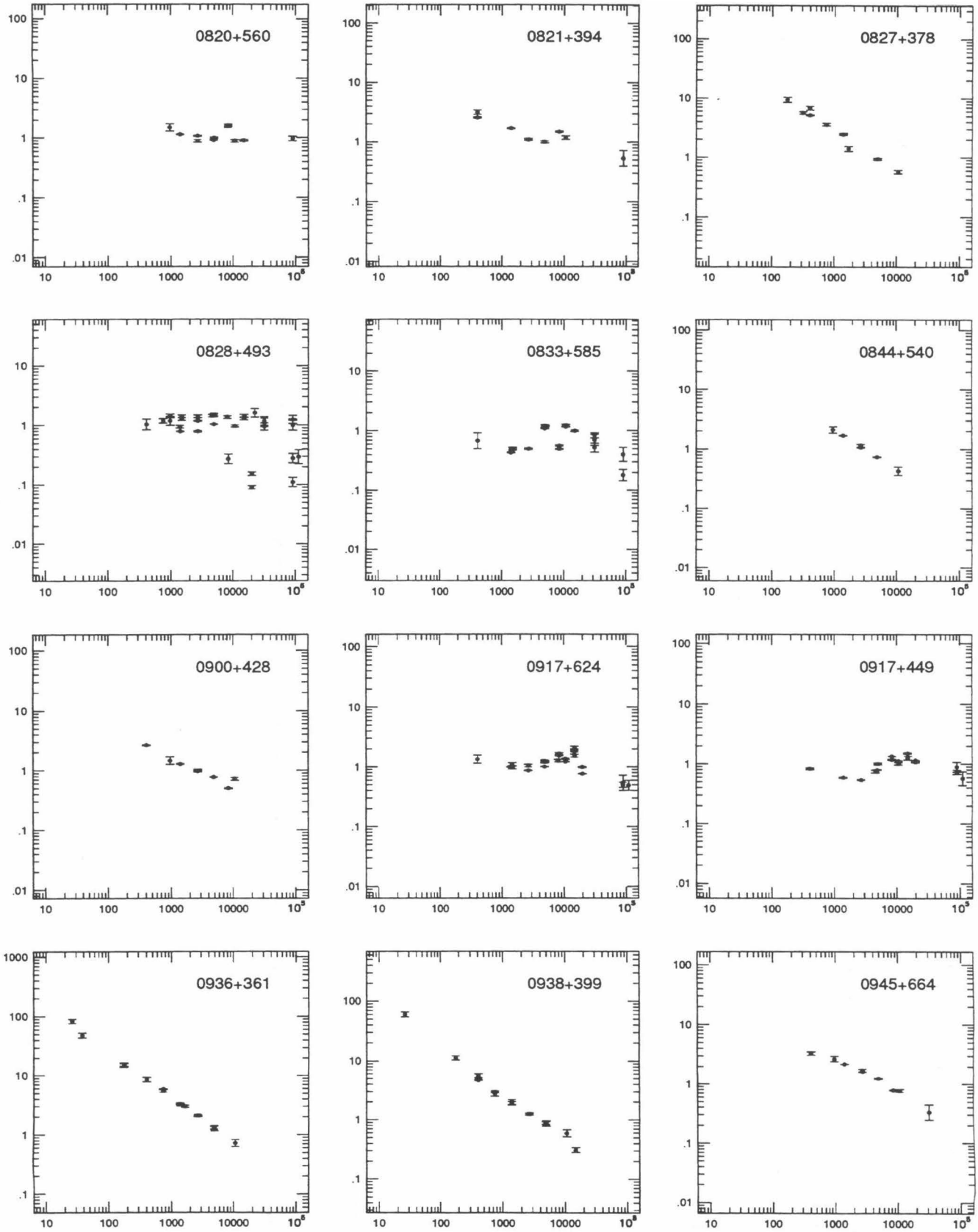

FIG. 7—*Continued*

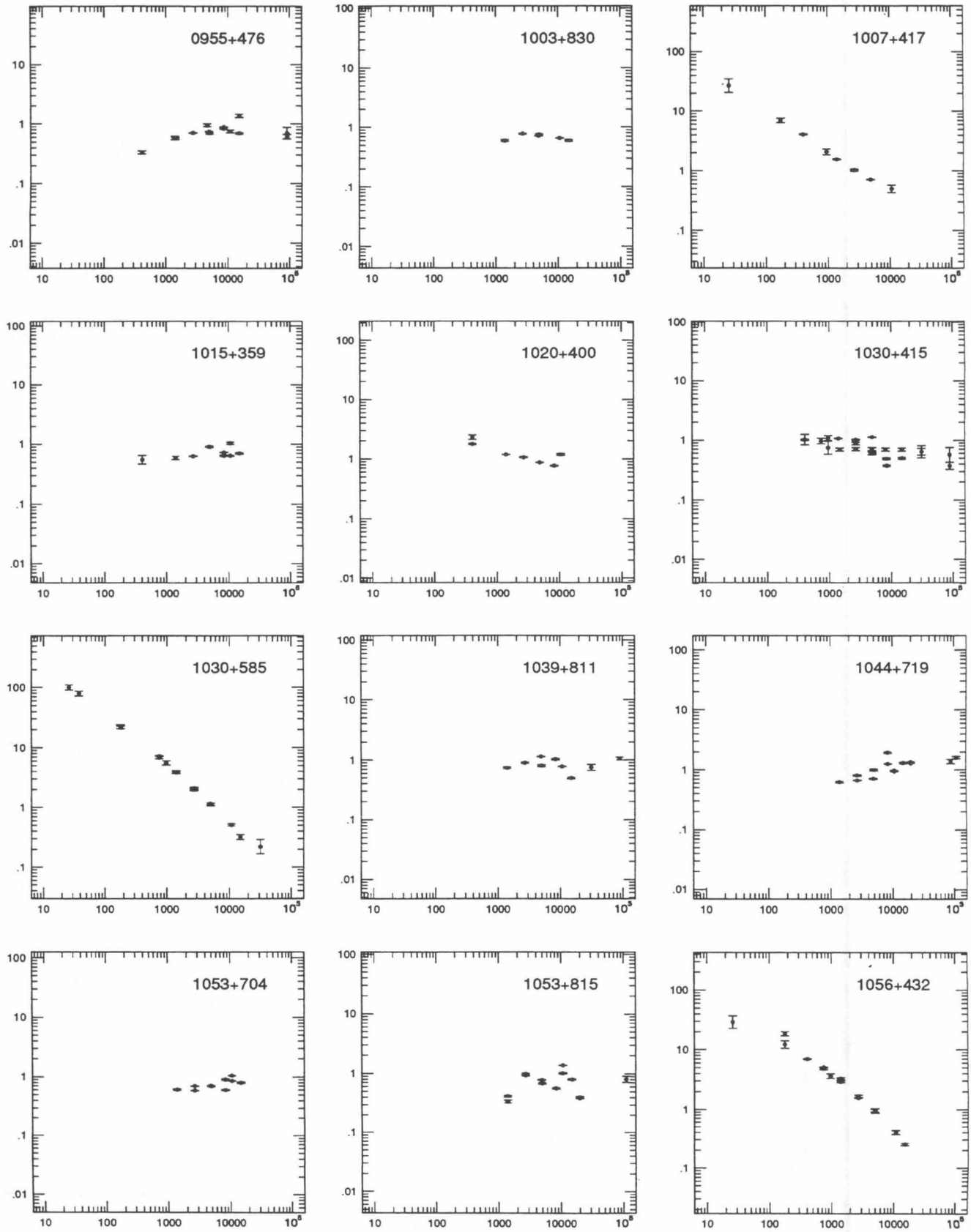

FIG. 7—*Continued*

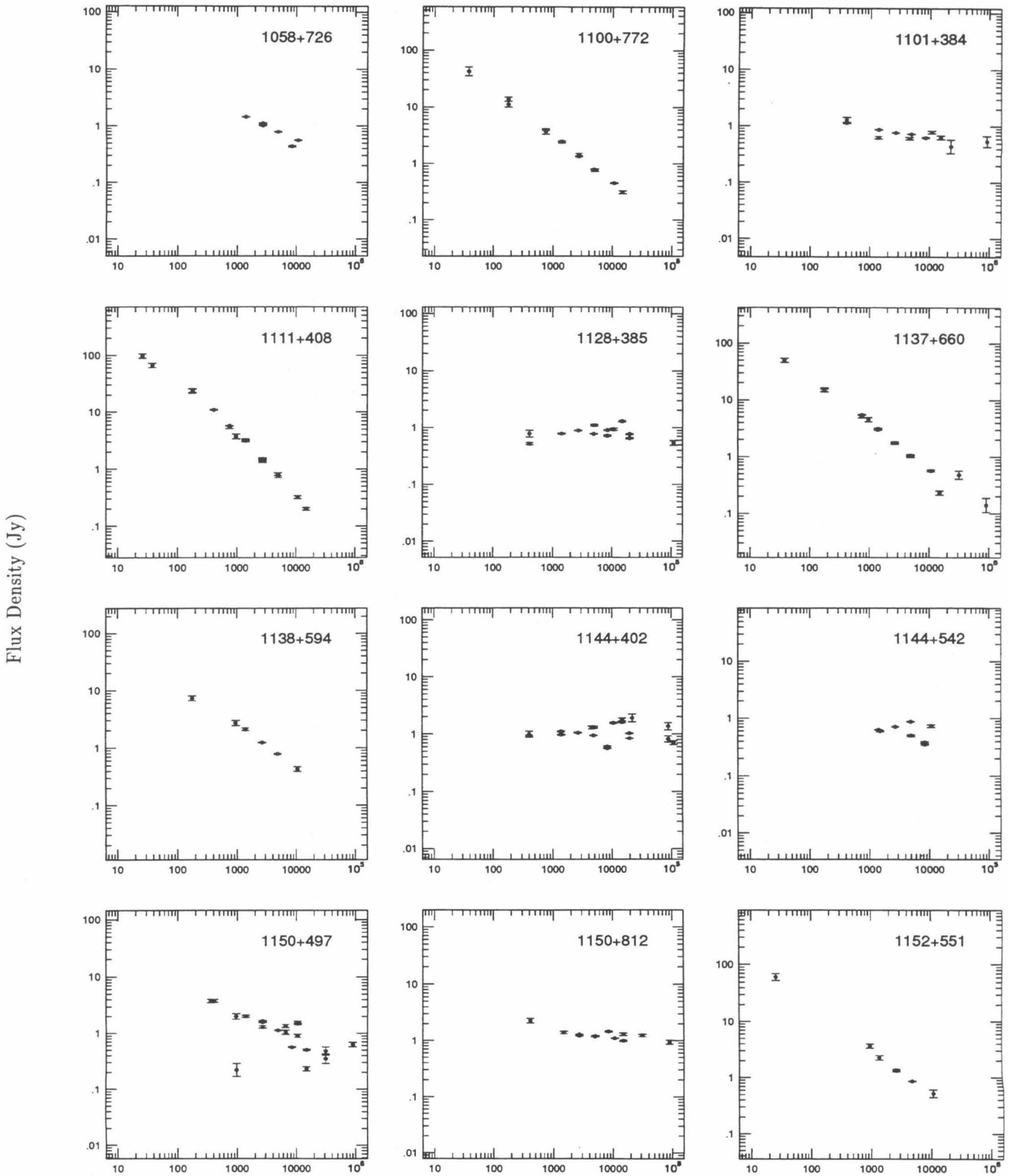

FIG. 7—*Continued*

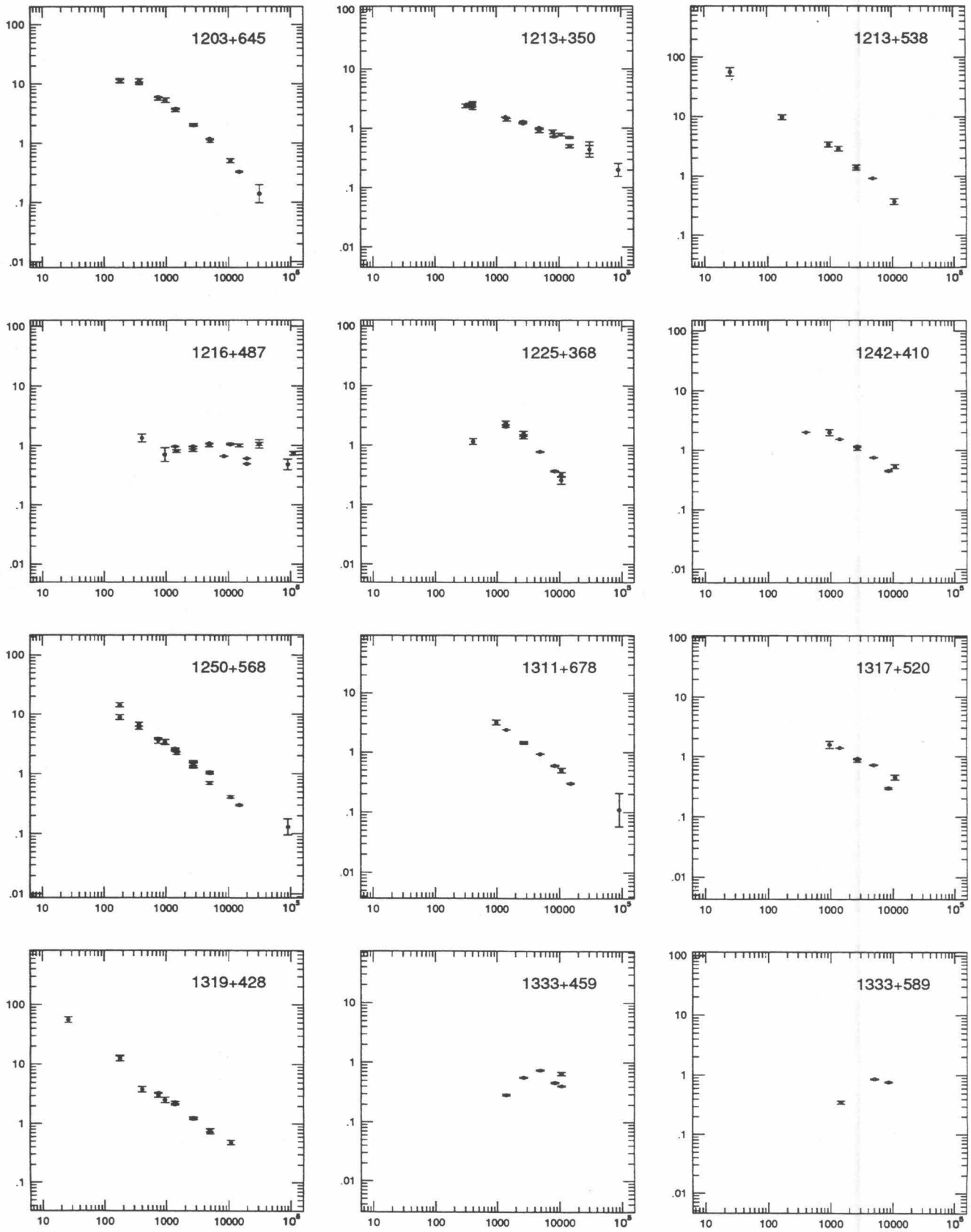

FIG. 7—*Continued*

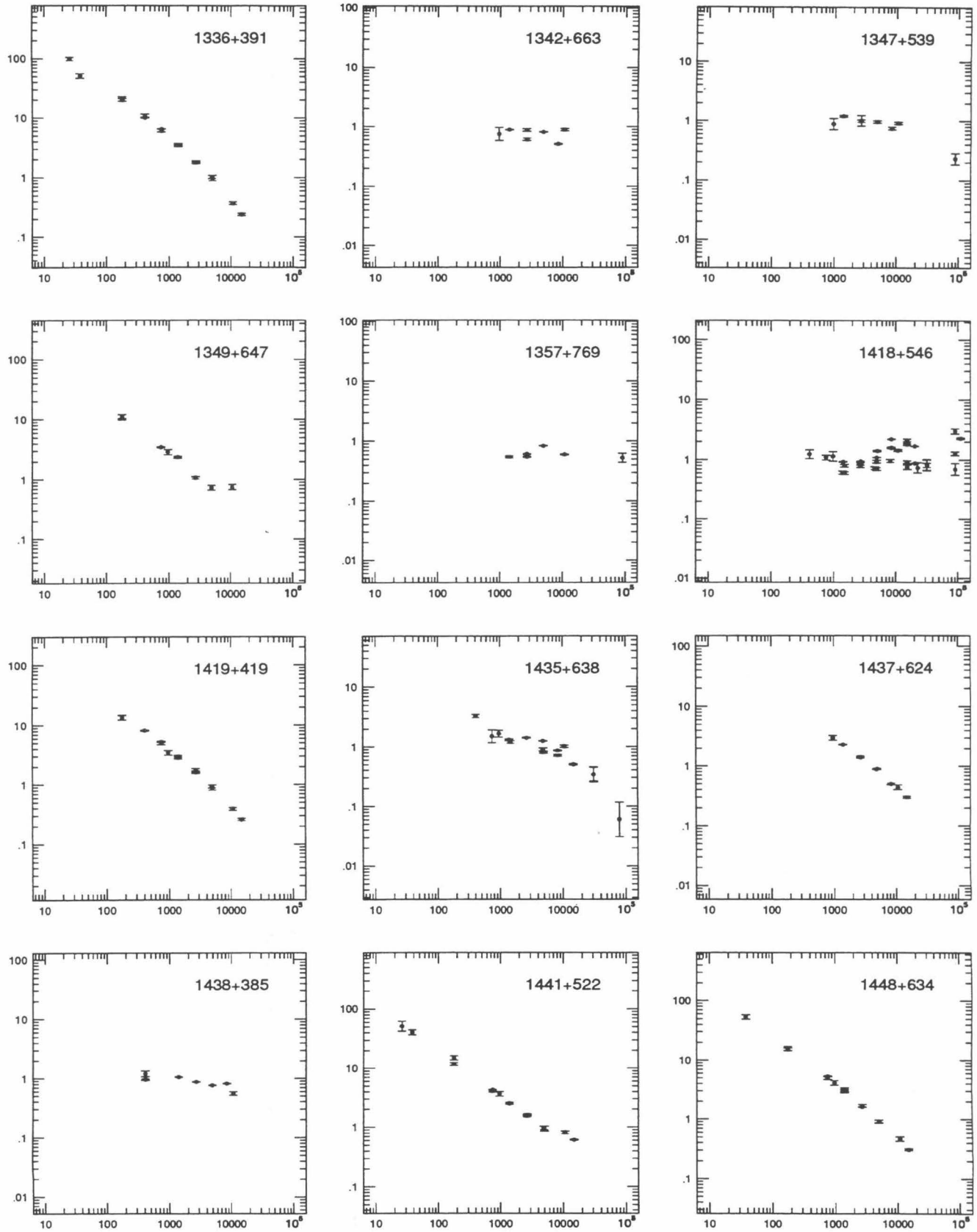

FIG. 7—*Continued*

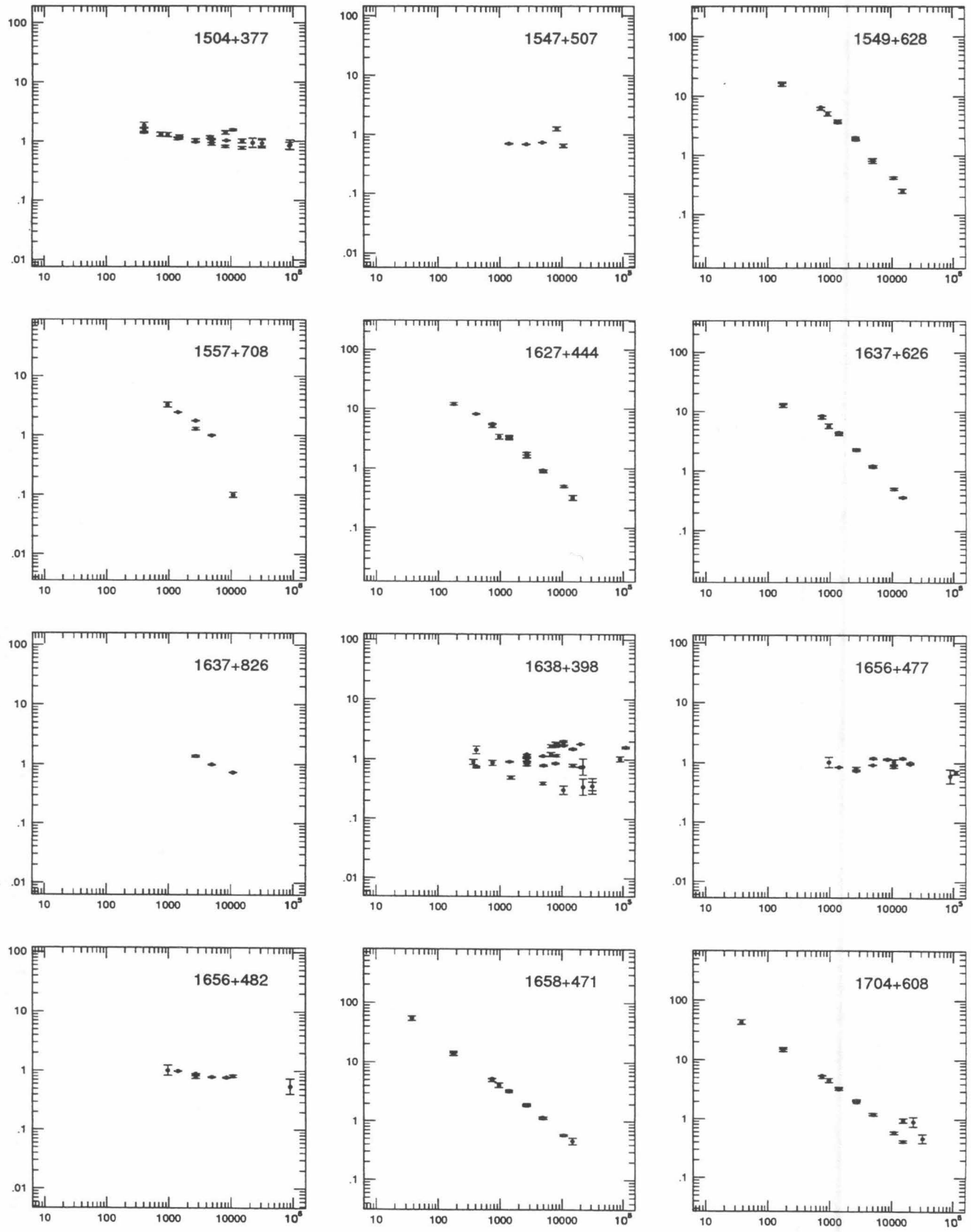

FIG. 7—*Continued*

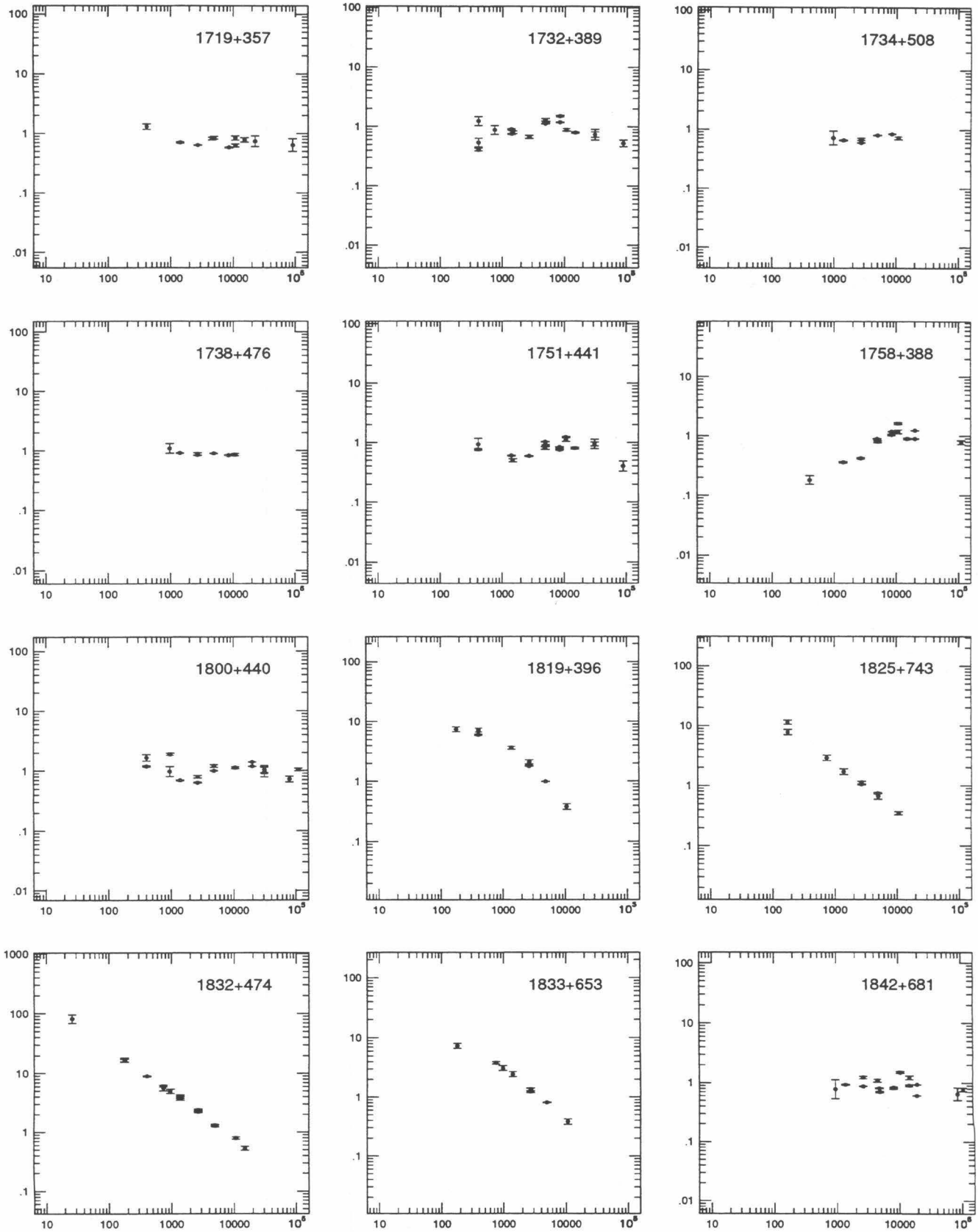

FIG. 7—*Continued*

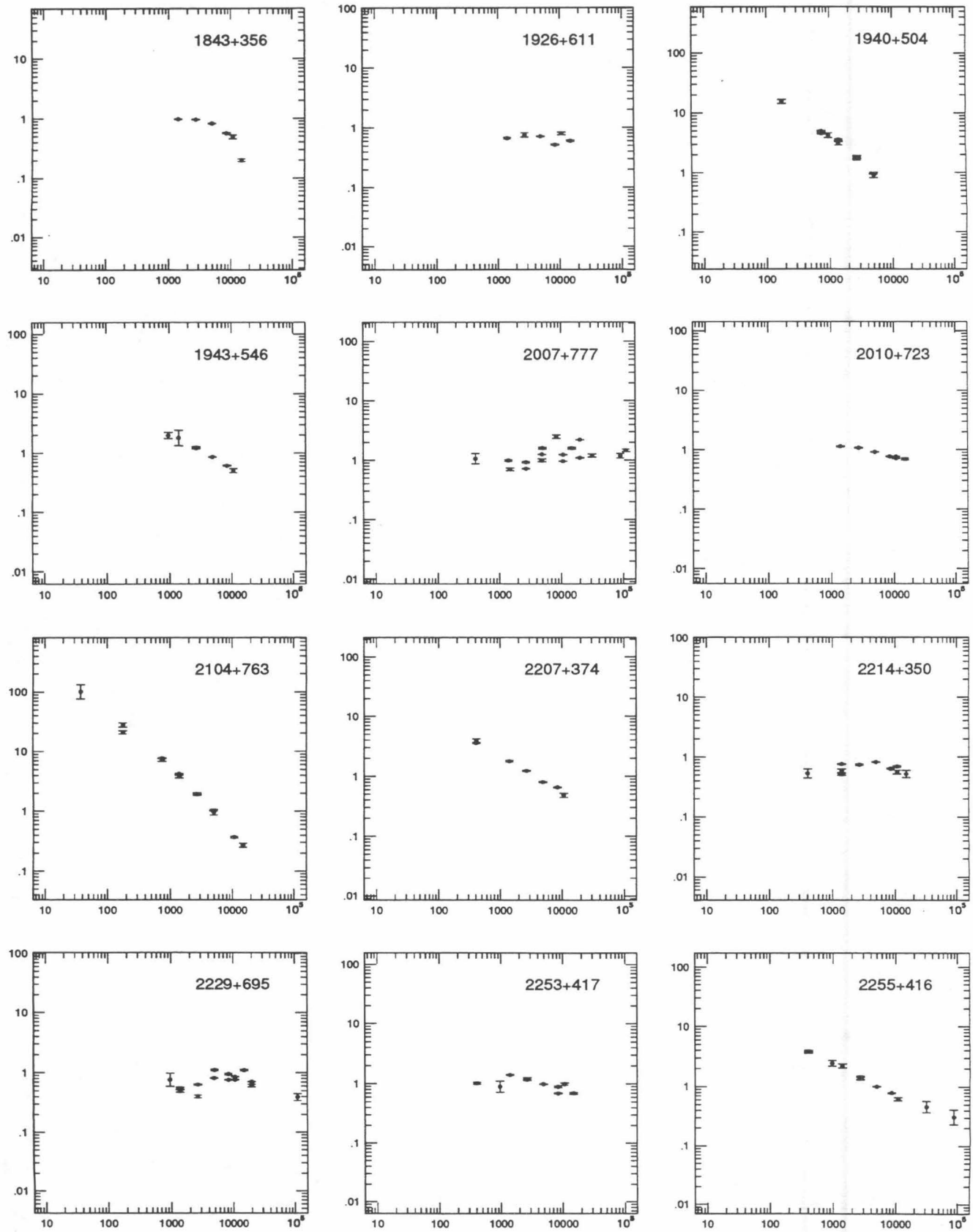

FIG. 7—*Continued*

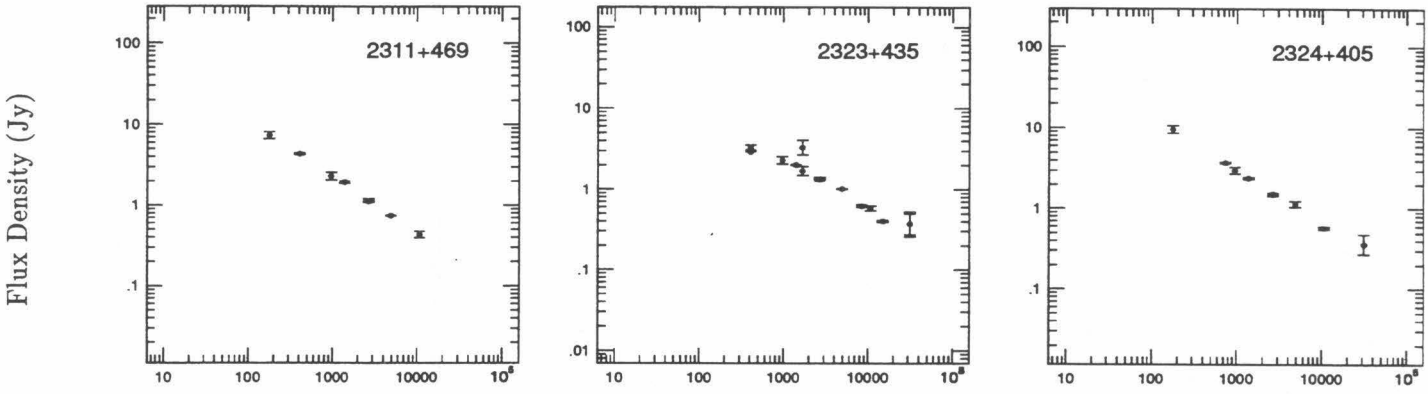

FIG. 7—*Continued*

2.3. *VLA Observations and Data Reduction*

Observations were made with the VLA in the A configuration at *L* band on 1992 November 5. Two IFs centered on 1464.9 and 1364.9 MHz, with a bandwidth of 50 MHz each, were used. The 92 objects observed are listed in Table 5. Each object was observed with three 2 minute snapshots, which were separated by 1.5 hr to improve the *uv* coverage. A typical *uv* coverage is shown in Figure 5. The data were reduced in the AIPS package. The object 3C 286 was used as the flux density calibrator. The MX program was used to make the maps and the CALIB program was used to perform self-calibration. In most cases the final maps were convolved with a circular Gaussian beam of FWHM 1.″5. For objects dominated by large-scale structure, the final maps were convolved with a larger beam (3″ or 5″).

In VLA observations at this frequency there are often other radio sources present in the field. These objects must also be mapped in order to achieve high dynamic range on the target object. Thus we mapped an $11' \times 11'$ field for each object to locate possible confusing sources. All sources brighter than $\sim$10 mJy were mapped. The rms noise of a blank area of sky in the maps ranges from 0.1 to 0.5 mJy for most objects (see Table 5). Several strong sources have large rms noise, and this could not be corrected with self-calibration. Of the 92 objects, 28 are unresolved, and for these we do not present maps. The maps of the other 64 objects are presented in Figure 6, and the parameters of the maps are listed in Table 5.

2.4. *Radio Spectra*

The spectra of all the CJ1 objects are presented in Figure 7. We collected flux density measurements at various frequencies from the literature. For the most part, the data were taken from the catalog of radio objects compiled by Kühr et al. (1979). Part of the catalog containing objects brighter than 1 Jy has been published (Kühr et al. 1981b). Other data were taken from the VLA calibrator list (1990 edition); Edelson (1987); Ficarra, Grueff, & Tomassetti (1985); Patnaik et al. (1992); Steppe et al. (1988); and White & Becker (1992). Many of the sources are variable, and the flux density measurements span several years, so much of the apparent structure in the spectra can be attributed to variability.

3. CONCLUSION

In this third paper of the series, we have reported 5 GHz VLBI and MERLIN observations and 1.4 GHz VLA observations of objects in the CJ1 and PR samples. We now have a large body of observational data on the majority of objects in the complete sample of 200 objects with $S_{5\,\mathrm{GHz}} \geq 0.7$ Jy, $\delta \geq 35°$, and $|b| \geq 10°$, including VLBI images at 1.6 GHz (Papers I and II), VLBI images at 5 GHz (this paper and Pearson & Readhead 1988), MERLIN and VLA images (this paper and published results), and radio spectra (this paper). Optical observations to measure redshifts are in progress (Xu et al. 1994).

The CJ1+PR sample of 200 objects is large enough to refine the classification of compact radio objects presented by Pearson & Readhead and to undertake a number of important astrophysical and cosmological studies. These subjects will be addressed in subsequent papers in the series. A number of particularly interesting objects have already been identified, including several compact symmetric objects (e.g., 2352+495: Wilkinson et al. 1994; Readhead et al. 1995), gravitational lenses (e.g., 0218+357; Patnaik et al. 1993), and a high-redshift superluminal object (0642+449: Vermeulen et al. 1995).

While this paper completes the VLBI observations for the CJ1 survey, we are also in the process of enlarging the sample still further with the second Caltech–Jodrell Bank VLBI survey (CJ2) of flat-spectrum radio objects (Taylor et al. 1994; Henstock et al. 1995).

We thank the staffs of the observatories in the European and the US VLBI networks and the staff of the JPL/Caltech Block 2 correlator for their assistance during the CJ1 survey. We also thank R. C. Vermeulen and G. B. Taylor for their help with

fringe-fitting and automatic mapping and G. B. Taylor and D. R. Henstock for observing six objects for us. A. G. P. acknowledges the receipt of a British Council Fellowship for the year 1991. The work at the California Institute of Technology was supported by the National Science Foundation (grants AST-8814554 and AST-9117100). The VLA and VLBA are instruments of the National Radio Astronomy Observatory, which is operated by Associated Universities, Inc., under cooperative agreement with the National Science Foundation.

REFERENCES

Clark, B. G. 1973, Proc. IEEE, 61, 1242
Cohen, M. H., et al. 1975, ApJ, 201, 249
Edelson, R. A. 1987, AJ, 94, 1150
Ficarra, A., Grueff, G., & Tomassetti, G. 1985, A&AS, 59, 255
Henstock, D. R., Wilkinson, P. N., Browne, I. W. A., Taylor, G. B., Vermeulen, R. C., Pearson, T. J., & Readhead, A. C. S. 1995, ApJS, in press
Högbom, J. A. 1974, A&AS, 15, 417
Jones, D. L., et al. 1986, ApJ, 305, 684
Kühr, H., Nauber, U., Pauliny-Toth, I. I. K., & Witzel, A. 1979, MPIfR preprint 55
Kühr, H., Pauliny-Toth, I. I. K., Witzel, A., & Schmidt, J. 1981a, AJ, 86, 854
Kühr, H., Witzel, A., Pauliny-Toth, I. I. K., & Nauber, U. 1981b, A&AS, 45, 367
Patnaik, A. R., Browne, I. W. A., King, L. J., Muxlow, T. W. B., Walsh, D., & Wilkinson, P. N. 1993, MNRAS, 261, 435
Patnaik, A. R., Browne, I. W. A., Wilkinson, P. N., & Wrobel, J. M. 1992, MNRAS, 254, 655
Pauliny-Toth, I. I. K., Witzel, A., Preuss, E., Kühr, H., Kellermann, K. I., Fomalont, E. B., & Davis, M. M. 1978, AJ, 83, 451
Pearson, T. J. 1991, BAAS, 23, 991
Pearson, T. J., & Readhead, A. C. S. 1988, ApJ, 328, 114 (PR)
Polatidis, A. G., Wilkinson, P. N., Xu, W., Readhead, A. C. S., Pearson, T. J., Taylor, G. B., & Vermeulen, R. C. 1995, ApJS, 98, 1 (Paper I)
Readhead, A. C. S., Xu, W., Pearson, T. J., Taylor, G. B., Wilkinson, P. N., & Polatidis, A. G. 1995, in preparation
Schwab, F. R., & Cotton, W. D. 1983, AJ, 88, 688
Shepherd, M. C., Pearson, T. J., & Taylor, G. B. 1994, BAAS, 26, 987
Steppe, H., Salter, C. J., Chini, R., Kreysa, E., Brunswig, W., & Lobato Perez, J. 1988, A&AS, 75, 317
Taylor, G. B., Vermeulen, R. C., Pearson, T. J., Readhead, A. C. S., Henstock, D. R., Browne, I. W. A., & Wilkinson, P. N. 1994, ApJS, 95, 345
Thakkar, D. D., Xu, W., Readhead, A. C. S., Pearson, T. J., Taylor, G. B., Vermeulen, R. C., Polatidis, A. G., & Wilkinson, P. N. 1995, ApJS, 98, 33 (Paper II)
White, R. L., & Becker, R. H. 1992, ApJS, 79, 331
Wilkinson, P. N., Polatidis, A. G., Readhead, A. C. S., Xu, W., & Pearson, T. J. 1994, ApJ, 432, L87
Xu, W., Lawrence, C. R., Readhead, A. C. S., & Pearson, T. J. 1994, AJ, 108, 395
Vermeulen, R. C., et al. 1995, in preparation

THE ASTROPHYSICAL JOURNAL SUPPLEMENT SERIES, 95:345–369, 1994 December

THE SECOND CALTECH–JODRELL BANK VLBI SURVEY. I. OBSERVATIONS OF 91 OF 193 SOURCES

G. B. TAYLOR, R. C. VERMEULEN, T. J. PEARSON, AND A. C. S. READHEAD
California Institute of Technology, Owens Valley Radio Observatory, 105-24, Pasadena, CA 91125

AND

D. R. HENSTOCK, I. W. A. BROWNE, AND P. N. WILKINSON
University of Manchester, Nuffield Radio Astronomy Laboratories, Jodrell Bank, Macclesfield, Cheshire SK11 9DL, UK
Received 1994 April 26; accepted 1994 May 20

ABSTRACT

We define the sample for the second Caltech–Jodrell Bank VLBI survey. This is a sample of 193 flat- or gigahertz-peaked-spectrum sources selected at 4850 MHz. This paper presents images of 91 sources with a resolution of ~1 mas, obtained using VLBI observations at 4992 MHz with a global array. The remaining images and the integrated radio spectra will be presented in a forthcoming paper by Henstock et al.

Subject headings: galaxies: structure — quasars: general — radio continuum: galaxies — surveys — techniques: interferometric

1. INTRODUCTION

The second Caltech–Jodrell Bank VLBI survey (CJ2) is a Mark II snapshot VLBI survey of 193 flat- and peaked-spectrum radio sources. The survey extends the morphological study of the Pearson & Readhead (1988, hereafter PR) and the first Caltech–Jodrell Bank (Polatidis et al. 1994; Thakkar et al. 1994; Xu 1994; hereafter CJ1) surveys to 321 sources. With uniform observations of a large sample, it is possible to pursue classification and evolutionary issues in detail and to test unification schemes. The CJ2 survey also has three cosmological goals: (1) to search for small-separation gravitationally lensed systems and hence to look directly for mass concentrations in the unexplored range of 10^6–10^9 $M_\odot$, (2) to populate the proper motion–redshift diagram for superluminal sources, and (3) to populate the angular size–redshift diagram for compact sources (both diagrams can be used to estimate the deceleration parameter, q_0).

In this paper we define the CJ2 sample and report on the first three observing campaigns, during which 91 sources were observed and imaged. Results for the remainder of the sample and plots of the integrated radio spectra for the entire sample are presented in Henstock et al. (1994, hereafter Paper II). In § 2 we discuss how the source sample was derived. A brief description of the observations is presented in § 3, and the images are presented in § 4. Future work will concentrate on the morphological classification (Taylor et al. 1994) and the constraints which these observations place on gravitational lensing by objects in the mass range of 10^6–10^9 $M_\odot$ (Henstock 1994). A campaign to obtain redshifts and improved optical identifications for the CJ2 sample is underway.

2. THE CJ2 SAMPLE SELECTION

The CJ2 sample is drawn from the Jodrell Bank–VLA Astrometric Survey (Patnaik et al. 1992, and papers in preparation; hereafter JVAS), which contains ~920 compact flat-spectrum sources north of declination 35°. The primary goal of that survey was to identify strong, compact sources at 8400 MHz and to measure their positions accurately enough for use as phase calibrators for the Jodrell Bank MERLIN. For declinations between 35° and 75°, sources in the JVAS catalog were derived from the 1400 and 4850 MHz Green Bank surveys (Condon & Broderick 1985, 1986; Condon, Broderick, & Seielstad 1989; Gregory & Condon 1991). Sources north of declination 75° were selected from the MPI S5 catalog (Kühr et al. 1981). The JVAS sources were selected with spectral indices between 1400 and 4850 MHz flatter than $\alpha = -0.5$ (where $S_\nu \propto \nu^\alpha$). The vast majority of the JVAS sources are unresolved by the ~200 mas VLA beam at 8400 MHz.

The selection criteria for the CJ2 sample were:

1. Observed in JVAS;
2. Flux density at 4850 MHz (Gregory & Condon 1991), $S_{4850} \geq 350$ mJy;
3. Declination (B1950) $\delta \geq 35°$;
4. Galactic latitude $|b| \geq 10°$;
5. Spectral index (α_{8400}^{365} flatter than -0.5);
6. Not previously observed in the PR or CJ1 surveys.

To increase the sample size of CJ2 in the search for small-scale gravitational lenses, we also included 11 sources weaker than 350 mJy at 4850 MHz, 4 sources with α_{8400}^{365} steeper than -0.5, and one source, 0026 + 346, just below our declination limit. A similar number of flat-spectrum sources stronger than 350 mJy were not observed because of missing information at lower frequencies, or because they were not included in JVAS. By selecting the CJ2 sample from the observed JVAS sample, rather than from the Green Bank catalog, we made use of better source positions and increased the likelihood of observing sources with compact structure on the milliarcsecond scale. Since flat-spectrum sources are known to be more compact than steep-spectrum sources, we excluded sources with evidence for a steep spectrum ($\alpha < -0.5$) between 365 MHz (J. Douglas, private communication) and 8400 MHz (JVAS). The net result of our selection procedure is not a complete, flux and spectrally limited sample. A complete sample of sources imaged with VLBI and suitable for statistical studies will be formed using the PR, CJ1, and CJ2 surveys and discussed in a later paper.

Positions, flux densities, and optical identifications for all 193 sources in the CJ2 sample are listed in Table 1. Spectra for all sources are presented in Paper II. The optical identifications and estimates of the apparent magnitudes were made with the aid of the Automatic Plate Measuring Facility at the Institute of Astronomy, Cambridge, which was used to scan the POSS plates around the JVAS positions (McMahon 1994).

3. OBSERVATIONS

The observations took place on 1992 June 5–7, 1992 September 24–27, and 1993 March 1–2 using a global VLBI array. Results from a further observing session on 1993 June 9–16 will be presented in Paper II. The telescopes used include those in the European VLBI Network, the Very Long Baseline Array,[1] the Very Large Array,[1] the NRAO 140 foot (43 m),[1] and the Haystack Observatory. The observing frequency was 4992 MHz, and the Mark II recording scheme was used, providing a bandwidth of 2 MHz. Only the signals from telescopes successfully observing in left-circular polarization were used. These telescopes are listed for each observing session in Table 2.

The observing strategy employed was a "VLBI-snapshot" technique, in which each source was observed in three, or sometimes four, scans each of 20 minutes duration distributed over a wide hour-angle range. The typical *u-v* coverages obtained for sources at high, middle, and low declinations are shown in Figure 1. A more detailed discussion of the VLBI-snapshot technique may be found in Polatidis et al. (1994).

All data were correlated using the Block II Correlator at Caltech. Observations of strong calibrators, primarily 0552 + 398 and 1739 + 522, were used to find and monitor the clock offsets at intervals of ~12 hr during each run. Following correlation, global fringe fitting was performed using the AIPS task FRING, an implementation of the Schwab & Cotton (1983) algorithm. A solution interval of ~7 minutes was used allowing for three solutions of the delay and fringe rate during each 20 minute scan. The fringe fitting was performed using the least-squares option within FRING and assuming a point source model in all cases. Effelsberg was chosen to be the "reference telescope" whenever possible, otherwise the NRAO 140 foot telescope at Green Bank was used.

Amplitude calibration for each antenna was derived from measurements of the antenna gain and system temperature during the run. In addition the calibrators 0552 + 398 and 1739 + 522 were observed throughout the run to further refine the amplitude calibration by examining *u-v* crossing points as described by Polatidis et al. (1994). After phase self-calibration with a 10 s solution interval, and a point-source model, the data were coherently averaged to 1 minute integrations. All editing, imaging, deconvolution, and self-calibration of the data were performed using DIFMAP (Shepherd, Pearson, &

[1] The National Radio Astronomy Observatory is operated by Associated Universities, Inc., under cooperative agreement with the National Science Foundation.

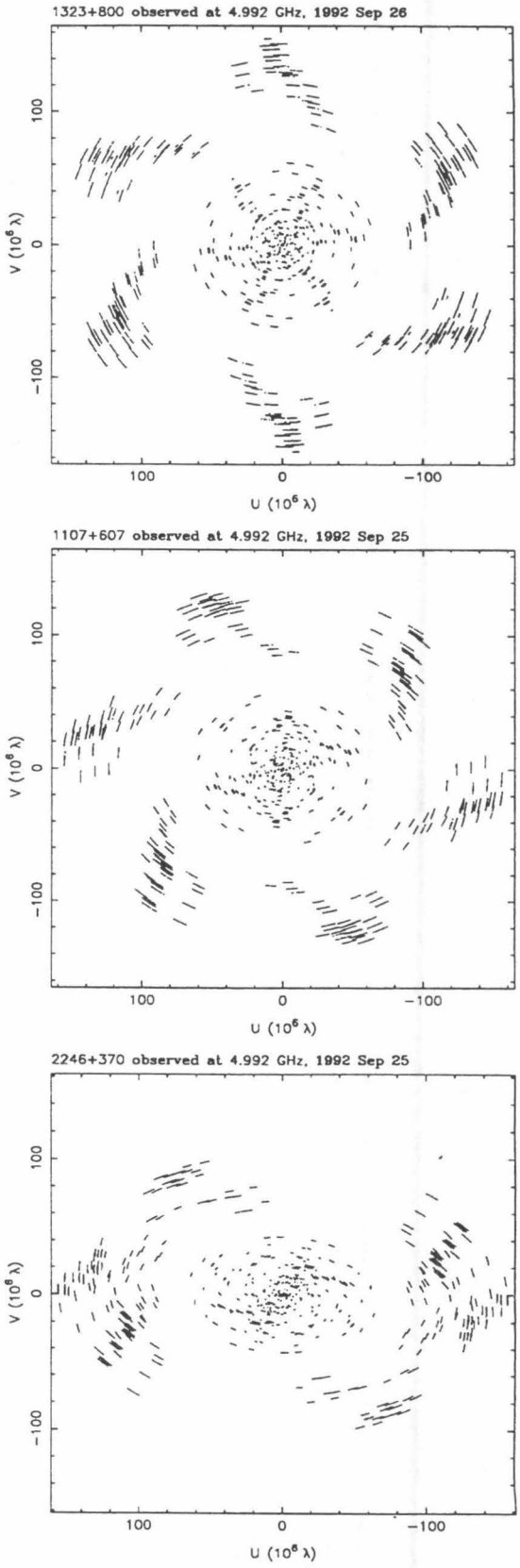

FIG. 1.—*u-v* coverage obtained for three sources at declinations of 80°, 60°, and 37°. The hexagonal pattern results from the three observations of 20 minutes each spaced over a wide range in hour angle.

TABLE 1

THE CJ2 SAMPLE

Source (1)	R.A. (2)	Declination (3)	S_{80cm} (4)	S_{20cm} (5)	S_{6cm} (6)	$S_{3.6cm}$ (7)	ID (8)	R (9)	z (10)	Date (11)
0003+380 ...	00 05 57.17550	38 20 15.1685	0.638	0.601	0.549	1.157	G	17.1	0.229	1993 Jun
0014+813 ...	00 17 08.47504	81 35 08.1365	–	0.676	0.551	1.355	Q	15.9[a]	3.384	1992 Sep
0018+729 ...	00 21 27.37784	73 12 41.9283	–	0.614	0.397	0.196	EF	–	...	1992 Jun
0026+346 ...	00 29 14.24355	34 56 32.2545	1.359	1.750	1.312	1.035	EF	–	...	1992 Jun
0035+413 ...	00 38 24.84498	41 37 06.0046	0.512	0.440	1.114	0.985	Q	19.4	1.353	1993 Jun
0109+351 ...	01 12 12.94503	35 22 19.2954	0.915	0.360	0.362	0.402	BS	17.8	...	1993 Jun
0110+495 ...	01 13 27.00695	49 48 24.0572	1.104	0.486	0.710	0.499	Q	17.5[b]	0.395	1993 Jun
0129+431 ...	01 32 44.12727	43 25 32.6667	–	0.216	0.347	0.235	BS	18.7	...	1993 Jun
0145+386 ...	01 48 24.37679	38 54 05.2227	0.209	0.293	0.370	0.343	Q	17.2	1.44	1993 Jun
0151+474 ...	01 54 56.29019	47 43 26.5392	0.384	0.353	0.505	0.690	EF	–	...	1993 Jun
0201+365 ...	02 04 55.59586	36 49 18.0007	0.460	0.590	0.349	0.263	Q	17.5	2.912	1993 Jun
0205+722 ...	02 09 51.79208	72 29 26.6686	–	0.842	0.560	0.549	RO	17.0[b]	...	1992 Sep
0227+403 ...	02 30 45.70679	40 32 53.0870	0.252	0.438	0.436	0.578	BS	17.0[b]	...	1993 Jun
0249+383 ...	02 53 08.88698	38 35 24.9867	0.970	0.781	0.450	0.454	BS	18.5	...	1993 Jun
0251+393 ...	02 54 42.63160	39 31 34.7140	–	0.297	0.408	0.367	BS	15.4	...	1993 Jun
0256+424 ...	02 59 38.38223	42 36 43.1192	0.685	0.616	0.366	0.320	EF	–	...	1993 Jun
0307+380 ...	03 10 49.88050	38 14 53.8452	–	–	0.760	0.453	EF	–	...	1993 Jun
0309+411 ...	03 13 01.96146	41 20 01.1903	0.474	0.467	0.516	0.673	G	16.0[b]	0.136	1993 Jun
0340+362 ...	03 43 28.95271	36 22 12.4404	0.454	0.282	0.376	0.620	EF	–[b]	...	1993 Jun
0346+800 ...	03 54 46.12577	80 09 28.8156	–	–	0.396	0.365	BO	21.3	...	1992 Sep
0444+634 ...	04 49 23.30971	63 32 09.4532	0.535	0.370	0.606	0.467	Q	19.0[b]	0.781	1992 Sep
0537+531 ...	05 41 16.17329	53 12 24.8379	1.115	0.656	0.665	0.747	Q	17.4[a]	1.275	1993 Mar
0546+726 ...	05 52 52.99716	72 40 45.1288	–	0.493	0.401	0.267	NS	17.0[b]	...	1992 Sep
0554+580 ...	05 59 13.39407	58 04 03.4432	0.630	0.373	0.906	0.501	BS	18.0[b]	...	1993 Mar
0600+442 ...	06 04 35.62972	44 13 58.5460	1.486	1.208	0.705	0.439	BS	17.0[b]	...	1993 Jun
0604+728 ...	06 10 48.86913	72 48 53.1885	–	1.015	0.654	0.391	EF	–	...	1992 Sep
0609+607 ...	06 14 23.86660	60 46 21.7540	1.562	1.060	1.059	0.750	BS	19.0[b]	...	1993 Mar
0627+532 ...	06 31 34.68599	53 11 27.7537	0.605	0.807	0.485	0.312	BS	18.5	...	1993 Jun
0633+734 ...	06 39 21.96228	73 24 58.0503	–	1.097	0.748	0.772	BS	17.8	...	1992 Sep
0633+596 ...	06 38 02.87300	59 33 22.2075	0.295	0.230	0.482	0.553	EF	–	...	1993 Mar
0636+680 ...	06 42 04.25682	67 58 35.6258	–	0.129	0.499	0.436	Q	16.2	3.174	1992 Jun
0641+393 ...	06 44 53.71000	39 14 47.5407	0.529	0.366	0.453	0.616	BS	19.5[b]	...	1993 Jun
0650+453 ...	06 54 23.71370	45 14 23.5410	0.466	0.590	0.420	0.372	BO	21.0	...	1993 Jun
0651+410 ...	06 55 10.02429	41 00 10.1479	–	–	0.425	0.373	G	14.0[b]	0.0201	1993 Jun
0700+470 ...	07 04 09.55875	47 00 56.0405	0.558	0.824	0.443	0.335	RO	20.0	...	1993 Jun
0702+612 ...	07 07 00.61645	61 10 11.5875	0.610	0.327	0.370	0.235	BS	17.0	...	1993 Mar
0714+457 ...	07 17 51.85314	45 38 03.2521	–	0.408	0.480	0.569	Q	17.7	0.940	1993 Jun
0718+793 ...	07 26 11.74592	79 11 31.0208	–	0.463	0.631	0.694	EF	–	...	1992 Sep
0724+571 ...	07 28 49.63210	57 01 24.3667	0.552	0.408	0.393	0.632	BS	17.0[b]	...	1993 Mar
0727+409 ...	07 30 51.34725	40 49 50.8263	0.242	0.413	0.468	0.377	Q	17.0[b]	2.501	1993 Jun
0730+504 ...	07 33 52.52117	50 22 09.0511	0.761	0.386	0.890	0.730	BS	19.0[b]	...	1992 Jun
0731+479 ...	07 35 02.31207	47 50 08.4202	0.351	0.432	0.533	0.450	Q	16.9	0.782	1993 Jun
0733+597 ...	07 37 30.08713	59 41 03.1948	0.862	0.553	0.357	0.235	G	14.9[c]	0.040	1993 Mar
0738+491 ...	07 42 02.75080	49 00 15.6021	–	–	0.352	0.483	EF	–	...	1993 Jun
0739+398 ...	07 43 09.88664	39 41 30.7813	1.286	0.770	0.410	0.327	Q	18.0	1.700	1993 Jun
0740+768 ...	07 47 14.62258	76 39 17.2644	–	–	0.592	0.550	EF	–	...	1992 Sep
0743+744 ...	07 49 22.45732	74 20 41.5949	–	0.354	0.479	0.394	Q	18.8	1.629	1993 Jun
0749+540 ...	07 53 01.38500	53 52 59.6370	–	0.791	0.877	1.162	BL	17.3	–	1993 Mar
0749+426 ...	07 53 03.33778	42 31 30.7631	0.760	0.702	0.461	0.280	RS	18.1	...	1992 Jun
0803+452 ...	08 06 33.47197	45 04 32.2740	0.272	0.389	0.414	0.423	BS	19.6	...	1993 Jun
0806+573 ...	08 11 00.60937	57 14 12.4939	0.927	–	0.405	0.348	BS	17.2	...	1992 Jun
0821+621 ...	08 25 38.61209	61 57 28.5773	1.066	0.652	0.615	0.608	Q	17.3	0.542	1992 Jun
0824+355 ...	08 27 38.58906	35 25 05.0807	1.832	0.866	0.746	0.657	Q	19.7	2.249	1993 Jun
0830+425 ...	08 33 53.88502	42 24 01.8494	0.405	–	0.341	0.553	NS	17.0	...	1993 Jun
0833+416 ...	08 36 36.89322	41 25 54.7062	0.473	0.425	0.385	0.279	BS	17.2	...	1993 Jun

TABLE 1—*Continued*

Source (1)	R.A. (2)	Declination (3)	S_{80cm} (4)	S_{20cm} (5)	S_{6cm} (6)	$S_{3.6cm}$ (7)	ID (8)	R (9)	z (10)	Date (11)
0843+575 ...	08 47 28.06159	57 23 38.3355	–	0.284	0.384	0.242	EF	–	...	1993 Mar
0859+681 ...	09 03 53.15590	67 57 22.6827	0.413	0.592	0.751	0.635	Q	18.2	1.499	1992 Jun
0900+520 ...	09 03 58.57582	51 51 00.6583	–	0.322	0.395	0.273	BS	19.6	...	1993 Mar
0902+490 ...	09 05 27.46476	48 50 49.9588	0.976	0.636	0.547	0.447	Q	17.2	2.690	1993 Jun
0913+391 ...	09 16 48.90469	38 54 28.1421	1.801	1.057	0.557	0.462	Q	19.0[b]	1.269	1993 Jun
0925+504 ...	09 29 15.44170	50 13 35.9782	–	0.266	0.558	0.692	BS	16.0	...	1993 Jun
0927+352 ...	09 30 55.27914	35 03 37.6082	1.053	0.422	0.383	0.472	NS	19.2	...	1993 Jun
0929+533 ...	09 32 41.15174	53 06 33.7851	0.483	0.537	0.384	0.380	Q	17.4	0.595	1993 Mar
0930+493 ...	09 34 15.76310	49 08 21.7164	0.488	0.733	0.574	0.398	BS	18.4	...	1993 Jun
0933+503 ...	09 37 12.32879	50 08 52.0753	–	–	0.347	0.352	G	18.0	...	1993 Jun
0941+522 ...	09 44 52.15670	52 02 34.2164	0.906	0.851	0.345	0.258	Q	17.8[b]	0.565	1993 Jun
0942+468 ...	09 45 42.09361	46 36 50.5928	0.403	0.278	0.354	0.356	EF	–	...	1993 Jun
0949+354 ...	09 52 32.02616	35 12 52.3929	0.510	0.344	0.403	0.337	Q	18.9	1.875	1993 Jun
0950+748 ...	09 54 47.44405	74 35 57.1405	–	1.186	0.738	0.411	EF	–	...	1992 Sep
1010+350 ...	10 13 49.61423	34 45 50.7817	0.469	0.418	0.597	0.367	G	18.6	1.414	1993 Jun
1014+615 ...	10 17 25.88496	61 16 27.4932	0.265	0.361	0.631	0.571	BS	18.1	...	1992 Sep
1030+398 ...	10 33 22.06179	39 35 51.0812	0.823	0.379	0.645	0.509	EF	–	...	1993 Jun
1030+611 ...	10 33 51.42726	60 51 07.3301	0.995	0.766	0.579	0.427	NS	19.3	0.336	1992 Sep
1038+528 ...	10 41 46.77999	52 33 28.2170	1.121	0.713	0.709	0.720	Q	16.3	0.677	1993 Jun
1041+536 ...	10 44 10.67165	53 22 20.5222	0.493	0.543	0.481	0.389	BS	19.0	...	1993 Jun
1058+629 ...	11 01 53.44908	62 41 50.5899	1.882	0.598	0.700	0.354	BS	17.7	...	1992 Sep
1105+437 ...	11 08 23.47791	43 30 53.6367	0.357	0.266	0.375	0.282	NS	19.5	...	1993 Jun
1107+607 ...	11 10 13.08711	60 28 42.5510	0.439	0.345	0.404	0.276	EF	–	...	1992 Sep
1124+455 ...	11 26 57.65509	45 16 06.2894	–	0.493	0.355	0.333	BS	17.0	...	1993 Jun
1124+571 ...	11 27 40.13530	56 50 14.7793	0.427	0.775	0.597	0.498	Q	18.0	2.890	1992 Sep
1125+596 ...	11 28 13.34150	59 25 14.7776	0.279	0.364	0.393	0.584	BS	20.0	...	1992 Sep
1143+590 ...	11 46 26.91199	58 48 34.2423	–	0.276	0.674	0.569	BS	19.6	...	1992 Sep
1144+352 ...	11 47 22.13022	35 01 07.5258	0.358	0.695	0.663	0.501	G	15.0	0.063	1993 Jun
1146+531 ...	11 48 56.56863	52 54 25.3311	–	–	0.304	0.597	BS	15.5	...	1993 Jun
1146+596 ...	11 48 50.35909	59 24 56.3620	0.327	0.415	0.627	0.516	G	11.0	0.0108	1992 Sep
1151+408 ...	11 53 54.65938	40 36 52.6172	0.949	0.698	0.380	0.361	NS	19.5	...	1993 Jun
1155+486 ...	11 58 26.76904	48 25 16.2350	0.309	0.484	0.445	0.424	BO	19.9	...	1993 Jun
1205+544 ...	12 08 27.49949	54 13 19.5292	–	0.463	0.397	0.280	EF	–	...	1993 Jun
1206+415 ...	12 09 22.78840	41 19 41.3688	–	0.323	0.515	0.486	BS	16.3	...	1993 Jun
1214+588 ...	12 17 11.02025	58 35 26.2283	0.710	0.422	0.307	0.473	BS	19.5	...	1992 Sep
1218+444 ...	12 21 27.04576	44 11 29.6635	0.662	0.601	0.478	0.435	BS	17.3	...	1992 Jun
1221+809 ...	12 23 40.49739	80 40 04.3239	–	0.726	0.518	0.454	BL	18.7	–	1993 Jun
1223+395 ...	12 25 50.57029	39 14 22.6806	0.544	0.540	0.438	0.377	EF	–	...	1993 Jun
1226+373 ...	12 28 47.42456	37 06 12.0820	0.263	0.192	0.953	0.868	BS	18.0[b]	...	1993 Jun
1239+376 ...	12 42 09.81383	37 20 05.6807	0.469	0.544	0.446	0.336	EF	–	...	1993 Jun
1240+381 ...	12 42 51.37049	37 51 00.0126	0.495	0.363	0.768	0.608	Q	19.1	1.316	1993 Jun
1246+586 ...	12 48 18.78472	58 20 28.7144	0.232	0.238	0.414	0.310	BS	14.0	...	1992 Sep
1250+532 ...	12 53 11.92132	53 01 11.7266	0.982	0.538	0.396	0.372	BS	16.4	...	1993 Jun
1254+571 ...	12 56 14.23440	56 52 25.2367	0.551	0.288	0.419	0.255	G	13.2[b]	0.041	1992 Sep
1258+507 ...	13 00 41.24832	50 29 36.7498	0.666	0.524	0.391	0.339	EF	–	...	1993 Jun
1300+580 ...	13 02 52.46490	57 48 37.6175	0.403	0.305	0.758	0.885	RO	20.0[b]	...	1992 Sep
1307+562 ...	13 09 09.75329	55 57 38.1932	0.319	0.294	0.416	0.302	BS	17.6	...	1992 Sep
1308+471 ...	13 10 53.59063	46 53 52.2192	–	–	0.393	0.361	BS	19.1	...	1993 Jun
1309+555 ...	13 11 03.20969	55 13 54.3298	0.595	0.207	0.677	0.505	BS	19.1	...	1992 Sep
1311+552 ...	13 13 37.85179	54 58 23.8943	1.645	1.173	0.542	0.302	EF	–	...	1992 Sep
1312+533 ...	13 14 43.82839	53 06 27.7274	–	0.232	0.433	0.303	EF	–	...	1993 Jun
1321+410 ...	13 24 12.09400	40 48 11.7728	–	0.357	0.413	0.246	NS	19.5	...	1993 Jun
1322+835 ...	13 21 45.59214	83 16 13.4365	–	–	0.506	0.267	EF	–	...	1992 Sep
1323+800 ...	13 23 51.57398	79 42 51.8592	–	0.492	0.458	0.564	EF	–	...	1992 Sep
1325+436 ...	13 27 20.97896	43 26 27.9969	0.660	0.703	0.533	0.462	Q	18.5	2.073	1993 Jun

TABLE 1—*Continued*

Source (1)	R.A. (2)	Declination (3)	S_{80cm} (4)	S_{20cm} (5)	S_{6cm} (6)	$S_{3.6cm}$ (7)	ID (8)	R (9)	z (10)	Date (11)
1335+552 ...	13 37 49.64084	55 01 02.1208	0.744	0.717	0.811	0.573	Q	17.8	1.096	1992 Sep
1337+637 ...	13 39 23.78121	63 28 58.4253	–	0.500	0.431	0.272	BS	18.5	...	1992 Sep
1342+662 ...	13 43 45.95763	66 02 25.7486	–	–	0.288	0.578	Q	18.8	0.766	1992 Jun
1413+373 ...	14 15 28.46657	37 06 21.1789	0.213	0.366	0.383	0.278	Q	17.3	2.36	1993 Jun
1415+463 ...	14 17 08.16081	46 07 05.4483	1.525	1.012	0.904	0.583	Q	17.5	1.552	1993 Jun
1417+385 ...	14 19 46.61407	38 21 48.4841	0.487	0.708	0.871	0.793	Q	18.5	1.832	1993 Jun
1421+482 ...	14 23 06.15619	48 02 10.8466	0.497	0.361	0.536	0.392	BS	18.9	...	1993 Jun
1424+366 ...	14 26 37.08764	36 25 09.5858	0.336	0.194	0.429	0.621	BS	18.3	...	1993 Jun
1427+543 ...	14 29 21.87958	54 06 11.1266	2.375	0.903	0.718	0.493	BS	20.7	...	1993 Jun
1436+763 ...	14 35 47.09760	76 05 25.8179	–	1.154	0.585	0.417	EF	–	...	1992 Sep
1442+637 ...	14 43 58.60200	63 32 26.3630	0.388	0.684	0.456	0.392	Q	17.3	1.380	1992 Jun
1448+762 ...	14 48 28.77822	76 01 11.5943	–	0.513	0.683	0.324	EF	–	...	1993 Jun
1456+375 ...	14 58 44.79492	37 20 21.6266	–	0.335	0.591	0.370	NS	18.2	...	1993 Jun
1459+480 ...	15 00 48.65431	47 51 15.5259	0.432	0.401	0.489	0.686	BS	17.1	...	1993 Jun
1505+428 ...	15 06 53.04195	42 39 23.0400	0.456	0.435	0.404	0.410	BS	21.5	...	1993 Jun
1526+670 ...	15 26 42.87323	66 50 54.6171	–	0.426	0.417	0.312	NS	17.1	...	1992 Sep
1531+722 ...	15 31 33.57679	72 06 41.2196	–	0.661	0.452	0.231	Q	16.5[b]	0.899	1992 Sep
1534+501 ...	15 35 52.03949	49 57 39.0837	–	0.229	0.359	0.312	BS	18.0	...	1993 Jun
1543+480 ...	15 45 08.53027	47 51 54.6667	0.835	0.665	0.441	0.347	EF	–	...	1993 Jun
1543+517 ...	15 45 02.82440	51 35 00.8780	0.614	0.485	0.544	0.629	BS	17.3	...	1993 Jun
1545+497 ...	15 47 21.13841	49 37 05.8100	1.690	0.936	0.549	0.360	RS	19.6	...	1993 Jun
1550+582 ...	15 51 58.20771	58 06 44.4659	–	0.226	0.367	0.305	BS	17.0[b]	...	1993 Jun
1602+576 ...	16 03 55.93111	57 30 54.4146	–	–	0.351	0.312	Q	16.8	2.858	1993 Jun
1619+491 ...	16 20 31.22632	49 01 53.2537	0.619	0.468	0.469	0.386	BS	17.8	...	1993 Jun
1623+569 ...	16 24 32.17968	56 52 28.0063	–	0.213	0.213	0.371	BS	17.0	...	1993 Mar
1629+495 ...	16 31 16.54118	49 27 39.5032	0.693	0.323	0.394	0.626	RS	18.3	...	1993 Jun
1636+473 ...	16 37 45.13069	47 17 33.8364	2.062	0.949	1.330	0.749	Q	17.0	0.740	1993 Jun
1638+540 ...	16 39 39.84349	53 57 47.1166	–	0.310	0.369	0.298	BS	19.7	...	1993 Jun
1645+410 ...	16 46 56.85906	40 59 17.1742	–	0.315	0.388	0.358	BS	20.6	...	1993 Jun
1645+635 ...	16 45 58.55338	63 30 10.9322	0.420	0.298	0.444	0.214	BS	19.4	...	1992 Sep
1656+571 ...	16 57 20.70951	57 05 53.5053	2.425	0.806	0.844	0.533	Q	16.8	1.290	1992 Sep
1700+685 ...	17 00 09.29376	68 30 06.9590	0.619	0.300	0.435	0.377	G	17.0	...	1992 Sep
1716+686 ...	17 16 13.93808	68 36 38.7403	–	0.412	0.988	0.829	Q	17.0	0.777	1992 Jun
1722+401 ...	17 24 05.42882	40 04 36.4605	1.040	0.551	0.532	0.284	BS	21.7	...	1993 Jun
1726+455 ...	17 27 27.65082	45 30 39.7339	0.654	0.425	1.066	1.331	Q	18.0[b]	0.714	1993 Jun
1734+363 ...	17 35 48.08683	36 16 45.6099	0.406	0.255	0.305	0.934	BS	19.4	...	1993 Jun
1738+499 ...	17 39 27.39025	49 55 03.3757	0.788	0.567	0.478	0.580	Q	17.5	1.545	1993 Mar
1742+402 ...	17 44 25.09586	40 14 48.1481	1.145	0.913	0.444	0.284	EF	–	...	1993 Jun
1745+624 ...	17 46 14.03324	62 26 54.7278	2.054	0.764	0.580	0.480	Q	18.3	3.886	1992 Sep
1746+470 ...	17 47 26.64725	46 58 50.9294	–	0.426	0.634	0.871	BS	21.3	...	1993 Mar
1747+433 ...	17 49 00.36037	43 21 51.2888	0.712	0.340	0.367	0.286	BS	17.0	...	1993 Jun
1755+578 ...	17 56 03.62851	57 48 47.9901	0.197	0.729	0.455	0.272	BS	18.0	...	1992 Sep
1806+456 ...	18 08 21.88567	45 42 20.8700	–	0.154	0.334	0.424	Q	18.6	0.830	1993 Mar
1809+568 ...	18 10 03.32027	56 49 22.9587	0.677	0.570	0.576	0.441	EF	–	...	1992 Sep
1811+430 ...	18 13 14.68906	43 04 15.6838	2.921	0.969	0.490	0.388	NS	19.4	...	1993 Mar
1812+412 ...	18 14 22.70825	41 13 05.6054	1.694	0.644	0.534	0.375	BS	18.9	...	1993 Jun
1815+614 ...	18 15 36.79199	61 27 11.6409	0.771	0.891	0.465	0.220	EF	–	...	1993 Mar
1826+796 ...	18 23 14.10905	79 38 49.0084	–	0.250	0.577	0.566	G	16.7	...	1992 Sep
1828+399 ...	18 29 56.52027	39 57 34.6902	–	0.127	0.353	0.234	EF	–	...	1993 Jun
1834+612 ...	18 35 19.67558	61 19 40.0233	1.014	0.448	0.590	0.492	BS	17.6	...	1992 Sep
1839+389 ...	18 40 57.15500	39 00 45.7119	–	–	0.476	0.221	BS	19.5[b]	...	1993 Jun
1849+670 ...	18 49 16.07136	67 05 41.6786	1.032	0.901	0.992	0.456	Q	16.0[b]	0.657	1992 Jun
1850+402 ...	18 52 30.37400	40 19 06.6006	0.554	0.546	0.535	0.616	Q	17.9[a]	2.12	1993 Jun
1851+488 ...	18 52 28.54751	48 55 47.4774	0.352	0.291	0.351	0.385	BS	18.5	...	1993 Mar
1856+737 ...	18 54 57.29825	73 51 19.9100	–	0.560	0.546	0.628	Q	15.9	0.460	1992 Sep

TABLE 1—*Continued*

Source (1)	R.A. (2)	Declination (3)	S_{80cm} (4)	S_{20cm} (5)	S_{6cm} (6)	$S_{3.6cm}$ (7)	ID (8)	R (9)	z (10)	Date (11)
1908+484 ...	19 09 46.56339	48 34 31.8265	0.620	0.575	0.423	0.244	NO	19.0[b]	...	1993 Mar
1910+375 ...	19 12 25.12308	37 40 36.6587	0.353	0.504	0.402	0.340	BS	18.5[b]	...	1993 Jun
1915+657 ...	19 15 23.81933	65 48 46.3946	0.833	0.772	0.372	0.221	RO	18.2	...	1993 Jun
1924+507 ...	19 26 06.32190	50 52 57.0209	1.423	0.656	0.354	0.434	Q	17.5[b]	1.098	1993 Jun
1936+714 ...	19 36 03.56036	71 31 31.7763	1.664	0.620	0.391	0.496	Q	18.9[b]	1.864	1992 Sep
1946+708 ...	19 45 53.51973	70 55 48.7226	0.392	0.921	0.645	0.477	G	16.7	0.101	1992 Sep
1950+573 ...	19 51 06.98368	57 27 17.1945	0.855	0.569	0.476	0.316	BS	18.0[b]	...	1992 Sep
2003+662 ...	20 03 54.51091	66 25 56.3889	1.218	1.152	0.490	0.313	EF	–	...	1992 Sep
2005+642 ...	20 06 17.69491	64 24 45.4226	–	0.174	0.739	0.973	RS	19.0[b]	...	1992 Sep
2007+659 ...	20 07 28.77132	66 07 22.5398	0.994	1.030	0.756	0.489	BS	16.4	...	1992 Jun
2015+657 ...	20 15 55.36830	65 54 52.6621	0.884	0.967	0.500	0.548	Q	19.1[a]	2.845	1992 Jun
2017+745 ...	20 17 13.07930	74 40 48.0020	–	0.472	0.500	0.341	BS	17.9	...	1992 Sep
2023+760 ...	20 22 35.58285	76 11 26.1814	–	0.383	0.426	0.374	BL	17.0[b]	–	1992 Sep
2054+611 ...	20 55 38.83705	61 22 00.6411	0.609	0.423	0.414	0.297	EF	–	...	1992 Sep
2136+824 ...	21 33 34.09726	82 39 06.0053	–	1.008	0.509	0.384	BO	18.9	...	1992 Sep
2138+389 ...	21 40 16.94765	39 11 44.8513	0.655	0.664	0.502	0.377	NS	19.0[b]	...	1993 Mar
2235+731 ...	22 36 38.60028	73 22 52.6646	–	0.300	0.424	0.346	EF	–[b]	...	1992 Sep
2238+410 ...	22 41 07.20544	41 20 11.6178	0.597	0.584	0.677	0.826	RS	17.9[b]	...	1992 Sep
2246+370 ...	22 48 37.91101	37 18 12.4680	1.251	0.906	0.414	0.307	BO	20.1	...	1992 Sep
2259+371 ...	23 01 27.73664	37 26 49.2445	0.780	0.596	0.406	0.379	BS	20.4	...	1992 Sep
2309+454 ...	23 11 47.41079	45 43 56.0250	–	0.306	0.597	0.610	EF	–	...	1993 Mar
2310+385 ...	23 12 58.79503	38 47 42.6683	0.293	0.693	0.484	0.327	Q	17.5	2.17	1993 Jun
2319+444 ...	23 22 20.35854	44 45 42.3727	0.356	0.305	0.366	0.366	NS	19.9	...	1993 Jun
2330+387 ...	23 33 02.53305	39 01 12.0185	1.252	0.844	0.394	0.357	EF	–	...	1993 Jun
2346+385 ...	23 49 20.82620	38 49 17.5725	0.259	0.322	0.640	0.286	Q	17.6	1.032	1993 Jun
2353+816 ...	23 56 22.79458	81 52 52.2669	–	0.395	0.476	0.492	BL	19.7[a]	–	1992 Sep
2356+390 ...	23 58 59.85538	39 22 28.3103	1.047	0.428	0.371	0.326	BS	20.6	...	1993 Jun
2356+385 ...	23 59 33.18089	38 50 42.3217	0.258	0.642	0.449	0.278	Q	18.6	2.704	1993 Jun

NOTES TO TABLE 1

Col. (1).—B1950 source name according to IAU convention. Cols. (2) and (3).—Right ascension and declination in J2000 coordinates from JVAS. These coordinates have an rms accuracy of ~12 milliarcsec. Cols. (4), (5), (6), and (7).—Total flux density (Jy) at wavelengths 80 cm, 20 cm, 6 cm, and 3.6 cm, from J. Douglas, private communication; White & Becker 1992; Gregory & Condon 1991; Kühr et al. 1981; JVAS. Col. (8).—Optical identification from automated scanning of the POSS plates unless otherwise noted. Key to identifications: Q—quasar; G—galaxy; BL—BL Lac object; EF—empty field; BS—blue stellar object; BO—blue object; RS—red stellar object; RO—red object; NS—neutral stellar object; NO—neutral object. Col. (9).—Apparent R magnitude of the object obtained by automated scanning of the POSS E plates, unless otherwise noted. The rms error is 0.3 down to magnitude 19.5 and increases to 0.5 by magnitude 20.0 (McMahon 1994). Col. (10).—Redshift; (–) indicates a featureless spectrum. Redshifts are taken from the catalog of Véron-Cetty & Véron 1993, except for the values quoted for 0651+410 from Merighi et al. 1991, 0733+597 from Stickel & Kühr 1994, 1144+352 from Morganti, Ulrich, & Tadhunter 1992, 1146+596 from Kelton 1980, and 1946+708 from Stickel & Kühr 1993. Col. (11).—Date of the VLBI observation.

Table 1 is published in computer-readable form in the AAS CD-ROM Series, Vol. 4.

[a] Identification and magnitude taken from Véron-Cetty & Véron 1993, and corrected to R magnitude using $\langle B - R \rangle = 0.6$.

[b] Identification and magnitude estimated by eye from the POSS plates.

[c] Identification and magnitude from Stickel & Kühr 1994.

Taylor 1994), part of the Caltech VLBI Programs. Several iterations of phase self-calibration and mapping were performed upon each source using uniform weighting, before switching to natural weighting. At each iteration, windows for clean components were added, if necessary, to provide support and reject sidelobes. Amplitude self-calibration was not performed with solution intervals smaller than 30 minutes unless the signal-to-noise ratio on all baselines was higher than ~8 (e.g., as for a compact component with flux density ≳400 mJy).

4. RESULTS

In Figure 2 we present the naturally weighted images for 91 CJ2 sources. For each image the FWHM contour of the Gaussian beam is drawn in the lower left corner and is listed in Table 3, along with the rms, peak flux density, and lowest contour level at 3 σ. The typical dynamic range in the images is 500:1. While the lowest contour may be affected by noise or small residual amplitude and phase errors, the second contour is reliable. Global fringe fitting and mapping proved difficult for three heavily resolved sources: 0733 + 597, 1436 + 763, and 2003 + 662. The north-south orientation of 0733 + 597 can be believed, but the second contour should not be trusted. The object 1436 + 763 has a flux density of 400 mJy on baselines of 5 Mλ but is undetected on baselines exceeding 50 Mλ. No naturally weighted image of 1436 + 763 at the full resolution is presented. Finally, 2003 + 662 is elongated east-west, but the second contour should not be trusted.

TABLE 2

TELESCOPE CHARACTERISTICS

Telescope	Code	Location	Diam (m)	1992 Jun	1992 Sep	1993 Mar	T_{sys} (K)	T_{sys} (Jy)	Sensitivity (K/Jy)
(1)	(2)	(3)	(4)	(5)	(6)	(7)	(8)	(9)	(10)
Cambridge	C	Cambridge, UK	32	√			32	140	0.23
Jodrell MKII	J2	Jodrell Bank, UK	26	√		√	44	366	0.12
Effelsberg	B	Germany	100		√	√	58	39	1.5
Onsala	S	Sweden	26	√	√	√	59	757	0.078
WSRT	W	Netherlands	5×25	√	√	√	105	133	0.86
Medicina	L	Bologna, Italy	32	√	√	√	36	225	0.16
Noto	N	Noto, Italy	32	√	√	√	35	221	0.16
Haystack	K	Westford MA, USA	36	√	√		97	606	0.16
NRAO	G	Green Bank WV, USA	43	√	√	√	34	126	0.27
VLA[a]	Y	New Mexico, USA	25	√	√	√	37	319	0.116
VLBA_BR	BR	Brewster IO, USA	25	√	√	√	37	281	0.133
VLBA_FD	FD	Fort Davis TX, USA	25	√	√		41	308	0.133
VLBA_HN	HN	Hancock NH, USA	25			√	34	259	0.133
VLBA_KP	KP	Kitt Peak AZ, USA	25	√	√	√	41	308	0.133
VLBA_LA	LA	Los Alamos NM, USA	25	√	√		38	270	0.142
VLBA_NL	NL	North Liberty IA, USA	25	√	√	√	40	300	0.133
VLBA_OV	OV	Owens Valley CA, USA	25	√	√	√	33	249	0.133
VLBA_PT	PT	Pie Town NM, USA	25	√	√	√	37	280	0.132
VLBA_SC	SC	Saint Croix VI, USA	25			√	34	255	0.133

NOTES TO TABLE 2

Cols. (1), (2), and (3).—Name, code used, and location of each telescope. Affiliations: B—Max-Planck-Institüt für Radioastronomie; O—Onsala Space Observatory; W—Westerbork Synthesis Radio Telescope, NFRA; J2, C—Nuffield Radio Astronomy Laboratories; L, N—Istituto di Radioastronomia; G—National Radio Astronomy Observatory; K—Haystack Observatory; BR, FD, HN, KP, LA, NL, OV, PT, SC—National Radio Astronomy Observatory VLBA: Y—National Radio Astronomy Observatory VLA. Col. (4).—Diameter of each telescope (in meters). Cols. (5), (6), and (7).—Tick indicates whether the telescope participated successfully in that session. Cols. (8), (9), and (10).—System temperature in K and in Jy and the sensitivity in K Jy^{-1} of each telescope. The values quoted are representative of the three sessions.

[a] The VLA was used in single-antenna mode.

Tapered images are presented in all cases where this image revealed additional information. The tapered images were produced using a Gaussian taper falling to 50% at 70 Mλ on the naturally weighted, self-calibrated data. All tapered images were restored with a circular 3 mas beam.

The rms noise in each naturally weighted image is plotted against the source declination and peak flux density in Figure 3 for all sources observed during the four sessions. There is a slight trend for higher declination sources, with correspondingly better *u-v* coverage, to have a lower noise. This result is biased, however, by the fact that many of the high-declination sources were observed during 1992 September, which had a large number of telescopes operating under favorable observing conditions. The lack of any correlation between the rms noise and the peak flux density in the map shows that the noise in the maps is predominantly limited by the thermal noise, and not by the dynamic range. The CJ2 sample is therefore an excellent, uniform sample of VLBI images.

Model fitting was performed on the self-calibrated amplitudes and phases of each source to extract quantitative information from the observations. Up to four Gaussian components were fitted to each source. The components are listed in Table 4 for all sources which produced a total agreement factor of 1.4 or better. The agreement factors are distributed as the square root of the reduced χ^2 and have an expected value of 1.0. Only two sources, 0604 + 728 and 1946 + 708, were too complex to model, and a good agreement factor could not be obtained for the heavily resolved and complex source 1436 + 763.

The average total agreement factor is 1.045. The amplitude agreement factors, presented in Table 4, are on average better by ~13% than the closure phase agreement factors. This is the result of performing the model fitting on the fully self-calibrated *u-v* data. Amplitude self-calibration at every integration period introduces N additional free parameters, where N is the number of antennas. The number of degrees of freedom is therefore reduced by a factor of approximately $(N - 3)/(N - 1)$ (Wieringa 1992). For 14 antennas this decreases the amplitude agreement factors by 9%.

5. SUMMARY

The CJ2 sample and its selection is described and 4992 MHz VLBI images and model fits are presented for 91 out of the 193 sources in the sample. The remaining images will be presented in Paper II (Henstock et al. 1994), along with a compilation of the integrated radio spectra. This highly uniform set of images should be well suited for morphological studies and cosmological tests. Future papers will provide interpretation of the results from the CJ2 and from statistically complete PR-CJ1-CJ2 subsamples and will present the results of a campaign to measure redshifts of the previously unobserved CJ2 sources.

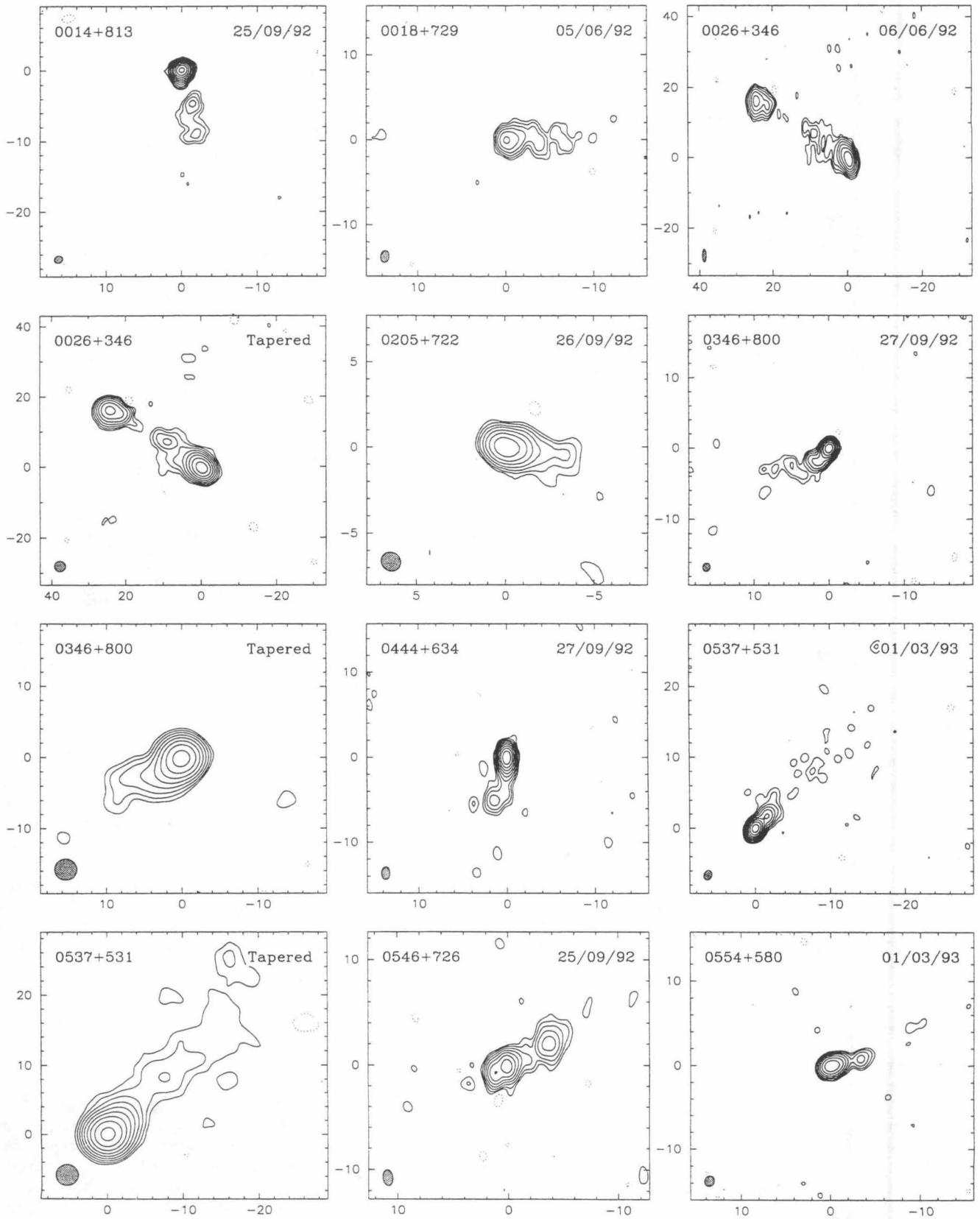

FIG. 2.—The 6 cm VLBI images for 91 sources in the CJ2 sample. Maps with the epoch of observation in the upper right corner are naturally weighted images, while those marked as "tapered" have been weighted by a Gaussian taper and restored with a 3 mas beam as described in the text. The FWHM contour of the Gaussian beam is drawn in the lower left corner and is listed in Table 3, along with the rms, peak flux density, and lowest contour level at 3 σ. Contours are drawn logarithmically at $-3\ \sigma$, $3\ \sigma$, $6\ \sigma$, $12\ \sigma$, etc., with negative contours shown as dashed lines.

FITS images corresponding to the maps presented in Fig. 2 are published in the AAS CD-ROM Series, Vol. 4.

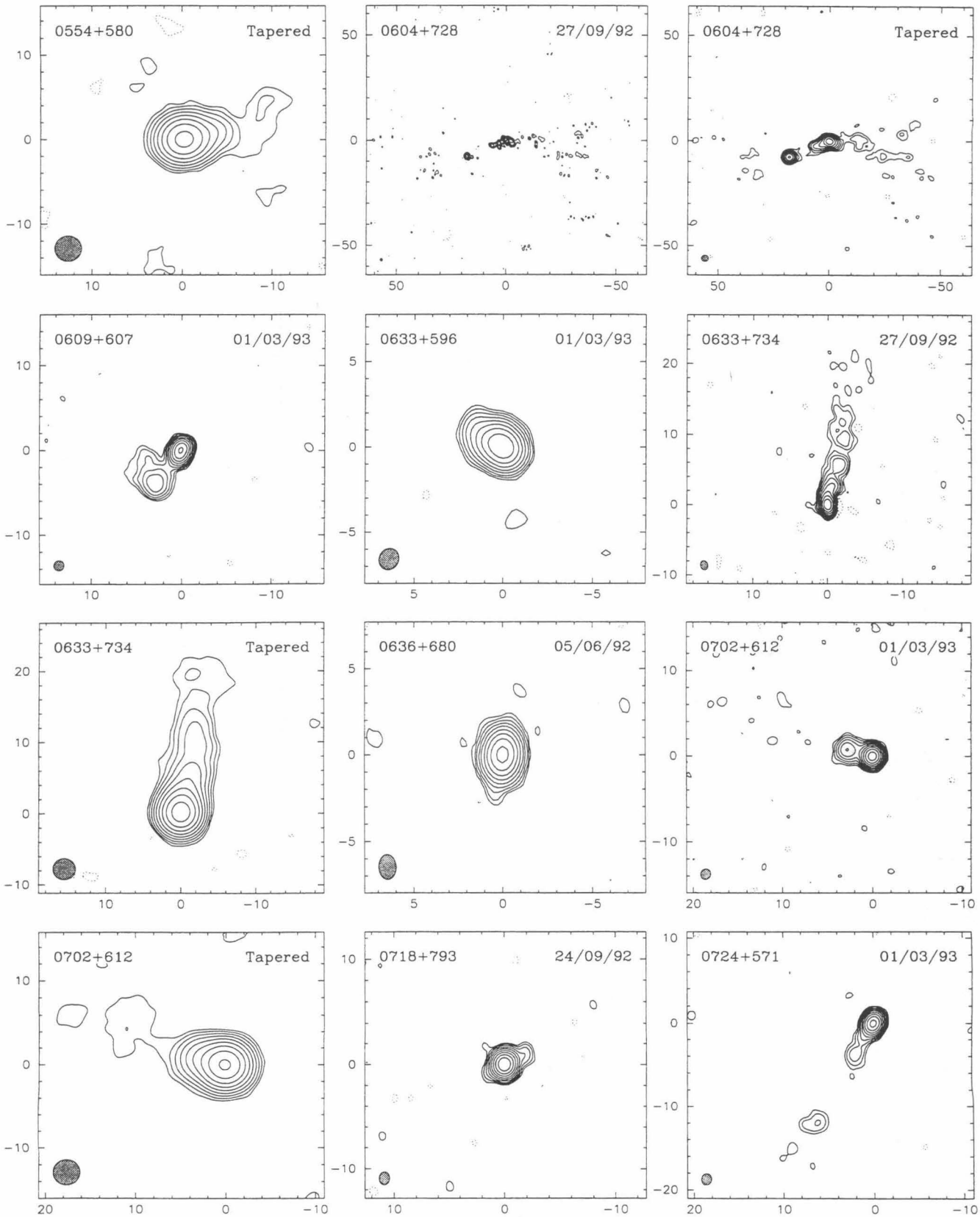

FIG. 2—*Continued*

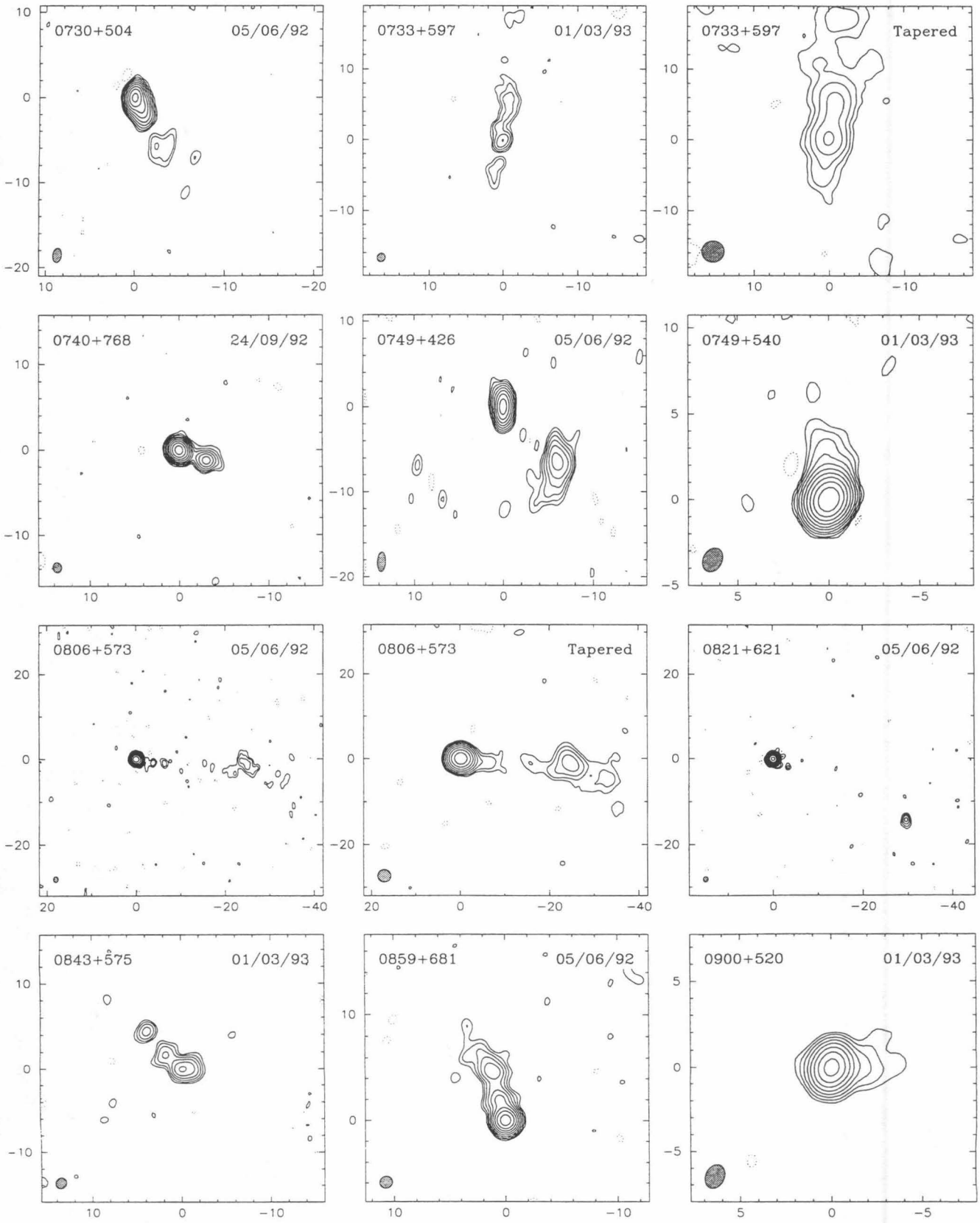

FIG. 2—*Continued*

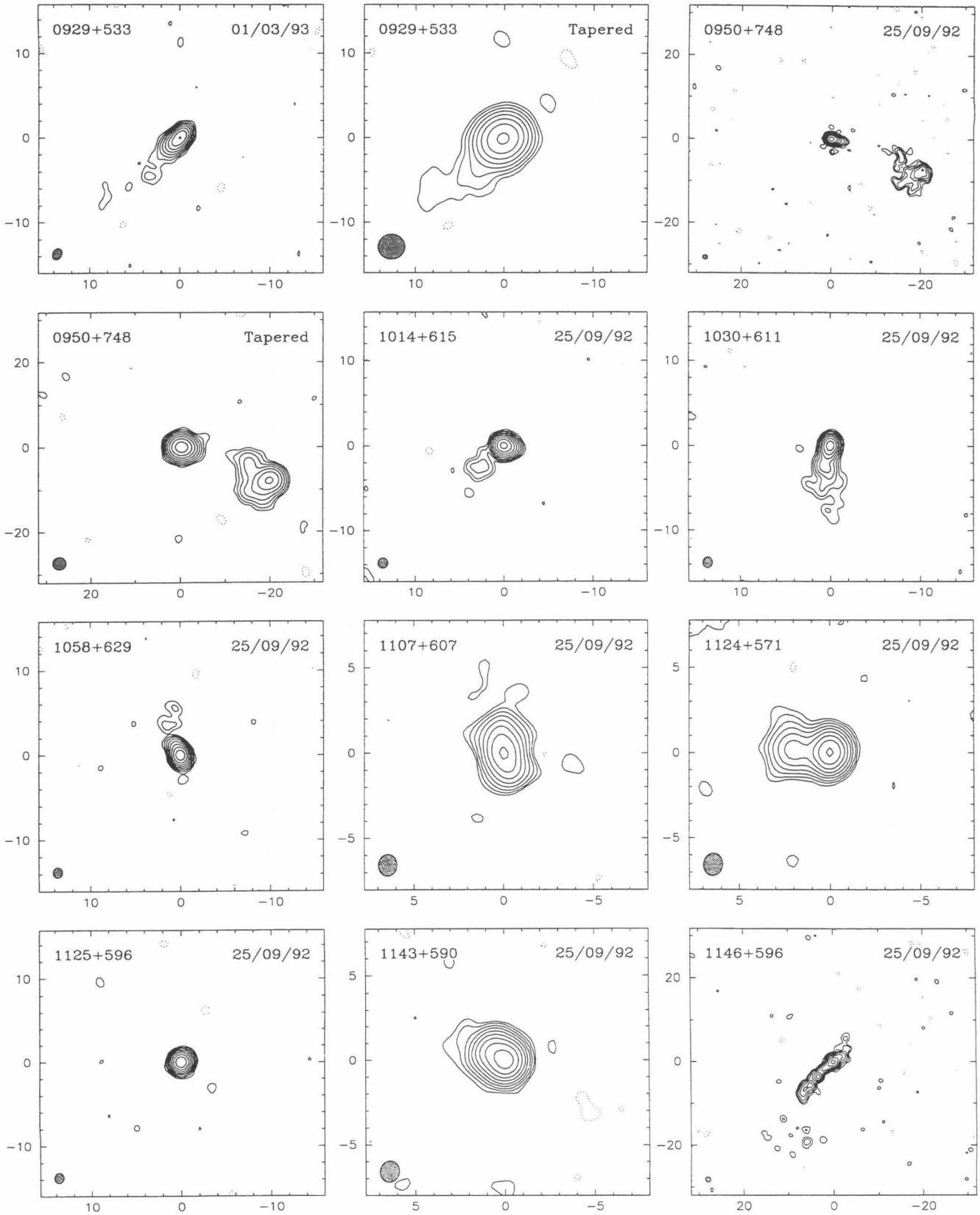

FIG. 2—*Continued*

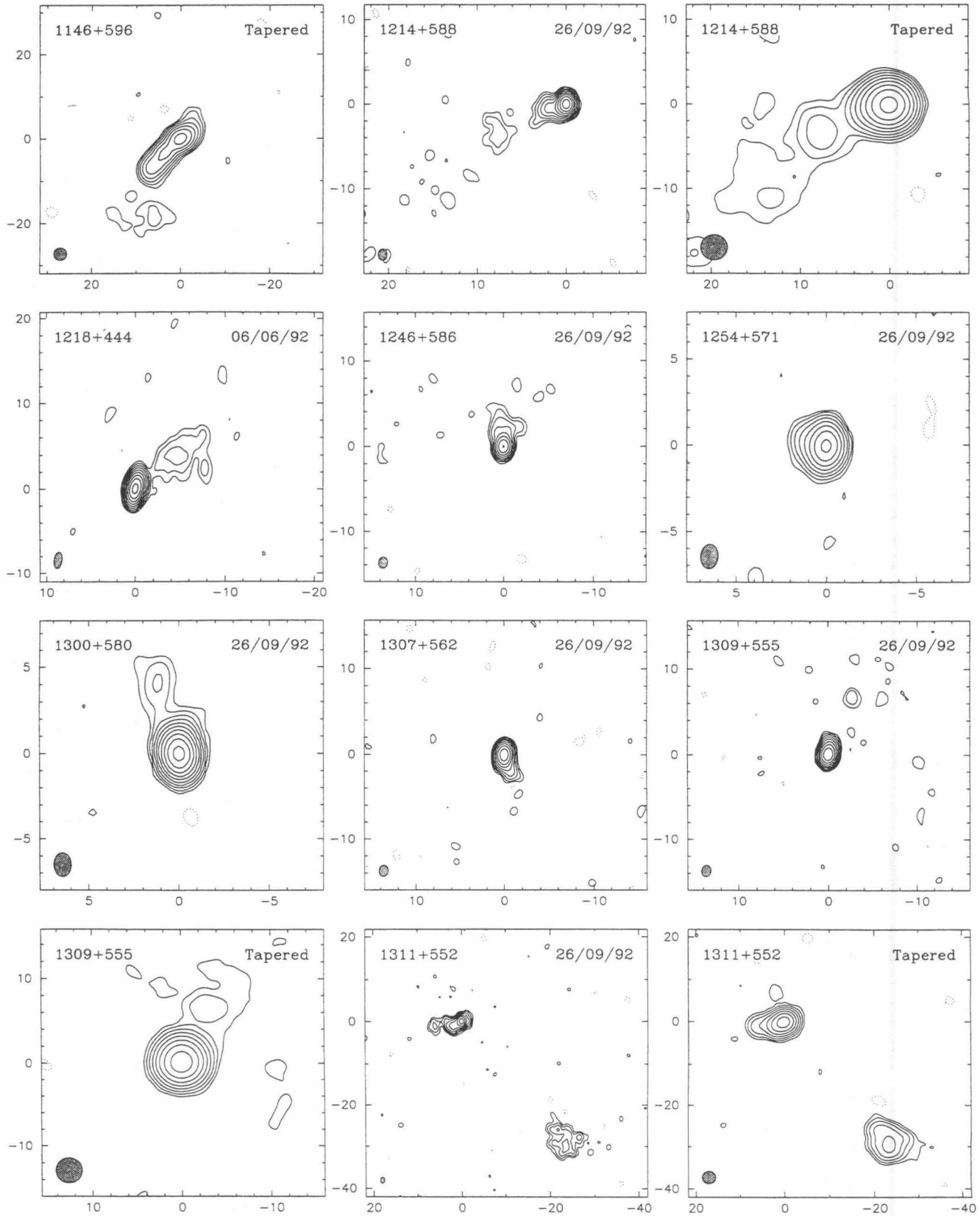

FIG. 2—*Continued*

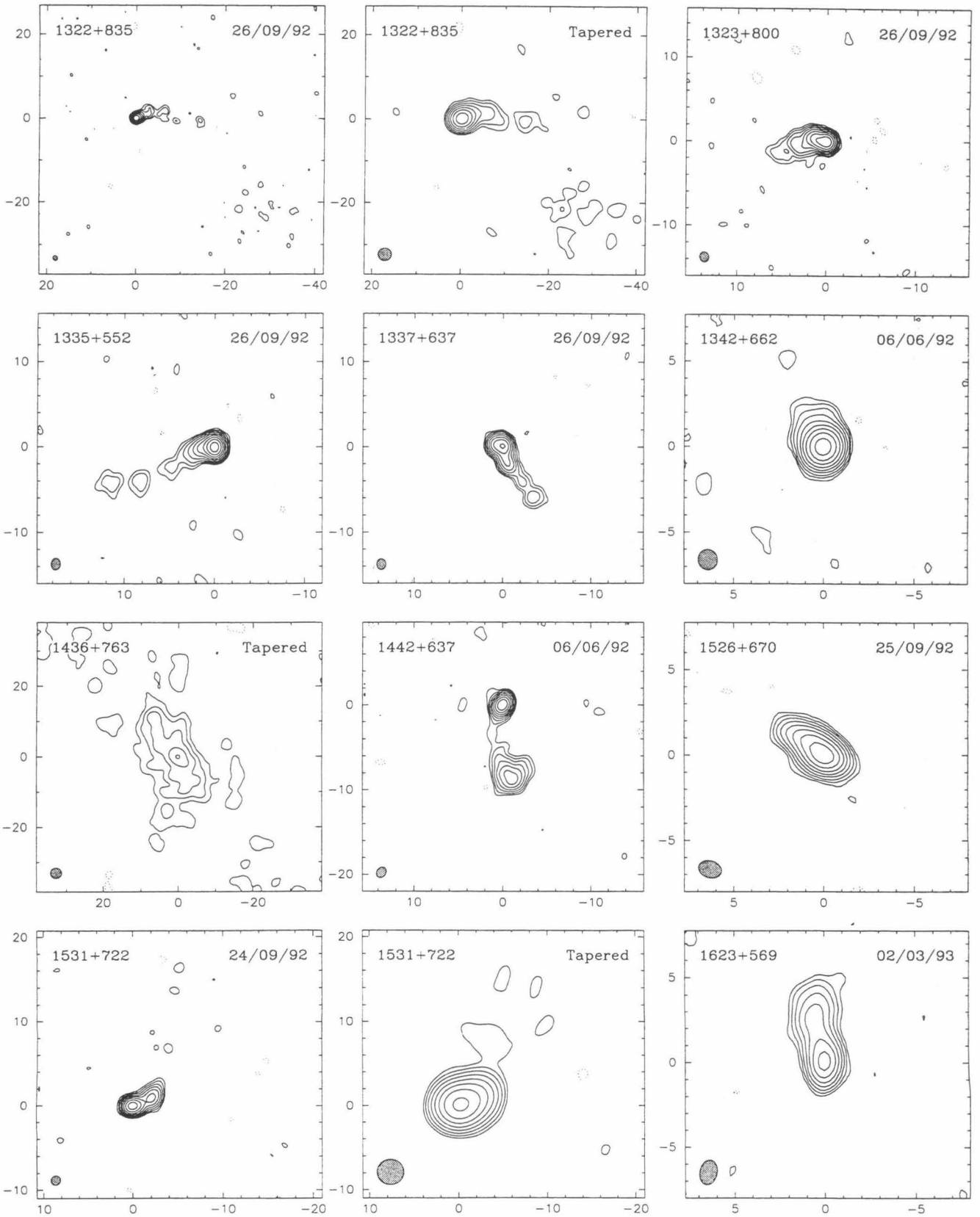

FIG. 2—*Continued*

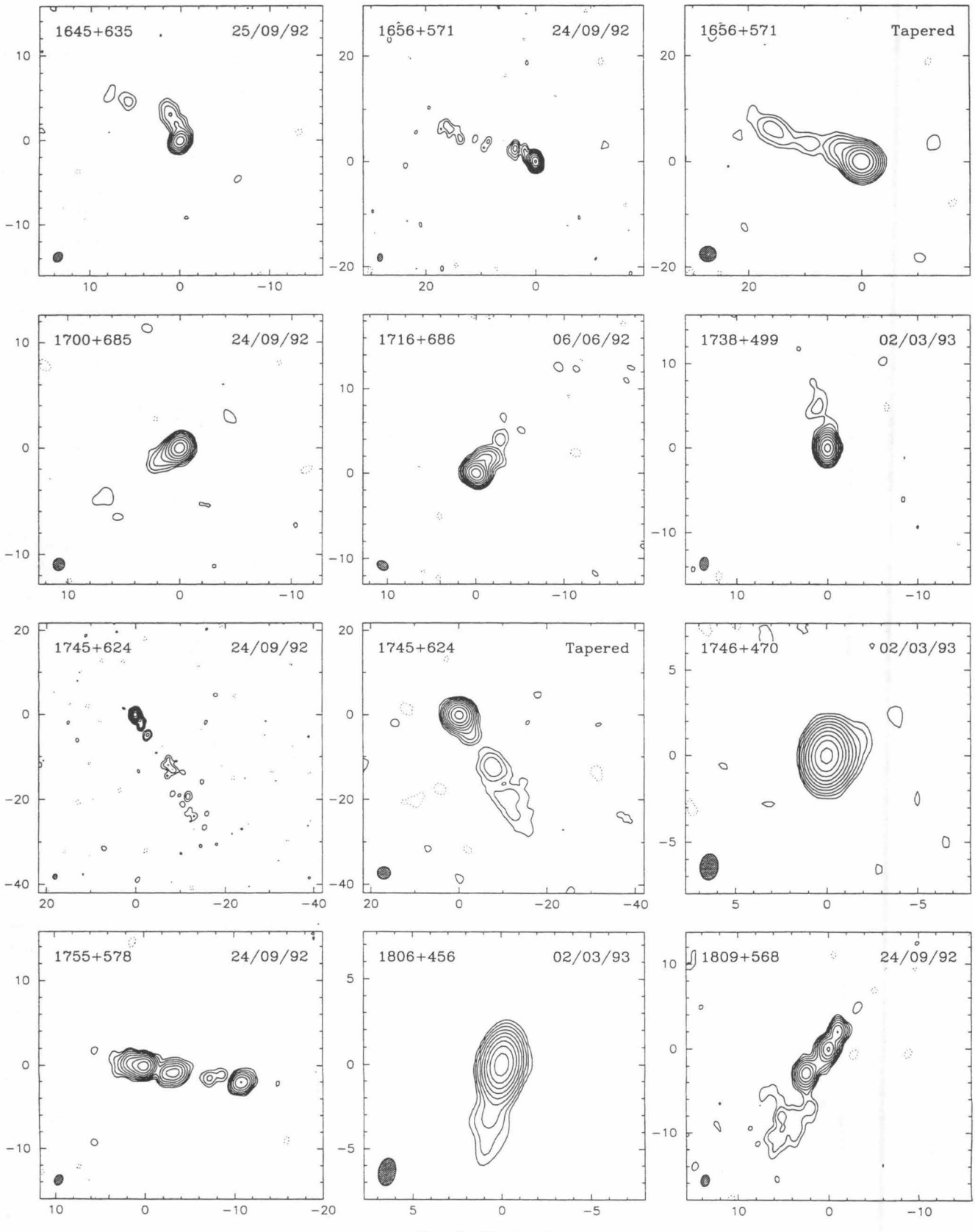

FIG. 2—*Continued*

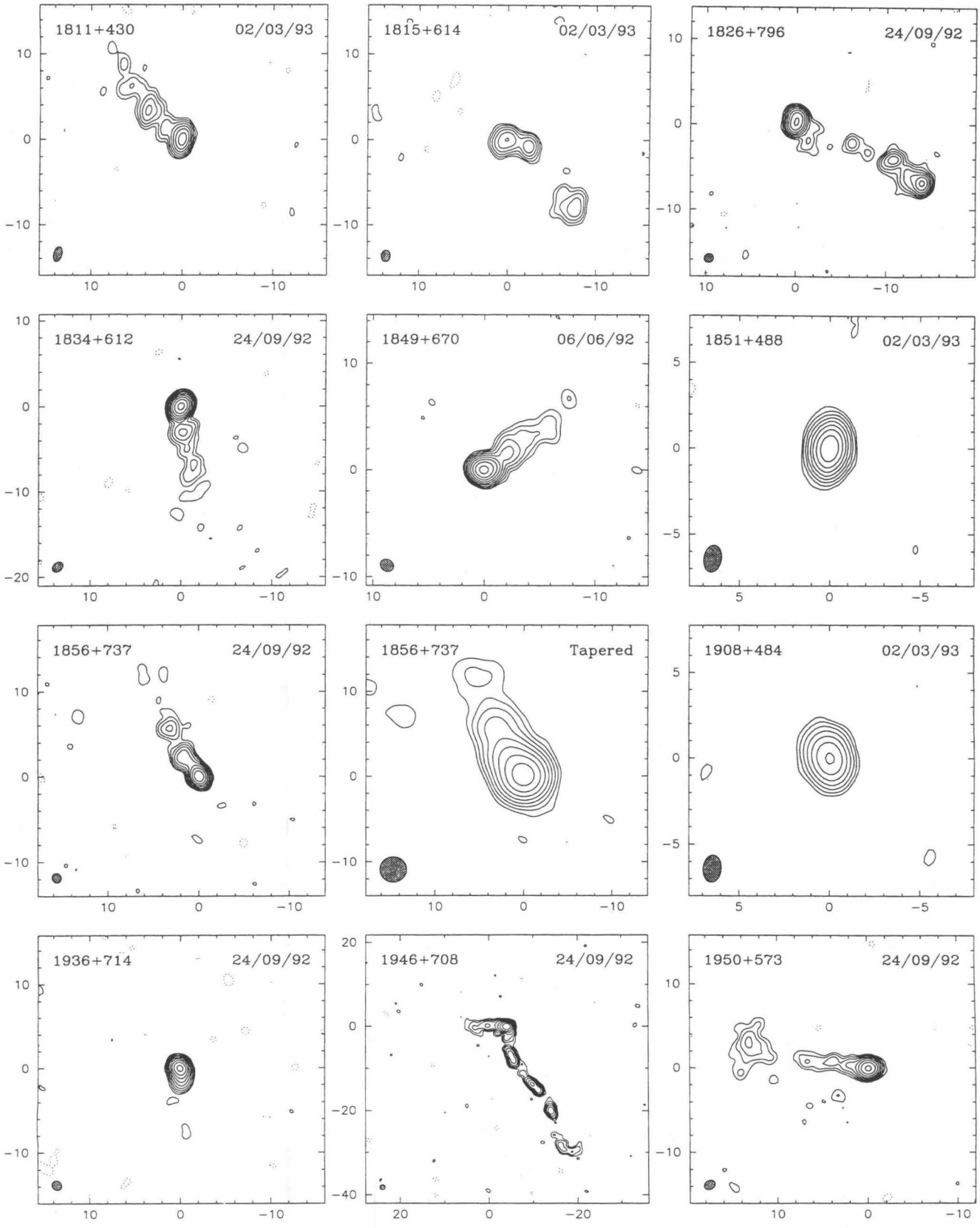

FIG. 2—*Continued*

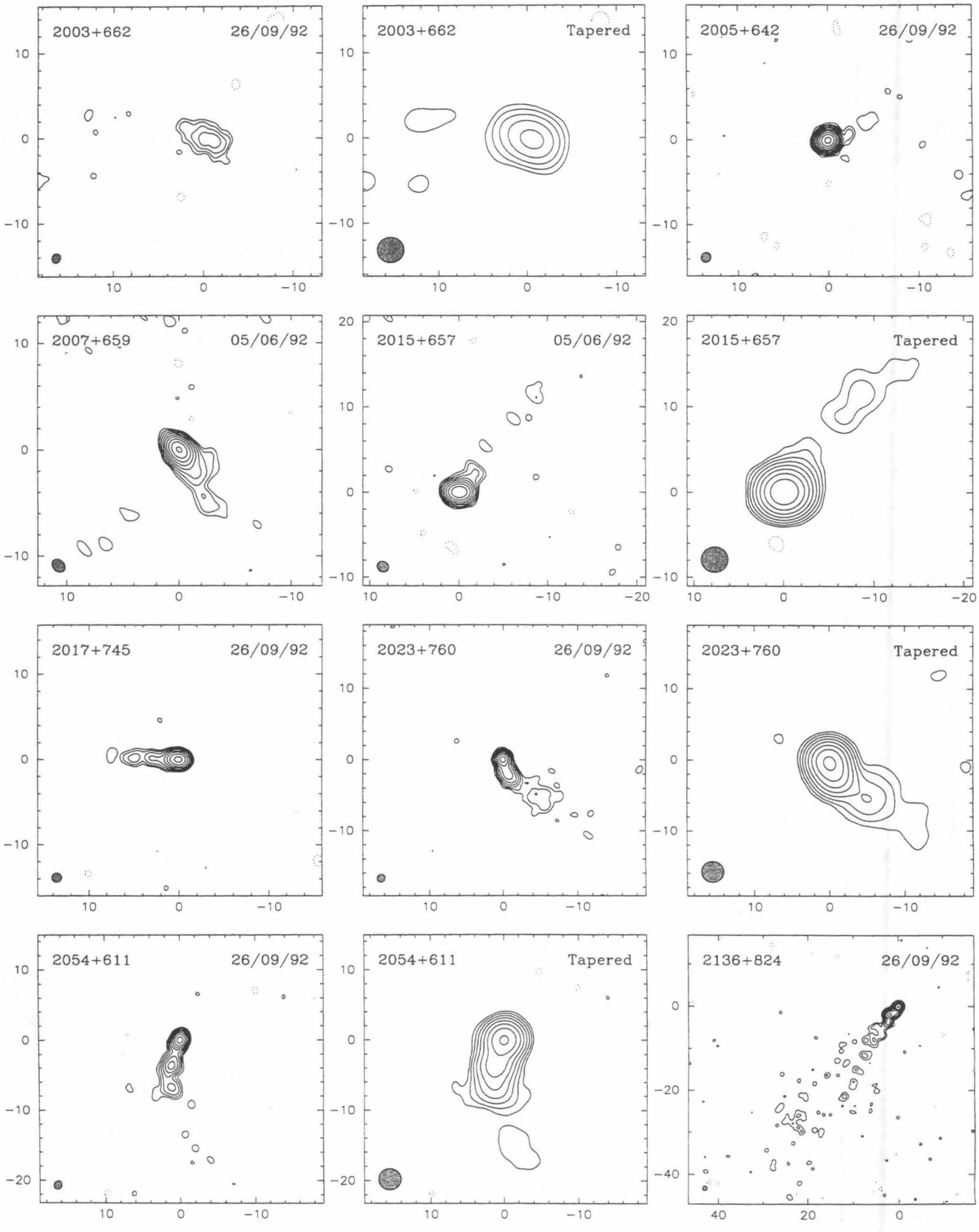

FIG. 2—*Continued*

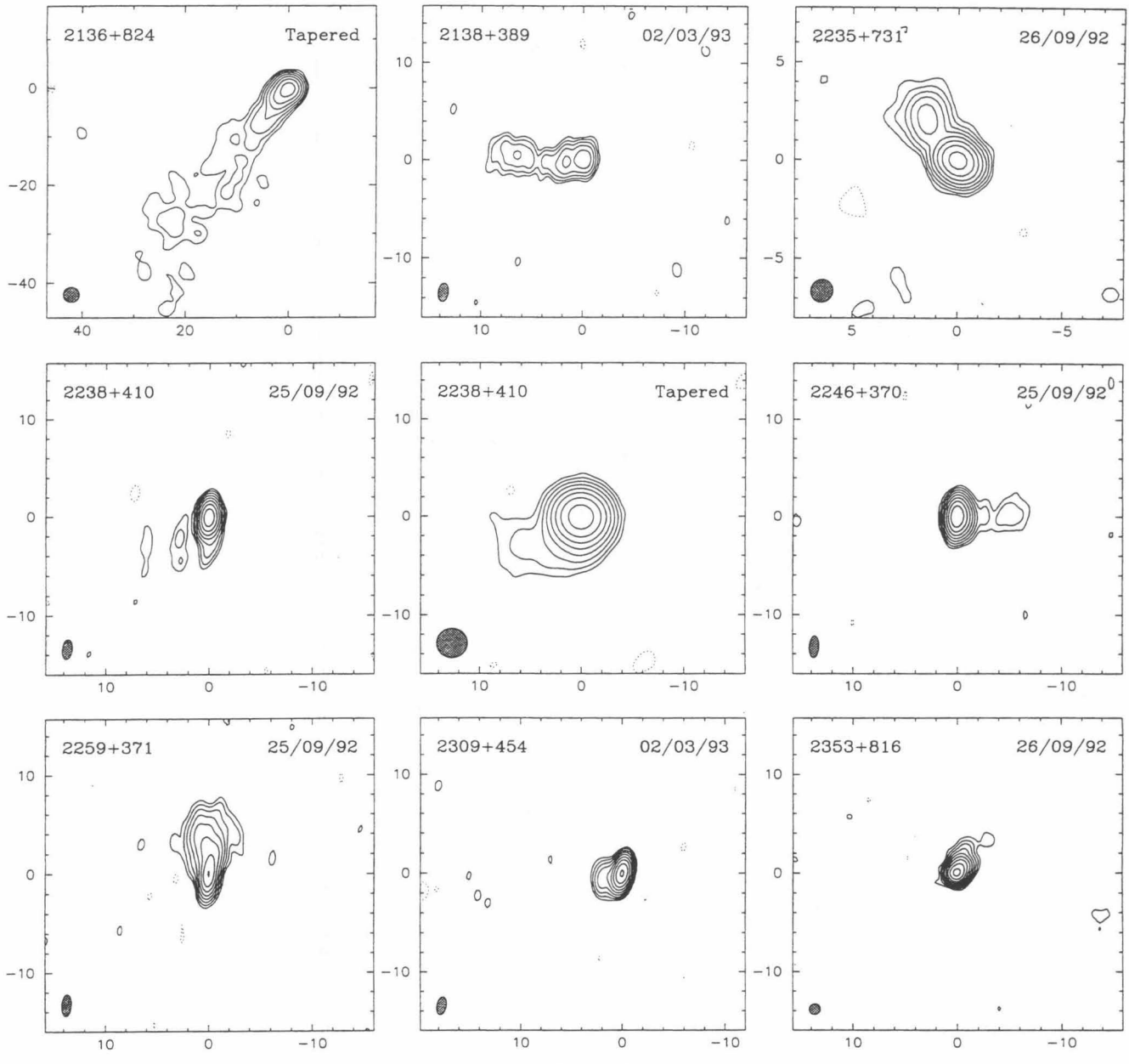

FIG. 2—*Continued*

TABLE 3

MAP PARAMETERS

Name	Obs.	Dur.	Beam			S_{nat}	rms	1st Cntr	S_{tap}	rms	1st Cntr
			a	b	θ						
		(min)	(mas)	(mas)	(°)	(mJy/beam)		(%Peak)	(mJy/beam)		(%Peak)
(1)	(2)	(3)	(4)	(5)	(6)	(7)	(8)	(9)	(10)	(11)	(12)
0014+813...	1992 Sep	72	1.18	1.00	−61	822	0.37	0.15			
0018+729...	1992 Jun	74	1.40	0.93	−7	64	0.58	2.70			
0026+346...	1992 Jun	73	3.64	1.00	0	269	0.72	0.80	451	0.74	0.50
0205+722...	1992 Sep	54	1.15	1.05	40	178	0.47	0.80			
0346+800...	1992 Sep	57	1.21	1.00	−7	262	0.36	0.40	305	0.54	0.55
0444+634...	1992 Sep	54	1.51	0.93	−1	548	0.37	0.20			
0537+531...	1993 Mar	60	1.41	1.05	−17	603	0.49	0.25	667	0.70	0.30
0546+726...	1992 Sep	72	1.50	0.89	7	97	0.32	1.00			
0554+580...	1993 Mar	57	1.28	1.07	−15	169	0.45	0.80	247	0.50	0.60
0604+728...	1992 Sep	54	1.35	0.94	11	93	0.44	1.40	172	0.55	0.95
0609+607...	1993 Mar	56	1.18	1.14	−30	444	0.50	0.35			
0633+596...	1993 Mar	61	1.27	1.09	−17	348	0.46	0.40			
0633+734...	1992 Sep	54	1.34	0.95	14	448	0.32	0.20	554	0.45	0.25
0636+680...	1992 Jun	59	1.47	0.96	2	399	0.40	0.30			
0702+612...	1993 Mar	57	1.27	1.10	−13	450	0.41	0.25	490	0.55	0.35
0718+793...	1992 Sep	56	1.23	0.93	−2	648	0.47	0.20			
0724+571...	1993 Mar	57	1.35	1.10	−7	454	0.43	0.30			
0730+504...	1992 Jun	54	1.70	0.97	−8	570	0.58	0.30			
0733+597...	1993 Mar	57	1.24	1.09	−16	25	0.50	6.00	44	0.80	5.45
0740+768...	1992 Sep	55	1.20	0.97	6	435	0.38	0.25			
0749+426...	1992 Jun	54	2.33	0.91	−2	244	0.39	0.50			
0749+540...	1993 Mar	57	1.46	1.05	−23	1310	0.51	0.10			
0806+573...	1992 Jun	55	1.43	1.00	0	241	0.37	0.45	331	0.49	0.45
0821+621...	1992 Jun	54	1.34	1.05	−9	425	0.41	0.30			
0843+575...	1993 Mar	57	1.35	1.17	−22	69	0.62	2.70			
0859+681...	1992 Jun	54	1.19	1.13	−43	458	0.40	0.25			
0900+520...	1993 Mar	57	1.49	1.05	−19	249	0.45	0.55			
0929+533...	1993 Mar	56	1.43	1.01	−21	159	0.40	0.75	225	0.53	0.70
0950+748...	1992 Sep	54	1.12	1.08	23	191	0.34	0.55	336	0.54	0.50
1014+615...	1992 Sep	54	1.22	1.12	−4	427	0.40	0.30			
1030+611...	1992 Sep	54	1.27	1.05	−3	258	0.42	0.50			
1058+629...	1992 Sep	54	1.23	1.06	−3	239	0.37	0.45			
1107+607...	1992 Sep	54	1.27	1.03	−4	200	0.47	0.70			
1124+571...	1992 Sep	54	1.31	1.04	−6	307	0.36	0.35			
1125+596...	1992 Sep	54	1.26	1.04	−5	274	0.37	0.40			
1143+590...	1992 Sep	54	1.27	1.06	−10	398	0.35	0.25			
1146+596...	1992 Sep	54	1.27	1.14	25	97	0.40	1.25	190	0.69	1.10
1214+588...	1992 Sep	57	1.35	1.01	0	399	0.33	0.25	443	0.43	0.30
1218+444...	1992 Jun	54	1.97	0.95	−8	429	0.43	0.30			
1246+586...	1992 Sep	54	1.35	1.02	−6	156	0.39	0.75			
1254+571...	1992 Sep	54	1.46	0.97	−4	151	0.32	0.65			
1300+580...	1992 Sep	54	1.41	0.99	0	814	0.43	0.15			
1307+562...	1992 Sep	51	1.34	1.03	−6	248	0.38	0.45			
1309+555...	1992 Sep	54	1.37	1.03	−8	253	0.36	0.45	282	0.46	0.50
1311+552...	1992 Sep	54	1.49	0.98	−1	113	0.39	1.05	194	0.68	1.05
1322+835...	1992 Sep	54	1.18	0.99	19	128	0.34	0.80	174	0.54	0.95
1323+800...	1992 Sep	54	1.22	1.00	9	268	0.38	0.45			
1335+552...	1992 Sep	54	1.40	1.00	−4	429	0.33	0.25			
1337+637...	1992 Sep	54	1.28	1.01	1	173	0.40	0.70			
1342+662...	1992 Jun	53	1.20	1.06	4	529	0.47	0.25			
1436+763...	1992 Sep	72	–	–	–	–	–	–	52	1.03	5.95
1442+637...	1992 Jun	59	1.34	1.02	−27	294	0.39	0.40			
1526+670...	1992 Sep	74	1.30	0.99	69	270	0.41	0.45			
1531+722...	1992 Sep	55	1.12	1.04	−26	216	0.37	0.50	277	0.60	0.65
1623+569...	1993 Mar	57	1.48	0.95	−10	120	0.47	1.20			

TABLE 3—*Continued*

Name	Obs.	Dur.	Beam			S_{nat}	rms	1st Cntr	S_{tap}	rms	1st Cntr
			a	b	θ						
		(min)	(mas)	(mas)	(°)	(mJy/beam)		(%Peak)	(mJy/beam)		(%Peak)
(1)	(2)	(3)	(4)	(5)	(6)	(7)	(8)	(9)	(10)	(11)	(12)
1645+635...	1992 Sep	51	1.26	1.00	−33	121	0.40	1.00			
1656+571...	1992 Sep	58	1.53	0.92	−4	299	0.33	0.35	370	0.51	0.40
1700+685...	1992 Sep	55	1.18	1.03	−13	191	0.32	0.50			
1716+686...	1992 Jun	55	1.38	1.04	51	554	0.45	0.25			
1738+499...	1993 Mar	57	1.58	0.99	−4	399	0.40	0.30			
1745+624...	1992 Sep	56	1.29	0.96	−11	364	0.29	0.25	422	0.42	0.30
1746+470...	1993 Mar	56	1.55	1.02	−5	707	0.38	0.15			
1755+578...	1992 Sep	56	1.34	0.91	−19	164	0.26	0.50			
1806+456...	1993 Mar	57	1.68	0.97	−9	480	0.38	0.25			
1809+568...	1992 Sep	57	1.45	0.94	−9	167	0.40	0.70			
1811+430...	1993 Mar	56	1.85	0.93	−13	147	0.48	1.00			
1815+614...	1993 Mar	57	1.40	1.01	−4	62	0.62	3.00			
1826+796...	1992 Sep	68	1.10	1.00	−23	173	0.41	0.70			
1834+612...	1992 Sep	56	1.37	0.99	−42	377	0.38	0.30			
1849+670...	1992 Jun	54	1.26	1.09	49	454	0.42	0.30			
1851+488...	1993 Mar	57	1.59	0.97	−8	261	0.36	0.40			
1856+737...	1992 Sep	55	1.17	1.01	10	279	0.37	0.40	331	0.57	0.50
1908+484...	1993 Mar	57	1.60	1.00	−5	97	0.44	1.35			
1936+714...	1992 Sep	75	1.16	1.04	32	328	0.35	0.30			
1946+708...	1992 Sep	55	1.20	1.20	0	133	0.35	0.80			
1950+573...	1992 Sep	55	1.30	1.04	−51	181	0.39	0.65			
2003+662...	1992 Sep	54	1.19	0.96	−17	38	0.95	7.50	132	2.13	4.85
2005+642...	1992 Sep	54	1.20	1.06	−19	728	0.42	0.15			
2007+659...	1992 Jun	55	1.36	1.04	40	384	0.47	0.35			
2015+657...	1992 Jun	56	1.36	1.22	46	313	0.42	0.40	419	0.57	0.40
2017+745...	1992 Sep	54	1.11	1.08	−76	203	0.40	0.60			
2023+760...	1992 Sep	54	1.13	1.05	−25	202	0.36	0.55	272	0.59	0.65
2054+611...	1992 Sep	54	1.24	1.05	−15	198	0.37	0.55	227	0.53	0.70
2136+824...	1992 Sep	54	1.11	1.04	−6	125	0.30	0.70	159	0.52	1.00
2138+389...	1993 Mar	55	1.86	0.98	−7	54	0.65	3.60			
2235+731...	1992 Sep	53	1.15	1.04	−14	209	0.38	0.55			
2238+410...	1992 Sep	59	2.01	0.93	−6	226	0.32	0.40	272	0.43	0.45
2246+370...	1992 Sep	54	2.23	0.91	−3	270	0.34	0.40			
2259+371...	1992 Sep	54	2.26	0.91	−4	145	0.37	0.75			
2309+454...	1993 Mar	60	1.87	0.92	−10	426	0.53	0.35			
2353+816...	1992 Sep	54	1.11	1.04	−17	346	0.33	0.30			

NOTES TO TABLE 3

Col. (1).—Source name. Col. (2).—Date of observations. Col. (3).—Total integration time on source in minutes. Cols. (4), (5), and (6).—Beam characteristics of the naturally weighted maps. The restoring beam is an elliptical Gaussian with FWHM major axis a mas and minor axis b mas, with major axis in position angle θ degrees. Col. (7).—Peak flux density of the naturally weighted maps (mJy beam^{-1}). Col. (8).—Rms noise in the naturally weighted maps (mJy beam^{-1}), measured off the source in the corners of the displayed image. Col. (9).—Lowest contour level of the map in percentage of the peak flux density. Cols. (10), (11), and (12).—Peak flux density, rms noise, and lowest contour level of the tapered map, if an image has been provided. All tapered maps have been restored with a 3 mas beam.

Table 3 is published in computer-readable form in the AAS CD-ROM Series, Vol. 4.

TABLE 4

GAUSSIAN MODELS

Source	S (Jy)	r (mas)	θ (°)	a (mas)	b/a	Φ (°)	Amp. A.F.	Phase A.F.	Total A.F.
0014+813 ...	1.012	0.00	0.0	0.61	0.55	−174.3	1.067	1.291	1.175
	0.059	3.64	−165.1	4.56	0.23	21.8			
	0.023	8.32	−173.2	2.56	0.30	143.9			
0018+729 ...	0.147	0.00	0.0	0.97	0.74	10.9	1.007	1.264	1.132
	0.091	2.43	−83.4	3.30	0.69	60.6			
	0.029	6.51	−86.2	3.65	0.56	−20.3			
0026+346 ...	0.649	0.00	0.0	2.82	0.41	36.8	1.272	1.408	1.334
	0.297	29.45	56.2	2.77	0.85	27.0			
	0.100	26.73	54.1	2.61	0.33	38.6			
	0.213	4.90	50.8	11.39	0.43	55.0			
0205+722 ...	0.196	0.00	0.0	0.65	0.25	−104.4	0.921	1.078	0.996
	0.052	0.88	−102.6	0.54	0.42	−17.1			
	0.024	2.16	−103.2	1.88	0.45	−88.7			
0346+800 ...	0.304	0.00	0.0	0.56	0.45	141.7	1.001	1.087	1.041
	0.066	2.63	143.0	1.68	0.37	87.4			
	0.017	5.66	112.7	1.51	0.26	36.5			
0444+634 ...	0.607	0.00	0.0	0.61	0.38	179.2	1.019	1.045	1.031
	0.046	4.23	164.2	4.02	0.20	151.3			
0537+531 ...	0.640	0.00	0.0	0.40	0.00	−39.0	0.914	1.127	1.016
	0.107	2.27	−41.9	1.51	0.54	−33.9			
0546+726 ...	0.121	0.00	0.0	0.49	0.61	101.3	1.010	1.231	1.118
	0.075	1.22	119.3	0.66	0.00	−52.8			
	0.065	4.18	−61.4	2.64	0.43	140.5			
0554+580 ...	0.264	0.00	0.0	1.20	0.25	−80.3	1.026	1.271	1.142
	0.030	3.42	−74.2	1.06	0.75	−45.3			
0609+607 ...	0.689	0.00	0.0	1.23	0.27	161.6	0.964	1.416	1.192
	0.160	4.62	142.4	2.33	0.69	17.1			
0633+596 ...	0.328	0.00	0.0	0.69	0.39	44.8	0.889	1.084	0.983
	0.196	0.72	55.1	1.08	0.36	64.6			
0633+734 ...	0.513	0.00	0.0	0.83	0.06	−5.1	1.013	1.170	1.088
	0.138	1.79	−3.2	2.25	0.32	−21.9			
	0.081	7.23	−12.2	8.16	0.18	−6.8			
0636+680 ...	0.482	0.00	0.0	0.66	0.56	−37.3	0.908	1.034	0.968
0702+612 ...	0.481	0.00	0.0	0.41	0.37	63.9	0.915	1.061	0.984
	0.075	2.82	75.2	1.15	0.90	124.9			
0718+793 ...	0.846	0.00	0.0	0.64	0.79	86.0	0.992	1.071	1.029
0724+571 ...	0.490	0.00	0.0	0.59	0.24	151.6	0.906	1.037	0.968
	0.050	1.71	152.6	3.68	0.16	150.2			
	0.015	13.70	151.9	1.93	0.47	102.6			
0730+504 ...	0.578	0.00	0.0	0.39	0.41	28.6	0.919	1.039	0.976
	0.215	1.40	−146.8	1.23	0.42	16.2			
	0.036	6.10	−153.7	4.79	0.51	22.9			
0733+597 ...	0.048	0.00	0.0	0.76	0.74	141.3	1.039	1.287	1.157
	0.084	3.80	−9.2	11.04	0.13	−8.0			
0740+768 ...	0.559	0.00	0.0	0.66	0.76	67.7	0.913	1.033	0.970
	0.086	3.23	−111.4	0.86	0.76	84.6			

TABLE 4—*Continued*

Source	S (Jy)	r (mas)	θ (°)	a (mas)	b/a	Φ (°)	Amp. A.F.	Phase A.F.	Total A.F.
0749+426 ...	0.284	0.00	0.0	0.53	0.58	63.5	0.951	1.044	0.995
	0.140	8.92	−137.5	2.40	0.58	14.1			
0749+540 ...	1.390	0.00	0.0	0.45	0.04	56.2	0.894	1.018	0.953
	0.098	0.92	10.8	1.07	0.75	−20.8			
0806+573 ...	0.354	0.00	0.0	0.96	0.37	86.8	1.037	1.171	1.101
	0.046	24.61	−92.8	3.89	0.80	54.4			
0821+621 ...	0.562	0.00	0.0	0.86	0.00	73.2	0.953	1.007	0.978
	0.021	32.74	−115.8	0.90	0.62	179.1			
0843+575 ...	0.143	0.00	0.0	1.54	0.56	−83.8	1.121	1.333	1.215
	0.028	2.52	49.1	1.08	0.00	6.2			
	0.025	6.01	41.7	0.48	0.50	169.4			
0859+681 ...	0.478	0.00	0.0	0.48	0.20	21.1	0.931	1.033	0.980
	0.123	1.52	12.6	1.99	0.51	26.4			
	0.073	4.94	14.1	1.82	0.47	47.7			
0900+520 ...	0.285	0.00	0.0	0.57	0.46	49.6	1.000	1.004	1.002
	0.017	1.51	−95.9	1.25	0.69	−2.6			
0929+533 ...	0.164	0.00	0.0	0.67	0.31	129.8	1.043	1.138	1.087
	0.091	1.08	137.5	0.81	0.67	90.4			
	0.015	5.11	144.7	4.83	0.14	119.2			
0950+748 ...	0.308	0.00	0.0	0.96	0.90	−77.6	1.031	1.256	1.140
	0.091	1.22	−92.8	1.22	0.62	14.2			
	0.027	16.37	−104.2	2.50	0.00	25.8			
	0.237	21.17	−112.6	3.99	0.57	−57.1			
1014+615 ...	0.468	0.00	0.0	0.51	0.78	47.8	0.883	1.025	0.951
	0.093	0.93	−105.5	0.58	0.00	−129.0			
	0.029	3.54	135.3	2.66	0.56	111.2			
1030+611 ...	0.321	0.00	0.0	0.74	0.50	165.0	1.079	1.148	1.112
	0.057	2.79	166.0	1.41	0.87	165.6			
1058+629 ...	0.224	0.00	0.0	0.27	0.69	11.8	0.910	1.052	0.978
	0.071	0.80	27.1	0.94	0.00	19.1			
	0.012	3.68	15.0	2.10	0.19	111.7			
1107+607 ...	0.389	0.00	0.0	1.43	0.50	18.3	1.133	1.228	1.177
1124+571 ...	0.321	0.00	0.0	0.36	0.83	72.5	0.962	1.022	0.990
	0.103	1.88	88.1	1.31	0.69	55.9			
1125+596 ...	0.330	0.00	0.0	0.59	0.68	88.4	0.863	1.026	0.941
1143+590 ...	0.438	0.00	0.0	0.51	0.70	66.5	0.889	1.023	0.953
	0.143	0.96	55.9	0.42	0.54	145.0			
1146+596 ...	0.187	0.00	0.0	1.38	0.74	43.5	1.204	1.331	1.263
	0.055	4.92	135.9	0.45	0.00	113.6			
	0.259	5.35	134.8	11.99	0.09	138.0			
1214+588 ...	0.395	0.00	0.0	0.31	0.00	119.6	0.891	1.012	0.948
	0.089	1.23	114.0	2.40	0.28	94.5			
	0.020	8.41	113.2	3.82	0.68	−4.0			
1218+444 ...	0.467	0.00	0.0	0.50	0.47	134.9	0.935	1.041	0.986
	0.074	4.93	−50.2	8.22	0.32	120.4			

TABLE 4—*Continued*

Source	S (Jy)	r (mas)	θ (°)	a (mas)	b/a	Φ (°)	Amp. A.F.	Phase A.F.	Total A.F.
1246+586 ...	0.177	0.00	0.0	0.56	0.67	178.7	0.942	1.051	0.993
	0.038	2.09	0.1	2.18	0.59	−6.9			
1254+571 ...	0.188	0.00	0.0	0.58	0.87	92.4	0.940	1.058	0.996
1300+580 ...	0.881	0.00	0.0	0.44	0.48	42.0	0.912	1.008	0.957
	0.022	2.93	18.9	2.04	0.59	19.3			
1307+562 ...	0.272	0.00	0.0	0.59	0.50	−2.7	0.940	1.008	0.972
	0.051	1.04	−178.1	0.10	0.72	−150.2			
1309+555 ...	0.292	0.00	0.0	0.71	0.23	−12.3	1.043	1.081	1.061
1311+552 ...	0.148	0.00	0.0	0.93	0.74	15.1	0.940	1.186	1.058
	0.142	1.86	120.2	2.76	0.59	103.0			
	0.152	36.87	−141.7	5.96	0.66	−157.1			
	0.019	6.39	103.1	2.12	0.37	137.5			
1322+835 ...	0.181	0.00	0.0	0.80	0.51	−63.6	1.052	1.145	1.095
	0.032	2.91	−76.3	1.37	0.44	3.6			
1323+800 ...	0.313	0.00	0.0	0.65	0.39	93.3	0.929	1.047	0.985
	0.162	1.23	75.6	0.86	0.69	54.3			
	0.068	2.91	97.1	2.35	0.83	123.8			
1335+552 ...	0.500	0.00	0.0	0.62	0.47	76.8	0.910	1.008	0.956
	0.095	1.37	96.4	1.18	0.56	103.4			
	0.032	8.56	113.1	9.05	0.13	104.2			
1337+637 ...	0.236	0.00	0.0	1.15	0.00	77.5	1.044	1.187	1.112
	0.106	1.34	−168.8	1.44	0.00	−173.6			
	0.031	4.53	−150.5	0.85	0.00	−16.9			
	0.016	7.16	−150.8	1.10	0.35	111.8			
1342+662 ...	0.609	0.00	0.0	0.48	0.76	−28.5	0.893	1.024	0.955
1442+637 ...	0.318	0.00	0.0	0.33	0.84	−14.6	0.975	1.051	1.011
	0.184	8.44	−173.5	2.08	0.85	48.2			
1526+670 ...	0.239	0.00	0.0	0.52	0.22	70.4	0.919	1.030	0.971
	0.175	1.02	39.7	1.20	0.17	56.1			
1531+722 ...	0.262	0.00	0.0	0.67	0.43	−80.9	0.915	1.064	0.986
	0.090	2.39	−63.6	1.30	0.55	−36.4			
1623+569 ...	0.118	0.00	0.0	0.59	0.41	11.2	1.029	1.090	1.057
	0.107	1.74	12.6	3.24	0.18	11.1			
1645+635 ...	0.133	0.00	0.0	0.39	0.64	7.2	0.991	1.086	1.036
	0.039	2.35	15.1	3.48	0.18	29.5			
	0.006	7.42	49.8	1.08	0.00	19.0			
1656+571 ...	0.377	0.00	0.0	0.74	0.49	41.0	0.981	1.067	1.021
	0.020	3.01	42.2	0.53	0.00	133.9			
	0.021	4.59	56.5	0.75	0.77	133.8			
1700+685 ...	0.191	0.00	0.0	0.27	0.11	148.5	0.984	1.025	1.003
	0.035	0.83	124.1	0.68	0.74	125.5			
1716+686 ...	0.638	0.00	0.0	0.64	0.00	150.3	0.894	1.043	0.965
	0.106	1.61	−31.0	1.89	0.26	133.3			
	0.007	5.39	−32.0	1.11	0.01	48.6			
1738+499 ...	0.464	0.00	0.0	0.65	0.55	21.2	0.907	1.020	0.960

TABLE 4—*Continued*

Source	S (Jy)	r (mas)	θ (°)	a (mas)	b/a	Φ (°)	Amp. A.F.	Phase A.F.	Total A.F.
1745+624 ...	0.421	0.00	0.0	0.60	0.46	−155.9	0.988	1.065	1.024
	0.037	2.52	−151.8	1.99	0.25	3.1			
	0.014	5.24	−155.2	0.81	0.58	−66.8			
1746+470 ...	0.756	0.00	0.0	0.33	0.94	94.0	0.937	1.043	0.987
1755+578 ...	0.240	0.00	0.0	0.86	0.43	67.1	0.992	1.131	1.058
	0.094	3.31	−104.6	1.78	0.36	−81.8			
	0.081	10.96	−100.7	0.96	0.00	−98.9			
	0.065	1.19	79.0	0.96	0.25	50.5			
1806+456 ...	0.492	0.00	0.0	0.35	0.39	172.9	0.875	1.001	0.935
	0.020	1.63	173.6	1.34	0.49	163.2			
1809+568 ...	0.196	0.00	0.0	0.56	0.71	27.7	1.157	1.242	1.197
	0.177	3.67	139.4	0.74	0.88	−15.5			
	0.101	2.29	−25.7	0.59	0.65	−5.8			
1811+430 ...	0.183	0.00	0.0	0.63	0.17	60.9	1.058	1.113	1.083
	0.015	1.35	54.7	1.50	0.39	21.2			
	0.060	5.02	47.5	2.06	0.44	−5.4			
	0.015	8.51	41.6	1.69	0.00	104.4			
1815+614 ...	0.182	0.00	0.0	1.07	0.83	−104.3	1.174	1.577	1.366
	0.033	3.27	−101.0	1.35	0.40	−32.5			
	0.092	10.09	−138.2	3.08	0.74	−118.1			
1826+796 ...	0.358	0.00	0.0	1.43	0.42	−11.8	1.416	1.608	1.507
	0.013	6.74	−104.3	0.00	0.16	−44.8			
	0.070	11.61	−110.9	0.93	0.36	−111.4			
	0.156	15.61	−116.4	1.04	0.51	−171.2			
1834+612 ...	0.466	0.00	0.0	0.78	0.25	−166.4	0.894	1.023	0.955
	0.046	2.92	−176.9	1.15	0.57	−117.8			
	0.040	7.48	−171.2	7.81	0.23	−176.9			
1849+670 ...	0.564	0.00	0.0	0.75	0.36	120.4	0.932	1.098	1.012
	0.075	2.75	−50.3	0.97	0.74	179.4			
	0.028	6.15	−51.9	3.50	0.34	−34.2			
1851+488 ...	0.273	0.00	0.0	0.31	0.73	38.4	0.990	1.008	0.998
1856+737 ...	0.291	0.00	0.0	0.49	0.00	23.6	0.959	1.036	0.995
	0.097	1.82	35.0	2.78	0.24	47.7			
	0.047	5.51	27.4	5.80	0.27	26.3			
1908+484 ...	0.145	0.00	0.0	0.97	0.64	42.6	0.853	1.170	1.007
1936+714 ...	0.284	0.00	0.0	0.28	0.00	39.4	0.905	1.041	0.970
	0.138	0.71	−166.1	1.45	0.24	0.6			
1950+573 ...	0.220	0.00	0.0	0.75	0.14	53.6	0.870	1.086	0.975
	0.053	2.58	82.2	6.04	0.12	83.7			
	0.050	13.23	78.4	3.23	0.71	19.5			
2003+662 ...	0.150	0.00	0.0	3.65	0.71	55.8	1.391	1.332	1.364
	0.100	1.58	−113.9	1.09	0.81	2.3			
2005+642 ...	0.802	0.00	0.0	0.43	0.64	−81.2	0.929	1.021	0.973
2007+659 ...	0.482	0.00	0.0	0.74	0.55	29.4	0.965	1.104	1.031
	0.045	2.65	−149.9	1.00	0.30	−38.6			
2015+657 ...	0.439	0.00	0.0	1.17	0.32	97.8	1.001	1.036	1.017
	0.028	1.59	−45.7	2.56	0.33	−33.7			

TABLE 4—*Continued*

Source	S (Jy)	r (mas)	θ (°)	a (mas)	b/a	Φ (°)	Amp. A.F.	Phase A.F.	Total A.F.
2017+745 ...	0.275	0.00	0.0	0.92	0.21	81.9	1.025	1.100	1.060
	0.037	2.83	85.4	3.12	0.00	80.2			
2023+760 ...	0.217	0.00	0.0	0.51	0.00	28.7	0.908	1.010	0.956
	0.152	2.01	−162.1	1.84	0.38	29.5			
	0.043	7.29	−135.4	5.78	0.60	−116.1			
2054+611 ...	0.228	0.00	0.0	0.56	0.42	148.3	0.910	1.037	0.971
	0.100	3.69	162.7	1.64	0.49	160.5			
	0.032	7.03	169.6	2.02	0.61	−134.0			
2136+824 ...	0.150	0.00	0.0	0.53	0.53	142.1	1.076	1.102	1.088
	0.064	2.75	134.8	1.08	0.52	111.5			
	0.070	8.08	147.7	19.93	0.10	149.6			
2138+389 ...	0.080	0.00	0.0	0.92	0.82	30.1	1.010	1.307	1.147
	0.163	3.54	91.4	7.25	0.23	87.0			
2235+731 ...	0.262	0.00	0.0	0.81	0.10	48.3	0.898	1.029	0.960
	0.058	2.54	35.0	1.66	0.40	19.3			
2238+410 ...	0.293	0.00	0.0	0.73	0.82	24.1	0.949	1.046	0.995
2246+370 ...	0.369	0.00	0.0	0.81	0.75	−95.1	1.060	1.058	1.059
	0.018	2.14	−85.2	2.56	0.20	−77.2			
2259+371 ...	0.192	0.00	0.0	1.20	0.40	168.4	0.910	1.095	0.999
	0.149	3.01	−1.0	2.92	0.57	42.2			
2309+454 ...	0.431	0.00	0.0	0.42	0.00	135.2	0.915	1.274	1.091
	0.072	1.07	116.4	2.23	0.13	93.8			
2353+816 ...	0.310	0.00	0.0	0.29	0.84	141.0	0.924	1.035	0.977
	0.174	0.85	−27.0	0.99	0.62	−32.2			

NOTES TO TABLE 4

Table reports parameters of each Gaussian component of the model brightness distribution: S, flux density; r, θ, polar coordinates of the center of the component relative to an arbitrary origin, with polar angle measured from north through east; a, b, major and minor axes of the FWHM contour; Φ, position angle of the major axis measured from north through east. The sources 0604+728, 1436+763, and 1946+708 were too complicated to model.

Table 4 is published in computer-readable form in the AAS CD-ROM Series, Vol. 4.

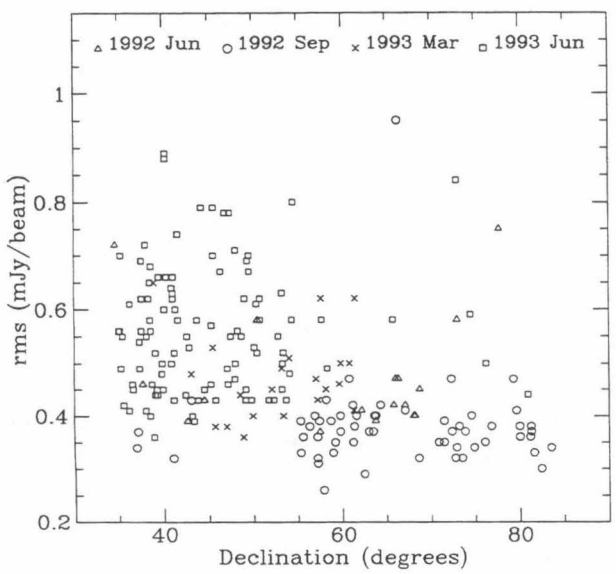

FIG. 3*a*

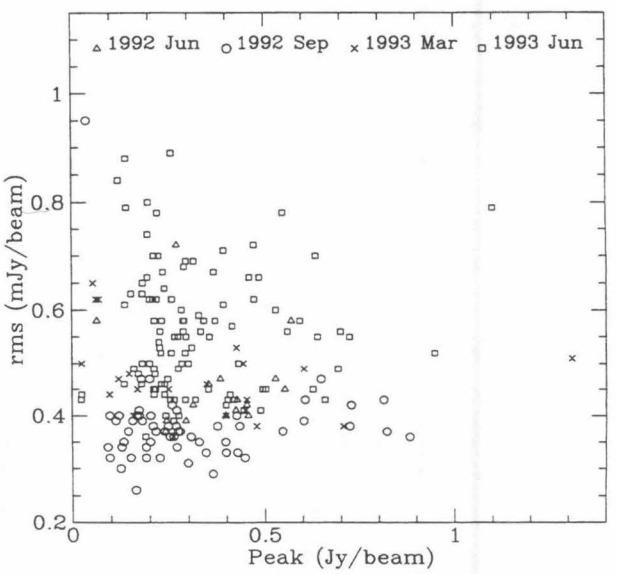

FIG. 3*b*

FIG. 3.—Rms noise from the naturally weighted maps is plotted (*a*) against the source declination and (*b*) against the peak in the map for all sources mapped during the four observing sessions, including the 1993 June session described in Paper II.

We thank the staffs at the observatories that took part in these observations and the staff of the JPL/Caltech Block II Correlator for their assistance. We thank R. McMahon for undertaking the APM scanning of the POSS plates and J. Douglas for supplying 365 MHz flux densities prior to publication. We also thank M. Shepherd for writing DIFMAP and for the many modifications he made on our behalf. The work done by the Caltech group was supported by NSF grant AST-9117100. D. R. H. gratefully acknowledges the receipt of a SERC research studentship. This research has made use of the NASA/IPAC Extragalactic Database (NED), which is operated by the Jet Propulsion Laboratory, Caltech, under contract with the National Aeronautics and Space Administration.

REFERENCES

Condon, J. J., & Broderick, J. J. 1985, AJ, 90, 2540
———. 1986, AJ, 91, 1051
Condon, J. J., Broderick, J. J., & Seielstad, G. A. 1989, AJ, 97, 1064
Gregory, P. C., & Condon, J. J. 1991, ApJS, 75, 1011
Henstock, D. R. 1994, Ph.D. thesis, Univ. Manchester
Henstock, D. R., Browne, I. W. A., Wilkinson, P. N., Taylor, G. B., Vermeulen, R. C., Pearson, T. J., & Readhead, A. C. S. 1994, ApJS, in preparation (Paper II)
Kelton, P. W. 1980, AJ, 85, 89
Kühr, H., Pauliny-Toth, I. I. K., Witzel, A., & Schmidt, J. 1981, AJ, 86, 854
McMahon, R. G. 1994, in preparation
Merighi, R., Basso, L., Vigotti, M., Lahulla, J. F., & Lopez-Arroyo, M. 1991, A&AS, 89, 225
Morganti, R., Ulrich, M.-H., & Tadhunter, C. N. 1992, MNRAS, 254, 546
Patnaik, A. R., Browne, I. W. A., Wilkinson, P. N., & Wrobel, J. M. 1992, MNRAS, 254, 655 (JVAS)
Pearson, T. J., & Readhead, A. C. S. 1988, ApJ, 328, 114 (PR)
Polatidis, A. G., Wilkinson, P. N., Xu, W., Readhead, A. C. S., Pearson, T. J., Taylor, G. B., & Vermeulen, R. C. 1994, ApJS, in press
Schwab, F. R. & Cotton, W. D. 1983, AJ, 88, 688
Shepherd, M. C., Pearson, T. J., & Taylor, G. B. 1994, BAAS, 26, 987
Stickel, M., & Kühr, H. 1993, A&AS, 100, 395
———. 1994, A&AS, 103, 349
Taylor, G. B., Vermeulen, R. C., Pearson, T. J., Readhead, A. C. S., Henstock, D. R., Browne, I. W. A., & Wilkinson, P. N. 1994, ApJ, in preparation
Thakkar, D. D., Xu, W., Readhead, A. C. S., Pearson, T. J., Taylor, G. B., Vermeulen, R. C., Polatidis, A. G., & Wilkinson, P. N. 1994, ApJS, in press
Véron-Cetty, M.-P., & Véron, P. 1993, ESO Sci Rep. No. 13
White, R. L., & Becker, R. H. 1992, ApJS, 79, 331
Wieringa, M. H. 1992, Exp. Astron., 2, 203
Xu, W. 1994, Ph.D. thesis, Caltech

THE ASTROPHYSICAL JOURNAL SUPPLEMENT SERIES, 100:1–36, 1995 September

THE SECOND CALTECH–JODRELL BANK VLBI SURVEY. II. OBSERVATIONS OF 102 OF 193 SOURCES

D. R. HENSTOCK, I. W. A. BROWNE, AND P. N. WILKINSON
University of Manchester, Nuffield Radio Astronomy Laboratories, Jodrell Bank, Macclesfield, Cheshire SK11 9DL, UK

AND

G. B. TAYLOR, R. C. VERMEULEN, T. J. PEARSON, AND A. C. S. READHEAD
California Institute of Technology, Owens Valley Radio Observatory, 105-24, Pasadena, CA 91125
Received 1994 November 21; accepted 1995 February 1

ABSTRACT

This is the second of two papers presenting the Second Caltech–Jodrell Bank VLBI survey (CJ2). The CJ2 sample consists of 193 flat- and gigahertz-peaked–spectrum sources selected at 4850 MHz. In this paper we present images of the remaining 102 sources with a resolution of ~1 mas, obtained using VLBI snapshot observations at 4992 MHz with a global array. We also present integrated radio spectra for the entire CJ2 sample.

Subject headings: quasars: general — radio continuum: galaxies — surveys

1. INTRODUCTION

The second Caltech–Jodrell Bank VLBI survey (CJ2) is a Mark II snapshot VLBI survey of 193 flat- and gigahertz-peaked–spectrum radio sources, observed at a frequency of 4992 MHz. The main aims of CJ2 are to extend the morphological classification started by the Pearson & Readhead survey (Pearson & Readhead 1988, hereafter PR), and first Caltech–Jodrell Bank VLBI survey (Polatidis et al. 1995; Thakkar et al. 1995; Xu et al. 1995; hereafter CJ1) and to address three cosmological goals. These goals are (1) to place significant limits on the mass in 10^6–10^9 $M_\odot$ condensed objects by searching for gravitational lenses with a separation of 1–200 mas, (2) to look for evidence of cosmological evolution in the proper motions of superluminal sources and place limits on q_0, and (3) to explore the possibility of using the angular diameter–redshift diagram for compact objects to constrain q_0.

In the first paper in this series (Taylor et al. 1994), we defined the CJ2 sample. We also reported on the first three observing sessions and presented VLBI images of 91 sources. We showed that the images, including those presented in this paper, are predominantly limited by thermal noise and not by dynamic range. Hence CJ2 is an excellent, uniform sample of VLBI images, ideal for the statistical tests which are the aims of the survey.

In this paper we present the second half of the results of the CJ2 survey. In § 2 we describe the fourth and final observing session, and in § 3 we present VLBI images of the remaining 102 sources. In § 4 we present integrated radio spectra, compiled from the literature, for all 193 sources in the CJ2 sample.

A redshift program of observations of CJ2 sources which have no measured redshift is well underway (Vermeulen & Taylor 1995); ~70% of CJ2 sources now have a measured redshift.

2. OBSERVATIONS

The observations presented in this paper were made from 1993 June 9 to June 16. Thirteen telescopes from the European VLBI Network (EVN), the US National Radio Astronomy Observatory's Very Large Baseline Array[1] (VLBA; Napier et al. 1994), and the VLA[1] participated successfully. Their characteristics are listed in Table 1. The observing frequency was 4992 MHz, and left-circular polarization was recorded using the Mark II system with 2 MHz bandwidth.

The VLBI snapshot technique was used, as in the previous sessions detailed in Paper I. Each source was observed for three to five scans of 20 minutes duration, the scans being approximately equally spaced over a wide range in hour angle. The sources observed in this session were mainly of low declination ($\delta \sim 35°$–$50°$), and since fewer telescopes observed successfully than in previous sessions, the u-v coverage was generally poorer than before. Figure 1 shows the typical u-v coverage for this session.

The data reduction procedure was identical to that given in Paper I, so only a brief outline will be given here. The data were correlated with the JPL/Caltech Block II correlator with clock offsets being monitored using strong calibrator sources. The data were then fringe-fitted using the AIPS task FRING, with a solution interval of ~7 minutes. Effelsberg was used as the reference telescope wherever possible; otherwise, the Hancock VLBA antenna was used. The amplitude calibration for each antenna, determined using measurements of antenna gain and system temperature, was adjusted by imaging strong calibrator sources and by examining the u-v crossing points. The relative amplitude calibration is accurate to ~2% rms, and the absolute flux calibration is accurate to better than 10%. The data were phase self-calibrated to a point-source model with a 10 s solution interval and then coherently averaged to 1 minute. Finally, the data were imaged with DIFMAP (Shepherd, Pearson, & Taylor 1994) using cycles of deconvolution and self-calibration.

3. RESULTS

In Figure 2 we present the naturally weighted images for the 102 CJ2 sources. While the lowest contour (3 σ) may be

[1] The National Radio Astronomy Observatory is operated by Associated Universities, Inc., under cooperative agreement with the National Science Foundation.

TABLE 1

TELESCOPE CHARACTERISTICS

Telescope	Code	Location	Diam (m)	T_{sys} (K)	T_{sys} (Jy)	Sensitivity (K/Jy)
(1)	(2)	(3)	(4)	(5)	(6)	(7)
Jodrell MKII	J2	Jodrell Bank, UK	26	45	375	0.12
Effelsberg	B	Germany	100	58	39	1.5
Onsala	S	Sweden	26	58	983	0.059
WSRT	W	Netherlands	5×25	64	128	0.5
Medicina	L	Bologna, Italy	32	44	275	0.16
Noto	N	Noto, Italy	32	30	183	0.164
Simeiz	U	Crimea, Ukraine	22	103	3433	0.030
VLA[a]	Y	New Mexico, USA	25	57	491	0.116
VLBA_BR	BR	Brewster WA, USA	25	33	282	0.117
VLBA_HN	HN	Hancock NH, USA	25	38	309	0.123
VLBA_NL	NL	North Liberty IA, USA	25	39	390	0.100
VLBA_OV	OV	Owens Valley CA, USA	25	38	302	0.126
VLBA_PT	PT	Pie Town NM, USA	25	45	308	0.146

NOTES.—Cols. (1)–(3): The name, the code used, and the location of each telescope. Affiliations: B, Max-Planck-Institüt für Radioastronomie; S, Onsala Space Observatory; W, Westerbork Synthesis Radio Telescope, NFRA; J2, Nuffield Radio Astronomy Laboratories; U, Space Research Institute, Moscow; L, N, Istituto di Radioastronomia; BR, HN, NL, OV, PT, National Radio Astronomy Observatory VLBA; Y, National Radio Astronomy Observatory VLA. Col. (4): The diameter of each telescope (in meters). Cols. (5)–(7): The system temperature in kelvins and in janskys and the sensitivity in kelvins per jansky of each telescope.

[a] The VLA was used in single antenna mode.

affected by residual systematic phase and amplitude errors, the second contour is reliable. The typical dynamic range, estimated as the ratio of the peak intensity to the rms in a blank area of sky, is ~500:1, the same as that for the first three sessions. Fringe-fitting and mapping proved difficult for only one source, 1545+497, which was barely detected on the shortest baselines. Any derived parameters for this source must be interpreted with caution. Another source, 0256+424, was initially weak because the original position given by Patnaik et al. (1992) and reproduced in Table 1 of Paper I was incorrect. This source was recorrelated at the correct position of $\alpha(J2000) = 02^h59^m37^s.6753$, $\delta(J2000) = 42°35'49''.9079$.

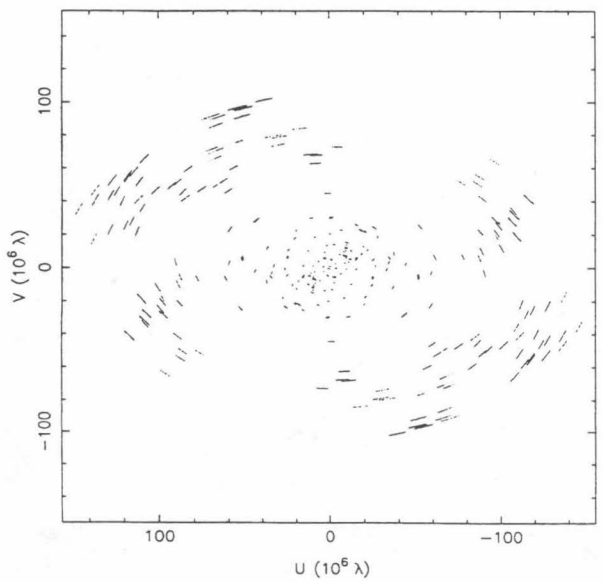

FIG. 1.—Typical u-v coverage for a source (1321+410) observed in the 1993 June session. The pattern is the result of three observations of 20 minutes each spaced over a wide range in hour angle.

Tapered images are shown in cases where they reveal additional information. These were produced by using a Gaussian taper falling to 50% at 70 Mλ on the naturally weighted self-calibrated data. All tapered images were restored with a circular 3 mas beam. The beam dimensions, rms, peak intensity, and lowest contour level (at 3 σ) for both the naturally weighted and tapered maps are shown in Table 2.

Model fitting was performed on the self-calibrated amplitudes and phases of each source in order to extract quantitative information, with up to four Gaussian components being fitted to each source. Model fitting was successful (total agreement factor < 1.2) for all 102 sources, and the model components are listed for each source in Table 3. The average total agreement factor is 1.004, slightly better than the value of 1.045 obtained for the previous three sessions. A description of the agreement factors is given in the Appendix.

4. SPECTRA

Integrated radio spectra for the entire CJ2 sample, covering the frequency range 151 MHz to 90 GHz, are given in Figure 3. These were compiled from various flux density catalogs in the literature, which are listed in Table 4. All the flux densities are on the absolute scale defined by Laing & Peacock (1980, hereafter LP),[2] and where necessary the original flux densities were converted to this scale, using correction factors that had already been determined by previous workers.

[2] The LP scale is identical to that of Baars et al. (1977) above 408 MHz (Riley 1988), and we have taken it to be identical above 327 MHz. At lower frequencies (178 MHz and below) the LP scale follows that of Roger, Bridle, & Costain (1973). Note that at 151 MHz the Baars et al. scale is ~0.95 times the LP scale.

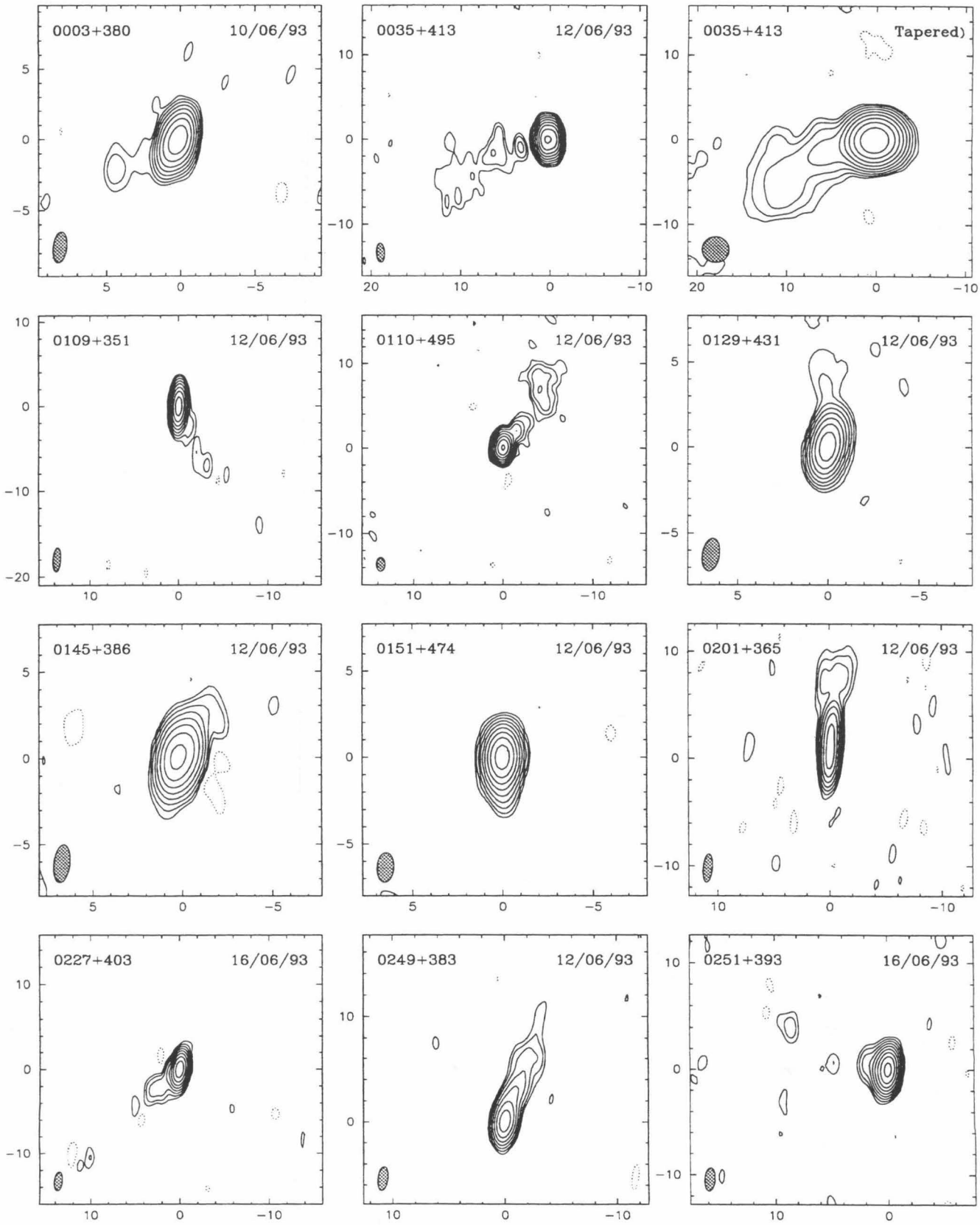

FIG. 2.—The 6 cm VLBI images for 102 sources in the CJ2 sample. Maps in which the epoch of observation is given in the upper right-hand corner are naturally weighted images, while those which are "tapered" have been weighted by a Gaussian taper and restored with a 3 mas beam as described in the text. The FWHM contour of the Gaussian beam is given in the lower left-hand corner and is listed in Table 2, along with the rms, peak intensity, and lowest contour level at 3 σ. Contours are logarithmic at $-3\ \sigma$, $3\ \sigma$, $6\ \sigma$, $12\ \sigma$, etc. Negative contours are shown as dashed lines. FITS images corresponding to the maps presented in Fig. 2 are published in the AAS CD-ROM Series, Vol. 4.

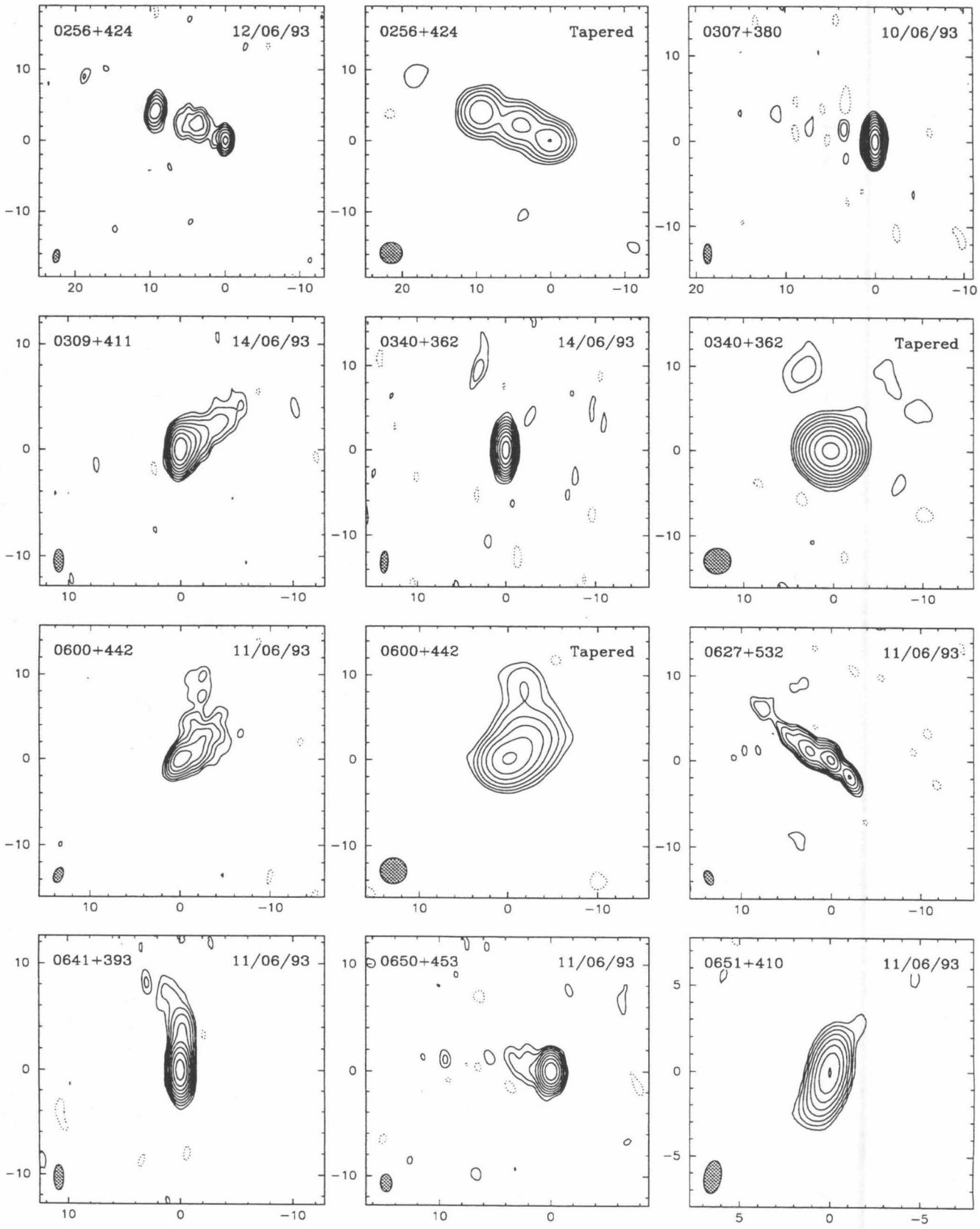

FIG. 2—*Continued*

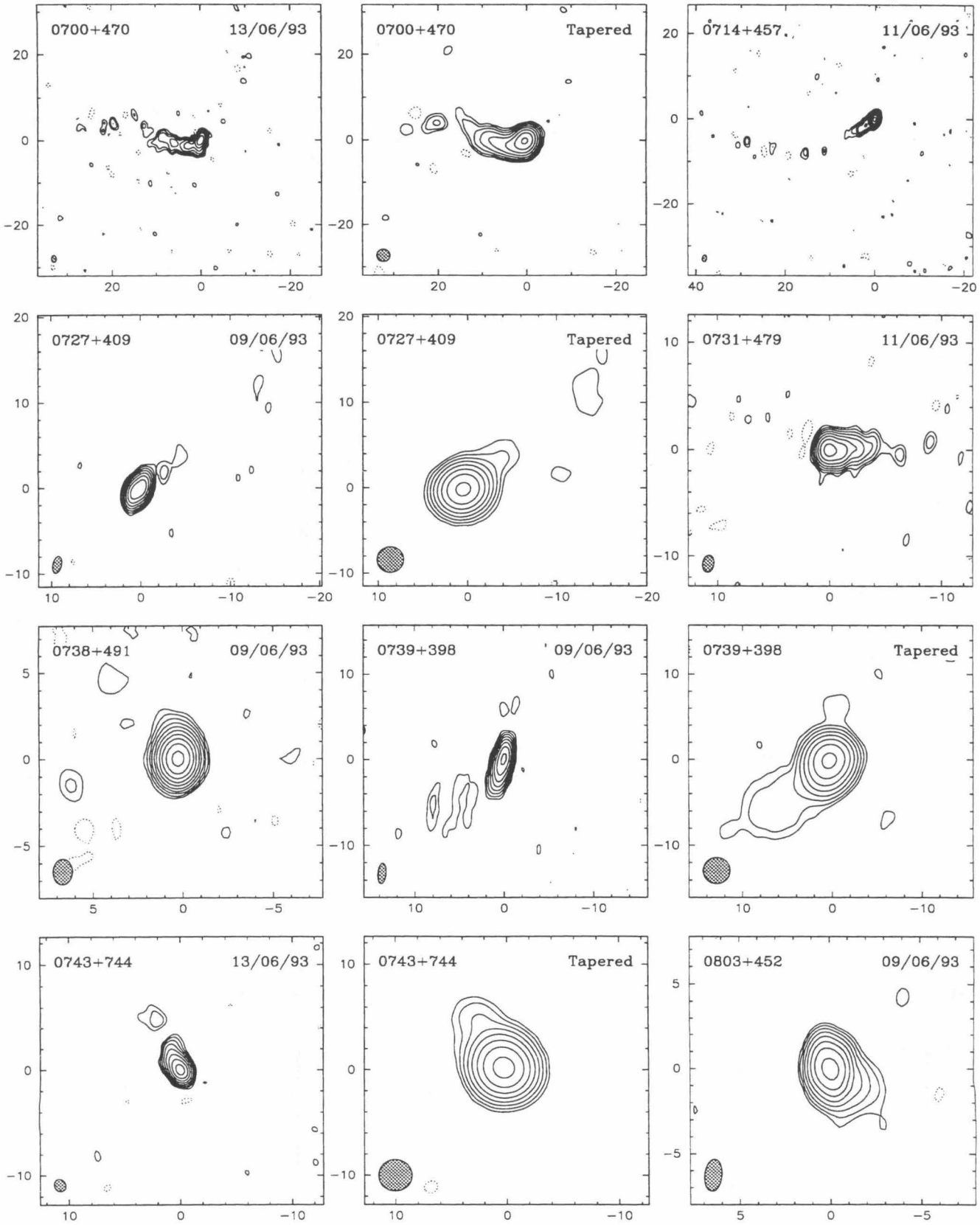

FIG. 2—*Continued*

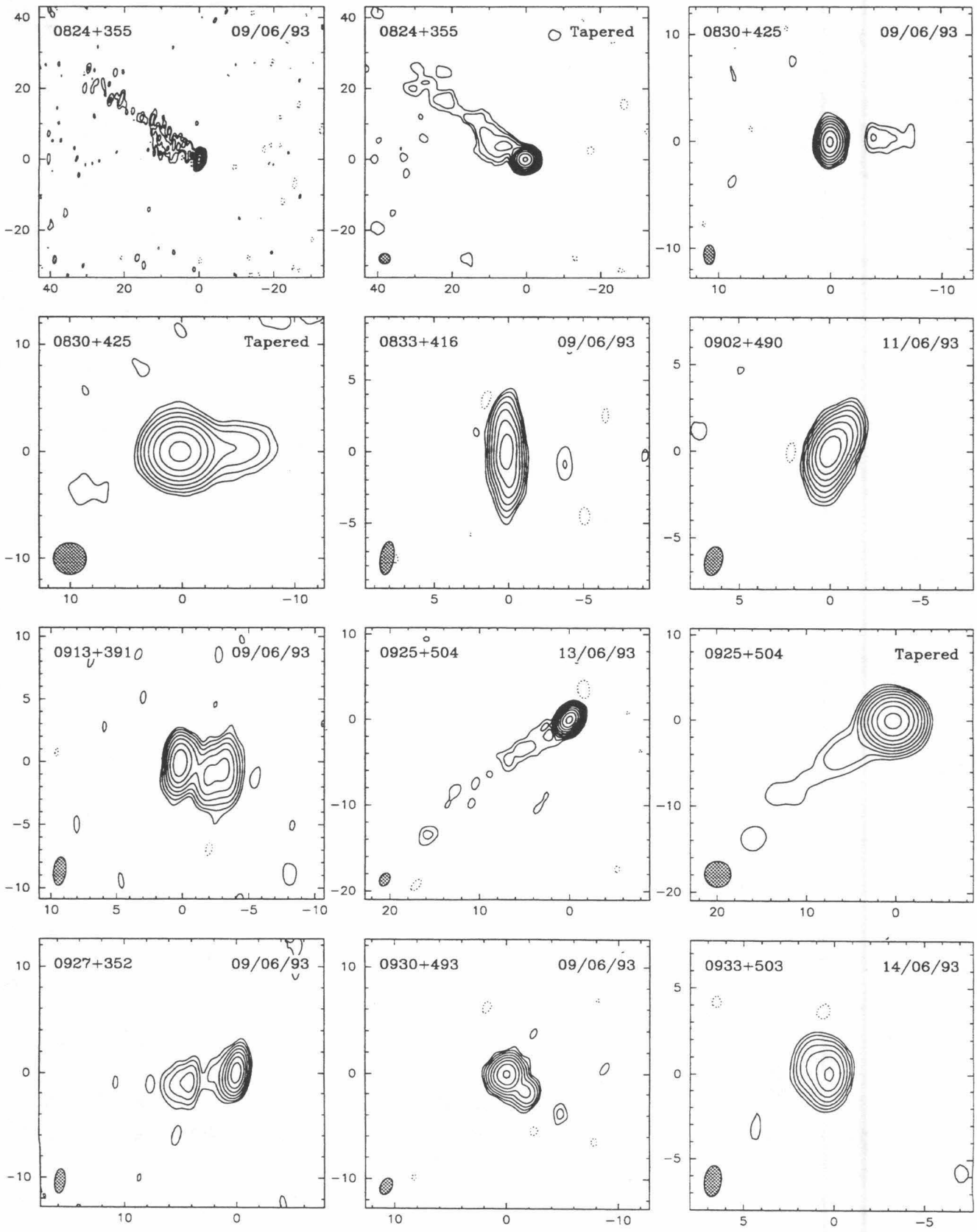

FIG. 2—*Continued*

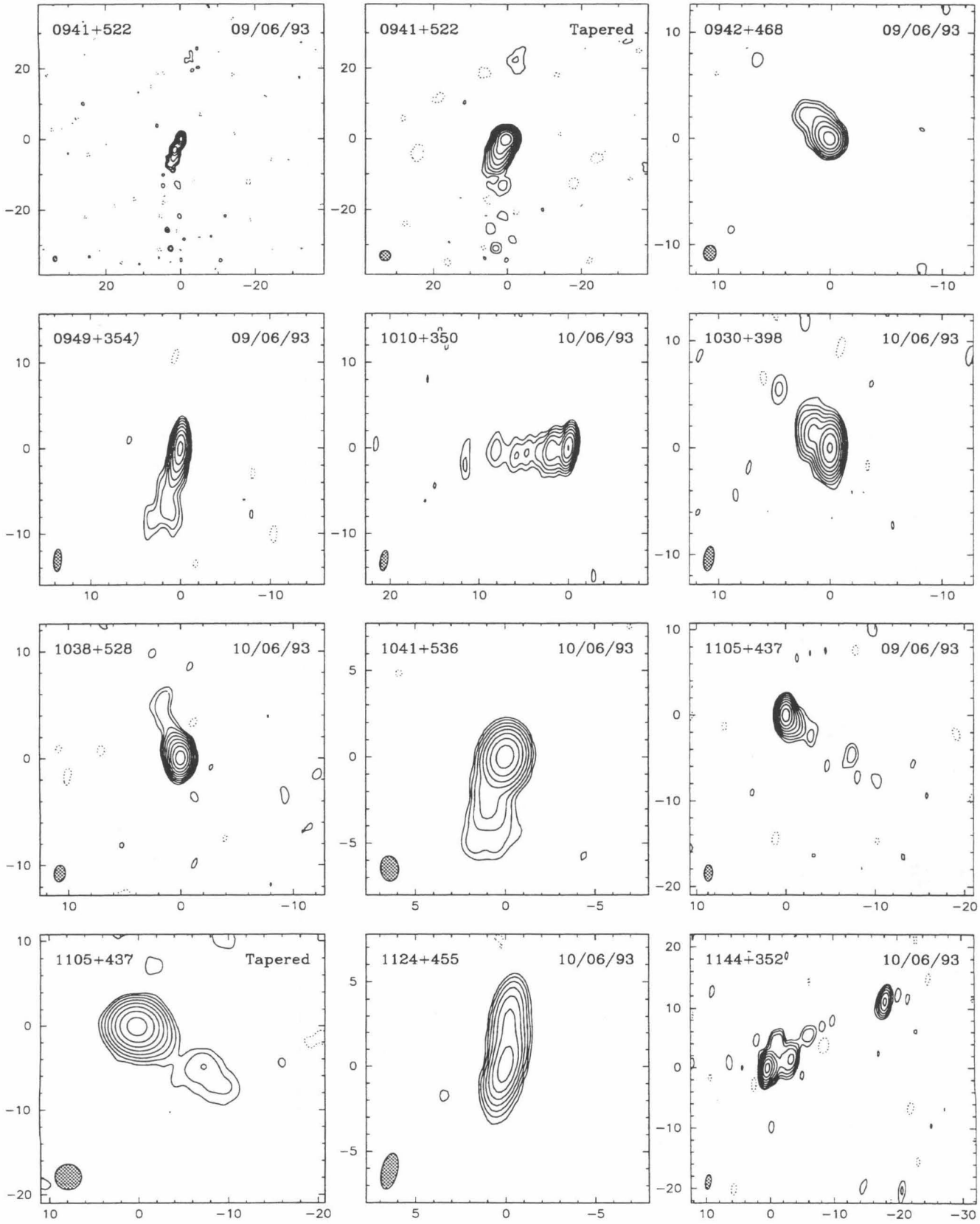

FIG. 2—*Continued*

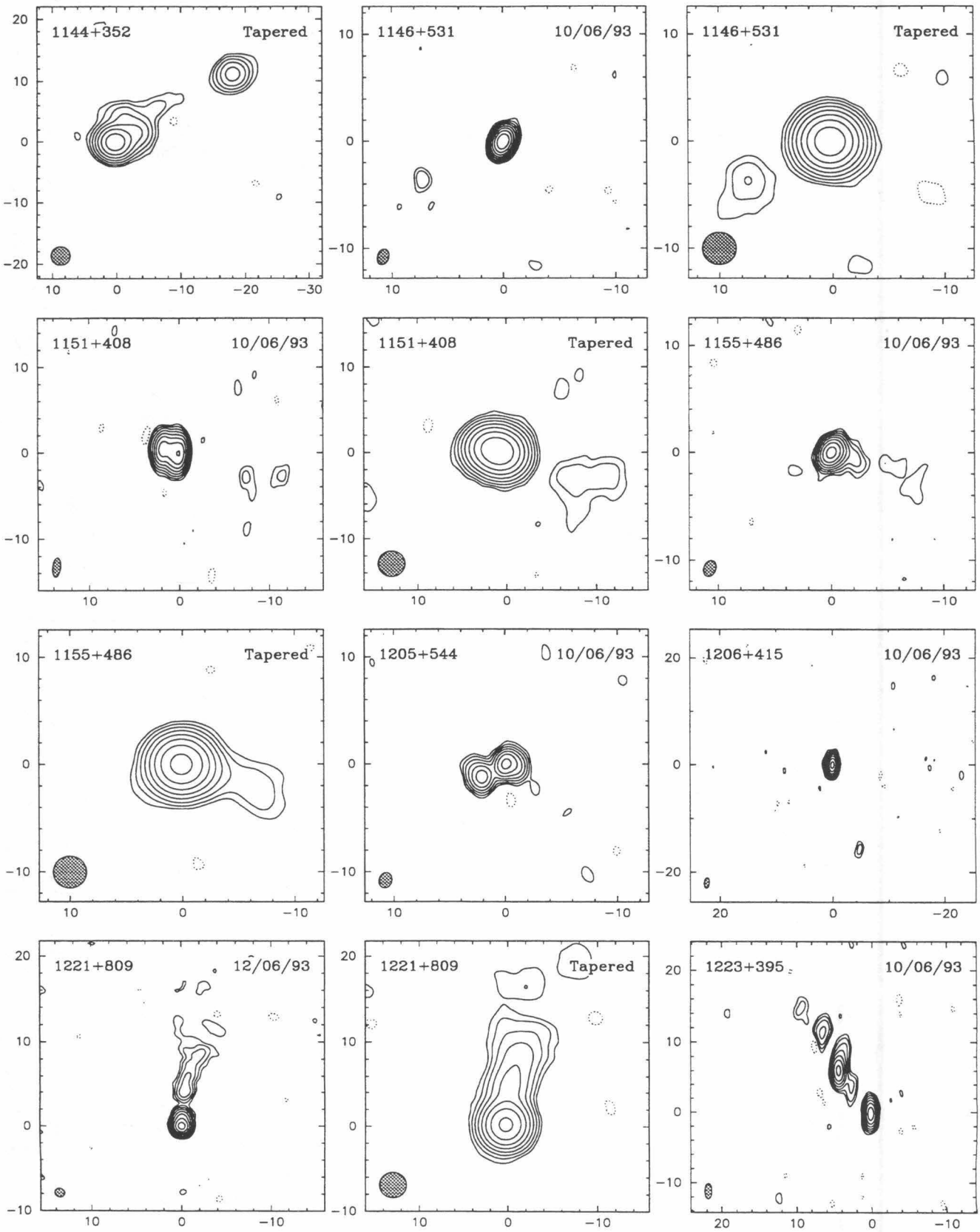

FIG. 2—*Continued*

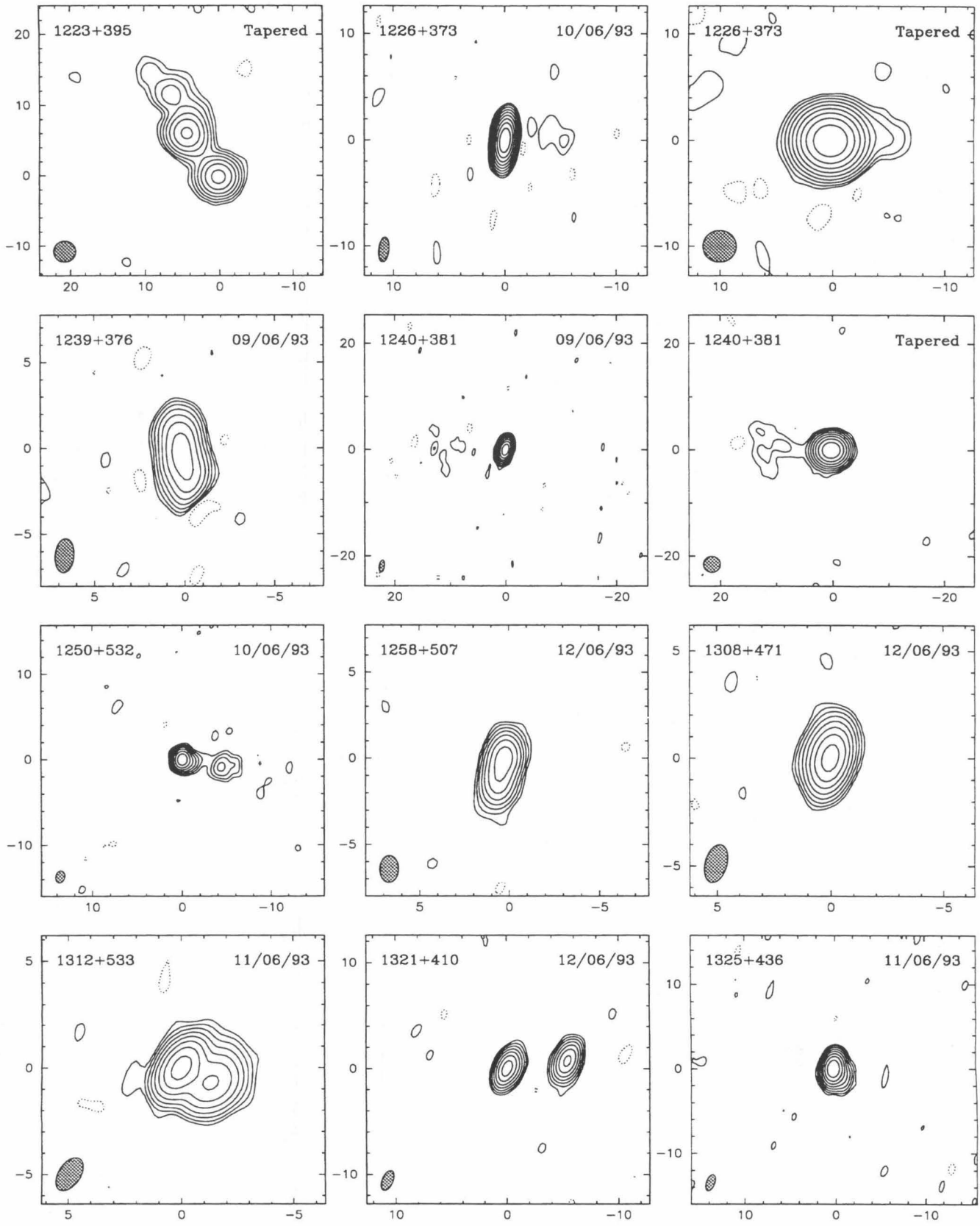

FIG. 2—*Continued*

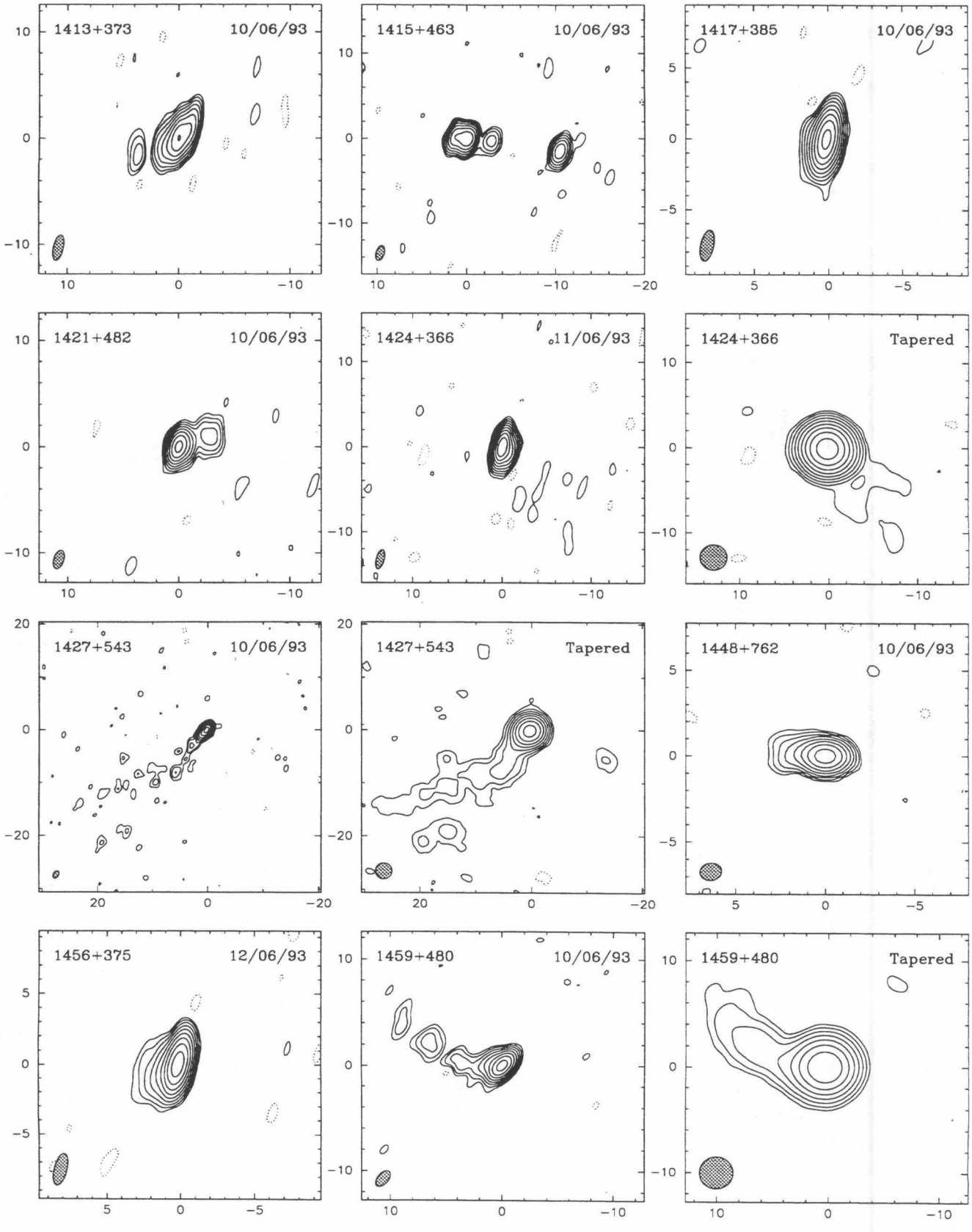

FIG. 2—*Continued*

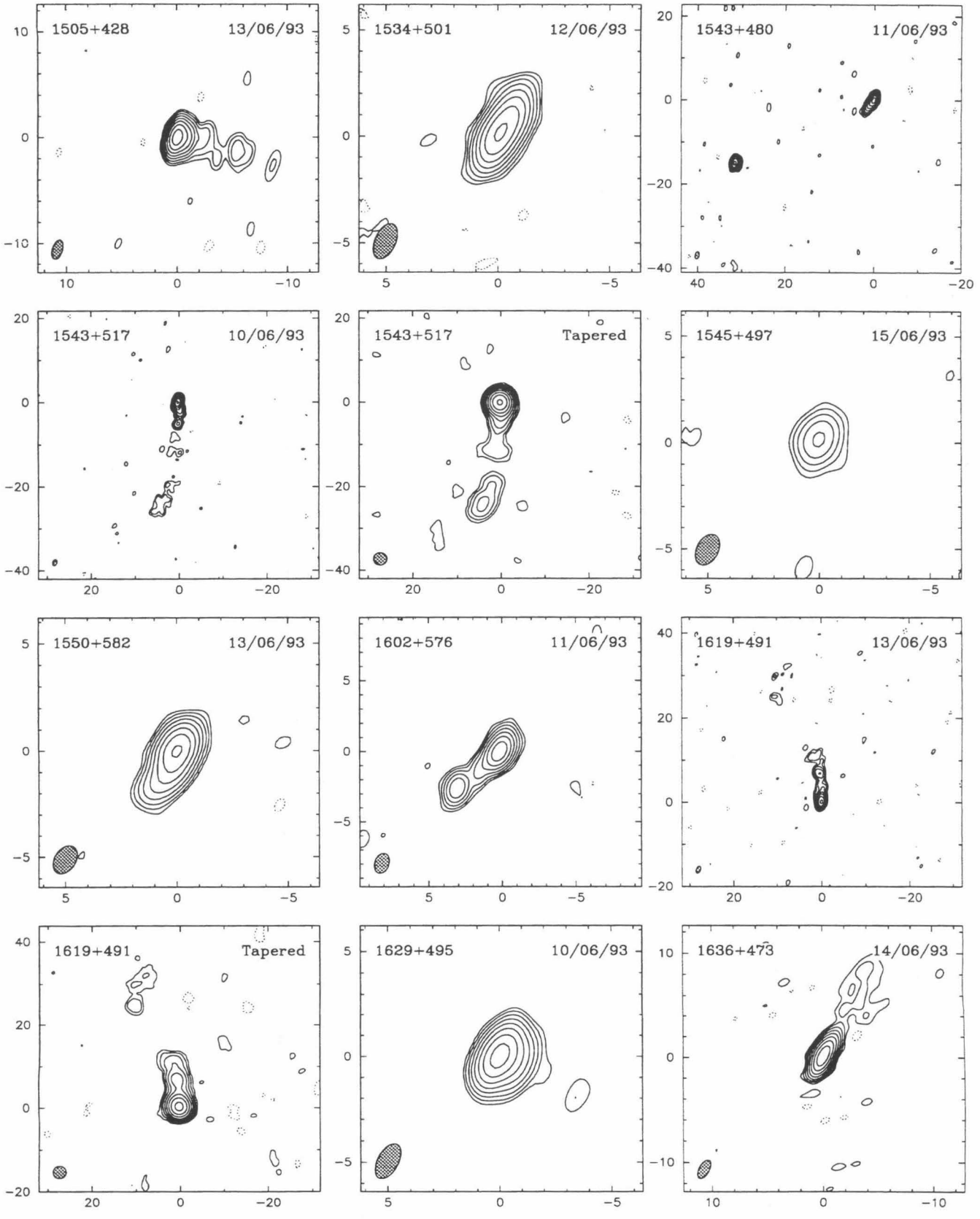

FIG. 2—*Continued*

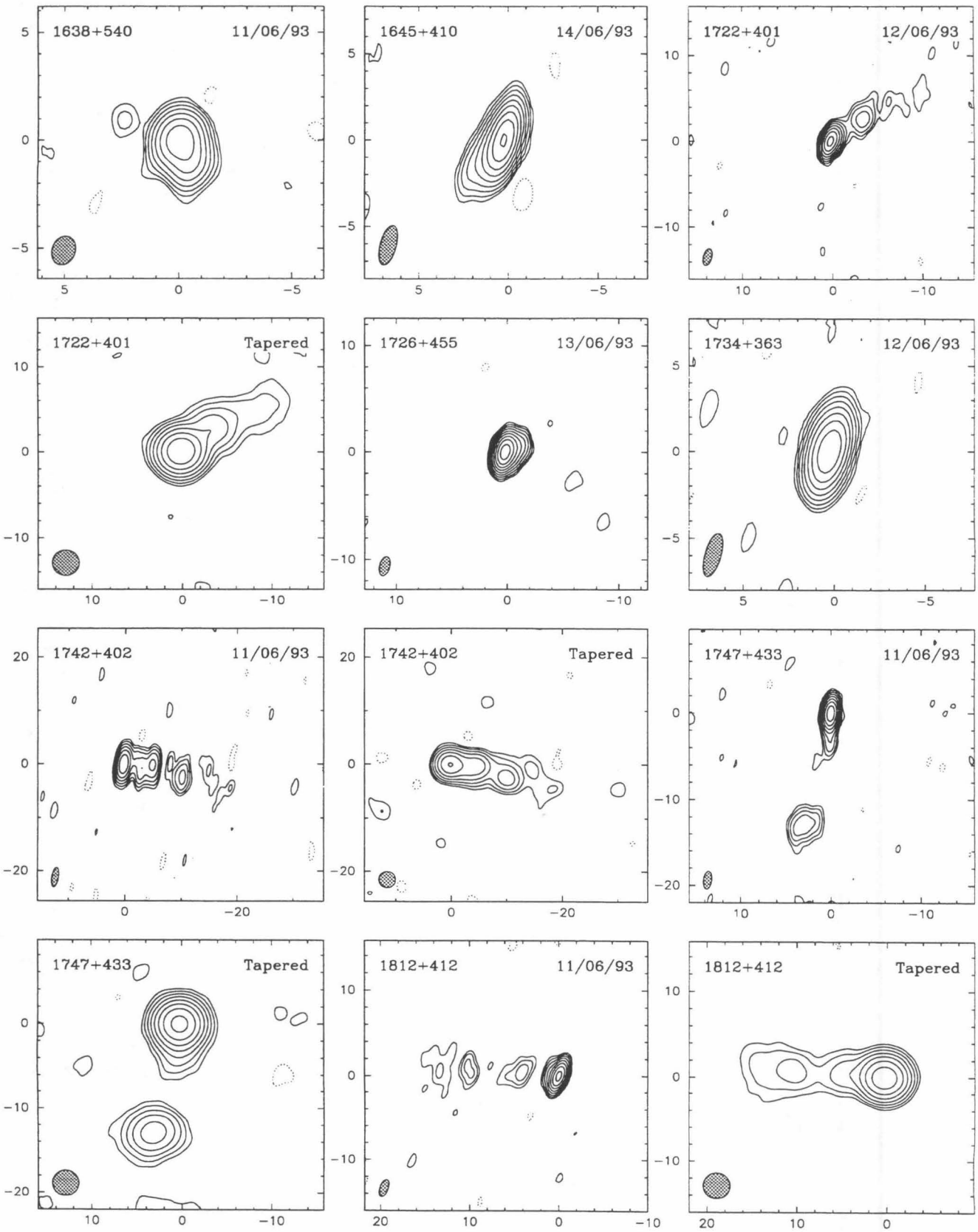

FIG. 2—*Continued*

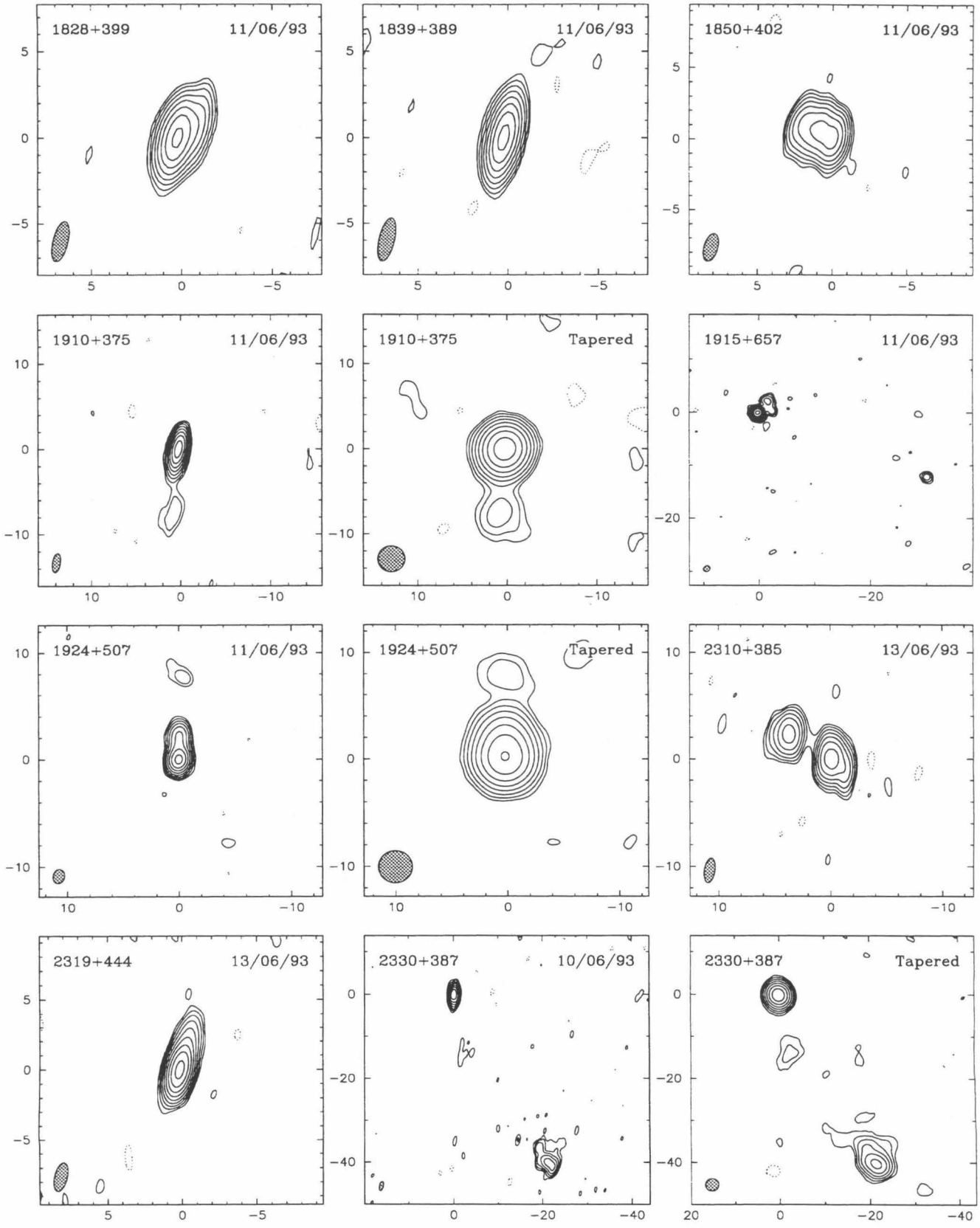

FIG. 2—*Continued*

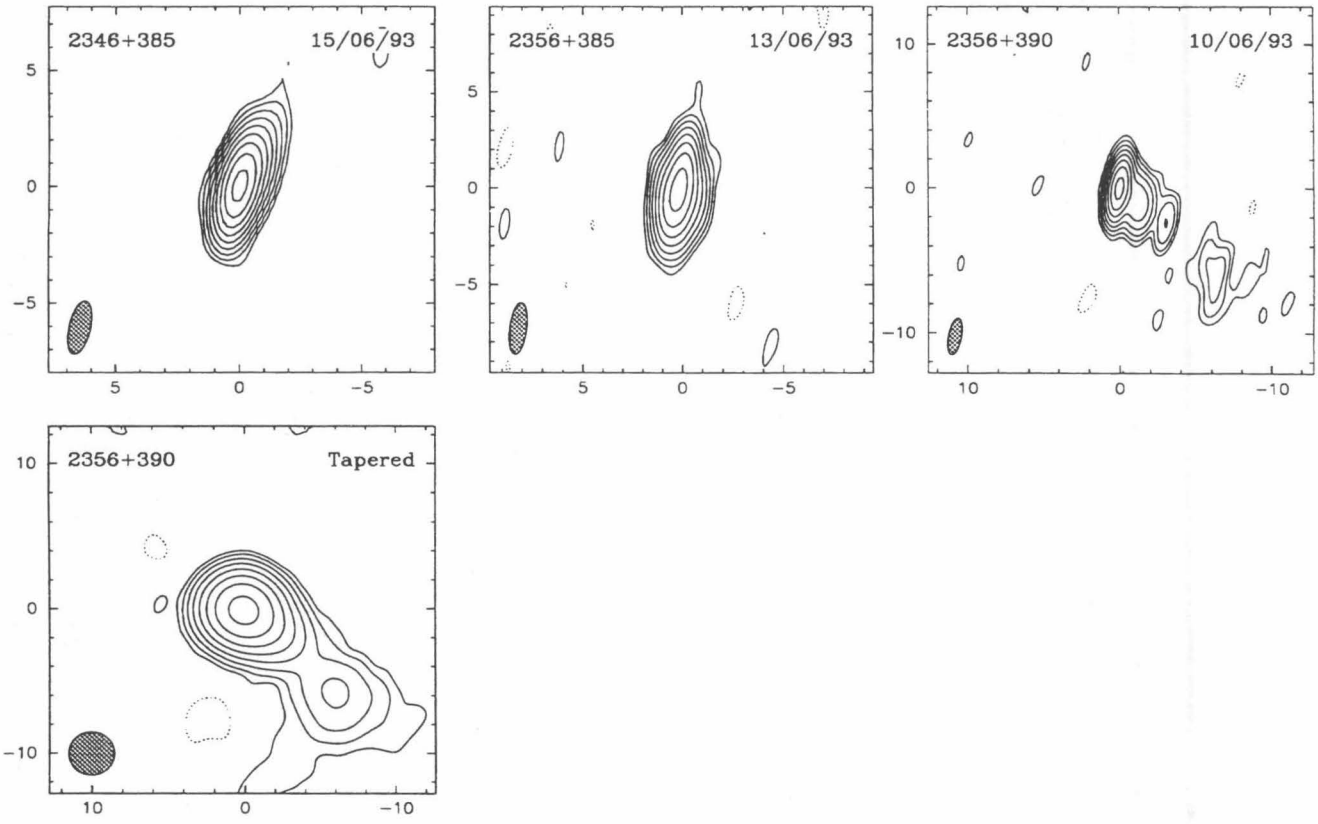

FIG. 2—*Continued*

TABLE 2

MAP PARAMETERS

Name	Dur.	Beam			S_{nat}	rms	1st Cntr	S_{tap}	rms	1st Cntr
		a	b	θ						
	(min)	(mas)	(mas)	(°)	(mJy/beam)		(%Peak)	(mJy/beam)		(%Peak)
(1)	(2)	(3)	(4)	(5)	(6)	(7)	(8)	(9)	(10)	(11)
0003+380...	57	2.17	0.92	−6	471	0.71	0.45			
0035+413...	62	2.24	0.92	3	530	0.61	0.35	869	0.63	0.20
0109+351...	57	2.80	0.85	−4	332	0.56	0.50			
0110+495...	57	1.61	0.98	0	633	0.70	0.35			
0129+431...	57	1.92	0.94	−8	275	0.40	0.45			
0145+386...	57	2.21	0.91	−6	288	0.59	0.60			
0151+474...	81	1.72	0.94	−4	723	0.55	0.25			
0201+365...	76	2.66	0.82	−5	134	0.46	1.05			
0227+403...	57	2.22	0.91	−6	459	0.66	0.45			
0249+383...	57	2.27	0.89	−6	200	0.62	0.95			
0251+393...	56	2.19	0.92	−4	410	0.44	0.30			
0256+424...	59	1.93	0.88	−9	93	0.74	2.40	118	1.21	3.10
0307+380...	95	2.41	0.90	0	490	0.41	0.25			
0309+411...	76	2.14	0.90	0	319	0.43	0.40			
0340+362...	76	2.56	0.88	−3	446	0.41	0.30	527	0.52	0.30
0600+442...	57	1.88	1.04	−21	141	0.79	1.70	240	1.11	1.40
0627+532...	76	1.79	0.98	20	152	0.63	1.25			
0641+393...	76	2.41	0.90	0	495	0.45	0.25			
0650+453...	57	1.68	1.03	2	415	0.57	0.40			
0651+410...	57	1.97	0.95	−9	257	0.62	0.70			
0700+470...	96	1.70	1.09	3	159	0.49	0.90	268	0.63	0.70
0714+457...	57	1.72	0.99	−8	421	0.43	0.30			
0727+409...	57	2.02	0.98	−12	238	0.64	0.80	364	0.76	0.65
0731+479...	57	1.61	1.00	−8	247	0.47	0.55			
0738+491...	57	1.46	1.07	−2	659	0.37	0.15			
0739+398...	76	2.37	0.91	−5	214	0.48	0.65	262	0.58	0.65
0743+744...	57	1.21	1.01	22	327	0.59	0.55	416	0.83	0.60
0803+452...	57	1.89	0.95	−5	230	0.46	0.60			
0824+355...	56	2.39	0.94	−7	400	0.42	0.30	512	0.58	0.35
0830+425...	56	1.84	1.00	0	264	0.55	0.65	300	0.61	0.60
0833+416...	57	2.38	0.92	−8	195	0.61	0.95			
0902+490...	58	1.73	0.98	−13	472	0.62	0.40			
0913+391...	57	2.26	0.94	−6	235	0.67	0.85			
0925+504...	97	1.60	1.07	−26	949	0.52	0.15	1020	1.02	0.30
0927+352...	57	2.35	0.95	−6	223	0.70	0.95			
0930+493...	57	1.65	1.01	−23	293	0.69	0.70			
0933+503...	57	1.84	0.96	−7	136	0.62	1.35			
0941+522...	57	1.56	1.03	−1	293	0.43	0.45	341	0.54	0.50
0942+468...	55	1.48	1.13	−6	220	0.78	1.05			
0949+354...	57	2.67	0.90	−4	273	0.55	0.60			
1010+350...	58	2.45	0.88	−9	227	0.56	0.75			
1030+398...	57	2.33	0.90	−8	432	0.50	0.35			
1038+528...	57	1.56	1.01	−6	639	0.55	0.25			
1041+536...	58	1.48	1.03	5	264	0.43	0.50			
1105+437...	57	1.92	0.96	−2	254	0.43	0.50	280	0.50	0.55
1124+455...	57	2.15	0.91	−12	210	0.70	1.00			
1144+352...	57	2.50	0.90	−7	250	0.49	0.60	329	1.00	0.90
1146+531...	57	1.49	1.00	−17	353	0.45	0.40	370	0.58	0.45
1151+408...	57	2.25	0.90	−6	200	0.50	0.75	423	0.57	0.40
1155+486...	57	1.55	1.08	−20	294	0.55	0.55	324	0.65	0.60
1205+544...	57	1.47	1.13	−13	197	0.80	1.20			
1206+415...	57	2.07	0.91	−5	286	0.58	0.60			
1221+809...	57	1.13	1.03	57	239	0.44	0.55	297	0.65	0.65
1223+395...	56	2.21	0.93	0	195	0.65	1.00	211	0.84	1.20
1226+373...	57	2.35	0.92	−6	693	0.49	0.20	723	0.50	0.20

TABLE 2—*Continued*

Name	Dur.	Beam			S_{nat}	rms	1st Cntr	S_{tap}	rms	1st Cntr
		a	b	θ						
	(min)	(mas)	(mas)	(°)	(mJy/beam)		(%Peak)	(mJy/beam)		(%Peak)
(1)	(2)	(3)	(4)	(5)	(6)	(7)	(8)	(9)	(10)	(11)
1239+376...	57	1.97	1.07	−5	208	0.69	1.00			
1240+381...	57	2.29	0.95	−9	355	0.55	0.45	489	0.64	0.40
1250+532...	57	1.44	1.02	−10	181	0.50	0.85			
1258+507...	57	1.56	1.04	−1	218	0.70	0.95			
1308+471...	57	1.81	0.97	−14	239	0.46	0.60			
1312+533...	57	1.71	0.99	−31	292	0.52	0.55			
1321+410...	57	2.00	0.97	−21	181	0.63	1.05			
1325+436...	76	1.99	0.93	−19	371	0.48	0.40			
1413+373...	76	2.45	0.92	−12	224	0.54	0.70			
1415+463...	57	1.85	0.93	−16	234	0.67	0.85			
1417+385...	57	2.25	0.88	−11	560	0.56	0.30			
1421+482...	57	1.83	0.91	−16	287	0.56	0.60			
1424+366...	76	2.36	0.90	−13	627	0.45	0.20	719	0.60	0.25
1427+543...	57	1.52	0.98	−28	340	0.61	0.55	410	0.76	0.55
1448+762...	57	1.20	1.00	−79	300	0.50	0.50			
1456+375...	57	2.32	0.88	−13	698	0.55	0.25			
1459+480...	57	1.76	0.98	−39	392	0.71	0.55	433	1.15	0.80
1505+428...	57	1.92	0.92	−16	309	0.53	0.50			
1534+501...	76	1.76	0.93	−22	226	0.53	0.70			
1543+480...	57	1.85	0.90	−14	283	0.50	0.55			
1543+517...	76	1.53	0.96	−17	404	0.46	0.35	479	0.56	0.35
1545+497...	57	1.55	0.98	−25	24	0.43	5.40			
1550+582...	57	1.43	0.95	−31	211	0.49	0.70			
1602+576...	57	1.45	0.96	−18	212	0.63	0.90			
1619+491...	57	1.70	0.95	−22	211	0.45	0.65	282	0.58	0.60
1629+495...	57	1.77	0.92	−26	366	0.67	0.55			
1636+473...	57	1.92	0.92	−28	547	0.78	0.45			
1638+540...	76	1.36	1.03	−20	171	0.48	0.85			
1645+410...	57	2.33	0.89	−14	497	0.56	0.35			
1722+401...	57	2.00	0.94	−14	283	0.57	0.60	319	0.83	0.80
1726+455...	57	1.83	0.92	−14	1080	0.82	0.25			
1734+363...	57	2.59	0.88	−15	392	0.55	0.40			
1742+402...	57	3.69	1.20	−9	139	0.79	1.70	182	0.90	1.50
1747+433...	95	2.05	0.91	−7	262	0.39	0.45	269	0.53	0.60
1812+412...	57	2.11	0.91	−19	256	0.52	0.60	272	0.84	0.95
1828+399...	76	2.40	0.84	−13	213	0.45	0.65			
1839+389...	76	2.57	0.86	−12	204	0.42	0.60			
1850+402...	58	2.02	0.92	−15	244	0.85	1.05			
1910+375...	57	2.25	0.90	−9	307	0.49	0.50	349	0.61	0.50
1915+657...	76	1.24	1.03	−53	241	0.46	0.55			
1924+507...	76	1.35	1.05	−13	289	0.58	0.60	341	0.84	0.75
2310+385...	57	2.34	0.95	−8	182	0.65	1.05			
2319+444...	97	2.09	0.88	−13	495	0.50	0.30			
2330+387...	58	2.30	0.89	−12	179	0.46	0.75	243	0.73	0.90
2346+385...	57	2.34	0.88	−12	592	0.58	0.30			
2356+385...	76	2.72	0.85	−7	243	0.47	0.60			
2356+390...	76	2.58	0.85	−10	212	0.44	0.60	244	0.48	0.60

NOTES.—Col. (2): Total integration time on source in minutes. Cols. (3)–(5): The beam characteristics of the naturally weighted maps. The restoring beam is an elliptical Gaussian with FWHM major axis a mas and minor axis b mas, with major axis in position angle θ°. Col. (6): The peak intensity of the naturally weighted maps (mJy beam^{-1}). Col. (7): The rms noise in the naturally weighted maps (mJy beam^{-1}), measured in the four corners of the displayed image. Col. (8): The lowest contour level of the map in percentage of the peak flux density. Cols. (9)–(11): The peak intensity, rms noise, and lowest contour level of the tapered map, if an image has been provided. All tapered maps have been restored with a 3 mas beam.

Table 2 is published in computer-readable form in the AAS CD-ROM Series, Vol. 4.

TABLE 3

GAUSSIAN MODELS

Source	S (Jy)	r (mas)	θ (°)	a (mas)	b/a	Φ (°)	Amplitude A.F.	Cl.Phase A.F.	Total A.F.
0003+380 ...	0.526	0.00	0.0	0.69	0.46	114.4	1.000	1.063	1.028
	0.183	0.89	122.4	0.61	0.14	146.2			
	0.013	4.62	111.9	1.67	0.53	7.4			
0035+413 ...	0.456	0.00	0.0	0.57	0.00	99.1	1.024	1.154	1.084
	0.474	0.83	95.8	0.60	0.50	−36.4			
	0.017	3.80	101.8	1.46	0.00	23.3			
	0.067	9.62	112.9	10.14	0.29	127.0			
0109+351 ...	0.300	0.00	0.0	0.45	0.00	−155.9	1.025	1.042	1.033
	0.065	0.58	−163.9	0.96	0.26	−150.3			
	0.014	5.54	−156.3	7.00	0.09	−155.8			
0110+495 ...	0.666	0.00	0.0	0.67	0.23	−27.8	1.012	1.093	1.049
	0.131	1.05	−39.8	2.78	0.29	−37.4			
	0.094	8.33	−30.9	4.11	0.46	0.1			
0129+431 ...	0.289	0.00	0.0	0.49	0.39	159.5	1.001	1.022	1.010
	0.013	1.95	−7.5	3.11	0.16	28.9			
0145+386 ...	0.401	0.00	0.0	0.95	0.61	122.1	0.917	1.153	1.030
	0.057	1.18	−45.5	0.85	0.32	23.6			
0151+474 ...	0.762	0.00	0.0	0.43	0.51	16.3	0.876	1.012	0.939
	0.036	1.67	−178.6	0.76	0.54	−3.8			
0201+365 ...	0.144	0.00	0.0	0.34	0.59	45.7	1.016	1.165	1.085
	0.108	2.45	−3.5	1.03	0.45	−11.7			
	0.035	7.24	−3.8	3.54	0.60	4.9			
0227+403 ...	0.502	0.00	0.0	0.75	0.39	162.1	0.950	1.053	0.997
	0.048	2.38	138.6	2.63	0.10	120.8			
0249+383 ...	0.199	0.00	0.0	0.61	0.86	165.1	1.050	1.042	1.047
	0.107	1.47	−12.8	2.01	0.37	−31.1			
	0.056	5.15	−19.7	3.44	0.33	−28.7			
0251+393 ...	0.438	0.00	0.0	0.43	0.35	90.9	0.977	1.016	0.994
	0.048	0.75	80.6	1.20	0.71	10.2			
	0.008	9.13	65.1	1.40	0.00	48.8			
0256+424 ...	0.113	0.00	0.0	0.74	0.00	35.0	1.040	1.244	1.135
	0.151	10.34	65.4	1.39	0.60	−51.8			
	0.106	4.57	55.7	1.74	0.46	−86.9			
0307+380 ...	0.515	0.00	0.0	0.32	0.44	80.2	0.915	1.002	0.955
	0.006	3.57	68.7	0.80	0.80	47.7			
0309+411 ...	0.318	0.00	0.0	0.44	0.82	135.9	0.895	1.029	0.957
	0.112	0.91	−51.5	1.19	0.00	−62.8			
	0.031	3.74	−55.2	3.26	0.00	−61.7			
0340+362 ...	0.470	0.00	0.0	0.53	0.55	54.8	0.896	1.039	0.963
	0.081	0.85	31.8	0.87	0.90	80.8			
	0.008	9.52	21.0	4.28	0.18	145.1			
0600+442 ...	0.222	0.00	0.0	1.08	0.70	−69.4	1.027	1.211	1.112
	0.159	2.52	−49.6	2.44	0.75	−26.6			
	0.080	5.04	−35.3	5.38	0.67	12.3			
0627+532 ...	0.215	0.00	0.0	1.21	0.23	65.6	1.043	1.146	1.090
	0.093	2.81	−132.1	0.77	0.01	−160.1			
	0.151	2.68	66.7	2.27	0.33	48.9			
	0.026	8.94	52.1	3.01	0.36	46.6			

TABLE 3—*Continued*

Source	S (Jy)	r (mas)	θ (°)	a (mas)	b/a	Φ (°)	Amplitude A.F.	Cl.Phase A.F.	Total A.F.
0641+393 ...	0.498	0.00	0.0	0.42	0.40	19.1	0.902	1.026	0.960
	0.063	1.77	−7.4	4.02	0.21	−1.6			
	0.016	4.70	1.4	3.05	0.13	32.1			
0650+453 ...	0.431	0.00	0.0	0.29	0.73	135.5	0.901	1.037	0.965
	0.037	1.04	100.1	2.17	0.39	53.2			
0651+410 ...	0.308	0.00	0.0	1.12	0.27	166.0	0.866	1.052	0.954
	0.033	1.56	156.4	0.79	0.00	72.4			
0700+470 ...	0.280	0.00	0.0	1.59	0.44	−24.2	1.084	1.310	1.188
	0.123	2.44	122.6	2.71	0.34	102.2			
	0.098	7.05	93.1	6.16	0.34	64.2			
	0.012	21.21	77.9	7.32	0.00	138.8			
0714+457 ...	0.424	0.00	0.0	0.41	0.08	148.7	0.909	1.047	0.974
	0.095	2.02	124.8	4.66	0.17	127.2			
	0.005	17.46	117.5	1.48	0.24	23.0			
0727+409 ...	0.213	0.00	0.0	0.49	0.57	−44.8	1.024	1.203	1.106
	0.197	1.12	124.1	0.74	0.44	139.3			
	0.007	2.89	−51.9	0.02	0.91	35.4			
0731+479 ...	0.231	0.00	0.0	0.37	0.72	61.1	1.009	1.063	1.034
	0.182	1.02	−103.6	0.84	0.34	−83.3			
	0.093	2.40	−87.9	1.87	0.08	−98.3			
	0.006	8.86	−85.7	1.01	0.38	−16.9			
0738+491 ...	0.691	0.00	0.0	0.28	0.94	174.1	0.879	1.009	0.939
0739+398 ...	0.209	0.00	0.0	0.76	0.38	161.6	1.000	1.080	1.037
	0.103	1.53	158.2	0.70	0.52	142.5			
	0.030	5.88	140.6	8.31	0.25	120.9			
0743+744 ...	0.368	0.00	0.0	0.71	0.20	24.8	0.891	1.064	0.972
	0.091	1.18	28.6	0.75	0.00	−17.9			
	0.015	5.32	28.5	1.88	0.33	127.9			
0803+452 ...	0.374	0.00	0.0	1.26	0.28	−125.8	0.997	1.207	1.096
	0.009	2.03	−123.6	0.00	0.55	125.4			
0824+355 ...	0.528	0.00	0.0	0.79	0.31	100.2	0.916	1.144	1.024
	0.131	11.07	52.8	22.05	0.19	52.7			
0830+425 ...	0.299	0.00	0.0	0.57	0.41	−74.9	0.994	1.040	1.015
	0.034	3.72	−84.1	6.02	0.00	−86.8			
0833+416 ...	0.238	0.00	0.0	1.41	0.24	5.0	0.987	1.162	1.069
	0.083	2.12	−171.9	0.44	0.05	−28.0			
0902+490 ...	0.480	0.00	0.0	0.39	0.76	−32.6	0.940	1.065	0.998
	0.141	1.18	−39.8	0.76	0.95	−37.8			
0913+391 ...	0.276	0.00	0.0	0.74	0.77	28.0	0.945	1.088	1.011
	0.125	2.32	−114.9	1.00	0.87	9.11			
	0.133	3.37	−97.9	1.13	0.74	29.1			
0925+504 ...	1.032	0.00	0.0	0.51	0.36	107.2	0.918	1.029	0.969
	0.035	5.24	126.4	7.65	0.24	128.5			
0927+352 ...	0.242	0.00	0.0	0.49	0.69	138.9	1.038	1.079	1.056
	0.078	4.36	103.0	3.95	0.43	102.1			
0930+493 ...	0.483	0.00	0.0	1.17	0.55	−133.6	0.863	1.122	0.985
	0.076	2.57	−136.3	1.12	0.30	−143.1			

TABLE 3—*Continued*

Source	S (Jy)	r (mas)	θ (°)	a (mas)	b/a	Φ (°)	Amplitude A.F.	Cl.Phase A.F.	Total A.F.
0933+503 ...	0.127	0.00	0.0	0.06	0.00	127.2	0.972	1.079	1.021
	0.065	0.92	64.0	0.92	0.43	58.4			
0941+522 ...	0.350	0.00	0.0	0.80	0.44	165.8	0.975	1.117	1.041
	0.122	3.50	150.8	1.21	0.65	166.4			
	0.074	5.82	163.9	6.45	0.13	158.0			
	0.009	30.82	175.4	1.57	0.00	118.0			
0942+468 ...	0.229	0.00	0.0	0.59	0.50	62.1	0.981	1.068	1.021
	0.075	1.01	47.4	0.68	0.56	14.8			
	0.049	2.62	31.1	1.94	0.71	72.0			
0949+354 ...	0.296	0.00	0.0	0.99	0.27	168.9	0.988	1.164	1.071
	0.078	3.11	167.0	5.11	0.13	169.9			
1010+350 ...	0.233	0.00	0.0	0.26	0.57	50.6	0.876	1.003	0.935
	0.088	1.83	98.0	1.22	0.70	32.0			
	0.033	5.40	99.1	4.47	0.22	78.6			
1030+398 ...	0.577	0.00	0.0	1.10	0.13	35.0	0.907	1.090	0.994
	0.108	2.04	47.6	0.95	0.33	87.4			
	0.007	7.58	40.9	0.61	0.00	65.1			
1038+528 ...	0.667	0.00	0.0	0.48	0.12	16.2	0.906	1.063	0.979
	0.055	1.25	27.1	0.16	0.17	132.8			
	0.027	2.71	18.3	3.88	0.24	27.4			
1041+536 ...	0.346	0.00	0.0	0.97	0.33	145.3	0.996	1.045	1.019
	0.053	2.58	160.1	3.28	0.34	178.7			
1105+437 ...	0.246	0.00	0.0	0.26	0.00	−133.5	1.000	1.049	1.022
	0.055	0.98	−136.5	1.45	0.47	−138.7			
	0.012	8.66	−125.6	3.27	0.29	−26.3			
1124+455 ...	0.213	0.00	0.0	0.81	0.00	−25.5	1.009	1.195	1.096
	0.145	2.48	−5.0	2.37	0.12	0.5			
1144+352 ...	0.297	0.00	0.0	0.60	0.86	31.9	0.962	1.159	1.055
	0.170	2.66	−58.2	3.99	0.86	−55.3			
	0.071	21.67	−58.5	0.55	0.78	−49.2			
1146+531 ...	0.378	0.00	0.0	0.37	0.70	122.4	0.884	1.046	0.960
1151+408 ...	0.365	0.00	0.0	1.08	0.83	64.3	0.919	1.184	1.047
	0.181	1.66	73.1	0.92	0.00	88.3			
1155+486 ...	0.310	0.00	0.0	0.46	0.40	−78.7	0.889	1.068	0.972
	0.041	1.53	−100.5	2.40	0.31	−132.0			
1205+544 ...	0.284	0.00	0.0	1.00	0.63	105.6	0.949	1.153	1.045
	0.141	2.48	121.5	0.91	0.32	58.2			
1206+415 ...	0.327	0.00	0.0	0.53	0.68	40.5	0.903	1.019	0.957
	0.007	16.36	−162.8	0.63	0.00	−54.7			
1221+809 ...	0.239	0.00	0.0	0.33	0.33	−22.2	0.887	1.036	0.956
	0.074	1.02	−3.5	0.65	0.63	−19.1			
	0.093	6.12	−6.6	6.06	0.18	−11.7			
1223+395 ...	0.206	0.00	0.0	0.56	0.41	18.6	0.906	1.188	1.041
	0.016	3.22	35.6	3.01	0.35	14.6			
	0.217	7.55	34.7	1.34	0.43	8.1			
	0.067	12.64	27.0	6.51	0.26	46.0			

TABLE 3—*Continued*

Source	S (Jy)	r (mas)	θ (°)	a (mas)	b/a	Φ (°)	Amplitude A.F.	Cl.Phase A.F.	Total A.F.
1226+373 ...	0.729	0.00	0.0	0.34	0.67	−51.4	0.886	1.014	0.946
	0.012	3.17	−70.7	2.09	0.00	−127.9			
1239+376 ...	0.231	0.00	0.0	1.51	0.34	2.3	0.863	1.100	0.974
	0.189	1.54	−159.8	0.80	0.78	107.7			
1240+381 ...	0.526	0.00	0.0	1.08	0.45	−66.3	0.892	1.106	0.994
1250+532 ...	0.207	0.00	0.0	0.59	0.19	−120.1	0.922	1.073	0.992
	0.063	4.28	−100.4	5.53	0.24	−96.4			
1258+507 ...	0.194	0.00	0.0	0.20	0.83	82.9	0.887	1.110	0.992
	0.152	1.30	162.9	0.63	0.50	159.8			
1308+471 ...	0.256	0.00	0.0	0.38	0.72	24.6	0.851	1.038	0.939
1312+533 ...	0.300	0.00	0.0	0.27	0.80	1.5	0.863	1.047	0.950
	0.170	1.53	−118.4	1.01	0.47	−110.8			
1321+410 ...	0.226	0.00	0.0	0.62	0.93	−90.9	0.865	1.194	1.022
	0.187	5.42	−82.5	0.74	0.85	20.1			
1325+436 ...	0.403	0.00	0.0	0.75	0.43	40.4	0.896	1.118	1.001
	0.181	0.78	−139.0	0.85	0.92	−173.3			
1413+373 ...	0.263	0.00	0.0	0.77	0.15	109.9	0.889	1.088	0.983
	0.096	1.56	−44.7	0.23	0.00	−1.0			
	0.023	1.65	116.9	0.72	0.26	21.2			
	0.010	4.25	116.5	0.54	0.01	29.7			
1415+463 ...	0.234	0.00	0.0	0.41	0.82	46.9	0.901	1.125	1.007
	0.232	1.14	76.2	1.02	0.00	87.0			
	0.043	2.53	−95.3	1.12	0.59	−3.3			
	0.155	10.47	−97.5	0.84	0.73	−54.4			
1417+385 ...	0.619	0.00	0.0	0.41	0.92	−10.7	0.972	1.036	1.001
1421+482 ...	0.324	0.00	0.0	0.52	0.75	−100.0	0.864	1.087	0.971
	0.074	2.24	−73.0	2.62	0.64	−72.9			
1424+366 ...	0.669	0.00	0.0	0.40	0.71	27.2	0.874	1.036	0.950
	0.090	1.13	−129.6	0.52	0.00	−37.7			
1427+543 ...	0.351	0.00	0.0	0.58	0.37	138.4	0.941	1.043	0.987
	0.100	1.28	136.7	0.76	0.54	119.9			
	0.038	6.20	141.5	7.43	0.16	154.4			
1448+762 ...	0.318	0.00	0.0	0.66	0.19	78.5	0.845	1.063	0.947
	0.088	0.77	81.5	1.08	0.43	82.8			
1456+375 ...	0.737	0.00	0.0	0.30	0.98	168.9	0.900	1.077	0.983
	0.045	1.36	112.8	1.42	0.56	9.4			
1459+480 ...	0.400	0.00	0.0	0.36	0.25	40.4	0.870	1.066	0.962
	0.067	1.43	86.0	1.74	0.19	82.0			
	0.059	6.66	72.9	5.97	0.10	50.4			
1505+428 ...	0.373	0.00	0.0	0.62	0.54	−101.5	0.892	1.058	0.970
	0.042	1.17	−97.8	0.00	0.70	−95.2			
	0.037	5.00	−103.8	4.35	0.00	−109.0			
1534+501 ...	0.315	0.00	0.0	1.43	0.13	−35.4	0.947	1.277	1.108

TABLE 3—*Continued*

Source	S (Jy)	r (mas)	θ (°)	a (mas)	b/a	Φ (°)	Amplitude A.F.	Cl.Phase A.F.	Total A.F.
1543+480 ...	0.299	0.00	0.0	0.46	0.80	97.8	0.914	1.051	0.978
	0.116	1.49	141.3	1.23	0.54	141.9			
	0.079	34.93	115.6	0.68	0.93	63.6			
1543+517 ...	0.358	0.00	0.0	0.42	0.52	177.9	0.893	1.044	0.964
	0.131	0.74	173.2	0.59	0.33	57.0			
	0.055	2.26	−169.4	1.15	0.54	23.4			
	0.022	5.34	179.4	1.19	0.62	120.3			
	0.057	23.39	172.1	8.21	0.24	149.9			
1545+497 ...	0.041	0.00	0.0	0.44	0.30	37.1	0.876	1.141	1.002
1550+582 ...	0.195	0.00	0.0	0.49	0.23	160.5	0.847	1.026	0.931
	0.093	1.03	163.2	1.33	0.00	143.6			
1602+576 ...	0.278	0.00	0.0	0.92	0.34	140.1	0.902	1.086	0.988
	0.076	3.87	130.9	0.53	0.67	12.2			
1619+491 ...	0.236	0.00	0.0	0.66	0.40	5.7	0.892	1.075	0.978
	0.087	1.30	9.0	0.47	0.01	96.6			
	0.052	6.51	2.5	1.66	0.59	38.4			
	0.033	10.26	8.2	3.75	0.63	−81.1			
1629+495 ...	0.415	0.00	0.0	0.53	0.31	−112.4	0.890	1.050	0.965
	0.033	1.12	−114.9	0.55	0.91	−8.1			
1636+473 ...	0.705	0.00	0.0	1.48	0.17	−20.7	1.048	1.086	1.065
	0.045	5.85	−31.3	6.99	0.15	−25.3			
1638+540 ...	0.229	0.00	0.0	0.79	0.72	−147.3	0.821	1.106	0.957
	0.056	1.22	−156.2	0.34	0.46	−31.9			
1645+410 ...	0.465	0.00	0.0	0.19	0.34	128.8	0.873	1.011	0.937
	0.085	0.89	136.1	0.81	0.60	111.5			
	0.020	2.22	132.2	0.60	0.00	98.8			
1722+401 ...	0.336	0.00	0.0	0.73	0.52	131.7	0.949	1.078	1.009
	0.055	4.41	−53.4	2.88	0.44	−44.6			
1726+455 ...	1.109	0.00	0.0	0.32	0.98	−80.0	0.932	1.042	0.983
	0.198	0.96	−76.5	0.92	0.62	−74.0			
1734+363 ...	0.534	0.00	0.0	0.80	0.59	71.7	0.873	1.041	0.952
1742+402 ...	0.217	0.00	0.0	1.20	0.83	15.3	0.845	1.259	1.031
	0.116	4.77	−94.6	2.57	0.54	−89.3			
	0.053	11.04	−104.5	4.68	0.63	−90.2			
1747+433 ...	0.252	0.00	0.0	0.10	0.00	104.0	0.883	1.036	0.955
	0.022	0.94	−171.2	1.10	0.00	−16.1			
	0.011	3.40	179.0	0.74	0.76	4.0			
	0.055	13.29	167.1	2.35	0.55	115.0			
1812+412 ...	0.275	0.00	0.0	0.41	0.83	138.0	0.881	1.038	0.954
	0.023	4.24	83.5	2.12	0.21	107.4			
	0.034	11.24	85.4	5.39	0.42	68.8			
1828+399 ...	0.222	0.00	0.0	0.44	0.79	−112.4	0.841	1.068	0.949
	0.072	0.98	−59.8	0.98	0.23	−62.5			
1839+389 ...	0.220	0.00	0.0	0.35	0.87	128.7	0.861	1.069	0.960
1850+402 ...	0.272	0.00	0.0	0.92	0.37	55.0	0.859	1.204	1.025
	0.376	1.41	61.8	1.64	0.19	69.2			

TABLE 3—*Continued*

Source	S (Jy)	r (mas)	θ (°)	a (mas)	b/a	Φ (°)	Amplitude A.F.	Cl.Phase A.F.	Total A.F.
1910+375 ...	0.388	0.00	0.0	1.33	0.25	159.8	0.892	1.045	0.964
	0.021	7.52	177.5	3.32	0.26	−49.5			
1915+657 ...	0.306	0.00	0.0	0.63	0.78	31.1	0.898	1.068	0.978
	0.045	2.68	−54.4	2.56	0.46	11.1			
	0.015	32.61	−111.8	0.86	0.60	7.7			
1924+507 ...	0.301	0.00	0.0	0.50	0.23	1.0	0.878	1.017	0.943
	0.110	2.00	−0.4	1.26	0.26	−1.9			
	0.011	8.41	3.0	3.11	0.38	77.2			
2310+385 ...	0.296	0.00	0.0	1.21	0.36	−121.1	0.876	1.190	1.026
	0.070	1.57	−131.1	1.90	0.00	−167.9			
	0.145	4.39	59.2	1.36	0.46	50.1			
2319+444 ...	0.509	0.00	0.0	0.26	0.61	2.5	0.873	1.007	0.935
	0.038	2.13	−16.5	0.70	0.39	−7.8			
2330+387 ...	0.250	0.00	0.0	1.00	0.58	24.8	1.037	1.230	1.126
	0.033	1.68	−161.0	0.00	0.80	0.0			
	0.182	45.20	−151.9	4.44	0.49	−144.9			
2346+385 ...	0.621	0.00	0.0	0.44	0.23	−47.3	0.905	1.029	0.962
	0.034	1.91	−28.7	0.66	0.00	51.7			
2356+385 ...	0.342	0.00	0.0	1.67	0.30	−21.4	0.893	1.232	1.059
	0.038	0.98	−136.4	0.826	0.00	31.5			
2356+390 ...	0.214	0.00	0.0	0.26	0.93	51.1	0.916	1.073	0.990
	0.057	1.71	−129.2	1.07	0.31	−139.0			
	0.012	3.71	−128.9	0.64	0.00	−95.2			
	0.031	8.82	−134.9	4.14	0.83	−130.7			

NOTES.—Parameters of each Gaussian component of the model brightness distribution: S, flux density; r, θ, polar coordinates of the center of the component relative to an arbitrary origin, with polar angle measured from north through east; a, b, major and minor axes (FWHM); Φ, position angle of the major axis measured from north through east.

Table 3 is published in computer-readable form in the AAS CD-ROM Series, Vol. 4.

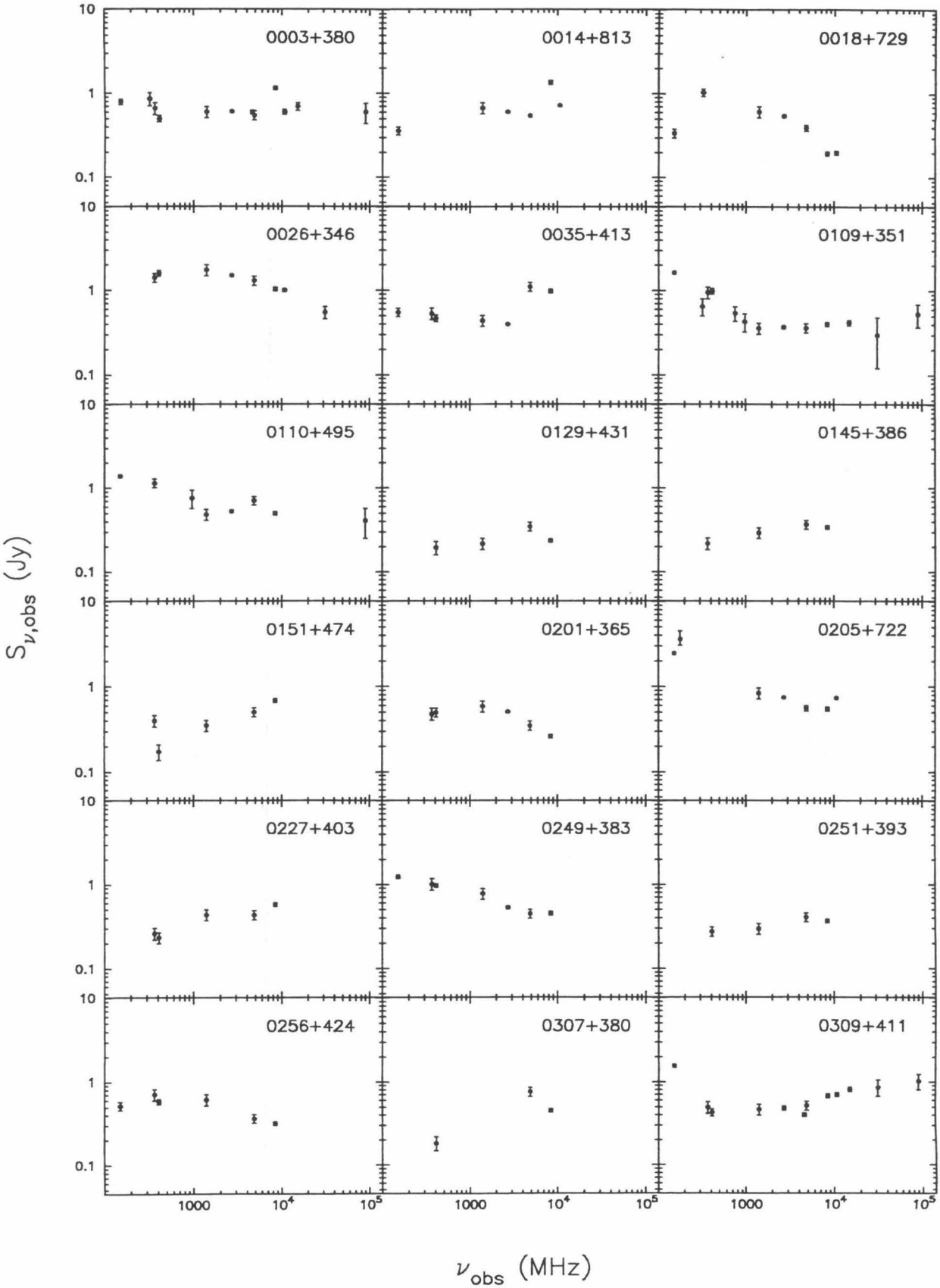

FIG. 3.—Integrated radio spectra for the entire CJ2 sample. All flux densities are on the scale of Laing & Peacock (1980). The error bars are $\pm 1\ \sigma$ and are mainly taken from the flux density catalogs, although we have estimated some of these.

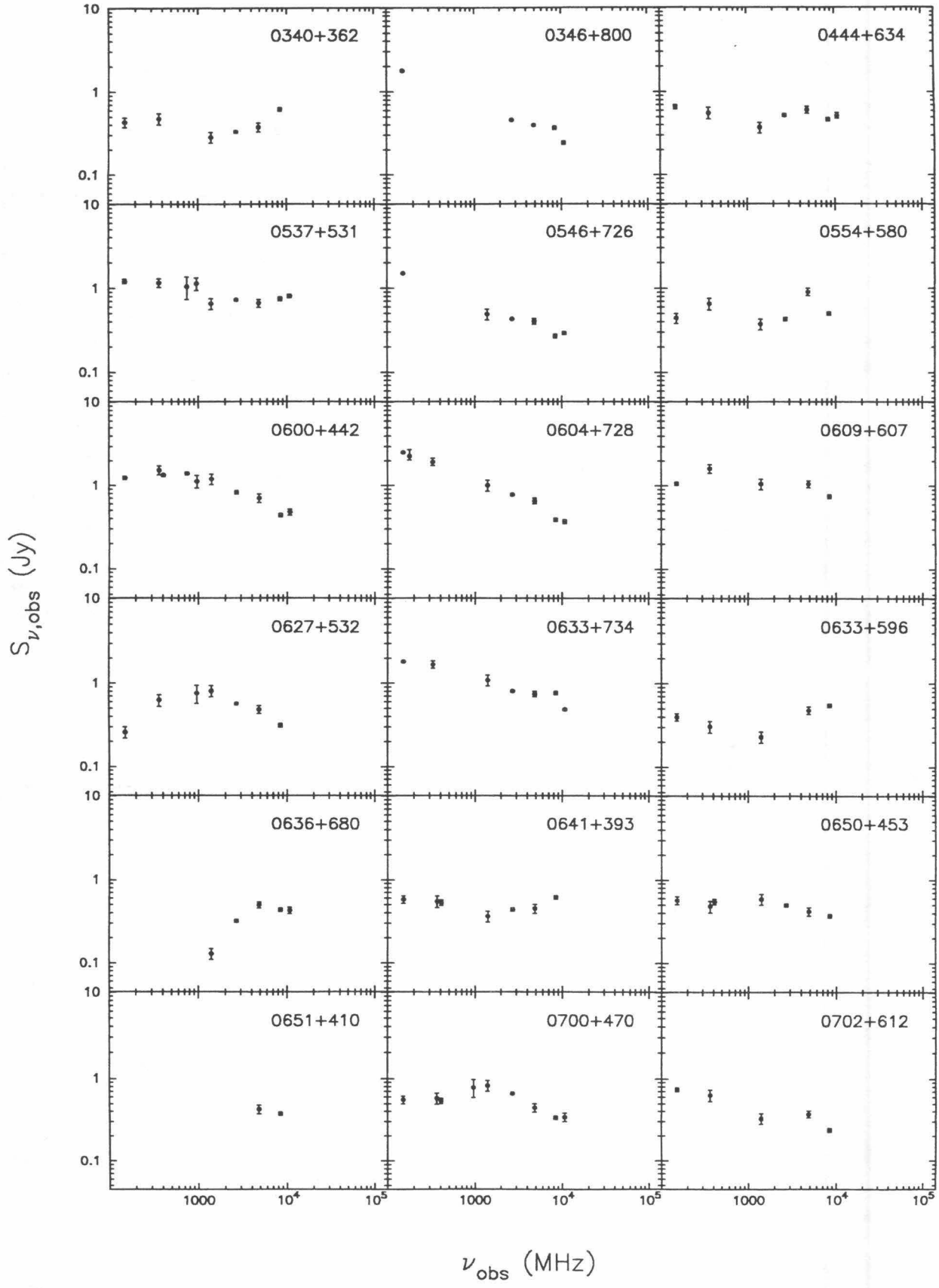

FIG. 3—*Continued*

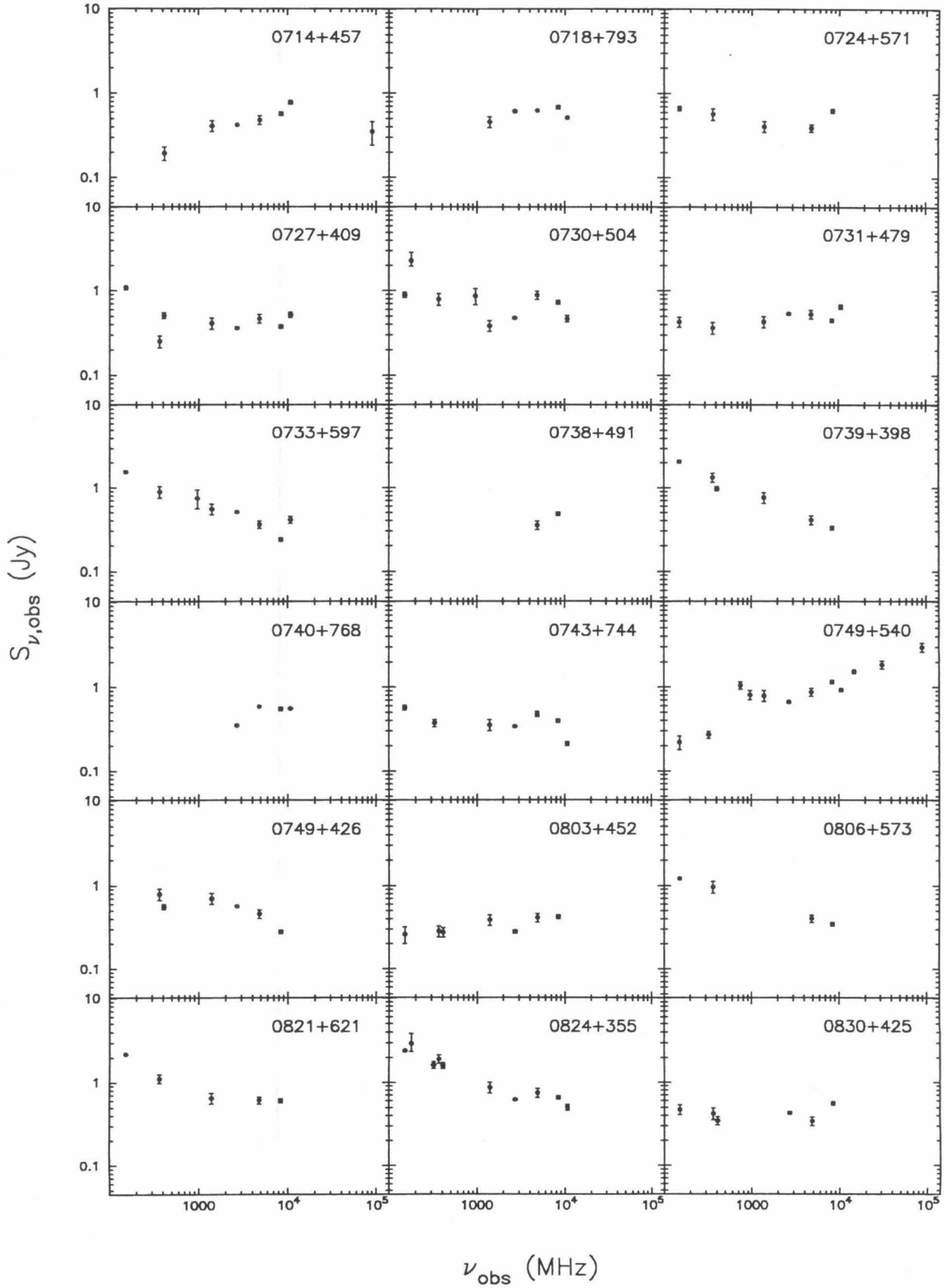

FIG. 3—*Continued*

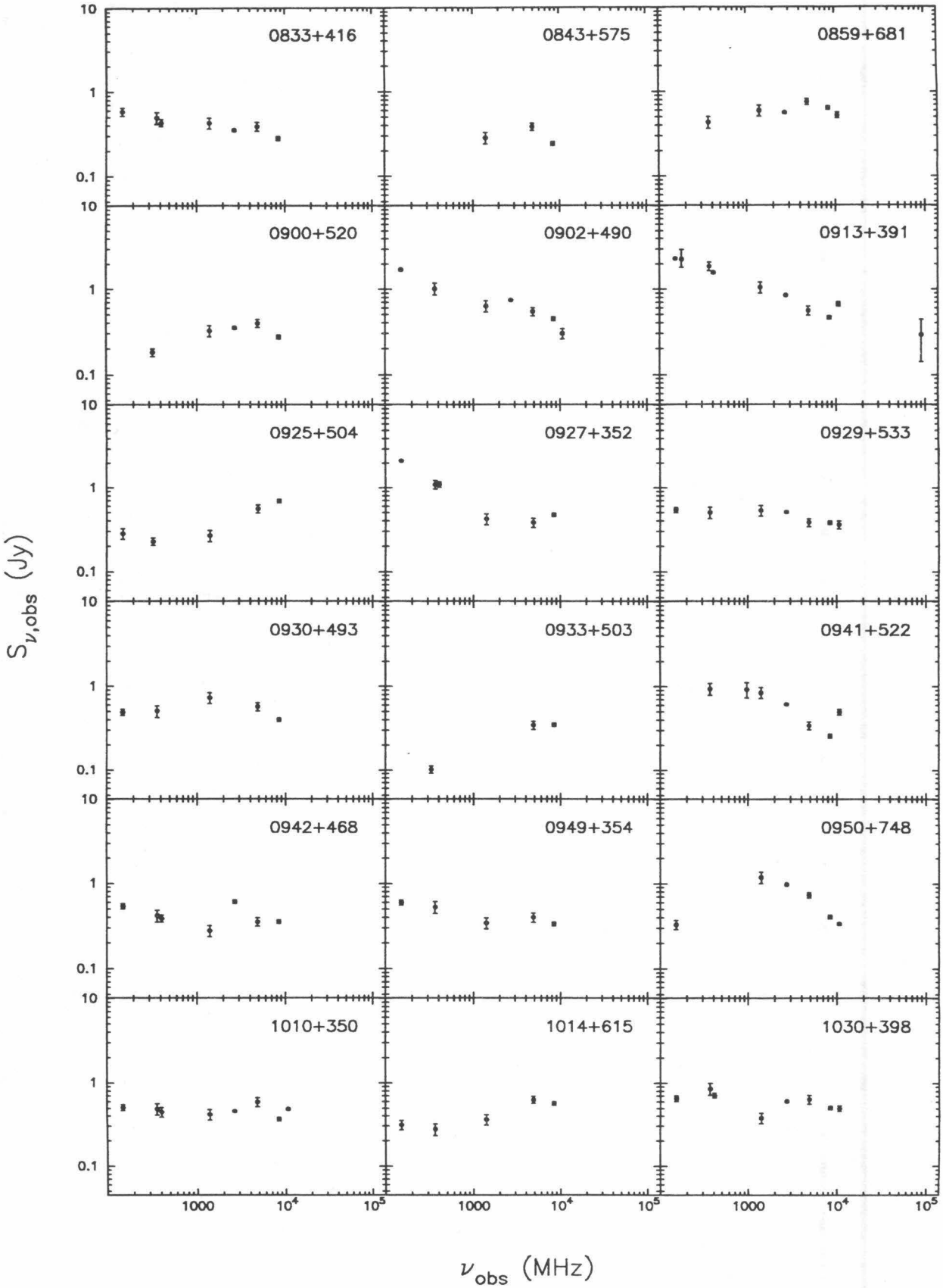

FIG. 3—*Continued*

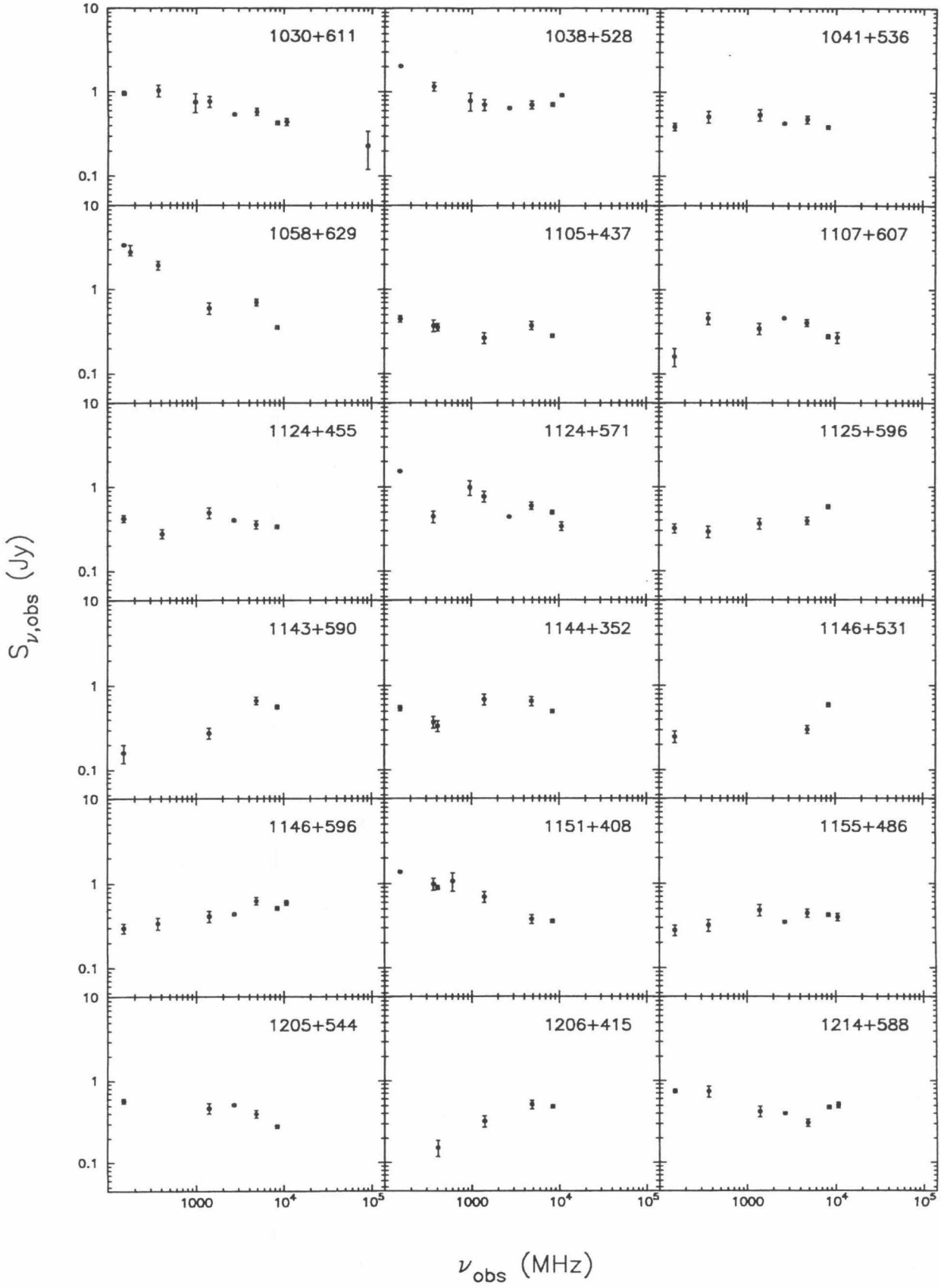

FIG. 3—*Continued*

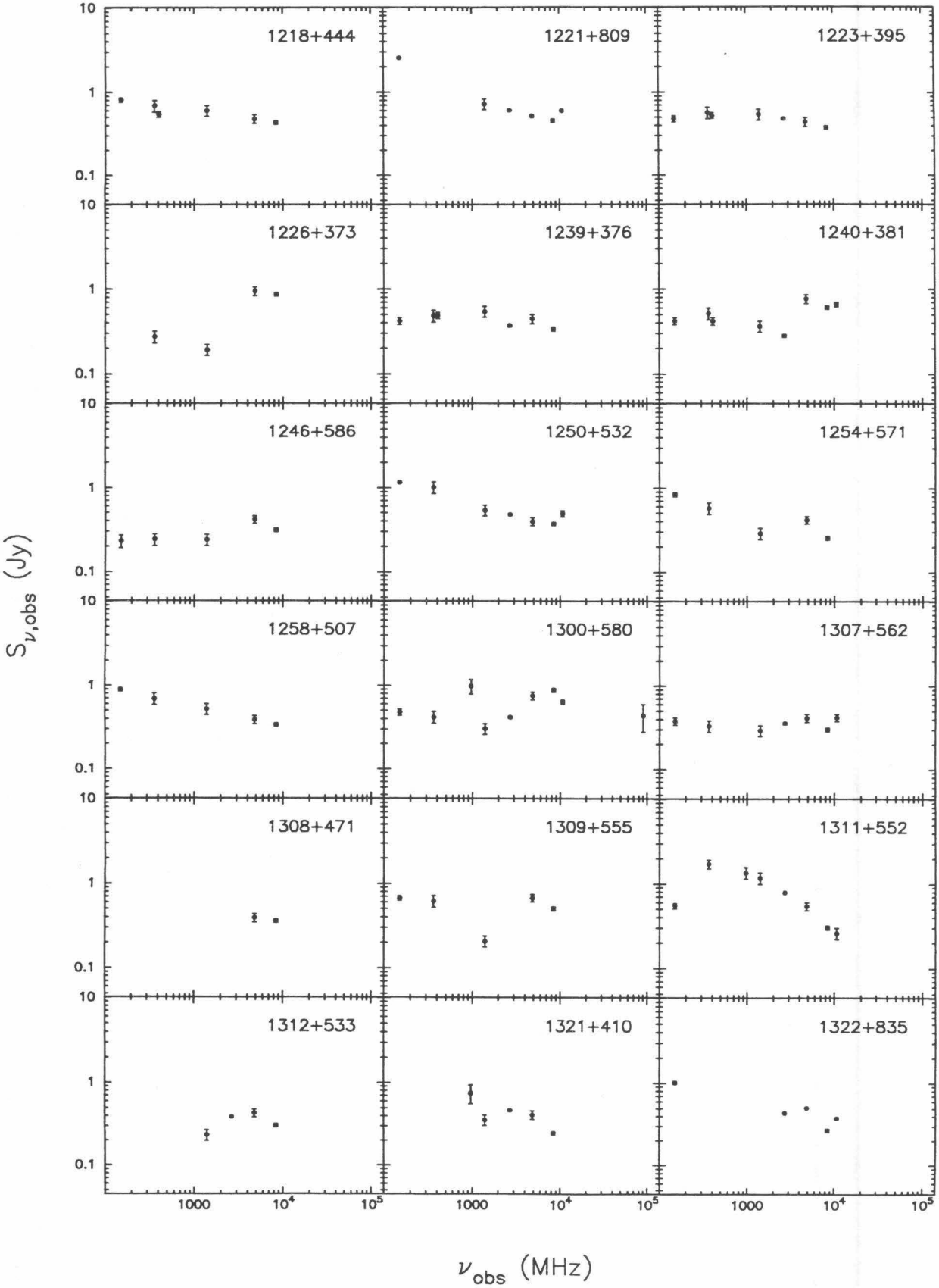

FIG. 3—*Continued*

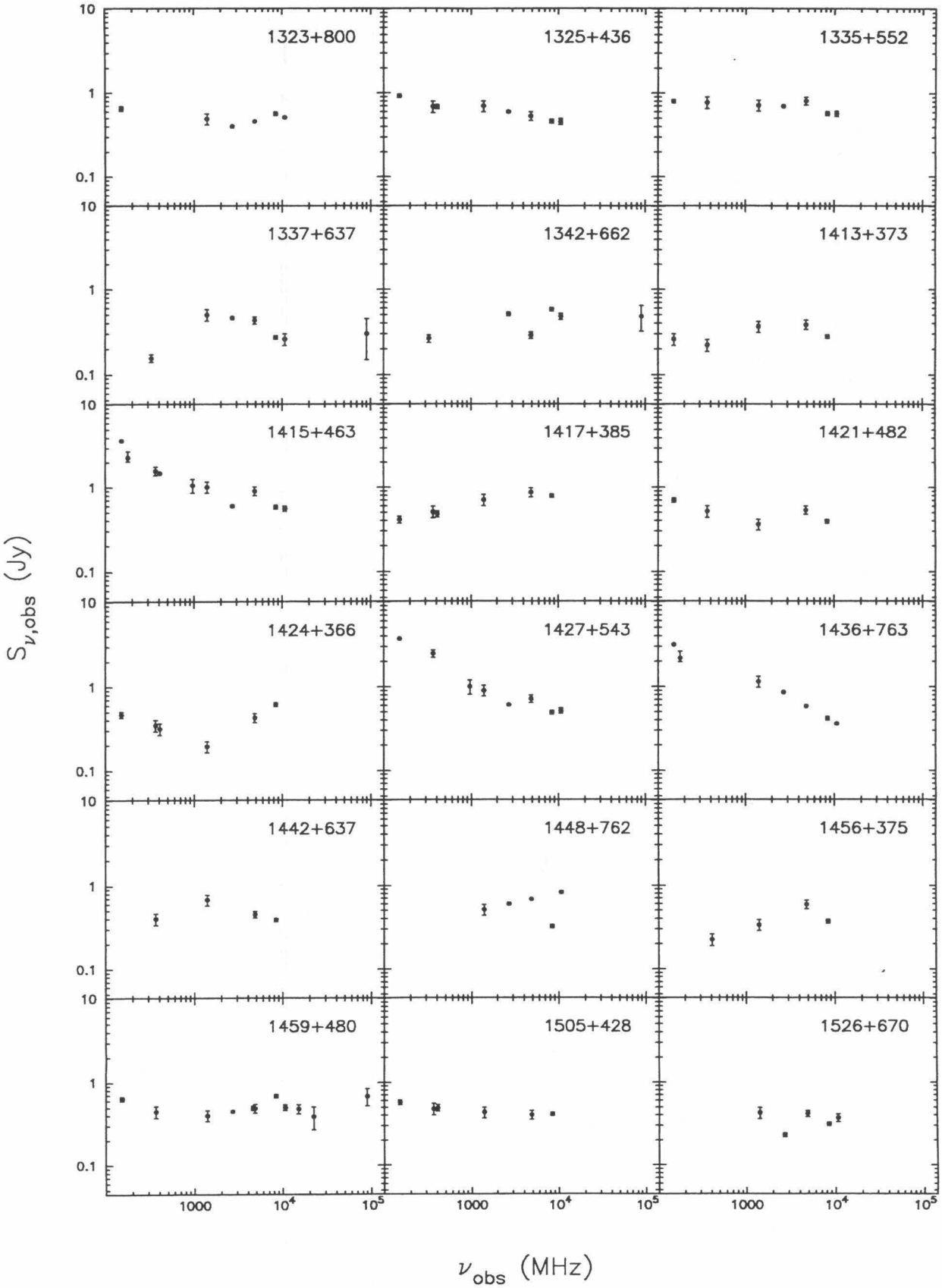

FIG. 3—*Continued*

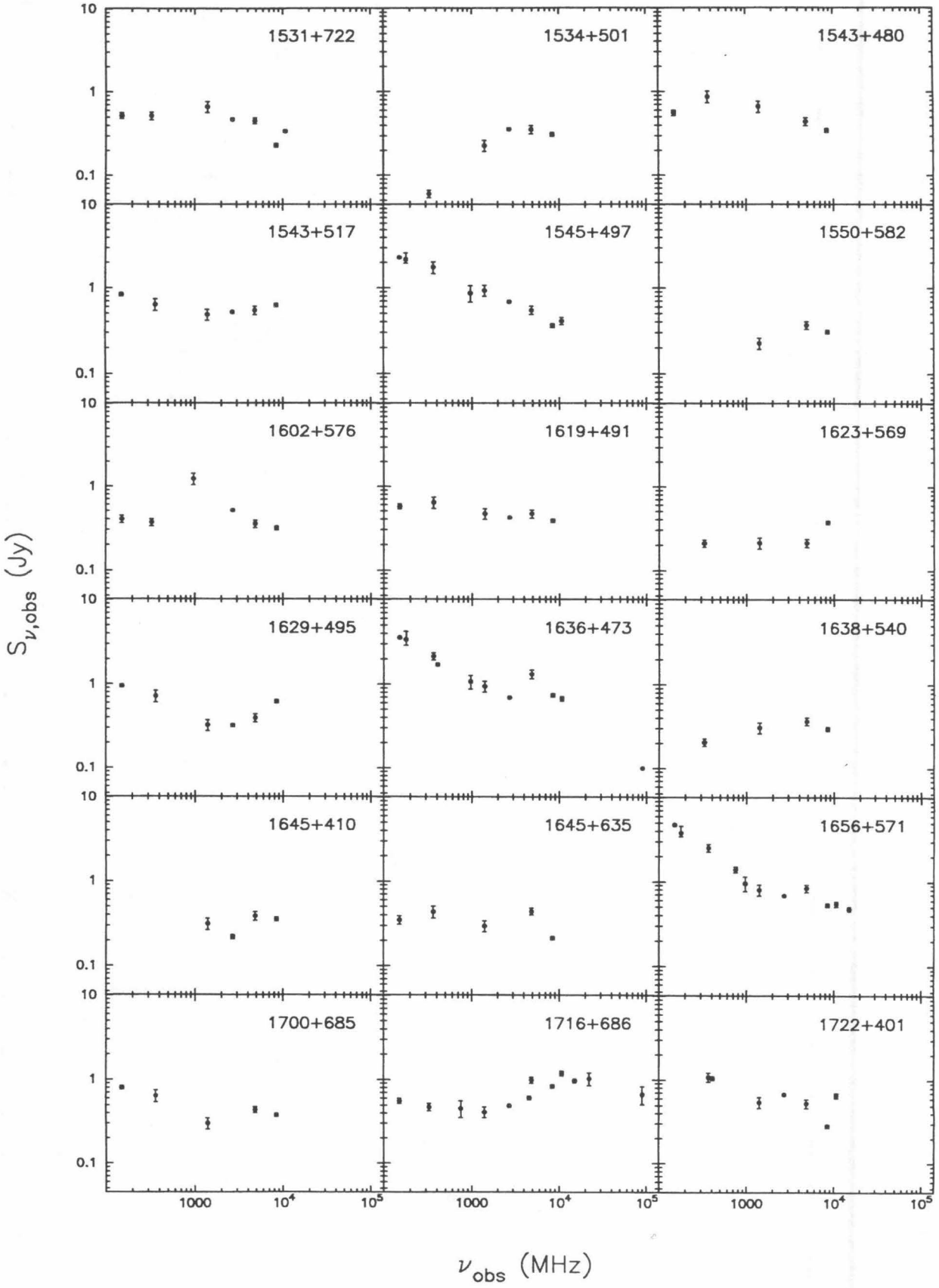

FIG. 3—*Continued*

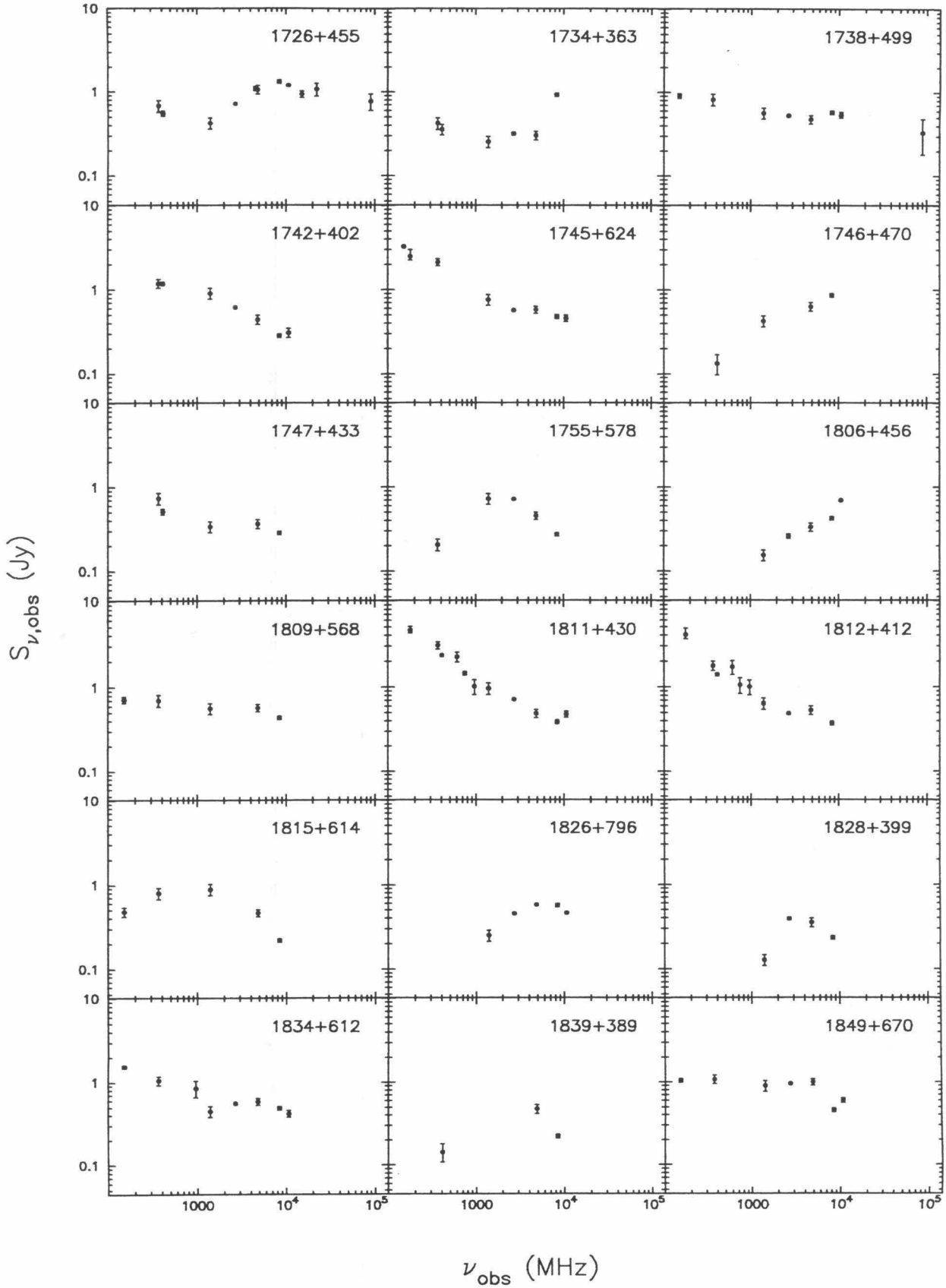

FIG. 3—*Continued*

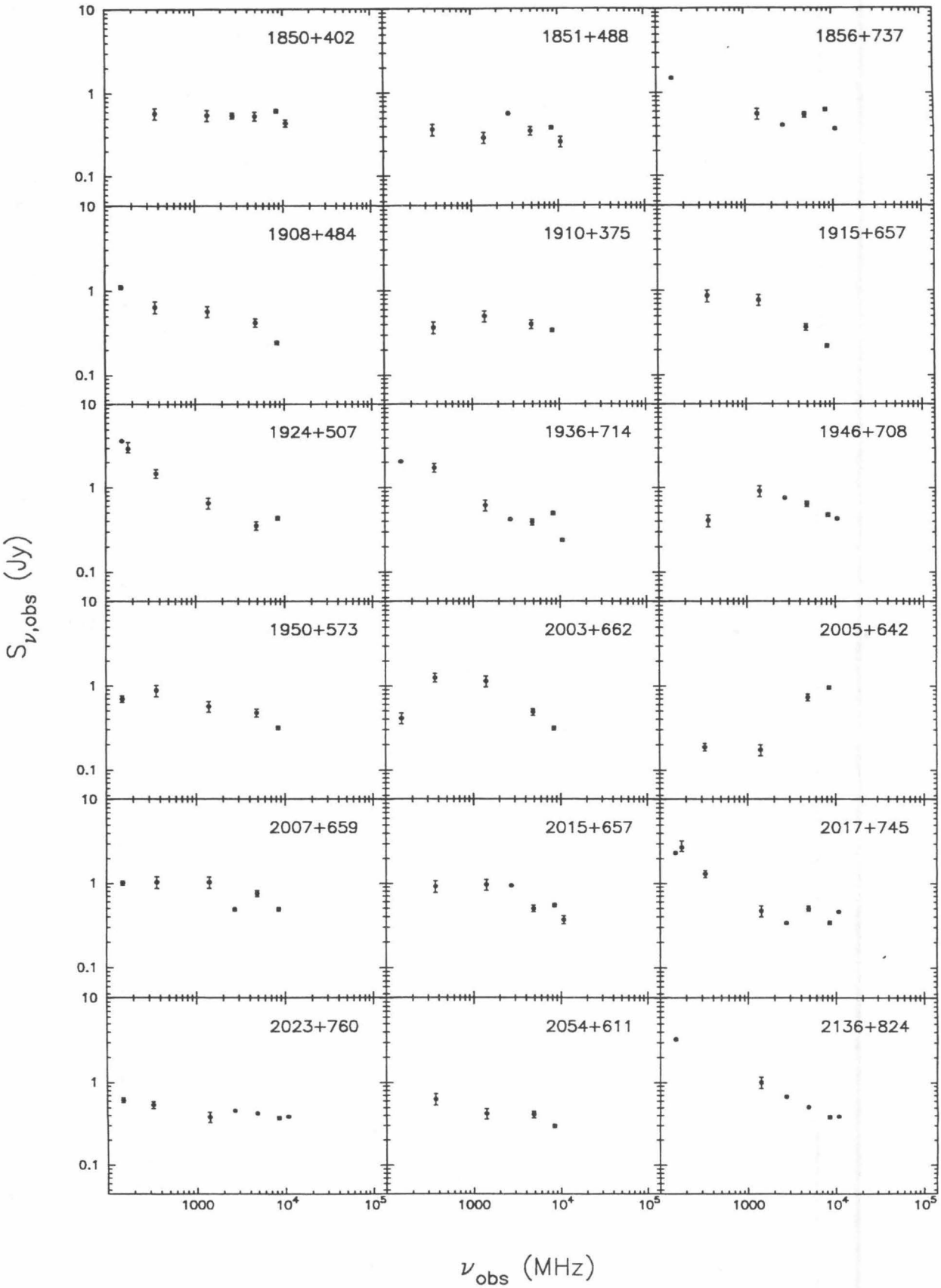

FIG. 3—*Continued*

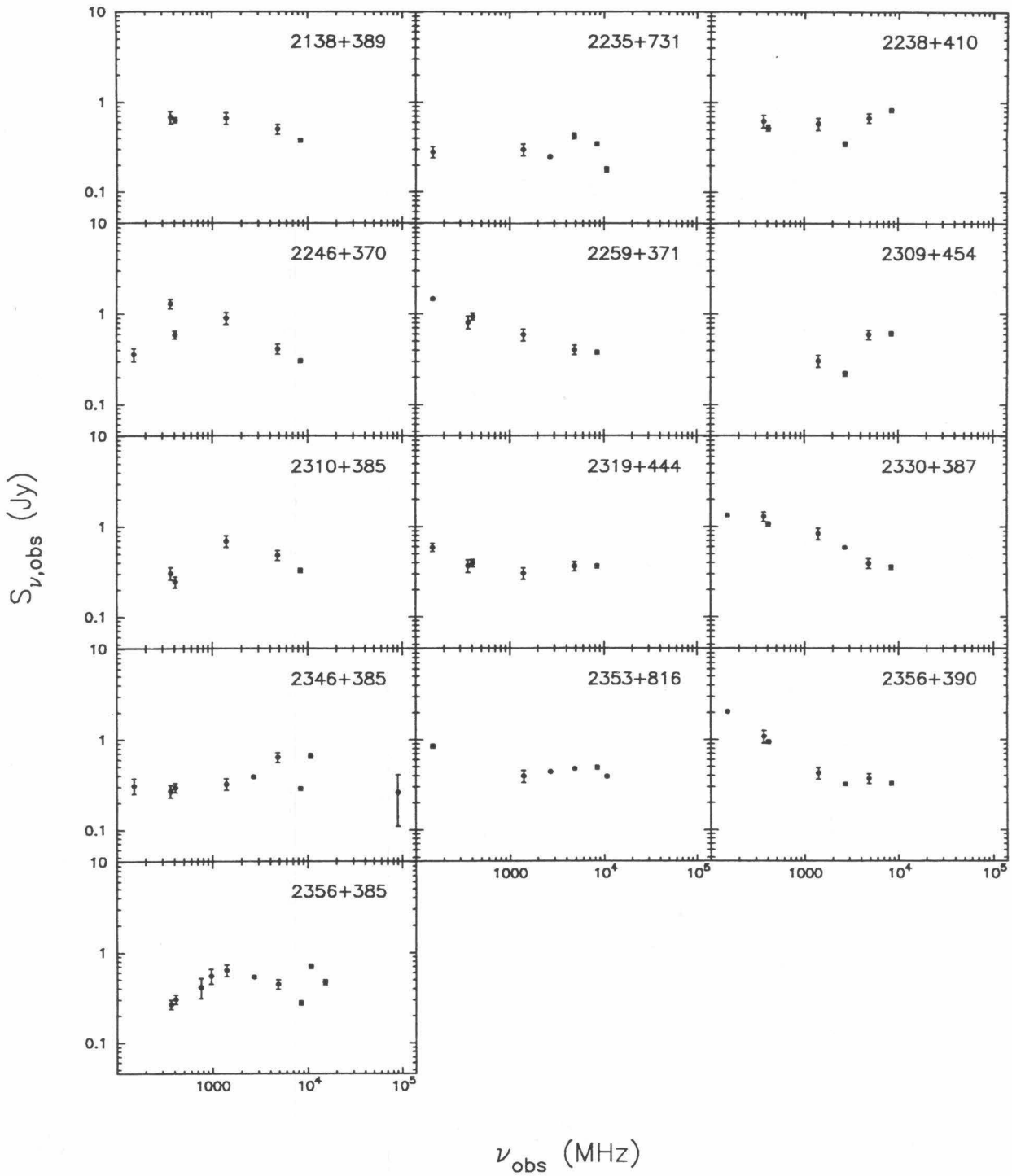

FIG. 3—*Continued*

TABLE 4

FLUX DENSITY CATALOGS

Frequency (MHz) (1)	Survey (2)	Reference(s) (3)	Typical Error (4)	Correction Factor (5)
151	6C	Baldwin et al. (1985), Hales, Baldwin & Warner (1988, 1993), Hales et al. (1990, 1991, 1993)	50 mJy	–
178	4C	Pilkington & Scott (1964), Gower, Scott & Wills (1967)	10%	1.09[a]
318		Kühr et al. (1979)	150 mJy	–
327	WENSS	WENSS team, 1994, priv. comm.	10%	–
365	Texas	Douglas et al. (1980)	15 mJy	1.041[b]
408	B2.3	Colla et al. (1973)	50 mJy	0.96 – 1.02[c]
408	B3	Ficarra et al. (1985)	50 mJy	0.96 – 1.02[c]
610	VRO	Macleod et al. (1965)	20%	1.065[d]
750		Pauliny-Toth, Wade & Heeschen (1966)	200 mJy	1.059[e]
750		Owen, Spangler & Cotton (1980)	100 mJy	1.035[e]
966		Kühr et al. (1979)		–
968		Owen, Spangler & Cotton (1980)	100 mJy	1.026[e]
1400		White & Becker (1992)	15%	–
2700		Kühr et al. (1979)	25 mJy	–
4585		Kühr et al. (1979)	40 mJy	–
4850	87GB	Gregory & Condon (1991)	15%	–
4890	S5	Kühr et al. (1981a)	5 mJy	–
8400	JVAS	Patnaik et al. (1992) and other JVAS papers in preparation	5%	–
10700		Kühr et al. (1979)	25 mJy	–
15000		Owen, Spangler & Cotton (1980)	40 mJy	–
15064		Kühr et al. (1979)	80 mJy	–
22185		Kühr et al. (1979)	150 mJy	–
31400		Kühr et al. (1979)	90 mJy	–
31400		Owen, Spangler & Cotton (1980)	200 mJy	–
90000		Kühr et al. (1979)	160 mJy	–
90000		Owen, Spangler & Cotton (1980)	200 mJy	–

NOTES.—Col. (1): The frequency of observation (in MHz). Col. (2): Name of the survey (if any); abbreviations are as follows: 6C, 6th Cambridge Survey; 4C, 4th Cambridge Survey; WENSS, Westerbork Northern Sky Survey; Texas, Texas Survey; B2.3, B3, Second Bologna Survey (Third Part) and Third Bologna Survey, respectively; VRO, Vermilion River Observatory Survey; 87GB, 1987 Green Bank Survey; S5, 5th Strong Source Survey; JVAS, Jodrell Bank–VLA Astrometric Survey. Col. (3): Reference(s) for the flux density catalog. A subsample of Kühr et al. 1979 containing only the sources stronger than 1 Jy at 5000 MHz was later published as Kühr et al. 1981b. Col. (4): Estimate of the typical uncertainty on the flux densities in the catalog, either in millijanskys or as a percentage of the flux density. Note that the error bars in Fig. 3 are taken predominantly from the uncertainties quoted for each flux density in the catalog, rather than these estimated values. Col. (5): The correction factor applied to the flux densities in the catalog to convert them to the absolute scale of Laing & Peacock 1980. Superscripts indicate source of correction factor: a, Roger, Bridle, & Costain 1973; b, J. Douglas, private communication; c, Riley 1988, correction factor depends on flux; d, Baars et al. 1977; e, Kühr et al. 1981b.

The flux density measurements for 1038+528 that were made with low-resolution instruments will be contaminated by a strong quasar, 1038+528B, located only 33″ to the northwest. VLBI observations of both quasars are reported by Marcaide & Shapiro (1984).

The spectral index distribution for the CJ2 sample is shown in Figure 4. Note that most flat-spectrum sources are variable, and since the flux density measurements at different frequencies were not simultaneous, the spectral indices derived are only representative and will differ from the instantaneous values. While the vast majority of the CJ2 sample have flat radio spectra, there are 13 "steep-spectrum" sources with $\alpha < -0.5$. Thus the CJ2 sample is not a perfect spectrally limited sample.

5. SUMMARY

Global VLBI images at 4992 MHz are presented for the 102 sources observed in the final observing session of the CJ2 survey. We also present integrated radio spectra for the entire CJ2 sample. Future papers will discuss the interpretation of these observations and of second-epoch observations. A concerted effort is underway to obtain redshifts for all objects in this sample.

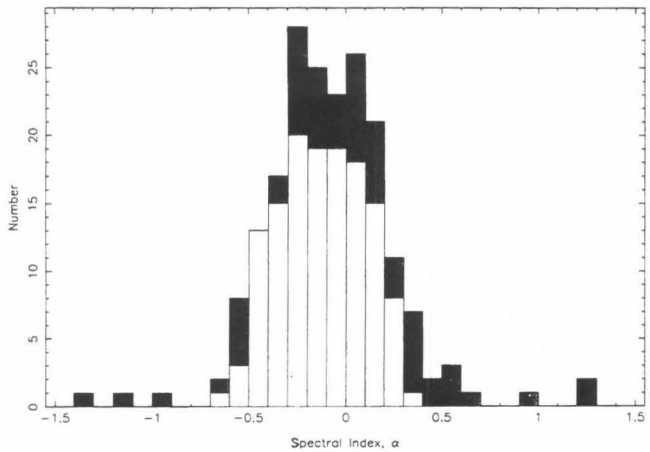

FIG. 4.—Distribution of spectral index (defined as $S_\nu \propto \nu^\alpha$) for the CJ2 sample. For most sources, α has been calculated between 365 MHz and 8400 MHz (shown with no shading). For 49 sources, with unknown 365 MHz flux densities, α has been calculated between 1400 MHz and 8400 MHz (*gray shading*); and for 12 sources, with both an unknown 365 MHz and 1400 MHz flux density, α has been calculated between 4850 MHz and 8400 MHz (*black shading*).

We thank the staff at the VLA, VLBA, and European VLBI Network observatories who took part in these observations and the staff of the JPL/Caltech Block II Correlator for their assistance. We also thank Sally Hales for help in obtaining the 151 MHz flux densities and for advice on the use of flux density scales. We are grateful to Jim Douglas for providing 365 MHz flux densities prior to publication and to Ger de Bruyn for providing 327 MHz flux densities from the WENSS prior to publication. We are indebted to Martin Shepherd for writing and maintaining DIFMAP and for the many modifications he made on our behalf. Thanks also to Roddy Calder for help with Figure 4. D. R. H. acknowledges the receipt of a SERC research studentship. The work done by the Caltech group was supported by the NSF under grant AST-9117100.

APPENDIX
AGREEMENT FACTORS

Table 3 lists *agreement factors* between the models and observed visibilities. Separate agreement factors are given for amplitude and closure phase. In addition a total agreement factor (a weighted average of the amplitude and closure-phase agreement factors) is given; this is the quantity that is minimized in the least-squares model-fitting procedure. The closure-phase agreement factor is useful because it is not affected by antenna phase calibration errors.

A1. AMPLITUDE AGREEMENT FACTOR

Denoting the model amplitude and phase at a sample point by A_m and ϕ_m and the observed amplitude and phase by A_0 and ϕ_0 with standard errors σ_A and σ_ϕ, the *amplitude agreement factor* is

$$Q_{\rm AMP} = \sqrt{\frac{1}{M}\sum_1^M \left(\frac{A_0 - A_m}{\sigma_A}\right)^2}, \qquad (1)$$

where the sum is over M measured visibility samples. Assuming that all the samples are independent and that the measured amplitudes have a Gaussian distribution (high-SNR approximation), the sum of squares in this expression is distributed as χ^2 with M degrees of freedom, and $Q^2_{\rm AMP}$ is a reduced χ^2 with expected value 1. (For a large number of degrees of freedom ν, the distribution of χ^2 is approximately normal with mean ν and standard deviation $\sqrt{2\nu}$.)

In the process of model fitting, a number m of parameters of the model are estimated from the data. This reduces the number of degrees of freedom from M to $M - m$, so the amplitude agreement factor, as defined above, is not strictly a reduced χ^2. For Gaussian model fitting, m is usually small compared with M, so this distinction can be ignored, but for a clean-component model with hundreds of parameters (component flux densities and positions), m may be large, and the expected value of the agreement factor may be significantly less than 1.

When the data are self-calibrated, additional parameters (unknown antenna gains) are estimated from the data, so the number of degrees of freedom is reduced. For example, if the data are taken on an array of N antennas and $N(N-1)/2$ baselines and if independent gains are estimated for each antenna for each integration, the number of degrees of freedom is reduced by a factor $(N-3)/(N-1)$, and the expected value of $Q_{\rm AMP}$ is $\sqrt{(N-3)/(N-1)}$ (e.g., 0.58 for $N = 4$ and 0.88 for $N = 10$). Wieringa (1992) has shown that for self-calibration with a perfect model, the noise in the visibility amplitudes after application of (noisy) gain solutions is *lower* than the noise in the input visibilities by a factor $\approx \sqrt{(N-3)/(N-1)}$. This leads to the reduction in the expected value of $Q_{\rm AMP}$ shown above.

A2. CLOSURE-PHASE AGREEMENT FACTOR

Closure phase is the sum of visibility phases around a triangle of baselines; e.g., for three antennas i, j, k,

$$\psi_0^{(ijk)} = \phi_0^{(ij)} + \phi_0^{(jk)} - \phi_0^{(ik)} . \tag{2}$$

In the high-SNR approximation, the variance of the closure phase is given by

$$(\sigma_\psi^{(ijk)})^2 = (\sigma_\phi^{(ij)})^2 + (\sigma_\phi^{(jk)})^2 + (\sigma_\phi^{(ik)})^2 . \tag{3}$$

In an array of N antennas in which all baselines are measured, there are $N(N-1)/2$ visibility phase measurements from which $N(N-1)(N-2)/6$ closure phases can be formed. However, only $(N-1)(N-2)/2$ of these are independent.

The *closure-phase agreement factor* is defined in a similar way to the amplitude agreement factor but allows for the fact that the closure phases are not all independent:

$$Q_{\mathrm{CLP}} = \sqrt{\sum_1^{M_{\mathrm{CLP}}} f\left(\frac{\psi_0 - \psi_m}{\sigma_\psi}\right) \Big/ \sum_1^{M_{\mathrm{CLP}}} f} , \tag{4}$$

where the sum is taken over all M_{CLP} available closure-phase samples, but the denominator $\sum f$ is now the number of independent closure phases, and the factor f is computed for each sampling interval as the number of independent closure phases divided by the total number of closure phases in that interval. If all baselines were observed, then $f = 3/N$.

REFERENCES

Baars, J. W. M., Genzel, R., Pauliny-Toth, I. I. K., & Witzel, A. 1977, A&A, 61, 99
Baldwin, J. E., Boysen, R. C., Hales, S. E. G., Jennings, J. E., Waggett, P. C., Warner, P. J., & Wilson, D. M. A. 1985, MNRAS, 217, 717
Colla, G., et al. 1973, A&AS, 11, 291
Douglas, J. N., Bash, F. N., Torrence, G. W., & Wolfe, C. 1980, Univ. Texas Publ. Astron., 17
Ficarra, A., Grueff, G., & Tomassetti, G. 1985, A&AS, 59, 255
Gower, J. F. R., Scott, P. F., & Wills, D. 1967, MmRAS, 71, 49
Gregory, P. C., & Condon, J. J. 1991, ApJS, 75, 1011
Hales, S. E. G., Baldwin, J. E., & Warner, P. J. 1988, MNRAS, 234, 919
———. 1993, MNRAS, 263, 25
Hales, S. E. G., Masson, C. R., Warner, P. J., & Baldwin, J. E. 1990, MNRAS, 246, 256
Hales, S. E. G., Masson, C. R., Warner, P. J., Baldwin, J. E., & Green, D. A. 1993, MNRAS, 262, 1057
Hales, S. E. G., Mayer, C. J., Warner, P. J., & Baldwin, J. E. 1991, MNRAS, 251, 46
Kühr, H., Nauber, U., Pauliny-Toth, I. I. K., & Witzel, A. 1979, MPIfR preprint, 55
Kühr, H., Pauliny-Toth, I. I. K., Witzel, A., & Schmidt, J. 1981a, AJ, 86, 854
Kühr, H., Witzel, A., Pauliny-Toth, I. I. K., & Nauber, U. 1981b, A&AS, 45, 367
Laing, R. A., & Peacock, J. A. 1980, MNRAS, 190, 903 (LP)
MacLeod, J. M., Swenson, G. W., Jr., Yang, K. S., & Dickel, J. R. 1965, AJ, 70, 756
Marcaide, J. M., & Shapiro, I. I. 1984, ApJ, 276, 56
Napier, P. J., Bagri, D. S., Clark, B. G., Rogers, A. E. E., Romney, J. D., Thompson, A. R., & Walker, R. C. 1994, Proc. IEEE, 82, 658
Owen, F. N., Spangler, S. R., & Cotton, W. D. 1980, AJ, 85, 351
Patnaik, A. R., Browne, I. W. A., Wilkinson, P. N., & Wrobel, J. M. 1992, MNRAS, 254, 655
Pauliny-Toth, I. I. K., Wade, C. M., & Heeschen, D. S. 1966, ApJS, 13, 65
Pearson, T. J., & Readhead, A. C. S. 1988, ApJ, 328, 114 (PR)
Pilkington, J. D. H., & Scott, P. F. 1964, MmRAS, 69, 183
Polatidis, A. G., Wilkinson, P. N., Xu, W., Readhead, A. C. S., Pearson, T. J., Taylor, G. B., & Vermeulen, R. C. 1995, ApJS, 98, 1
Riley, J. M. 1988, MNRAS, 233, 225
Roger, R. S., Bridle, A. H., & Costain, C. H. 1973, AJ, 78, 1030
Shepherd, M. C., Pearson, T. J., & Taylor, G. B. 1994, BAAS 26, 987
Taylor, G. B., Vermeulen, R. C., Pearson, T. J., Readhead, A. C. S., Henstock, D. R., Browne, I. W. A., & Wilkinson, P. N. 1994, ApJS, 95, 345 (Paper I)
Thakkar, D. D., Xu, W., Readhead, A. C. S., Pearson, T. J., Taylor, G. B., Vermeulen, R. C., Polatidis, A. G., & Wilkinson, P. N. 1995, ApJS, 98, 33
Vermeulen, R. C., & Taylor, G. B. 1995, AJ, 109, 1983
Wieringa, M. H. 1992, Exp. Astron., 2, 203
White, R. L., & Becker, R. H. 1992, ApJS, 79, 331
Xu, W., Readhead, A. C. S., Pearson, T. J., Polatidis, A. G., & Wilkinson, P. N. 1995, ApJS, 99, 297